Introduction

With the success of the first Faroe Islands Exploration Conference (FIEC) in 2004 as a forum for discussion for industry and academia professionals working within the Faroese area and the North Atlantic in general, it was decided to keep the impetus and a second conference was held in 2006 and this proceedings volume contains a large portion of the presentations given.

The first initial phase of exploration within the Faroese Continental Shelf focused on the non-basalt covered Judd Basin, with some disappointing and surprising results. Some aspects of the outcome from this first phase is discussed here, with some interesting results relating to the effect intrusives can have on reservoir sections and a unique example of how band-limited impedance inversion can help in understanding sill emplacement.

The period between the two conferences has been focusing on raising the prospectivity in the large areas on the Faroese Continental Shelf, which are covered with various thicknesses of volcanics and some encouraging results from the UK side has emerged, with the drilling of Cambo and the intra-basalt Rosebank discoveries close to the Faroese area. Results from the Rosebank discovery were presented at the second conference for the first time and a contribution in this proceedings volume is presenting some of the aspects of this important discovery.

Over the years a major obstacle in de-risking prospects within these volcanic covered areas has been the difficulty in seismic imaging and much effort and attention has focused on this issue in the period between the two conferences. Some of the results are presented in this volume and the contributions shows some pronounced improvements using both novel acquisition techniques and processing techniques which all has helped in improving the mapping of sub-basalt structures.

With the new exploration efforts focusing on the basalt covered areas of the Faroese Continental Shelf, a better understanding of the spatial and temporal development of the volcanic section and its interaction with non-volcanic sedimentary systems has also been the centre of attention and this proceedings volume present some interesting results and insights gained from mapping of the exposed volcanic pile onshore Faroes and an example of post-basalt delta systems sourced from the Faroese area into the Faroe-Shetland Channel and the mixing with non-volcanic sediments from the Shetland side is presented.

Also the link between different volcanic facies observed onshore and the responses seen on offshore seismic data and wireline logs is offered here.

Another important contribution emphasises the importance and difficulties with age dating basalts and the discrepancy between the obtained ages from radiometric dating and biostratigraphy.

In a regional context, important results from wide-angle seismic experiments, inversion of S-wave arrivals and inversion of satellite gravity data points out the importance of understanding the larger picture in assessing an area's prospectivity.

A number of contributions in this volume describes in close detail specific prospects within the Faroese area and the effort that has gone into de-risking these, some to such a degree that wells have been committed to and the next couple of years should be an interesting period in the exploration history on the Faroese Continental Shelf.

Thomas Varming

Crustal structure of the Norwegian-Greenland Sea from Satellite Gravity Inversion Incorporating a Correction for the Lithosphere Thermal Gravity Anomaly

ALEX R. CHAPPELL[1*] AND NICK J. KUSZNIR[1]

[1] Department of Earth and Ocean Science, University of Liverpool, Jane Herdman Laboratories, 4 Brownlow Street, Liverpool, Merseyside L69 3GP, UK

* Email: alex_chappell@hotmail.com

ABSTRACT

We have used gravity inversion, incorporating a lithosphere thermal gravity anomaly correction, to produce maps of the maximum bound of crustal thickness in the North Atlantic between Iceland and the Jan Mayen Fracture Zones in order to assess the accuracy and validity of proposed plate reconstruction models. The lithosphere thermal gravity anomaly and crustal thickness depend on the thermal equilibration age given by the assumed plate reconstruction model. We predict the ocean-continent transition location in the Norway Basin and use it to assess the applicability of plate reconstruction models. For the Iceland Plateau, we test 3 plate reconstruction hypotheses. We test a model that assumes that the Jan Mayen Basin is oceanic and two models that assume continental crust in the Jan Mayen Basin; one assumes spreading at the Kolbeinsey Ridge only and one assumes that an early Miocene spreading axis existed within the Iceland Plateau. We find no evidence for a second spreading axis in the Iceland Plateau.

Introduction

In this paper, we present an appraisal of current plate reconstruction models for the region of the North Atlantic between Iceland and the Jan Mayen Fracture Zones (Figures 1 and 2) by generating crustal thickness maps for each model using a 3D satellite gravity inversion for Moho depth (Greenhalgh and Kusznir, 2007; Chappell and Kusznir, 2008a). The inversion method makes a correction for the variations in lithosphere temperature and density associated with the thinning of the lithosphere at rifted continental margins and the formation of oceanic lithosphere. In generating this correction, using a cooling-plate lithosphere model (McKenzie, 1978) to estimate present-day lithosphere temperature, we assume a particular plate reconstruction model to predict the age of the oceanic lithosphere and the age of the rifted continental margins; thus, the Moho depth estimate is dependent on the plate reconstruction model. We can exploit this property in a number of ways to test and refine plate reconstruction models. (1) Where the plate reconstruction model is open to question and modern wide-angle seismic observations of the Moho exist, we use the gravity inversion method to predict Moho depth according to each alternative plate reconstruction model and compare these predictions to the seismic data to determine which plate reconstruction model produces a valid Moho depth estimate. (2) Where the plate reconstruction model is more established, but observations of the ocean-continent transition (OCT) location are widely spaced, we can predict the ocean continent transition in the intervening areas based on crustal thickness and thinning factor (1-1/ß). (3) In oceanic lithosphere we can compare predictions of crustal thickness to that expected from models of partial melting (e.g. Bown and White, 1994) for the spreading rate assumed in the plate reconstruction model (Greenhalgh and Kusznir, 2007).

Faroe Islands Exploration Conference: Proceedings of the 2nd Conference.
Annales Societatis Scientiarum Færoensis, Supplementum 50, 2009: 9-29

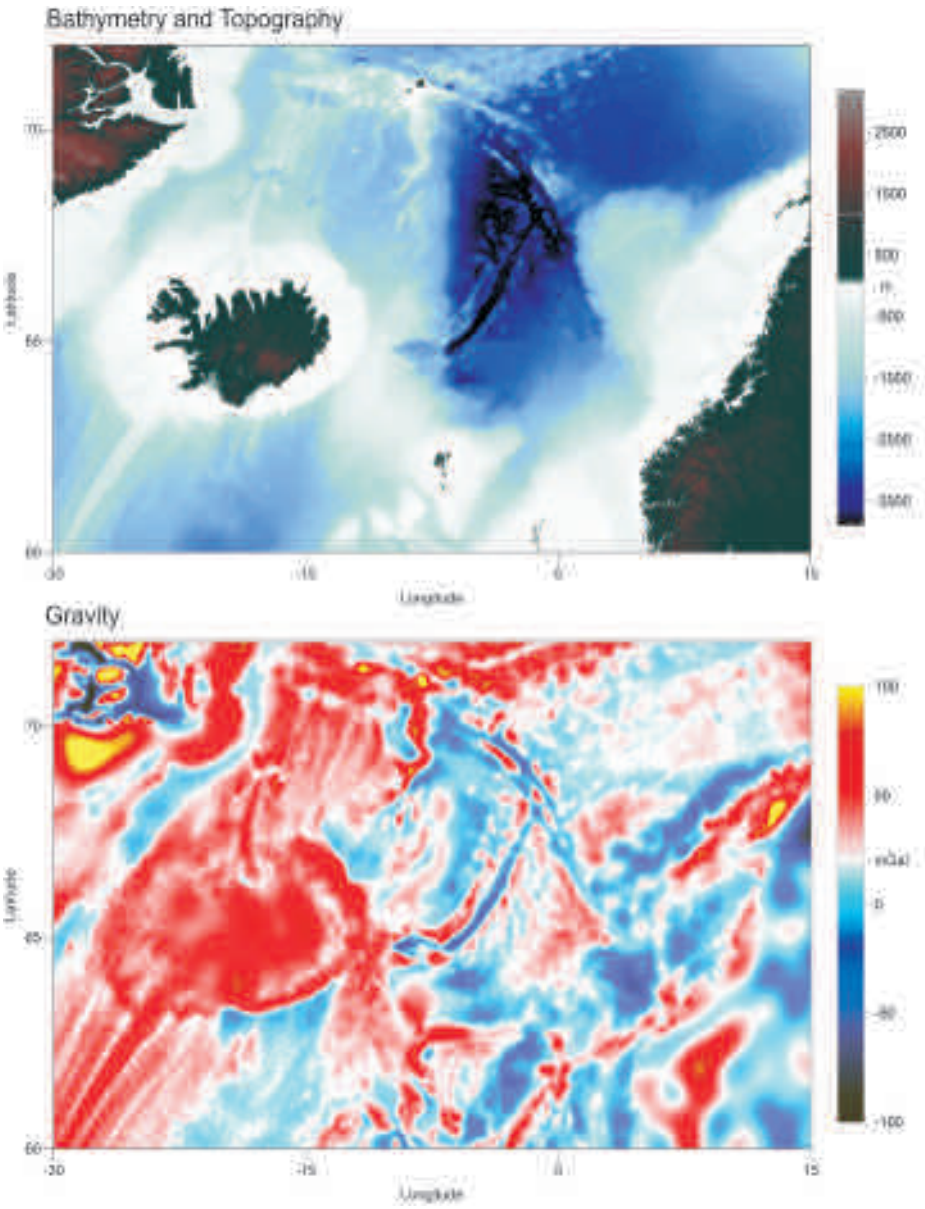

Figure 1. Bathymetry (IOC 2003) and free air gravity (Sandwell & Smith 1997) of the North Atlantic between Norway and Greenland.

In the region of interest (Figures 1 and 2), between the Jan Mayen Fracture Zones to the north and Iceland and the Iceland-Faroes Ridge to the south, the Atlantic consists of two physiographic regions, the Norway Basin and the Iceland Plateau, separated by a narrow region of shallow bathymetry, the Jan Mayen Ridge. In this paper, we use the term "Iceland Plateau" to describe the region of shallow bathymetry (< 2 km depth) to the west of the Jan Mayen Basin, which is itself on the western side of the Jan Mayen Ridge (Figure 2).

In the North Atlantic, the early Eocene break-up between the Jan Mayen microcontinent, then still part of the Greenland plate, and Norway marks the

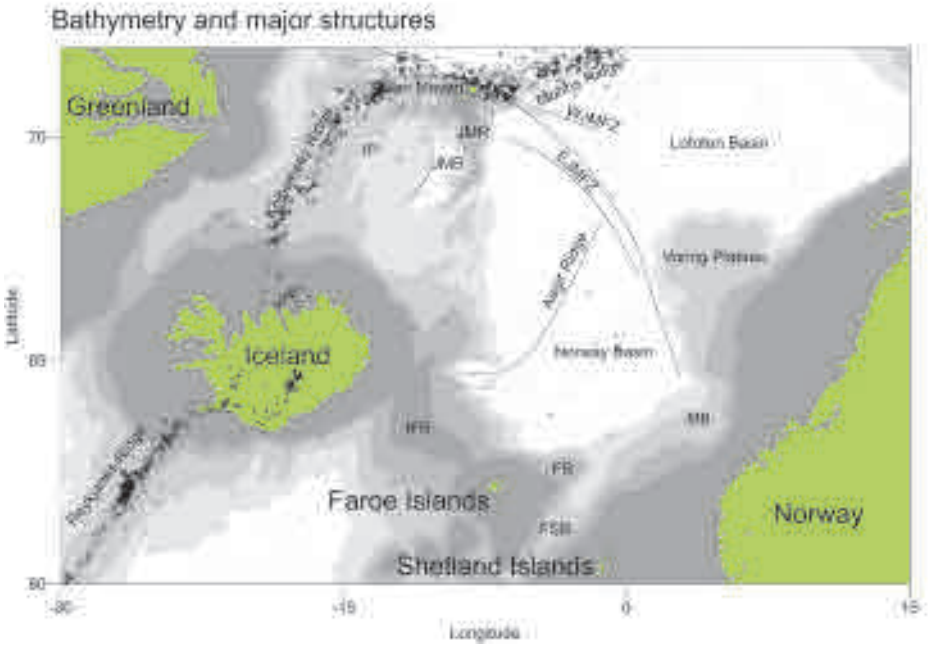

Figure 2. Major bathymetric and topographic structures of the Norway-Greenland Sea. EJMFZ - East Jan Mayen Fracture Zone; WJMFZ - West Jan Mayen Fracture Zone; JMB - Jan Mayen Basin; JMR - Jan Mayen Ridge; IP - Iceland Plateau; IFR - Iceland-Faroes Ridge; FSB - Faroe-Shetland Basin; FR - Fugloy Ridge; MB - Møre Basin. Small circles are earthquake locations marking the present day active spreading ridge and transforms faults.

end of a protracted post-Variscan history of intracontinental extension in the region (e.g. Doré *et al*., 1999). During this period, the locus of extension mostly jumped westwards towards the present-day margin, with the greatest subsidence occurring in the Cretaceous in the Rockall, Faroes-Shetland, Møre and Vøring Basins.

Several spatially and temporally discrete magmatic events affected the margins prior to break up, beginning in the late Cretaceous (O'Connor *et al*., 2000; Morton *et al*., 1995) and continuing into the Palaeocene. The events become more widespread and more intense during the Palaeocene. The presence of large volumes of basaltic magmatism during continental extension and break-up is associated with elevated upper mantle temperatures (e.g. White and McKenzie, 1989). Associated uplift, due to transient regional dynamic effects and permanent underplating of continental crust, is responsible for the generation of unconformities and the renewed supply of clastic material into many basins during the Palaeocene (e.g. Archer *et al*., 2005; White and Lovell, 1997).

Sea floor spreading between Faroes-Møre margin and the Jan Mayen microcontinent initiated during magnetic chron A24r (53.3-55.9 Ma) forming the Aegir spreading ridge (Parkin *et al*., 2007; Breivik *et al*., 2006; Mosar *et al*., 2002). The oldest oceanic crust has an observed thickness of ~14.5 km on the iSIMM seismic profile across the Faroes Shelf decreasing to ~10 km by A20 (43.2 Ma) (Parkin *et al*., 2007). Adjacent to the Møre margin the oldest oceanic crust has an observed thickness of ~11 km decreasing to ~4 km by A20 (43.2 Ma) (Breivik *et al*., 2006). Initial spreading rates were high, exceeding 2 cm a^{-1}, decreasing until the Aegir ridge finally became extinct around anomaly A7 time (25 Ma) (Mosar *et al*., 2002). Spreading rates on the NW flank of the Aegir Ridge are generally less than on the SE flank indicating greater accretion of oceanic crust onto the European plate; they also decrease from NE to SW, in response to the anticlockwise rotation of the western margin during opening. After anomaly

A13 (33.3 Ma), spreading rates become ultra-slow on the Aegir Ridge in response to extension in the Greenland margin ahead of the northward propagating tip of the Reykjanes Ridge (Müller *et al*. 1997; Müller *et al*., 2001). Apart from the East Jan Mayen Fracture Zone, the Norway Basin does not display any clear fracture zones in either gravity or bathymetry data. A lack of segmentation is often associated with thin oceanic crust formed at slow spreading rates (e.g. Cannat, 1993; Jokat *et al*., 2003).

The Aegir Ridge finally became extinct by anomaly A7 (25 Ma) (Lundin and Doré, 2002; Mosar *et al*., 2002). Extension continued to propagate northwards into the Greenland margin and progressed to sea-floor spreading, transferring the Jan Mayen microcontinent from the North American (Greenland) plate to the European plate by anomaly A6 (19.6 Ma). The Oligocene timing of the ridge-jump is part of a reorganisation of both absolute and relative plate motion in the North Atlantic (Torsvik *et al*., 2001) and the appearance of the Iceland mantle plume near the spreading axis. Sea floor spreading has continued between the Jan Mayen microcontinent and Greenland to the present day.

The geometry, nature and precise timing of opening between the Jan Mayen microcontinent and Greenland are unclear (e.g. Lundin and Doré, 2002). The relative position of Europe, including the Jan Mayen microcontinent, with respect to North America (Greenland) is constrained by the clear magnetic anomalies formed by the adjoining Reykjanes and Mohns Ridge segments. The data that is available from the Jan Mayen Basin and the Iceland Plateau is relatively sparse and present interpretations lead to a number of possible models. There are several published models based on interpretations of the observed magnetic anomaly pattern (Johnson *et al*., 1972; Talwani and Eldholm, 1977; Grønlie *et al*., 1979; Vogt *et al.,* 1980; Müller *et al*., 1997, 2001; Torsvik *et al*., 2001; Lundin and Doré, 2002; Mosar *et al*., 2002) and one from seismic data (Kodaira *et al*., 1997, 1998a, 1998b; Mjelde, 2002); however, no consensus has emerged on the location of the OCT, the location, timing and number of spreading axes and the extent of oceanic crust.

Between anomalies A13 (33.3 Ma) and A7 (25 Ma) models either extend sea floor spreading at the Kolbeinsey Ridge across the Jan Mayen Basin to an OCT close to the Jan Mayen Ridge (Vogt *et al*., 1980; Müller *et al*., 1997, 2001; Lundin and Doré, 2002) or assume that the OCT is at the western edge of the Jan Mayen Basin (Talwani and Eldholm, 1977; Grønlie *et al*., 1979; Kodaira *et al*., 1998a, 1998b; Torsvik *et al*., 2001; Mjelde, 2002; Mosar *et al*., 2002;). The latter hypothesis infers that the Jan Mayen Basin forms part of the Jan Mayen microcontinent. A number of seismic observations exist in this region (Kodaira *et al*., 1998a, 1998b; Mjelde, 2002), which are interpreted to show that the majority of the Jan Mayen Basin is floored by continental crust. However, part of line L6 lies within the region of clear magnetic anomalies (Olafsson, 1983) in the SW Jan Mayen Basin and indicates the possibility of thin (5 km) oceanic crust.

Between anomalies A7 (25 Ma) and A5 (10.3 Ma) we can divide models into two groups: those that invoke continuous spreading at the Kolbeinsey Ridge and those that invoke spreading at a second axis located within the Iceland Plateau to the east of the Kolbeinsey Ridge (Johnson *et al*., 1972; Talwani and Eldholm, 1977; Grønlie *et al*., 1979). The latter group of models are best summarised by the model of Talwani and Eldholm (1977) which locates a second axis within a bathymetric low on the Iceland Plateau bounded by escarpments close to anomaly A5 to the west and a ridge at the western edge of the Jan Mayen Basin to the east. In our single axis models, this is the region occupied by anomalies A5-A6 [10.3-25 Ma]. In this region, seismic observations show 8-9 km thick oceanic crust with < 1 km sedimentation (Kodaira *et al*., 1998b) and no structures that suggest an extinct axis of the form seen elsewhere (Grevemeyer *et al*., 1997; Osler and Louden, 1995). However, given that a second axis would presumably have propagated northwards as the Kolbeinsey Ridge has, we cannot rule out the possibility that it may not have reached the latitude of this seismic line.

All models agree that between A5 (10.3 Ma) and present day spreading has been at the Kolbeinsey Ridge and spreading rates are slow (< 1.05 cm a^{-1}). Seismic observations show 8-9 km thick

oceanic crust with little sedimentation in this region (Kodaira *et al*., 1998b). An increased melt supply, associated with the high lithosphere temperatures in the region of the Iceland mantle plume, dominates over spreading rate dependence (Bown and White 1994) to produce anomalously thick oceanic crust at both the Reykjanes and Kolbeinsey Ridges (Smallwood and White, 1999; Hooft *et al*., 2006). The observation of thin (5 km) oceanic crust in the SW Jan Mayen Basin suggests this crust may have formed before the Iceland mantle plume coincided with the spreading axis.

In this paper, we use a 3D gravity inversion method (Greenhalgh and Kusznir, 2007; Chappell and Kusznir, 2008a) to address separate problems in the Norway Basin and in the region of the Iceland Plateau. In the Norway Basin, the plate reconstruction model is established; however, observations of the OCT location in both seismic and magnetic data are sparse, so we use the gravity inversion method to predict and refine the OCT location. In the Iceland Plateau region, we predict crustal thickness and thinning factors based on age estimates representing the three main plate reconstruction hypotheses, in order to test the validity of the models by comparing our results with seismic observations of Moho depth.

Gravity Inversion Method

Crustal thickness mapping from satellite gravity data involves isolating the mantle residual gravity anomaly, g_{mra}, the component of the gravity anomaly due to changes in Moho depth, and inverting to recover Moho topography (Greenhalgh and Kusznir, 2007; Chappell and Kusznir, 2008a). The largest contributions to the free air gravity in rifted margin and oceanic lithosphere are usually from bathymetry, sediments and the lithosphere thermal gravity anomaly, so we can assume that the mantle residual gravity anomaly, g_{mra}, is given by

$$g_{mra} = g_{faa} - g_b - g_t - g_s, \quad (1)$$

where g_{faa} is the observed free air gravity (e.g. Sandwell and Smith, 1997); g_b is the gravity anomaly from bathymetry, calculated from IOC (2003; figure 1a); g_t is the lithosphere thermal gravity anomaly and g_s is the gravity anomaly from sediments. If accurate sediment thickness and density data is available, we calculate the sediment gravity anomaly using the methods of Chappell and Kusznir (2008b) and subtract this from the free air gravity anomaly. However, where available sediment thickness data is sparse, or inconsistent, it is preferable to omit the sediment correction in order to simplify interpretation. These assumptions produce maximum bounds of Moho depth and crustal thickness and a minimum bound of thinning factor.

We invert the mantle residual anomaly using the method of Oldenburg (1974)

$$F[h(x,y)] = -\frac{F[\Delta g_{mra}(x,y)]e^{|k|z}}{2\pi G\rho} - \sum_{n=2}^{\infty} \frac{|k|^{n-1}}{n!} F[h(x,y)^n] \quad (2)$$

in which F [ ] represents a 2D discrete Fourier transform; $h(x,y)$ is Moho topography at the geographic coordinates x,y; $\varnothing g_{mra}(x,y)$ is the corrected mantle residual gravity anomaly (see below) at the geographic coordinates x,y; G is the universal gravitational constant (6.672×10^{-11} Nm^2kg^{-2}); ρ is the density contrast between crust and mantle; $|k|$ is the absolute value of the wave-vector and z is the inversion reference depth, chosen to ensure convergence, from which $h(x,y)$ is measured (Oldenburg, 1974). The densities we use for seawater, crust and mantle are 1030 kgm^{-3}, 2850 kgm^{-3} and 3330 kgm^{-3} respectively.

We cannot use the mantle residual gravity anomaly as computed with equation (1) directly, since it contains a short wavelength component, from crustal sources, and the reference crustal thickness, tc_{ref} is not the same as the inversion reference depth z. For these reasons, we must subtract the gravity anomaly of a Bouguer slab with density contrast ρ and thickness $tc_{ref} - z$ from the mantle residual gravity anomaly calculated with equation (1) and low-pass filter to remove the short wavelength (crustal) components of the data. We use the zero-bounded cosine filter of Oldenburg (1974) with limits set at 150 km and 75 km wavelength. The reference crustal thickness, tc_{ref}, is chosen to calibrate the inversion against seismic refraction results and deserves particular attention in this application. The value of tc_{ref} varies at regional scale since it is dependent on (1) dynamic

topography, (2) the assumption of pre-thinning crustal thickness (which is not necessarily tc_{ref}) used to calculate thinning factors for the lithosphere thermal gravity anomaly and (3) the recent extensional history of the lithosphere. In this application, we have large present-day dynamic topography from the Iceland mantle plume (Conrad *et al*., 2004), which we would expect to reduce tc_{ref}. The rift basins now seen on the margins of the North Atlantic and the final break-up, have developed across the Caledonian orogeny, which will have introduced large variations in pre-extension crustal thickness which will affect our estimated thinning factors. The North Atlantic margins have a protracted Mesozoic extensional history. The timescale for the decay of the thermal effects of thinning continental lithosphere is longer than the observed period of rifting; so, in calculating the lithosphere thermal gravity anomaly for the final extensional event by assuming that we are rifting equilibrium lithosphere, we are going to overestimate the magnitude of the thermal anomaly due to rifting and break-up. By comparison with published seismic estimates (Kodaira *et al*., 1998a; Hooft *et al*., 2006; Breivik *et al*., 2006; Parkin *et al*., 2007) we find that a value of 32 km for both tc_{ref} and the pre-thinning crustal thickness used to calculate thinning factors provides a reasonable calibration of Moho depth for the simple regional models used in this paper.

The Lithosphere Thermal Gravity Anomaly

Rifted continental margin and oceanic lithosphere have elevated geotherms. At the ocean ridge, the calculated lithosphere thermal gravity anomaly, g_t, may reach -320 mGal, with lower, but non-negligible, values in rifted continental margins (Greenhalgh and Kusznir, 2007; Chappell and Kusznir, 2008a). The cause of the lithosphere thermal gravity anomaly is lateral density variations in the lithosphere caused by thermal expansion in regions with elevated geotherms. To estimate the temperature and density perturbations from which we calculate the lithosphere thermal gravity anomaly we calculate an estimate of the temperature field using a cooling-plate model (McKenzie, 1978). The temperature anomaly in °C, T_z, at depth z is given by

$$T_z = \frac{2T_m}{\pi}\sum_{n=1}^{\infty}\frac{(-1)^{n+1}}{n}\left[\frac{\beta}{n\pi}\sin\left(\frac{n\pi}{\beta}\right)\right]\times\exp\left(\frac{-n^2 t}{\tau}\right)\sin\left(\frac{n\pi z}{a}\right) \quad (3)$$

in which T_m is base-lithosphere temperature; β is the lithosphere stretching-factor equal to equilibrium lithosphere thickness divided by the initial thinned lithosphere thickness; τ is the lithosphere cooling thermal decay constant and a is equilibrium lithosphere (plate) thickness. The values we use for τ and a are 62.8 Myr and 125 km.

The two unknowns required to solve equation (3) are an estimate of the lithosphere stretching factor, β (McKenzie, 1978), and the lithosphere thermal equilibration time, t. In oceanic lithosphere, $\beta = \infty$, so the magnitude of the anomaly is only dependent on t, which is the age of the lithosphere and readily obtained from magnetic isochrons (e.g. Müller *et al*., 1997).

In continental margin lithosphere, $\beta = tl_0/tl_r$, where tl_0 is equilibrium lithosphere thickness and tl_r is the immediately post-rift lithosphere thickness. The lithosphere equilibration time t is the break-up age at the margin of interest; therefore, the magnitude of the anomaly is dependent on both β and t. In order to estimate β in continental lithosphere, we assume that lithosphere stretching is equal to crustal stretching (i.e. pure shear) and that decompression melting occurs during rifting making a magmatic addition to the stretched continental crust where β exceeds β_{crit}, the stretching factor at which decompression of the upwelling mantle is sufficient to generate melt.

$$\beta = tc_0/tc_{now} \qquad 1 < \beta < \beta_{crit} \quad (4)$$

$$\beta = tc_0/(tc_{now} - tc_{mag}) \qquad \beta > \beta_{crit} \quad (5)$$

in which tc_0 is the pre-stretching continental crustal thickness; tc_{now} is total present day crustal thickness and tc_{mag} is the thickness of magmatic addition to the crust. The decompression-melting model of McKenzie and Bickle (1988) allows us to estimate β_{crit} as a function of mantle potential temperature. We estimate an appropriate mantle potential temperature using seismic observations of oceanic crustal thickness at the OCT and the seafloor spreading model of White and McKenzie

(1989). We can then find the thickness of magmatic addition as a function of lithosphere thinning factor ($1-1/\beta$) by interpolating between the lithosphere thinning factor for the onset of melt ($1-1/\beta_{crit}$), at which $tc_{mag} = 0$, and a lithosphere thinning factor of 1, representing oceanic lithosphere, at which $tc_{mag} = tc_{now}$ (Figure 3).

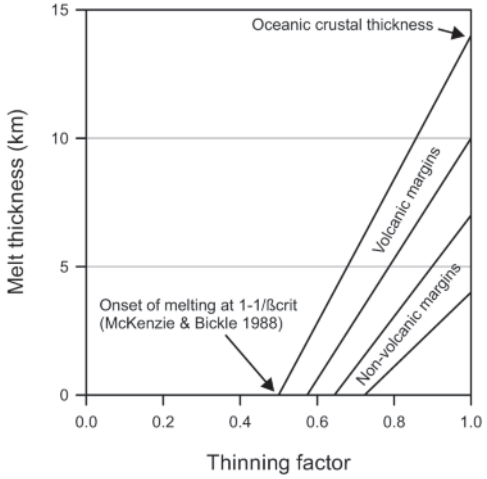

Figure 3. The relationship between melt thickness produced by decompression melting during continental break-up and thinning factor used in equation (5). We use an observation of oceanic crustal thickness at the OCT to estimate mantle potential temperature (White & McKenzie 1989) and the corresponding value of β_{crit} is found using McKenzie & Bickle (1988).

The solution of equation (2) is recursive (Oldenburg, 1974), involving a repeating cycle of inversion for Moho topography. We add the solution for g_t into this cycle so that it becomes: inversion for Moho topography, calculation of crustal thickness and lithosphere thinning factors, estimation of g_t and re-calculation of the mantle residual gravity anomaly using equation (1) (Figure 4). This inversion method usually converges to final values of g_t and $h(x,y)$ within 10 iterations.

Predicting OCT location

In the method as described above, it is assumed that the OCT is known and accurately located in the plate reconstruction being used to estimate the

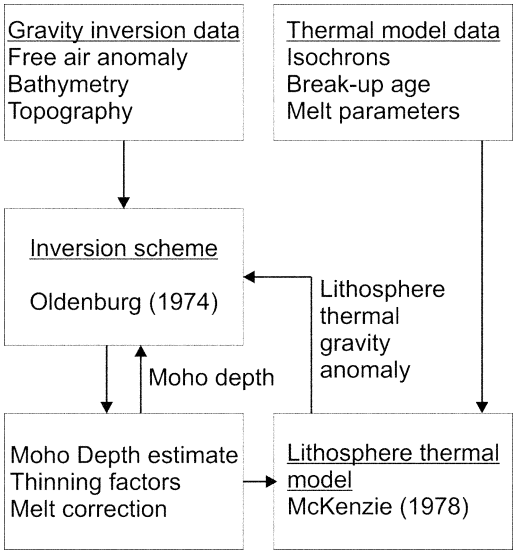

Figure 4. Workflow for the gravity inversion method we use in this paper (Greenhalgh & Kusznir 2007; Chappell & Kusznir 2008). In parallel to the normal recursive inversion of the Oldenburg (1974) method we also use inversion derived crustal thinning estimates, corrected for melt addition, to calculate the lithosphere thermal gravity anomaly.

thermal equilibration time, t. We use the OCT as the division between oceanic lithosphere, in which $\beta = \infty$ and the lithosphere thermal gravity anomaly is substantial, and continental lithosphere in which β is finite and the lithosphere thermal gravity anomaly is smaller (Figure 5a). If we rely on the plate reconstruction model to locate the OCT and the OCT is mis-located some distance into the continental margin, we risk assigning oceanic stretching factors to areas where, in fact, stretching factors are much smaller. The consequence of this is a large overestimate of the lithosphere thermal gravity anomaly in the margin and an erroneously shallow Moho depth prediction (Figure 5b). Unfortunately, plate reconstruction models always generate overlaps at plate boundaries to account for the extension at rifted continental margins, making the oldest isochrons lie over continental lithosphere. In many cases, we can avoid this situation by setting the OCT to lie at isochron corresponding to the oldest observed sea-floor spreading anomaly; however, at some margins, especial-

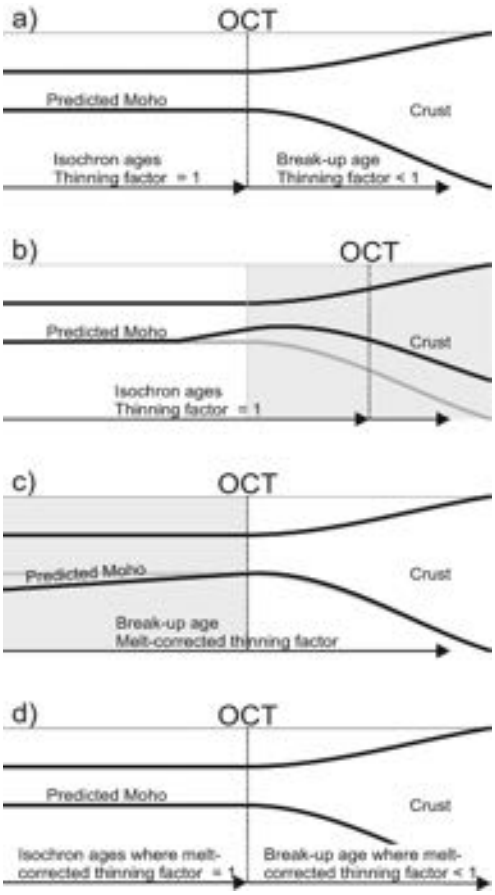

Figure 5. Models for conditioning the lithosphere thermal model when using gravity inversion to predict OCT location. (**a**) The ideal situation is where the position of the OCT is known and correctly located in the isochron model, with the correct age, allowing us to assign oceanic thinning factors to oceanic lithosphere and break-up age in the continental margin and recover Moho depth estimates that match observations. (**b**) The OCT is often mis-located in the isochron model or has the wrong age. If we use the OCT to define oceanic lithosphere in this situation, we risk assigning oceanic thinning factors to the continental margin, severely overestimating the lithosphere thermal gravity anomaly, which produces a shallow Moho depth estimate. (**c**) When we use a constant break-up age and melt corrected thinning factors, we overestimate the thermal equilibration time in young oceanic lithosphere, which reduces the lithosphere thermal gravity anomaly and produces a deep Moho depth estimate. At the continental margin, we correctly represent the break up age and thinning factor. With calibration against seismic OCT observations to calibrate the melt addition correction and reference depth, this model will predict Moho depth and OCT estimates which match observations. (**d**) If this calibration is robust and isochrons are available, isochrons can be used where the inversion indicates that the thinning factor is oceanic, refining the lithosphere thermal gravity estimate to produce correct Moho depth estimates throughout.

ly non-volcanic margins, there is no consensus on identifying the oldest sea-floor spreading anomalies.

An alternative strategy to using magnetic data is to use the gravity inversion to predict the OCT location. To achieve this, we treat the entire model as if it is continental lithosphere making no assumptions about OCT location and calculate stretching factors using equations (4) and (5) based on observations of oceanic crustal thickness at the OCT. In this way, the stretching factor estimate will become infinite, defining oceanic lithosphere, where the predicted crustal thickness reduces below the observed value at the OCT. Since we are only using the inversion to predict OCT location, we can simply use the break-up age of the margin to estimate the thermal equilibration time, *t*. Because the magnitude of the lithosphere mass deficiency and thermal gravity anomaly are more dependant on the thinning factor value than the age estimate in rifted margins (Figure 6) we are not introducing large errors if we use a constant age to estimate *t*. However, in young oceanic lithosphere, away from the margin, this approach overestimates the thermal equilibration time, reducing the magnitude of the lithosphere thermal gravity anomaly and overestimating Moho depth (Figure 5c).

A refinement of how we define the age of the lithosphere is to use isochrons in oceanic lithosphere only where the stretching factor has become infinite. In the rest of the model, we use margin break-up age (Figure 5d). In this way, we are utilising the information from the isochrons to ensure that all of the oceanic lithosphere has an appropriate thermal equilibration time and the inversion still defines the OCT based on crustal thickness.

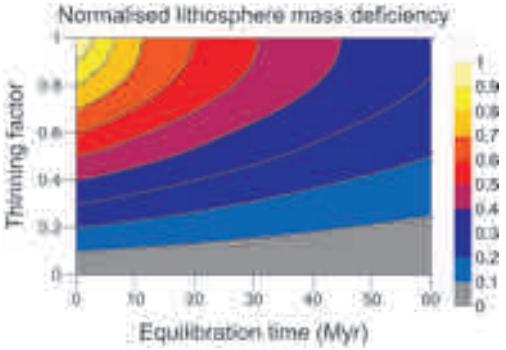

Figure 6. The lithosphere mass deficiency, which is proportional to the long-wavelength lithosphere thermal gravity anomaly, plotted as a function of lithosphere thinning factor ($1-1/\beta$) and age. Values are normalised to the ocean ridge value ($1-1/\beta=1$, age = 0 Myr). In large areas of rifted margins, where thinning factors are below $1-1/\beta_{crit}$, the mass deficiency and the lithosphere thermal gravity anomaly are less sensitive to changes in equilibration time than to changes in thinning factor. At higher thinning factors (> 0.8) sensitivity to thinning factor decreases markedly; however, this represents a very small model region at most margins.

Inversion parameters to predict OCT location in the Norway Basin

In the Norway Basin our aim is to predict OCT location around the Basin since seismic observations are sparse (Breivik *et al*., 2006; Parkin *et al*., 2007) and ship-track magnetic anomaly data is widely spaced (e.g. Breivik *et al*. 2006; figure 8). We show results using the 10 km and 14 km observations of oceanic crustal thickness at the OCT (Breivik *et al*., 2006; Parkin *et al*., 2007) to generate the melt-addition correction. Firstly, for each of these values, we show simple models with a fixed break up age of 55 Ma throughout. Secondly, we show model results that assume oceanic lithosphere and use isochrons where the stretching factor has become infinite. In the remainder of this model, where the stretching factor is finite, we use break up age of 55 Ma. In the surrounding basins, this result in oceanic lithosphere being defined, which is important since the long-wavelength thermal gravity anomaly, will affect the Norway Basin. Parameters for these models are summarised in table 1.

Inversion parameters to test plate reconstruction models for the Jan Mayen Basin and Iceland Plateau

To the west of the Jan Mayen microcontinent, our aim is to generate Moho depth estimates to test the validity of the proposed plate reconstruction models. We show results from three models. Firstly, a model according to the hypothesis that sea-floor spreading has occurred since anomaly A13 (33.3 Ma) with an OCT at the eastern edge of the Jan

Model	≤55 Ma in Müller *et al.* (1997) isochrons		>55 Ma in Müller *et al.* (1997) isochrons	
	Age	OCT crust	Age	OCT crust
1	55 Ma	10 km	55 Ma	10 km
2	55 Ma	14 km	55 Ma	14 km
3	Isochron age if $\beta = \infty$ 55 Ma if $\beta \neq \infty$	10 km	55 Ma	10 km
4	Isochron age if $\beta = \infty$ 55 Ma if $\beta \neq \infty$	14 km	55 Ma	14 km

Table 1. Model parameters used to condition Models 1 to 4 (Norway Basin).

Mayen Basin, close to the Jan Mayen Ridge. Since this is essentially the model indicated by the Müller *et al*. (1997) isochrons, we use this isochron dataset without modification with the OCT at 33.3 Ma and a break-up age of 33.3 Ma in continental lithosphere. Secondly, we show a model according to the hypothesis that continental crust floors the Jan Mayen Basin and the OCT lies on the western edge of the physiographic feature. This location is coincident with the location of anomaly A7 (25 Ma) in the Müller *et al*. (1997) isochrons so we use isochrons younger than 25 Ma and a break-up age of 25 Ma. Thirdly, we show a model according to the hypothesis that a second sea-floor spreading axis existed within the Iceland plateau between anomalies A5 (10.3 Ma) and A7 (25 Ma) and that continental crust floors the Jan Mayen Basin. For ages younger than anomaly A5 (10.3 Ma) we use the Müller *et al*. (1997) isochrons. To represent the extinct ridge axis we assume that the extinct axis lies midway between the 10.3 Ma and 25 Ma isochrons and modify the isochron dataset so that the extinct axis has an age of 10.3 Ma and the lithosphere at the edges of this region have an age of 25 Ma. We use a break-up age of 25 Ma in the remainder of the model. Since unequivocal oceanic crust in the region is thicker than average (Kodaira *et al*., 1998; Hooft *et al*., 2006), we use a melt-addition correction based on an oceanic crustal thickness of 10 km in these models. In the surrounding basins, we use the melt-corrected stretching factor to define oceanic lithosphere and estimate the lithosphere thermal gravity anomaly, since the long-wavelength thermal gravity anomaly will affect the Iceland Plateau and Jan Mayen Basin. Parameters for these models are summarised in table 2.

Model	0-10.3 Ma in Müller et al. (1997) isochrons		10.3-25 Ma in Müller et al. (1997) isochrons		25-33.3 Ma in Müller et al. (1997) isochrons		>33.3 Ma in Müller et al. (1997) isochrons	
	Age	**Beta**	**Age**	**Beta**	**Age**	**Beta**	**Age**	**Beta**
5	Isochron age	∞	Isochron age	∞	Isochron age	∞	Isochron age if $\beta = \infty$ 33.3 Ma if $\beta \neq \infty$	Melt corrected crustal
6	Isochron age	∞	Isochron age	∞	25 Ma	Melt corrected crustal	Isochron age if $\beta = \infty$ 25 Ma if $\beta \neq \infty$	Melt corrected crustal
7	Isochron age	∞	10.3 Ma at centre of area to 25 Ma at edges	∞	25 Ma	Melt corrected crustal	Isochron age if $\beta = \infty$ 25 Ma if $\beta \neq \infty$	Melt corrected crustal

Table 2. Model parameters used to condition Models 5 to 7 (Iceland Plateau).

Results

All of the models omit a correction for sediment thickness since a consistent sediment thickness map is not available. The presence of flood basalts and igneous intrusions within the sedimentary sequence produces a shallow acoustic basement in many places. Omitting the sediment correction from the gravity inversion makes our thinning factor estimate a minimum bound which gives maximum bounds of Moho depth and crustal thickness. In calculating the thermal model to generate the lithosphere thermal gravity anomaly, we assume that a stretching factor of 25 represents oceanic lithosphere to avoid the inversion becoming computationally slow. Where we plot the OCT, we are plotting the corresponding thinning factor ($1-1/\beta =$ 0.96). This approximation makes little or no difference to our results or conclusions.

Norway Basin

The four models we show predict the location of the OCT based on crustal thickness. Table 1 summarises the parameters used to condition the lithosphere thermal model used to generate the lithosphere thermal gravity anomaly in each model.

Model 1 (Figure 7a) uses a fixed break up age of 55 Ma throughout and consequently the magnitude of the lithosphere thermal gravity anomaly is ~-100 mGal in oceanic lithosphere. The model overestimates crustal thickness by 2-3 km at the Aegir Ridge because it overestimates the lithosphere thermal equilibration time, thereby reducing the lithosphere thermal gravity anomaly correction. At the margins, the model uses an assumption of 10 km as the initial oceanic crustal thickness, which leads to an improbable OCT location which is too oceanward. The predicted OCT cuts across the western end of the Aegir Ridge and corresponds to the rapid drop in crustal thickness from ~10 km to <6 km observed on the P1-00 seismic line (Breivik *et al*., 2006) at anomaly A23 (51.3 Ma) rather than the observed OCT locations. In not making a correction for sediment thickness, it is likely that we are underestimating the thinning factor close to the margins, which pushes the predicted OCT oceanwards.

Model 2 (Figure 7a) is identical to Model 1 apart from using an assumption of 14 km as initial oceanic crustal thickness. In oceanic lithosphere, results are similar to those predicted by Model 1. However, the predicted OCT location from the model is in agreement with observations (Breivik *et al*., 2006; Parkin *et al*., 2007). There is little sediment over the OCT on the iSIMM seismic line and crustal thickness, including sediments, drops below 14 km at the OCT on the P1-00 seismic line (Breivik *et al*., 2006).

Model 3 (Figure 7b) uses isochrons where the thinning factor has become oceanic (≥ 0.96) and a break up age of 55 Ma where the thinning factor is continental (< 0.96). In regions where the Müller *et al*. (1997) isochrons have ages older than 55 Ma and oceanic crust is indicated, break up age has also been used since the Müller *et al*. (1997) dataset locates the 55 Ma isochron to the north of the observed OCT on the Møre Margin. The lithosphere thermal gravity anomaly is more sensitive to the stretching factor than age (Figure 6), so the errors introduced by this mis-location are small. West of -2° longitude, the oldest isochrons intersect the predicted OCT, which indicates that either the plate reconstruction OCT is in error or the plate reconstruction model itself is in error. The lithosphere thermal gravity anomaly is close to -150 mGal at the Aegir Ridge, producing thin (4km) crust similar to that observed by Breivik *et al*. (2006). The slightly greater lithosphere thermal gravity in the centre of the Norway Basin also affects the margins, pushing the OCT more continentwards than in the equivalent fixed-age model (Model 1). However, the OCT still cuts across the western end of the Aegir Ridge and picks out the rapid drop in crustal thickness from ~10 km to <6 km observed on the P1-00 seismic line (Breivik *et al*. 2006) at anomaly A23 (51.3 Ma).

Model 4 is identical to Model 3 apart from using an assumption of 14 km as initial oceanic crustal thickness. In oceanic lithosphere, results are similar. The predicted OCT location is in agreement with observations (Breivik *et al*., 2006; Parkin *et al*., 2007). There is little sediment over the OCT on the iSIMM seismic line and crustal thickness, including sediments, drops below 14 km at the OCT on the P1-00 seismic line (Breivik *et al*., 2006). The small differences in OCT loca-

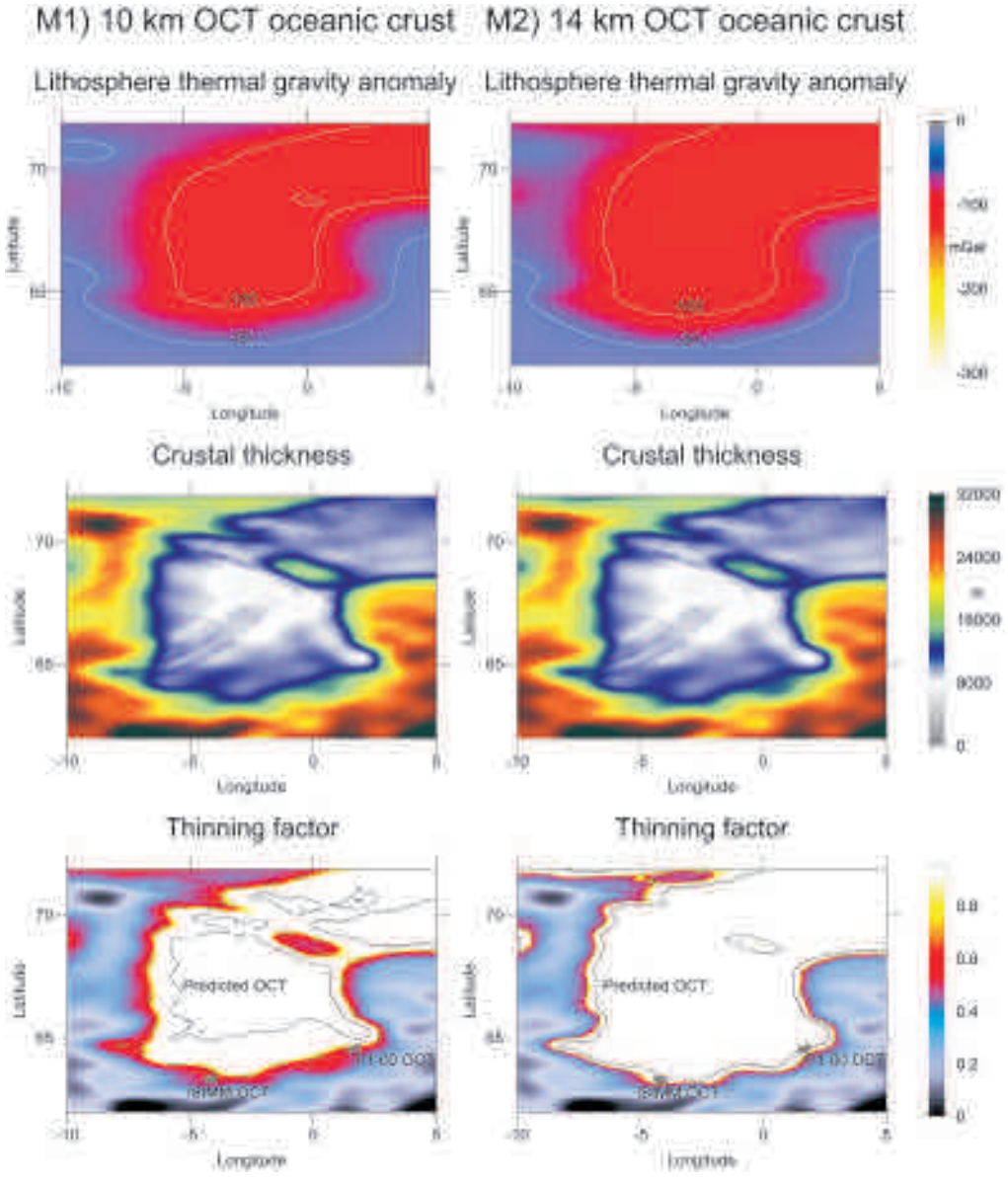

Figure 7. (**a**) Lithosphere thermal gravity anomaly, crustal thickness and thinning factor predictions from gravity inversion for Models 1 and 2 (table 1). The solid black line is the OCT predicted from the gravity inversion. The long dashed line is the thinning factor at which melt addition begins ($1-1/\beta_{crit}$) predicted from the gravity inversion. iSIMM OCT is the OCT location observed on the iSIMM seismic line (Parkin *et al*. 2007) and P1-00 OCT is the OCT location observed on the P1-00 seismic line (Breivik *et al*. 2006) on which we calibrate our OCT prediction.

tion between Model 2, using a fixed age (55 Ma), and Model 4 are negligible, apart from north of the Jan Mayen Fracture Zones near the Mohns Ridge, indicating that the fixed age approximation is reasonable and highlighting the stronger dependence on stretching factor than on thermal equilibration age. This feature allows us to use the method in other regions where isochrons are not available.

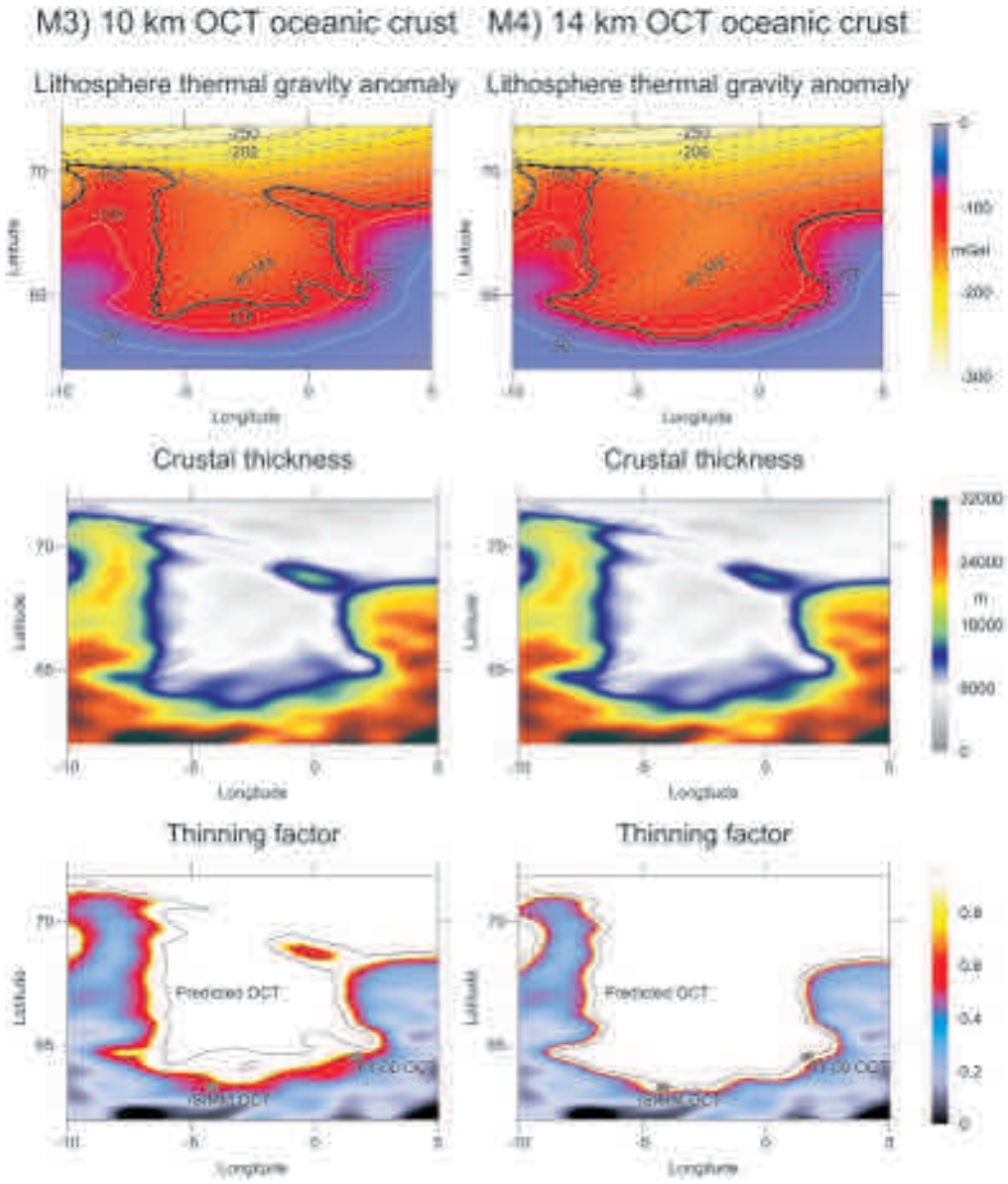

Figure 7. (**b**) Lithosphere thermal gravity anomaly, crustal thickness and thinning factor predictions from gravity inversion for Models 3 and 4 (table 1). Isochrons, where used, are shown as dashed black lines at 8 Myr spacing in the lithosphere thermal gravity anomaly plots. Other details are as for figure 7a.

Iceland Plateau

The three models we show predict crustal thickness assuming a fixed OCT and prescribed isochrons according to the plate reconstruction hypotheses that we are testing. Table 2 summarises the parameters used to condition the lithosphere thermal model used to generate the lithosphere thermal gravity anomaly in each model. In each case we are using a model to investigate the area north of Iceland and to the east of the Kolbeinsey Ridge. In perturbing the OCT and isochrons to do this, we are introducing errors at the Greenland

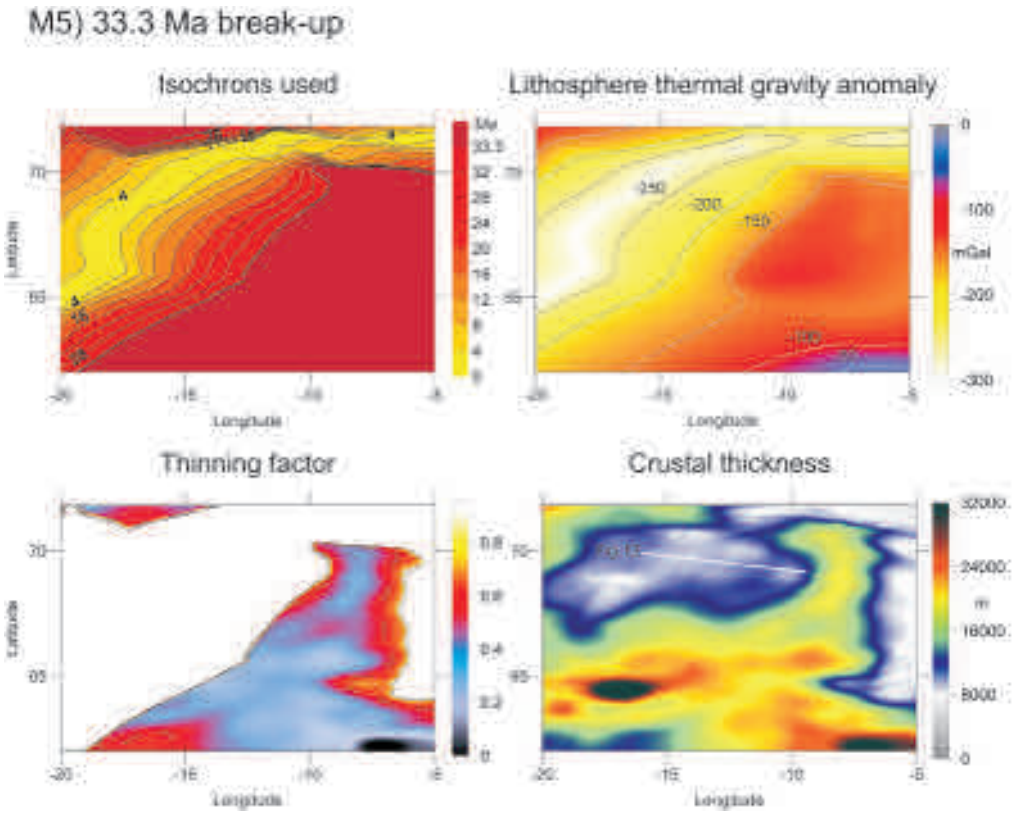

Figure 8. Model 5 (table 2). The isochrons used with Model 5 to represent a 33.3 Ma break-up, assuming the Jan Mayen Basin is oceanic; lithosphere thermal gravity anomaly, crustal thickness and thinning factor predictions from gravity inversion. The position of seismic line L3S (Kodaira *et al.* 1998b) used to compare models in figure 12 is shown.

Margin and south of the Jan Mayen Basin, so we do not consider crustal thickness and thinning factor estimates from these areas to be representative. Predicting representative crustal thickness estimates from gravity inversion at the Greenland Margin is not possible due to the large volumes of igneous and sedimentary addition (Olesen *et al*., 2007). Also, assigning a break up age is problematic because we do not know whether the majority of stretching occurred during Palaeocene break up or during the Oligocene separation of the Jan Mayen microcontinent. Likewise, the assumption of a single rift event at the Jan Mayen Margin to calculate the temperature field for the lithosphere thermal gravity anomaly may introduce errors into our results. However, we are able to calibrate the inversion against seismic observations of Moho depth on the Iceland Plateau, so, by choosing an appropriate value of tc_{ref}, we should be accounting for any systematic errors.

Model 5 (Figure 8) uses a 33.3 Ma break up age and assumes the Jan Mayen Basin to be oceanic. On the western side of the Jan Mayen Ridge, there is a rapid change in thinning factor close to where we prescribe the OCT, with melt-addition starting close to the OCT. Oceanic crustal thickness estimates are close to the observation of Kodaira *et al*. (1998b). We do not predict the thin crust observed by Kodaira *et al*. (1998b) in the Jan Mayen Basin; however, crustal thickness predicted from the gravity inversion is less than that observed on the Iceland Plateau.

Model 6 (Figure 9) moves the OCT further to the west and assumes a younger (25 Ma) break up age, which increases the lithosphere thermal gravity anomaly in the region of the Jan Mayen micro-

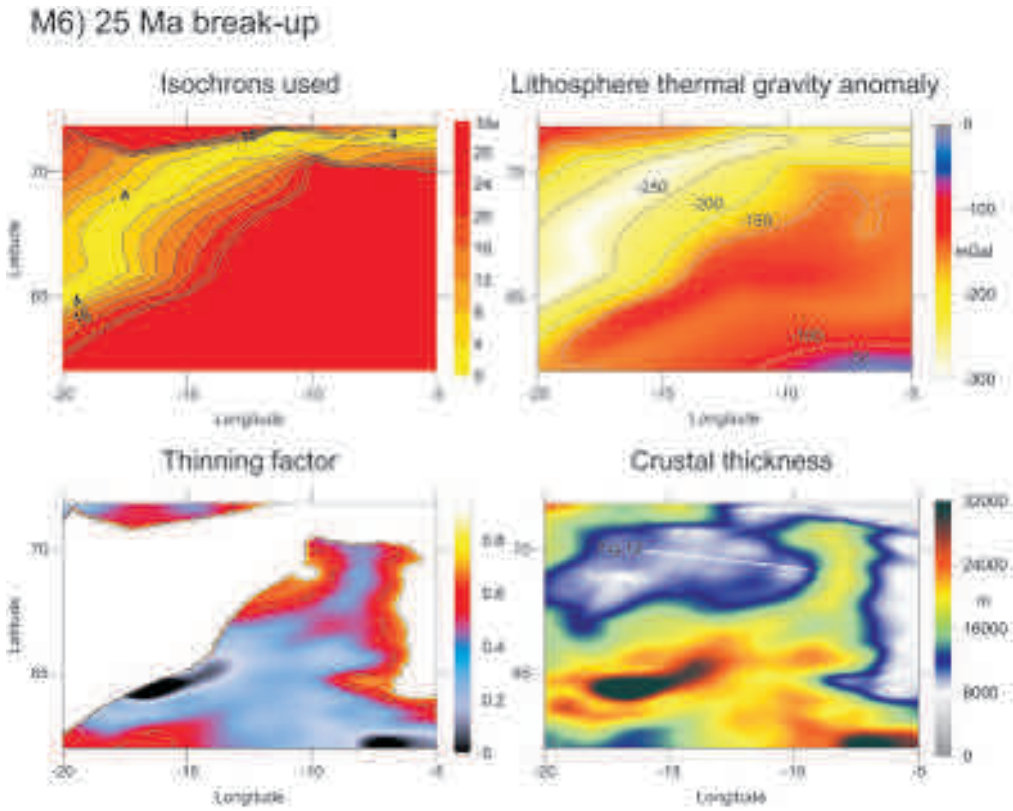

Figure 9. Model 6 (table 2). The isochrons used with Model 6 to represent a 25 Ma break-up, assuming the Jan Mayen Basin is continental; lithosphere thermal gravity anomaly, crustal thickness and thinning factor predictions from gravity inversion. The position of seismic line L3S (Kodaira *et al.* 1998b) used to compare models in figure 12 is shown.

continent and slightly reduces the predicted crustal thickness; however, results are similar to Model 5. The position of the onset of the melt-addition correction is similar to Model 5, despite the revised OCT location. Thinning factors are 0.58 or greater in the Jan Mayen Basin. In Models 5 and 6, the position of the OCT in the Norway Basin is identical.

Model 7 (Figure 10) assumes a second spreading axis existed in the Iceland Plateau between 25 Ma and 10.3 Ma. The differences between the results from this model and Model 6 are small. We assume younger lithosphere, 10.3 Ma as opposed to ~18 Ma, at the proposed Iceland Plateau axis, which increases the lithosphere thermal gravity anomaly and thinning factor and slightly reduces crustal thickness in the adjacent Jan Mayen Basin compared to Model 6.

Discussion in relation to plate reconstruction models

Norway Basin

In the Norway Basin, our aim has been to produce a model that predicts the location of the OCT. Using the 10 km oceanic crustal thickness at the OCT observed on seismic line P1-00 (Breivik *et al.*, 2006) the inversion does not predict an OCT that agrees with the observations. These inversions (Models 1 and 3) underestimate the thinning factor at the margins because of the lack of sediment correction and we do not use them for interpretation. Both Models 2 and 4 predict an OCT that agrees with observations; however, Model 4 has a better representation of the lithosphere thermal gravity anomaly than Model 2 and predicts oceanic crustal thickness in agreement with seismic observations, so we use it for interpretation (Figure 11). We

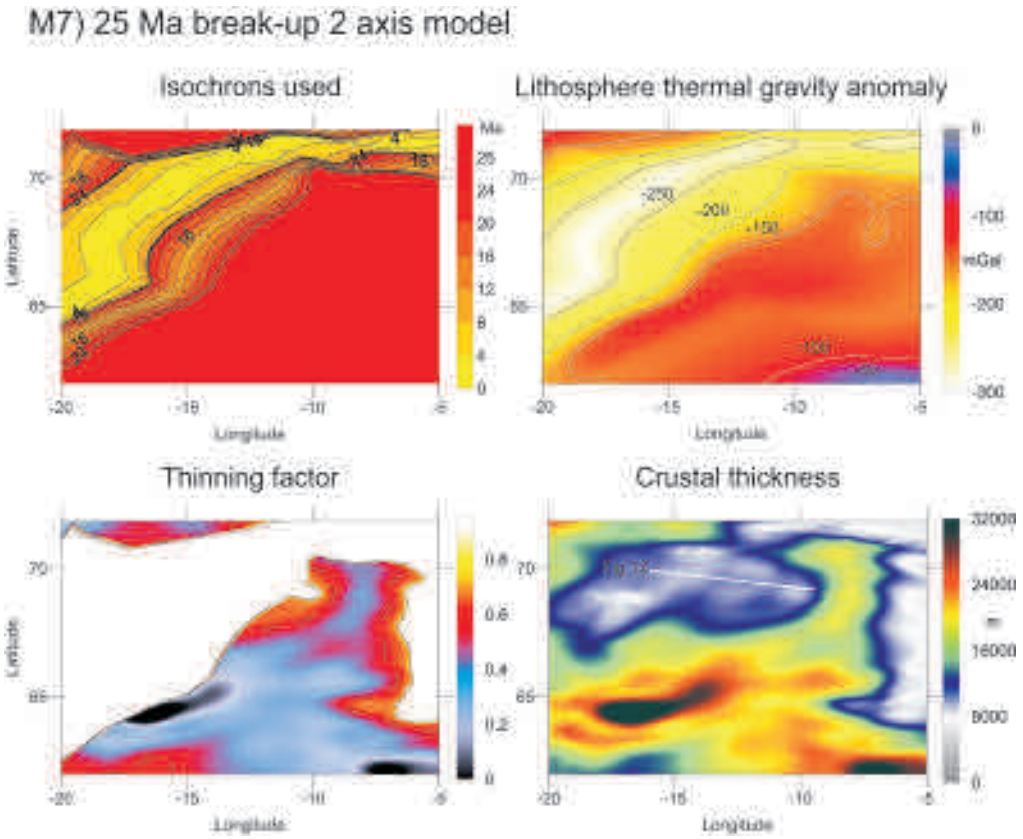

Figure 10. Model 7 (table 2). The isochrons used with Model 7 to represent a 25 Ma break-up and an intermediate axis, assuming the Jan Mayen Basin is continental; lithosphere thermal gravity anomaly, crustal thickness and thinning factor predictions from gravity inversion. The position of seismic line L3S (Kodaira *et al.* 1998b) used to compare models in figure 12 is shown.

compare our results with the Müller *et al*. (1997) isochron model, which we assume is representative of plate reconstruction models for the Norway Basin.

On the East Jan Mayen Margin, between 67° and 70° latitude our predicted OCT lies close to the 55 Ma isochron in the Müller *et al*. (1997) model. Our predicted OCT is more irregular, due to crustal thickness changes associated with the segmentation of this margin (Gudlaugsson *et al*., 1988). On the conjugate Møre Margin between -2° and 2° longitude, the 55 Ma isochron in the Müller *et al*. (1997) model is up to 135 km northwest of our predicted OCT. The geometry of the predicted OCT is similar on both margins.

At 66° latitude, the 55 Ma isochron in the Müller *et al*. (1997) model cuts into thick continental crust (~26 km) at the southern end of the Jan Mayen microcontinent (Figure 11). We suggest that a fracture zone may cross the margin to the north of the thicker block of crust, causing the ~100 km sinistral offset between this block and the ~21 km thick crust of the Jan Mayen Ridge. A similar drop in crustal thickness occurs in the conjugate margin at -2° longitude, between the end of the Fugløy Ridge and the northeastern part of the Faroe-Shetland Basin. To the southwest of this discontinuity, the Müller *et al*. (1997) model assumes that the Iceland-Faroes Ridge is oceanic, and to the south of the Aegir Ridge isochrons cross the Denmark Straight Fracture Zone (Lundin and Doré, 2002) into what Bohnhoff and Makris (2004) interpret as continental crust. It is interesting to note the negligible thin oceanic crust and the

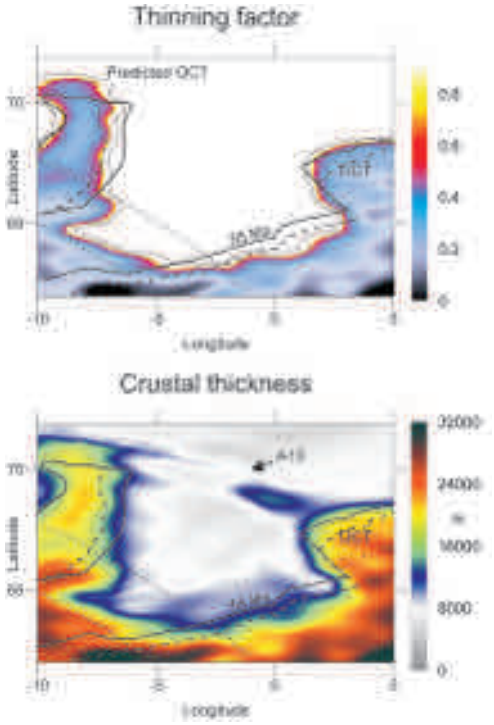

Figure 11. Thinning factor and crustal thickness for Model 4 from gravity inversion, which we use to assess the timing, OCT location and geometry of the Müller *et al.* (1997) plate reconstruction model for consistency with crustal thickness predictions. The thin black line is our predicted OCT from gravity inversion. The thick black line is the 55 Ma isochron and the dashed line is the OCT from the Müller *et al.* (1997) plate reconstruction model. The position of the Denmark Straight Fracture Zone (Lundin & Doré 2002) and the postulated fracture zone discussed in the text are indicated by dotted lines.

extremely asymmetric position of the Aegir Ridge in this southwestern sector of the Norway Basin. This is consistent with the extremely asymmetric accretion measured by Mosar *et al.* (2002) further east. The lack of thin oceanic crust may also suggest that sea-floor spreading jumped westwards from the southwest Aegir Ridge into the Iceland Basin at an early stage. Further east, oceanic crustal thickness reduces markedly at anomaly A23 (51.3 Ma) (Breivik *et al.*, 2006).

The terminations of magnetic anomalies at the edge of the Vøring Plateau clearly define the north-eastern boundary of the Norway Basin, the East Jan Mayen Fracture Zone (e.g. Lundin and Doré, 2002). Further west, interpretations vary, with the fracture zone either passing to the south of Jan Mayen Island (e.g. Müller *et al.*, 1997; Breivik *et al.*, 2006) or to the north (e.g. Mosar *et al.*, 2002; Olesen *et al.*, 2007). The former interpretation implies that the region of Jan Mayen Island is either oceanic or rifted from the Vøring Plateau rather than from the Møre Margin as the Jan Mayen Ridge region must have done. Volcanism on Jan Mayen Island shows an oceanic affinity, which is not surprising given the proximity of the Mohns Ridge system; however, this does not preclude an underlying continental fragment (Haase *et al.*, 1996 and references therein).

The Müller *et al.* (1997) isochrons assume that the northern 100 km of the Jan Mayen microcontinent is oceanic. We predict an OCT that runs to the north of Jan Mayen Island and a sizeable region of thick crust suggesting continuity with the Jan Mayen Ridge, or a continental fragment rifted from the Vøring Plateau (Figure 11).

Oceanwards of the Vøring Plateau, we predict a region of thicker than typical oceanic crust within ~60 km of the East Jan Mayen Fracture Zone that extends as far west as anomaly A13 (33.3 Ma), at which time the West Jan Mayen Fracture Zone is initiated. Magnetic anomalies in the region of thicker crust are not linear (e.g. Olesen *et al.*, 2007). This may represent underplating of existing oceanic crust as the Aegir Ridge moves past the transform margin.

Iceland Plateau

On the western side of the Jan Mayen microconti-

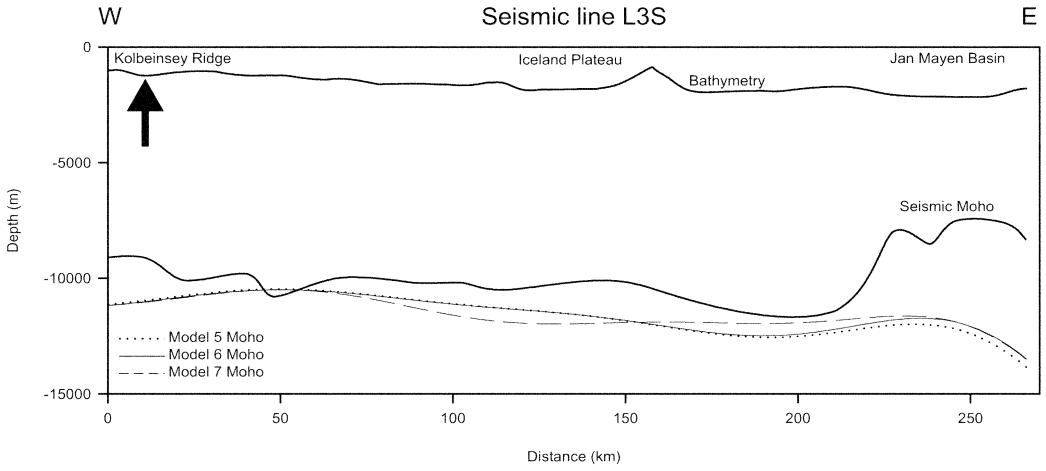

Figure 12. Crustal section along seismic line L3S (Kodaira *et al.* 1998b) showing bathymetry, seismic Moho and predicted Moho for Models 5 to 7. The position of the Kolbeinsey Ridge is shown by an arrow.

nent our aim has been to test whether any of the three main plate reconstruction variants can be ruled out by the gravity inversion. We do this by comparing the Moho estimate for each plate reconstruction model with the seismic Moho estimate for seismic line L3S (Kodaira *et al*., 1998b) (Figure 12). If a significant discrepancy exists in the plate reconstruction model we have assumed, it will result in a corresponding discrepancy between predicted Moho depth and the seismic Moho depth through use of incorrect lithosphere thermal equilibration ages to generate the lithosphere thermal gravity anomaly. We have calibrated our inversions against the data of Hooft (2006), Parkin (2007) and unpublished data from the iSIMM line all of which show that a reference crustal thickness of 32 km is appropriate.

Within the Jan Mayen Basin, the predicted Moho from Models 5-7 is ~4 km deeper than the seismic Moho (Figure 12). Such a discrepancy may result from either a geological cause such as a drop in crustal density or a low-density sedimentary basin being present, for which we make no correction, or a model specific cause, such as underestimating thinning factors and the lithosphere thermal gravity anomaly. Features causing a gravity anomaly of less than 75 km wavelength are not resolvable by the gravity inversion method we use. We can rule out underestimating thinning factors since Model 5 prescribes an infinite thinning factor across the Jan Mayen Basin, maximising the lithosphere thermal gravity anomaly. The wavelength of the Moho is greater than 100 km on this line across the shortest extent of the basin, so by considering that continuation of the Moho anomaly from the mean depth (~10 km) will increase the wavelength further we can eliminate a model specific cause. Kodaira *et al.* (1998a) interpret their results to show a deep sedimentary basin beneath the Jan Mayen Basin, which would be consistent with what we predict; however, their velocity structure is also consistent with thin oceanic crust and a veneer of Cenozoic sediment. In this case, the negative density anomaly could result from a difference in crustal composition between relatively dense, high temperature oceanic crust, on which we have calibrated our inversion and pre-Iceland mantle plume oceanic crust formed under cooler conditions with a lower MgO content (White and McKenzie, 1989).

Beneath the Iceland Plateau, the deepest seismic Moho occurs immediately to the west of the Jan Mayen Basin. The difference between the seismic and predicted Moho results from the lack of sediment correction in the inversion and the presence of a thin layer of Cenozoic of sediment. Nevertheless, the geometry of the predicted Moho generated by Models 5 and 6 is similar to the seismic Moho, with a maximum depth close to the Jan Mayen Basin. Model 7 produces a maximum

Moho depth mid-way between the Kolbeinsey Ridge and the Jan Mayen Basin. Thin oceanic crust typifies extinct ridge axes (Osler and Louden, 1995; Grevemeyer *et al*., 1997), for which we see no evidence. Our results show a worse agreement with observed Moho geometry when we assume a 2- axis model, although the differences are small and may be within the error of the method. We believe that our results do not show evidence for an extinct ridge axis in the Iceland Plateau along the seismic line L3S transect.

Conclusions

In the Norway Basin, we have used gravity inversion to predict crustal thickness and the OCT location around the Basin. We can identify segmentation of the OCT on the East Jan Mayen Margin and see the same features in the conjugate Møre Margin. From this, we suggest that the geometry of the basin is more complex than that assumed by many plate reconstruction models.

Gravity inversion models of the Iceland Plateau are similar for each of the three plate reconstruction variants we have tested. There is no structure indicating the presence of the proposed second Iceland Plateau axis when we assume this model. All three models show a significant discrepancy when compared to seismic data in the Jan Mayen Basin with the Moho being ~4 km deeper than the seismic Moho. We suggest that there is ambiguity in the interpretation of the seismic velocity structure and we can explain the discrepancy in our gravity inversion results by the presence of either thin oceanic crust or a sedimentary basin.

This paper demonstrates that crustal thickness mapping can a powerful tool for interpreting large-scale geological features that are critical to producing accurate kinematic plate models of continental break up and sea-floor spreading. We are able to identify the OCT, fracture zones, salients of continental crust and regions likely to be underplated oceanic crust. However, where structures are complex and the scale approaches the resolution of the method, we see that results can be inconclusive.

Acknowledgements

This work forms part of the NERC ocean margins iSIMM (integrated Seismic Imaging and Margin Modelling) project. The iSIMM team comprises researchers from the Universities of Liverpool and Cambridge, Badley Geoscience and Schlumberger and is funded by a consortium of NERC, DTI, Eni UK, BP, Amerada Hess, Anadarko, ConocoPhillips, Shell, Statoil and WesternGeco.

The authors would like to thank Robert Hunsdale and Geoff Kimbell for their reviews of an earlier version of this paper.

References

Archer, S.G., Bergman, S.C., Iliffe, J., Murphy, C.M. and Thornton, M. 2005. Palaeogene igneous rocks reveal new insights into the geodynamic evolution and petroleum potential of the Rockall Trough, NE Atlantic Margin. *Basin Res.* 17(2): 171-205.

Bohnhoff, M. and Makris, J. 2004. Crustal structure of the southeastern Iceland-Faeroe Ridge (IFR) from wide aperture seismic data. *J. of Geodynamics* 37(2): 233-252.

Bown, J.W. and White, R.S. 1994**.** Variation with spreading rate of oceanic crustal thickness and geochemistry. *Earth planet. Sci. Lett.*, 121: 435-449.

Breivik, A.J., Mjelde, R., Faleides, J.I. and Murai, Y. 2006. Rates of continental breakup magmatism and seafloor spreading in the Norway Basin- Iceland plume interaction. *J. Geophys. Res.* 111: B07102.

Cannat, M. 1993. Emplacement of Mantle rocks in the sea-floor at mid-ocean ridges. *J. Geophys. Res.* 98: 4163-4172.

Chappell, A.R. and Kusznir, N.J. 2008a. Three-dimensional gravity inversion for Moho depth incorporating a correction for the Lithosphere Thermal Gravity Anomaly. *Geophys. J. Int.* 174: 1-13.

Chappell, A.R. and Kusznir, N.J. 2008b. An algorithm to calculate the gravity anomaly of sedimentary basins with exponential density-depth relationships. *Geophys. Prospecting* 56: 249-258.

Conrad, C.P., Lithgow-Bertelloni, C. and Louden, K.E. 2004. Iceland, the Farallon slab, and dynamic topography of the North Atlantic. *Geology* 32(3): 177-180.

Doré, A.G., Lundin, E.R., Jensen, L.N., Birkeland, Ø., Eliassen, P.E. and Fichler, C. 1999. Principal tectonic events in the evolution of the northwest European Atlantic margin. *In*: Fleet, A.J. and Boldy, S.A.R. (eds) *Petroleum Geology of Northwest Europe: proceedings of the 5th Conference, 1999*. Geological Society, London: 41-61.

Greenhalgh, E.E. and Kusznir, N.J. 2007. Evidence for thin oceanic crust on the extinct Aegir Ridge, Norwegian Basin, N.E. Atlantic derived from satellite

gravity inversion. *Geophys. Res. Lett*., 34 (6): Art. No. L06305.

Grevemeyer, I., Weigel, W., Whitmarsh, R.B., Avedik, F. and Dehghani, A.G. 1997. The Aegir Rift: crustal structure of an extinct spreading axis. *Marine Geophysical Researches* 19: 1-23.

Grønlie, G., Chapmann, M., and Talwani, M. 1979. Jan Mayen Ridge and Iceland Plateau. *Origin and evolution, Norsk Polarinstitutt Skrift* 170: 201-224.

Gudlaugsson, S.T., Gunnarsson, K., Sand, M., and Skogseid, J. 1988. Tectonic and

volcanic events at the Jan Mayen Ridge microcontinent. *In*: Parson, L.M. and Morton, A.C. (eds) *Early Tertiary Volcanism and the Opening of the NE Atlantic*. Geological Society, London, Special Publications 39: 85-93.

Haase, K.M., Devey, C.W., Mertz, D.F., Stoffers, P. and Garbe-Schonberg, D. 1996. Geochemistry of lavas from mohns Ridge, Norwegian-Greenland Sea: Implications for melting sources and magma sources near Jan Mayen. *Contrib. Min. Pet.* 123 (3): 223-237.

Hooft, E.E.E, Brandsdottir, B., Mjelde, R., Shinamura, H. and Murai, Y. 2006. Asymmetric plume-ridge interaction around Iceland: The Kolbeinsey Ridge Iceland Seismic Experiment. *Geochemistry Geophysics Geosystems* 7: Art no. Q05015.

Intergovernmental Oceanographic Commission, International Hydrographic Organization, and British Oceanographic Data Centre (2003), Centenary Edition of the GEBCO Digital Atlas [CD-ROM], Br. Oceanogr. Data Cent., Liverpool, U. K.

Johnson, G.L., Southall, J.R., Vogt, P.R. and Young, P.W. 1972. Origin and Structure of Iceland Plateau and Kolbeinsey Ridge. *J. Geophys. Res.* 77(29): 5688-.

Jokat, W., Ritzmann, O., Schmidt-Aursch, M.C., Drachev, S., Gauger, S. and Snow, J. 2003. Geophysical evidence for reduced melt production on the Arctic ultraslow Gakkel mid-ocean ridge. *Nature (London)* 423 (6943): 962-965.

Kodaira, S., Mjelde, R., Gunnarsson, K., Shiobara, H., and Shimamura, H. 1998a. Structure of the Jan Mayen micro-continent and implications for its evolution. *Geophysical Journal International* 132: 383-400.

Kodaira, S., Mjelde, R., Gunnarsson, K., Shiobara, H., and Shimamura, H. 1998b. Evolution of oceanic crust on the Kolbeinsey Ridge, north of Iceland, over the past 22 Myr. *Terra Nova* 10: 27-31.

Kodaira, S., Mjelde, R., Gunnarsson, K., Shiobara, H., and Shimamura, H. 1997. Crustal structure of the Kolbeinsey Ridge, North Atlantic, obtained by use of ocean bottom seismographs. *J. Geophys. Res.* 102: 3131-3151.

Lundin, E.R. and Doré, A.G. 2002. Mid-Cenozoic post-breakup deformation in the 'passive' margins bordering the Norwegian-Greenland Sea. *Marine and Petroleum Geology* 19: 79-93.

McKenzie, D.P. and Bickle, M.J. 1988. The Volume and Composition of Melt Generated by Extension of the Lithosphere. *Journal of Petrology* 29: 625-679.

McKenzie, D.P. 1978. Some remarks on the development of sedimentary basins. *Earth planet. Sci. Lett.* 40: 25-32.

Mjelde, R., Aurvag, R., Kodaira, S., Shimamura, H., Gunnarsson, K., Nakanishi, A. and Shiobara, H. 2002. Vp /Vs -ratios from the central Kolbeinsey Ridge to the Jan Mayen Basin, North Atlantic; implications for lithology, porosity and present-day stress field. *Marine Geophysical Researches* 23:125-14.

Morton, A.C., Hitchen, K., Ritchie, J.D., Hine, N.M., Whitehouse, M., and Carter, S.G. 1995. Late Cretaceous Basalts from Rosemary Bank Northern Rockall Trough. *J. Geol. Soc. Lon.* 152: 947-952.

Mosar, J., Lewis, G. and Torsvik, T.H. 2002. North Atlantic sea-floor spreading rates: implications for the Tertiary development of inversion structures of the Norwegian-Greenland Sea. *J. Geol. Soc. Lon.* 159: 503-515.

Müller, R.D., Roest, W.R., Royer, J.-Y., Gahagan, L.M. and Sclater, J.G., 1997. Digital isochrons of the world's ocean floor. *J. of Geophys. Res.* 102: 3211-3214.

Müller, R.D., Gaina, C., Roest, W.R. and Hansen, D.L. 2001. A recipe for microcontinent formation. *Geology* 29(3): 203-206.

O'Connor, J.M., Stoffers, P., Wijbrans, J.R., Shannon, P.M. and Morrissey, T. 2000. Evidence from episodic seamount volcanism for pulsing of the Iceland plume in the past 70 Myr. *Nature (London)* 408 (6815): 954-95

Olafsson I. 1983. The Jan Mayen Ridge and surrounding areas—a marine geophysical study. Cand. real. thesi. University of Bergen.

Oldenburg, D.W. 1974. The inversion and interpretation of gravity anomalies. *Geophysics* 39: 526-536.

Olesen, O., Ebbing, J., Lundin, E., Mauring, E., Skilbrei, J.R., Torsvik, T.H., Hansen, E.K., Henningsen, T., Midboe, P., and Sand, M. 2007. An improved tectonic model for the Eocene opening of the Norwegian-Greenland Sea: use of modern magnetic data. *Marine and Pet. Geol.* 24(1): 53-66.

Osler, J.C. and Louden, K.E. 1995. Extinct spreading center in the Labrador Sea-crustla structure from a 2-dimensional seismic-refraction velocity model. *J. Geophys. Res.* 100 (B2): 22612-2278.

Parkin, C.J., Lunnon, Z.C., White, R.S., Christie, P.A.F. and the iSIMM team. 2007. Imaging the pulsing Iceland mantle plume through the Eocene. *Geology* 35(1): 93-96.

Sandwell, D.T. and Smith, W.H.F. 1997. Marine gravity anomaly from Geosat and ERS 1 satellite altimetry.

J. Geophys. Res. 102: 10039-10054.

Smallwood, J.R. and White, R.S. 1998. Crustal accretion at the Reykjanes Ridge, 61 degrees-62 degrees N. *J. Geophys. Res.* 103(B3): 5185-5201.

Talwani, M. and Eldholm, O. 1977. Evolution of the Norwegian-Greenland Sea. *Geological Society of America Bulletin* 88(7): 969-999.

Torsvik, T.H., Mosar, J. and Eide, E. 2001. Cretaceous-Tertiary geodynamics: a North Atlantic exercise. *Geophys. J. Int.* 146(3): 850-866.

Vogt, P.R., Johnson, G.L. and Kristjannson, L. 1980. Morphology and Magnetic Isochrons North of Iceland. *Journal of Geophysics* 47: 67-80.

White, N., and Lovell, B. 1997. Measuring the pulse of a plume with the sedimentary record. *Nature (London)* 387(6636): 888-891.

White, R.S. and McKenzie, D.P. 1989. Magmatism at Rift Zones: The Generation of Volcanic Continental Margins and Flood Basalts, *J. Geophys. Res.* 94: 7685-7729.

Crustal structure of the Shetland-Faeroe Basin from long offset seismic data

JANNIS MAKRIS [1*], IOANNA PAPOULIA [2] AND HERI ZISKA [3]

[1] GeoPro GmbH, St. Annenufer 2, 20457 Hamburg, Germany

* Email: info@geopro.com; Tel: +49 4030 399576

[2] Hellenic Centre for Marine Research, Athens, Greece

[3] Faroese Earth and Energy Directorate, Brekkutún 1, P.O. 3059, FO-110 Tórshavn, Faroe Islands

ABSTRACT

In 1993 we shot 2 long seismic lines across the Shetland-Faeroe Basin and a 3D array of 42 x 31 km^2 area using 50 Ocean-Bottom Seismographs and a low-frequency tuned air-gun array of 7300 cuin volume. Both lines are NW-SE oriented, crossing the basin perpendicular to its strike. Data evaluation was accomplished in 2 steps: First, we applied a τ-P inversion that allowed us to obtain 1D velocity models for each OBS position. We interpolated first-order discontinuities from the 1D velocity models and developed a 2D velocity section for each profile by forward modelling.

We obtained the following results:

Crustal thickness below the Shetland Islands is approximately 28 km. The crust is separated by an upper, middle and lower crust, which is typical for the Caledonides. The Moho is mapped by a 1st order discontinuity, separating a lower crust of Vp = 7 km/s from the upper mantel of Vp = 8 km/s. The same type of crust occurs in the basin again towards the Faeroe Islands, although the crust here is thinner and the Moho was encountered at 20 km depth. This includes at least 4 to 6 km sediments above the igneous crust. The crustal structure in the basin is dominated by a 2-layer continental crust of an upper and a lower domain. The Moho in the central part of the basin, below the Corona Ridge, is only 14 km thick. Sediments on top of the crust have their maximum thickness at the south-eastern part of the basin exceeding 10 km, and thin to the northwest to about 6 km north of the Corona Ridge. The Mesozoic sediments extend over the complete depression, which is covered by Paleocene-Eocene and Oligocene series. The north-western part of the basin is covered by basaltic flows that extend to the Corona Ridge and limit the Oligocene-Eocene sequences from those of the Paleocene. The basalt flows along the profiles have maximum thickness to the northwest (more than 1000 m), thinning towards the central part of the basin where they gradually deteriorate into thin discontinuous flows. Thickening of the igneous crust below the Corona Ridge with simultaneous uplift of the Moho indicates inversion of the tectonic regime sometime during the Mesozoic, as well as thickening of the igneous crust by compression.

Introduction

The Shetland-Faeroe Basin is one of the areas having the capacity to help sustain oil and gas production within Europe. In the United Kingdom sector of the basin, production is already undergoing and discoveries have proven the tremendous hydrocarbon potential of the region. Research was initiated in the mid-1990's with the Foinaven (Cooper *et al*., 1999) and Schiehallion (Leach *et al*., 1999) Fields, and the Clair Field has recently come on-stream almost 30 years after it was discovered. Recent discoveries, such as Cambo and Rosebank (this volume), have also proven the hydrocarbon potential within the basin. The main question at the moment is how to understand the development and structure of the basins to the northwest, and particularly those on the Faeroese Continental Shelf, covered by the flood basalts of the North Atlantic Igneous Province e.g. (Hinz *et al*., 1993, Eldholm and Grue, 1994). These basalts have a detrimental effect on conventional imaging techniques (White *et al*., 2005), which prevents a thorough understanding of the underlying crustal geometry and nature. The technique that seismically permits

Faroe Islands Exploration Conference: Proceedings of the 2nd Conference.
Annales Societatis Scientiarum Færoensis, Supplementum 50, 2009: 30-42

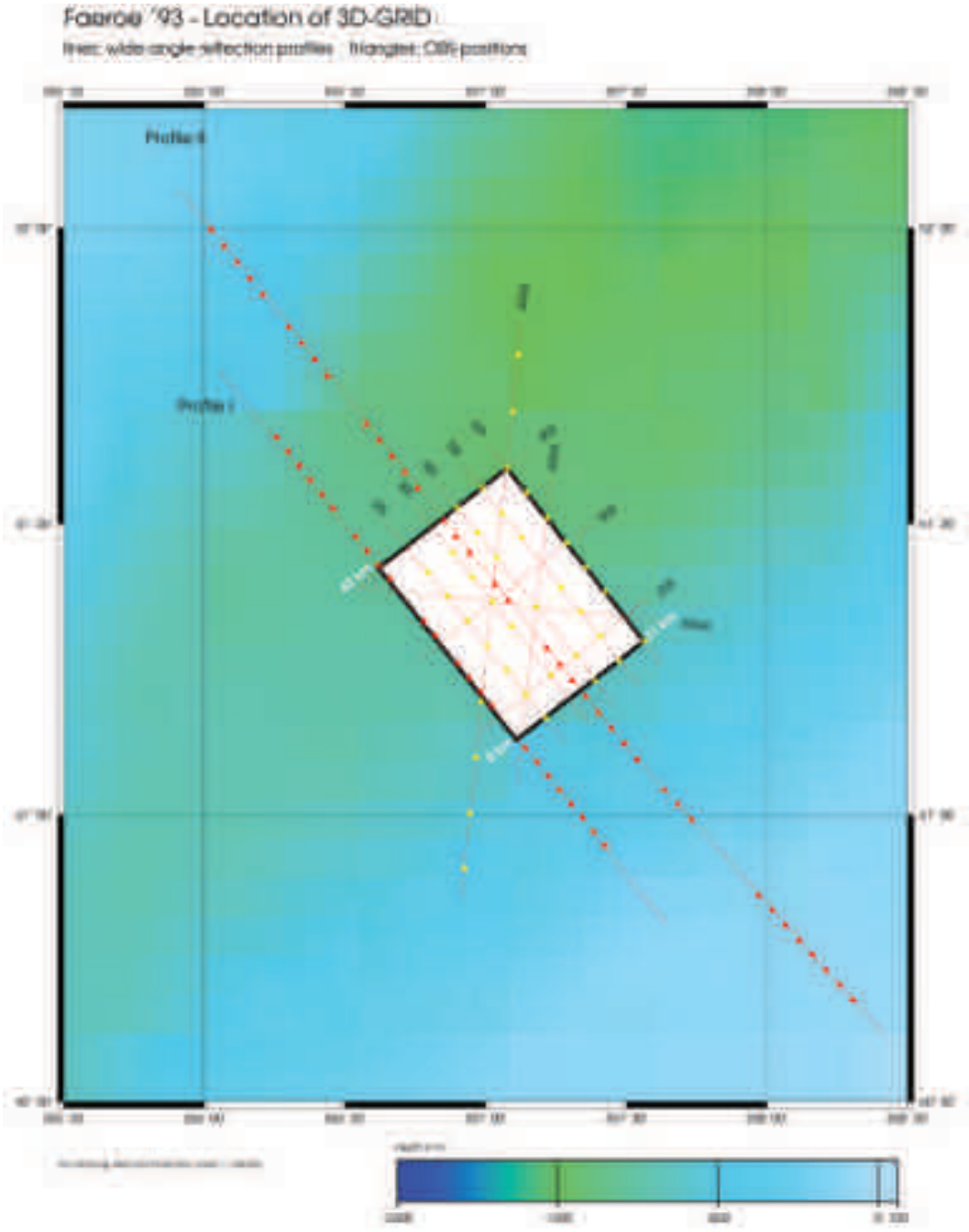

Figure 1. Location of Profiles and OBS locations along the 2D lines and the 3D array in the Faeroe-Shetland Basin.

penetration of the basalts and provides the wave speed of the structures below them is that of WARRP (Wide Aperture Reflection Refraction Profiling, (Makris *et al*., 1999). It requires expanded active seismic arrays beyond the length of commercially available streamers or ocean bottom cables

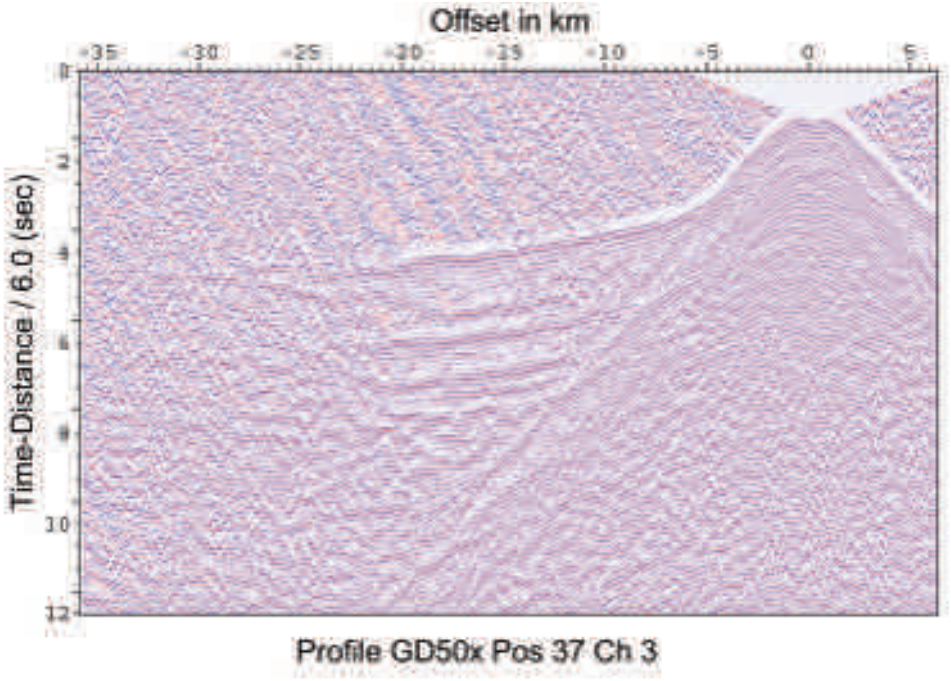

Figure 2. Example of a Common Station Gather (CSG) of OBS position 37, vertical component, of Profile DD50X of the 3D array. We have applied a linear moveout using 6 km/s as reduction velocity. This holds for all CSGs used in developing the velocity models.

(OBC), in order to record wide- angle reflections and diving waves in addition to the conventional wave field observed by the state-of-the-art procedures.

GeoPro undertook a seismic survey, on behalf of Mobil Oil in 1996, with the goal to penetrate the basalts and better understand the deeper geology across the Corona Ridge. In the following, we will present modelling results of WARRP data that delineate the deeper part of the Shetland-Faeroe Basin and crust, by using large numbers of ocean bottom seismographs (OBS's) and long offsets. Line length of these experiments extended to 210 km, and guaranteed that crustal structure as well as sub-basalt mapping of the sedimentary basin could be obtained over the entire area.

The Experiment

We used 50 3C OBS's and observed two 2D lines perpendicular to dominant NE/SW structural grain within the Faeroe-Shetland Basin. The 2D lines are centred on the Corona Ridge, where data density is increased by a 3D OBS array consisting of 5 x 8 OBS's and one N-S line of 10 OBS's crossing this array (Figure 1). Spacing of the OBS's was 5 km in the 3D array, 3.5 km along Profile I and 3.8 km along Profile II. The seismic energy was generated by air gun shots fired every 126 m at 1 min. time intervals. The air gun array consisted of two sleeve guns of 60 lt. each, which were synchronized and placed at 20 m water depth. The dominant frequency of the shots was 8 Hz. The length of the lines was 120 km and 210 km along Profile I and II, respectively.

Data were compiled in Common Station Gathers (CSGs). A linear moveout was applied using 6 km/s as reduction velocity. An AGC of 2 s was applied in order to enhance later arrivals. Examples of two sections are presented in figures 2 and 3.

Figure 2 shows OBS position 37 along line GD50X of the 3D array. At km 25 we can recognize a PmP reflection from the crust/mantle boundary at 5 s reduced traveltime. First-break ar-

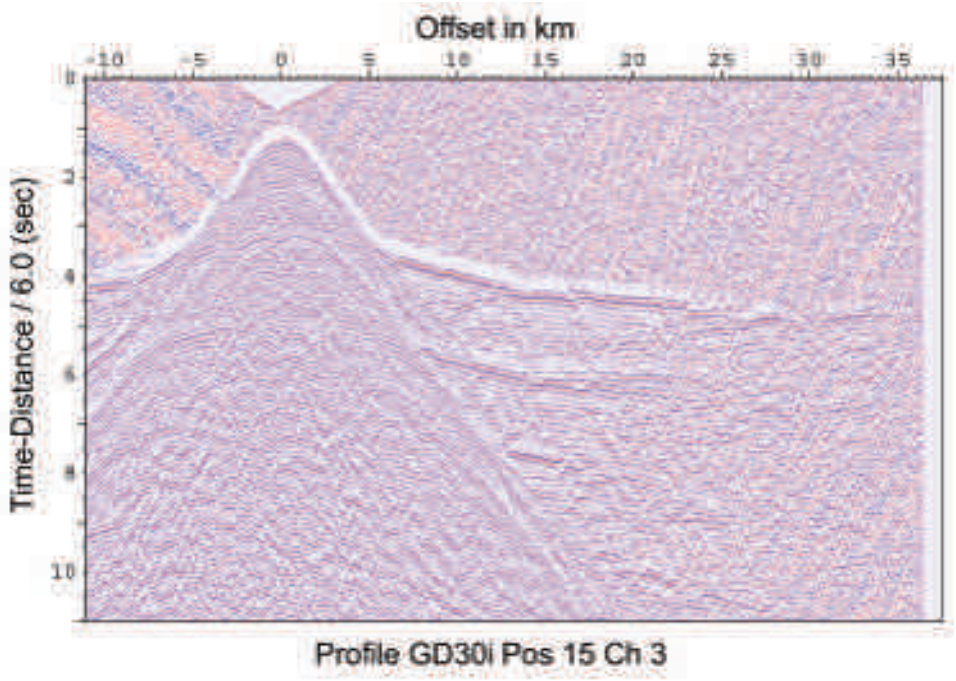

Figure 3. Example of a Common Station Gather (CSG) of OBS position 15, vertical component, of Profile GD 301 of the 3D array. Data are presented as described in figure 2 and in the text.

rivals are clearly recorded over offsets exceeding 40 km that permit the development of the velocity distribution over the entire sedimentary basin and crust. Figure 3 shows a CSG along line GD30I of the 3D array. Here, PmP arrivals are also clearly identified at km 28, and first breaks are recorded up to 40 km offsets. At a distance of 12 km to the southeast, a wide-angle reflection from the basis of the sediments can be seen at 4.5 s reduced traveltime. We used this type of CSGs to develop the velocity depth models along all observed seismic lines. We calculated synthetic traveltimes by using the SEIS 83 algorithm, (Cervený and Psencyk, 1983).

Seismic Modelling and Results

The evaluation of the seismic data was accomplished in two steps: First, we applied a τ-P inversion of the first breaks of each OBS position and developed 1D velocity depth functions. From these, we interpolated first-order discontinuities defined by step-like changes of the velocity values. Examples are presented in figures 4 and 5. Using these models as input for two-point ray-tracing, we computed synthetic traveltimes and compared them with the observed data.

We developed the models from top to bottom by fitting the computed to the observed traveltimes until their alignment was within the picking accuracy. Examples of this procedure are presented in figures 6 to 8.

In figure 6, the ray-traced traveltimes show arrivals of seismic signals that have propagated through the upper part of the sediments, as well as wide-angle reflections visualized by rays that were reflected from intercalated basaltic flows. Different arrivals are colour-coded for clarity.

In figure 7, we present the ray paths of seismic energy that have travelled as wide-angle reflections through the Shetland Basin to the southeast, and parts of the Corona Ridge to the northwest. The OBS position in the middle of the figure was placed at 1 km water depth. In figure 8, we show

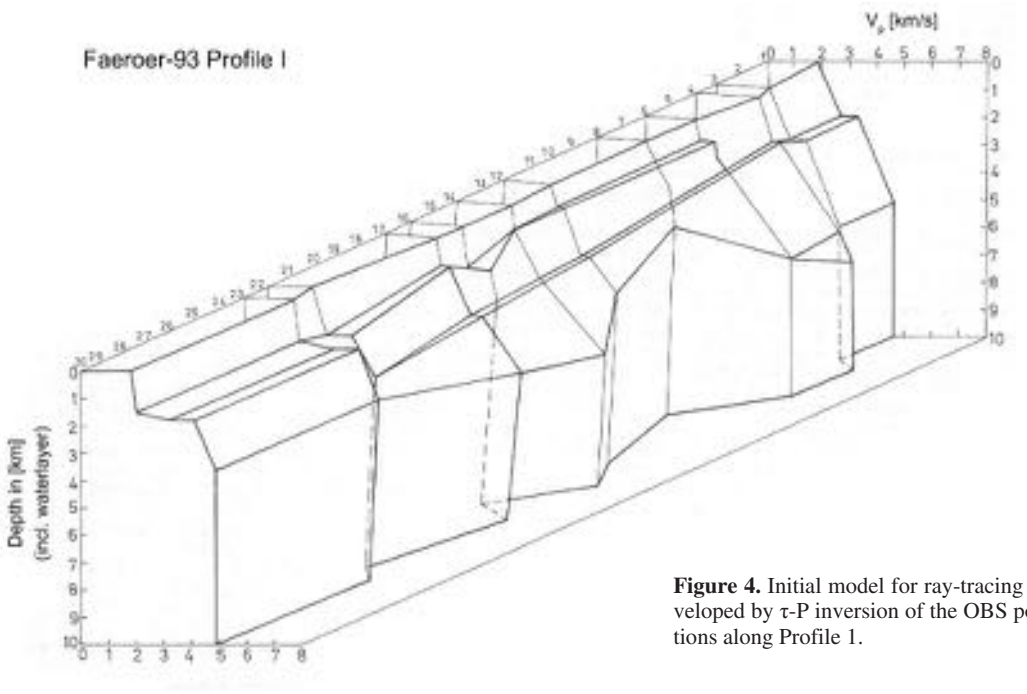

Figure 4. Initial model for ray-tracing developed by τ-P inversion of the OBS positions along Profile 1.

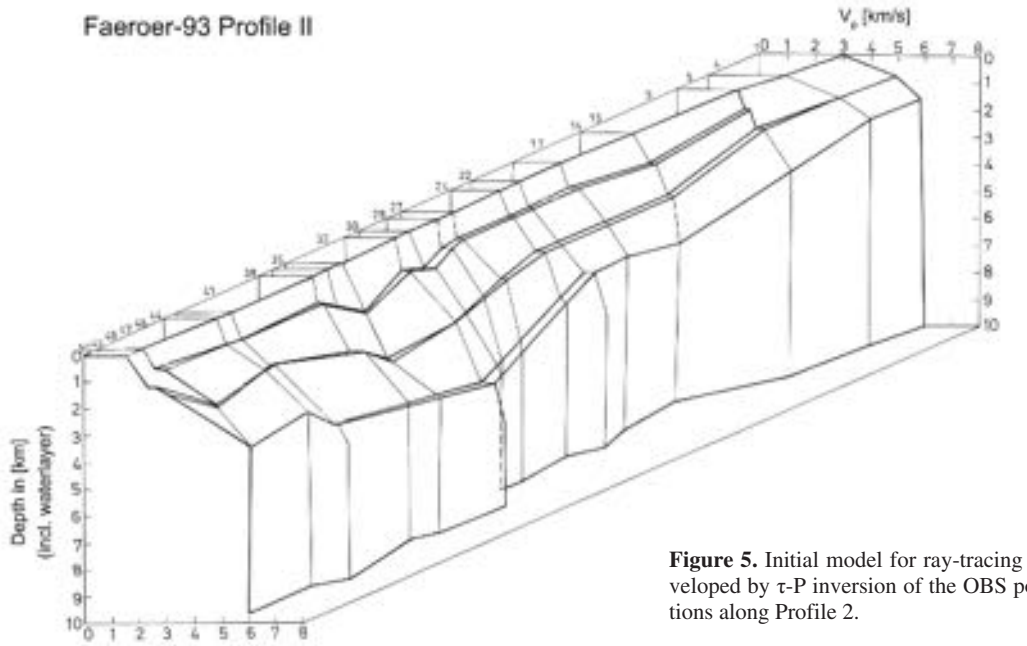

Figure 5. Initial model for ray-tracing developed by τ-P inversion of the OBS positions along Profile 2.

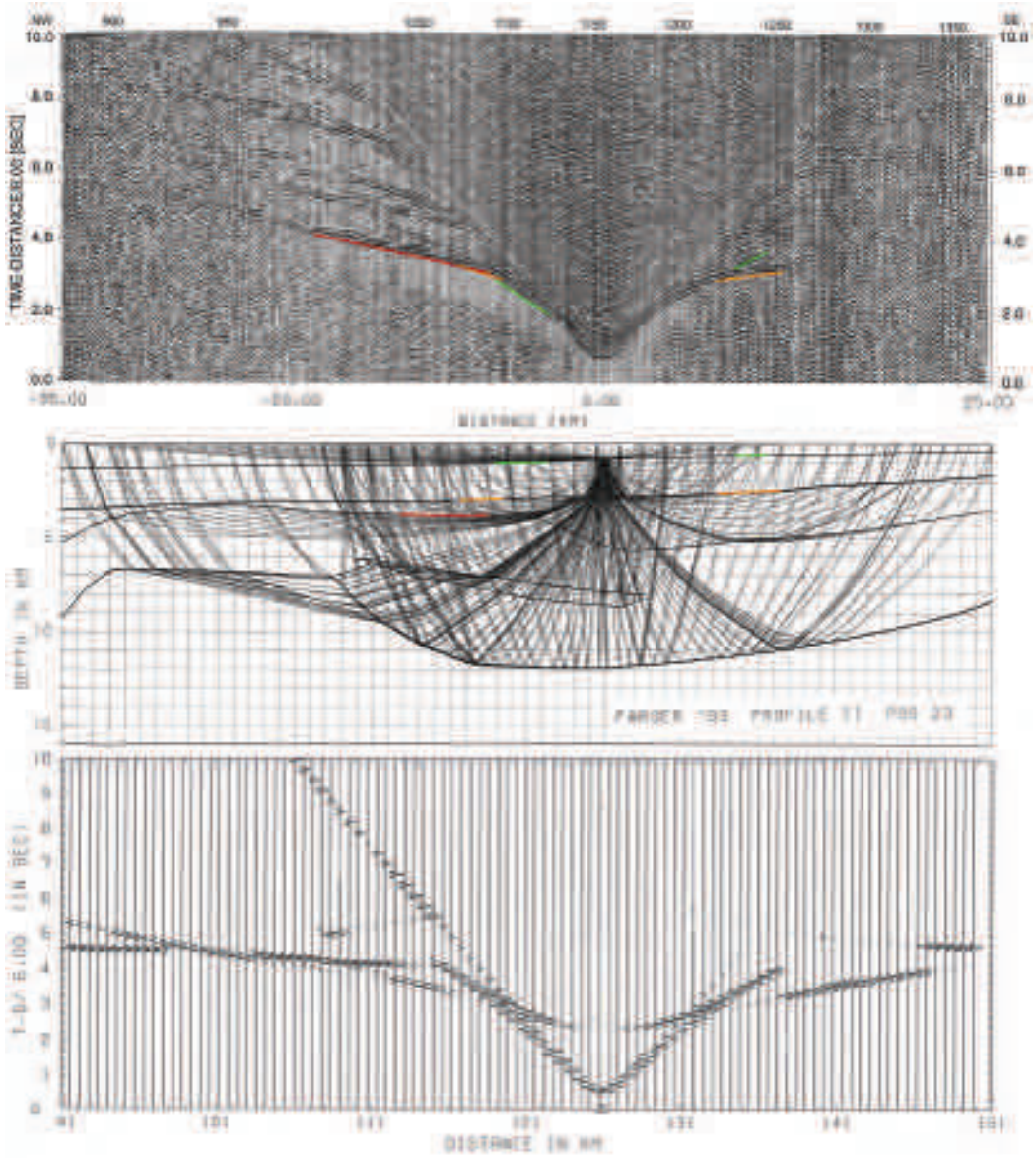

Figure 6. Example of ray-tracing of the upper sediments of Profile 2, OBS Position 20, vertical component. Synthetic amplitudes computed by forwards modelling are given at the lower part of the figure. Further explanations are given in the text.

the example of an OBS position in the Shetland Basin and synthetic rays that have mapped the basis of the sediments and the top of the continental crust. Synthetic traveltimes are presented at the lower part of figures 6 to 8.

Using the procedure described above, we developed wave-speed models for the two 2D lines of figure 1, which are presented below (figures 9 and 10). The accuracy obtained in defining wave speeds and depth to discontinuities depends on the distribution of the OBS's along the seismic lines and the quality of picks. We have estimated that our results, depending on the depth of the models, are about 2 to 4% accurate.

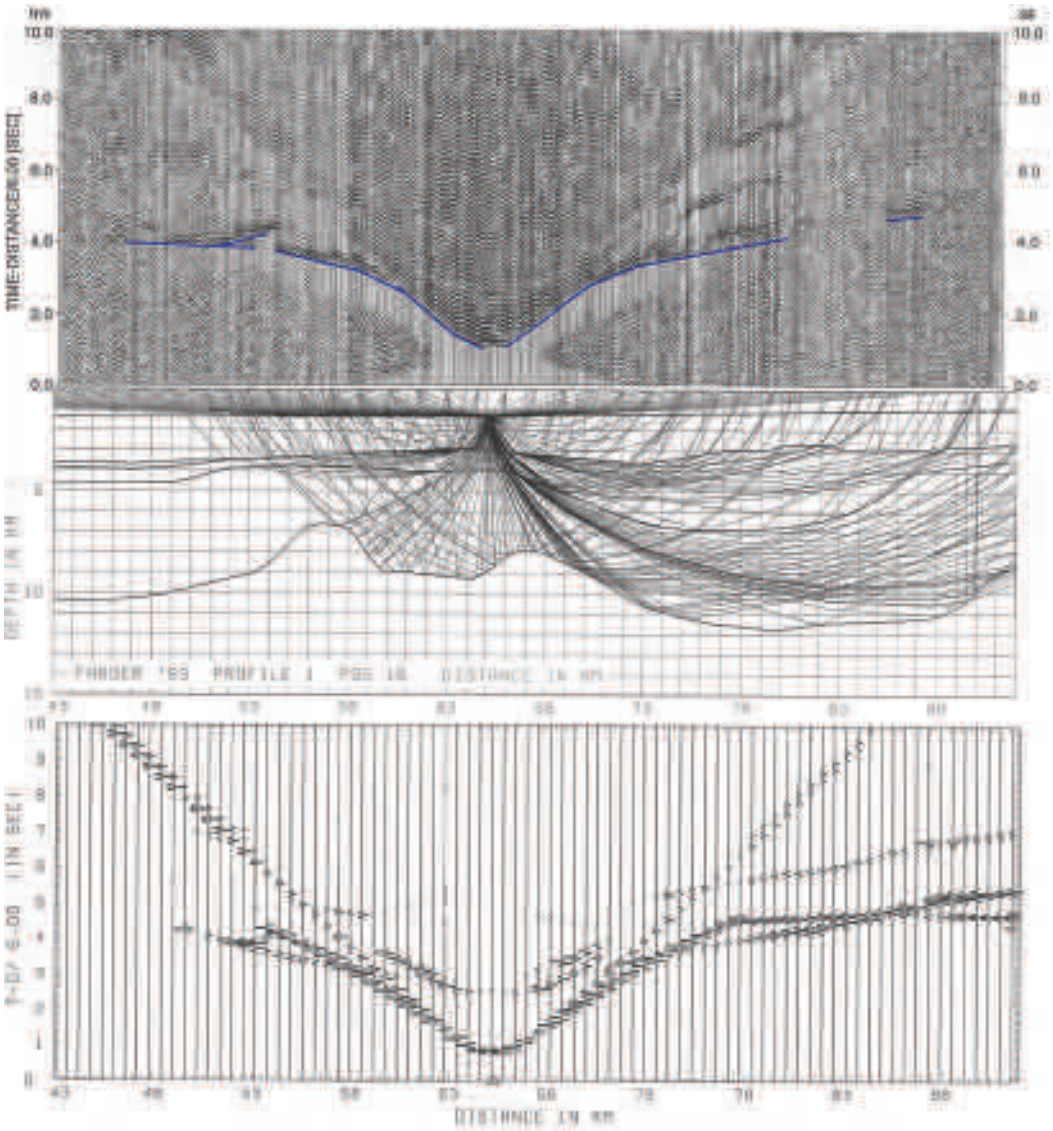

Figure 7. Example of ray-traced sediments to top basement of Profile 1, OBS position 16, vertical components. Synthetic traveltimes and amplitudes are given at the lower part of the figure. (See also text).

Figure 9 presents the velocity model of the P-waves along Profile I. OBS positions are numbered from 1 to 30, with position 1 being furthest towards the SE. The upper part of the sediments consists of Oligocene-Eocene formations with velocities varying between 2.2 km/s to 2.6 km/s. Wells drilled in the basin have confirmed the sedimentary nature of the younger section towards the south-western part of the Profile. The nearest well further to the northwest is 213/23-1 located on the Corona Ridge, about 17 km off the line. The well was terminated after reaching crystalline basement at a depth of 4309 m which, considering the distance to the well, is close to the 4.5 km suggested by our modelling. Top Cretaceous was reached at a depth of 3046 m, which is about the same as

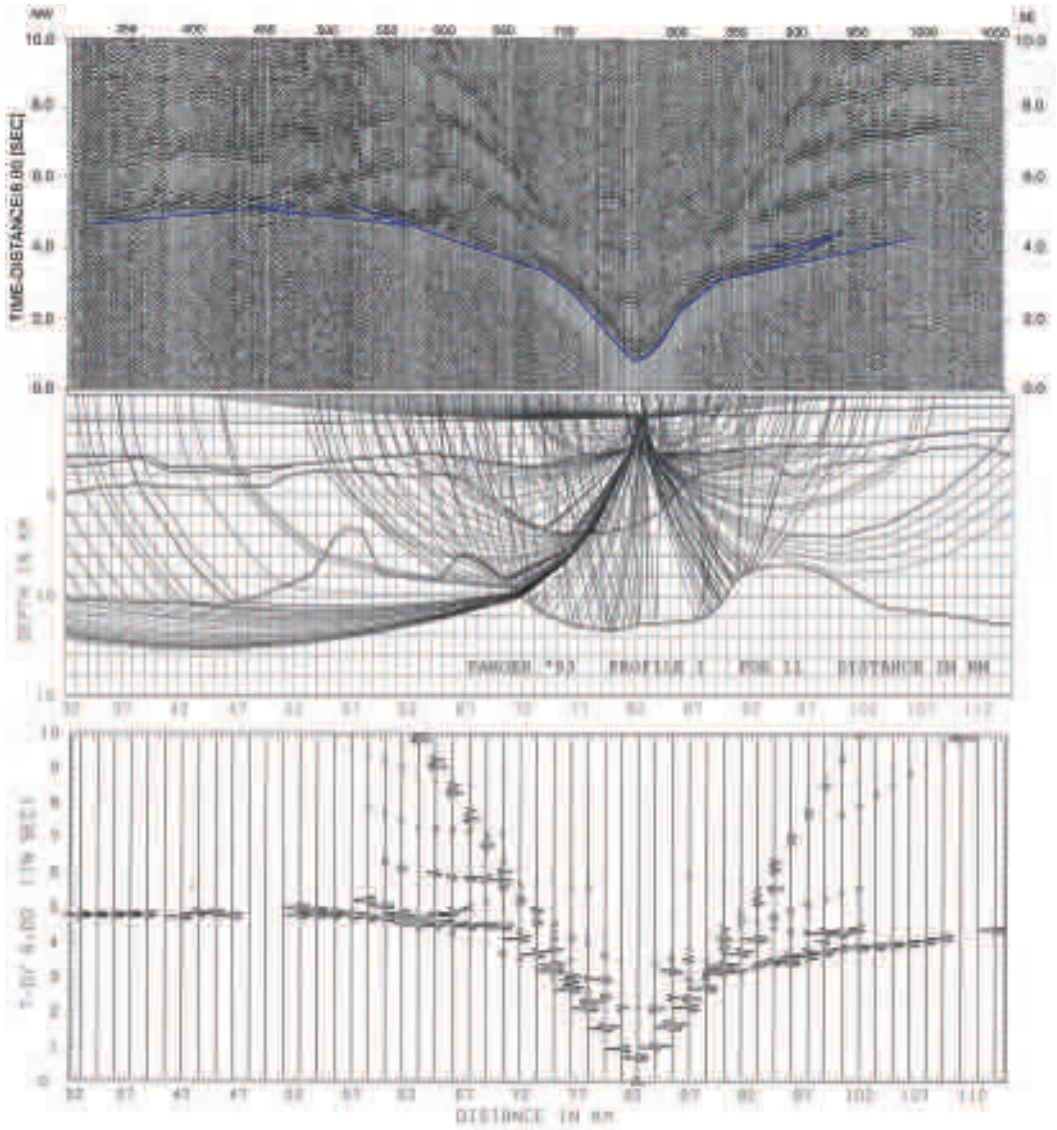

Figure 8. Ray-tracing of sediments and upper crust of Profile 1, OBS position 11, vertical component. Explanations in figures 6 and 7, and in the text.

found in our modelling. At the north-western part of the model, that is northwest of the Corona Ridge, a basalt flow was mapped which thins from northwest to southeast. It covers the Mesozoic sedimentary basins located northwest of the Corona Ridge (Guðrun and Corona Basins). The sediments below the basalts extend to a maximum depth of 9 km and are up to 5 km thick. The Corona Ridge to the southeast indicates either the termination of the basalts or a significant thinning of it. This indicates that either the Corona Ridge was a positive feature during the time of volcanism, or that the extrusion rates were not sufficient to reach any further than the Corona Ridge. We favour the second possibility.

The basin is separated into a Faeroese part to the

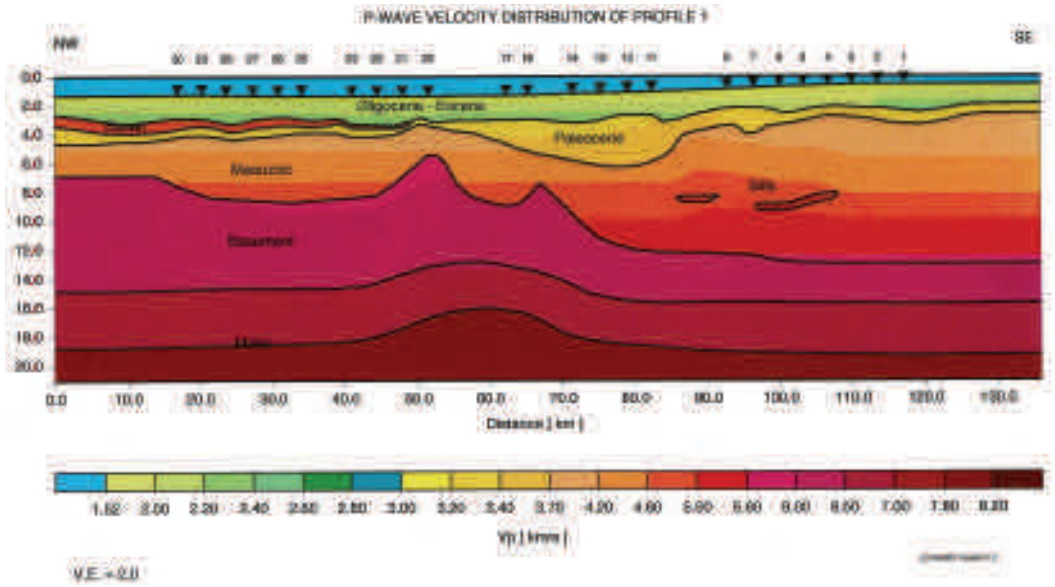

Figure 9. 2D model of the compressional velocities of Profile 1. See the discussion in text.

NW and a Shetland one to the SE, which in its central part is covered by more than 10 km of Oligocene to Mesozoic sediments. Crustal thickness increases from the Corona Ridge to the northwest towards the Faeroe Islands, from 14 km at the Corona Ridge to 19 km at a distance of 50 km north of the Ridge. The crust is continental and composed of an upper and a lower part with veloc-

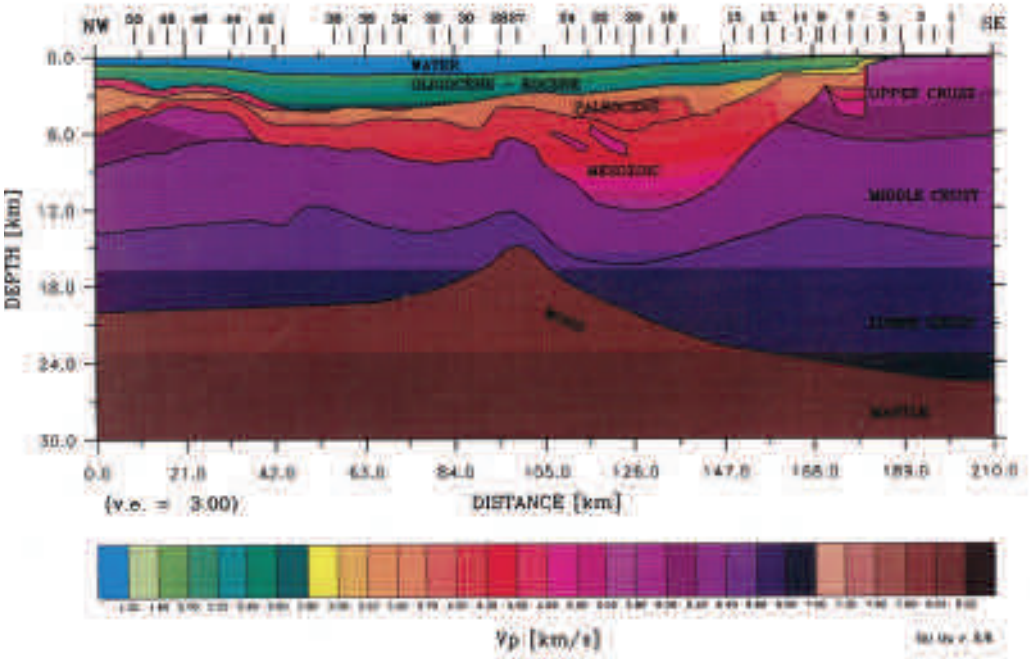

Figure 10. 2D model of the compressional velocities of Profile 2. See the discussion in text.

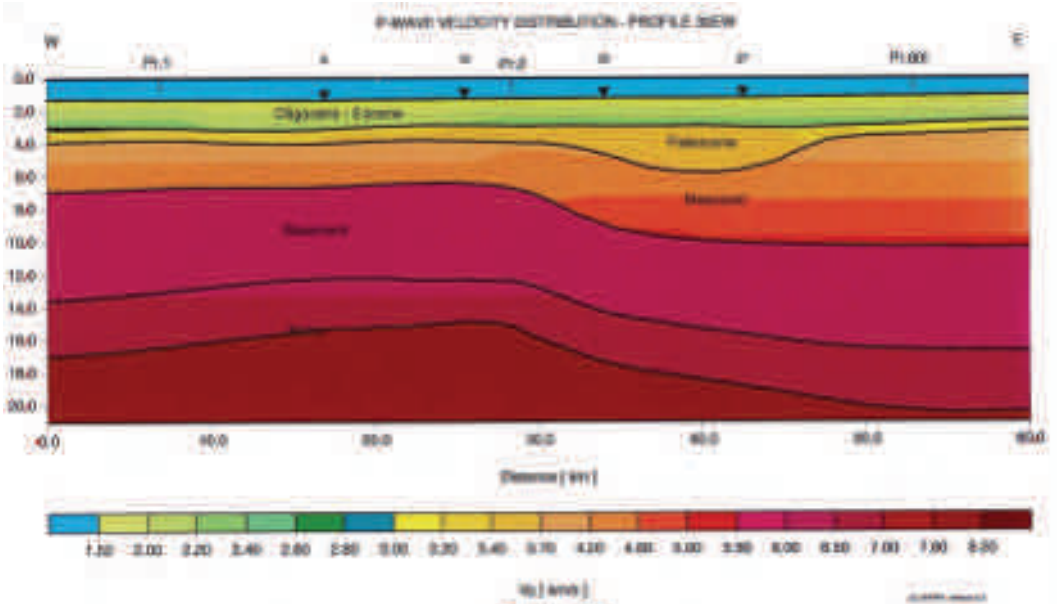

Figure 11. 2D model of the compressional velocities of Profile 30 EW of the 3D array. See the discussion in text.

ities ranging from 5.8 to 6.5 km/s and 6.8 to 7.2 km/s, respectively. This is similar to the findings of Raum *et al*. (2004) further to the west - southwest, the primary difference being that there are less variations in the defined velocities. Below the Faeroe Islands, Casten (1974) calculated the crustal thickness to about 31 km by evaluating wide- angle seismic data. The published Pn value of 7.6 km/s is an apparent velocity, not reversed, and definitely too low. Due to the fact that the asthenosphere thermal anomaly below the Faeroe Islands was active during the Paleocene (Clift and Turner, 1988), the Pn velocity has increased since then by cooling to approximately 7.9 to 8 km/s. Basaltic flows were also located within the Mesozoic sediments in the Shetland basin at a depth of about 9 km.

Profile II (figure 10) is a longer section observed by 50 OBS positions. It is located 16 km further to the northwest. It maps the continental crust of the Shetland Islands over the complete Faeroe-Shetland Basin. The shallow section in the central part has similarities to Profile I. Crustal thickness mapped below the Shetland Islands is approximately 26 km, consisting of three layers: The upper one has Vp values ranging from 5.6 to 6.2 km/s, followed by a middle crust of 6.4 to 6.6 km/s and a lower one with Vp values from 6.6 to 7.0 km/s. This type of crust has also been mapped below the British Caledonides (see e.g. Roberts et al., 1988). To the northwest of the Shetland Islands, the Mesozoic basin is fully developed exceeding 10 km of sediments from Oligocene to early Mesozoic. Well 214/17-1 was drilled on a shallow structure at approximately OBS position 16/17 (Figure 10) and confirmed the presence of young sediments. The thick sedimentary basin is limited to the northwest by the Corona Ridge.

The Moho depth has its smallest value of approximately 14 km at the Corona Ridge, and it deepens towards the Shetland Islands. In some locations the sediments-crust transition occurs at 9 km depth that also coincides with the deepest part of the ocean of 1.8 km. To the northwest, towards the area where the basalt flows occur, at the Eocene-Paleocene transition, the Mesozoic basin thins to not more than 3 km. The crustal type mapped below this part of the basin has the same structure as that observed below the Caledonides, consisting of three igneous layers. In contrast to the Caledonian crustal type, we have the stretched continental crust of the basin that consists only of an upper and a lower crust. This type of crust in the basin has been mapped along all the basins ex-

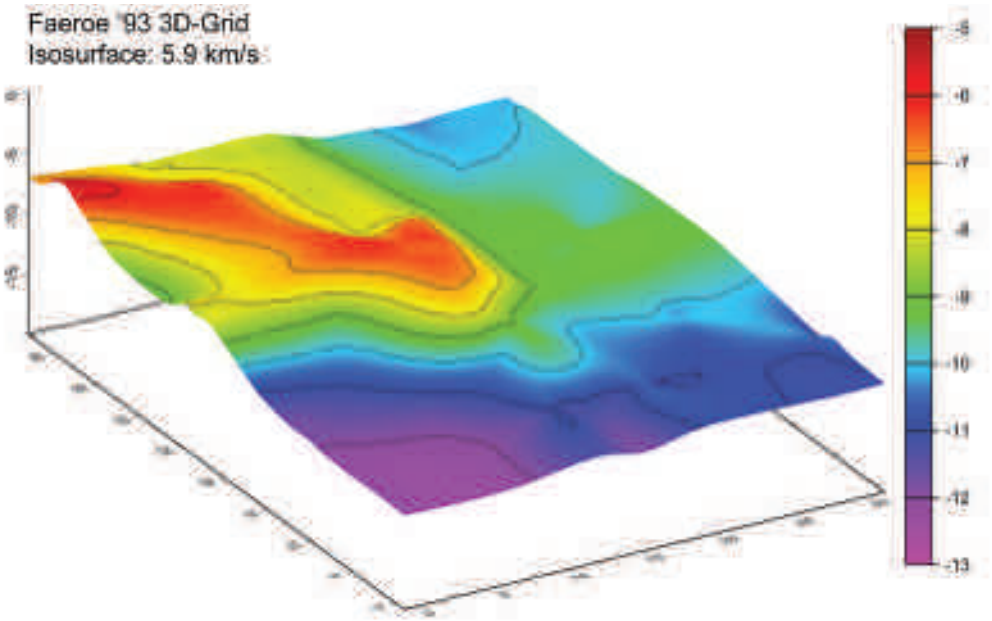

Figure 12. 3D model of the Corona Ridge, 5.8 km/s interface, derived by interpolating all the results of the 2D profiles.

tending from the Shetlands to Ireland in the Porcupine and Rockall troughs (Makris *et al*., 1991; Vogt *et al*., 1998; Klingelhöfer *et al*., 2005). The fact that the thinnest part of the basin exists below the Corona Ridge, which is an uplifted block, is explained by the inversion of the tectonic regime from extensional to compressional sometime during the Mesozoic. In this way, the south-eastern part of the basin deepened, while to the northwest, behind the Corona Ridge, the basin was elevated.

In figure 11 we present an example of one E-W oriented profile from the 3D OBS array. This profile is constrained to the west by the crustal model of Profile I, and to the east by that of Profile II and Profile 60l. Four OBS positions are marked by triangles and numbers. The crustal structure is similar to that described for Profiles I and II and the sediments, particularly those of the Mesozoic sequence, thicken eastwards, which is in line with the general trend of the basin.

By combining the 2D velocity models of the 8 NE-SW profiles with 7 NW-SE oriented, and by also using the results from the NS long profiles, we interpolated the 3D geometry of the Corona Ridge and the underlying Moho. In figure 12 we present the 3D geometry of the Corona Ridge (5.9 km/s interface), which is the top of the continental crust. The Ridge is nearly E-W oriented. It marks the separation between the Corona Basin to the north and the Shetland Basin to the south.

In figure 13 we have plotted the crust-mantle boundary as an isosurface presentation of the 7.8 km/s layer. The trend of this surface is parallel to the Ridge. This indicates that the crustal deformation processes that formed the Ridge are also responsible for the Moho geometry. These processes are likely to be compression due to inversion of the tectonic evolution of the basin sometime during the Mesozoic.

Conclusions

The OBS WARRP survey of the Faeroe-Shetland Basin revealed the geometry of the basin as well as the crustal geometry and thickness below it. We mapped the Eocene to recent sediments down to the Mesozoic and demonstrated that the thickest part of the sediments is located at the Shetland site,

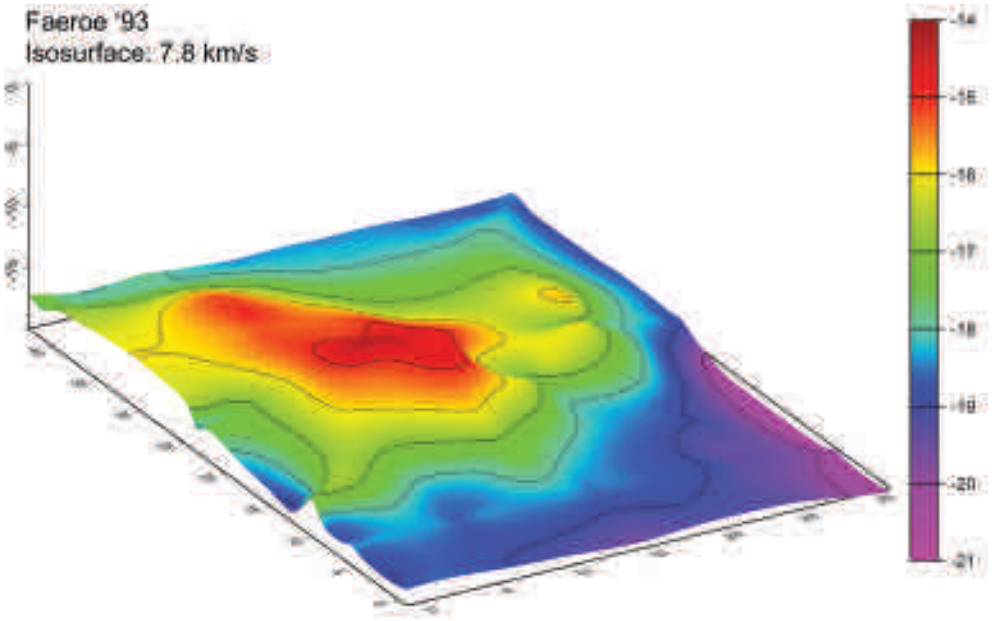

Figure 13. 3D model of the Moho discontinuity, 7.8 km/s interface, below the Corona Ridge. Derived by interpolation of all 2D results.

exceeding 10 km of thickness. The Mesozoic sediments thin to the northwest, and are covered by basaltic flows that terminate northwest of the Corona Ridge, marking the transition from the Eocene to the Paleocene. The Paleocene is better developed to the Shetland side than that to the Faeroe Islands. It extends below the basaltic flows and, together with the Mesozoic sequence, is more than 4 km thick. Towards the Shetlands, this part of the basin thins significantly. The asymmetry of the basin is expressed by the geometry of the Corona Ridge, as well as by an uplift of the Moho discontinuity separating the Shetland Basin sediments and crust from those of the Faeroese side of the basin. Exploration for oil and gas is easier at the Shetland side, which is nearly free of basaltic flows and better accessible to seismic mapping techniques. On the contrary, the Faeroese side, with significant basaltic flows intercalated in the sediments thus marking the Eocene-Paleocene transition, is prohibiting the application of standard reflection mapping. It is necessary to use large-offset OBS data and WARRP techniques in order to map sub-basalt and constrain velocity and structure of the sediments by Vp as well as Vs velocity models (see also Hughes et al., 1998). Prestack depth migration of WARRP data is now available and is the only way to obtain the velocity structure of the sediments below the basalts and delineate their tectonization.

Acknowledgements

We thank the Captain and crew of the "R/V PROF. SHTOKMAN" and Dr. K. Lange for their efforts during the field operations to optimize the work and obtain useful data under difficult weather conditions. We appreciate the input of Mr. L. Akentiev, who developed the 60 lt. sleeve guns, and advised us in generating low-frequency tuned seismic signals.

References

Casten, U., 1974. Analysis of seismic measurements from the Faeroer Islands. *Hamburger Geophysikalische Einzelschriften*: Hamburg: 109.

Cervený, V. and Psencyk, I. 1983. 2-D Seismic ray tracing program package: Charles University.

Clift, P.D. and Turner, J.D. 1988. Paleogene igneous underplating and subsidence anomalies in the Rockall-Faeroes-Shetland area. *Marine and Petroleum Geology* 15: 223-243.

Cooper, M.M., Evans, A.C., Lynch, D.J., Neville, G., and Newley, T. 1999. The Foinaven Field: managing reservoir development uncertainty prior to start-up. *In*: Fleet, A.J. and Boldy, S.A.R. (eds) *Petroleum Geology of Northwest Europe: Proceedings of the 5th Conference*. Geological Society, London: 675-682.

Eldholm, O. and Grue, K., 1994. North Atlantic volcanic margins: dimensions and production rates. *Journal of Geophysical Research* 99: 2955-2988.

Hinz, K., Eldholm, O., Block, M., and Skogseid, J. 1993. Evolution of North Atlantic volcanic continental margins. *In*: Parker, J.R. (ed.) *Petroleum Geology of Northwest Europe: Proceedings of the 4th Conference*. Geological Society, London: 901-913.

Hughes, S., Barton, P.J. and Harrison, D. 1998. Exploration in the Shetland-Faeroe Basin using densely spaced arrays of ocean-bottom seismometers. *Geophysics* 63: 490-501.

Leach, H.M., Herbert, N., Los, A. and Smith, R.L. 1999. The Schiehallion development. *In*: Fleet, A.J. and Boldy, S.A.R. (eds) *Petroleum Geology of Northwest Europe: Proceedings of the 5th Conference*. Geological Society, London: 683-692.

Klingelhöfer, F., Edwards, R.A., Hobbs, R.W. and England, R.W. 2005. Crustal structure of the NE Rockall Trough from wide-angle seismic data modeling. *Journal of Geophysical Research* 110: B11105, doi:10.1029/2005JB003763.

Makris, J., Ginzburg, A., Shannon, P.M., Jacob, A.W.B., Bean, C.J. and Vogt, U. 1991. A new look at the Rockall region, offshore Ireland. *Marine and Petroleum Geology* 8: 410-416.

Raum, T., Mjelde, R., Berge, A.M., Paulsen, J.T., Digranes, P., Shimamura, H., Shiobara, H., Kodaira, S., Larsen, V.B., Fredsted, R., Harrison, D.J. and Johnson, M. 2004. Sub-basalt structures east of the Faeroe Islands revealed from wide-angle seismic and gravity data. *Petroleum Geoscience* 11(4): 291-308.

Roberts, D.G., Ginzburg, A., Nunn, K. and McQuillin, R. 1988. The structure of the Rockall Trough from seismic refraction and wide-angle reflection data. *Nature* 217: 632-635.

Vogt, U., Makris, J., O'Reilly, B.M., Hauser, F., Readman, P.W., Brian Jacob, A. W., and Shannon, P.M. 1998. The Hatton Basin and continental margin: Crustal structure from wide-angle seismic and gravity data. *Journal of Geophysical Research* 103(B6): 12545-12566.

White, R.S., Spitzer, R., Christie, P.A.F., Roberts, A., Lunnon, Z., Maresh, J. and iSIMM group 2005. Seismic Imaging through Basalt Flows on the Faroes Shelf. *In*: Ziska, H., Varming, T. and Bloch, D. (eds) *Faroe Islands Exploration Conference: Proceedings of the 1st Conference*. *Annales Societatis Scientiarum Færoensis*, Supplementum 43, Tórshavn: 11-31.

Insight into sub-basalt lithology from wide-angle converted shear wave analysis

JENNIFER D. ECCLES[1,2*], ROBERT S. WHITE[1], PHILIP A.F. CHRISTIE[2], ALAN W. ROBERTS[1] AND THE iSIMM TEAM[3]

[1] Bullard Laboratories, University of Cambridge, Madingley Rise, Cambridge CB3 0EZ

* Email: jde29@cam.ac.uk; Tel:+44 (0) 1223 721589; Fax: +44 (0) 1223 360779

[2] Schlumberger Cambridge Research, High Cross, Madingley Road, Cambridge CB3 0EL

[3] The iSIMM team: R.S. White, P.A.F. Christie, N.J. Kusznir, A.M. Roberts, D. Healy, R. Spitzer, A. Chappell, J.D. Eccles, R. Fletcher, N. Hurst, H. Lau, Z. Lunnon, C.J. Parkin, A.W. Roberts, L.K. Smith and V.J. Tymms.

ABSTRACT

A high quality wide-angle seismic profile was acquired across the Faroes volcanic rifted continental margin as part of the integrated Seismic Imaging and Modelling of Margins (iSIMM) project. Eighty-five 4-component ocean bottom seismometers (OBS) were deployed along the 375 km profile, from continental to oceanic crust, at 2-6 >km spacing. Penetration of seismic energy beneath the extensive Tertiary flood basalts, semi-opaque to conventional seismic reflection techniques, was achieved using a low frequency seismic source. We discuss a subsection of the profile across the Fugloy Ridge, where compressional (P-) wave tomographic modelling has revealed low velocity material lying beneath 2-7 km of layered basalt flows.

Clear converted shear (S-) wave crustal refractions are observed on rotated radial geophone components of the OBS. These are distinguished from P-waves by their slow linear move-out velocity, late arrival times, and particle motions. Travel-time modelling shows that the dominant conversion interface within this region is the sediment-basalt boundary at the top of the basalt flows. Data are of highest quality in the northwest of the region while S-wave arrivals in the Faroe-Shetland trough are severely attenuated and/or the P- to S-wave conversion efficiency at the sediment-top basalt interface is reduced with distance from the rift. Across the Fugloy Ridge step-backs of the P- and S-wave refractions indicate that both the P- and S-waves encounter a sub-basalt low velocity zone.

An S-wave velocity model along the iSIMM profile has been produced by inverting S-wave arrivals assuming the same layered crustal structure as determined by the P-wave analysis. A more detailed analysis of the sub-basalt layer was then made. Determination of the Vp/Vs ratio in the low velocity zone is less sensitive to the velocity-thickness ambiguity than is the determination of either the P- or S-wave velocity alone. A robust measurement of Vp/Vs in the sub-basalt material was therefore calculated from the relative P- and S- wave travel-time step-backs of refractions turning above and below the low velocity zone. A Vp/Vs ratio of 1.81 ± 0.11 was calculated for the best sampled region of the low velocity zone from 180-200 km along the profile. This Vp/Vs ratio, and a P-wave velocity of 3.9-4.7 km/s for the low velocity zone lies just within the calculated uncertainty bounds for interbedded basalt and hyaloclastite but is more indicative of sedimentary rock which would be likely to be Paleocene in age.

Introduction

Tertiary continental break-up between northwest Europe and Greenland caused the rapid production of large volumes of extrusive basalt (> 1 million km^3; Eldholm and Grue, 1994) in the North Atlantic Igneous Province (NAIP), due to decompression of elevated temperature mantle during rifting (White and McKenzie, 1989). Lava flowed across sedimentary basins up to 150 >km away from the rift while intrusion into the crust of large

Faroe Islands Exploration Conference: Proceedings of the 2nd Conference.
Annales Societatis Scientiarum Færoensis, Supplementum 50, 2009: 43-60

volumes of melt caused permanent crustal thickening and uplift across the continent-ocean transition (White *et al*., 2005). The possible existence of sedimentary rock beneath the basalt flows on the Faroes shelf is of considerable interest to the petroleum industry as any such sedimentary rocks, likely to be of the same age as those in the nearby Foinaven field (Loizou, 2005), may be hydrocarbon bearing. However, exploration in this region has proved to be problematic as the basalt is semi-opaque to conventional seismic reflection techniques and few wells currently penetrate beneath the basalt in the NAIP. Other examples of sub-basalt sedimentary basins include Western India, Karoo (southern Africa), Paraná Basin (Brazil), Columbia Basin (USA) and East Siberia.

On the Faroe Islands basalts have an exposed stratigraphic thickness of 3 km and a further 3.5 km has been drilled by the Lopra-1/1A borehole (for location see Figure 1). Most of the lavas were extruded at or near sea-level (Waagstein, 1988; Ellis *et al*., 2003). Individual basalt flows, interbedded with sediment, tuff or hyaloclastites and with vesiculated or altered margins around a dense core (Planke and Cambray, 1998), are often too thin to be seismically resolved (Barton and White, 1997). Reflectors observed within the basalt represent a complex interference pattern except where flows are > 50 m thick (Smallwood *et al*., 1998). The high effective attenuation of the basalt (Bais *et al.*, this volume; Shaw *et al*., 2008) is attributed to the cyclical nature of the basalt structure (Rutledge and Winkler, 1989; Maresh and White, 2005). Energy scattering from rugose surfaces (Martini and Bean, 2002; Maresh *et al*., 2006) also inhibits the sub-basalt penetration of high frequency seismic energy.

The joint industry and university iSIMM project aimed to improve sub-basalt imaging (White *et al*., 2002). Data acquisition was specifically tailored to this problem, achieving improved sub-basalt seismic reflection profiles and high-quality, wide-angle seismic data. The use of converted shear (S-) waves, that is energy transformed from compressional (P-) waves to S-waves at a crustal interface, provides further constraint on the crustal, and particularly the sub-basalt, composition. The combination of P-wave velocity and the ratio of P- to S- wave velocities (Vp/Vs), or equivalently Poisson's Ratio, is more diagnostic of the lithology than is the P-wave velocity alone. One question of immediate relevance is whether the thick hyaloclastite unit found on the Faroe Islands at the base of the deep Lopra-1/1A well beneath the basalts (Christie *et al*., 2006a) is widely distributed or whether more prospective sub-basalt sedimentary rock can be found elsewhere.

Data Acquisition

A seismic profile, crossing the volcanic rifted continental margin northeast of the Faroe Islands (Figure 1), was acquired in 2002 as part of the iSIMM project (White *et al*., 2002). The Faroes profile was approximately 375 km long and eighty-five 4-component GeoPro OBS (Geopro, 2007) were deployed at 2 or 6 km intervals in water depths of up to 3.5 km. A coincident seismic reflection profile was also acquired using a 12 km long single-sensor streamer (Martin *et al*., 2000). Low frequency energy has been identified as being more effective than high frequency energy in penetrating basalt flows (Ziolkowski *et al*., 2003; Maresh and White, 2005). To generate seismic energy with a low peak frequency of 9 Hz, we used bubble tuning (Avedik *et al*., 1996, Lunnon *et al*., 2003), a large 14 gun, 6300 in^3 (103 l) source array, and deep (18-22 m) towing of the source for this survey. The towing depth, with the optimum tradeoff between the effect of the ghost response and increased hydrostatic pressure, was found to be of greater importance in generating this low frequency energy than the tuning mode (Christie *et al*., 2006b).

The gimballed 4-component OBS, recording the vertical and two orthogonal horizontal components as well as a hydrophone allows wide-angle (Samson *et al*., 1995) scalar and vector wavefield data to be recorded. This enables deeply-turning P-wave refractions and wide-angle reflections to be recorded and converted wave arrivals to be distinguished from other energy. Low velocity sediments in the near surface beneath the OBS cause upcoming energy to be refracted towards the vertical and thus provide a natural separation between the P- and S-waves on the vertical and horizontal components due to the fundamental differences of

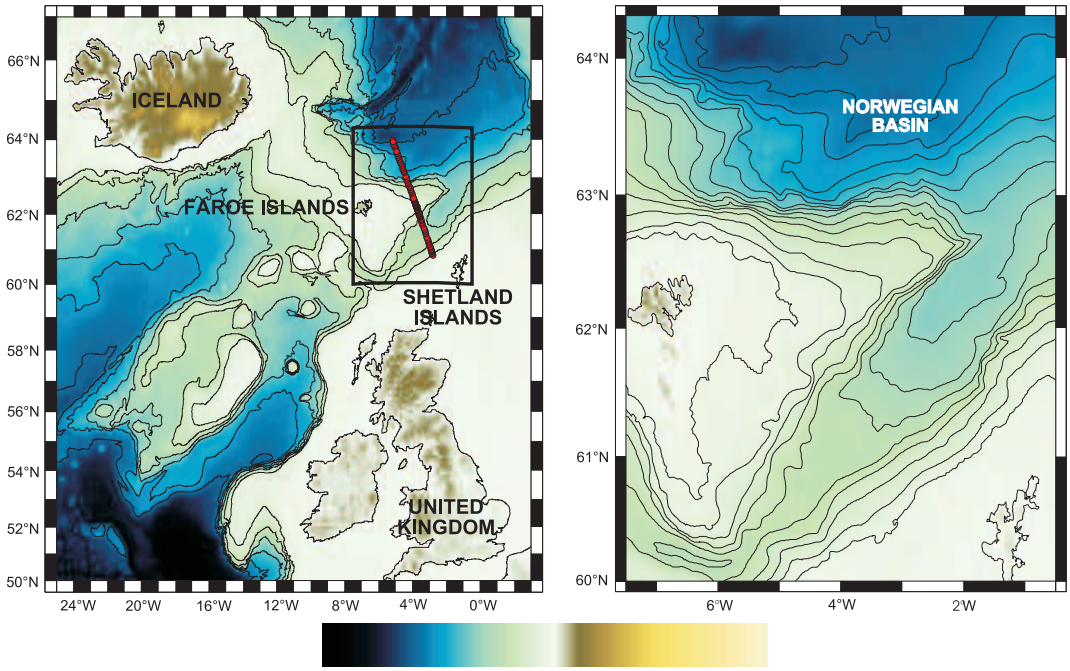

Figure 1.: (A). Location map of the iSIMM OBS profile over the Faroes continental margin. (B). Enlargement of the Faroes profile. The yellow line represents the multi-channel seismic profile and circles the successfully recorded and recovered OBS. The orange box indicates the sub-section of the profile concentrated in this paper. Red filled circles represent OBS used in the detailed analysis of the sub-basalt low velocity zone described in this paper. OBS48, shown in Figure 2, and OBS53, Figure 3, are highlighted in white.

P- and S-wave propagation (that is, particle motion parallel and perpendicular to the direction of wave propagation respectively). OBS data can have a lower ambient noise level than streamer data as they are not being towed through the water and, at the sea-floor, are less affected by sea-surface wave or weather noise. On the other hand current noise, due to the vigorous North Atlantic deep-water circulation, may be significant on some OBS records.

The large offsets recorded capture the arrivals with large angles of incidence that show greatest conversion from P- to S-wave energy. Generally the S-wave velocity structures of oceanic crust and of continent-ocean transition zones are only poorly defined as they are difficult to study using conventional marine seismic surveys reliant on double mode conversion back to a P-wave for propagation through the water column to the streamer (Minshull, 2002). However, multi-component OBS data, such as those reported here, make it possible to directly record incident S-waves. The low frequency iSIMM source combined with the relatively high density OBS deployment along the profile and the unusually long streamer used to collect the multi-channel seismic data, allows more detailed study of the crust beneath the basalts flows than has previously been achieved (Spitzer *et al.*, 2005).

Methodology

OBS data quality was good with wide-angle converted S-waves visible from shots located up to 150 km from the seismometers and P-wave arrivals visible to even greater offsets. S-wave crustal refractions were identified by their characteristically slow linear move-out (Figures 2 and 3). Although visible on the vertical component (Figures 2A and 3A), S-wave arrivals are strongest on the horizontal components. To improve the signal

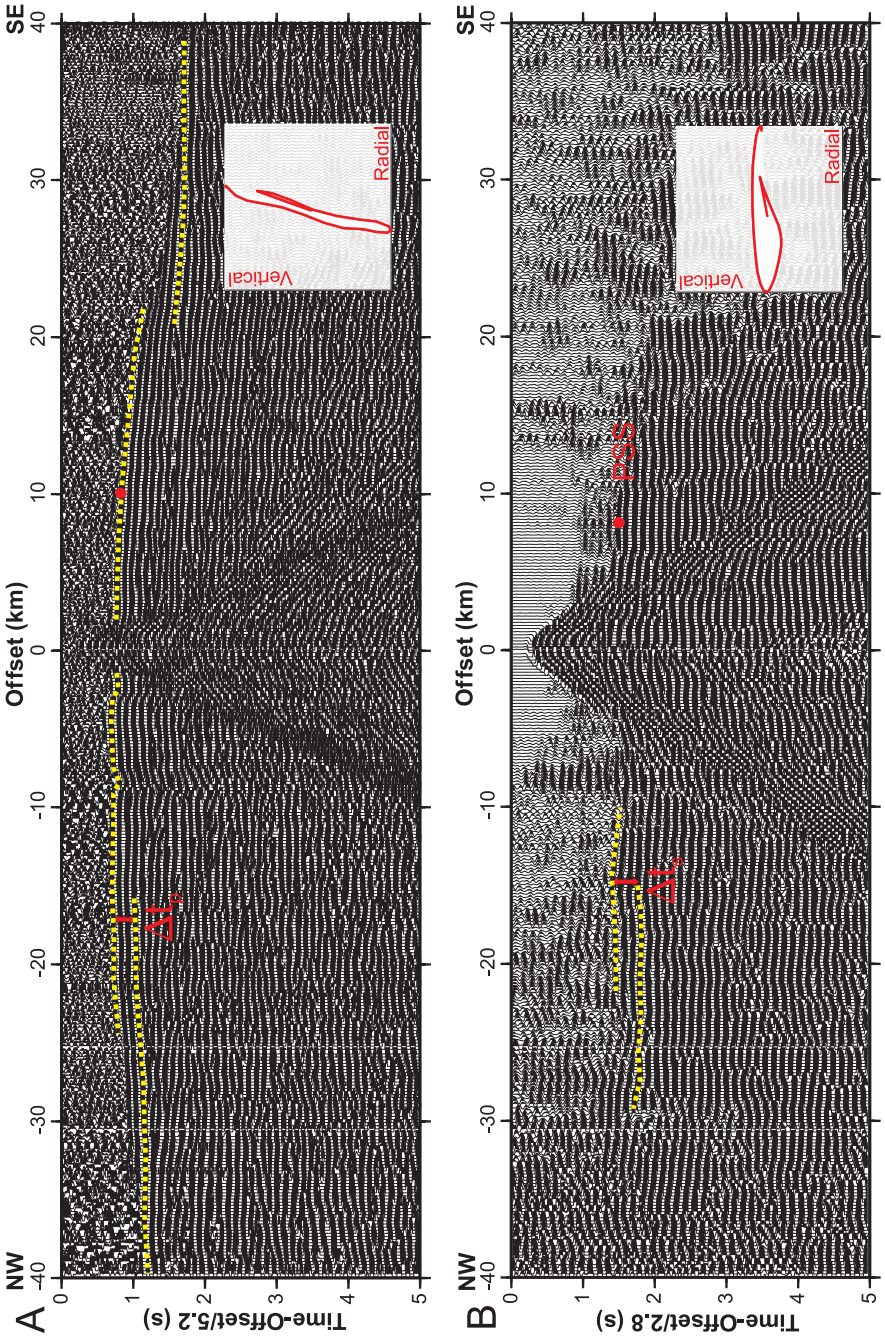

Figure 2.: OBS48 seismic data with a 3-20 Hz bandpass filter. (A). Vertical geophone component displayed with a reduction velocity of 5.2 km/s. Step-backs are highlighted in yellow. Converted S-wave arrivals can be seen steeply dipping from 5-15 km and 2-5 s. Inset is the particle motion of the P-wave arrival with energy dominantly on the vertical component. (B). Radial geophone component displayed with a reduction velocity of 2.8 km/s. To remove interfering P-wave energy an FK-filter of 3.2 km/s has been applied. Step-backs are highlighted in yellow and amplitude variation was very important in the identification of the refraction at wide offsets. Both the PSP and PSS conversion phases are visible on this instrument. Inset is the particle motion of one cycle of the converted S-wave arrival with energy dominantly on the radial component.

to noise ratio these arbitrarily-orientated components (due to free fall of the OBS through the water column during deployment) were rotated into radial (in-line) and transverse (cross-line) components based on the polarisation of the direct wave (Kragh and Peardon, 1995). FK-filters that cut out energy above 3.2-4.0 km/s were also applied to the radial component to reduce interference by the earlier P-wave phases (Figures 2B and 3B). Despite this processing the clarity of the converted S-wave phases was variable as exhibited by Figures 2 and 3.

Particle motions of the arrivals were examined by cross-plotting the vertical and radial components. As expected, P-wave arrivals (Figures 2A and 3A) are dominated by energy on the vertical components and S-wave arrivals by energy on the radial components (Figures 2B and 3B). Particle motions of those arrivals with an S-wave move-out gave insight into whether conversions were occurring at the source or receiver end. Picking the travel-times of the weaker secondary S-wave arrivals is more problematic than picking the times of the equivalent P-wave arrivals because the first onset of the S-wave is less well defined due to interference with the earlier P-wave, and with its multiples/reverberations. S-wave arrivals are generally less continuous and extensive due to higher attenuation of the slow S-wave, variable, large amplitude S-wave statics and the variability of the P- to S- conversion efficiency (Figures 2 and 3).

We use a P-wave velocity model of the entire Faroes profile (Figure 1) as a starting model for S-wave analysis. Figure 4 shows the P-wave velocity model for the area (Roberts, 2006), centred on the Fugloy Ridge, on which we focus in this paper. This P-wave model was produced using a three stage travel-time tomography approach on travel-time picks made from the vertical geophone components (Roberts, 2006). Initially the P-wave crustal refractions were inverted for upper crustal structure using a first arrival travel-time tomography code (Zelt and Barton, 1998), then the poorly-resolved, sub-basalt low velocity zone (LVZ) was forward modelled using a computer ray-tracing program that allows crustal interfaces (Zelt and Smith, 1992). This forward modelling entailed matching the carefully picked basalt refraction terminations and step-back times to the basement refraction. As illustrated by Figure 5, in the presence of a sub-basalt LVZ the basalt refraction terminates when the turning ray meets the base of the basalt. The offset at which this termination occurs is dependent on the basalt thickness and its velocity gradient, and the magnitude of the step-back to the later basement refraction is dependent on the thickness and velocity of the intervening LVZ (Fliedner and White, 2001). Reflections from the base of the LVZ were also used to constrain the LVZ velocity and thickness. The sub-basalt LVZ feathers out beneath the northwest flank of the Fugloy Ridge at the continent-ocean transition (Figure 4). Finally, the lower crustal velocity structure and crustal thickness were constrained by inversion of the travel-times of Moho reflections and, for oceanic crust and the continent-ocean transition, by deep crustal refractions.

For most previous studies converted S-wave arrivals have been sparse, so Vp/Vs analyses have been carried out by forward modelling assuming a constant Vp/Vs ratio within each layer or block (e.g. Raum *et al*., 2005). This strategy was initially used, assuming the underlying P-wave velocity model of Roberts (2006), to establish approximate Vp/Vs ratios for each layer and to determine the conversion interfaces. It was found that the arrival times of the S-waves in this area are consistent with conversion of the downward propagating wave from a P- to an S-wave at the sediment-top basalt interface, the boundary at which solutions to the Zoeppritz equations (Aki and Richards, 2002) indicate the most theoretically efficient conversion will occur. Due to the large number of OBS deployed and the high data quality achieved in this survey, inversion of the S-wave travel-time data was feasible. Over 35,500 S-wave travel-time picks were inverted for the entire profile, 29,500 of these having some portion of their raypath within the 140-240 km range. This is in contrast to the 88,000 picks used to constrain the 250 km sub-section of the P-wave model, 55,000 of these having some portion of their raypath within the 140-240 km range.

For the converted S-wave tomographic inversion it was assumed that the S-wave crustal boundaries occurred at the same place as for P-waves and

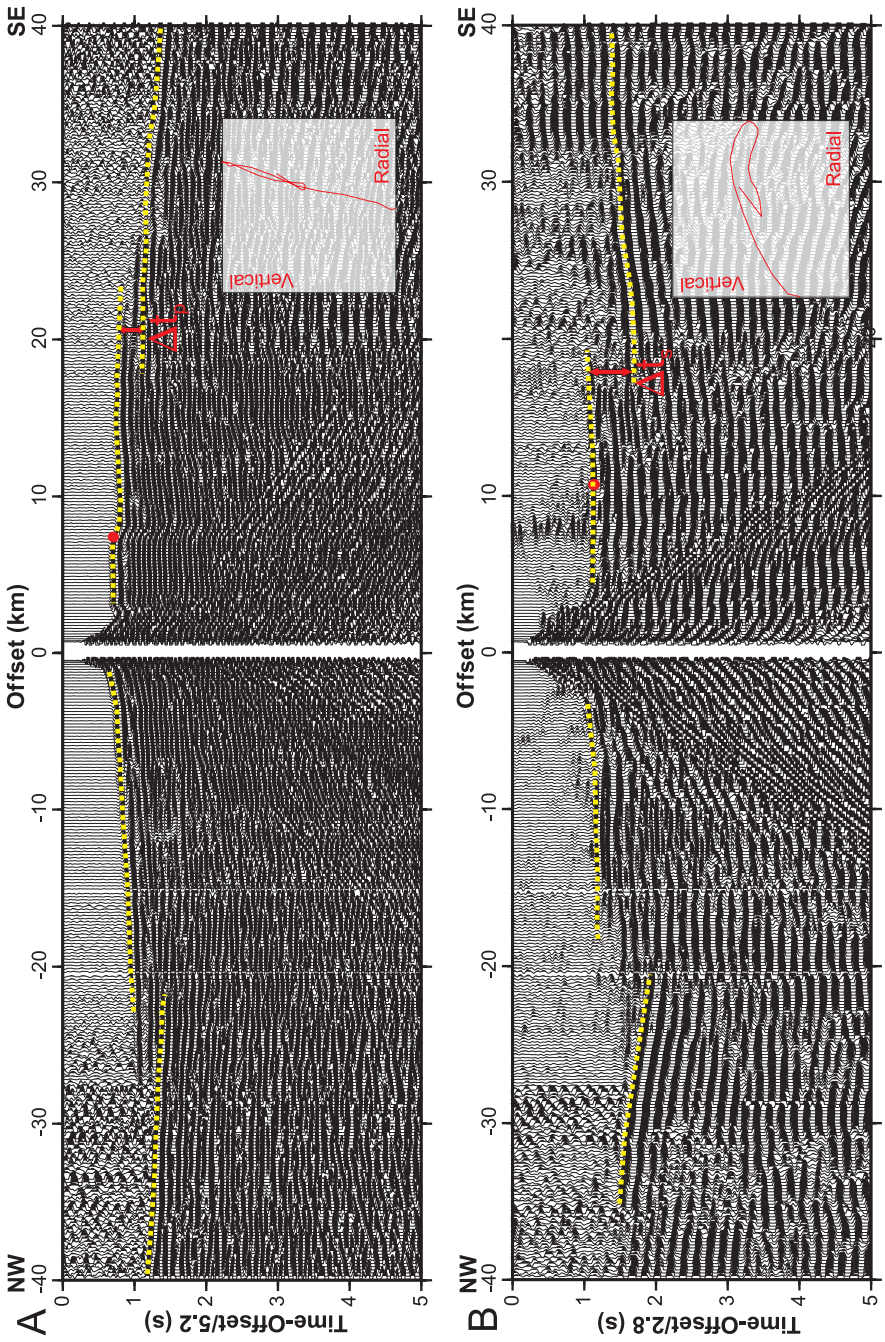

Figure 3.: OBS53 seismic data with a 3-20 Hz bandpass filter. (A). Vertical geophone component displayed with a reduction velocity of 5.2 km/s. Step-backs are highlighted in yellow. Converted S-wave arrivals can be seen steeply dipping from 5-15 km and 2-5 s. Inset is the particle motion of the P-wave arrival with energy dominantly on the vertical component. (B). Radial geophone component displayed with a reduction velocity of 2.8 km/s. To remove interfering P-wave energy an FK-filter of 3.2 km/s has been applied. Step-backs are highlighted in yellow. Inset is the particle motion of one cycle of the converted S-wave arrival with energy dominantly on the radial component.

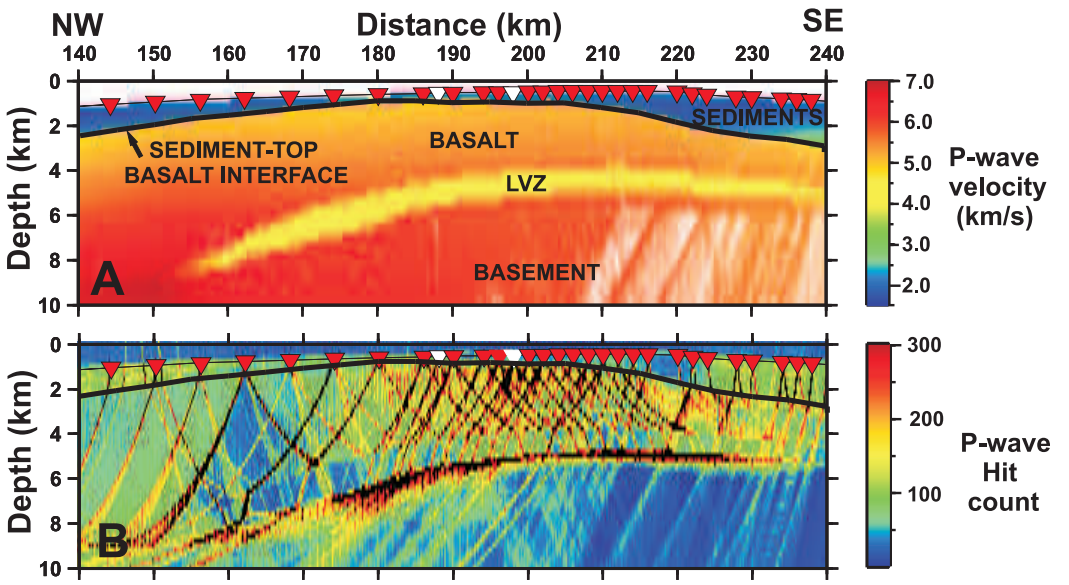

Figure 4. (A). Sub-section of the profile wide P-wave velocity model from Roberts (2006). OBS positions are shown with red triangles. Major crustal units are labelled, LVZ=Low Velocity Zone. (B). Ray coverage of the P-wave velocity model with many rays penetrating deeply beneath the basalt. OBS 48, at 198 km profile distance, and OBS 53, at 188 km profile distance, (Figures 2 and 3) are highlighted in white. The different regions of the model discussed in the text, the continent-ocean transition (COT), the Fugloy Ridge and the Faroe-Shetland Trough are defined.

hence the positions of interfaces from the higher quality P-wave model (Roberts, 2006) were held fixed. A starting model was generated by converting the P-wave velocity model beneath the sediment-top basalt interface to S-wave velocities using a simple Vp/Vs structure with constant Vp/Vs ratios of 1.87, 1.81 and 1.76 for the areas interpreted to be basalt, lower oceanic crust and lower continental crust respectively. The robustness of the inversion was also tested by using a starting model with a single crustal Vp/Vs ratio, which yielded very similar results. The bulk Vp/Vs ratio of the sedimentary sequence beneath each OBS was analysed by modelling the PPS refractions i.e. those arrivals propagating through the crust as a P-wave, and hence having a P-wave moveout, yet being converted on the way up to an S-wave at the top basalt-sedimentary rock interface. These arrivals are subject to a travel-time delay compared to the P-wave first arrival. The sediment Vp/Vs was also determined by comparing travel-times of P-wave and target converted S-wave reflections from the top basalt interface on each OBS. Using the calculated sediment S-wave velocity and water depth, the crustal travel-times were corrected to allow a reciprocity analysis to be performed for quality control of the arrivals picked. The effect of errors in sediment Vp/Vs were quantified by calculating the travel-time difference between arrivals corrected using the limits of allowable Vp/Vs ratios from the analysis of PPS arrivals. Large sediment Vp/Vs uncertainty at the top of the Fugloy Ridge had little impact due to the thin sediments however sediment Vp/Vs uncertainty in the Faroe-Shetland Trough, associated with poor quality PPS picks, had a significant effect on the corrected arrival time of crustal S-wave refractions or, similarly, the calculated travel time through the model. These errors were combined with an estimate of picking uncertainty and assigned to each arrival prior to inversion.

The inversion was carried out using Rayinvr (Zelt and Smith, 1992), which had previously been used for P-wave forward modelling of the LVZ and inversion of the lower crustal structure. The Vp/Vs structure of the sediments was defined in

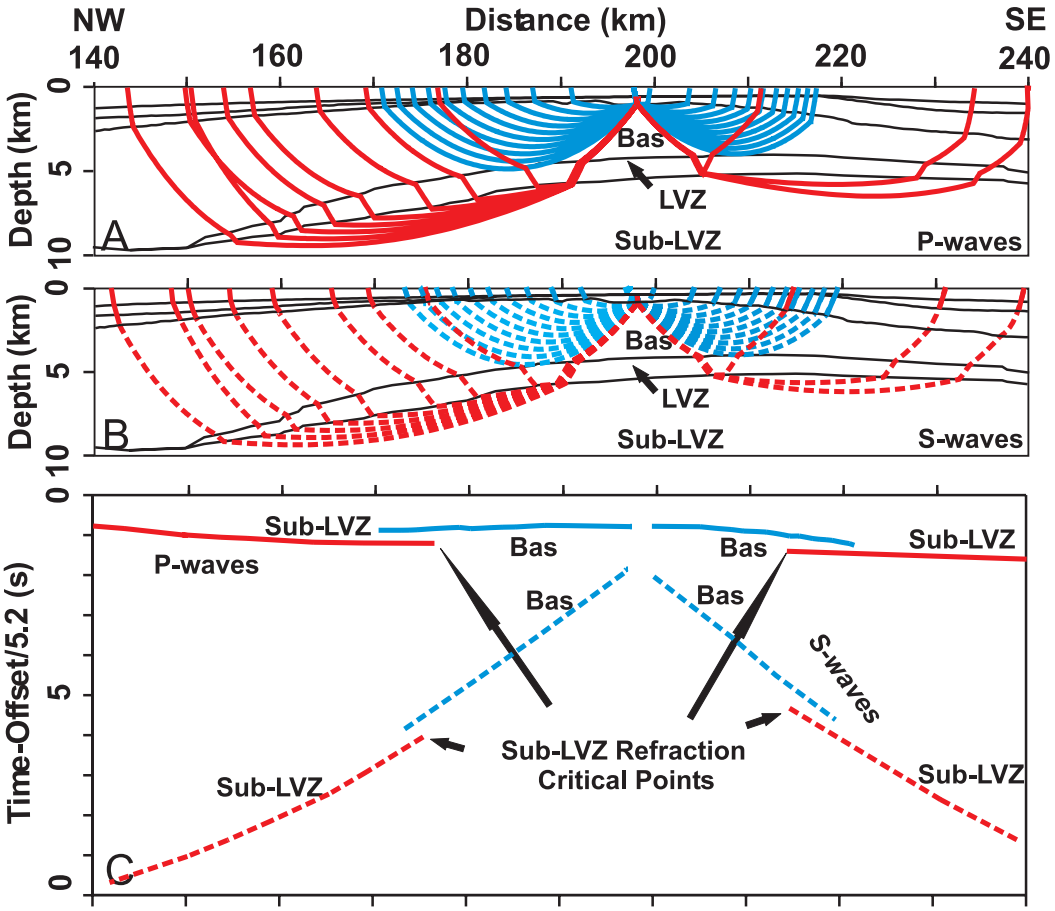

Figure 5. (A). Ray tracing of refractions through the P-wave velocity model (Figure 3) for OBS 48. (B). Ray tracing of S-waves, converted at the top basalt interface, through the S-wave velocity model. (C). Calculated travel-times of the ray tracing in A and B including 'step-backs' associated with the LVZ. Solid lines denote P-wave arrivals while dotted lines are S-wave arrivals. The basalt (Bas) refraction terminates when the turning rays reach the base of the basalt layer while refractions from beneath the low velocity zone (Sub-LVZ) are delayed and persist to greater offsets.

0.5 km wide blocks and rays converted at the sediment-top basalt interface at the source end of each ray path. With the geometry of the LVZ fixed from the P-wave analysis a measure of the Vp/Vs ratio in the LVZ was made within the model by varying the Vp/Vs ratio in the LVZ from 1.60 to 2.1 at increments of 0.05 with the inversion run to completion for the deeper structure for each value of Vp/Vs in the LVZ. This process allowed the S-wave step-back time (e.g. Figure 2B and 3B) to be fitted well.

Although a velocity-thickness ambiguity is inherent in the P-wave forward modelling of the LVZ, if we can assume the same LVZ thickness for S-waves as for P-waves, the calculated Vp/Vs ratio is almost insensitive to the thickness. To give a simple example, if the thickness of the LVZ were halved, the velocity within the layer would have also have to be halved to maintain the same travel-time through it (for a fixed raypath) and hence the same step-back in time to the basement refraction. This principle holds for both the P- and S-wave velocities and hence the Vp/Vs ratio would remain unchanged.

A more detailed analysis of the Vp/Vs ratio in the LVZ than that gained from the S-wave modelling of the entire line can be achieved by considering the relative P- and S- wave step-backs (taking into account the ~90 degree phase delay due to the LVZ) at the critical point of the basement refraction. As shown by Equation 1 (below) the relationship between the Vp/Vs ratio of the LVZ and the step-back times is dependent on the P- and S-wave velocity relationships between the LVZ and the underlying basement velocity because of ray-bending; in our case basement velocities are well resolved. This analysis was restricted to the flat lying, approximately constant thickness portion of the LVZ at profile distances of 180-200 km. This region had the lowest modelled P-wave velocities and is best sampled by S-wave step-backs.

$$\frac{Vp_{LVZ}}{Vs_{LVZ}} = \frac{\Delta t_s \sqrt{1 - \frac{Vp_{LVZ}^2}{Vp_{Sub-LVZ}^2}}}{\Delta t_p \sqrt{1 - \frac{Vs_{LVZ}^2}{Vs_{Sub-LVZ}^2}}} \qquad \text{(Equation 1)}$$

or to simplify

$$\frac{Vp_{LVZ}}{Vs_{LVZ}} = A\frac{\Delta t_s}{\Delta t_p} \qquad \text{(Equation 2)}$$

Vp_{LVZ} and Vs_{LVZ} are the P- and S-wave velocities of the low-velocity zone, $Vp_{Sub\text{-}LVZ}$ and $Vs_{Sub\text{-}LVZ}$ the P- and S-wave velocities directly beneath the low-velocity zone, and Δt_p and Δt_s the P- and S-wave step-back times respectively at the critical points of the refractions turning beneath the low-velocity zone.

From Equation 2 the Vp/Vs ratio of the LVZ cannot be entirely independently calculated using the relative step-back times. Given modelled errors in $Vp_{Sub\text{-}LVZ}$ of ±0.03 km/s (Roberts, 2006), an estimated error in $Vs_{Sub\text{-}LVZ}$ of ±0.1 km/s, and a possible range of LVZ P-wave velocities of 3.9-4.7 km/s, the allowable range of Vp/Vs values, and hence that for the bulk multiplier, A, which corrects for the different P- and S-wave paths through the LVZ was explored. The bulk multiplier, A, can be determined to within 5-8% at any single location within the model, exhibiting 3% spatial variation. However the step-back times provide additional errors in the calculated Vp/Vs ratio. Step-backs were analysed from ten instruments deployed over the top of the Fugloy Ridge (Figure 1B). The critical point of the basalt refraction, at which the magnitude of the step-back was measured, was determined by ray tracing through the global model (e.g., Figure 5). The analysis was repeated with a different global model (with an appropriate Vp/Vs ratio in the LVZ) until the Vp/Vs ratio in the LVZ of the global model and that calculated in the step-back analysis converged.

Results

A 250 km long 'global' S-wave velocity model of the Faroes profile from the Norwegian Sea to the northwest side of the Faroe-Shetland Trough has been generated successfully by tomographic inversion followed by iterative forward travel-time modelling. The relevant sub-section across the Fugloy Ridge is displayed in Figure 6A. Low velocity Tertiary sedimentary rock, displayed with a P-wave velocity consistent with the down going ray path, overlies thick basalt. The subaerially extruded basalt sequence on the Fugloy Ridge was modelled as having a Vp/Vs ratio of 1.8-1.9 (Figure 7). The distinctive LVZ occurs at 5 km depth, deepening towards the continent-ocean transition. The associated ray coverage (Figure 6B) shows that S-waves do not penetrate deeply into the basement beneath the LVZ. The Vp/Vs ratio of the material immediately beneath the LVZ was modelled to be 1.80-1.88 (Figure 7). Ray coverage decreases with thickening sedimentary rock and thinning basalt in the Faroe-Shetland Trough to the south. That converted S-wave arrivals from shots to the NW fail to propagate to these instruments indicates that these sediments or the underlying stretched continental crust highly attenuate S-waves. The failure to record arrivals from shots in the Faroe-Shetland Trough could also be attributed to the attenuation of the S-waves in the continental crust or to less efficient conversion from P- to S-wave energy. This variation in conversion efficiency is largely due to increasing sediment velocities and decreasing basalt velocities caused by individual flows thinning with distance from the rift and a higher pro-

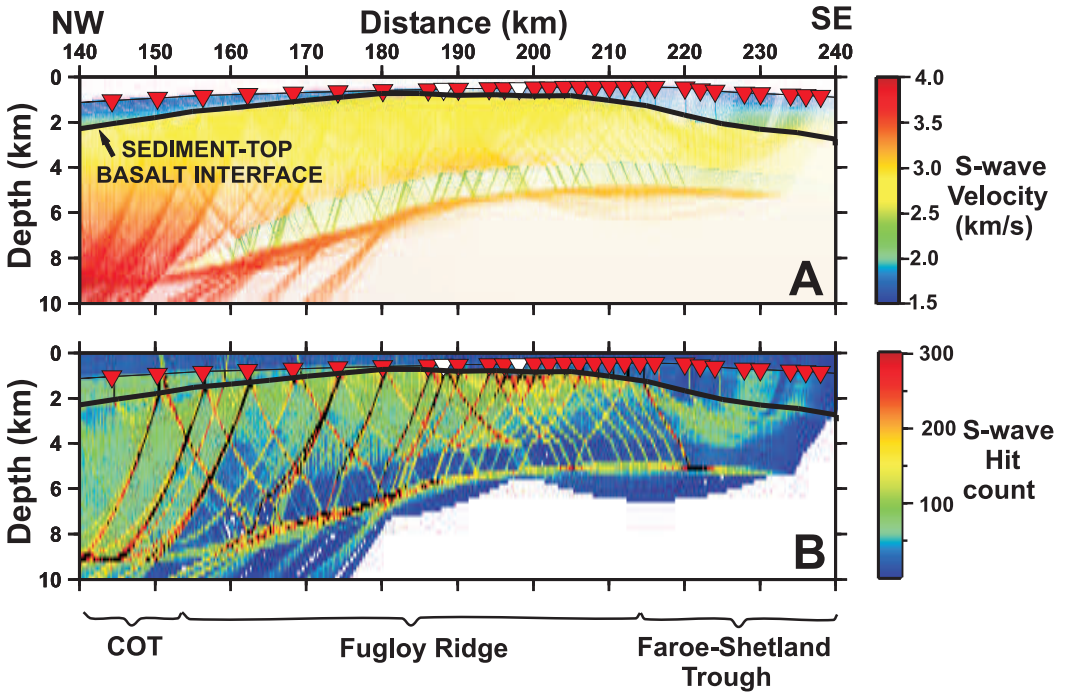

Figure 6. (A). Composite P- and S-wave velocity model. Sediments, with P-wave velocities < 3 km/s, are shown above the sediment-top basalt interface (bold horizon). The Vp/Vs ratio of these sediments constrained from wide-angle data PPS refractions and PS reflections from the top basalt. Crustal S-wave velocities are shown beneath this interface (B). Ray coverage of the converted S-wave model. Few rays penetrate deeply into the basement beneath the low velocity zone. OBS 48, at 198 km profile distance, and OBS 53, at 188 km profile distance, (Figures 2 and 3) are highlighted in white.

portion of vesicular or fractured flow margins and interbedded sediments than seen to the northwest. Thus the identification of converted S-wave arrivals is limited to within the modelled 250 km section of the profile. The Vp/Vs ratio, determined from comparison of the 'global' P- and S-wave velocity models is presented schematically in Figure 7. The best fit global model has a constant LVZ Vp/Vs ratio of 1.80 while a LVZ Vp/Vs ratio of 1.75 provides the best fit to sub-LVZ refractions.

Analysis of the relative P- and S-wave step-back times from the ten OBS across the Fugloy Ridge with step-backs occurring at the LVZ in the region 180 km to 200 km profile distance gives an average Vp/Vs ratio of 1.81±0.11 (Table 1) for a LVZ Vp/Vs ratio of 1.8.

Discussion

The resolution of basalt P-wave velocities (Figure 4) is very good, but first arrival or refraction travel-time inversion codes cannot resolve low velocity zones. The computationally intensive waveform inversion technique, which includes amplitude information, represents a promising development in the resolution of such features (Sirgue and Pratt, 2004). Careful modelling of basalt refraction terminations, step-backs to the basement refraction and reflections from the base of the LVZ can allow estimation of the location and properties of the LVZ, although due to the velocity-thickness ambiguity and potential for bias during forward modelling, the uncertainty remains higher in the LVZ than elsewhere in the model (Roberts, 2006). The picking of the offsets at which the basalt refractions terminate is difficult because, although the termination is generally marked by a rapid de-

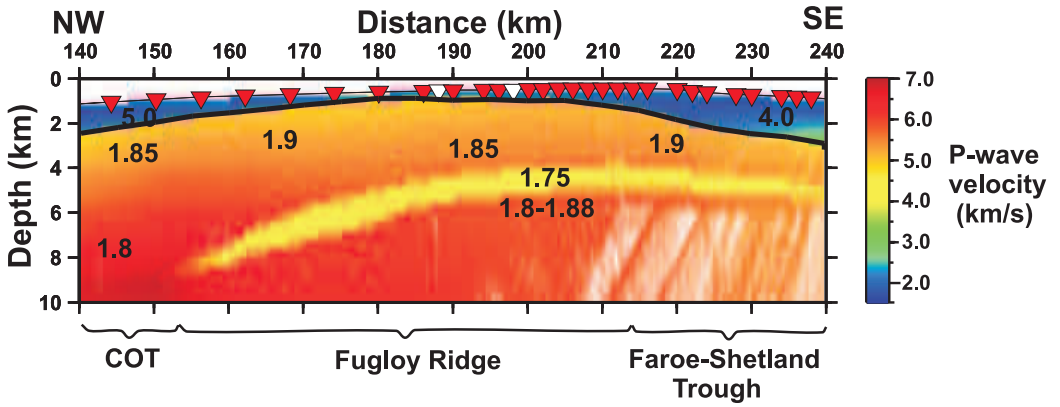

Figure 7.: Vp/Vs values superimposed on the P-wave velocity model. OBS 48, at 198 km profile distance, and OBS 53, at 188 km profile distance (Figures 2 and 3) are highlighted in white.

crease in amplitude to below the noise levels, the exact offset can be affected by the processing applied, particularly the display parameters, and noise levels. The basalt termination defines the upper boundary of the LVZ (i.e., the base of the basalt), and although we endeavour to implement consistent picking, variation in the depth to the top of the LVZ of ~200 m may exist. While the velocity-thickness ambiguity is a major problem for the LVZ, some constraint on the velocity modelled can be gained from places where the LVZ deviates from horizontal towards the feather edge near the continent-ocean transition. The extrapolation of velocity results from beneath the thinner basalt further to the southeast (Spitzer et al., 2005) also provides some guidance to a suitable velocity within the LVZ. Although modelled P-wave velocities cover a wide range of interpretations the associated changes in thickness make little difference to the structural interpretation of the LVZ as a thin, laterally extensive unit.

When considering converted S-waves, not only is the uncertainty in travel-time picking larger than for P-waves due to the secondary nature of these arrivals and reduced signal to noise ratios, but additional variables are also involved in travel-time modelling, such as variability in the conversion interface. Effective conversion of P- to S-wave energy requires a sharp change in seismic velocity (occurring over a distance of less than half a seismic wavelength) while a rough interface, or the alteration or weathering of a paleo-surface can degrade conversion efficiency (White and Stephen, 1980). Along the portion of the profile we consider here, P- to S-wave conversion mainly occurs on the way down at the top of the sub-aerially extruded basalt sequence and energy thereafter propagates through the crust to the OBS as S-waves (PSS wave, Figure 2B). An earlier arriving converted S-wave phase is also identified, observable on Figure 2B at 1 s reduced time at an offset of 5 km: this phase (PSP) is associated with a second conversion, back to a P-wave, at the top basalt interface as the wave propagates upwards. Although conversion primarily occurs at the sediment-top basalt interface (either on the way up or down) the late Oligocene unconformity within the sedimentary section provides some potential for conversion, as observed from arrivals converted on reflection at this interface. Due to the increased travel-time caused by conversion at the seafloor or at an unconformity within the sedimentary section, these phases arrive after the top-basalt conversion and are difficult to distinguish from reverberations associated with the top-basalt converted S-wave phase.

Cycle skipping, in which the picked high amplitude peak is not the first onset of the arrival, has been identified as a problem for calculating the travel-times of converted S-waves. In the case of P-waves the velocity of the overburden (the sedimentary units which overlie the basalt), has been

independently and more accurately determined through semblance analysis of reflections on the 12 km long, single-sensor, multi-channel seismic data. In the converted S-wave case no such accurate constraint exists and uncertainty in picks due to cycle skipping of the PPS arrival may be incorporated into the modelled sediment velocity. Timing errors due to this, or cycle skipping within the PSS picking, are compensated by unrealistic velocities in the top of the basalt layer.

Commonly, crustal Vp/Vs ratios are determined from sparse converted S-wave data by forward modelling using a constant Vp/Vs ratio within each model layer or vertically bounded block within the layer (e.g. Raum *et al.*, 2005). A consequence of this approach is that S-wave velocity discontinuities are introduced at layer interfaces if differing Vp/Vs are modelled in the two layers, even if the underlying P-wave velocity gradient is continuous across the interface. Multiple conversion interfaces within a region are also commonly used to fit the travel-times of observed arrival phases. For the dataset described here, with over 35,500 arrivals that have been converted on the way down, forward modelling becomes unmanageable. Only the most obvious PSS S-wave arrivals, namely those converted while propagating downward, and travelling the remainder of the path as an S-wave giving an S-wave move-out velocity, were inverted. S-wave reflections from the Moho are used to constrain the structure of the lower crust and although these arrivals are common on oceanic crust, to the SE they appear over decreased offset ranges and finally disappear due to increased attenuation along the lengthening ray path to the Moho beneath the Fugloy Ridge continental block. Few converted S-waves penetrate deeply into the basement beneath the LVZ and hence the deeper structure in the centre and southeast of our profile (Figure 6) cannot be interpreted in terms of S-wave velocity or Vp/Vs ratio.

As travel-time inversions provide little constraint on the velocity within the LVZ and picking errors associated with the S-waves are larger than for P-waves the Vp/Vs ratio was assumed to be constant within the LVZ (i.e., any lateral lithological differences are below the level of resolution). During the global inversion the Vp/Vs ratio of the LVZ was set between 1.60 and 2.10 in increments of 0.05 and the inversion carried to completion for the underlying layers. The global results show a best fit overall for a model with a Vp/Vs ratio in the LVZ of 1.80 while the misfit of the refractions turning beneath the LVZ was minimised with a Vp/Vs ratio of 1.75. However, little statistical difference was found between models with a LVZ Vp/Vs of 1.70 to 1.90. The north-western feather edge of the LVZ was found to be most sensitive to variation in the Vp/Vs ratio of the LVZ. High Vp/Vs ratios of 1.90-1.95 were found to improve the ability of the ray tracing algorithm (Zelt and Smith, 1992) to propagate rays through this zone, although, as the problem of ray propagation was encountered for the P-wave modelling in this area, the feather edge of the LVZ remains the least robust area of the model. The variation of the Vp/Vs ratio in the LVZ during inversion explored the effect with fixed LVZ thickness however the full range and fits of possible S-wave models derived from the family of possible P-wave velocities in the LVZ and the associated optimum thicknesses have not been explored.

Ideally we would like a measure of the Vp/Vs ratio in the LVZ that is entirely independent of the global model. However this is not possible, as previously explained. As shown in Equation 1, to use the relative P- and S-wave step-backs several parameters must be extracted from the global model, including the P- and S-wave velocity ratios between the LVZ and the underlying basement and the position of the critical point for the basement refraction for both P- and S-waves. Although not algebraically separable, the allowable range of Vp/Vs solutions given modelled uncertainties in LVZ and sub-LVZ velocities was numerically calculated for a simplified model. This assumed step-back times were free of error and that P- and S-wave velocities in each unit would be linked i.e., increase or decrease together. The calculated uncertainty in Vp/Vs, and hence A, was 5% for a Vp/Vs ratio in the global model LVZ of 1.80. The value of bulk multiplier, A, did vary dependant on the Vp/Vs ratio of the LVZ as did the step-back times picked however the calculated Vp/Vs proved to be relatively stable. Limited lateral variation (3%) in the multiplier, A, calculated from the

global model is observed within the 180-200km interval. However this variation is found to be less than the calculated uncertainty in A and so A is assumed to be laterally constant.

Additional errors in the calculated low velocity zone Vp/Vs ratio are associated with measuring the step-back times themselves. Picking errors may be involved, particularly for the lower signal to noise ratio S-wave arrivals. However cycle skipping is unlikely to be a problem as generally only one combination of P- and S-wave picks yielded a geologically reasonable Vp/Vs value. One-dimensional synthetic modelling of a LVZ show that the actual source signature (centred on 9 Hz), as well as higher frequency content Ricker wavelets, could resolve the modelled Vp/Vs ratio exactly using noise-free synthetic seismograms generated using a 1D model as at 200 km profile distance with a Vp/Vs ratio in the LVZ of 1.80. The determination of the basement refraction critical point is reliant on the global model and although the velocity-thickness ambiguity in the LVZ should cause minimal variations in critical distance, the ratio of step-back times and hence Vp/Vs, is sensitive to variations associated, via the critical distance, with the velocity uncertainty assigned for the modelled thickness. The modelled basalt and sub-LVZ velocities, uncertainties of 100 m and 500 m in the critical distances for P- and S-waves lead to uncertainties in step-back times of 10 ms and 15 ms respectively. This effect, combined with picking uncertainty in the P-wave step-back of the order of 30 ms and S-wave step-backs of 50 ms, accounts for much of the observed scatter in the results. Combining errors leads to an estimated error of between 19-27% for the determination of the Vp/Vs ratio in the LVZ from individual OBS step-back times.

The population of Vp/Vs values between 180-200 km along the profile, determined from the ten OBS gives an average Vp/Vs ratio of the LVZ of 1.81±0.36 using a starting LVZ Vp/Vs ratio of 1.80. However, since systematic spatial heterogeneity within the low velocity zone was not resolvable, Vp/Vs is assumed to be constant and thus treating the calculated Vp/Vs values as sample estimates, the Vp/Vs sample population has a mean of 1.81±0.11 for a starting LVZ Vp/Vs ratio in the global model of 1.80 (Table 1).

The bulk properties of the LVZ determined by this analysis are plotted against relevant sedimentary rock and hyaloclastite measurements in Figure 8. Hyaloclastite values (grey dots) from the Lopra-1/1A well cluster into two populations representing large scale hyaloclastite units with and without interbedded basalt flows (Christie *et al*, 2006a), with averages shown by a black circle and square respectively. The Paleocene Lopra-1/1A hyaloclastite units are deeply buried at 2.4-3.5 km and have undergone significant compaction and lithification.

Laboratory and well studies (Eberhart-Phillips *et al*., 1989; Storvoll *et al*., 2005) indicate that for sandstone the most rapid increase in velocity with depth occurs with the initial mechanical compaction, after which a linear increase in velocity occurs with depth as chemical compaction occurs. For comparison of these well log measurements with wide-angle seismic analysis of the LVZ at ~5 km depth we have to consider the effect of further

OBS	Global Vp/Vs=1.80
56	1.87
55	1.88
54	1.63
53	1.79
50	1.85
49	1.97
48	1.67
47	1.92
46	1.70
44	1.83
Average	1.81
Standard Deviation	0.11

Table 1.: Vp/Vs results from the step-back analysis for the area of the LVZ from 180 km to 200 km profile distance. The starting model for the calculation of critical distances and the factor 'A' was the global inversion with the Vp/Vs ratio in the LVZ set to 1.80.

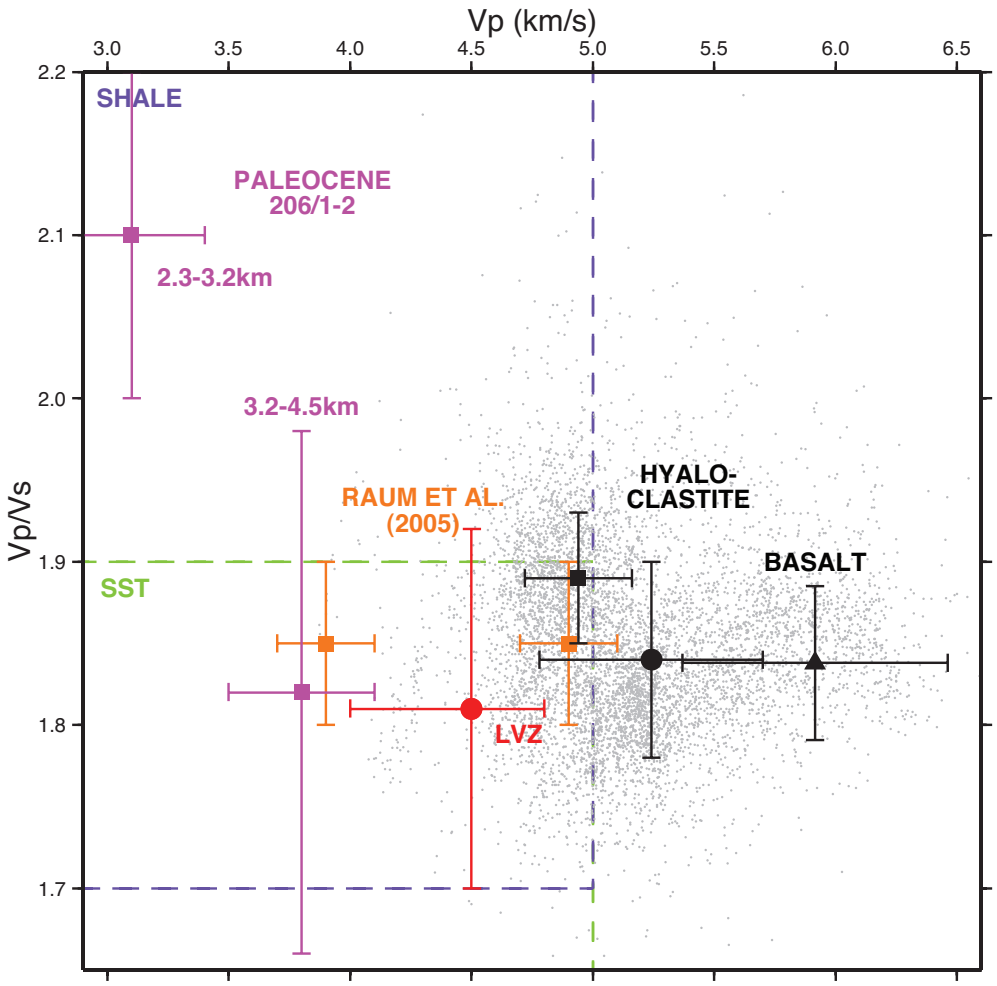

Figure 8. Vp versus Vp/Vs plot. The average result of detailed analysis of the LVZ with associated uncertainty is shown by the large red dot. Well log measurements of hyaloclastites from the Faroes Island Lopra-1/1A well are shown by grey dots; the black square represents the average Lopra-1/1A hyaloclastite without interbedded basalt flows and the black circle includes units with some interbedded flows (Christie *et al.*, 2006a) with one standard deviation error bars. The properties of basalt (at 200 MPa; Christensen, 1996) are plotted by a black triangle. Zones defining clean sandstone, limestone and shale (Domenico, 1984; Tatham, 1982; Tatham and McCormack, 1991) are shown in green, blue and purple respectively. The physical properties of the 206/1-2 well in 2.3-3.2 km and 3.2-4.5 km depth intervals are shown in pink, the Vp/Vs ratio has been calculated from the P-wave logs using Castagna's mudrock relation (Castagna *et al*., 1985). Also plotted are wide-angle seismic derived values for sub-basalt sedimentary rock in the Faroes region (Raum *et al*., 2005; orange squares), although the errors associated with these measurements are believed to be underestimated as they were not specifically assigned to address the velocity-depth ambiguity present in the LVZ.

burial on such samples already at high confining pressure in the Lopra-1/1A well. We surmise that we may see a continued increase in P-wave velocity due to reduced porosity while the Vp/Vs ratio is likely to remain approximately constant (Eberhart-Phillips *et al.,* 1989). Another factor to consider is the effect of frequency dispersion when comparing well log (sonic) velocities and lower frequency seismic velocities. For Lopra-1/1A basalts the sonic velocities were found to be only 3% higher than seismic velocities (Christie *et al.*, 2006a). Thus Lopra-1/1A measurements should provide a reasonably good proxy for what we would expect to see were the LVZ entirely composed of hyaloclastite.

The physical properties of Paleocene sedimentary units measured in the 206/1-2 well (see Figure 1 for location) from the south-eastern flank of the Faroe-Shetland Trough in two depth ranges have been plotted in Figure 8. Because only P-wave logs were measured in this well an S-wave log was constructed using Castagna's mudrock relation (Castagna *et al*., 1985). Hence the Vp/Vs ratios shown have not been directly measured. Within the Paleocene the P-wave velocity increases and Vp/Vs ratio decreases with increasing depth and compaction. The Faroe-Shetland Trough has been a deep water depocentre since the Cretaceous (Stoker *et al*, 1993) and the sediments within the 206/1-2 well are largely shale (which has a high Vp/Vs ratio, Figure 8). In the Kangerlussuaq Basin, East Greenland, coarser middle to late Paleocene shallow marine and fluvial sedimentary rocks are observed associated with significant thermal uplift of the region in response to arrival of the proto-Iceland mantle plume (Peate *et al.* 2003). Prior to rifting the Fugloy ridge would have been located less than 100 km from East Greenland (Peate *et al.* 2003) and hence the Fugloy Ridge could have experienced relatively shallow marine deposition as an extension of the coeval fluvial systems observed in Greenland.

Also plotted on Figure 8 are values from wide-angle seismic work for what has been interpreted to be sub-basalt sedimentary rock in the Faroes region (Raum *et al*., 2005); the errors assigned to these measurements are believed to be underestimated since the LVZ was assigned the same errors as elsewhere in the model and the effect of the velocity-depth ambiguity of the LVZ was neglected. Although a sub-basalt layer modelled by Raum *et al*. (2005), with a Vp of 4.9 km/s (orange square on Figure 8), plots within the expected values for hyaloclastite, this layer represents the deeper of two sub-basalt low velocity layers. The upper layer, with a Vp of 3.9 km/s (orange square) is far slower than would be expected for hyaloclastite. Were hyaloclastites to be present beneath the basalt they would have been deposited on top of any pre-existing sedimentary basin.

Due to its relatively low Vp/Vs ratio and slow P-wave velocity, the LVZ under the Fugloy Ridge is likely to represent at least some proportion of clastic sedimentary rock. Although calculated uncertainty bounds do overlap with hyaloclastites, particularly those with interbedded or intruded basalt, by comparison with data from the Lopra-1/1A well the mean properties of the LVZ lie within the slowest 4% of the interbedded units P-wave velocities and lowest 24% of the Vp/Vs ratios. Careful P-wave analysis using move-out to 12 km offset indicates the presence of sedimentary rock underlying hyaloclastites beneath thinner flood basalts of the Faroe-Shetland Trough (Spitzer *et al.,* 2005). The P-wave velocity of hyaloclastites modelled (~5.2 km/s) is higher than that measured for pure hyaloclastite in the Lopra-1/1A well (Figure 8) and is perhaps indicative of interbedded basalt flows and hyaloclastite (Figure 8) from the earliest eruptive phase. In the case of a lateral continuation of this model, the wide-angle analysis is may not be able to resolve the subtle difference between basalt or interbedded basalt and hyaloclastite, particularly if hyaloclastite is less voluminous than found in the Lopra-1/1A well, and hence some hyaloclastites may be incorporated into the basalt layer of the model.

The material underlying the LVZ was initially thought of as 'basement'. However the modelled Vp/Vs ratio of 1.80-1.88 is higher than would be expected for crystalline continental crust. For example, the upper crust of an averaged continental crustal model (Christensen and Mooney, 1995) exhibits an average Vp/Vs ratio of 1.74. Granite has a Vp/Vs of 1.71 while diorite has a Vp/Vs ratio of 1.77 (Christensen, 1996). Low P- and S-wave ve-

locities and high Vp/Vs ratio may be associated with a period of prolonged exposure of the Lewisian basement prior to the Paleocene that allowed significant weathering and mineral hydration to occur (as exposed in northern Scotland, Hall and Simmons 1979), while basaltic sill intrusion into the gneissic basement may also raise the observed Vp/Vs ratio. Rifting in the North Atlantic was a multi-phase process with initiation of rifting in the Devonian (Coward, 1995) and while localised Permo-Triassic sedimentary rocks of a pre-existing sedimentary basin have been mapped, widespread material of a Cretaceous age is more likely to be present. These well-consolidated sedimentary rocks could be the unit sampled by the converted S-waves as 'acoustic basement' beneath the low velocity zone. The Vp/Vs ratio is high for such deeply buried sediments and hence the sediment is likely to be Cretaceous shales or mudstones as observed in both the Faroe-Shetland Trough (Stoker et al. 1993) and in the Kangerlussuaq Basin, East Greenland (Peate et al. 2003). As the P-wave velocity of the sub-basalt material exceeds that expected for quartzo-feldspathic sedimentary rocks (up to 5 km/s, Figure 7), basaltic or doleritic intrusions, consistent with those seen within the Faroe-Shetland Trough (e.g., Smallwood and Maresh, 2002) are interpreted to occur within the basalt buried flank of the trough on the Fugloy Ridge and these intrusions would also help to raise the observed Vp/Vs ratio.

Conclusions

High-quality, wide-angle seismic data acquired with a low frequency seismic source have been recorded across the Faroes volcanic rifted continental margin, with energy penetrating beneath thick basalt sequences. Ocean bottom seismometers allowed converted S-wave data to be collected that was used to construct a S-wave velocity model and hence, when combined with a pre-existing P-wave model, to determine the crustal Vp/Vs ratio. Step-backs between basalt and basement refractions for both P- and S-waves are indicative of a sub-basalt velocity inversion or low velocity zone. A velocity-thickness ambiguity is inherent in the travel-time analysis of sub-basalt low velocity zones but the direct determination of the Vp/Vs ratio in these zones is robust and is not strongly dependent on the modelled thickness of the LVZ or the absolute P- or S-wave velocities. The calculated Vp/Vs ratio is consistent within the calculated uncertainty bounds to both interbedded hyaloclastites and basalt flows as observed in the Lopra-1/1A well on the Faroes Islands and Paleocene clastic sedimentary rock. However, the mean properties are more indicative of clastic sedimentary rock. Beneath the LVZ, intruded Permo-Triassic or Cretaceous sediments are likely to occur above the inferred continental basement. A sedimentary interpretation of the LVZ and sub-LVZ units is consistent with continuation of the sedimentary systems of the Cretaceous-Paleocene Faroe-Shetland Trough over the thinned continental crust of the present Fugloy Ridge prior to continental break-up in the late Paleocene.

Acknowledgements

The iSIMM project was supported by Liverpool and Cambridge Universities, Schlumberger Cambridge Research, Badley Geoscience Limited, WesternGeco, Amerada Hess, Anadarko, BP, ConocoPhillips, ENI UK, Statoil, Shell, the Natural Environment Research Council and the Department of Trade and Industry. However, the views expressed here are those of the authors who are solely responsible for any errors. Thank you to Richard Hobbs, University of Durham and an anonymous reviewer for their comments. Department of Earth Sciences, Cambridge contribution number ES.8683.

References

Aki, K. and Richards, P. 2002. Quantitative Seismology. Second Edition, University Science Books, Sausalito, CA.

Avedik, F., Hirn, A., Renard, V., Nicolich, R., Olivet, J.L. and Sachpazi, M. 1996. "Single-bubble" marine source offers new perspectives for lithospheric exploration. *Tectonophysics* 267: 57-71.

Bais G., White R. S., Worthington M. H., Andersen M. S. and Seifaba Group. Seismic properties of Faroe basalts from borehole and surface data. *In*: Varming and Ziska (eds) *Faroe Islands Exploration Conference: Proceedings of the 2nd Conference.,* Annales

Societatis Scientiarum Færoensis, (Faroese Society of Sciences and Humanities), Tórshavn, this issue.in press.

Barton, A.J. and White, R.S. 1997. Volcanism on the Rockall continental margin. *Journal of the Geological Society of London* 154: 531-536.

Castagna, J.P., Batzle, M.L. and Eastwood, R.L. 1985. Relationships between compressional-wave and shear-wave velocities in clastic silicate rocks. *Geophysics* 50: 571-581.

Christensen, N.I..1996. Poisson's ratio and crustal seismology. *Journal of Geophysical Research - Solid Earth* 101: 3139-3156.

Christensen, N.I. and Mooney, W.D. 1995. Seismic velocity structure and composition of the continental crust: A global view. *Journal of Geophysical Research - Solid Earth* 100: 9761-9788.

Christie, P., Gollifer, I. and Cowper, D. 2006a. Borehole Seismic Studies of a Volcanic Succession from the Lopra-1/1A Borehole in the Faroe Islands, NE Atlantic. *Geology of Denmark Survey* 9: 23-40.

Christie, P., Lunnon, Z.C., White, R.S., Kusznir, N., Roberts, A., Roberts, A.W., Parkin, C., Smith, L., Eccles, J., Healy, D., Hurst, N., Tymms, V., Chappell, A. and Fletcher, R. 2006b. iSIMM Experience with Peak- and Bubble Tuned Sources for Generating Low Frequencies. *EAGE 68th Conference and Exhibition. Vienna, Austria, 12-15 June 2006:* A034.

Coward, M.P. 1995. Structural and tectonic setting of the Permo-Triassic basins of northwest Europe. *In*: Boldy, S.A.R. (ed) *Permian and Triassic Rifting in Northwest Europe*. Geological Society, London, Special Publications 91: 7-39.

Domenico, S.N. 1984. Rock Lithology and porosity determination from shear and compressional wave velocity. *Geophysics* 49:1188-1195.

Eberhart-Phillips, D., Han, D-H. and Zoback, M. 1989. Empirical relationships among seismic velocity, effective pressure, porosity, and clay content in sandstone. *Geophysics* 54: 82-89.

Eldholm, O. and Grue, K. 1994. North Atlantic volcanic margins: Dimensions and production rates. *Journal of Geophysical Research* 99(B2): 2955-2968.

Ellis, D., Bell, B.R., Jolley, D.W. and O'Callaghan, M. 2003. The stratigraphy, environment of eruption and age of the Faroes Lava Group, NE Atlantic Ocean. *In*: Jolley, D.W. and Bell, B.R. (eds.) *The North Atlantic Igneous Province: Stratigraphy, Tectonic, Volcanic and magmatic Processes*. Geological Society Special Publications 197: 253-269.

Fliedner, M.M. and White, R.S. 2001. Seismic structure of basalt flows from surface seismic data, borehole measurements, and synthetic seismogram modelling. *Geophysics* 66: 1925-1936.

Geopro., 2007. www.geopro.com

Hall, J. and Simmons, G. 1979 Seismic velocities of Lewisian metamorphic rocks at pressures to 8 >kbar: relationship to crustal layering in North Britain. *Geophysical Journal of the Royal Astronomical Society* 58: 337-347.

Kragh, E. and Peardon, L. 1995. Ground roll and polarisation. *First Break* 13: 369-378.

Loizou, N. 2005. West of Shetland exploration unravelled - an indication of what the future may hold. *First Break* 23: 53-59.

Lunnon, Z.C., Christie, P.A.F. and White, R.S. 2003. An evaluation of peak and bubble tuning in sub-basalt seismology: modelling and results from OBS data. *First Break* 21: 51-56.

Maresh, J. and White, R. S. 2005. Seeing through a glass, darkly: strategies for imaging through basalt. *First Break* 23: 27_32.

Maresh, J., White, R. S. Hobbs, R.W. and Smallwood, J.R. 2006. Seismic attenuation of Atlantic margin basalts: observations and modeling *Geophysics 71*: 211-221.

Martin, J., Ozbek, A., Combee, L., Lunde, N., Bittleston, S. and Kragh, E. 2000. Acquisition of marine point receiver seismic data with a towed streamer. *70th Annual International Meeting, Society of Exploration Geophysicists*, 37-40.

Martini, F. and Bean, C.J. 2002. Application of pre-stack wave equation datuming to remove interface scattering in sub-basalt imaging. *First Break* 20: 395-403.

Minshull, T.A. 2002. Seismic Structure of the oceanic Crust and Passive Continental Margins. *In International Handbook of Earthquake and Engineering Seismology* 81A: 1-14.

Peate, I.U., Larsen, M. and Lesher, C.E. 2003. The transition from sedimentation to flood volcanism in the Kangerlussuaq Basin, East Greenland: basaltic pyroclastic volcanism during initial Palaeogene continental break-up. *Journal of the Geological Society*, London 160: 759-772.

Planke, S. and Cambray, H. 1998. Seismic properties of flood basalts from Hole 917A downhole data, Southeast Greenland volcanic margin. *In*: Saunders, A.D., Larsen, H.C. and Wise, S.W. (eds) *Proceedings of the Ocean Drilling Program, Scientific Results* 152: 453-462.

Raum, T., Mjelde, R., Berge, A.M., Paulsen, J.T., Digranes, P., Shimamura, H., Shibara, H., Kodaira, S., Larsen, V.B., Fredsted, R., Harrison, D.J., and Johnson, M. 2005. Sub-basalt structures east of the Faroe Islands revealed from wide-angle seismic and gravity data. *Petroleum Geoscience* 11: 291-308.

Roberts, A.W. 2006. *Crustal Structure of the Faroes North Atlantic Margin from Wide-Angle Seismic Data*. PhD Dissertation, University of Cambridge.

Rutledge, J.T. and Winkler, H.. 1989. Attenuation measurements from vertical seismic profile data: Leg 104, site 462. *In*: Eldholm, O., Thiede, J. and Taylor, E. (eds) *Proceedings of the Ocean Drilling Program, Scientific Results* 104: 965-972.

Samson, C., Barton, P.J, and Karwatowski, J. 1995. Imaging beneath an opaque basaltic layer using densely sampled wide-angle OBS data. *Geophysical Prospecting* 43: 509-527.

Shaw, F., Worthington, M. H., White, R. S., Andersen, M. S., Petersen, U. K. and the SeiFaba Group. 2008. Seismic attenuation in Faroe Islands Basalts. *Geophysical Prospecting* 56: 5-20.

Sirgue, L. and Pratt, G. 2004. Efficient waveform inversion and imaging: A strategy for selecting temporal frequencies. *Geophysics* 69: 231-248.

Smallwood and Maresh, J. 2002, The properties, morphology and distribution of igneous sills: modelling, borehole data and 3D seismic from the Faroe-Shetland area. *In*: Jolley, D.W. and Bell, B.R. (eds) T*he North Atlantic Igneous Province: Stratigraphy, Tectonic, Volcanic and Magmatic Processes.* Geological Society Special Publications 197: 271-306.

Smallwood, J. R., White, R. S. and Staples, R. K. 1998. Deep crustal reflectors under Reydarfjördur, eastern Iceland: Crustal accretion above the Iceland mantle plume. *Geophysical Journal International* 134: 277-290.

Spitzer, R., White, R.S. and iSIMM Team. 2005. Advances in seismic imaging through basalts: a case study from the Faroe-Shetland Basin. *Petroleum Geosciences* 11: 147-156

Stoker, M.S., Hitchen, K. and Graham, C.C. 1993 The geology of the Hebrides and West Shetland shelves, and adjacent deep-water areas. British Geological Survey United Kingdom Offshore Regional Report.

Storvoll, V., Bjørlykke, K. and Mondol, N.H. 2005. Velocity-depth trend in Mesozoic and Cenozoic sediments from the Norwegian Shelf. *AAPG Bulletin* 89: 359-381.

Tatham, R.H. 1982. Vp/Vs and lithology. *Geophysics* 47: 336-344.

Tatham, R.H. and McCormack, M.D. 1991. Rock Physics Measurements. *In Multicomponent Seismology in Petroleum Exploration.* Investigations in Geophysics No. 6. SEG: 43-91.

Waagstein, R. 1988. Structure, composition and age of the Faeroe basalt plateau. *In*: Morton, A.C. and Parson, L.M. (eds.) *Early Tertiary volcanism and the opening of the NW Atlantic.* Geological Society Special Publication 39: 225-238.

White, R.S. and Stephen, R.A. 1980. Compressional to shear wave conversion in oceanic crust. *Geophysical Journal of the Royal Astronomical Society* 63: 547-565.

White, R. and McKenzie, D. 1989. Magmatism at Rift Zones: Generation of Volcanic Continental Margins and Flood Basalts. *Journal of Geophysical Research - Solid Earth* 94: 7685-7729.

White, R.S., Christie, P.A.F., Kusznir, N.J., Roberts, A., Davies, A., Hurst, N., Lunnon, Z., Parkin, C.J., Roberts, A.W., Smith, L.K., Spitzer, R., Surendra, A. and Tymms, V. 2002. iSIMM pushes frontiers of marine seismic acquisition. *First Break* 20: 782-786.

White, R. S., Spitzer, R., Christie, P. A. F., Roberts, A., Lunnon, Z., Maresh, J. and iSIMM Working Group. 2005. >Seismic imaging through basalt flows on the Faroes Shelf. In Ziska, H., Varming, T. & and Blotch, D. (eds.). *Faroe Islands Exploration Conference: Proceedings of the 1st Conference, Annales Societatis Scientiarum Færoensis (Faroese Society of Sciences and Humanities),* Supplementum 43: 11_31.

Zelt, C.A. and Smith, R.B. 1992. Seismic traveltime inversion for 2D crustal velocity structure. *Geophysical Journal International* 108: 16-34.

Zelt, C.A. and Barton, P.J. 1998. Three-dimensional seismic refraction tomography; a comparison of two methods applied to data from the Faeroe Basin. *Journal of Geophysical Research - Solid Earth* 103:7187-7210.

Ziolkowski, A., Hanssen, P., Gatliff, R., Jakubowicz, H., Dobson, A., Hampson, G., Li, X. and Liu, E. 2003. Use of low frequencies for sub-basalt imaging. *Geophysical Prospecting* 51: 169-182.

Imaging Below Faroese Basalts Using Over/under Acquisition

MARGARET LEATHARD[1*], STEPHEN MCHUGO[1] AND RUPERT HOARE[2]

[1] Schlumberger House, Buckingham Gate, Gatwick Airport, West Sussex, RH6 0NZ, UK
* Email: margaret.leathard@slb.com; Tel: +44 (0)1293 556158; Fax: +44 (0)1293 557151
[2] WesternGeco, Schlumberger Completions, Units 18-22, Kirkton Avenue, Pitmedden Road Industrial Estate, Dyce, Aberdeen, AB21 0BF, UK

ABSTRACT

Imaging through basalt is a well-known problem that has proven difficult to solve. Potential hydrocarbon reservoirs lying beneath basalt are a target for exploration. Stacked basalt flows in the offshore Faroes area consist of many thin layers, and the reflection and transmission of energy within each of these layers leads to the loss of high-frequency information. Therefore, it is crucial that the input signal contain as much low-frequency energy as possible in order to penetrate beneath the basalt.

Conventional deep-tow seismic data has been acquired in the Faroes area, but was largely unsuccessful at imaging the fault blocks beneath the basalt. A multi-cable/source acquisition technique, known as over/under was designed to boost the low frequencies to improve reflection energy below basalt.

In 2005, approximately 3,500 km of 2D over/under data were acquired in the West of Shetlands and Faroes region. The acquisition, processing and subsequent inversion of this data show that the over/under dataset produces a more reliable and interpretable seismic image.

Introduction

In order to image beneath stacked basalt flows, low frequencies are required. This is due to the weathering of each of the basalt layers, which causes low velocities and densities at the flow boundaries. The scattering at these sharp boundaries causes the loss of high frequency information. Conventional deep source/deep cable techniques have been tried in this area with limited success (Hoare *et* al., 2004). Over/under seismic acquisition and processing has been designed to increase the input low frequency energy whilst maintaining a broad-band signal by filling in the ghost notches in the amplitude spectrum. The effect of the ghosts on conventional acquisition and the benefits of the reduction of these notches in over/under acquisition are discussed in detail by Davies *et al*. (2006).

Acquisition

Conventionally, in order to enhance the low frequencies needed to image below basalt, seismic data has been acquired with a deep source/deep cable and long offset configuration (Hoare *et al*., 2004). This has the advantage of enhancing low frequencies and increasing the signal-to-noise ratio. However, the trade-off to this technique is the lack of high frequency data and the effect this has on the resolution of shallow events due to the ghost notch.

To maximize the advantages of both shallow tow and deep tow seismic acquisition, a technique known as over/under acquisition is deployed. Over/under seismic acquisition consists of towing paired sources and paired cables, keeping the cables vertically above each other. The depths of the sources and cables are deeper than that usually used for conventional acquisition and the over and under cables must remain vertically aligned for the duration of the acquisition, in order for the subse-

Faroe Islands Exploration Conference: Proceedings of the 2nd Conference.
Annales Societatis Scientiarum Færoensis, Supplementum 50, 2009: 61-66

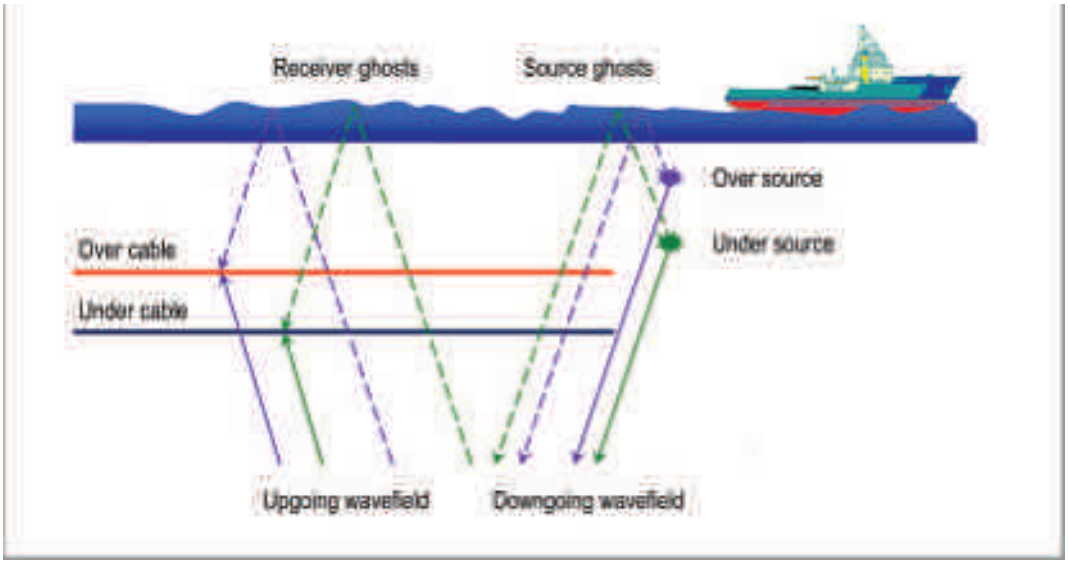

Figure 1. Acquisition configuration of source and streamer arrangement. Over source and under source are at depths of 12.5 m and 20 m, respectively. Over and under cables are at depths of 20 m and 30 m, respectively.

quent up and down-going wavefield separation to work.

In 2005 over 3,500 km of over/under seismic data was acquired in a region east of the Faroe Islands and west of the Shetland Islands. Figure 1 shows the acquisition configuration of the over/under source/streamer arrangement. The over and under cables are at 20 m and 30 m depth, respectively and the over and under sources are at 12.5 m and 20 m, respectively. The shot-point interval is 25 m, with the sources firing alternately, and the single sensor separation is 3.125 m.

Processing

The bandwidth of offshore seismic data is restricted by notches in its amplitude spectrum caused by the interference of source and receiver ghosts. The source ghost occurs due to energy from the source radiating upward and reflecting from the sea surface. Equally, energy traveling upward, which has been reflected from the subsurface, also reflects down from the sea surface, is recorded and is known as the receiver ghost. Both the source and receiver ghosts have the opposite polarity to the up-going wavefield. During over/under processing, the wavefield is separated into its up-going and down-going components with the up-going containing the primary wavefield and the down-going containing the ghosts. The up-going wavefield is free from notches in its amplitude spectrum, thus giving it a flatter bandwidth and lower frequencies than the conventional comparison. The Posthumus (1993) technique was used for the source and receiver combination, in this case. This combined dataset has the advantage of high frequencies due to the shallow source and streamer combination and low frequencies due to the deep source and streamer.

The key processing steps are outlined below,

1. Input the field data records at a 3.125 m group interval

2. Data regularization
   Align the receivers in the over cable with the receivers in the under cable.

3. Over source and over/ under cable combination
   The over source ghost remains in dataset, but the directional cable ghost is completely removed.

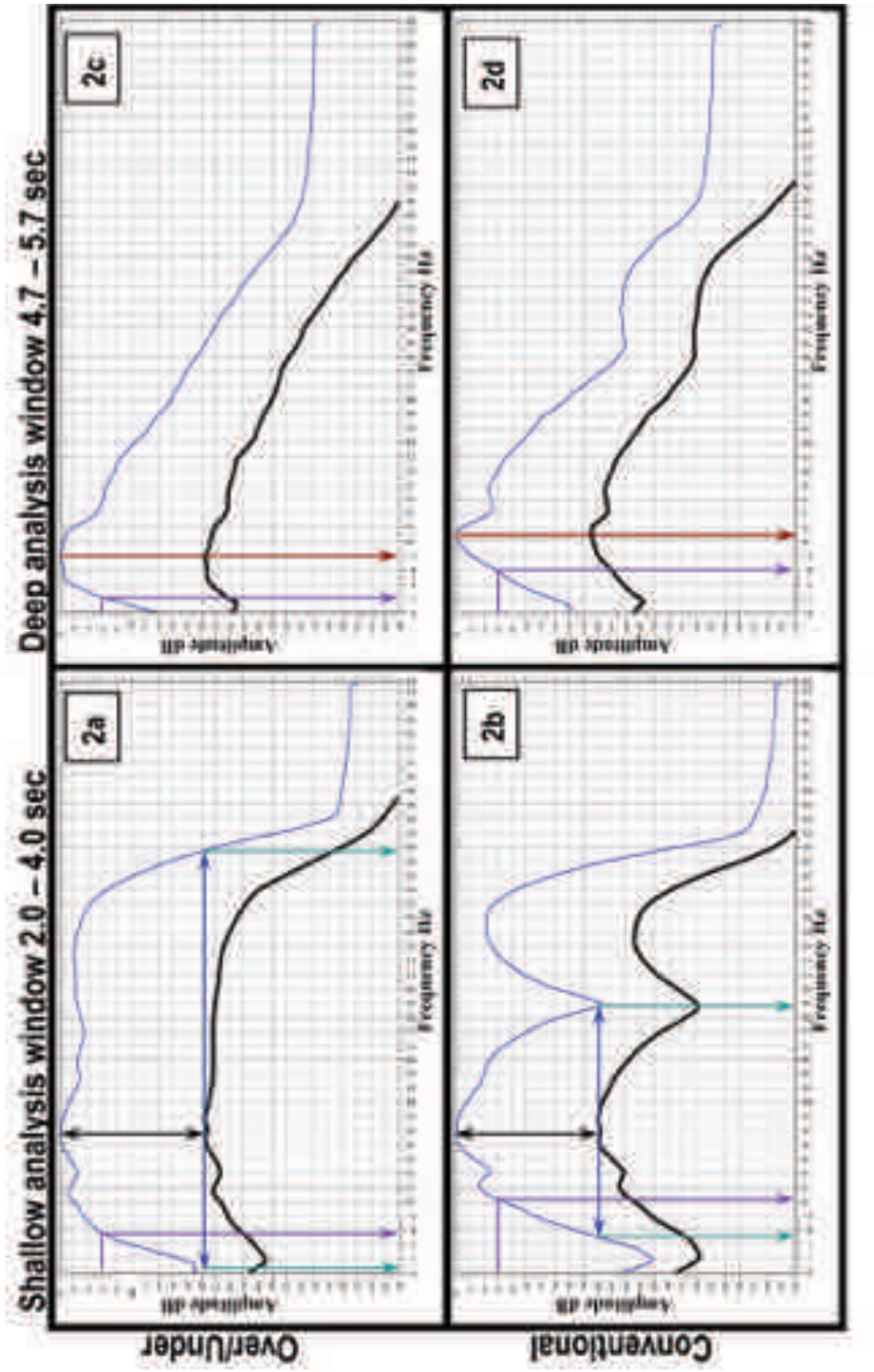

Figure 2. Amplitude spectra for over/under and conventional data. The blue curve is the signal and the black curve is the noise estimate. In the shallow window, useable bandwidth of over/under data is 1 to 60 Hz compared to 5 to 37 Hz for conventional data. For the deeper window, peak frequency is 8 Hz for over/under and 11 Hz for conventional. At -6 dB, frequency is 2 Hz for over/under and 8 Hz for conventional.

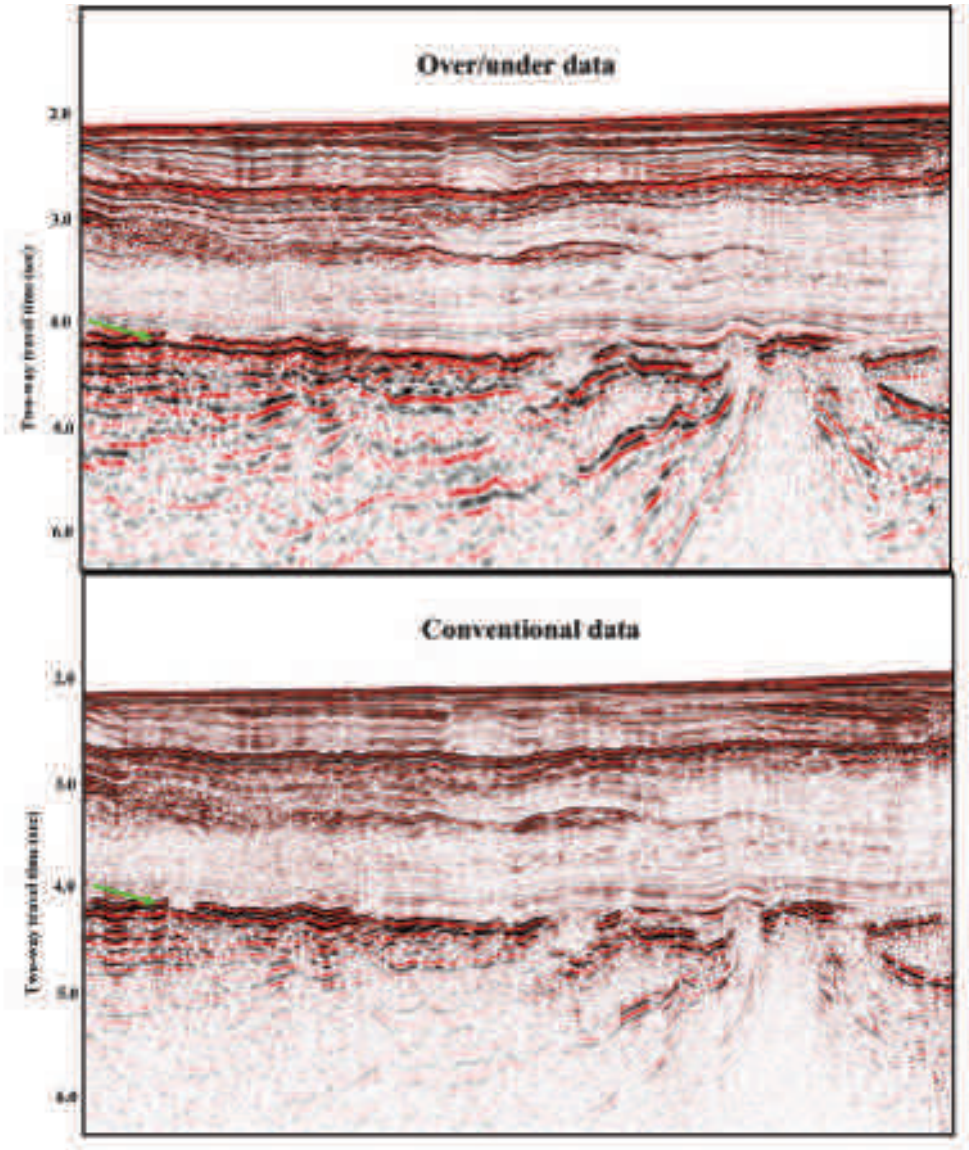

Figure 3. Over/under contains more low frequencies at depth, whilst not losing shallow resolution. Top basalt is indicated by green arrow. Beneath basalt, more reflection events give a clearer image of the potential hydro-carbon bearing zones.

4. Under source, over/ under cable combination
   The under source ghost remains in this dataset, but the directional cable ghost is completely removed.

5. Shot interpolation to increase the sampling in the common receiver domain. The data is then sorted to the common receiver domain.

6. Over/ under combination of over source and under source
   The data from Steps 3 and 4 are now combined, resulting in the complete removal of the directional source ghost.

7. After the over/ under combinations are complete, both the source and receiver ghosts have been removed. The data processing sequence then follows a more conventional route, but parameterized in such a way as to maximize the benefits of the enhanced bandwidth delivered in the over/ under combination steps.

The data processing sequence is also designed to preserve relative amplitudes, thus making the data suitable for further amplitude inversion work.

Data Examples

In order to fully evaluate the effectiveness of the over/under data, several comparison datasets were made. Two of these comparisons are shown here. The first comparison was chosen to simulate conventional deep-tow acquisition in this area. Data was taken from the over cable and over source and processed using the same sequence as the over/under data. This will be referred to as conventional data. The conventional data has source and receiver depths of 12.5 m and 20 m, respectively. This was compared to the full over/under combination which consists of all sources recorded into all cables. This will be referred to as over/under data. For other combinations, see Davies *et al*. (2006).

Figure 2 shows amplitude spectra for the over/under and conventional data. The spectra on the left are for a shallow window from 2.0 - 4.0 s and on the right are spectra from a deeper window, 4.7 - 5.7 s. The blue curve is the signal and the black curve is the noise estimate. It can be seen that for the shallow window, the useable bandwidth of the over/under data is 1 to 60 Hz compared to 5 to 37 Hz for the conventional data. For the deeper window, the signal peak frequency is 8 Hz and the frequency at -6 dB is 2 Hz for over/under, whereas the signal peak frequency is 11 Hz and the frequency at -6 dB is 8 Hz for the conventional.

Figure 3 illustrates the imaging benefits of over/under data. The top image is the over/under data and the bottom image is conventional data. The over/under dataset is far richer in lower frequencies and beneath the basalt, at approximately 4 s, there are more interpretable reflections which give a clearer image of the potential hydro-carbon bearing zones. It is important to note that the resolution in the shallow section has not been compromised on the over/under data.

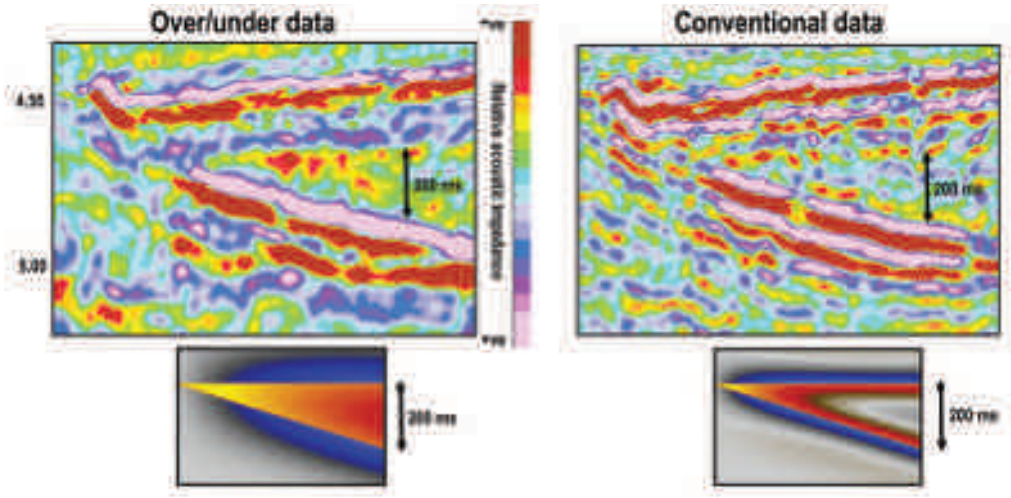

Figure 4. Inverted wedge models and RAI (relative acoustic impedance) from the inverted seismic data. The over/under RAI shows the true thickness of wedge, which is not interpretable from conventional RAI. The over/under and conventional wedge models confirm this. The conventional wedge model shows false layers within the wedge.

Amplitude Inversion

Low-frequency information (i.e., 0-6 Hz) is crucial for reliable, quantitative seismic inversion to rock parameters. However, we rarely acquire and preserve seismic signal frequencies less than 5 to 6 Hz during conventional seismic acquisition and processing. This lack of low-frequency information is known to cause uncertainty during inversion, particularly when computing absolute parameters (e.g., acoustic impedance). To account for this deficiency in the seismic data we usually add the missing low-frequency information through use of a low-frequency model built from sparsely (spatially) sampled well data. However, opinion is divided on the reliability of this approach because it can introduce both uncertainty and errors due to the sparseness of the data used to build the background low-frequency model. Therefore, recording and preserving low frequencies in the seismic data will improve confidence and usefulness of the inverted result. Over/under seismic technology provides the broader bandwidth and improved signal-to-noise ratio required to improve amplitude inversion.

In order to assess the effectiveness of the over/under data for amplitude inversion, wedge modeling was performed prior to inverting the two datasets. A model was constructed consisting of a sand wedge surrounded by shale. Two synthetic datasets were created using wavelets with a low-cut of 2 Hz and with a low-cut of 5 Hz, corresponding to over/under and conventional data frequency ranges. These models were inverted to relative acoustic impedance (RAI) and the results are shown in Figure 4 along with a small part of the actual inverted seismic also showing a wedge feature. The conventional wedge model inversion shows evidence of high frequency layers within the wedge which are not present on the over/under wedge model inversion. These false layers are artifacts caused by the lack of low frequencies and have the effect of making the inversion appear higher frequency. The splitting the relatively thick uniform bodies can lead to an incorrect interpretation. This can be seen, in practice, by examining the inversions of the seismic data. The over/under inversion, on the right, accurately reflects the true thickness of the wedge, whereas the conventional seismic data inversion is harder to interpret. This has significant implication in geo-body volume estimation.

Conclusions

Over/under technology has proven superior to conventional acquisition in scenarios where broader bandwidth, lower frequency content and higher signal-to-noise are required. Stacked basalt flows in the offshore Faroes absorb high frequencies leading to imaging problems beneath them and thus benefit from the increased low frequencies. These extra low frequencies give added benefit to amplitude inversion. Thick sand bodies are better resolved and uncertainty in the inversion is decreased. This leads to more confidence in amplitude inversion as an exploration tool.

Acknowledgements

The authors would like to thank David Hill, Robert Godfrey, Hüseyin Özdemir, Alex Cooke, John Sansom and Neil Woods for their contribution to this paper.

References

Davies K., Hampson G., Reilly A., Swanston A. 2006. Sub-basalt Imaging Using Over Under Sources and Receivers. *Petr. Soc. Great Britain Mtg., PETEX 2006, London.* Extended Abstracts

Hoare R., Schearer P., Langridge A., Saragoussi E. and Christie P. 2004. Imaging sub-basalt with deep towed streamer: A case study from the Faroe Islands. *In*: Ziska, H., Varming, T. and Bloch, D. (eds) *Faroe Islands Exploration Conference: Proceedings of the 1st Conference*. Annales Societatis Scientiarum Færoensis, Tórshavn, Supplementum 43: 168-175.

Posthumus, B.J. 1993. De-ghosting Using A Twin Cable Configuration. *Geophysical Prospecting*, 41, 267-286.

Seismic properties of Faroe basalts from borehole and surface data

GIOVANNI BAIS[1], ROBERT S. WHITE [1*], MICHAEL H. WORTHINGTON [2], MORTEN S. ANDERSEN.[3,4] AND THE SEIFABA GROUP[5]

[1] Department of Earth Sciences, Bullard Laboratories, Madingley Rd., Cambridge, CB3 OEZ, UK
* Email: rsw1@cam.ac.uk; Tel: +44 1223 337187; Fax: +44 1223 360779
[2] Department of Earth Sciences, Oxford University, Parks Road, Oxford, OX1 3PR, UK
[3] Geological Survey of Denmark and Greenland, Østervold Gade 10, Copenhagen DK-1350, Denmark
[4] Faculty of Science and Technology, Nóatún 3, Box 2109, FO-165, Faroe Islands
[5] See Acknowledgements for full list of members

ABSTRACT

The seismic velocities, anisotropy and reflectivity of layered basalts in the Faroe Islands were studied using borehole data and vertical seismic profiles from the Vestmanna borehole, combined with reflection and wide-angle seismic data recorded by arrays of both borehole and land multicomponent receivers. The correlation of in-situ downhole ultrasonic-scale velocity and density measurements, borehole logs and core samples with the seismic-scale velocities and reflection data allows us to build a model of the seismic properties across a range of scales. The match of observed travel-times of wide-angle P-wave data into borehole and surface seismometers with those predicted from the borehole sonic measurements suggests that the basalts are homogenous over horizontal distances on the kilometre scale. We find that any P-wave transverse anisotropy in the basalts is less than 5%, and probably lower than half that. A pronounced intra-basalt reflector visible on the surface seismometer data is likely to be caused by thick flows near the top of the Beinisvørð Formation, but is not precisely at the geological boundary between the Malinstindur Formation and the Beinisvørð Formation. Using full-waveform synthetic seismogram models, we demonstrate that strong intra-basalt reflections are likely to be caused by interference of the seismic signal with the layered sequence rather than necessarily representing specific stratigraphic or lithological boundaries.

Introduction

In this paper, we analyse borehole and surface seismic data acquired in 2004 around the Vestmanna-1 borehole as part of the SeiFaBa project to obtain detailed data about the seismic velocity, anisotropy and reflection character of extrusive basalts from the Faroe Islands in the North Atlantic (Japsen *et al*., 2005). Imaging through the basalt cover in the Faroe-Shetland Basin presents a challenge for conventional seismic surveys, but better knowledge of the basalt properties allows acquisition strategies to be designed to optimise signal penetration.

A typical succession of lava flows in the Faroes is characterized by many sub-horizontal layers (Waagstein, 1988; Passey and Bell, 2007). The tops and bases of the lava flows produce sharp impedance contrasts (e.g., Planke, 1994). O'Doherty and Anstey (1971) showed that reverberations within well-layered sequences cause low-pass filtering of seismic energy. This low-pass filtering effect is also produced by well-layered basalts (Pujol and Smithson, 1991; Mack, 1997; Maresh and White, 2005), and at seismic frequencies the layering produces interference effects from the numerous thin basalt layers (e.g., Planke and Eldholm, 1994; Smallwood *et al.*, 1998). This makes it difficult to locate precisely the depth of any particular intra-basalt reflection.

Seismic properties of basalt have been reported

Faroe Islands Exploration Conference: Proceedings of the 2nd Conference.
Annales Societatis Scientiarum Færoensis, Supplementum 50, 2009: 67-83

from a number of studies: attenuation and scattering studies have been made by, among others, Pujol and Smithson (1991), Martini and Bean (2002), Maresh and White (2005), Maresh *et al.* (2006) and Christie *et al.* (2006). Shaw *et al.* (2008) demonstrated severe effective seismic attenuation in the succession penetrated by the Vestmanna borehole with effective quality factors, Q_{eff} as low as 20 derived from the VSP data.

Petersen *et al.* (2006) argue for a seismic processing approach driven by well data, demonstrating that signal attenuation and scattering as well as the reflection character of basalt sequences can be related to lava morphology as sampled by borehole logs. Fliedner and White (2001) and Spitzer *et al.* (2005) developed and tested seismic imaging techniques for sub-basalt exploration and showed that a source rich in low frequencies and recorded to large offsets improves sub-basalt imaging in the Faroe Region. Pre-stack depth migration, including an anisotropy correction, is suggested as a method to collapse scattered energy (Silva and Cocoran, 2002). In a review of seismic imaging below the Deccan basalts in the Kutch Basin it was proposed that model-driven imaging using low frequency sources, accurate velocity data (including anisotropy if possible), multiple attenuation, pre-stack depth migration and inverse Q-filtering should be used to improve the seismic image below the basalt succession (Kumar *et al.*, 2004).

There are few existing published measurements of seismic anisotropy in layered basalts, even though their extensive lateral nature means that some VTI anisotropy might be expected. Reported measurements mainly compare the average vertical velocity from a VSP or sonic measurements with the average sub-horizontal velocity from refraction experiments. The two reported values from Tertiary basalts in the North Atlantic give conflicting results. Planke and Eldholm (1994) found average vertical velocities from a VSP and sonic measurements that are some 10-20% lower than refraction velocities from a nearby (though not coincident) seismic refraction profile, which they explain by sub-horizontal refractions travelling faster through the high-velocity cores of laterally continuous thick basalt flows than do the vertical reflections sampled by the VSP. On the other hand, Kiørboe and Petersen (1995) report the average vertical velocity from the upper 800 m of the Lopra-1 well through basalts in the Faroes as being about 10% higher than the sub-horizontal propagation velocity from surface recordings, which they attribute to the presence of sub-vertical cooling cracks and joints.

Layering induced VTI anisotropy around the Lopra-1 borehole was estimated using Backus upscaling of dipole sonic and bulk density logs acquired during deepening of the borehole in 1996. Thomsen's (1986) anisotropy parameters were estimated as: $0 < \varepsilon < 0.05$ and $\delta \approx 0$ (Christie *et al.* 2006). Only weak azimuthal anisotropy was reported by Christie *et al.* (2006). It is difficult to reconcile the observations made by Christie *et al.* (2006) with those by Kiørboe and Petersen (1995). It could be argued that the volumes sampled by the sonic log are too small to be affected by columnar jointing in the lava cores. However, Kiørboe and Petersen's (1995) refraction profile was un-reversed and was shot in a down-dip direction without additional structural control. Furthermore, Kiørboe and Petersen (1995) may have overestimated vertical seismic velocities in the upper part of the well, as seismic waves may have propagated along sub-vertical dolerite intrusions found in the well at 600 and 800 m depth. It thus remains possible that the apparent difference between their measured refraction velocities and those from the Lopra VSP is an artefact.

In this study we use log data, VSP and surface seismic data to investigate seismic VTI anisotropy in the Vestmanna area. We then analyse the reflection character of normal moveout corrected surface seismic data using shots fired offshore in the fjord as well as at the site of the onshore Vestmanna borehole, and investigate the cause of the reflectivity using synthetic seismogram modelling. Finally, we calculate the average Poisson's ratio of the basalt sequence using converted S-wave arrivals recorded by a 3-component seismometer in the borehole.

Geological setting

Extrusive igneous rocks dominate the northwestern flank of the Faroe-Shetland Basin and the

Faroe Shelf, at the edge of which are the Faroe Islands. Flood basalts created at the time of break-up between the Faroe Islands and east Greenland extend over 250,000 km^2 (Andersen 1988; Waagstein 1988; Larsen *et al.* 1999), at least 40,000 km^2 of which lie in the Faroe-Shetland Basin (Naylor *et al.,* 1999). The basalt formations on the Faroe Islands can be correlated with units on East Greenland, with both lava morphology and geochemistry being the same throughout each pair of correlative units (Larsen *et al.*, 1999). The extrusive basalts attain a thickness of more than 7 km on the Faroe Islands themselves, and extend some 150 km eastwards from the islands to feather out in the Faroe-Shetland Trough (Richardson *et al.*, 1999). The extrusive basalt thickness and distribution in the Faroes area has been reported by White *et al.* (2003) and Sørensen (2003). The volcanic rocks in the Faroes region are part of a much larger igneous province with up to 10 million km^3 of igneous rock extending from the northern tip of Norway to the southern part of Rockall Plateau on the eastern side of the North Atlantic, and down the east coast of Greenland on the conjugate margin (White and McKenzie, 1989; Eldholm and Grue, 1994).

In and around the Faroe Islands the basalts are mainly parallel and sub-horizontally layered (e.g., Rasmussen and Noe-Nygaard, 1970; Andersen, 1988). The basalts were originally divided into three series separated by distinct marker horizons (Rasmussen and Noe-Nygaard, 1970): the Lower basalt series, Middle basalt series and Upper basalt series. In more recent literature Rasmussen and Noe-Nygaard's (1970) basalt series have been treated as formations (Waagstein, 1988), and the stratigraphy has been further revised (Passey and Bell, 2007). In this paper, we will only consider the formations present in the Vestmanna borehole.

The Beinisvørð Formation (BF) is ca. 3300 m thick, and corresponds to the lower basalt formation. It is composed of around 20 m thick laterally extensive sheet flows, typically separated by intercalated thin volcaniclastic units (Rasmussen and Noe-Nygaard, 1970; Waagstein, 1988; Passey and Bell, 2007). Seismic experiments by Kiørboe and Petersen (1995) and by Christie *et al.* (2006) were carried out in and around the Lopra-1 borehole which penetrates the lower ca. 2400 m of the Beinisvørð Formation. The most northerly occurrence of the Beinisvørð Formation is in the Vestmanna borehole, where the formation comprises five aphyric and sparsely plagioclase-phyric basalt layers (6-37 m thick) intercalated by 2-4 m thick shaley sediment layers, 100 m thick in total (Waagstein and Hald, 1984).

The Beinisvørð Formation is overlain by the 3-15 m thick Prestfjall Formation (PF) which consists mainly of shales and coals on Suðuroy. The Prestfjall Formation thins and changes character to the north (Rasmussen and Noe-Nygaard, 1970). The northernmost known occurrence of the Prestfjall Formation is in the Vestmanna borehole, where it comprises a ~ 2.5 m thick shale with a thin basal conglomerate (Waagstein and Hald, 1984). In the Vestmanna borehole the Prestfjall Formation is overlain by the ~ 1350 m thick Malinstindur Formation (MF), which consists of numerous 0.5-4 m thick lava lobes and occasional infilled lava-tubes (Rasmussen and Noe-Nygaard, 1970; Waagstein and Hald, 1984; Passey and Bell, 2007). This corresponds to the Middle basalt formation. Individual flow lobes in the Malinstindur Formation can be grouped into laterally continuous compound flows averaging ca. 20 m in thickness based on their petrography, chemistry and the occurrence of interflow sediments or oxidised flow tops (Rasmussen and Noe-Nygaard, 1970; Waagstein, 1988; Passey and Bell, 2007). Overall they have the characteristics of Jerram's (2002) compound-braided facies architecture (Passey and Bell, 2007). The lowermost 555 m of the Malinstindur Formation is sampled in the Vestmanna borehole.

Data acquisition

The seismic experiments in the harbour adjacent to the Vestmanna borehole (Fig. 1) were carried out with a clamped 3-component geophone in the borehole and a 395 m long, 120-channel geophone string with vertical and 3-component seismometers deployed on outcropping basalts, every fourth position being a 3-component geophone with vertical component geophones only in the intervening 3 locations. The borehole receiver was a custom-made I/O 3-component sensor containing SM-7M

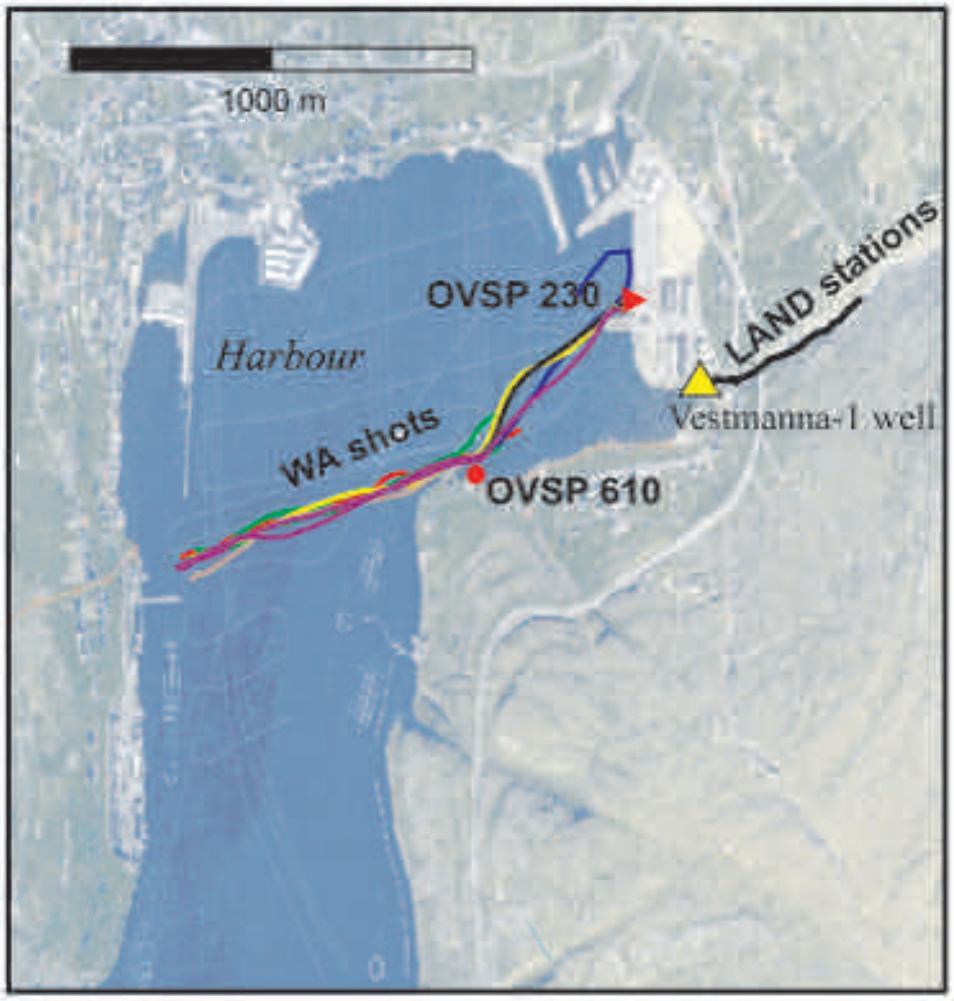

Figure 1. Location map of seismic data acquisition. The LAND data were acquired using the same shots in the harbour as fired for the Walk Away data and for the zero offset VSP data. Pale blue lines show the high-resolution boomer tracks used to map sediment thickness.

10Hz geophones and a hydraulic bow spring with a clamping pressure of approximately 2000 psi. A zero offset VSP (VSP), two offset-VSP (OVSP) profiles and eight walk-away (WA) profiles were recorded by a 3-component receiver in the Vestmanna borehole. All shots were also recorded on the surface geophone array (LAND).

The seismic source consisted of three 0.7 litre (40 cu. in.) sleeve guns, towed behind a small boat for the WA profile or moored at a fixed position for the OVSP. For the VSP only two guns were used in the cluster due to the restricted size of the water pool in which they were shot. Key data acquisition parameters are listed in Table 1. Positions of the borehole, the three VSP shot locations and all geophones were measured by a differential GPS using a local reference station operated by Landsverk Føroya, which was set up for this purpose. The absolute precision is thus significantly better than 0.25 m for the borehole and the geophone positions and ca. 0.25 m for the VSP shot locations. The position of the offshore airgun

source was measured using a standard mobile differential GPS system (Ashtech G12 GPS with Shipmate RS5660 on the gun boat). As the height relative to the geoid is well known, this system provides absolute precision of ca. 1-2 m.

A boomer survey of Vestmanna harbour was made in order to obtain accurate information on the nature and thickness distribution of sediments. These data (e.g., Fig. 2) were filtered between 800-2300 Hz. The shot interval was 100 ms and sediment thicknesses were found to vary between 0-40 m. In most of the fjord, the sediment thicknesses varied little, typically between 10 and 15 m.

Eight WA profiles along one of the boomer

Source: OVSP and WA	Cluster of three 0.7 litre (40 cubic inches) Halliburton sleeveguns (0.5 m gun separation) fired simultaneously and towed at a depth of 3 m
Source: VSP	Cluster of two 0.7 litre (40 cubic inches) Halliburton sleeveguns (0.5 m gun separation) fired simultaneously at a depth of 3 m
Gun positioning, WA	Ashtech G12 GPS receiver with antenna-gun distance correction.
Trigger and telemetry	Airgun first break recorded by hydrophone in the middle of the cluster and telemetered to acquisition units.
Geophone string for surface data	Total length 395 m, 5 m geophone separation.
	60 1-component vertical geophones: I/O Sensor SM6; 14 Hz
	20 3-component geophones GeoSpace GS-30CT; 10 Hz with the first horizontal component oriented towards magnetic north. Every fourth geophone is three-component.
Acquisition unit for surface data	2 Geometrics 60 channels StrataView R60
dynamic range	110 dB
record length	5 sec
sampling interval	0.5 ms
filters	built-in anti-alias: 825 Hz, no other filters.
Acquisition unit for down-hole data	Geometrics 8 channel Geode
Down-hole tool	Custom made 3-component sensor; hydraulic clamped
Geophones	I/0 sensor type SM7; 10 Hz
Near field hydrophone	Fixed at 20 m depth in borehole (only for VSP)
Geophone depths	Every 5 m from 50-500 m (VSP)
	Every 10 m from 50-500 m (OVSP)
	100, 200, 300, 400, 500m (WA)

Table 1. Key data acquisition parameters

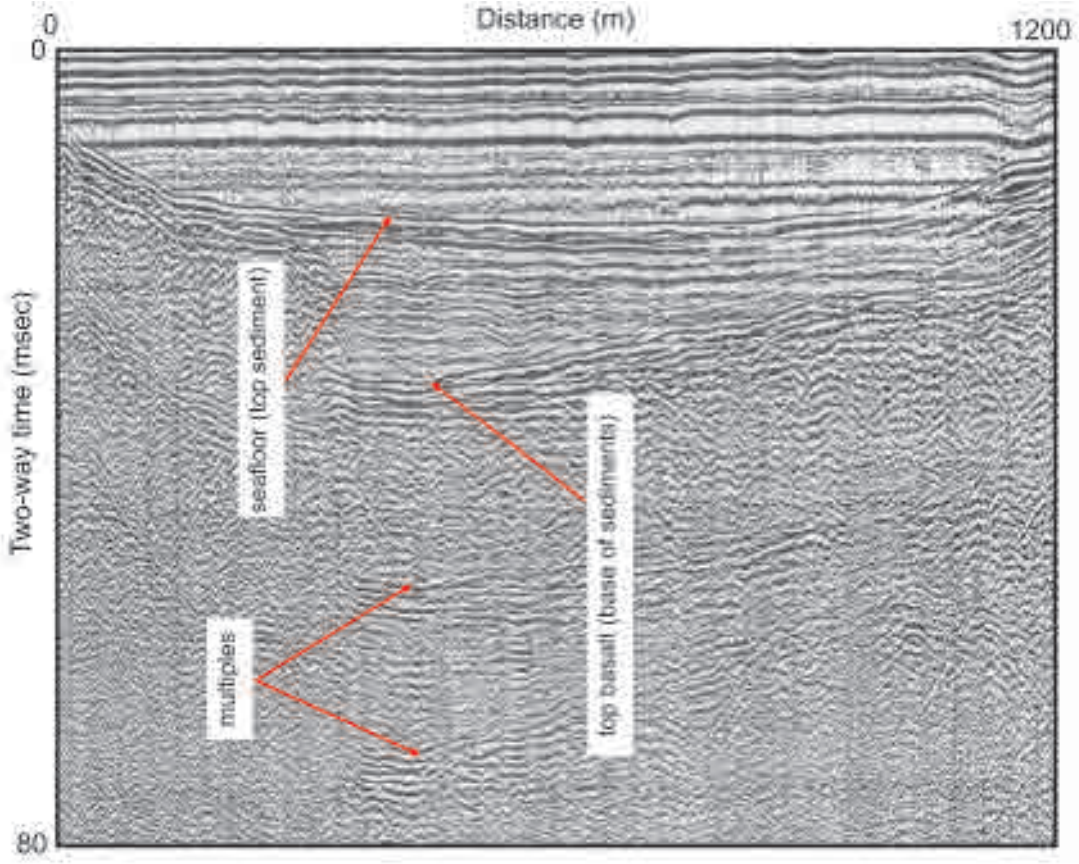

Figure 2. Example of boomer survey data recorded in Vestmanna harbour for mapping sediment thicknesses.

transects (from 200 - 1500 m offset, with 0.5 ms sampling interval), two fixed-offset VSPs (OVSP) (at 230 m and 610 m offset, 0.5 ms sampling interval), and one zero-offset VSP (in which the 3-component seismometer was clamped at 5 m depth intervals in the borehole from 50-500 m depth, with two 0.7 litre sleeve guns for the source) were acquired. Multiple shots were fired in the same location during the OVSP acquisition, which has allowed stacking and, consequently, a significant increase in the signal-to-noise (S/N) ratio. Similarly, it was possible to stack data acquired on the 120 channel LAND array during the individual walk-away profiles. All shots fired during the VSP acquisition were recorded on the LAND array and stacked to a single gather with improved signal/noise ratio.

Ray tracing and anisotropy

Due to the sub-horizontal (dips of less than 2º in the Vestmanna area), layered nature of the basalt sequences, some seismic velocity anisotropy with a vertical axis of symmetry might be expected. However, as mentioned in the introduction, there is conflicting field evidence concerning the magnitude and orientation of the seismic anisotropy of basalts in the North Atlantic region.

We have carried out Backus averaging of the borehole logs (Backus, 1962), from which we obtain mean values of the Thomsen weak anisotropy parameters and of -0.003 and 0.01 respectively (Thomsen, 1986). Fig. 3 shows histograms of these two parameters. The window length used in the analysis was 10 m. This is sufficiently long compared to the individual bed thicknesses (0.5-

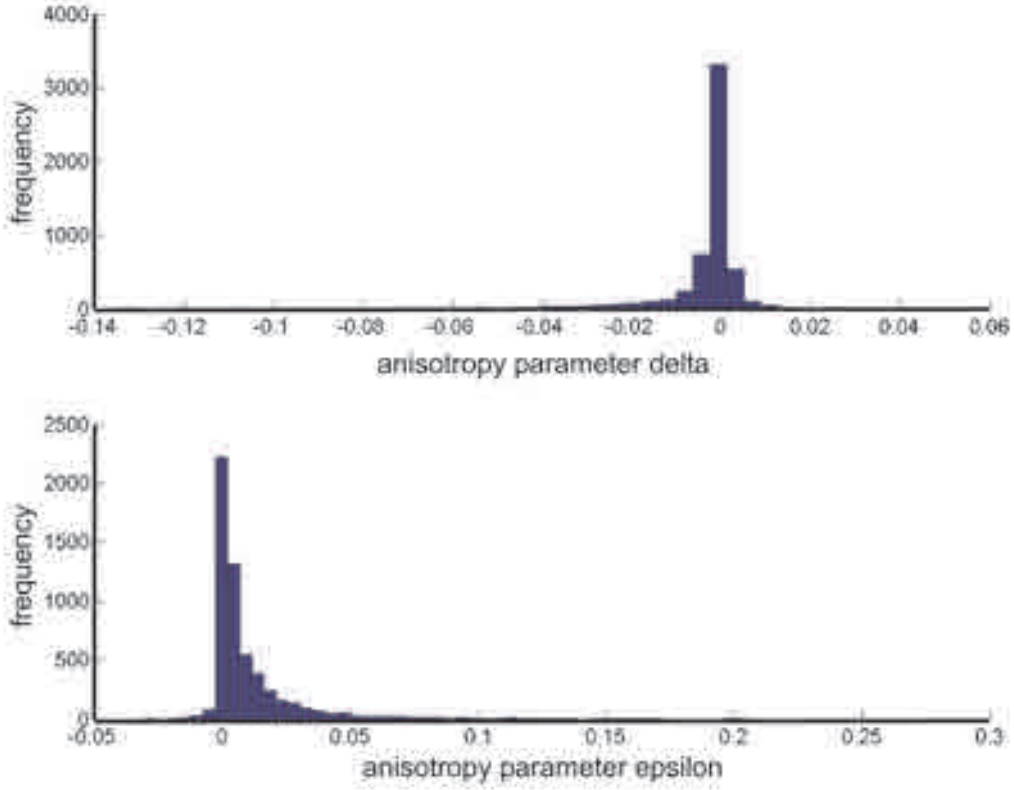

Figure 3. Thomsen's anisotropy parameters and estimated from log data using Backus upscaling (Backus, 1962). Upper diagram is the histogram for anisotropy parameter , with a mean value of -0.003. Lower diagram is the histogram for anisotropy parameter , with a mean value of 0.010. The window length for the upscaling is 10 m. The mean and median values of both anisotropy parameters are stable for window lengths varying from 5 to 50 m.

4.0 m) to account for nearly all anisotropy caused by layering. We assume that each basalt layer is itself isotropic. Mean and median values of the anisotropy parameters are stable for window lengths varying from 5 to 50 m. There is a tail to the values of d which has fallen to negligible values by approximately 0.05.

Seismic data for a wide range of ray directions from vertical to horizontal have been recorded with the combination of VSP, offset VSP and wide angle walk away surveys at the Vestmanna borehole. We have compared the observed first arrival traveltimes from these surveys with calculated ray-traced traveltimes based on an isotropic horizontal plane-layered P wave velocity model. The model is obtained from the Vestmanna borehole sonic log, which has been calibrated using the zero offset VSP data. We have also calculated ray-traced traveltimes for a transversely isotropic velocity model with a vertical axis of symmetry to determine whether it would be possible to detect the presence of 5% P-wave velocity anisotropy ($\varepsilon = 0.05$) given the measurement error and uncertainties in the earth model.

Figure 4 shows (blue stars) the first arrival traveltimes of the VSP data and the 230 m and 610 m offset VSP data. The red crosses are the isotropic ray-traced traveltimes for a horizontal earth model. A ten-layer average velocity model with 50 m thick layers was calculated from the sonic log. Velocities of the layers ranged from 5808 m/s to 5135 m/s with an average of 5443 m/s. Agreement between observed and calculated times for the vertical VSP survey is always better than +/- 0.25 ms.

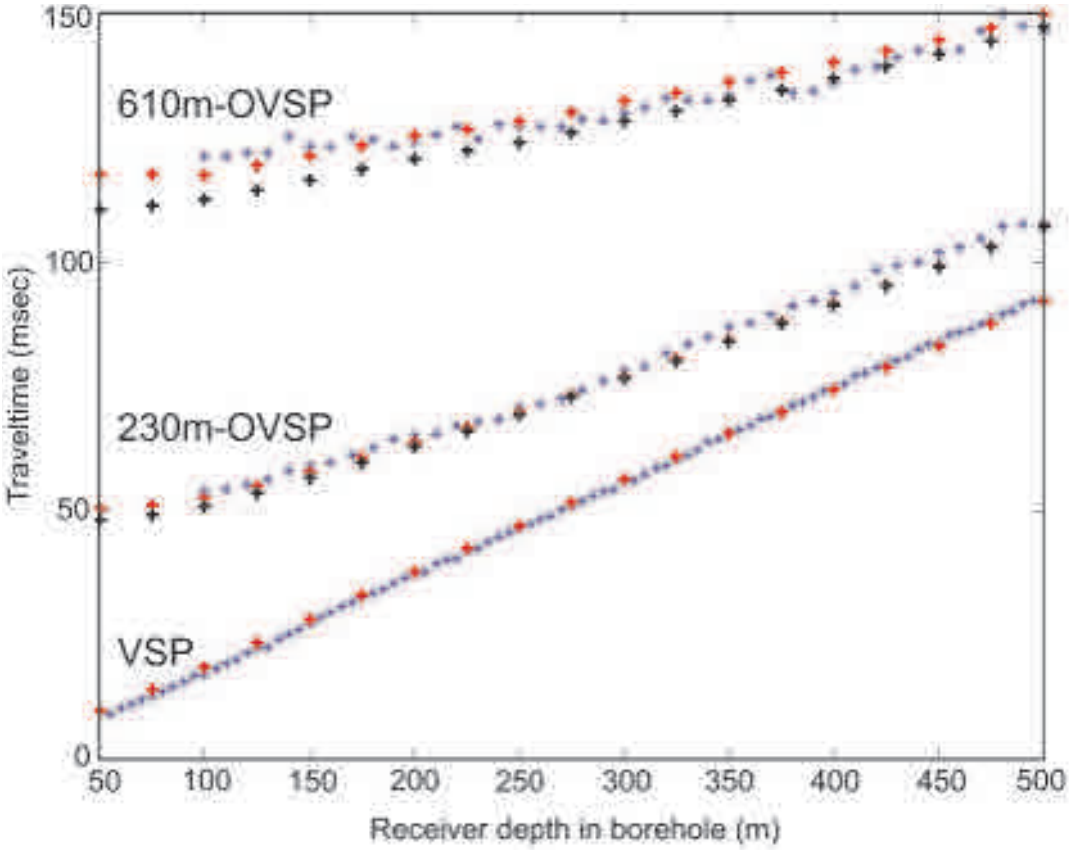

Figure 4. First arrival traveltime data picked from the VSP, 230 m offset-VSP and 610 m offset-VSP data (blue stars). Red crosses are the calculated traveltimes for a horizontally layered isotropic basalt model. Black crosses are traveltimes for a transversely isotropic model with $\varepsilon = 0.05$ and $\delta = 0.0$. Note that no anisotropy is apparent in the vertical ray paths of the VSP, so the red crosses are coincident with the black crosses for the VSP. See text for details.

The match in Fig. 4 between observed and calculated times for the offset VSP surveys was only achieved by introducing a variable near surface sedimentary layer, differing by 3 m between the two locations, that effectively introduced static time shifts to the data. We had no boomer data at the locations of the offset VSP shot positions, so cannot be certain that this model adjustment is valid. However, the only conclusions that we wish to draw from the offset VSP data are that a laterally invariant earth model is not inconsistent with the data and that these data do not enable us to draw any firm conclusions about the transverse isotropy of the basalts. The black crosses show the ray-traced times for a transversely isotropic earth model. The vertical velocities are the same as for the isotropic case, but with $\varepsilon = 0.05$ and $\delta = 0.0$ in all the basalt layers. At 230 m offset, there is little difference between isotropic and anisotropic times. At 610 m offset, the uncertainty in traveltime picking and static shift adjustment of approximately 3 ms is of the same order as the difference between the theoretical isotropic and anisotropic times. Times were calculated using code based on the work of Chapman and Pratt (1992) and Pratt and Chapman (1992).

Figure 5 shows the isotropic ray-traced paths for the offset VSP surveys described above and the five walk-away VSP surveys with receiver depths fixed at 100, 200, 300, 400 and 500 m depth. In this case, isotropic ray tracing was performed using code based on the work of Zelt and Smith

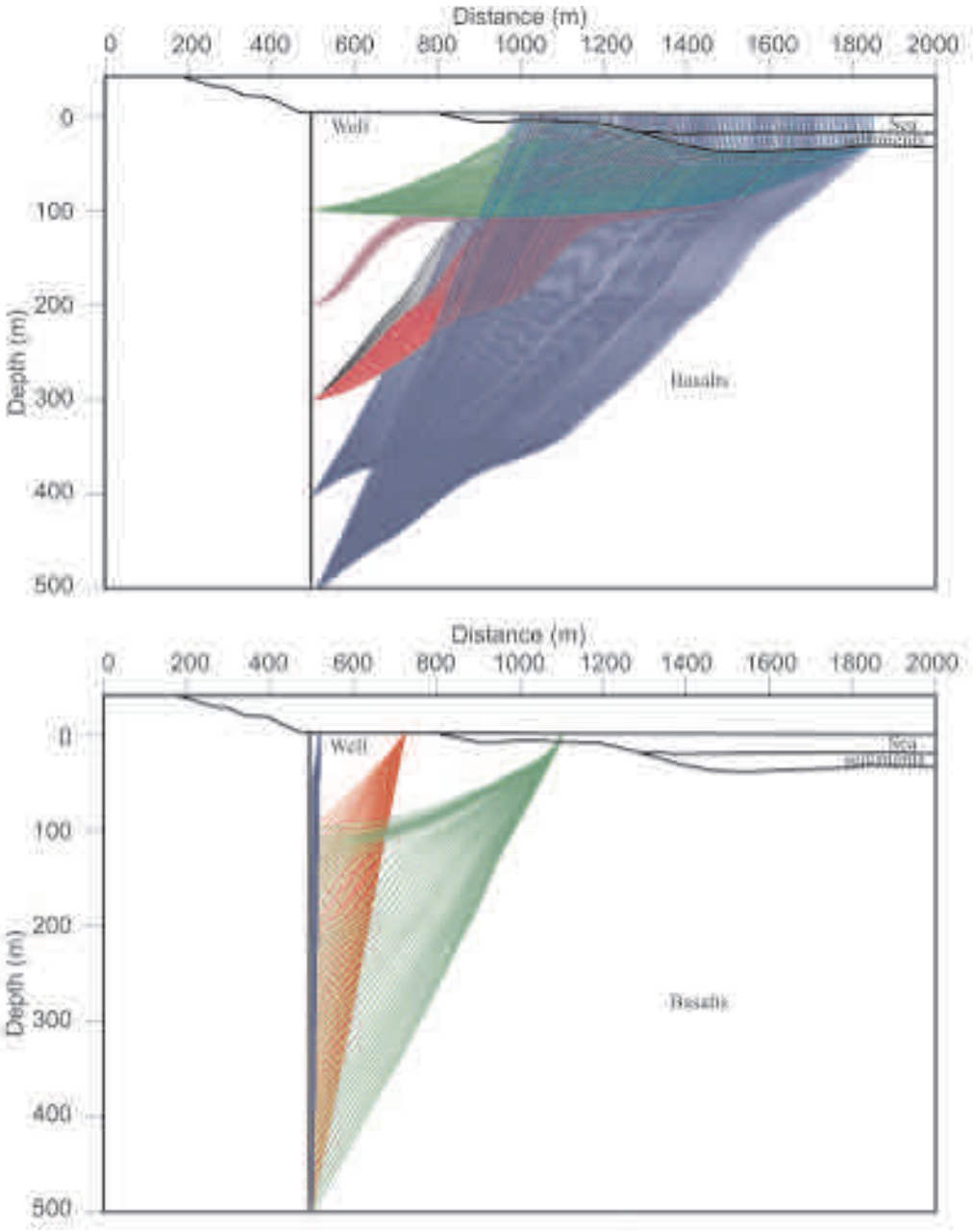

Figure 5. Ray tracing of WA data (top) and VSP & OVSP data (bottom) through the best fitting velocity model. The Vestmanna-1 borehole is located at 500 m from the origin. The velocity of the sedimentary layer is 1600 m/s.

(1992). The sonic log was averaged to obtain 10 m thick layers. In each layer, a very small vertical velocity gradient was introduced to permit accurate tracing of turning rays. In order to model the irregular sedimentary thickness in the harbour beneath the shooting lines, the sediment thickness was calculated from the traveltime picks read from the boomer data (e.g., Fig. 2).

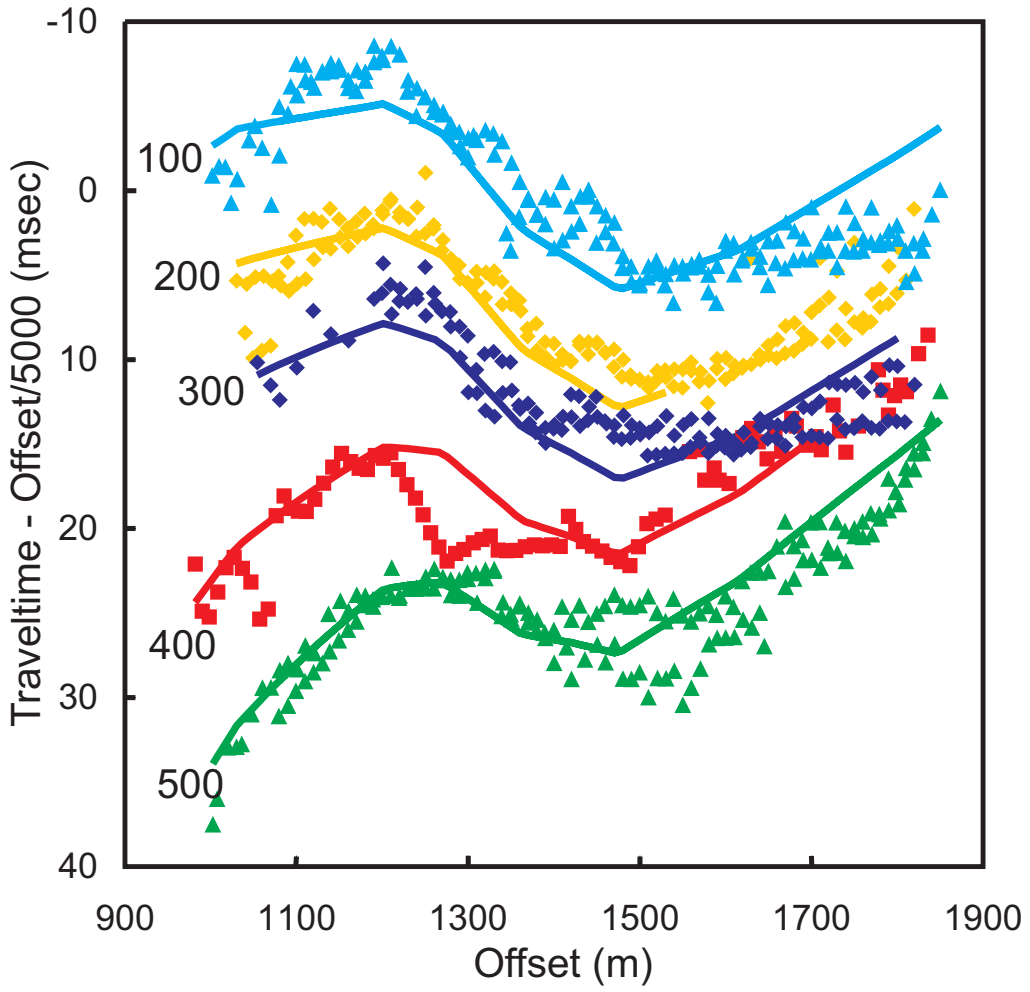

Figure 6. WA picked traveltimes (coloured symbols, receiver depth in borehole marked against each line) compared to theoretical traveltimes (lines of same colour) plotted with a velocity reduction of 5000 m/s.

Figure 6 shows the match between observed and calculated first arrival travel times for the walk-away VSP surveys. Scatter in the data can be attributed to picking error and shot mislocation. Misfits between observed and calculated times could easily be resolved by introducing lateral variations in a combination of water depth and sediment thickness of 5 m or less, or possibly broader lateral variations in the basalt velocity. However, these data are consistent with an isotropic horizontally layered basalt model.

Figure 7 shows the differences in traveltimes between an isotropic and a transversely isotropic velocity model with a vertical axis of symmetry and $\varepsilon = 0.05$ and $\delta = 0.0$, obtained using code based on the work of Chapman and Pratt (1992) and Pratt and Chapman (1992). The coarser layered velocity model described above has again been used for this anisotropic calculation. One observes the predictable result that the difference in traveltimes between the isotropic and anisotropic models increases with offset, since the ray paths are becoming more horizontal, and the difference at maximum offset is approximately 5% of the total traveltimes, corresponding to a transverse velocity anisotropy of 5%. The key observation is

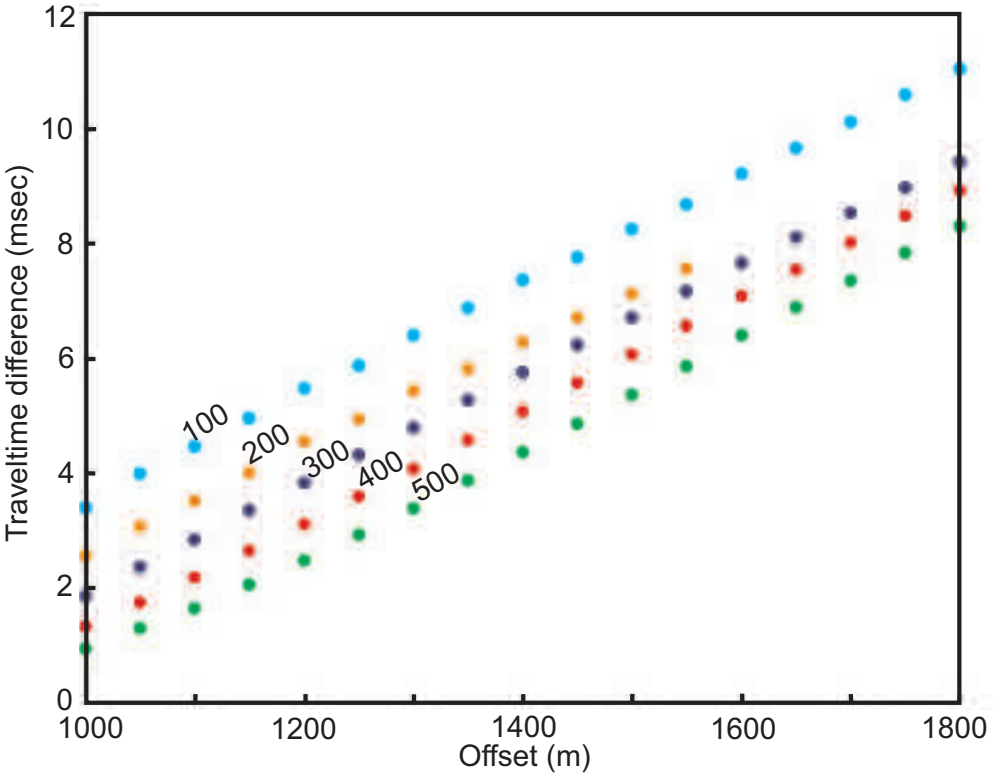

Figure 7. Difference between the traveltimes that would be observed for the walk-away (WA) surveys if the earth were transversely isotropic with $\varepsilon = 0.05$ and $\delta = 0.0$, compared to traveltimes for an isotropic earth. Colours for each receiver depth in the borehole are the same as in Fig. 6, with receiver depth marked against each set of data. See text for details.

that 5% anisotropy would result in approximately 10 ms delay at our maximum offsets and would produce a delay that varies linearly with offset. It would be possible to construct some combination of velocity anisotropy and significant lateral variation in basalt structure that would satisfy the traveltimes from our walk-away data. However, the model would be highly contrived. The simplest conclusion that satisfies the data is that there is no evidence for velocity anisotropy in the basalts in the Vestmanna region at the 5% level and arguably not at half that value.

Shear wave analysis

Airguns fired in the water generate a purely compressional wave-field but strong mode converted shear waves are generated at the seafloor and are observed on the 3-component borehole seismometer. We rotated the 3 components of the borehole seismometer into in-line and transverse components, and picked P-wave traveltimes from the former and S-wave arrivals from the latter. By ray-tracing through an S-wave velocity model generated from the P-wave model with a constant Poisson's ratio for the sediments and a different constant Poisson's ratio for the basalts, we optimised the values of the Poisson's ratios until a best traveltime fit was achieved to the S-wave arrivals.

Assuming that the main mode conversion from P-waves to S-waves occurred at the seabed, we find a Poisson's ratio of 0.47 for the sediments, and 0.28 ± 0.01 ($V_p/V_s \sim 1.78$ -1.83) for the basalt sequence. These results are consistent with Poisson's ratios calculated from offshore profiles over originally subaerial basalts near the Faroe Islands (Eccles *et al.*, 2007; Eccles *et al.*, this volume), and

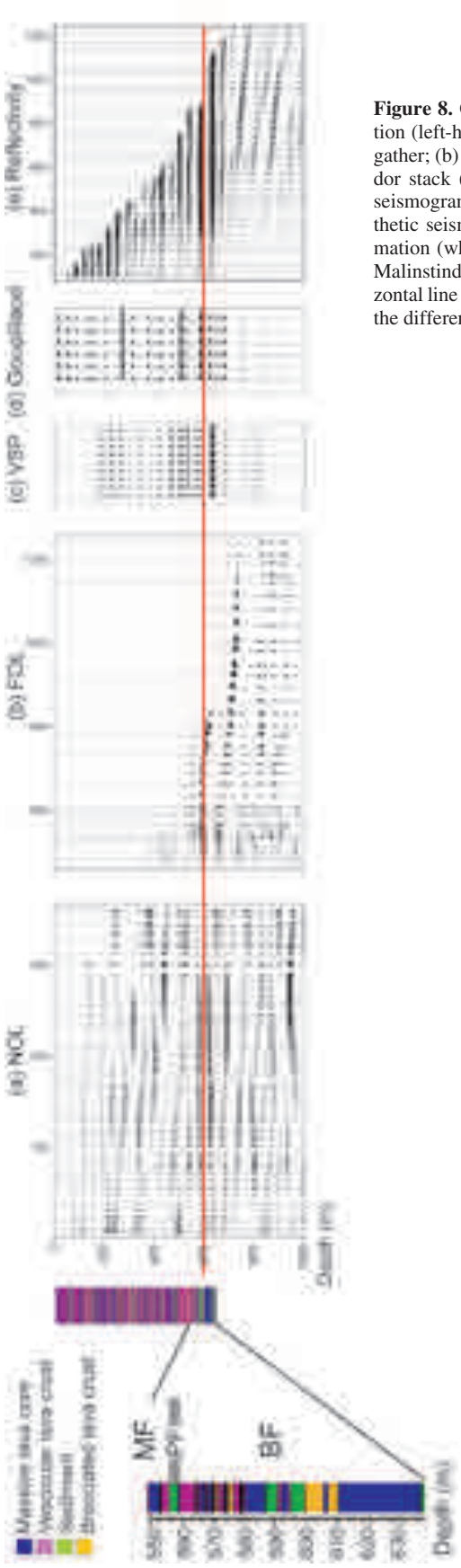

Figure 8. Comparison between Vestmanna borehole stratigraphic section (left-hand side of figure); (a) the near offset land (NOL) data shot gather; (b) the far offset land (FOL) data stacked section; (c) VSP corridor stack (single trace repeated for clarity); (d) Goupillaud synthetic seismograms (zero offset trace repeated for clarity); (e) reflectivity synthetic seismograms. BF is Beinisvørð Formation; PF is Prestfjall Formation (which is only 2.5 m thick in the Vestmanna borehole); MF is Malinstindur Formation. See the text for processing applied. The horizontal line correlates the main event at 600 m depth on the sections. Note the different horizontal scales (labelled in m) of the different panels.

from the Lopra-1A borehole on the Faroe Islands (Christie *et al.*, 2006).

Reflection seismogram study

The seismic data acquired on the surface geophone array were processed in order to study the seismic reflection response and intra-basalt reflectivity for comparison with the stratigraphy determined from coring, the borehole velocity measurements and synthetic seismograms generated from the borehole logs. The aim was to understand how the distribution of lava flow thicknesses, the intercalation of sediments and the igneous compositional variations within the lavas affect the seismic reflectivity.

We have processed two different seismic reflection datasets: a Far Offset Land (FOL) dataset composed from all the shot gathers fired in the harbour for the wide-angle borehole dataset and recorded on the 80 land geophones. The second seismic dataset (Near Offset Land, NOL) was acquired by recording on the same geophone array using the shots fired in the pond close to the borehole for the zero-offset VSP survey. The NOL is a single shot gather acquired using 80 channels, but with a stack of many shots after a hyperbolic normal moveout correction. The high fold of the FOL data (574 shots into 80 seismometers) allowed us to gather them in common offset bins of 10 m size with subsequent stacking to improve the signal to noise ratio (maximum stack fold of 240). We made an elevation static correction to a final datum at sea level with a replacement velocity of 5000 m/s appropriate for the basalts, then applied an F-K filter and an Orsmby band pass filter of 4-20-120-200 to enhance the signal to noise ratio of the data.

The velocity applied for the hyperbolic move-

out correction was derived from the smoothed log velocity profile. The lack of heterogeneity noticed during the ray tracing analysis allowed us to use a 1D velocity model. CDPs from 400 to 2000 m from the FOL data were stacked after a conventional hyperbolic moveout correction, with a maximum allowable normal moveout stretch of 60%. Finally the amplitudes were adjusted with an automatic gain control using a window length of 500 ms. For the NOL dataset, the maximum normal moveout stretch is 30%.

To synthesize a seismic velocity profile suitable for calculating the ID synthetic seismograms we used the sonic velocity logs from the borehole with an assumed Quality Factor of 50. We have filled the missing sonic values for the deepest part of the borehole by extrapolating the borehole logs using the lithological section. In doing so, an average velocity was derived for each of the four main lithologies: massive lava core, vesicular lava crust, sediment, and brecciated lava crust.

To study the behaviour of the reflection amplitudes we calculated synthetic seismograms using two different codes. The first synthetic modelling algorithm was based on the reflectivity method (Fuchs and Müller, 1971; Kennett, 1979), which computes the complete solution to the wave equation including all multiples and phase conversions. The traces were generated using a Ricker wavelet with a pulse length of 40 ms, 1 ms sampling and 2048 samples, then band pass filtered and normal moveout corrected with the same parameters as were used for the real data. Synthetic traces were also generated using a 1D all-multiples impulse response method based on a Goupillaud medium (Ganley, 1981; Cohen and Stockwell, 2000), with a 40 Hz peak-frequency source wavelet to match the real data.

Figure 8 shows the FOL and NOL data compared with both types of 1D synthetic seismogram and with the stratigraphic column from the borehole at the left-hand side. The main feature on the FOL stacked section is a strong subhorizontal reflection at about 600 m depth (Fig. 8a). A later event (at 650 m depth on the left and moving deeper to the right, Fig. 8a,b) is also evident. On the Goupillaud synthetic (Fig. 8d) there is a strong reflection at the same depth as that on the FOL data.

Comparing the reflectivity seismograms (Fig. 8e) with the FOL stacked data, there is a good correlation around the main reflection at 600 m: the position in depth of this event and the arrival on the real data match well with the event on the synthetic dataset. The main event at about 600-610 m depth is easily detectable on the NOL dataset, FOL dataset and reflectivity synthetic traces. It is deeper by at least 40 m than the interface between the Malinstindur and Beinisvørð basalt Formations. It is apparently associated with the transition from the low impedance contrast of sediment and lava breccia in the 588-600 m interval to the 30 m thick massive lava layer at 610 m depth (see stratigraphic column in Fig. 8). Correlating the NOL data (Fig. 8a) with the reflectivity synthetic seismogram (Fig. 8e) we also see a coherent reflection at 225-250 m depth which is confirmed by the Goupillaud synthetics (Fig. 8d). This is interpreted as caused by another strong impedance contrast.

We also made synthetic studies with the reflectivity method to investigate the influence of the frequency content on the reflectivity response. The panel in Figure 9 shows synthetic traces made with the same parameters as for the previous model but varying the source pulse length. The impulse length variation does not affect the presence of a main reflection at 600 m depth; in contrast the interference pattern at 410-430 m is considerably influenced by the frequency content of the seismic wave used to investigate it.

This behaviour can be explained by the vertical resolution of the signal: thin layers are not resolvable by long wavelength signals and thus sequences of thin basalt may give rise to a "reflection" event as the result of an interference pattern of strong impendence contrasts (e.g., Smallwood *et al.*, 1998). Conversely, the seismic response of a sharp and strong isolated impedance contrast, like that at 600 m is not affected so strongly by the frequency of the source.

Conclusions

We have studied the seismic characteristics of the lower part of the Malinstindur Formation, and the topmost part of the Beinisvørð Formation in the Faroe Islands by processing seismic data acquired

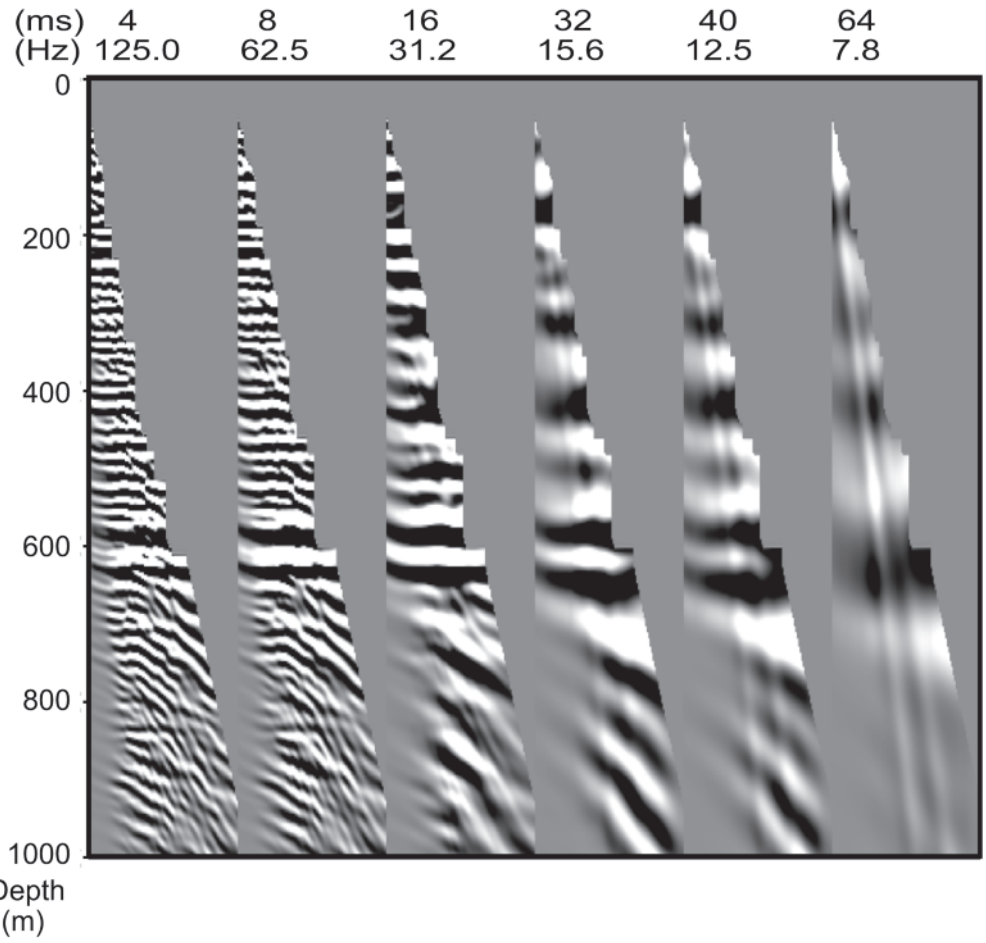

Figure 9. Synthetic seismograms computed by the reflectivity code for different pulse lengths (dominant frequency) as written at the top of each panel. Signal frequency content does not affect the presence of a strong reflector at 600 m depth.

in the Vestmanna area with coincident borehole information. Using a combination of VSP and land seismic data we have placed constraints on the velocity of the basalts and their Poisson's ratio, on the maximum possible P-wave velocity anisotropy, and on intra-basalt reflectivity.

The transverse isotropy of the basalts is constrained as lower than 5%, and probably less than half of that, which is consistent with calculations based on Backus upscaling of the logs through layered basalts in the Vestmanna borehole. The results from the Malinstindur Formation sampled in Vestmanna are similar to those obtained from the much coarser bedded Beinisvørð Formation investigated by Christie *et al.* (2006) in the Lopra borehole. Hence introducing a VTI anisotropic term into normal moveout corrections when processing seismic reflection data through basalts in this area would have little effect. The average Poisson's ratio of the basalts is 0.28 ± 0.01 (V_p/V_s ~ 1.78 - 1.83).

Synthetic seismogram analysis shows that the seismic response of the layered basalts is due primarily to interference patterns produced by the layered flows which are considerably thinner than the seismic wavelength. The reflectivity is therefore dependent on the frequency of the seismic waveform that samples the flows. However, there

is a strong reflection in the Vestmanna area which occurs at the same depth of 600 m across a wide range of incident seismic frequencies, from 8 - 125 Hz. This prominent reflector is caused by the contrast between a 10 m thick layer of low impedance sediments and an unusually thick (40 m) lava core layer with a high impedance. Although this layer is close to the boundary between the Malinstindur and Beinisvørð basalt Formations and might therefore be a candidate for regional mapping, in detail it lies some 40 m below that interface. The integration of seismic data and core analysis provides insights into the identification of some properties of the layered basalts which may otherwise have been missed from core descriptions alone. In particular, the response of the necessarily long-wavelength source signal is the integrated effect of the multiple thin layers of the basalt flows, and prominent reflectors may not always correlate one to one with lithological layers.

Acknowledgments

We thank the Sindri Group for financial support and for permission to publish the results in this paper. The SeiFaBa project is funded collectively by oil companies operating in the Faroese sector. Members of the SeiFaBa research group are Morten-Sparre Andersen, Peter Japsen, Dan Olsen, Niels Springer, Rasmus Rasmussen and Regin Waagstein (Geological Survey of Denmark and Greenland), Claus Andersen (Faroes Geological Survey), Felicia Shaw and Michael H. Worthington (University of Oxford), Lars Boldreel (University of Copenhagen), Giovanni Bais and Robert S. White (University of Cambridge), and Uni K. Petersen (University of the Faroe Islands). We thank Gerhard Pratt (Queen's University, Canada) for the use of his anisotropic ray-trace modelling code. Department of Earth Sciences, Cambridge contribution no. ES8769.

References

Andersen, M.S. 1988. Late Cretaceous and early Tertiary extension and volcanism around the Faeroe Islands. *In*: Morton, A.C. and Parson, L.M. (eds) *Early Tertiary Volcanism and the Opening of the NE Atlantic*. Geological Society Special Publications 39: 115-112.

Backus, G.E. 1962. Long-wave elastic anisotropy produced by horizontal layering. *Journal of Geophysical Research* 67: 4427-4440.

Chapman, C.H. and Pratt, R.G. 1992. Traveltime tomography in anisotropic media - I. Theory. *Geophysical Journal International* 109: 1-19.

Christie, P., Gollifer, I. and Cowper, D. 2006. Borehole seismic studies of a volcanic succession from the Lopra-1/1A borehole in the Faroe Islands, NE Atlantic. *Geology of Denmark Survey* 9: 23-40.

Cohen, J.K. and Stockwell, Jr. J.W. 2000. CWP/SU: Seismic Unix Release 34: a free package for seismic research and processing, Center for Wave Phenomena, Colorado School of Mines.

Eccles, J.D., White, R.S., Roberts, A.W., Christie, P.A.F., and the iSIMM Team 2007. Wide angle converted shear wave analysis of a North Atlantic volcanic rifted continental margin: constraint on subbasalt lithology. *First Break* 25.10 (October 2007): 63-70.

Eccles, J.D., White, R.S., Christie, P.A.F., Roberts, A.W. and iSIMM Team. Discrimination of subbasalt sediments and hyaloclastites by Vp/Vs. *In*: Varming, T. and Ziska, H. (eds) *Faroe Islands Exploration Conference: Proceedings of the 2nd Conference*. Annales Societatis Scientiarum Færoensis, Tórshavn, this volume.

Eldholm, O. and Grue, K. 1994. North Atlantic volcanic margins: dimensions and production rates. *Journal of Geophysical Research* 99: 2955-2988.

Fliedner, M.M. and White, R.S. 2001. Sub-basalt imaging in the Faroe-Shetland Basin with large offset data. *First Break* 19: 247-252.

Fuchs, K. and Müller, G. 1971. Computation of synthetic seismograms with the reflectivity method and comparison with observations. *Geophysical Journal of the Royal Astronomical Society* 23: 417-433.

Ganley, D.C. 1981. A method for calculating synthetic seismograms which include the effects of absorption and dispersion. *Geophysics* 46(8): 1100-1107.

Japsen, P., Andersen, C., Andersen, H.L., Andersen, M.S., Boldreel, L.O., Mavko, G., Mohammed, N.G., Pedersen, J.M., Petersen, U.K., Rasmussen, R., Shaw, F., Springer, N., Waagstein, R., White, R.S. and Worthington, M. 2005. Sub-basalt imaging - new insight from investigations of petrophysical and seismic properties of Faroes basalts (SeiFaBa project). *In*: Doré, A.G. and Vining, B.A. (eds) *Petroleum Geology: North-West Europe and Global Perspectives - Proceedings of the 6th Petroleum Geolo-*

gy Conference. Geological Society, London: 1461–1470.

Jerram, D.A. 2002. Volcanology and facies architecture of flood basalts, *In*: Menzies, M.A., Klemperer, S.L., Ebinger, C.J., Baker, J. (eds) *Volcanic Rifted Margins*. Geological Society America Special Paper 362: 119-132

Kennett, B.L.N. 1979. Theoretical reflection seismograms for elastic media. *Geophysical Prospecting*: 27: 301-321.

Kiørboe, L. and Petersen, S.E. 1995. Seismic investigation of the Faeroe basalts and their substratum, *In*: Scrutton, R.A., Stoker, M.S., Shimmield, G.B. and Tudhope, A.W. (eds) *The tectonics, Sedimentation and Palaeoceanography of the North Atlantic Region*. Geological Society Special Publications 90**:** 111-123.

Kumar, D., Bastia, R. and Guha, D. 2004. Prospect hunting below Deccan basalt: imaging challenges and solutions. *First Break* 22: 35-39.

Larsen, L.M., Waagstein, R., Pedersen, A.K. and Storey, M. 1999. Trans-Atlantic correlation of the Palaeogene volcanic successions in the Faeroe Islands and East Greenland. *Journal of the Geological Society* 156: 1081-1095.

Mack, H. 1997. Seismic response of Tertiary basalt flows in Northeast Atlantic - a modelling study. *EAGE 59th Conference and Technical Exhibition*, Geneva: Paper B017.

Maresh, J. and White, R.S. 2005. Seeing through a glass, darkly: strategies for imaging through basalt. *First Break* 23: 27–32.

Maresh, J., White, R.S., Hobbs, RW. and Smallwood, J.R. 2006. Seismic attenuation of Atlantic margin basalts: observations and modelling. *Geophysics* 71: B211-B221, doi: 10.1190/1.2335875

Martini, F. and Bean C. J. 2002. Application of pre-stack wave equation datuming to remove interface scattering in sub-basalt imaging. *First Break* 20: 395-403.

Naylor, P.H., Bell, B.R., Jolley, D.W., Durnall, P. and Fredsted, R. 1999. Palaeogene magmatism in the Faeroe-Shetland Basin: influences on uplift history and sedimentation. *In*: Fleet, A.J. and Boldy, S.A.R (eds.) *Petroleum Geology of Northwest Europe: Proceedings of the 5th Conference*. Geological Society, London: 545-558.

O'Doherty, R.F. and Anstey, N.A. 1971. Reflections on amplitudes. *Geophysical Prospecting* 19: 430-458.

Passey, S.R. and Bell, B.R. 2007. Morphologies and emplacement mechanisms of the lava flows of the Faroe Islands Basalt Group, Faroe Islands, NE Atlantic Ocean. *Bulletin of Volcanology* 70: 139-156.

Petersen, U.P., Andersen M.S., White R.S. and the SeiFaBa Group. 2006. Seismic imaging of basalts at Glyvursnes, Faroe-Islands - Hunting for future exploration methods in basalt covered areas. *First Break* 24: 45-52.

Planke, S. 1994. Geophysical response of flood basalts from analysis of wire line logs: Ocean Drilling Program Site 642, Vøring volcanic margin. *Journal of Geophysical Research* 99: 9279-9296.

Planke, S. and Eldholm, O. 1994. Seismic response and construction of seaward dipping wedges of flood basalts: Vøring volcanic margin. *Journal of Geophysical Research* 99: 9263-9278.

Pratt, R.G and Chapman, C.H. 1992. Traveltime tomography in anisotropic media - II. Application. *Geophysical Journal International* 109: 20-37.

Pujol, J. and Smithson, S. 1991. Seismic wave attenuation in volcanic rocks from VSP experiments. *Geophysics* 56: 1441-1455.

Rasmussen, J. and Noe-Nygaard, A. 1970. Geology of the Faeroe Islands. *Geological Survey of Denmark I. Series*. 25: 142pp.

Richardson, K.R., White, R.S., England, R.W. and Fruehn, J. 1999. Crustal structure east of the Faroe Islands. *Petroleum Geoscience* 5: 161-172.

Shaw, F., Worthington, M.H., White, R.S., Andersen, M.S., Petersen, U.K. and the SeiFaBa Group. 2008. Seismic attenuation in Faroe Islands basalts. *Geophysical Prospecting*: 56, 5-20. doi: 10.1111/j.1365-2478.2007.00665.x

Silva, R. and Cocoran, D. 2002. Sub-basalt imaging via pre-stack depth migration - an example from the Slyne Basin, offshore Ireland. *First Break* 20: 295-299.

Smallwood, J.R., White, R.S. and Staples R.K. 1998. Deep crustal reflectors under Reydarfjördur, eastern Iceland: crustal accretion above the Iceland mantle plume. *Geophysical Journal International* 134: 277-290.

Sørensen, A.B. 2003. Cenozoic basin development and stratigraphy of the Faroes area. *Petroleum Geoscience* 9: 189-207.

Spitzer, R., White, R.S. and iSIMM Team. 2005. Advances in seismic imaging through basalts: a case study from the Faroe-Shetland Basin. *Petroleum Geoscience* 11(2): 147-156.

Thomsen, L. 1986. Weak elastic anisotropy. *Geophysics* 51: 1954-1966.

Smallwood, J.R., Fliedner, M.M., Boslaugh, B., Maresh, J. and Fruehn, J. 2003. Imaging and regional distribution of basalt flows in the Faroe-Shetland Basin. *Geophysical Prospecting* 51: 215-231.

Waagstein, R. 1988. Structure, composition and age of the Faeroe basalt plateau. *In*: Morton, A.C. and Parson, L.M. (eds.) *Early Tertiary Volcanism and the Opening of the NE Atlantic*. Geological Society Special Publications 39: 225-238.

Waagstein, R. and Hald, N. 1984. Structure and petrography of a 660 >m lava sequence from the Vestmanna-1 drill hole, lower and middle basalt series, Faeroe Islands, *In*: Berthelsen, O., Noe-Nygaard, A. and Rasmussen, J. (eds.) *The deep drilling project*

1980-1981 in the Faeroe Islands, *Annales Societatis Scientiarum Færoensis*, Supplementum IX: 39-70.

White, R. and McKenzie, D. 1989. Magmatism at rift zones: The generation of volcanic continental margins and flood basalts. *Journal of Geophysical Research* 94: 7685-7729.

White, R.S., Smallwood, J.R., Fliedner, M.M., Boslaugh, B., Maresh, J. and Fruehn, J. 2003. Imaging and regional distribution of basalt flows in the Faroe-Shetland Basin. *Geophysical Prospecting* 51: 215-231.

Zelt, C.A. and Smith R.B. 1992. Seismic traveltime inversion for 2-D crustal velocity structure. *Geophysical Journal International* 108: 16-34.

Understanding the facies architecture of flood basalts and volcanic rifted margins and its effect on geophysical properties

CATHERINE E. NELSON[1]*, DOUGAL A. JERRAM[1], RICHARD T. SINGLE[2] AND RICHARD W. HOBBS[1]

[1] Dept. of Earth Sciences, The University of Durham, South Rd., Durham DH1 3LE, UK.
[*] Email: c.e.nelson@durham.ac.uk
[2] Senior Geofysiker, Det norske oljeselskap ASA, Bryggegata 9, 0250 Oslo, Norway

ABSTRACT

A review is presented of the current developments in our understanding of the facies architecture of flood basalts and volcanic rifted margins. Basalt sequences are sometimes considered to consist of uniform, homogeneous layers of basalt; however heterogeneity in basalt sequences exists at every scale from that of a lava flow, through lava flow stacking patterns, up to the basin or province scale. The main scales addressed in this review comprise: intrafacies - heterogeneity on a lava flow scale; facies/facies associations – variations on a lava field scale; and seismic facies – the sub-province scale. These scales of heterogeneity are important in the interpretation of flood basalt sequences from a variety of different settings. Examples from the North Atlantic Igneous Province, Paranã-Etendeka, Deccan and Ethiopia are presented, which suggest that there are common facies elements in the generation of flood basalt provinces associated with volcanic rifted margins. Research into facies architecture has the potential to improve imaging beneath basalt sequences through better understanding of the loss of seismic energy caused by the basalt sequence. This is due to both the high impedance contrast between the basalt sequence and the overlying sedimentary succession, and the scattering and production of multiples by the heterogeneity within the basalt sequence. Recent studies have shown that the internal heterogeneity causes more energy loss than the impedance contrast at the surface of the basalt sequence. Accordingly, characterising this internal heterogeneity and incorporating it into 3D models allows the generation of synthetic seismic data, and hence improved strategies for data acquisition and processing.

1 Introduction

Three quarters of the Atlantic rifted margins are estimated to be volcanic, and perhaps as much as 90% of rifted margins worldwide (Menzies *et al*., 2002). In places along these margins, subaerial lava flows were erupted to form flood basalt provinces, especially where the positions of mantle melting anomalies were coincident with the rifted margin (e.g. North Atlantic Igneous Province, Paranã-Etendeka, White and McKenzie, 1989, Jerram and Widdowson, 2005). Substantial volumes of material were also added to the underside of the continental crust via magmatic underplating (Cox 1980; 1993). The distribution of several of the main Cenozoic and Mesozoic flood basalt provinces is highlighted in Figure 1a. These provinces contain enormous volumes of lava; for example the Deccan Volcanic Province has an estimated maximum extrusive volume of c. $1x10^6$ km^3 (Self *et al*., 2006). The North Atlantic Igneous Province (NAIP) (Figure 1b), when its volcanic rifted margins are included, is estimated to have a volume of $1.8x10^6$ km^3 covering an area of $1.3x10^6$ km^2 (Eldholm and Grue, 1994). Provinces such as the NAIP cover some sedimentary basins which are thought to have a high potential for hydrocarbon discovery. Volcanism coincided with the deposition of Palaeocene sediments in the Faroe-Shetland Basin, which contain the Foinaven and

Faroe Islands Exploration Conference: Proceedings of the 2nd Conference.
Annales Societatis Scientiarum Færoensis, Supplementum 50, 2009: 84-103

Schiehallion fields in areas without basalt cover (Naylor *et al*. 1999), and the Rosebank discovery within the edge of the basalts. Similar areas are associated with other flood basalt provinces, such as the Kudu Gas Field, offshore Namibia (Jerram *et al*., 1999), associated with the Paranã-Etendeka flood basalts. Areas covered by the Deccan Volcanic Province such as the Saurashtra Peninsula, western India (Sain *et al.*, 2002) and the Kutch Basin, offshore to the west of India (Kumar *et al*., 2004) have also been identified as sub-basalt hydrocarbon prospects. Therefore, a major target in hydrocarbon exploration is to exploit areas with flood basalt cover, which specifically requires good seismic imaging of the structure beneath the basalt sequence, often over 1 km thick.

The aim of this overview is to look at how a facies architecture approach to the study of flood

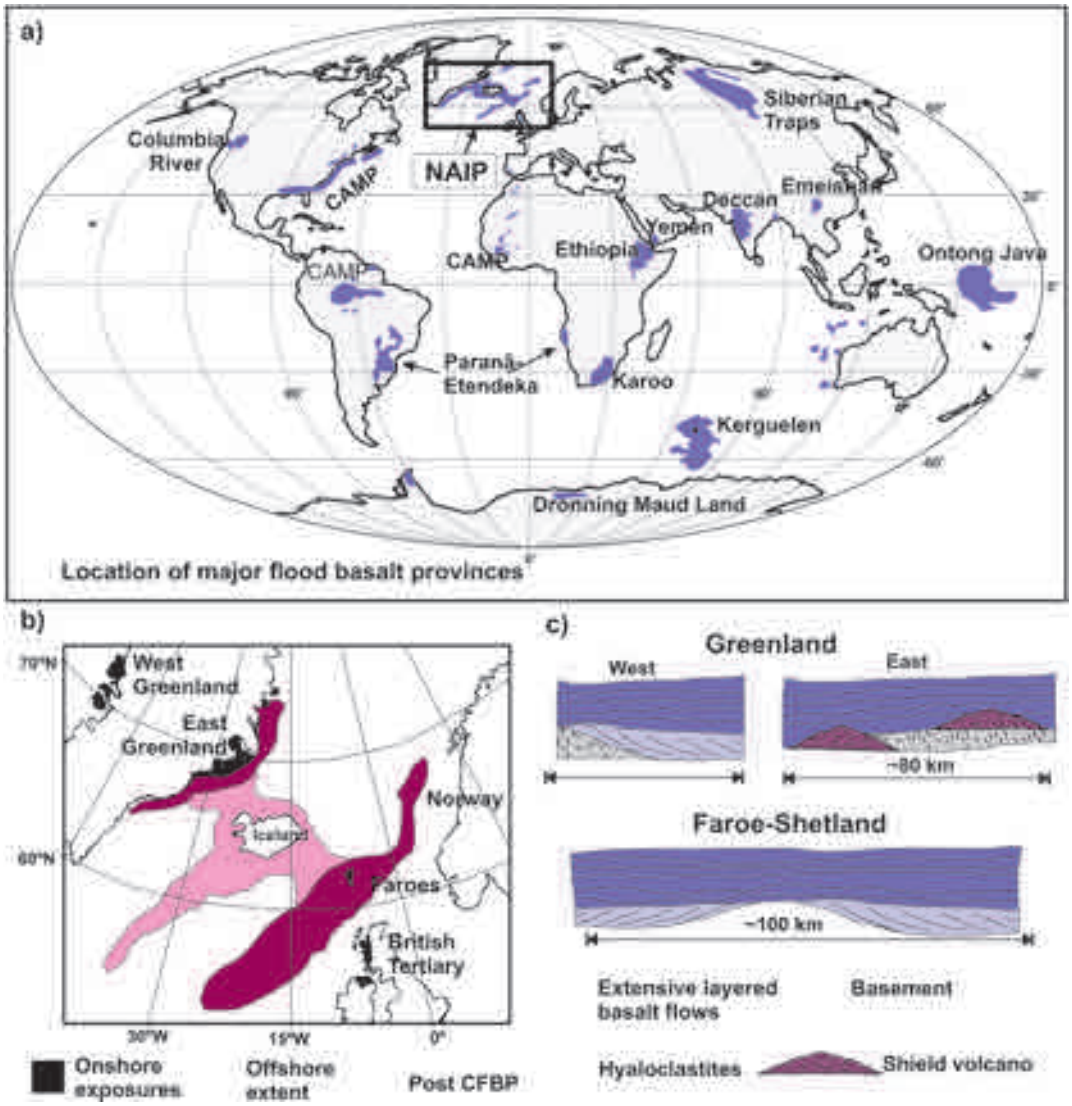

Figure 1. a) Location map of major flood basalt provinces, North Atlantic Igneous Province (NAIP) is highlighted. **b**) Schematic map of the NAIP showing location of onshore exposure. **c**) Schematic E-W cross-section from Greenland to Shetland, showing large scale lateral facies variations (adapted from Jerram and Widdowson, 2005).

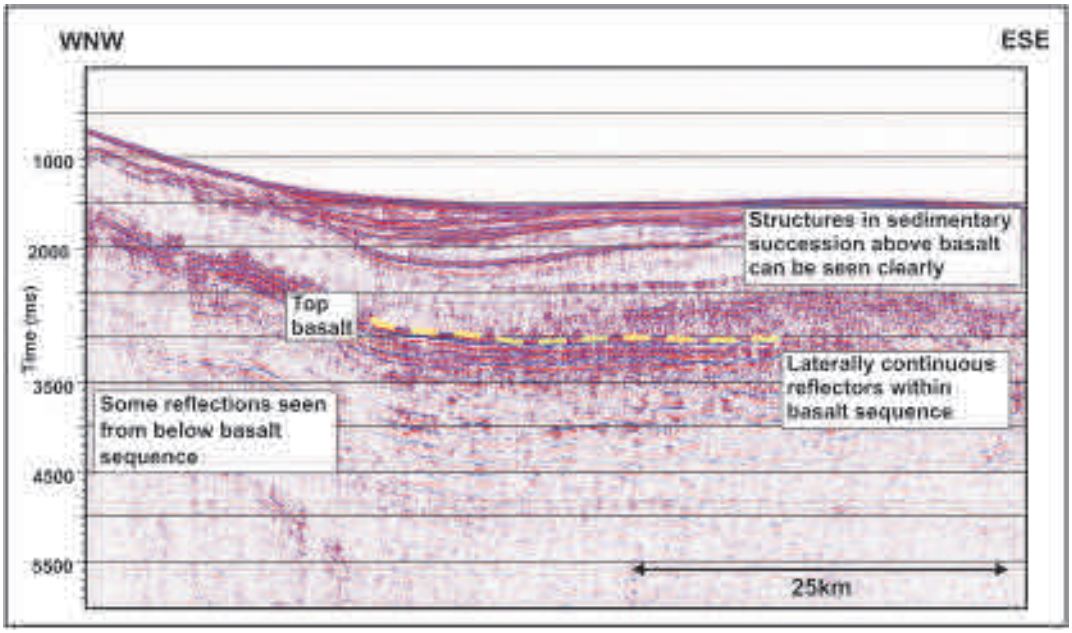

Figure 2. Seismic reflection data from the FAST profile, Faroe-Shetland Basin (England *et al*., 2005). The source was designed to maximise penetration through basalts, using large airguns to increase low-frequency energy. A long offset was used, allowing better multiple suppression by normal moveout strategies.

basalts is of importance in understanding their temporal and spatial evolution in a basin wide context, with specific focus on the potential problems and implications to the successful exploration of sub-basalt basins. Firstly, we will outline some of the problems associated with exploration in flood basalt terrains, and introduce the developing field of flood basalt facies analysis. Focus will then be on the different scales of heterogeneity through the volcanic pile, which will have major effects on remote sensing techniques through such media. These range from heterogeneities at the 0.1 to 10 metre, or lava flow scale (intrafacies), through flow facies variations at the metre to kilometre scale and facies associations up to the seismic scale (km to 10 km). Figure 1c shows schematically how extensive these facies variations can be on a basin-wide scale. Finally, the potential effect of these heterogeneities on geophysical surveying is presented.

1.1 Exploration problems in flood basalts, volcanic rifted margins and associated basins

Seismic reflection surveying has proved good at sub-surface imaging in layered sedimentary sequences. Unfortunately, the presence of thick, layered basalt sequences (consisting predominantly of lava flows and associated lithologies) in flood basalt provinces and volcanic rifted margins creates an environment where very few clear reflections are returned from below the basalt sequence, as demonstrated in Figure 2. The poor imaging below the basalt sequence is due to loss of seismic energy by scattering and attenuation. This is caused by the high impedance contrast between sediments and basaltic lava flows at the top of the basalt succession, and by energy loss within the basalt sequence from its internal heterogeneity. This internal heterogeneity causes more of a problem than the high impedance contrast (Martini and Bean, 2002), causing the production of multiples, scattering due to layering and rubbly flow tops, and transmissions and mode conversions at flow boundaries (Maresh *et al*.,

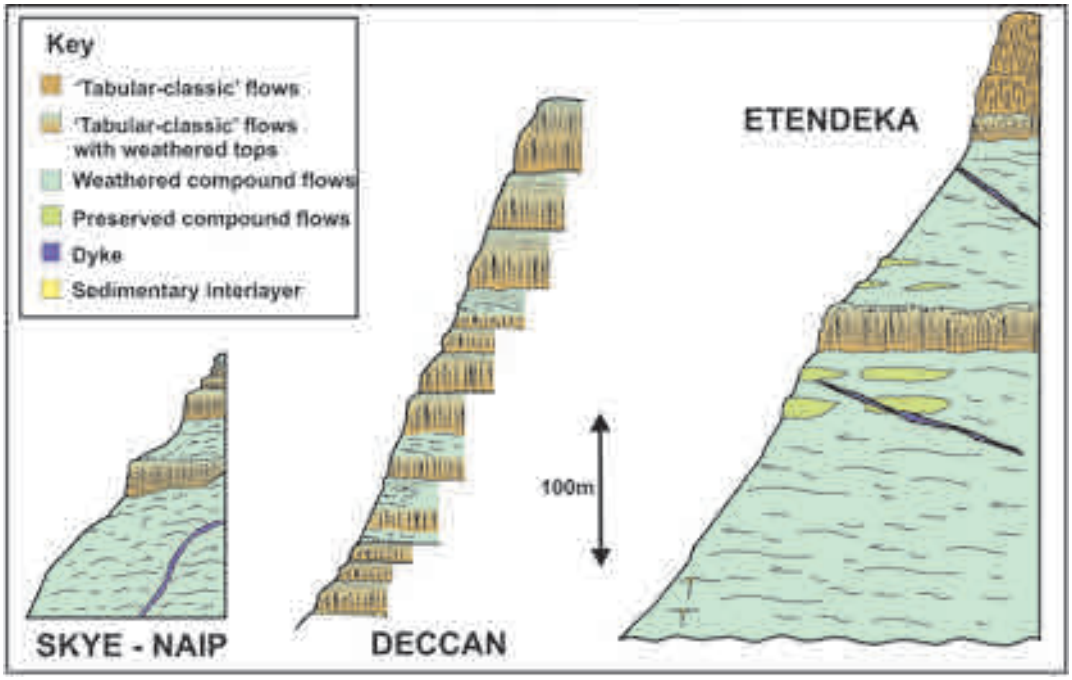

Figure 3. Examples of the internal heterogeneity present in flood basalt provinces. Sections were produced from field sketches. Note that the scale is the same for each example. It can be seen that there is a wide variation in the internal architecture of a flood basalt province - flow thicknesses, numbers and associations all vary within a province and between provinces. Provinces are, however, made of the same "building blocks" allowing classification schemes to be developed, as discussed in Section 2.

2006). The net effect is that higher frequencies are preferentially attenuated.

Recent research by Maresh *et al*. (2006) investigated the cause of the attenuation in layered basaltic lava flows, using a vertical seismic profile from Well 164/07-1. The measured attenuation was considerably higher than predicted from laboratory basalt samples, indicating that either the impedance contrasts caused by layering, or the scattering caused by the rugose interfaces between flows, contributed to the attenuation. Modelling synthetic seismograms showed that the layering caused more attenuation than the rubbly surfaces, and the layering alone could account for the observed attenuation in the borehole data. However, this study only considered the effect of one rubbly surface, and the combined effect of many such interfaces may be significant.

Due to the loss of high frequencies through attenuation, strategies for imaging below basalt sequences have concentrated on the use of low frequencies. Wide-angle surveys have also had some success in imaging the base of the basalt sequence, as fewer interbed multiples are present in long-offset data (White *et al*., 2005). Work has also focussed on optimizing the source and receivers to obtain better low frequency data. Ziolkowski *et al*. (2003) argued for the use of larger airguns and for towing both the seismic source and receiver at a depth of around 20 m below the sea surface. Towing the source at a greater depth allows a reflection from the sea surface, to increase constructive interference at low frequencies (Maresh and White, 2005).

Martini *et al*. (2005) highlighted the need for synthetic seismic data based on realistic 3D geology. A 3D model of a basalt succession could be used for the simulation of realistic seismic data, to test seismic acquisition and processing techniques. This would help to improve imaging

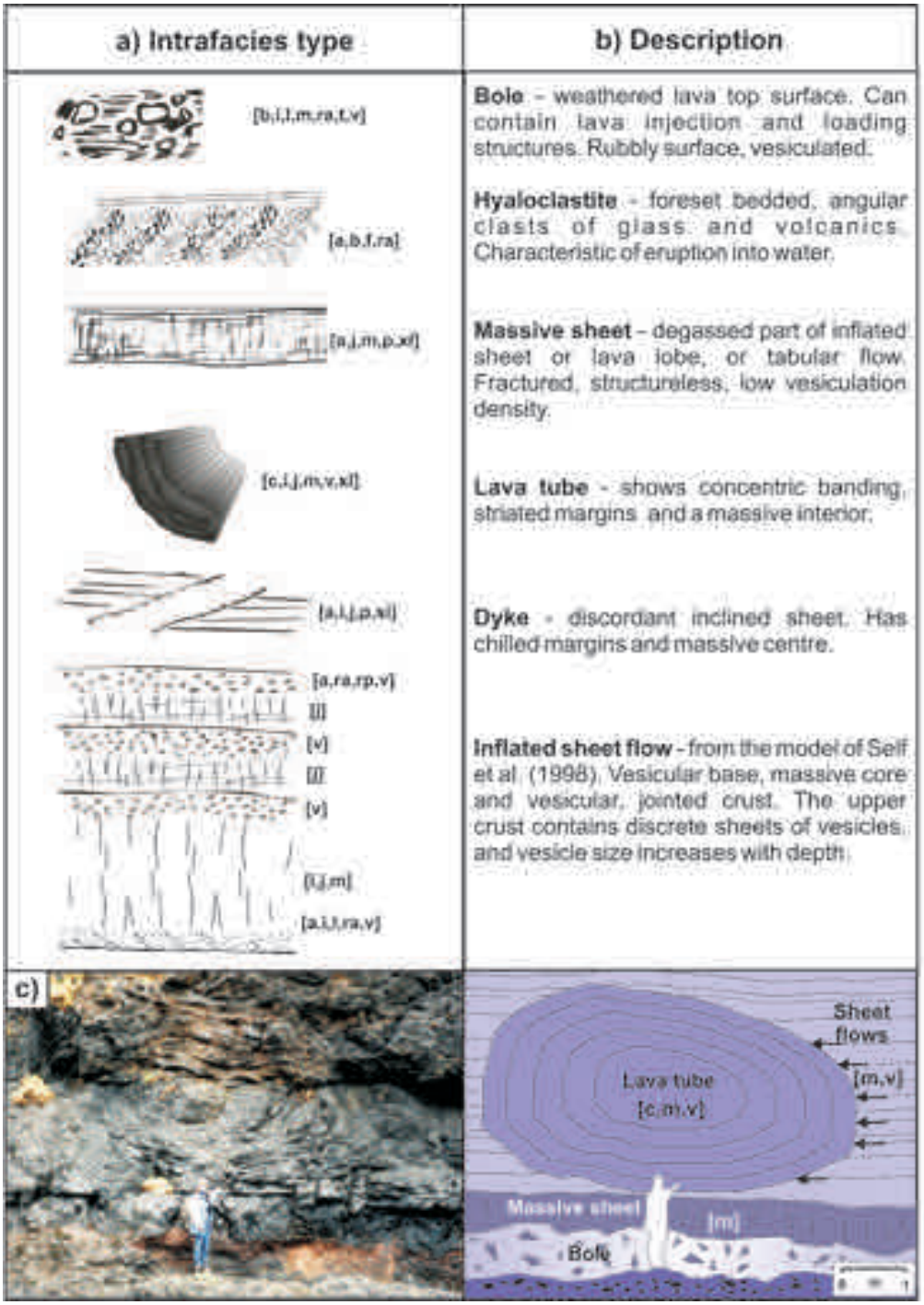

Figure 4. The intrafacies classification scheme. **a**) The components which make up the various facies are indicated next to the diagrams. The abbreviations are as follows: **a** aphanitic margin, **b** bole material, **c** concentric banding, **f** foreset bedding, **i** injection structure, **j** regular jointing, **l** loading structure, **m** massive, **p** porphyritic texture, **ra** rubbly surface, **rp** ropy surface, **si** inclined sheet, **t** tuffaceous material, **v** vesiculated, **xl** medium to coarsely crystalline. Other intrafacies include Flow base, Flow top (unweathered), Sill, Pillow lava and Volcaniclastic. **b**) Descriptions of the different intrafacies shown in a). **c**) An example of various intrafacies from Talisker Bay, Skye, NAIP. There is a high degree of complexity evident in this one small area. For further details on all the intrafacies and their components, see Single and Jerram, 2004.

below the basalt sequence, and provides the purpose for current work outlined in this contribution.

1.2 The developing field of detailed facies analysis in flood basalt terrains

As discussed above, it is the internal heterogeneity of the flood basalt provinces and volcanic rifted margins that give rise to imaging problems. Figure 3 shows three logged sections highlighting the vertical stacking of lava flows preserved in onshore examples of flood basalt sequences. Each lava flow contains internal heterogeneities and this, together with the stacking variations, would give rise to complex seismic characteristics in the offshore setting. Clearly, a simple solid block of massive basalt would present very different seismic characteristics (e.g. an intrusive sill). Characterising this internal heterogeneity would give valuable information on the effect of the basalt sequence on the passage of seismic energy. An additional problem affecting exploration of such areas is the prediction of inter- and intraflow variations. Here, a clear understanding of the volcanic facies distributions and their physical properties is of vital importance.

Although borehole data gives a vertical section, the existence of lateral variations (e.g. Passey, 2004) requires us to use onshore analogues where much more data is available to characterise the 3D nature. Recent studies have investigated the physical characteristics of continental flood basalt provinces, and classification schemes have been developed (see below). No onshore analogues are available for the parts of volcanic rifted margins found further offshore; facies here (such as the outer seaward dipping reflectors facies of Planke *et al*., 2000) have been classified based on their shape and characteristic reflections in seismic data. However, the use of 3D seismic data has led to successful imaging of the structure of sill complexes (e.g. Corfield *et al*., 2004; Thomson, 2005, Smallwood and Maresh, 2002).

The facies concept, used extensively in describing sedimentary rocks, was first applied to volcanic rocks by Cas and Wright (1987). A facies is defined as a body of rock with specified characteristics (Reading, 1986), and these characteristics are definable and distinguish the rock from other facies. The facies is considered to

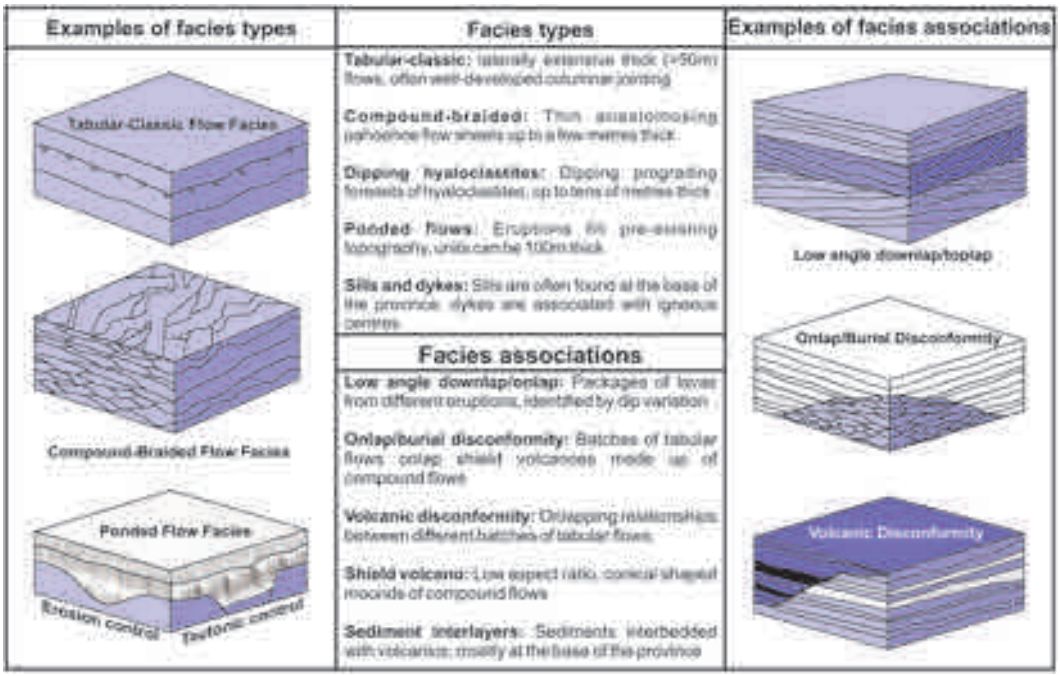

Figure 5. The facies classification scheme. 3D examples of different facies are shown, together with a list of the facies from the classification scheme of Jerram (2002).

be the product of a particular set of conditions (Cas and Wright 1987). In volcanic successions different styles of volcanism, different magma compositions, topographic variations or differences in rates of eruption, produce the various facies (e.g. Jerram, 2002). An understanding of the evolution of a province can thus be gained from facies analysis.

Facies variation has been observed at scales from the individual lava flow to the seismic scale. Classification schemes have been developed by Single and Jerram (2004) (Figure 4) at the intrafacies scale (flow scale variation), at the facies scale (e.g. Jerram, 2002) (Figure 5) and at the seismic scale (e.g. Planke *et al*., 2000) (Table 1). Although these schemes are not fully inclusive of all facies types found in flood basalt provinces, they provide a conceptual means of defining volcanic heterogeneities and comparing between different flood basalt provinces, thus providing a systematic framework for observations. In the following section we will summarise these conceptual facies models and show key examples from a number of onshore flood basalt provinces.

2 Flood basalts and volcanic rifted margins – a facies architecture approach

2.1 How to define key volcanic facies

Cas and Wright (1987) suggested that facies should be defined by two major groups of characteristics. Firstly, the geometry of the facies should be considered - the volume, shape, pre-existing relief and flow direction. Secondly, the lithology is equally important - the composition and the texture. The lithology is subject to later modification by processes such as erosion and alteration. Deformation may also be important as flood basalt provinces are often situated at sites of later rifting. Flood basalt provinces are massive outpourings of predominantly tholeiitic basalt, but also basaltic andesite lava which cover several thousands of square kilometres, and build to a thickness of up to a few kilometres. Yet they are made up of many hundreds or thousands of individual lava flows, with associated sills and dyke facies which vary on the scale of metres and in some cases centimetres. Therefore, it is useful to consider the heterogeneities present at different scales of observation. Below, we consider scales of heterogeneity from 1) intrafacies variations, 2) facies variations and associations and 3) seismic scale variations.

2.1.1 Scales of heterogeneity 1 - intrafacies

To understand the volcanology and physical characteristics of flood basalts it is important to look beyond their geochemical variations, and quantify them from a volcanological perspective. For example, in attempting to understand lava emplacement mechanisms, Self *et al*. (1996; 1997) divided flows into an upper crust, core and basal zone, based on vesicle patterns, jointing style and petrographic texture. The abundance of flows with this three-part structure led to an emplacement model of inflating pahoehoe flows whereby liquid lava is injected under a solidifying crust. This model was proposed as the standard way of emplacing large pahoehoe lava fields (e.g. Self *et al*., 1996).

A similar approach was taken by Single and Jerram (2004), who developed a classification scheme for small-scale heterogeneity within lava flows, which built on the core-crust observations to include bole horizons, lava tubes, small intrusions and so on. Within this scheme, known as the 'intrafacies' scheme (Single and Jerram, 2004), information on rock properties important for geophysical modelling are also included, providing a systematic method of characterising features in lava sequences and allowing comparisons to be made between provinces. A summary of the different intrafacies components is shown in Figure 4.

This intrafacies classification scheme is based on field observations and covers heterogeneities visible at the smallest scale of field observation: the 0.1-10 m scale. These intrafacies can provide information on the method of emplacement, for example if vesicle patterns characteristic of inflated pahoehoe flows are present (e.g. Cashman and Kauahikaua, 1997), and give information on the association of flow breakouts, inflation textures and lava feeder systems (e.g. Single and

Jerram, 2004). Intrafacies components are identified by changes in properties such as fracturing, vesiculation, shape of the feature, and the presence of palaeosols. The effect of these properties on geophysical parameters such as seismic velocity, density and magnetic susceptibility is discussed further in Section 3.1.

2.1.2 Scales of heterogeneity 2 - flow facies and facies associations

Studies of heterogeneity at the facies scale are somewhat more common than those at the intrafacies scale, but they are still relatively few in number. Walker (1972) proposed the terms "simple" and "compound" for describing two very different types of lava flow, based on observations of numerous recent and ancient lava flows. Compound flows are defined as those that are divisible into smaller flow lobes, whereas simple flows are composed of only one flow unit.

Jerram (2002) outlined the major facies types and facies associations providing a systematic way of describing heterogeneity at the metre to kilometre scale (summarised in Figure 5). Facies types described in this scheme include different types of lava flow (incorporating the terminology of Walker, 1972), hyaloclastites, ponded flows, sills and dykes, based on observations made in the Etendeka, Karoo, Columbia River, Ethiopia, Deccan and British Palaeogene provinces. Sedimentary units may also be present as interbeds, and would thus be included in this

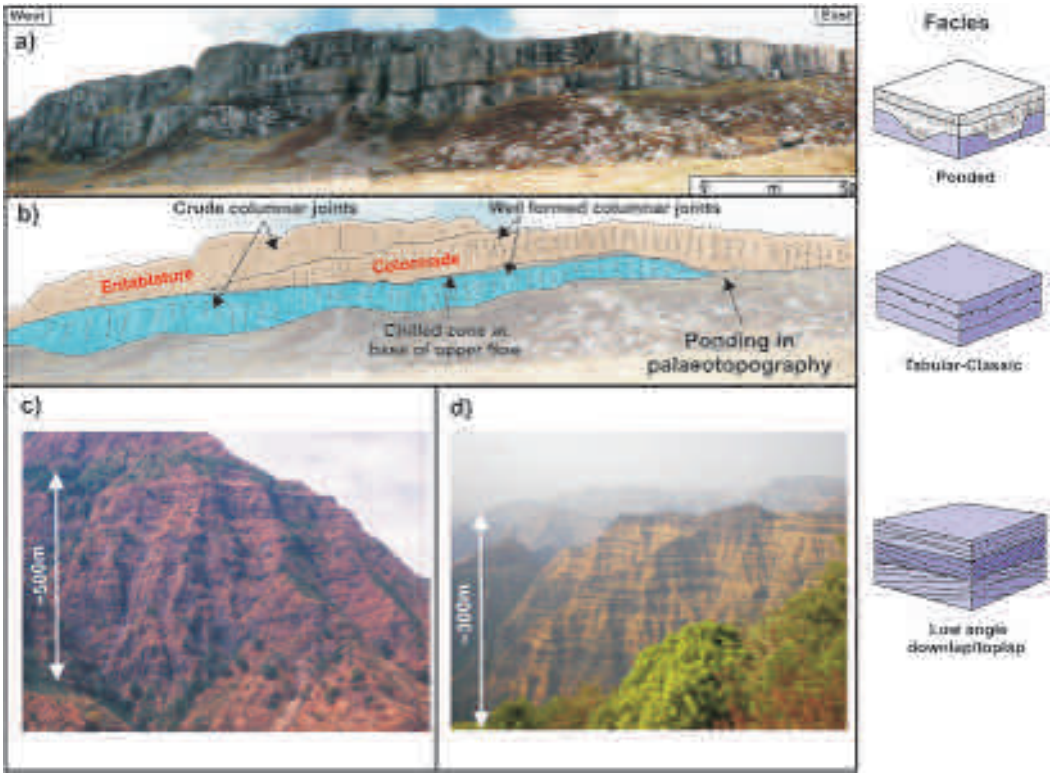

Figure 6. Examples of facies types. **a**) is a cliff section from Talisker Bay, Skye, NAIP. **b**) shows the interpretation. Two flows are present, both showing the tabular-classic facies type. The upper flow shows a well-developed entablature and colonnade structure. The ponded flow facies type is also present here, on the right of the photograph. Also note the onlapping relationship between the two flows a) and b) Examples of ponding and pinch out in thick flows Talisker area, NAIP. Examples of facies associations: Large scale onlap-offlap facies variations in Ethiopia and Deccan. **c**) is from the Ethiopian Traps, Africa. **d**) is from the Deccan Traps, India. Note that the scale is similar - in both areas, this facies association is present on a scale of hundreds of metres. Modified from Jerram 2002; Jerram and Widdowson 2005.

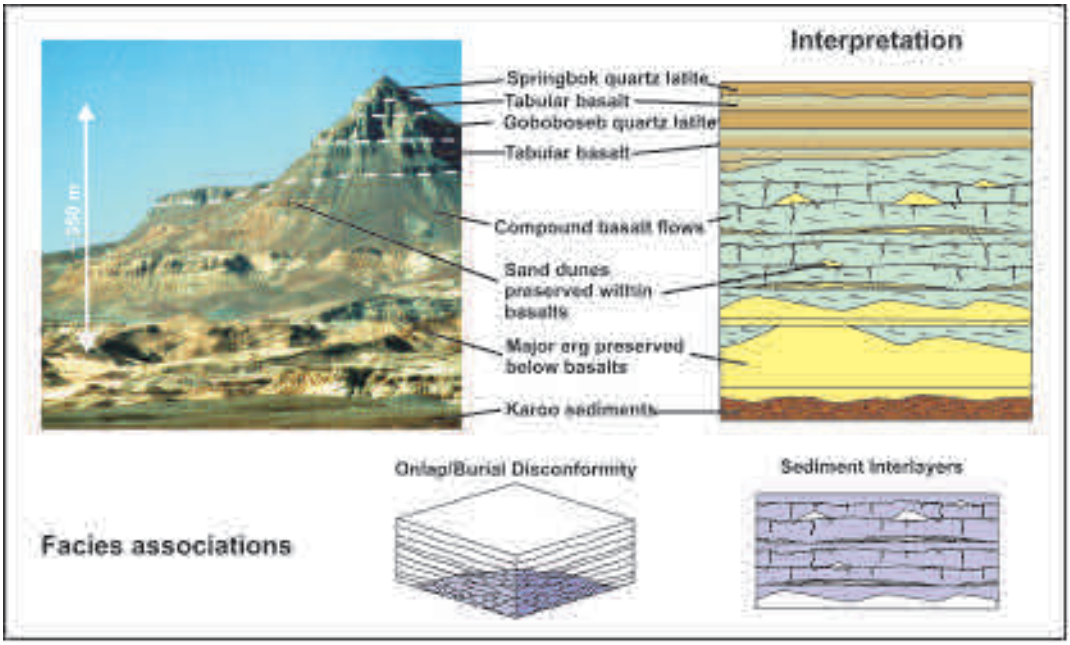

Figure 7. Section through the Etendeka flood basalts, NW Namibia. Compound-braided and tabular-classic flow facies can both be observed here, as well as onlap disconformity and sediment interlayer facies associations.

classification scheme. Examples are shown in Figures 6 and 7. These facies are identified by their characteristic physical properties, and are made up of the intrafacies described above. In common with facies analysis in sedimentary successions, their interpretation is based on analogues with present-day examples. The eruptions of Kilauea, Hawaii, and Laki, Iceland, are the most commonly used analogues, with preserved flood basalt lavas which range in size from examples similar to modern day occurrences to flows that are orders of magnitude larger (Jerram, 2002), with the largest flows having volumes of 1000s of km^3 (e.g. the Roza Member, Columbia River, Self *et al*., 1997).

The study of the relationships between these facies is particularly important when considering offshore examples. Geometrical stacking patterns may be seen on seismic scales, so if we know what causes these patterns in well-exposed onshore examples, we can then begin to identify facies offshore. Characteristic stacking patterns include disconformities, downlap and shield volcanoes. Examples are given in Figures 6 and 7.

The facies classification scheme has been applied successfully in several flood basalt provinces. In the NAIP, Passey and Bell (2007) characterised the morphologies of the Faroe Islands Basalt Group, incorporating a facies approach such as the scheme of Jerram (2002). The three main eruptive sequences (the Beinisvørð, Malinstindur and Enni formations) demonstrate a variety of different facies architectures. The Beinisvørð (previously Lower) Formation is dominated by a 'tabular-classic' facies architecture, which is interpreted as indicating that the flows were erupted as single continuous flows from fissure systems. In contrast, the Malinstindur (previously Middle) formation consists mainly of 'compound-braided' flows, suggesting a different eruptive style whereby flows were not erupted continuously, but at longer time intervals from separate shield volcanoes. The Enni (previously Upper) formation has a mixture of the two facies architectures. Hyaloclastite and sill facies are also present (Ellis *et al.*, 2002; Rasmussen and Noe-Nygaard, 1970). Single (2004) also studied the NAIP - in this case, the facies architecture of the Talisker Bay area, Skye.

A series of tabular-classic flows was found overlying compound-braided flows, with a transitional sequence in between.

Jerram and Widdowson (2005) showed how facies variations may successfully be compared across different provinces. The architecture of the Deccan, the Paranã-Etendeka and the NAIP was considered; despite many differences between the provinces, there are some key similarities. All show initial low-volume eruptions followed by a main phase of relatively short duration (1-5Ma). This main phase is often characterised by large volume, extensive tabular flows.

The characteristic associations of these facies are important in developing models of the basin as a whole. In the NAIP and the Paranã-Etendeka, early shield volcanoes were buried by later large-volume flat-lying tabular flows, creating volcanic disconformities (Jerram and Widdowson, 2005). The Ethiopian flood basalt province, where the top of the flood basalt sequence is preserved, contains a series of flood basalts overlain by large shield volcanoes (Kieffer *et al*., 2004). Clearly the relative abundance and distribution of key facies within flood basalt sequences will help define their evolution both spatially and temporally, particularly below the resolution of or in the absence of geochronological markers.

2.1.3 Scales of heterogeneity 3 - seismic scale

Seismic imaging can pick out features greater than 50 m thick, so individual lava flows (typically 5-30 m thick) cannot be identified. A certain amount of heterogeneity is, however, still apparent within processed seismic data. This has been characterised by Planke *et al*. (1999; 2000) who developed a facies classification scheme at the seismic scale (1 to 10's of kilometres). Their scheme is summarised in Table 1, and is based on seismic reflection data from the Atlantic and Western Australia volcanic rifted margins. The different facies were identified by their gross form, and the reflection characteristics of their boundaries and internal reflections.

In order to gain a better understanding of offshore basaltic successions, the use of onshore

Facies	**Shape**	**Characteristics**	**Probable flow scale components**
Inner flows	Sheet	High amplitude top reflector, high amplitude parallel internal reflectors	Mixture of compound and tabular facies and volcaniclastics; subaqueous.
Lava delta	Bank	Prograding clinoform internal reflectors	Hyaloclastites and volcaniclastics; coastal
Landward flows	Sheet	High amplitude top reflector, high amplitude parallel internal reflectors	Mixture of compound and tabular facies; subaerial.
Inner Seaward Dipping Reflectors (SDR)	Wedge	Divergent-arcuate internal reflectors, toplap seen on top reflector	Mixture of compound and tabular facies; subaerial.
Outer high	Mound	Strong top reflector, chaotic internal reflector	Hyaloclastites and volcaniclastics; shallow marine
Outer SDR	Wedge	Divergent-arcuate internal reflectors, weaker than Inner SDR	Deep marine compound facies, pillow lavas, sediments and sills.

Table 1. Summary of the seismic scale facies of Planke *et al.* (1999; 2000) and their probable flow scale components (e.g equivalents of Jerram 2002).

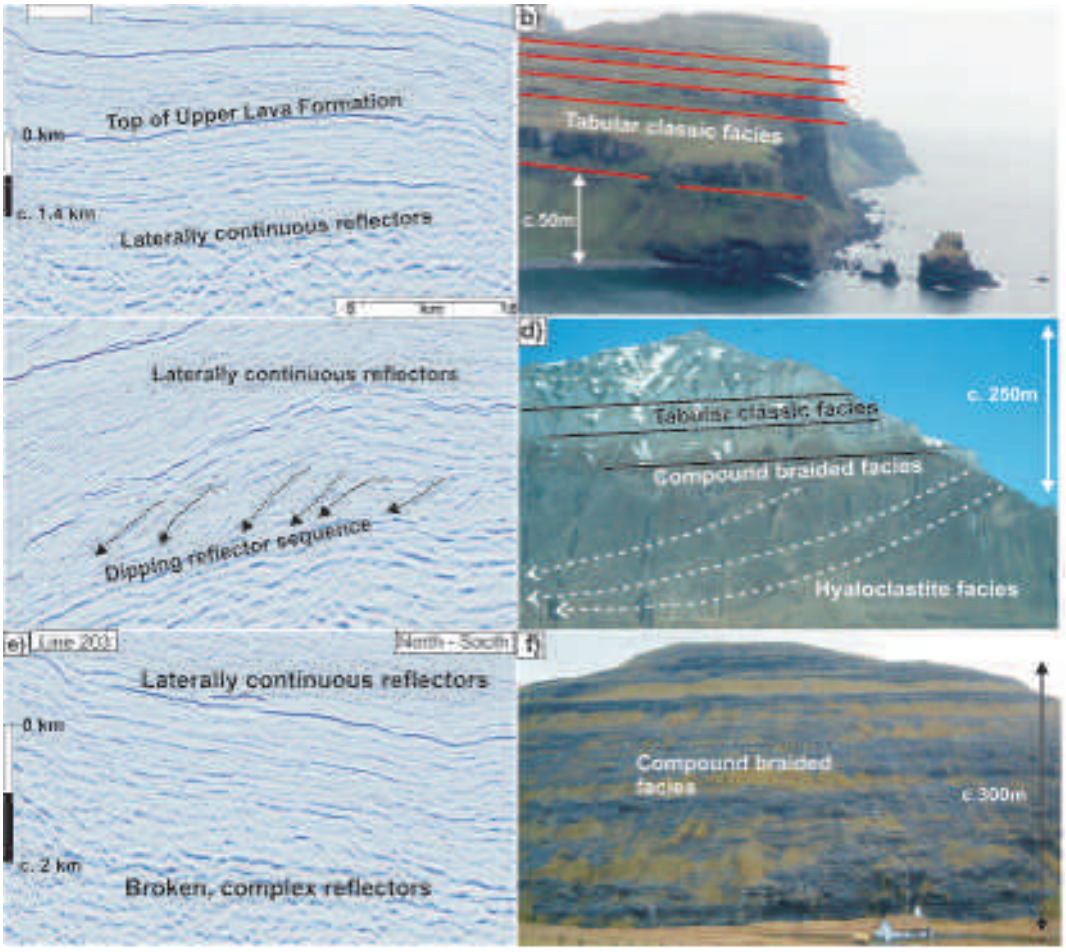

Figure 8. Facies observed in seismic sections and onshore analogues. **a**) Section of GFA-99 line 205 interpreted as showing tabular-type facies. The GFA-99 seismic data was collected approximately 60km SE of the Faroe Islands in the Faroe-Shetland Basin. **b**) Example of thick tabular flows from Talisker Bay, Skye. **c**) Section of GFA-99 line 107 showing dipping reflector sequences interpreted as hyaloclastite facies. Section changed from W-E to E-W for comparison with onshore analogue. **d**) Cliff section in the Nausuaq area, West Greenland shows hyaloclastites dipping and prograding eastwards onto Jurassic sediments. The hyaloclastites are covered by subaerial compound and tabular flows; this section is interpreted as filling a water-filled basin. Photograph courtesy of D.G. Pearson. **e**) Section of GFA-99 line 203 showing contrasting seismic signatures. **f**) These different seismic signatures are interpreted as compound braided facies overlain by tabular classic facies. An example of compound braided facies is shown from NW Streymoy, Faroe Islands. Seismic data courtesy of Western-Geco.

analogues is crucial to the interpretation of seismic data. In table 1 we consider the possible flow scale components which make up the seismic scale facies described by Planke *et al*. (1999; 2000). In the offshore region around the Faroe Islands, it has proved possible to correlate onshore observations with offshore seismic data. Ellis *et al*. (2002) determined the offshore extent of the Lower, Middle and Upper Lava Formations from seismic data. Passey (2004) correlated material from Well 214/04-1 (240 km east of the Faroe Islands) with the Lower Basalt Formation, based on geochemical data, although there is also evidence of a lateral facies change. Seismic interpretation

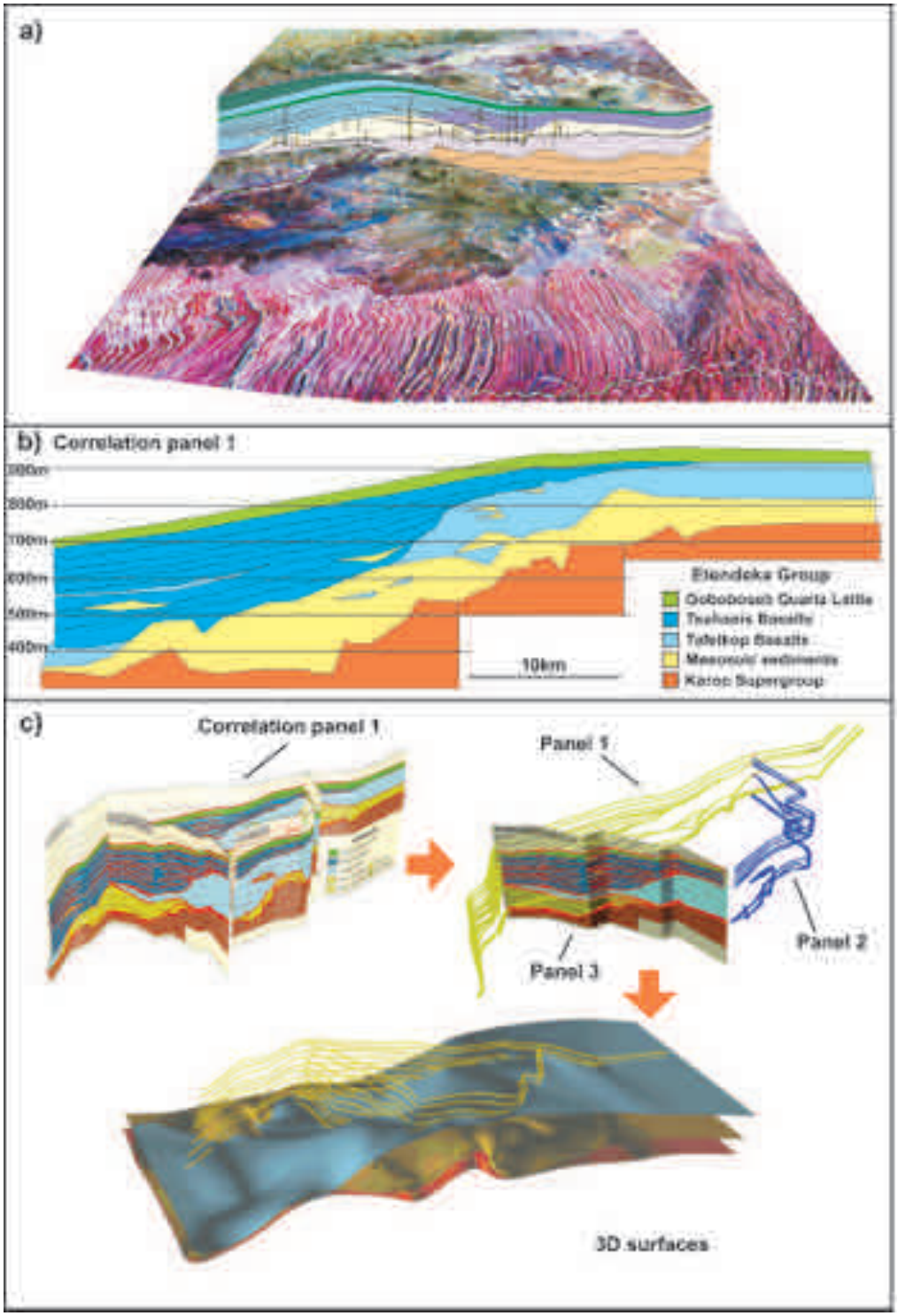

Figure 9. Construction of a 3-D model from surfaces identified on correlation panels. **a**) Fully geo-spatially constrained logs and correlation panels. Data based on detailed satellite located logs. 3D data collected for key surfaces through the lava sequence can include many types of data such as satellite, laser scanning, 3D located logs and so on. **b**) A correlation panel of key surfaces is constructed through logged data (e.g. Jerram *et al*., 1999). **c**) Panels orientated into true 3-D position, key surfaces identified from the 3 correlation panels, and 3-D surfaces reconstructed as GoCad™ interpolated surfaces (adapted from Jerram and Robbe, 2001).

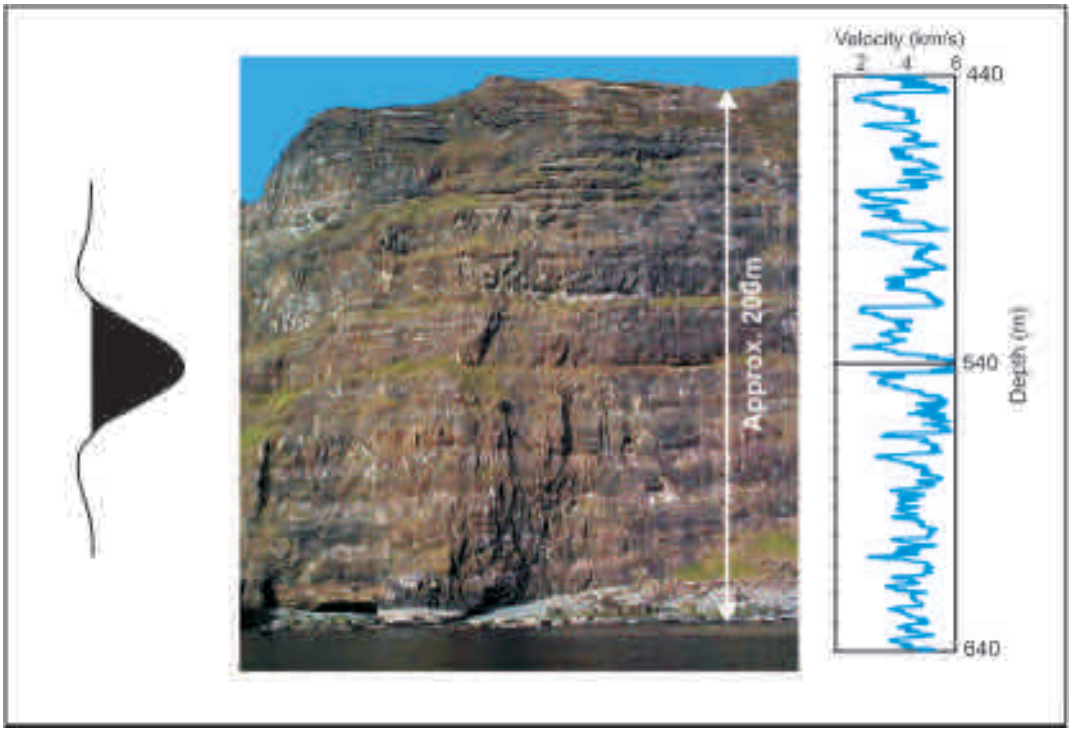

Figure 10. Schematic representation of the effects of basalt heterogeneity on the velocity profile through a lava pile. All elements of this diagram are on approximately the same scale. Photo from Skye Main Lava Series showing a typical layered basalt sequence. A seismic wavelet is included for comparison. The velocity profile is taken from ODP Hole 642E (Eldholm *et al*., 1987) and shows the wide and rapid variation in P-wave velocity.

by Single (2004) identified tabular lavas, delta fans, compound braided flows and hyaloclastites, with direct analogues onshore (Figure 8). These facies were identified by their characteristic shapes and internal reflections. The thickness and areal extent of these facies were also calculated with the aid of gravity models along the seismic lines.

2.2 3D geological models

As can be seen from the facies associations of Jerram (2002), heterogeneity within a flood basalt sequence is not limited to 1D layering. The protracted build-up of lava packages results in marked lateral variations within the provinces (e.g. Jerram and Widdowson, 2005). These lateral facies variations exist and must be taken into account in geophysical modelling of areas with flood basalt cover. Constructing 3D models allows improved geophysical modelling (see Section 3), as well as improved understanding of the evolution of flood basalt provinces. As yet, limited examples of 3D geological models of flood basalt basins exist. However, there is promising initial work on reconstructing onshore flood basalt basin analogues. This aims to capture further information on heterogeneities and facies distributions as well as providing realistic geometries for geophysical modelling. Jerram and Robbe (2001) produced a 3D geological model in GoCad™ for the Etendeka region in Namibia (Figure 9), and were able to use this to map out a palaeo-shield volcanic feature in the sequence. Further detailed examples have been constructed for the Skye lavas in the British Palaeogene (e.g. Single and Jerram, 2004), and for the offshore Faroe-Shetland (Single 2004).

3 A geophysical perspective

To improve sub-basalt imaging, it is necessary to understand the effect of a layered, heterogeneous basalt sequence on the seismic wave. This is currently poorly constrained; it is known that a flood basalt sequence causes scattering and preferentially attenuates high frequencies (Maresh *et al*., 2006). Knowledge of how the heterogeneity within the basalt sequence affects the seismic wave will enable optimisation of the seismic method. Figure 10 schematically highlights some of the geophysical problems that a thick basalt sequence would cause. Accordingly, in the following section some of the issues related to the geophysical response of basaltic sequences will be explored.

3.1 Relating basaltic facies to geophysical properties

To ascertain how the geological heterogeneity affects geophysical data, it becomes necessary to link physical rock properties to the different facies. Methods to distinguish between facies include the amount of vesiculation, jointing, flow thickness, colour, shape of the feature and so on. We must determine which of these also affect geophysical data. The different physical properties that affect geophysical surveying methods are summarised in Table 2.

We can say qualitatively that these rock properties affect the various geophysical methods, based on our knowledge of, for example, the relationship between jointing and seismic velocity. Unfortunately, no studies have yet quantified the relationship between the physical properties and the geophysical data. The rock properties are complex and change dramatically over centimetre scales.

However, the effect of the variations in rock properties can be observed in borehole data. Both commercial and academic boreholes have penetrated thick basalt sequences and wireline logs recorded include sonic, density, gamma ray and resistivity. Site 642 of Ocean Drilling Program (ODP) Leg 104, on the Vøring margin, was one of the first drill holes to penetrate deeply into a volcanic margin sequence. Approximately 687m of basaltic lava flows were cored and logged, and 137 individual lava flows were identified (Eldholm *et al.*, 1987). The internal structure of the lava flows was identified from the core, and Planke (1994) correlated variations in logging measurements with the internal structure of the lava flows. A cyclic pattern was observed in the velocity, density, resistivity, porosity and gamma ray logs, and an example of the cyclicity present in the velocity log is presented in Figure 10.

This cyclic pattern has also been observed in other drill holes. Planke and Cambray (1998) reported similar data from Hole 917A (East

Geophysical method	Operative physical property	Rock properties which may affect this
Seismic	Seismic velocity and density	Vesicularity, jointing, geochemistry, degree of alteration, size of flow, shape of flow
Gravity	Density	Vesicularity, geochemistry, degree of alteration
Resistivity	Electrical conductivity	Vesiculation, geochemistry, degree of alteration, jointing, pore fluid
Magnetic	Magnetic susceptibility and remanence	Geochemistry, degree of alteration

Table 2. Adapted from Kearey *et al*. (2002) and Single (2004).

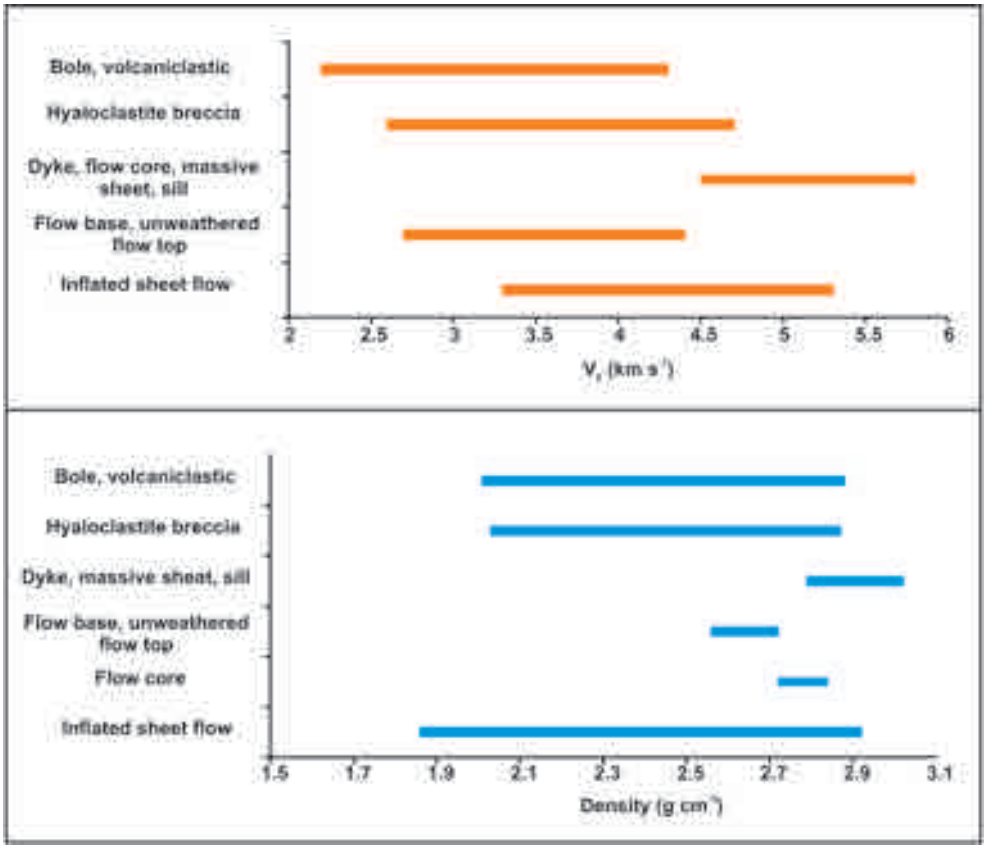

Figure 11. Physical properties of different intrafacies. **a**) P-wave velocities for the different intrafacies. It can be seen that there is a wide velocity range. Massive intrafacies such as dykes and flow cores are faster, while more vesicular intrafacies such as boles are slower. The inflated sheet flow shows a range. **b**) Densities for the different intrafacies. Again, there is a wide range, from high density flow cores to low density boles. Data from the SIMBA database.

Greenland Margin). Bücker *et al*. (1998) summarised the data from ODP Holes 553A and 990A, where the cyclic pattern is also observed. A similar pattern can also be seen in Well 164/7-1 in the Rockall Trough (Archer *et al*., 2005) and the Lopra 1/1A borehole on the Faroe Islands (Boldreel, 2006).

In all cases where core was also recovered, a strong correlation was found between the flow structure and the log responses. The log response reflects the three-part structure commonly observed in basalt flows, described by Self *et al*. (1997) and summarised in Section 2.1.1 above. The flow core corresponds to a high velocity, high density, and low gamma ray interval on the wireline log data (e.g. Planke 1994; Boldreel 2006). The flow crust is correlated to a lower velocity, lower density, and high gamma ray interval. This correlation is possible because the internal structure of the basalt flows is present as variations in the amount of vesicles, jointing and weathering of the basalt. These variations also indicate the boundaries between flows and strongly affect conventional logging tools.

As yet, few studies have linked this borehole data to the facies observed onshore. The EU 5th Framework SIMBA (ENK6-CT-2000-00075) project collated a database from various wells in the North Atlantic (Single, 2004). From this, the range of P-wave velocities and densities present for the different intrafacies has been identified, and the results are shown in Figure 11. It is

immediately apparent that there is a wide velocity range within a basalt succession, which must be taken into account in geophysical models involving basalt sequences. Boles, volcaniclastics, flow bases and flow tops all have a relatively low P-wave velocity (around 2.5-4.5 km s^{-1}) whereas dykes, flow cores and sills have a relatively high P-wave velocity (around 4.5-6 km s^{-1}. A similar pattern is observed for density, although boles, volcaniclastics and hyaloclastites have a wide range. It can also be seen that the different intrafacies cannot be distinguished by the range of velocities and densities alone. Fully characterising the different facies in terms of their logging properties would be an important step towards building accurate geophysical models of basalt sequences.

3.2 How does heterogeneity affect seismic data?
We have seen in previous sections that basalt sequences are heterogeneous at a variety of scales. As discussed in section 1.1, a basalt sequence causes attenuation of high frequency seismic waves by scattering and the production of multiples. In this section, the theoretical basis for the effect of heterogeneity on the seismic wave is examined, focussing in particular on the different types of scattering caused by different scales of heterogeneity. A heterogeneity, as discussed in this section, is for example a lava flow crust, which is different to the flow core above and below it. A flow crust is typically of the order of one to ten metres thick, depending on the overall flow thickness, so an average heterogeneity for a lava crust could be considered as 5 m.

Figure 12 shows the interplay between the size of the heterogeneity, the seismic wavelength of the input pulse, and the length of the travel path of the seismic wave. The labelled boxes correspond to the approximations that can be used to correct for the scattering, and thus obtain clear reflections. "Geometric optics" are the simple rules of reflection and refraction. The heterogeneity (a) is large relative to the wavelength (λ) and the travel path (L). Therefore, a coherent reflection is received from the boundary of the heterogeneity, and it can be imaged. In the "Diffraction theory" region, it is still possible to image the heterogeneity, provided that diffraction is taken into account and single scattering approximations (e.g. Born theory, Aki and Richards, 1980) can be used.

"Quasi-homogeneous" means that the seismic wave only responds to the average properties of the region it travels through - the heterogeneity is so small relative to the wavelength that it does not affect the seismic wave. No measurable reflection is received from the boundary of the heterogeneity.

In the "Saturated region", the seismic wave encounters a large number of heterogeneities that are large relative to the wavelength. The seismic energy undergoes multiple reflection events creating a complex path, which can no longer be analysed by conventional approximations. The saturated region expands or contracts depending on the scattering strength - this is greater if the heterogeneities exhibit a large velocity and density contrast. Figure 12 shows how the saturated region expands for a material with a high scattering strength such as a layered basalt sequence.

If we consider a layered basalt sequence with a thickness of 2000 m, the two-way travel path of a seismic wave through this sequence (L) has a value of 4000 m. A typical heterogeneity size (a), for example a flow crust as described above, would be around 5 m. $\frac{L}{a}$ in this case is 800, which plots on the y-axis of Figure 12. If a high frequency seismic wave, with a frequency of 40 Hz, passes through the basalt sequence, λ is 100m if the average velocity is 4000 m s^{-1}. ka (on the x-axis) is thus approximately 0.3 (Point A on Figure 12). If a low frequency seismic wave (10 Hz) passes through this basalt sequence, ka is approximately 0.79 (Point B on Figure 12). It can be seen that a low frequency wave (Point B) falls within the "Diffraction regime", whereas a high frequency wave falls on the boundary of the "Saturated region". This more complex scattering at high frequencies explains why low frequency waves have produced better imaging through basalt sequences.

Figure 12 may also be able to predict which approximations could be used when attempting to image the different facies. It may be able to give information on which facies can be better imaged.

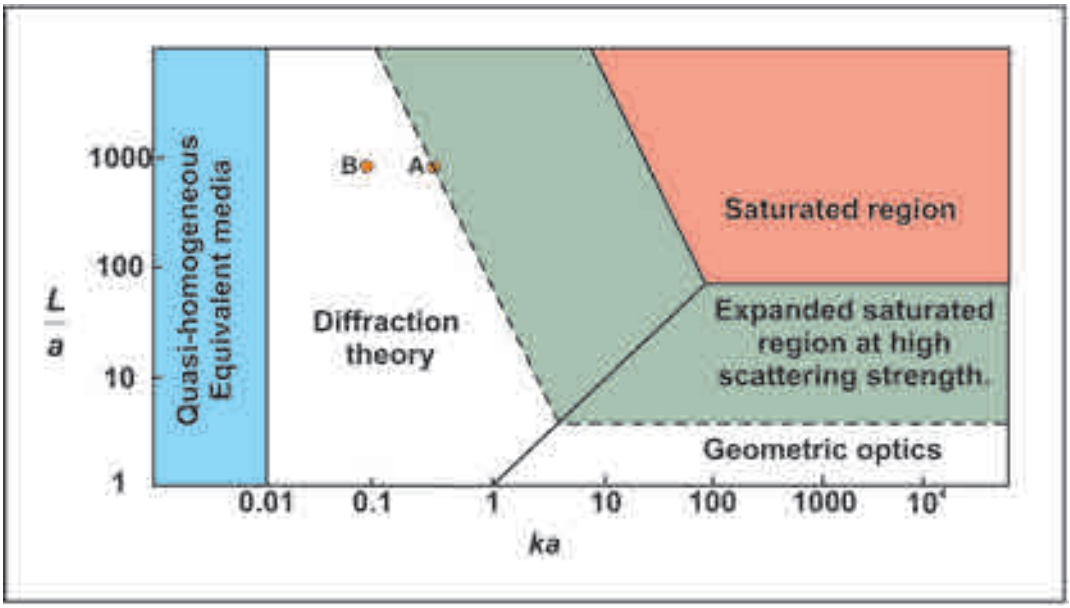

Figure 12. Classification of scattering problems in heterogeneous media. Regions where different methods of analysis can be used are highlighted. *L* is the extent of the heterogeneous region, or the distance the seismic wave travels (the travel path). *a* is the size of the heterogeneity. *k* (the wavenumber) is where λ is the wavelength. Adapted from Wu and Aki, 1988.

For example, a hyaloclastite sequence has small internal impedance contrasts, so it has a weak scattering strength. The saturated region is smaller in this case, so the likelihood of clear imaging is greater. A sequence comprising compound-braided facies would contain many strong impedance contrasts between the flow crust and the flow core. Its scattering strength would therefore be stronger, and the saturated region would be larger. More work is needed to characterise the size of the heterogeneities in the different facies, the average velocity within the facies, and the thickness of the sequence. This will allow the construction of diagrams similar to Figure 12, with appropriately sized regions depending on the scattering strength.

4 Summary and closing remarks

Understanding flood basalts and volcanic rifted margins in terms of their properties (size and geometry of key facies, physical properties of the rocks) and how these relate to their geophysical responses is an important emerging subject. It is also useful to consider whether the inverse is possible: can we derive information on facies from geophysical data? There are still relatively few studies of the facies architecture of flood basalts and volcanic rifted margins, but they have the potential to help improve sub-basalt imaging and our knowledge of the development of the lava sequences.

Improved data on geometric and facies changes within basalt sequences will enable the creation of more robust models of flood basalt provinces, which in turn will help us understand how they relate to geophysical problems. This will facilitate better data acquisition and processing. Within this context, much more information is required about the scale of flood basalt lavas. Current information is often skewed to data from the few largest lava flows (e.g. Roza Mbr, Columbia River Basalts; Self *et al*., 1996), as these have been well mapped out. Current data on 3D geometries and volumes is limited for the various facies types described in this contribution.

The role of hyaloclastites in the onset of flood

volcanism should be another focus for future research. In many cases, for example in the NAIP, the occurrence of thick hyaloclastite sequences (up to 700 m in Greenland) requires deep waterways. The presence of such deep waterways needs to be accounted for in our models of uplift due to plume impact (e.g. White and McKenzie, 1989). They can also be mapped out to define the palaeo-environments immediately prior to flood basalt eruption. Additionally, the role of hyaloclastites as potential hydrocarbon reservoirs warrants further investigation.

The incorporation of additional imaging techniques such as MT and Gravity (e.g. Hautot *et al*., 2007) has proved successful, and multidisciplinary studies such as SIMBA (CONTRACT N°: ENK6-CT-2000-00075; EU 5th Framework), have provided a template for the integrated approach we must take to understanding flood basalts and associated basins in the offshore setting. Strength may be gained by the combined approach to characterising flood volcanic sequences and their associated margins. With geologists and geophysicists working together, it will be possible to overcome some of the main issues and to develop new strategies for further exploration.

Acknowledgements

DAJ is the TOTAL lecturer at Durham University. This work was supported by funding provided to DAJ by Elf/TOTAL GRC and the EU 5th Framework Project SIMBA (CONTRACT N°: ENK6-CT-2000-00075). The GFA-99 survey data were acquired by WesternGeco and made available to the SIMBA project researchers. RWH is a NERC Advanced Research Fellow (NERC/J/S/2002/00745).

References

Aki, K. and Richards, P.G. 1980. *Quantitative seismology: theory and methods Volume II*. W.H Freeman and Company, San Francisco.

Archer, S.G., Bergman, S.C., Iliffe, J., Murphy, C.M. and Thornton, M. 2005. Palaeogene igneous rocks reveal new insights into the geodynamic evolution and petroleum potential of the Rockall Trough, NE Atlantic Margin. *Basin Research* 17: 171-201.

Boldreel, L.O. 2006. Wireline log-based stratigraphy of flood basalts from the Lopra-1/1A well, Faroe Islands. *In*: Chalmers, J.A. and Waagstein, R. (eds) *Scientific results from the deepened Lopra-1 borehole, Faroe Islands*. Geological Survey of Denmark and Greenland Bulletin 9: 7-22.

Bücker, C.J., Delius, H., Wohlenberg, J. and Leg 163 Shipboard Scientific Party. 1998. Physical signature of basaltic volcanics drilled on the northeast Atlantic volcanic rifted margins. *In*: Harvey, P.K. and Lovell, M.A. (eds) *Core-Log Integration*, Geological Society, London, Special Publications 136: 363-374.

Cas, R.A.F. and Wright, J.V. 1987. *Volcanic successions: modern and ancient.* Allen and Unwin, London.

Cashman, K.V. and Kauahikaua, J.P. 1997. Reevaluation of vesicle distributions in basaltic lava flows. *Geology* 25: 419-422.

Corfield, S.M., Wheeler, W., Karpuz, R., Wilson, M. and Helland, R. 2004. Exploration 3D seismic over the Gjallar Ridge, Mid-Norway: visualization of structures on the Norwegian volcanic margin from Moho to seafloor. *In*: Davies, R.J., Cartwright, J.A., Stewart, S.A., Lappin, M., Underhill, J.R. (eds) *3D Seismic Technology: Application to the Exploration of Sedimentary Basins*. Geological Society, London, Memoirs 29: 177-185.

Cox, K.G. 1980. A model for flood basalt volcanism. *Journal of Petrology* 21: 629-650.

Cox, K.G. 1993. Continental magmatic underplating. *Philosophical transactions of the Royal Society of London A* 342: 155-166.

Eldholm, O., Thiede, J., Taylor, E. and Shipboard Scientific Party, 1987. *Proceedings of the Ocean Drilling Program, Initial Reports* 104: College Station, TX (Ocean Drilling Program).

Eldholm, O. and Grue, K. 1994. North Atlantic volcanic margins: dimensions and production rates. *Journal of Geophysical Research* 99: 2955-2968.

Ellis, D., Bell, B. R., Jolley, D. W. and O'Callaghan, M. 2002. The stratigraphy, environment of eruption and age of the Faroes Lava Group, NE Atlantic Ocean. *In*: Jolley, D.W. and Bell, B.R. (eds) *The North Atlantic Igneous Province: Stratigraphy, Tectonic, Volcanic and Magmatic Processes*. Geological Society, London, Special Publications 197: 253-269.

England, R.W., McBride, J.H. and Hobbs, R.W. 2005. The role of Mesozoic rifting in the opening of the NE Atlantic: evidence from deep seismic profiling across the Faroe-Shetland Trough. *Journal of the Geological Society, London* 162: 661-673.

Hautot, S., Single, R. T., Watson, J., Harrop, N., Jerram, D. A., Tarits, P., Whaler K. and Dawes, G. 2007 3-D magnetotelluric inversion and model validation with gravity data for the investigation of flood basalts and associated volcanic rifted margins *Geophys. J. Int*. 170: 1418-1430.

Jerram, D.A., Mountney, N. and Stollhofen, H. 1999. Facies architecture of the Etjo Sandstone Fm. and its interaction with the Basal Etendeka flood basalts of NW Namibia: implications for offshore analogues. *In*: Cameron, N., Bate, R. and Clure, V. (eds) *The oil and gas habitats of the South Atlantic*. Geological Society, London, Special Publications 153: 367-380.

Jerram, D.A. and Robbe, O. 2001. Building a 3-D geologic model of a Flood Basalt: an example from the Etendeka, NW Namibia. *Electronic Geosciences* 6:1.

Jerram, D.A. 2002. Volcanology and facies architecture of flood basalts. *In*: Menzies, M.A., Klemperer, S.L., Ebinger, C.J. and Baker, J. (eds) *Volcanic Rifted Margins*. Geological Society of America Special Paper 362: 121-135.

Jerram, D.A. and Widdowson, M. 2005. The anatomy of Continental Flood Basalt Provinces: geological constraints on the processes and products of flood volcanism. *Lithos* 79: 385-405.

Kearey, P., Brooks, M. and Hill, I. 2002. *An Introduction to Geophysical Exploration*. Third Edition, Blackwell Science Publications, Oxford.

Kieffer, B., Arndt, N. Lapierre, H. Bastien, F., Bosch, D., Pecher, A., Yirgu, G., Ayalew, D., Weis, D., Jerram, D.A., Keller, F. and Meugniot, C. 2004. Flood and Shield Basalts from Ethiopia: Magmas from the African Superswell. *Journal of Petrology* 45: 793-834.

Kumar, D., Bastia, R. and Guha, D. 2004. Prospect hunting below Deccan basalt: imaging challenges and solutions. *First Break* 22: 35-39.

Maresh, J. and White, R.S. 2005. Seeing through a glass, darkly: strategies for imaging through basalt. *First Break* 23: 27-33.

Maresh, J., White, R.S., Hobbs, R.W. and Smallwood, J.R. 2006. Seismic attenuation of Atlantic margin basalts: Observations and modelling. *Geophysics* 71: B211-B221.

Martini, F. and Bean, C.J. 2002. Application of pre-stack wave equation datuming to remove interface scattering in sub-basalt imaging. *First Break* 20: 395-403.

Martini, F., Hobbs, R.W., Bean, C.J. and Single, R.T. 2005. A complex 3D volume for sub-basalt imaging. *First Break* 23: 41-51.

Menzies, M.A., Klemperer, S.L., Ebinger, C.J. and Baker, J. 2002. Characteristics of volcanic rifted margins. *In*: Menzies, M.A., Klemperer, S.L., Ebinger, C.J. and Baker, J. (eds) *Volcanic Rifted Margins*. Geological Society of America Special Paper 362: 1-14.

Naylor, P.H., Bell, B.R., Jolley, D.W., Durnall, P. and Fredsted, R. 1999. Palaeogene magmatism in the Faroe-Shetland Basin: influences on uplift history and sedimentation. *In*: Fleet, A.J. and Boldy, S.A.R. (eds) *Petroleum Geology of Northwest Europe: Proceedings of the 5th Conference*: 545-558.

Passey, S.R. 2004. *The Volcanic and Sedimentary Evolution of the Faroe Plateau Lava Group, Faroe Islands and Faroe-Shetland Basin, NE Atlantic.* PhD thesis, University of Glasgow.

Passey, S.R. and Bell, B.R. 2007. Morphologies and emplacement mechanisms of the lava flows of the Faroe Islands Basalt Group, Faroe Islands, NE Atlantic Ocean. *Bulletin of Volcanology* DOI: 10.1007/s00445-007-0125-6.

Planke, S. 1994. Geophysical response of flood basalts from analysis of wireline logs: Ocean Drilling Project Site 642, Vøring volcanic margin. *Journal of Geophysical Research* 99: 9263-9278.

Planke, S., Cambray, H. 1998. Seismic properties of flood basalts from Hole 917A downhole data, Southeast Greenland volcanic margin. *In*: Saunders, A.D., Larsen, H.C. and Wise, S.W. (eds) *Proceedings of the Ocean Drilling Program, Scientific Results*. Volume 152: 453-462.

Planke, S., Alvestad, E. and Skogseid, J. 1999. Seismic characteristics of basaltic extrusive and intrusive rocks. *The Leading Edge* 18: 342-348.

Planke, S., Symonds, P.A., Alvestad, E. and Skogseid, J. 2000. Seismic volcanostratigraphy of large-volume basaltic extrusive complexes on rifted margins. *Journal of Geophysical Research* 105: 19335-19351.

Rasmussen, J. and Noe-Nygaard, A. 1970. *Geology of the Faeroe Islands (Pre-Quaternary).* Trans: Henderson, G. Geological Survey of Denmark, Copenhagen 1/25.

Reading, H.G. 1986. *Sedimentary Environments and Facies*. Second Edition, Blackwell Scientific Publications, Oxford.

Sain, K., Zelt, C.A. and Reddy, P.R. 2002. Imaging of subvolcanic Mesozoics in the Saurashtra peninsula of India using traveltime inversion of wide-angle seismic data. *Geophysical Journal International* 150: 820-826.

Self, S., Thordarson, T., Kesthelyi, L., Walker, G.P.L., Hon, K., Murphy, M.T., Long, P. and Finnemore, S. 1996. A new model for the emplacement of Columbia River basalts as large, inflated pahoehoe lava flow fields. *Geophysical Research Letters* 23: 2689-2692.

Self, S., Thordarson, T. and Keszthelyi, L. 1997. Emplacement of continental flood basalt lava flows. In: Mahoney, J. J. and Coffin, M. F. (eds) *Large Igneous Provinces: Continental, Oceanic, and Planetary Flood Volcanism*. American Geophysical Union Geophysical Monograph 100: 381-410.

Self, S., Widdowson, M., E Thordarson, T. and Jay, A.E. 2006. Volatile fluxes during flood basalt eruptions and potential effects on the global environment: A Deccan perspective. Earth and Planetary Science Letters, Volume 248, Issues 1-2, Pages 518-532.

Single, R.T. 2004. *The facies architecture of large ig-*

neous provinces: an integrated geological and geophysical approach to the characterisation of volcanic successions in 3-D. PhD thesis, University of Durham.

Single, R.T. and Jerram, D.A., 2004. The 3-D facies architecture of flood basalt provinces and their internal heterogeneity: examples from the Palaeogene Skye Lava Field. *Journal of the Geological Society, London,* 161: 911-926.

Smallwood, J.R. and Maresh, J. 2002. The properties, morphology and distribution of igneous sills: modelling, borehole data and 3D seismic from the Faroe-Shetland area. *In*: Jolley, D.W. and Bell, B.R. (eds) *The North Atlantic Igneous Province: Stratigraphy, Tectonic, Volcanic and Magmatic Processes*. Geological Society, London, Special Publications 197: 271-306.

Thomson, K. 2005. Volcanic features of the North Rockall Trough: application of visualisation techniques on 3D seismic reflection data. *Bulletin of Volcanology* 67: 116-128.

Walker, G.P.L., 1972. Compound and Simple Lava Flows and Flood Basalts. *Bulletin of Volcanology* 35: 579-590.

White, R.S. and McKenzie, D. 1989. Mantle plumes and flood basalts. *Journal of Geophysical Research* 100: 17543-17585.

White, R.S., Spitzer, R., Christie, P.A.F., Roberts, A., Lunnon, Z., Maresh, J. and iSIMM Working Group 2005. Seismic imaging through basalt flows on the Faroes Shelf. *In*: Ziska, H., Varming, T. and Bloch, D. (eds) *Proceedings of the 1st Faroe Islands Exploration Conference* Annales Societatis Scientiarum Færoensis (Faroese Society of Science and Humanities), Tórshavn, Supplementum 43: 11-31.

Wu, R.S. and Aki, K., 1988. Introduction: Seismic Wave Scattering in Three-dimensionally Heterogeneous Earth. *Pure and Applied Geophysics* 128: 1-6.

Ziolkowski, A., Hanssen, P., Gatcliff, R., Jakubowicz, H., Dobson, A., Hampson, G., Li, X.-Y. and Liu, E. 2003. Use of low frequencies for sub-basalt imaging. *Geophysical Prospecting* 51: 169-182.

New seismic imaging methods, dating, intrusion style and effects of sills: A drilled example from the Faroe-Shetland Basin

JOHN R. SMALLWOOD[1*] AND ALYSON HARDING[1,2]

[1] Hess Ltd., Level 9, The Adelphi Building, 1-11 John Adam St, London, WC2N 6AG, UK.
* Email: john.smallwood@hess.com; Tel: +44 (0) 207 331 3123
[2] Now at: Atlantic Petroleum, P.O. Box 1228, Gongin 9, FO-110 Tórshavn, Faroe Islands.
Email: alysonh@petroleum.fo

ABSTRACT

Much of the eastern part of the Faroe Islands' continental shelf is affected by the intrusion of igneous sills. Where there are no overlying lavas to degrade the deeper seismic image, excellent 3D seismic imaging quality is achieved, including that of the sill penetrated by Well 6004/16-1z. Whereas published techniques such as opacity rendering allow good visualisation of sills, improved interpretations are shown here using band-limited impedance inversion, dip-steered filtering and automatic geobody extraction. The stratigraphically highest sill in the 6004/16-1z area has a 'saucer' morphology and is 8-12 km in diameter. The inner sill of this "Trykleývari" intrusion consists of three smaller bowls, and was emplaced into Early Paleocene Danian (T10) sandstones which form the reservoir in the 6004/16-1z Marjun discovery 2 km along strike. The sill was apparently sourced from the centre of one or more of the three sub-bowls, and possibly also from a peripheral inclined sheet, an observation new to 3D seismic sill studies. The inclined sheets surrounding the inner sill transgress through younger (T20s) shales to the peripheral lobes of the outer sill which lie at the base of Selandian-age (T28) sandstones. Ar/Ar dating from an apophysis (offshoot) of the sill complex encountered in 6004/16-1z returned an age of 56.0±1.2 Ma, confirming the period of intrusion as Early Eocene, coincident within error with the latest of the Faroes lavas and continental break-up to the west. The intrusion has not degraded the porosity of the T10 sand in 6004/16-1z, which at 3000-3200 m below mudline, is 11-13%, matching expectations from the local porosity-depth trend. The sill complex has, however, caused elevated heat flows though the reservoir and overlying rocks, with vitrinite reflectance values raised locally up to 1.0 %. Although associated diagenetic changes have reduced the permeability of the Marjun reservoir to a mean of 3.6 mD, dolerite intervals penetrated within the T34 interval of Well 6005/15-1, previously interpreted as sills, are reinterpreted as extrusives, assuaging possible concerns of intrusive degradation of reservoir quality in that area.

Introduction

The Faroe-Shetland area is characterised by an extensive suite of intrusive igneous rocks, both central complexes and small-scale bodies (e.g. Naylor *et al*., 1999). Gibb and Kanaris-Sotiriou (1988) referred to the small-scale intrusions collectively as the "Faroe-Shetland sill complex", and cite earlier workers to delineate the southeast edge of the main complex, although some individual sills lie outside this boundary (Figure 1). The northwest edge of the sill complex lies beneath the extrusive lava province and is therefore determined more speculatively (Smallwood and Maresh, 2002; Figure 1). The attenuative effects of the lava pile on the seismic wavefield (Maresh *et al*., 2006) mean that only strong underlying reflectors, such as sills, are imaged (e.g. Archer *et al*., 2005) assisting this process. Within the Flett Basin, the uppermost sills lie mainly within Mesozoic strata, although a few lie within strata of the Paleocene Shetland Group (Smallwood *et al*., 2001; Figure 2). To the south, in the Judd Basin, however, the uppermost

Faroe Islands Exploration Conference: Proceedings of the 2nd Conference.
Annales Societatis Scientiarum Færoensis, Supplementum 50, 2009: 104-123

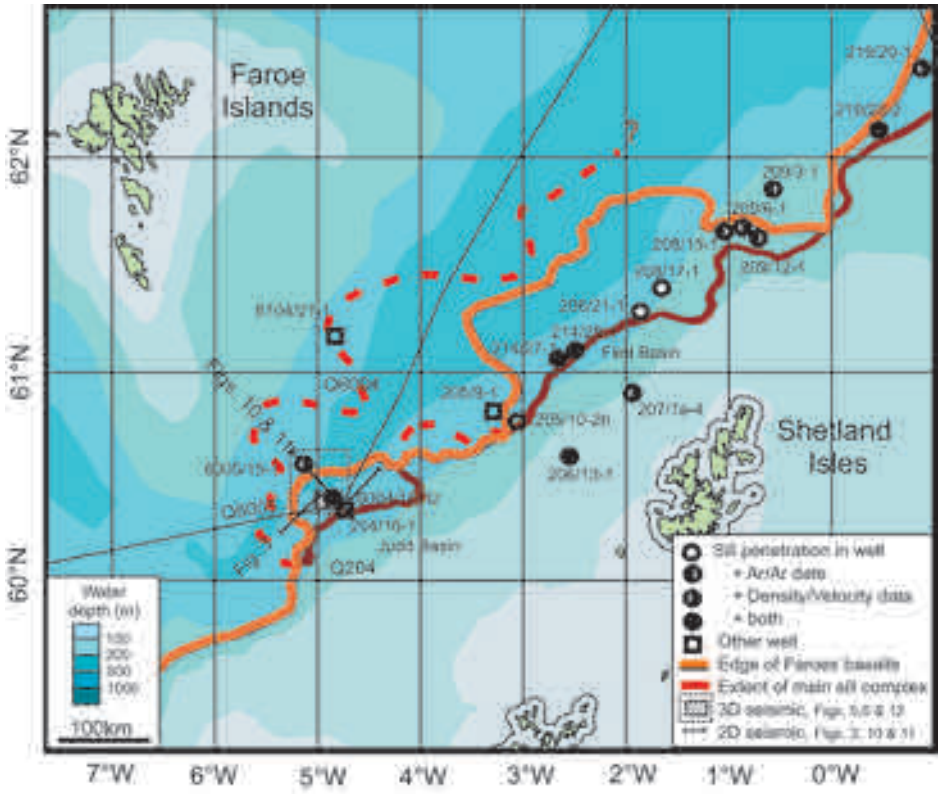

Figure 1. Faroe-Shetland area with bathymetry shaded. Location of the Faroe-Shetland Sill Complex is outlined in red. The northwestern edge of the sill complex (dashed) is uncertain due to the deterioration of seismic quality beneath the Faroes basaltic lavas (outlined in orange). Some well penetrations of sills and wells discussed in text marked with circles and squares. Seismic data line and map locations of Figures 3, 5, 6, 10, 11 and 12 are shown.

sills are more commonly hosted within strata of the Paleocene Shetland and Faroe Groups (Lamers and Carmichael, 1999; Figure 3). The general structural level of the shallowest sills follows a trend of increasing height with thicker crust and shallower basement (Smallwood and Maresh, 2002).

Several boreholes or wells have penetrated sills in the Flett Basin area (Figure 1). Samples from many of these sill borehole penetrations have provided evidence of the petrology, geochemistry and physical properties of the sills (Gibb and Kanaris-Sotiriou, 1988; Smallwood and Maresh, 2002). Petrographically, the sills are dolerites or olivine dolerites, with modal normative mineralogy indicating that they are olivine tholeiites. Such lithologies are universally denser and of higher sonic velocity than host sedimentary rocks (e.g. Planke, 1999). Such physical properties result in strong seismic reflections and excellent imaging in 3D seismic datasets (e.g. Bell and Butcher, 2002; Smallwood and Maresh, 2002; Hansen *et al*., 2004; Trude, 2004; Thomson, 2004; Figure 3). Such studies rely on a combination of detailed manual or automatic interpretation of conventional seismic reflection data or opacity rendering of these data.

In this paper, some new strategies for improved seismic interpretation of sill bodies are discussed. These strategies are illustrated by application to a compound sill in the southeast corner of the Faroes' continental shelf near Well 6004/16-1z. The sill appears to have been fed from below at one or more point sources at the periphery of un-

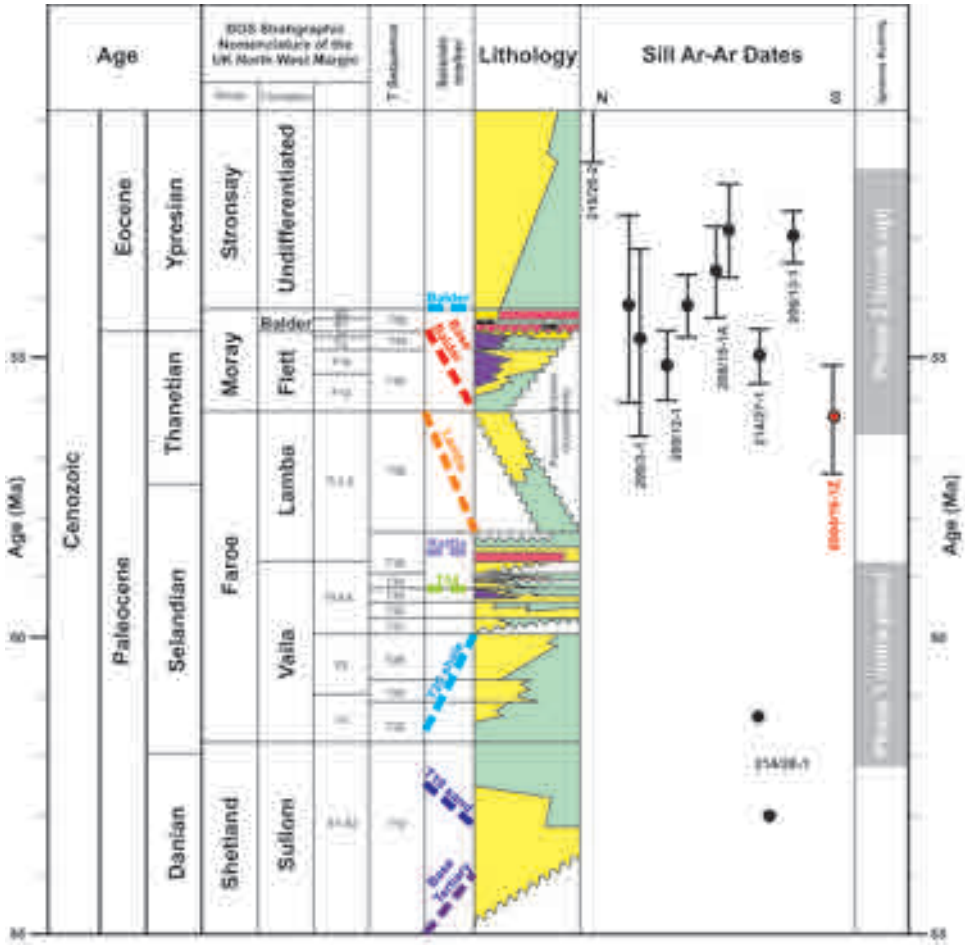

Figure 2. Stratigraphy, indicative Judd Basin lithology, approximate timescale (from Shaw-Champion *et al*. (2008) and references therein) and selected radiometric sill dates from Hitchen and Ritchie (1993), Ritchie and Hitchen (1996) and this study (6004/16-1z). Although radiometric dates range from 63.5 Ma (Early Paleocene) to 48 Ma (Late Eocene), most of the reliable dates cluster around the 56-53 Ma interval (Early Eocene). The BGS nomenclature is from Knox *et al*. (1997). T sequence scheme is based on Ebdon *et al*. (1995) and Lamers and Carmichael (1999). North Atlantic Igneous Province igneous activity phases from Saunders *et al*. (1997). The lithology column shows the approximate constituent lithologies encountered within the sequences with indicative positions of the main Figure 11 seismic horizons (dashed): Green indicates fine-grained clastics, yellow indicates sand-grade clastics, purple indicates lava, red indicates volcanic tuff and black indicates coal (not to scale). At the Paleocene-Eocene transition there is an error bar of at least 1 Ma between the absolute timescale and the stratigraphy shown (Clarke, 2002).

derlying discordant intrusions, as well as perhaps from a peripheral inclined sheet, and displays a variety of characteristic intrusion geometries. Part of the same sill complex was penetrated by Well 6004/16-1z, and igneous rock samples have undergone radiometric dating. Since the wellbore intersected the sill within the reservoir interval of the "Marjun" discovery, local and more regional effects of the intrusion on the reservoir sandstones will be discussed. Finally, the evidence for the interpretation of dolerite intervals in Well 6005/15-1 as either intrusive or extrusive is discussed.

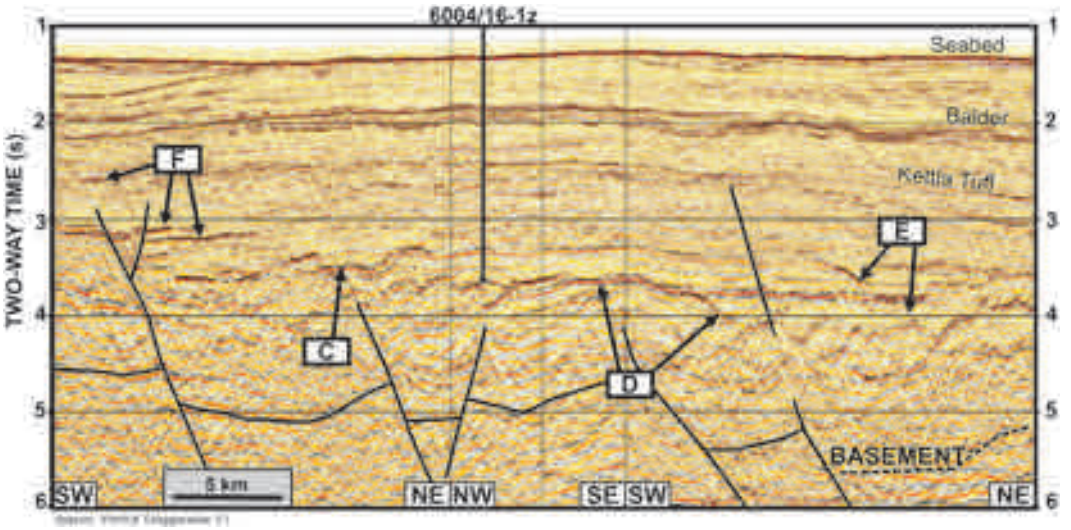

Figure 3. Seismic line in the Quads 204/6004 area, location shown in Figure 1. Plate-like and trumpet-like sills (marked "D" and "E") intrude the Lower Paleocene section. The Trykleývari sill, also shown in Figures 4, 5, 6, and 7 is marked "C". Image quality deteriorates to the southwest under the "T34" laterally extensive reflectors interpreted as lavas and associated volcanic rocks (marked "F"; Figures 10, 11 and 12). Modified after Smallwood and Maresh (2002), and shown by kind permission of Veritas DGC.

Imaging and interpretation methods

Since the physical property that gives rise to the bright reflections observed within many 3D seismic datasets is the high relative acoustic impedance of the sills, carrying out an acoustic impedance inversion to give a more physically relevant product for interpretation is an obvious step, although it has not been used in published 3D seismic sill studies to date. A quick (and inexpensive) option is to run a band-limited inversion (or combination of post-stack phase-rotation and low-cut filter) on a conventional reflection dataset (Lancaster and Whitcombe, 2000).

The dataset used here for example purposes is the 2002 survey shot by PGS and processed by CGG for operator Hess on behalf of companies including the Faroes Licence 001 and 004 partner groups (Figures 1 and 4-7). The acquisition equipment included dual airgun sources and 6 km hydrophone streamers. Unusually for the area, this survey was acquired with a north-south shooting direction. Since the processing flow targeted true amplitude preservation, band-limited impedance inversion has advantages over model-driven inversion approaches with their inherent small contrast assumptions and requirements for local well calibration. The processing flow included pre-stack time migration. Although contributing to excellent quality data, the migration can introduce a few artefacts which could be misinterpreted as intrusion features (Figures 4a and 6e).

The sill selected to illustrate the suggested visualisation and interpretation technique is the structurally highest sill in a sill complex near the centre of the Paleocene Judd Basin (Figures 1 and 3). Broadly, this sill has a 'saucer' morphology, 8-12 km across, and in cross section on the reflection data displays a wide outer sill and discordant inclined sheet surrounding an inner sill (Figure 3; cf Thomson and Hutton, 2004). The name "Trykleývari" sill (Faroese for shamrock) is used here as the inner sill consists of three sub-bowls. The seismic reflection from the Trykleývari sill lies above a stacked sequence of other bright reflections, both continuous and discontinuous (Figure 4a), which makes manual or automatic horizon-style interpretation potentially quite subjective and time consuming, with multi-z value capability a minimum requirement for successful interpretation.

Inverting the data to an impedance volume, to-

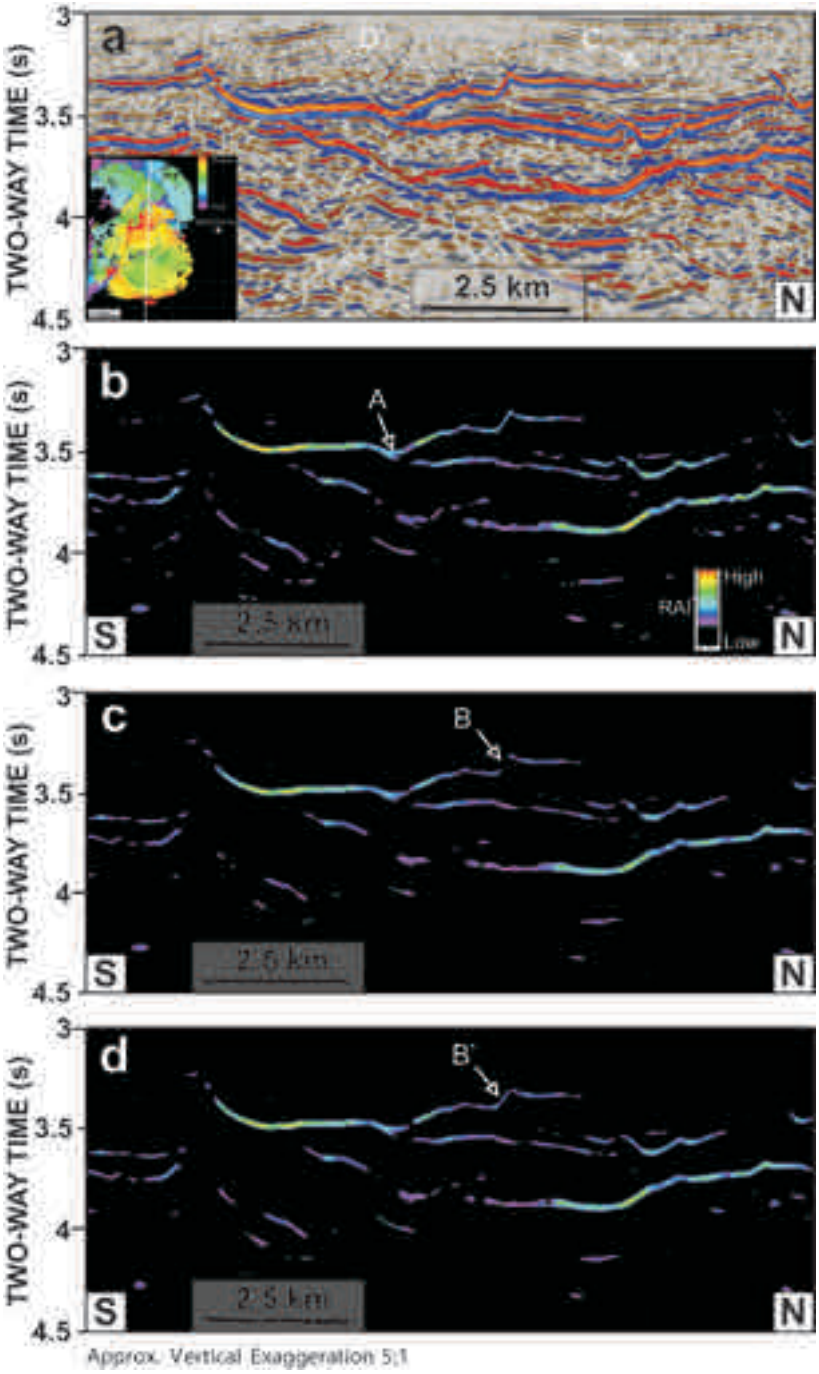

Figure 4. Band-limited impedance inversion for imaging sills: **a**) Conventional seismic line (from 3D volume) through Trykleývari sill. Location shown in inset (TWT map of geo-body extracted sills). Peripheral dyking (e.g. Thomson, 2004) appears to be present (C), but must be distinguished from migration artefact parabolas (D). **b**) Relative impedance inversion product generated from (**a**). The deepest point of the Trykleývari sill (A) is a branch-point where magma appears to have been fed from an underlying intrusion sheet. **c**) Smoothed version of (**b**), which contains less noise but at the expense of steep-dipping sill limbs (B). **d**) Dip-steered smoothed version of (**b**), in which noise is suppressed but steep dips are maintained (B').

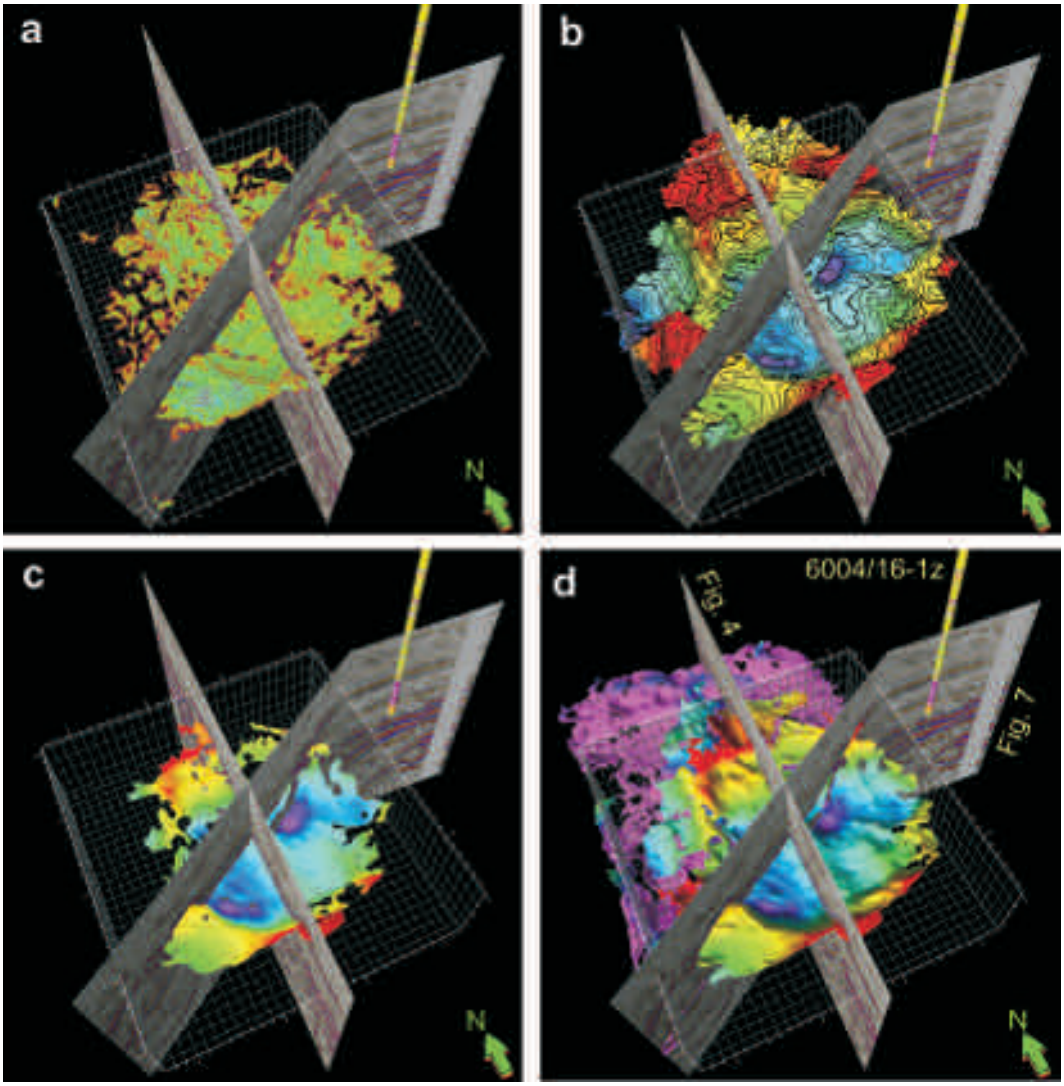

Figure 5. 3D view comparing interpretation methods for the Trykleývari sill. Horizontal Scale: Long frame ticks on X and Y axis 2 km. Vertical scale: Long frame ticks on Z axis 100 ms two-way time. Seismic lines Figures 4 and 7 and well trajectory of 6004/16-1z coloured by Gamma Ray (Yellow=low GR) included on all panels. **a**) Opacity rendering of data subcube (extent shown by grey axes) **b**) Single seed autotracked horizon from conventional 3D seismic data cube coloured by two-way time (scale as Figure 6a, red = shallow, purple = deep) **c**) Geobody extraction from band-limited inversion volume, low threshold, same colouring as (**b**). **d**) Geobody extraction from same data volume, with higher threshold, same colouring as (**b**). Underlying seismically connected sills were included during the geobody extraction.

gether with selection of a suitable colour bar, isolates the events associated with impedance values likely to be associated with sills (Figure 4b), although some relatively incoherent noise is still present in the section. This can be removed with a (horizontal) smoothing filter (Figure 4c). The disadvantage of such a process is that steeply-dipping discordant intrusive limbs have quite a similar character to the type of noise such an operator is designed to remove. The solution is to run a dip-

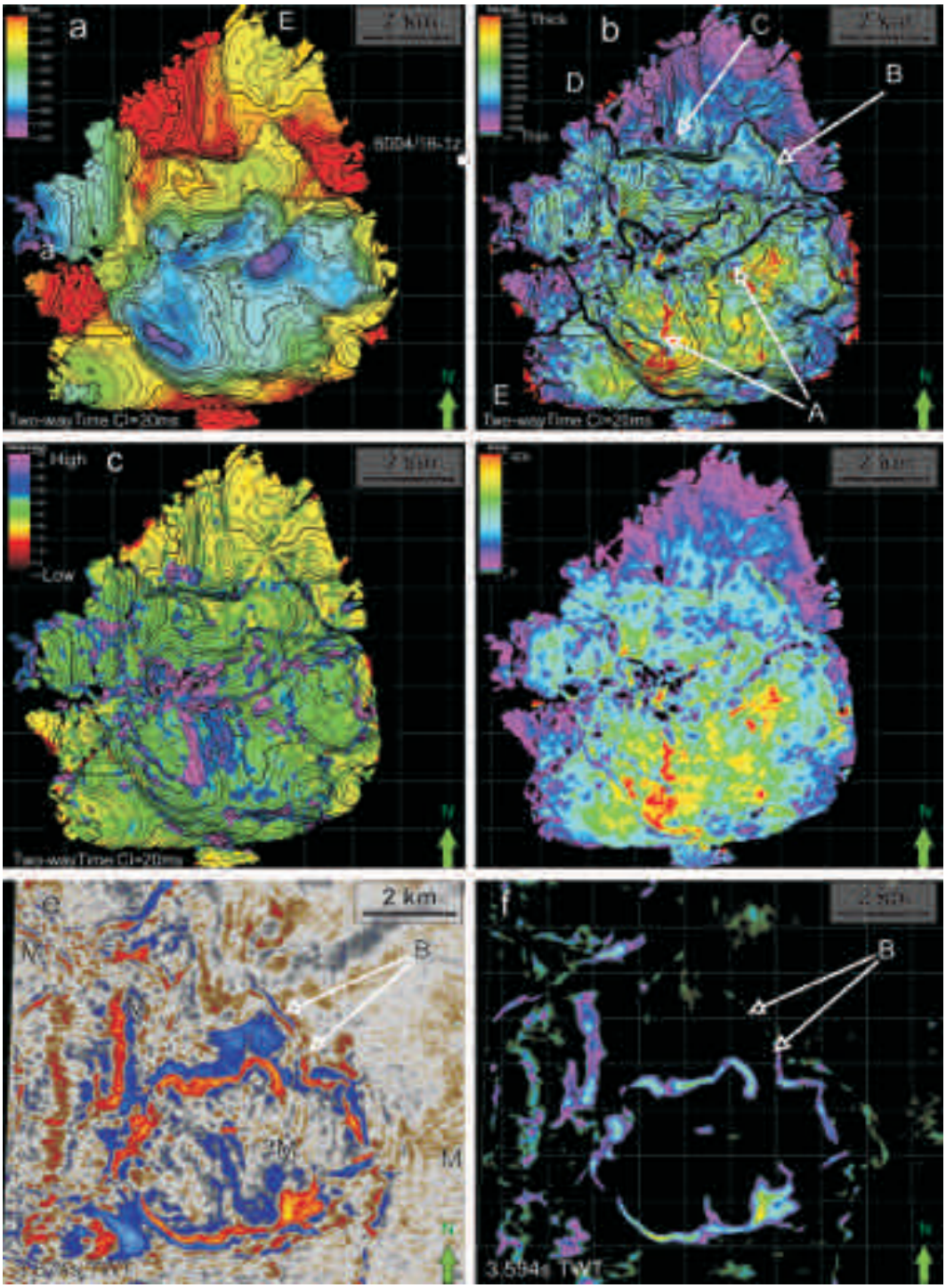

Figure 6. Map views of Trykleývari sill. **a**) Two-way time map. The central, lower inner sill consists of three sub-bowls, whereas the discontinuous peripheral fringing outer sill itself consists of partial saucers (E). **b**) Proxy for sill thickness: product of two-way time thickness (**c**) and relative impedance of sill reflector (**d**) with two-way time contours (black). See text for discussion. **c**) Two-way time thickness of sill reflector with two-way time contours (black). **d**) Relative impedance of sill reflector. **e**) Time-slice at 3574ms through conventional seismic cube showing arcuate migration artefacts (M) as well as bright sill reflector. **f**) Time-slice at 3594 ms through relative seismic impedance volume, colour bar designed to show high impedance bodies. See text for discussion. (B) indicates inclined ?feeder sheet.

steered smoothing filter (Figure 4d), which maintains the coherent intrusive limbs but removes isolated noise patches.

Although opacity rendering (Smallwood and Maresh, 2002; Thomson and Hutton, 2004) is an extremely quick way of visualising high strength reflections within a seismic cube (Figure 4a), it can require time-consuming colour-bar adjustment and sub-cube cropping. It can also be difficult to use for the commonly observed stacked sill sequences where lower or higher opaque patches obscure the feature of interest (e.g. Figure 4a). An alternative and quicker way of visualising sills can be to seed 3D autotrackers (e.g. Bell and Butcher, 2002) or to use geobody extraction. The Trykleývari sill is used as an example: 3D autotracking on the impedance inversion volume (Figure 5b) or automatic geobody detection (following a common contour surface around a body through 3D impedance space; Figure 5c) are each achieved in a few seconds. A second geobody detection run with a lower impedance threshold captured the linkages between the Trykleývari sill and its underlying connected seismic bodies, interpreted to be earlier intrusive (feeder?) inclined sheet systems and dykes (Figure 5d).

The data preparation and interpretation techniques described here allow removal of some noise from the data, and may advance the process of sill study from visualisation of the sill with an opacity technique to objective confirmation of connections within the seismic volume indicative of magmatic plumbing. If absolute impedance inversion, calibrated to wells, were to be undertaken, then selection of impedance surface thresholds for the geobody edges should allow still more quantitative assessment of sill thicknesses and body volumes. However, attention would have to be paid to ensure that small velocity perturbation assumptions do not invalidate the process of such model-driven impedance inversion processes. Since the processing flow of the dataset discussed here targeted true amplitude preservation, the band-limited impedance inversion shown here is not vulnerable to this problem. Future studies could in principle use a pre-stack inversion process to ameliorate the effect of offset-dependent tuning. Interpretation of both reflectivity and impedance data could be affected by physical property changes within the aureole (see Berndt *et al*., 2000; Smallwood and Maresh, 2002; Svensen *et al*., 2007).

A second innovation is the suggestion of calculation of the product of sill time thickness (Figure 6c) with impedance "amplitude" (Figure 6d) to allow extension of the range of thicknesses over which sill thickness can be assessed (Figure 6b). The Trykleývari sill is too thin for a separate top and base reflection to be resolved (cf Hansen and Cartwright, 2006a), so seismic attributes can yield thickness information. Reflector peak amplitude (and therefore band-limited inverted impedance "amplitude") alone increases approximately linearly with thickness up to the tuning thickness (half wavelength λ; Smallwood and Maresh, 2002; Thomson, 2005) whereas peak-trough separation measures sill thickness beyond the thickness when amplitude no longer varies (approximately 3λ/4). The product of the two attributes therefore increases with sill thickness below λ/2 (c. 25 m) and beyond 3λ/4 (c. 40 m), with the intervening thickness interval having an approximately flat response. Some caution naturally applies to interpretation of this product, as offset-dependent tuning variations are not accounted for in the post-stack inversion employed here, but the product should give a better indication of thickness variation than amplitude alone.

Morphology

The Trykleývari sill, illustrated in Figures 3 to 7, shares a number of common features with sills observed elsewhere on the Atlantic Margin. It is a compound sill, part of a sill complex (*sensu* Hansen *et al*., 2004). The inner sill consists of three bowls, two separated by a ridge and the other edges characterised by steps in intrusion level, aligned with the semi-regional intra-Paleocene east-west to west-southwest to east-northeast faulting trend.

The indicative map of sill thickness highlights a number of features of the sill morphology. There are some thicker lineaments within both the inner (e.g. C, Figure 6b) and the outer sill. The edges of the outer sill (D, Figure 6b) generally appear thinner than the inner sill. The areas of greatest sill

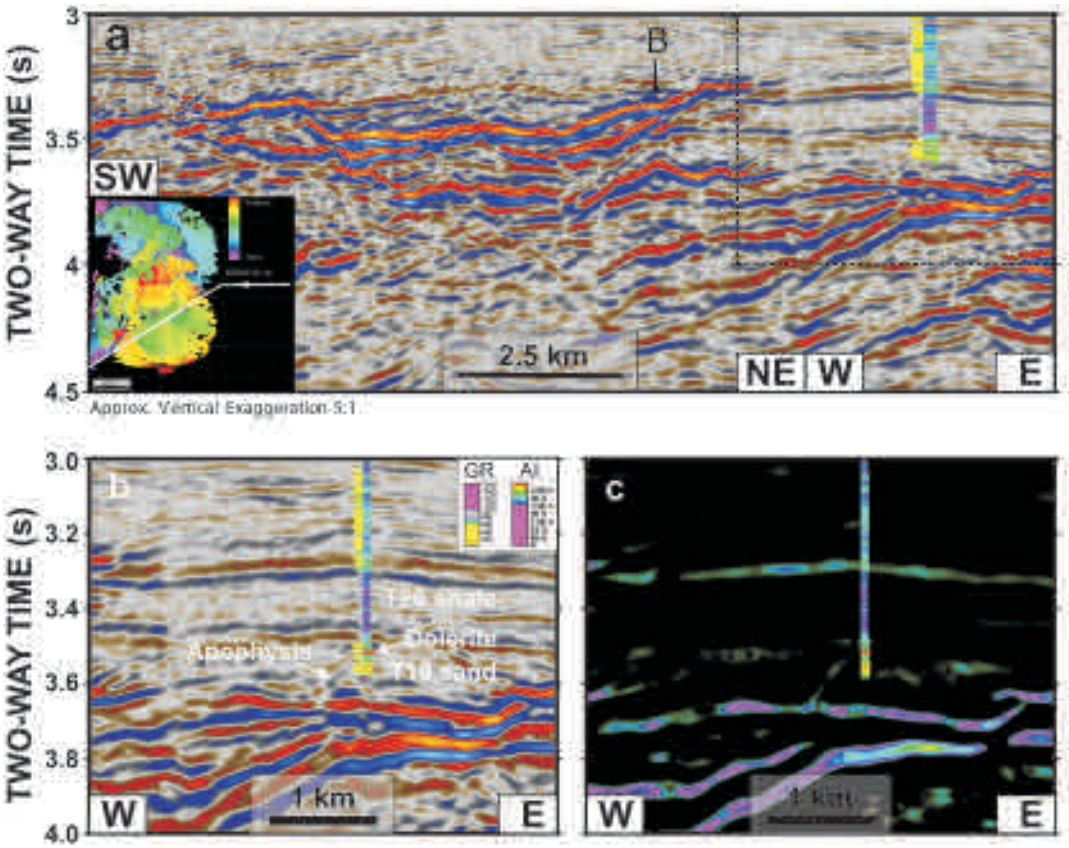

Figure 7. Seismic line across Trykleývari sill tying to Well 6004/16-1z. Line location shown in inset to (**a**), which is a map of the Trykleývari and underlying sills coloured by two-way time. Wireline log curves shown along the wellbore: Gamma Ray on left, Acoustic Impedance calculated from Density and Sonic logs on right, key as inset to (b). **a**) Conventional seismic data. The Trykleývari sill is emplaced within rocks of Danian-Selandian age, the inner sill at T10 level, inclined sheet within the T20 shales and the outer sill within sandstones of T28 age. Dashed box shows section expanded in (**b**) and (**c**). **b**) Blow-up of (**a**) with steeply-dipping reflection from apophysis (offshoot) of sill penetrated in 6004/16-1z indicated. The 6m dolerite encountered in the well had a high acoustic impedance (red). **c**) Relative impedance inverted version of (**b**). High impedance bodies include basal T28 sand, weak upper T10 sand and sill complex, including apophysis encountered in the well.

thickness occur in the deepest points of the three constituent parts of the inner sill. Such overall outward thinning of the inner sill has been observed previously both in outcrop (e.g. Francis, 1982) and in 3D seismic studies from direct mapping of top and base reflectors (e.g. Hansen and Cartwright, 2006a) but not derived from seismic attributes alone, as illustrated here.

One feature of particular interest is the relatively thick rim around much of the outer edge of the inner sill (B, Figure 6b). Examination of this feature suggests that it marks a sill junction between the Trykleývari sill and underlying inclined sheets arranged in an irregular cone (B, Figure 7). Other linear swells in sill thickness are interpreted to record the conduits of the magmatic plumbing system within the intrusion (e.g. Thomson, 2004; C, Figure 6b).

The tri-partite inner sill is flanked by steep discordant inclined sheets, which display seismic impedance lineations (B, Figure 6b). The outer sill is discontinuous and composed of concave-upwards partial saucers to the north and southwest (Figures 5 and D, Figure 6). The extreme periphery of the

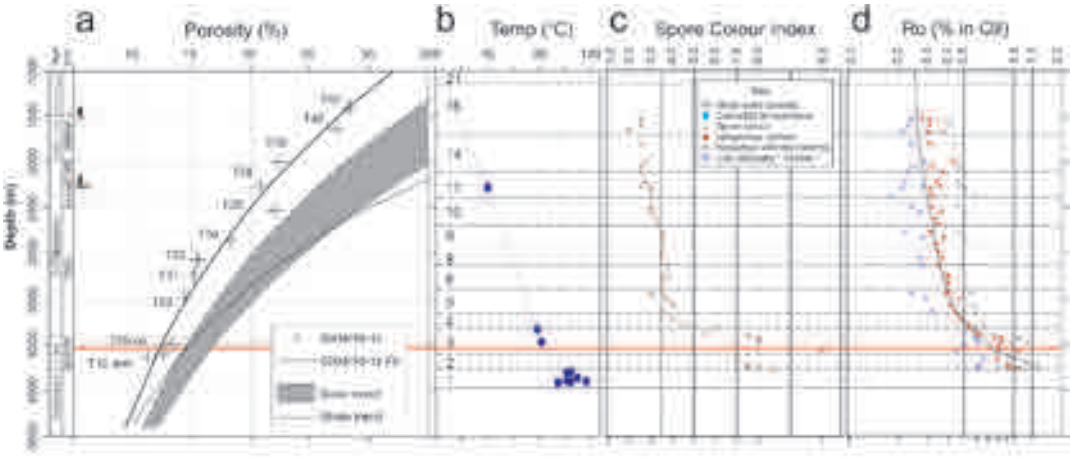

Figure 8. Data from Well 6004/16-1z, red line indicates position of sill encountered in the well-bore (water depth at well 974.5 m). **a**) Mean sand porosity with best-fit exponential decay curve (solid line). Grey area shows range of regional sand porosity-depth trends for non-exhumed wells West of Shetland and dotted line shows typical regional shale trend (from Smallwood, 2005). **b**) Corrected temperature data with 55 mWm^{-2} present-day heat flow line. **c**) Spore colour index data (Roberson Research, 2002). Extrapolation of the 1500-3500 m gradient suggests c. 0.5-1 km of exhumation. **d**). Vitrinite reflectance data (Robertson Research, 2002) with fit resulting from model shown in Figure 9.

outer sill is composed of irregular lobes as observed elsewhere (e.g. Thomson, 2004; Hansen and Cartwright, 2006b), with an outer fringe consisting of branching lobes with decreasing scale (C, Figure 5b). The magma front is interpreted to advances by inflation and break-out, forming a hierarchy of lobes towards the margin (Thomson, 2004; Hansen and Cartwright, 2006b; D, Figure 6b).

Intrusion and uplift dating

Well 6004/16-1z penetrated a 6 m-thick offshoot (apophysis) of the Judd Basin sill complex at 3113 m below the mudline, within the Early Paleocene Danian T10 reservoir of the Marjun discovery (Figures 2, 7 and 8; Oljumálaráðið, 2001a; Smallwood and Kirk, 2005). Ar/Ar dating yielded an age of 56.0±1.2 Ma for this dolerite. This result suggests that at least part of the Judd Basin sill complex was coincident within error with the majority of the intrusions within the Flett Basin (Figures 1 and 2). This Early Eocene sill intrusion phase occurs towards the end of period of volcanic activity on the Faroes and much of the North Atlantic Igneous Province and corresponds to the time of continental break-up to the west (Ritchie *et al*., 1999; Figure 2). Tying the radiometric dates with the stratigraphy is not straightforward, but the preferred models of Clarke (2002) and Shaw-Champion *et al*. (2008) suggest that the main period of sill intrusion was distinct from and later than the major uplift evidenced locally by sub-aerial erosion of a valley system into rocks of Upper Paleocene age (Smallwood and Gill, 2002; Shaw-Champion *et al*., 2008; Figures 2, 3, 8).

Comparison of the 6004/16-1z porosity-depth trend with functions fitted to more regional data (Smallwood, 2005), suggests that 0.5 to 1 km of post-Paleocene overburden has been eroded at the well location, comparable with estimates from seismic interpretation (Figure 8c; Smallwood, 2004). Upward extrapolation of the spore-colour index trend in 6004/16-1z also suggests that there is approximately 0.5-1 km of missing section at the well location (Figure 8). There are several candidate epeirogenic, compressional uplift and deep-water erosion events for this exhumation, which are manifest in the Base Balder, Top Lower Eocene and younger coincident erosional unconformities in the well (Figure 9; Smallwood, 2004).

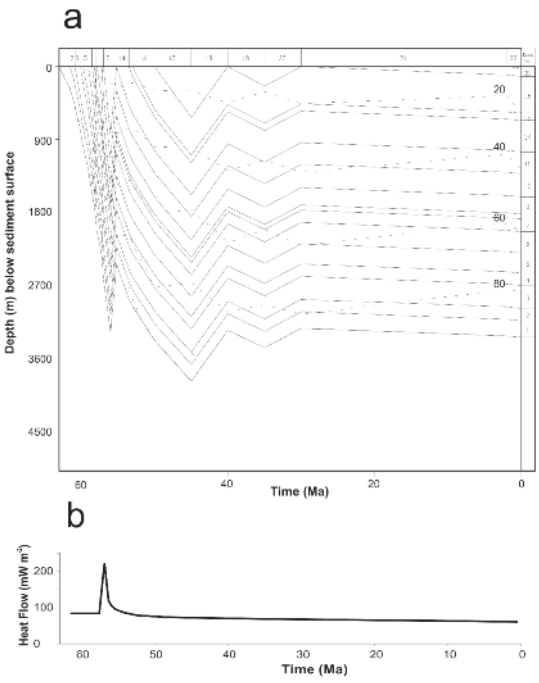

Figure 9. Well 6004/16-1z models resulting in fit to vitrinite reflectance data shown in Figure 8d. **a**) Subsidence/uplift model (Robertson Research, 2002). Numbered units correspond to labelling in Figure 8b. Rapid burial of Paleocene strata was interrupted by a Late Paleocene uplift event (Smallwood and Gill, 2002). Continued subsidence was punctuated by [at least two] Cenozoic compressional inversion events (Smallwood 2004). **b**) Heat flow model including short but intense heating event at North Atlantic Igneous Province breakup phase time (Figure 2).

Emplacement

Hansen and Cartwright (2006b) and Thomson (2007) interpreted saucer-shaped sills imaged on 3D seismic surveys on the Atlantic Margin to have grown upwards and outwards from feeder points within the inner sill. Thomson (2007) describes this as a "laccolith"-type model (e.g. Bradley, 1965), in which, following growth of the inner sill, peripheral steep magma tubes climb away, exploiting fractures in the hinges of the peripheral forced fold above the sill edges. These magma tubes coalesce to form the inclined sheet and the outer sill may form if a suitable overlying horizon is encountered. Experimental and numerical simulations have reproduced this emplacement style (Malthe-Sørenssen *et al*., 2004; Galland *et al*., 2006).

The extraction of a continuous high impedance "geobody" including the Trykleývari sill and underlying features from the impedance volume suggests that there is physical connectivity between the seismically reflective igneous bodies. Underlying intrusions intersect the floor of the each of the three sub-bowls of the inner sill (point A, Figure 4b, Figure 6b; Junction Type B, Hansen *et al*., 2004). An initial assessment, therefore, suggests that the morphology of the Trykleývari sill is consistent with the "laccolith" mechanism model, with emplacement commencing from a central magma feeder at the deepest point (or points?) and magma propagation upwards and outwards (A, Figure 6a).

Several observations, however, suggest a second contributory mechanism for the intrusion of the Trykleývari sill. Firstly, the merging of the three sub-bowls into an apparently conjoined single body suggests that either magma input was simultaneous from each of the basal feeders, or that one or more of the imaged sill junctions were not active magma feeder points. The second novel and important observation from the Trykleývari sill is that it appears to connect with, and therefore may have been fed from, the inclined sheet of a deeper saucer (Figures 6e and f, 7). The increase in sill thickness in a lineament around the edge of the inner sill (D, Figure 6b) indicates the position of the intersection between the Trykleývari sill and this cone-like underlying inclined sheet. At least some parts, and maybe all, of the Trykleývari sill may therefore have formed following magma supply from an inclined sheet (Figure 6b), that continued to supply magma upwards to form parts of the outer sill and simultaneously or subsequently collapsed back to form the inner sill, a model also formerly favoured for the Karoo sills (Chevallier and Woodford, 1999).

More recent work on flow indicators within the Karoo sills, including anisotropy of magnetic susceptibility, supports an emplacement model where the saucers are fed from the centre and transgress

around the edges of the sub-horizontal inner sill (Polteau *et al*., 2005). Localized shearing of the magnetic fabric and undulations on the outer sill suggests a late phase of inward magma flow during cooling and contraction of the saucer.

The Trykleývari sill displays thickness variations (Figure 6d) relevant to intrusion mechanism discussions. The partial saucers composing the outer sill and the inner sill are all thickest towards their centres (Figure 6). This observation is consistent with down-dip magma ponding under gravity. Goulty (2005) followed Francis (1982) in preferring such a model for the Great Whin and Midland Valley sills, invoking a thickening-with-depth/hydrostatic equilibrium mechanism. An alternative view, the central source "laccolith" model, would be to associate the radial thinning with increasing distance from the feeder. Menand (2008) discusses the thickening of a sill during growth, arguing for propagation acceleration towards the thinner leading edge as viscous dissipation increases.

Controls on intrusion depth

Kavanagh *et al*. (2006) showed experimentally that lithological discontinuities and rigidity contrasts can control the formation of sills at interfaces between upper, rigid strata and lower, weaker, strata. Upward, transgressive propagation is expected as a consequence of lateral expansion and interaction of the stress field over a sill with a free surface (Malthe-Sørenssen *et al*. 2004).

One aspect of the Trykleývari sill unusual in seismic studies is the knowledge of the host-rock lithological column provided by Well 6004/16-1z. The inner sill occurs within the Danian-age T10 sands (the Marjun discovery reservoir, Smallwood and Kirk, 2005), the inclined sheet cuts up through Selandian-age T22-T28 shales (the Marjun topseal) and the outer sill is formed near the base of the Selandian-age lowest T28 sands (Figures 2 and 7; Fig. 1 of Smallwood, 2008). This lithological variation is in contrast to that discussed by Thomson (2007), who suggested ductile layers such as overpressured shales may provide more suitable host horizons for the concordant elements of the sill.

Various favoured host lithologies for sills have been documented (e.g. Larsen *et al*., 1999; Lamers and Carmichael, 1999), and Francis (1982) commented that for the sills in Scotland and northeast England, there was "no evidence to show that any particular lithology had any influence in determining preferred horizons of intrusion". Generalised preferential lithologies for intrusion can therefore be discounted. Rather, as Kavanagh *et al*. (2006) investigated, the mechanical stratigraphy of the host succession is important, and for sedimentary successions this varies with burial as compaction and diagenesis progresses. Sands and shales have different compaction-depth trends (Figure 8a), and if a sill is to create space for itself at least partly by local compaction of the sediments, then this difference may partially control the ease with which the sill may intrude into each lithology. Considering pore-space available to compaction only, at greater depths it is likely to be preferable for the sills to intrude coarser-grained section, but finer-grained sediments will become easier to intrude closer to the seabed. Exponential porosity decay curves (Sclater and Christie, 1980) fitted to compilations of local data (Smallwood, 2005) show this cross-over to lie between 1.5 and 3.0 km below the sea-bed for non-exhumed rocks (Figure 8a).

Allowing for the 0.5-1.0 km of missing post-Eocene section and applying a normal decompaction correction to the 2.75 km of Paleocene rocks above the Trykleývari sill suggests that it was intruded 3-3.5 km below the contemporary seabed. At these depths more porosity would have been preserved in the coarse-grained sediments than in fine-grained ones, possibly explaining the difference between the preferred lithology for concordant intrusion of the Trykleývari sill and the sills studied by Thomson (2007). The sills lying beneath the Trykleývari sill are within Cretaceous strata, which are probably largely fine-grained, but unusually do include some sand beds (e.g. UK Well 204/16-1, Figure 1), which may explain the development of the sill complex in this part of the basin. The Trykleývari sill forms a useful constraint on further work in this field, which may have application in lithology prediction in offshore areas away from well control.

Polteau *et al*. (2007) show a compilation linking inner sill diameter with emplacement depth ranging up to 1.6 km, from numerical modelling, seismic and field measurements. The Trykleývari sill would appear to form an outlier to this compilation, as it was emplaced 3-3.5 km below contemporary seabed. If the mechanism driving inclined sheet transgression invoked by Malthe-Sørenssen *et al*. (2004) applies, it appears that, unusually, the Trykleývari sill might have started to experience significant free-surface interaction prior to inner sill diameter exceeding the overburden thickness. Structural restoration is required to investigate this further.

Effects of intrusion

During emplacement and cooling of intrusions, local heat flow is elevated. Direct evidence of this process is found in the spore colour and vitrinite reflectance values recorded in Well 6004/16-1z (Figure 8). The vitrinite reflectance values increase with depth at a roughly constant rate from 0.3 to 0.4 % at a depth of 2500 m below the mudline. The gradient then increases and values of over 1 % are recorded near the 6 m-thick sill at 4100 m depth. It is unlikely that the anomalous heat input to the system originates only from the 6 m-thick sill itself, as the seismic data show that there has not been a significant throughput of magma (Figure 7). The elevated vitrinite reflectance gradient is more likely to have been caused by the thermal aureole of the whole sill complex itself, which is well-developed and at least 200 m in vertical extent just beneath the TD of the well (Figure 7). Elevated paleotemperatures at the well location are confirmed by Apatite Fission Track Analysis (AFTA). The AFTA data are not discussed further here, but an absence of apatite in the lower part of the well was tentatively attributed to dissolution by hot fluids related to intrusion (P. Green pers. comm.).

Several examples have been documented in which vents on contemporary seafloor above sills prove extrusion of magma or hydrothermal fluids (e.g. Davies *et al*., 2002; Bell and Butcher, 2002; Hansen *et al*., 2004; Planke *et al*., 2005). In the 6004/16-1z area there are various seismic chimneys but these are thought to be associated with hydrocarbons rather than high temperature fluids (Smallwood and Gill, 2002). The extremely high sand net-to-gross ratio of the Paleocene-age rocks locally (Smallwood and Kirk, 2005) would have allowed hydrothermal fluid circulation without requiring as much sediment deformation as in a finer-grained system. However, 10-20 kilometres to the south-east, in UK Quad 204 (Figure 1), small circular seismic anomalies, of the type interpreted elsewhere to represent high temperature fluid escape structures (Planke *et al*., 2005), have been observed.

Elevated temperatures and convection of hot fluids driven by the heat input of the intrusion affect the process of diagenesis. This has a complex influence on the preservation or degradation of porosity and permeability in the vicinity of intrusions. The porosities encountered within the 6004/16-1z T10 reservoir sand of around 13% in the oil leg and 11% in the thin water leg fall on a normal compaction trend, based on the porosities of the other sands in the well (Figure 8a). The intrusion event does not, therefore, appear to have degraded porosity in the Marjun reservoir, over and above the relatively low porosity for the depth, which can be attributed to burial and exhumation. A similar result was recorded by Mckinley *et al*. (2001) for a Triassic Sherwood Sandstone example.

Mean permeability of the Marjun reservoir was determined to be 3.6 mD from MDT mobilities and CMR logging. Although not discussed in detail here, this figure is considered to have been adversely affected by the intrusion-related diagenetic sequence.

Lavas or sills in Well 6005/15-1?

Well 6005/15-1 (Figure 1; Oljumálaráðið, 2001b) also penetrated several intervals of dolerite within Paleocene strata. There are six dolerite intervals between 3310 and 3420 m TVDSS, average thickness 6.5 m, four dolerite intervals between 3500 and 3605 m TVDSS, average thickness 15 m, dolerite from 3800 to 3830 m TVDSS and a dolerite at least 25 m thick from 3978 m TVDSS to well TD. These dolerite intervals, like the 27 m-thick

lava package in the well at 2120 m TVDSS in the well, have high acoustic impedance and return strong, continuous seismic reflections (Figure 10).

Although the dolerite intervals are interpreted on the composite log as sills, several lines of evidence suggest an extrusive origin for at least some of these "dolerites". Firstly, the reflections tying the dolerite packages in the well are laterally extensive and perfectly concordant, with a lobate edge to the south and east (Figures 11 and 12), like that observed in the 205/9-1 lavas (Smallwood *et al*. 2004; Figure 1). To the west, the reflections continue concordantly until losing strength beneath the thickening T40-age lava package. Secondly, the dolerite reflectors have a totally different character to those from the deeper sill complex towards 6004/16-1z, in that the offsets on the dolerite reflector match offsets caused by normal faulting of overlying strata of T34 to T38 age (Figure 11). Thirdly, although there is some hole

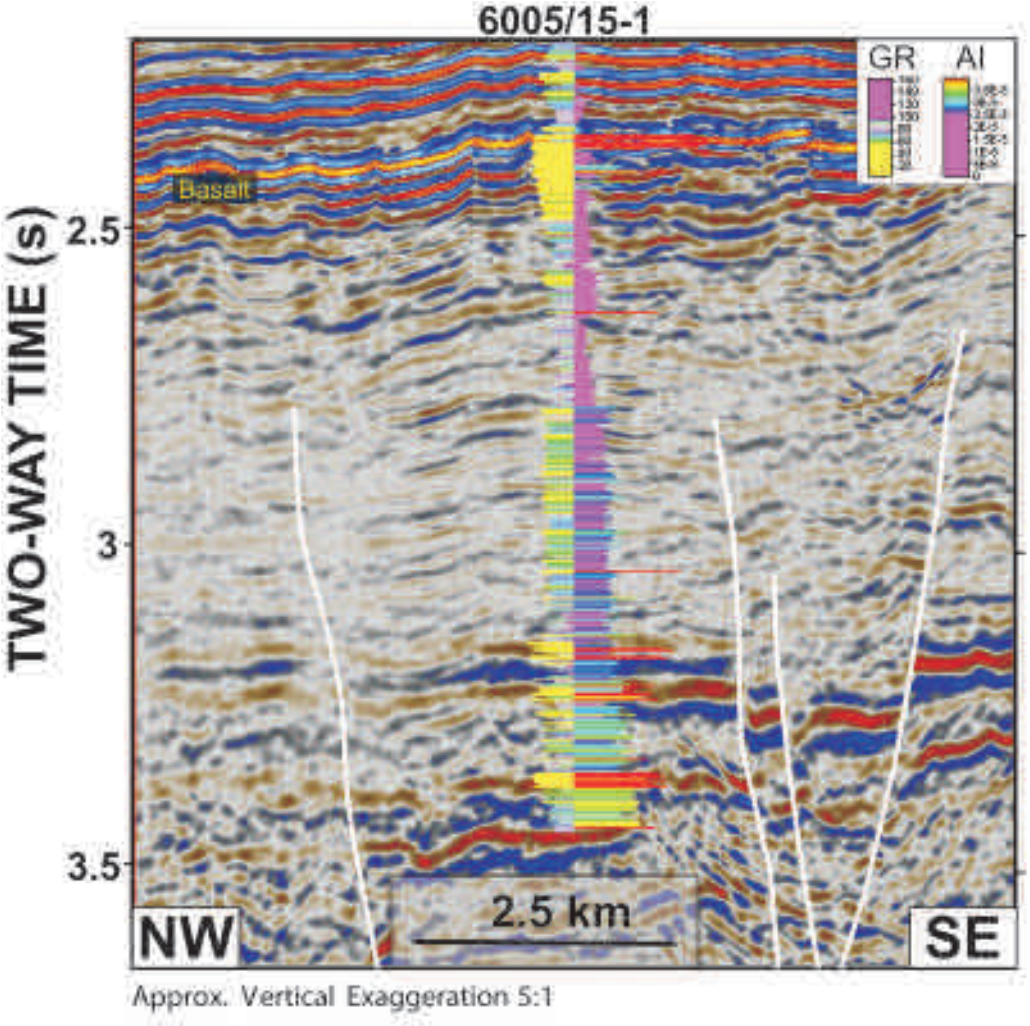

Figure 10. Seismic line through Well 6005/15-1. Line location shown Figures in 1 and 12. Log curves shown along the well-bore: Gamma Ray on left, Acoustic Impedance calculated from Density and Sonic logs on right, key as inset. The basalt lavas encountered (reflector at 2.4 s two-way time) have the highest impedance in the well, followed by the four "dolerite" packages at 3.2 to 3.5 s two-way time. The seismic reflections caused by these igneous rocks are concordant and offset by Paleocene normal faults (white). Image quality deteriorates to the northwest of the well under thickening lavas and overlying igneous layers.

washout and mixed lithologies around the dolerite intervals at the wellbore, the wireline logs across the dolerite intervals show neither the symmetrical internal character or the aureole "wings" normally associated with intrusions (Bell and Butcher, 2002; Smallwood and Maresh, 2002). Fourthly, the presence of volcaniclastic sandstones and siltstones adjacent to at least three of the four dolerite intervals is strong evidence for contemporary extrusive activity, and has to be ascribed to coincidence if these are just host volcaniclastic rocks providing a suitable horizon for mechanical exploitation by intrusives.

Further circumstantial evidence for an extrusive origin comes from the physical properties of the dolerite intervals, which are more akin to lavas than sills logged elsewhere in the region. The mean density of the dolerite intervals in 6005/15-1, where not washed out, is c. 2750 kg m^{-3} and velocity rarely above 5000 m s^{-1}, whereas sills from the Flett Basin have a mean density of 2950 kg m^{-3} and modal P-wave velocity over 6000 m s^{-1} (Smallwood and Maresh, 2002).

Possible intrusion timing is not a particularly helpful diagnostic for the question of intrusive or extrusive. The offsets of the dolerite reflector matching offsets of ?T32 to T38-age strata by the T35 to T38-age faulting appear to either require pre-T38-age concordant intrusion or an extrusive origin. While many sill radiometric ages and the 6004/16-1z sample cluster round Early Eocene Ypresian times (Figure 2), earlier sill activity in (Vaila-Flett Formation times), has been proved further north from stratigraphic relationships (e.g. Smallwood and Maresh, 2002; Trude *et al*., 2003). Intrusion of dolerite sheets post-faulting is unlikely but not geometrically impossible and would require exploitation of weakness at common stratigraphic levels in faulted strata across a very wide area (cf Lee *et al*., 2006). Given the multiple levels of dolerite encountered in the well, concordant intrusion across the fault swarm would seem unlikely. The intercalation of sedimentary rocks and dolerites is likewise non-diagnostic for the dolerite origin, as multiple levels of sill intrusion and lavas intercalated with sedimentary rocks are both well-documented (e.g. Smallwood and Maresh, 2002; Smallwood *et al*., 2004). A final piece of evidence weakly corroborating an extrusive origin of the dolerites is the absence of any hydrothermal disruption of overlying sediments and absence of associated volcanic structures.

A possible objection to the interpretation that the dolerite intervals in the well are extrusive would be that paleogeographies and fauna suggest deep-water conditions in the area at T34 times, so if extrusive, sheets of submarine lava have to be invoked. However, deep-water seabed lava sheets are not unusual: for example they are interpreted to be present on the west flank of the Flett Basin to the northwest (Figure 2 of Trude, 2004). Submarine lava flows are widely documented elsewhere (e.g. Sinton et al. 2002), and at high eruption rates a smooth sheet morphology is expected (Griffiths and Fink, 2002). The seismic amplitude map on the uppermost high amplitude T34 reflection near Well 6005/15-1 (Figures 10 and 11) shows a character suggestive of a meandering channel, 2 km-wide, and showing nested crescent-shaped lineations (Figure 12). Such lineations may develop on both subaerial and submarine erupted lavas and shallow sills, as a partially frozen upper magma crust is deformed during continued flow (Trude, 2004).

Overall, an interpretation of the dolerites as sills, as suggested on the 6005/15-1 composite log, therefore seems unlikely, at least for the upper dolerite packages, and the presence of relatively early (Vaila Formation) lavas is suggested, corresponding to the intra-plate phase of the North Atlantic Igneous Province (Saunders et al. 1997; Figure 2). Confirmation of this hypothesis awaits publication of petrological and more detailed seismic and wireline log interpretation. The importance of this conclusion for hydrocarbon prospectivity is that nearby clastic potential reservoir sandstones will not have been adversely affected by diagenesis associated with upward-transmitted heat or hydrothermal fluids.

Conclusions

The development of the Faroe-Shetland Channel area has been strongly influenced by the magmatic events of the North Atlantic Tertiary Igneous Province. This study, focussing on the intrusion of

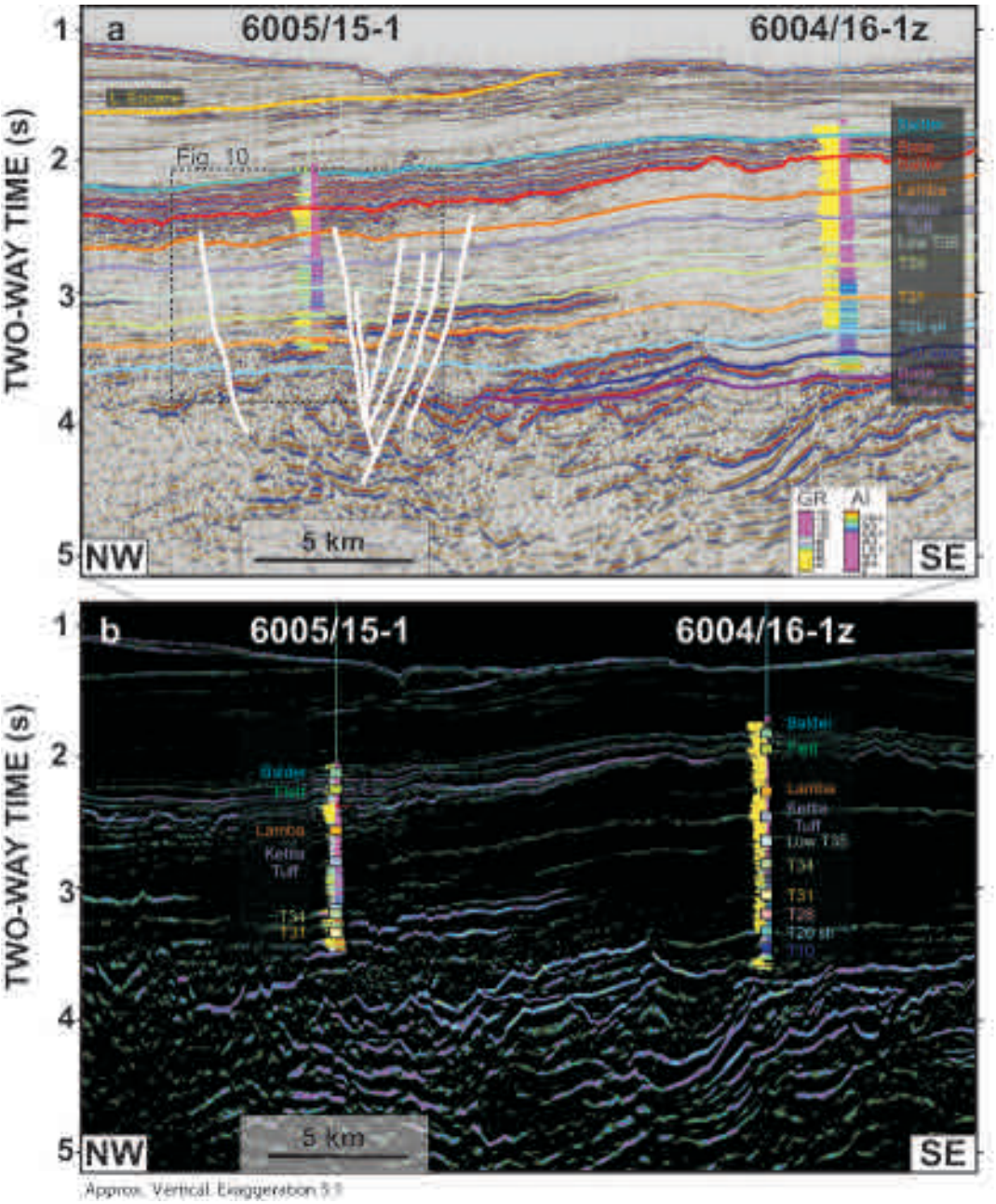

Figure 11. Seismic line through wells 6005/15-1 and 6004/16-1z. Line location shown in Figures 1 and 12. Log curves shown along the well-bores: Gamma Ray on left, Acoustic Impedance calculated from Density and Sonic logs on right, key as inset to (**a**). **a**) Conventional seismic data, with interpreted seismic horizons (as dashed on Figure 2 lithology column) and Paleocene normal faults (white). Image quality deteriorates to the northwest of the well under thickening lavas and overlying igneous layers. Dashed box shows extent of Figure 10. **b**) Impedance data. Relatively high impedance interfaces/layers in purple/blue, such as seabed, Balder and Kettla tuffs, lavas and sills. Biostratigraphically constrained well tops marked (squares).

a sill complex into Upper Cretaceous and Paleocene rocks to the southeast of the Faroe Islands' continental shelf, offers a rare opportunity for direct confirmation of the timing and host stratigraphy within a prospective sedimentary section.

Seismic processing and interpretation techniques developed primarily for hydrocarbon exploration are ideal for studying sills because of their robust seismic character. In this paper, dip-steered filtering of inverted seismic reflection data conditions the seismic volume for automatic interpretation. Sills make ideal targets for autotracking and geobody extraction, and semi-quantitative dimension measurements. The attenuation of the seismic signal below the highest sills of the complex is still problematic, however, and to fully appreciate the magmatic plumbing system requires a combination of automatic and manual interpretation (e.g. Hansen and Cartwright, 2006a).

The Trykleývari sill, which was intruded into sandstones at a depth of 3-3.5 km below contemporaneous seabed, appears to display some intriguing characteristics more similar to sills mapped at outcrop (Chevallier and Woodford, 1999; Polteau *et al*., 2005) than those studied remotely (e.g. Thomson and Hutton, 2004; Hansen *et al*., 2004). The inward thickening of both inner sill and partial saucers of the outer sill may reflect a late phase of inward magma flow as observed for the Karoo sills (Polteau *et al*., 2005). In addition, a component of magma source may have been supplied by a rising inclined sheet which is observed to intersect the edge of the inner sill. These observations have important implications for other sills where point or line sill junctions have been interpreted to be the magma feeder points. As steep structures are extremely hard to image with time-migrated seismic data, inclined sheet feeders may be more important than previously recognised in seismic data. Recent advances in seismic depth imaging have begun to allow examination of near-vertical structures beneath sills (Hardy *et al*., 2008).

Seismic attributes, such as those discussed here, together with experimental and numerical simulations and fieldwork are likely to play an important role in further study of sill emplacement mechanisms. Each has strengths, examination of complete sill complex geometry, thickness variations and intact overburden being those of 3D seismic data.

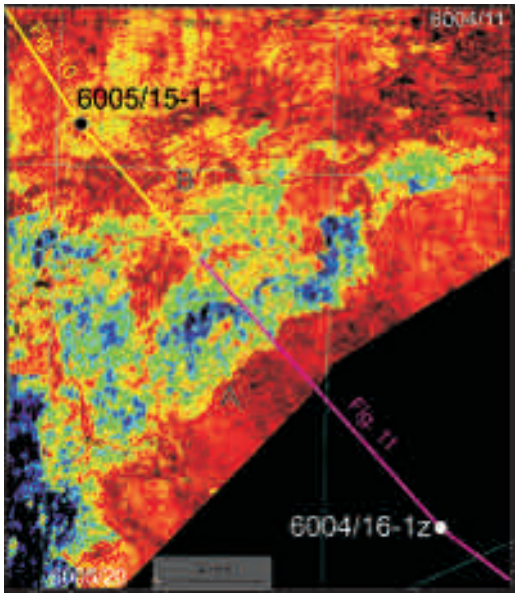

Figure 12. Seismic amplitude map on T34 peak pick (Figure 11). The seismic event corresponds to the upper of the T34 igneous packages in the well. Blue = strong event, red = weak to no event. Wells 6005/15-1 & 6004/16-1z indicated. The strong events terminate midway between the two wells. Dark-light blue feature possesses a 2 >km-wide meandering form to the northwest, and "ropey" cuspate lineations within (A). A band of dark, thin east-west to westsouthwest-eastnortheast lineations through the north part of Block 6005/20 and southern 6005/15 indicate the position and pattern of Paleocene normal faults (Figure 11). Image quality deteriorates to the northwest of Well 6005/15-1 under thickening lavas.

The hot fluids associated with the sill complex have affected the diagenesis of the host sandstones but the porosity of the T10 Marjun reservoir has not been adversely affected by the intrusion. Finally, as illustrated by the 6005/15-1 case, distinguishing extrusive and intrusive rocks within seismic data can be difficult, and careful interpretation of bright reflector packages in sedimentary basins near igneous provinces may result in improved perceptions of nearby hydrocarbon prospectivity.

Acknowledgements

Thanks is due to the Licence 001 partner group (Hess, DONG, BG and Atlantic Petroleum) for permission to publish the data included here: E. Kaslin (Robertson Research) made the maturity indicator measurements and initial thermal modelling on Well 6004/16-1z, S. Mahdi (Robertson Research) carried out the biostratigraphy study and S. Kelley (Open University) carried out the Ar-Ar dating on the dolerite in 6004/16-1z. The seismic line in Figure 3 is shown by kind permission of Veritas DGC. Thanks to Dorthe Hansen and Ken Thomson for discussions and supply of pre-publication material, and for constructive reviews by Brian Bell and an anonymous reviewer from the University of Oslo/VBPR group. Although the opinions and interpretations expressed herein are not necessarily theirs, thanks are also due to Hess for permission to publish.

References

Archer, S., Bergman, S., Iliffe, J., Murphy, C.M. and Thornton, M. 2005. Paleogene igneous rocks reveal new insights into the geodynamic evolution and petroleum of the Rockall Trough, NE Atlantic Margin, *Basin Research* 17: 171-201.

Bell, B. and Butcher, H. 2002. On the emplacement of sill complexes: evidence from the Faroe-Shetland Basin. *In*: Jolley, D.W. and Bell, B.R. (eds) *The North Atlantic Igneous Province: Stratigraphy, Tectonic, Volcanic and Magmatic Processes.* Geological Society, London, Special Publications 197: 307-329.

Berndt, C., Skogly, O.P., Planke, S., Eldholm, O. and Mjelde, R. 2000. High-velocity breakup-related sills in the Vøring Basin, off Norway. *Journal of Geophysical Research* 105: 28443-28454.

Bradley, J. 1965. Intrusion of Major Dolerite Sills. *Transactions of the Royal Society of New Zealand* 3: 27-54.

Chevallier L. and Woodford, A. 1999 Morph-tectonics and mechanism of emplacement of the dolerite rings and sills of the western Karoo, South Africa. *South African Journal of Geology* 102: 43-54.

Clarke, B.J. 2002. *Early Cenozoic denudation of the British Isles: a quantitative stratigraphic approach.* Ph.D. dissertation, University of Cambridge, UK.

Davies, R., Bell, B.R., Cartwright, J.A. and Shoulders, S. 2002. Three-dimensional seismic imaging of Paleogene dike-fed submarine volcanoes from the northeast Atlantic margin. *Geology* 30: 223-226.

Ebdon, C.C., Granger, P.J., Johnson, H.D. and Evans, A.M. 1995. Early Tertiary evolution and sequence stratigraphy of the Faeroe-Shetland Basin: Implications for hydrocarbon prospectivity. *In*: Scrutton, R.A., Stoker, M.S., Shimmield, G.B. and Tudhope, A.W. (eds) *The Tectonics, Sedimentation and Palaeoceanography of the North Atlantic Region*. Geological Society, London, Special Publication 90: 51-69.

Francis, E.H. 1982. Emplacement mechanism of late Carboniferous tholeiite sills in Northern Britain. *Journal of the Geological Society of London* 139: 1-20.

Gibb, F.G.F. and Kanaris-Sotiriou, R. 1988. The geochemistry and origin of the Faeroe-Shetland sill complex. *In*: Morton, A.C. and Parson, L.M. (eds) *Early Tertiary Volcanism and the Opening of the NE Atlantic*. Geological Society, London, Special Publications 39: 241-252.

Griffiths, R.W. and Fink, J.H. 1992. Solidification and morphology of submarine lavas: A dependence on extrusion rate, *Journal of Geophysical Research,* **97,** 19,729-19,737.

Goulty, N.R. 2005. Emplacement mechanism of the Great Whin and Midland Valley dolerite sills, *Journal of the Geological Society* 162: 1047-1056.

Hansen, D.M., Cartwright, J.A. and Thomas, D. 2004. 3D seismic analysis of the geometry of igneous sills and sill junction relationships. *In*: Davies, R.J., Stewart, S.A., Cartwright, J.A., Lappin, M. and Underhill, J.R. (eds) *3D Seismic Technology: Application to the Exploration of Sedimentary Basins*. Geological Society, London, Memoirs 29: 199-208.

Hansen, D.M. and Cartwright, J. 2006a. The three-dimensional geometry and growth of forced folds above saucer-shaped igneous sills. *Journal of Structural Geology* 28: 1520-1535.

Hansen, D.M. and Cartwright, J.A. 2006b. Saucer-shaped sill with lobate morphology revealed by 3D seismic data: implications for resolving a shallow-level sill emplacement mechanism. *Journal of the Geological Society* 163: 509-523.

Hardy, R., Bednar, J.B., Bednar, C., Fernandes K. and Jones, S.M. 2008. Imaging beneath igneous sills using reverse time depth migration, H040, 70th EAGE Conference, Rome.

Hitchen, K. and Ritchie, J.D. 1993. New K-Ar ages, and a provisional chronology, for the offshore part of the British Tertiary Igneous Province. *Scottish Journal of Geology* 29: 73-85.

Knox, R.W.O'B, Holloway, S. and Baily, H.E. 1997. Stratigraphic nomenclature of the UK North West Margin: 2. Early Paleogene lithostratigraphy and sequence stratigraphy. British Geological Survey, Nottingham.

Lamers, E. and Carmichael, S.M.M. 1999. The Paleocene deepwater sandstone play west of Shetland. *In*: Fleet A.J. and Boldy S.A.R. (eds) *Petroleum Ge-*

ology of Northwest Europe: Proceedings of the 5th Conference. Geological Society, London: 645-659.

Lancaster, S. and Whitcombe, D.N. 2000. Fast-track 'coloured' inversion, *SEG August 2000, Calgary, Abstracts*.

Larsen, M., Hamburg, L., Olaussen, S, Norgaard-Pedersen, N. and Stemmerik, L. 1999. Basin evolution in Southern East Greenland: An outcrop analog for Cretaceous-Paleogene Basins on the North Atlantic Volcanic margins, *Bulletin of the American Association of Petroleum Geologists* 83: 1236-1261.

Lee, G.H., Kwon, Y.I., Yoon, C.S., Kim, H.J. and Yoo, H.S. 2006. Igneous complexes in the eastern Northern South Yellow Sea Basin and their implications for hydrocarbon systems. *Marine & Petroleum Geology* 23: 631-645.

Malthe-Sørenssen, A., Planke, S., Svensen, H. and Jamtveit, B. 2004. Formation of saucer-shaped sills. *In*: Breitkreuz, C. and Petford, N. (eds) *Physical Geology of High-Level Magmatic Systems*. Geological Society, London, Memoirs 234: 215-227.

Maresh, J., White, R.S., Hobbs, R.W. and Smallwood, J.R. 2006. Seismic attenuation of Atlantic margin basalts: Observations and modelling, *Geophysics* 71: B211-B221.

Mckinley, J.M., Worden, R.H. and Ruffell, A.H. 2001. Contact diagenesis: The effect of an intrusion on reservoir quality in the Triassic Sherwood Sandstone Group, Northern Ireland, *Journal of Sedimentary Research* 71: 484-495.

Menand, T. 2008. The mechanics and dynamics of sills in layered elastic rocks and their implications for the growth of laccoliths and other igneous complexes. *Earth and Planetary Science Letters* 267: 93-99.

Naylor, P.H., Bell, B.R., Jolley, D.W., Durnall, P. and Fredsted, R. 1999. Palaeogene magmatism in the Faeroe-Shetland Basin: influences on uplift history and sedimentation. *In*: Fleet, A.J. and Boldy, S.A.R. (eds) *Petroleum Geology of Northwest Europe: Proceedings of the 5th Conference*. Geological Society, London: 545-558.

Oljumálaráðið, 2001a. Amerada Hess Well 6004/16-1z, *Faroe Islands Ministry of Petroleum Press Release* 19th November.

Oljumálaráðið, 2001b. Statoil Well 6005/15-1, *Faroe Islands Ministry of Petroleum Press Release* 3rd September.

Polteau, S., Planke, S., Neumann, E.R., Ferré, E.C., Galerne, C., Malthe-Sørenssen, A., Podladtchikov, Y., Svensen, H., Marsh, J., Chevallier, L.,and Liss, D. 2005. Emplacement of saucer-shaped sills and long dykes: constrains from detailed field work and AMS analyses in the Karoo Basin, South Africa, *Eos Transactions AGU* 86(48), Fall Meeting Supplement.

Polteau, S., Mazzini, A., Galland, O., Planke, S. and Malthe-Sørenssen, A. 2008. Saucer-shaped intrusions: Occurrences, emplacement and implications. *Earth and Planetary Science Letters* 266: 195-204.

Planke, S., Alvestad, E. and Eldholm, O. 1999. Seismic characteristics of basaltic extrusive and intrusive rocks. *The Leading Edge* 18: 342-348.

Planke, S., Rasmussen, T., Rey, S.S. and Myklebust, R. 2005. Seismic characteristics and distribution of volcanic intrusions and hydrothermal vent complexes in the Vøring and Møre basins, *In*: Doré, A. G. and Vining, B. (eds) *Petroleum Geology: North-West Europe and Global Perspectives - Proceedings of the 6th Petroleum Geology Conference*. Geological Society, London: 833-844.

Ritchie, J.D., Gatliff, R.W. and Richards, P.C. 1999. Early Tertiary Magmatism in the offshore Northwest U.K. margin and surrounds. *In*: Fleet A.J. and Boldy S.A.R.(eds) *Petroleum Geology of Northwest Europe: Proceedings of the 5th Conference*. Geological Society, London: 573-584.

Ritchie, J.D. and Hitchen, K. 1996. Early Paleogene offshore igneous activity to the northwest of the UK and its relationship to the North Atlantic Igneous Province, *In*: Knox, R.B.O'B., Corfield, R.M. and Dunay, R.E. (eds) *Correlation of the Early Paleogene in Northwest Europe*. Geological Society, London, Special Publications 101: 63-78.

Robertson Research 2002. Maturity evaluation of the interval 1519m-4271m in the 6004/16-1, 1z well, offshore Faroe Islands, proprietary report no. 8577/ic for Amerada Hess Ltd.

Saunders, A.D., Fitton, J.G., Kerr, A.C., Norry, M.J. and Kent, R.W. 1997. The North Atlantic Igneous Province, *In*: Mahoney, J.J. and Coffin, M.F. (eds) *Large Igneous Provinces: Continental, Oceanic, and Planetary Flood Volcanism*. Geophysical Monograph 100, American Geophysical Union: 45-93.

Sclater, J.G. and Christie, P.A.F. 1980. Continental stretching: an explanation of the post-mid-Cretaceous subsidence of the Central North Sea Basin. *Journal of Geophysical Research* 85: 3711-3739.

Shaw-Champion, M.E., White, N.J., Jones, S.M. and Lovell, J.P.B. 2008. Quantifying transient mantle plume uplift in the Faroe-Shetland basin, *Tectonics* 27: TC1002, doi:10.1029/2007TC002106.

Sinton, J., Bermanis, E., Rubin, K., Batzika, R., Gregg, T.K.P., Grönvold, K., Macdonald, K.C. and White, S.M. 2002. Volcanic eruptions on mid-ocean ridges: New evidence from the superfast-spreading East Pacific Rise, 17°-19° S, *Journal of Geophysical Research* 107: 2115, ECV 3-1 - 3-20. doi:10.1029/2000JB000090.

Smallwood, J.R. 2004. Tertiary inversion in the Faroe-Shetland Channel and the development of major erosional scarps. *In*: Davies, R.J., Stewart, S.A., Cartwright, J.A., Lappin, M. and Underhill, J.R. (eds) *3D Seismic Technology: Application to the Ex-*

ploration of Sedimentary Basins. Geological Society, London, Memoirs 29: 187-198.

Smallwood, J.R. 2005. Lithology prediction from velocity data: Paleocene sediments in the Faroe-Shetland area. *In*: Ziska, H., Varming, T and Bloch, D. (eds) *Faroe Islands Exploration Conference: Proceedings of the 1st Conference*, *Annales Societatis Scientiarum Færoensis*, Supplementum 43, Tórshavn: 70-81.

Smallwood, J.R., Towns, M.J. and White, R.S. 2001. The structure of the Faroe-Shetland Trough from integrated deep seismic and potential field modelling. *Journal of the Geological Society of London* 158: 409-412.

Smallwood, J.R. and Gill, C.E. 2002. The rise and fall of the Faroe-Shetland Channel: evidence from seismic mapping of the Balder Formation. *Journal of the Geological Society of London* 159: 627-630.

Smallwood, J.R. and Maresh, J. 2002. The properties, morphology and distribution of igneous sills: Modelling, borehole data and 3D seismic from the Faroe-Shetland area. *In*: Jolley, D.W. and Bell, B.R. (eds) *The North Atlantic igneous province: stratigraphy, tectonics, volcanic and magmatic processes*. Geological Society, London, Special Publications 197: 271-306.

Smallwood J.R. and Kirk, W.J. 2005. Exploration in the Faroe-Shetland Channel: Disappointments and Discoveries. *In*: Doré, A. G. and Vining, B. (eds) *Petroleum Geology: North-West Europe and Global Perspectives - Proceedings of the 6th Petroleum Geology Conference*. Geological Society, London: 977-992.

Smallwood, J.R., Prescott, D. and Kirk, W. J. 2004. Alternatives in Paleocene exploration West of Shetland: A case study. *Scottish Journal of Geology* 40: 131-143.

Smallwood, J.R. 2008. Comment on "Determining magma flow in sills, dykes and laccoliths and their implications for sill emplacement mechanisms by K. Thomson [*Bulletin of Volcanology* 70: *183-210*.]", *Bulletin of Volcanology* 71: *DOI: 10.1007/s00445-008-0203-4*.

Svensen, H., Planke, S., Chevallier, L., Malthe-Sørenssen, A., Corfu, B. and Jamtveit, B. 2007. Hydrothermal venting of greenhouse gases triggering Early Jurassic global warming. *Earth and Planetary Science Letters* 256: 554-566.

Thomson, K. 2004. Sill complex geometry and internal architecture: a 3D seismic perspective. *In*: Breitkreuz, C. and Petford, N. (eds) *Physical Geology of High-Level Magmatic Systems*. Geological Society, London, Special Publications 234: 364-375.

Thomson, K. 2005. Volcanic features of the North Rockall Trough: application of visualisation techniques on 3D seismic reflection data. *Bulletin of Volcanology* 67: 116-128.

Thomson, K. 2007. Determining magma flow in sills, dykes and laccoliths and their implications for sill emplacement mechanisms. *Bulletin of Volcanology* 70: *183-210*.

Thomson, K. and Hutton, D. 2004. Geometry and growth of sill complexes: insights using 3D seismic from the North Rockall Trough, *Bulletin of Volcanology* 66: 364-375.

Trude, K.J. 2004. Kinematic indicators for shallow level igneous intrusions from 3D seismic data: evidence of flow direction and feeder location. *In*: Davies, R.J., Stewart, S.A., Cartwright, J.A., Lappin, M. and Underhill, J.R. (eds) *3D Seismic Technology: Application to the Exploration of Sedimentary Basins*. Geological Society, London, Memoirs 29: 209-217.

Trude, J., Cartwright, J., Davies, R.J. and Smallwood, J. 2003. New technique for dating igneous sills. *Geology* 31: 813-816.

Pore fluid and hydrocarbon migration histories in North Atlantic basins intruded by Tertiary sills

JOHN PARNELL* AND DAVID W. J. MIDDLETON

Department of Geology and Petroleum Geology, University of Aberdeen, Aberdeen AB24 3UE, U.K.
*Email: J.Parnell@abdn.ac.uk; Tel. +44 1224 273464; Fax +44 1224 272785

ABSTRACT

Exploration risk in the North Atlantic region, including in Faroese waters, has been compounded by the presence of Tertiary igneous intrusions in many basins, leading to complex pore fluid and hydrocarbon migration histories. In both the Triassic/Jurassic of East Greenland and the Jurassic of Skye, igneous activity during the Paleocene caused advection of hot (~200º C) pore fluids, and the extensive precipitation of quartz cement within reservoir intervals. Subsequent, cooler (~165º C) fluid flow was responsible for volumetrically minor cementation in both regions. Finally, a late phase of fluid flow characterized by relatively low temperatures (~130ºC) was caused by regional exhumation and basin inversion in the Neogene. Multiple hydrocarbon charge events are also recorded in both study areas. In East Greenland, an early charge occurred between the Albian/Cenomanian and Paleocene, followed by a separate charge of Paleocene to Oligocene age. In Skye, an early oil generated due to Paleocene igneous intrusion within source rocks was followed by a later regional oil charge event. In both regions, hydrocarbon potential was not destroyed by the emplacement of the sills.

Introduction

There is currently much interest in the effects of igneous intrusions (sills, dykes) into sedimentary successions. The subject is particularly pertinent to the basins of the Atlantic Margin west of the British Isles and in Faroese waters, where Tertiary intrusions are often encountered at a range of stratigraphic levels (e.g. Ritchie *et al*., 1999; Bell and Butcher, 2002; Smallwood and Maresh, 2002; Archer *et al*., 2005), and may have diverse consequences for hydrocarbon prospectivity (Price *et al*., 1997; Linnard and Nelson, 2005; Archer *et al*., 2005; Smallwood and Kirk, 2005). Important aspects include models of emplacement, resultant fracture patterns, creation of fluid flow barriers, influence on contemporaneous seafloor sedimentation, potential destruction of reservoired oil, influence on heat flow/thermal maturation, and diagenetic alteration. Several of these aspects involve changes in the pore fluids present in the host sediments. Onshore exposures of Atlantic Margin basins allow detailed study of pore fluid histories in the vicinity of early Tertiary intrusions. This account reports studies of two successions at different states of thermal maturation; Skye, where the Jurassic source rocks were immature before intrusion and remain immature where not intruded (Thrasher, 1992), and East Greenland, where intrusions penetrated pre-existing oil reservoirs in a mature sequence (Price and Whitham, 1997). The studies are based upon fluid inclusion data, ultraviolet microscopy, cathodoluminescence microscopy, scanning electron microscopy and petrographic studies of sandstones in intruded sections.

Geological Setting

The Mesozoic basins of Skye and East Greenland form part of the extensive system of elongate NE-SW trending fault-bounded basins, floored by highly attenuated continental crust, along the North Atlantic seaboard (figure 1). This system of basins extends from offshore Iberia to the Norwegian Arctic on the European margin, and from East Canada to Greenland on the North American margin (Roberts *et al*., 1999). Widespread rift events on the Atlantic Margin are recognised in the Per-

Faroe Islands Exploration Conference: Proceedings of the 2nd Conference.
Annales Societatis Scientiarum Færoensis, Supplementum 50, 2009: 124-155

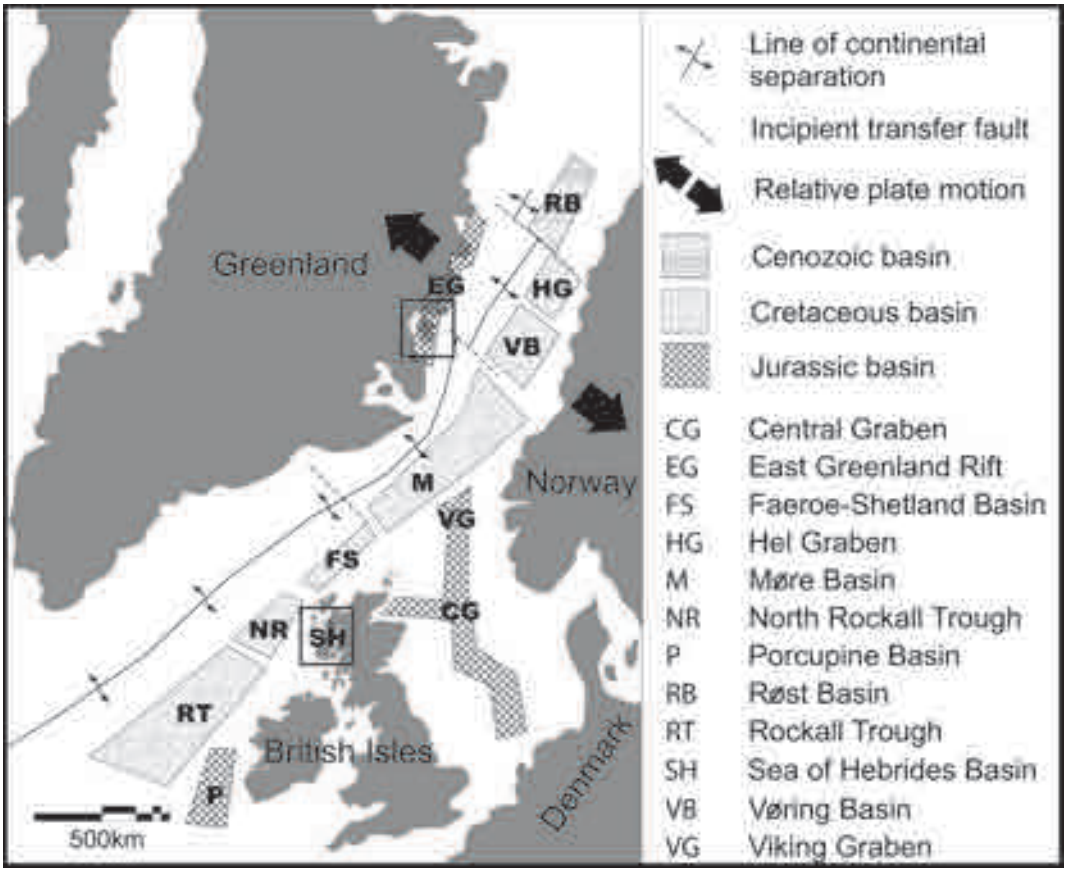

Figure 1. Plate reconstruction showing the relative positions of the Skye and East Greenland study areas (boxed) during the Palaeocene-Early Eocene, just prior to the onset of continental separation and seafloor spreading in the North Atlantic. The two areas form part of an extensive system of elongate basins developed along the North Atlantic Margins. Modified in part after Doré *et al.* (1999).

mo-Triassic, Jurassic, Early Cretaceous, Middle Cretaceous and latest Cretaceous-Early Eocene (Doré *et al*., 1999.) Repeated episodes of basin inversion are evident in the presence of multiple unconformities in the Late Paleozoic to Cenozoic stratigraphy of many basins on the Atlantic Margin.

East Greenland

The geology of East Greenland (figure 2) has much in common with many basins on the North Atlantic Margins. Precambrian and other Caledonian basement rocks are overlain by syn-rift fluviolacustrine sediments of Middle Devonian age (Price and Whitham, 1997). Further rift events in the end Devonian-Visean and Westphalian-Stephanian resulted in fault-block rotation and low regional dips of strata in the Traill Ø area (Surlyk *et al*., 1986; Larsen, 1990).

A period of regional uplift and peneplanation was followed by marine transgression in response to thermal subsidence, resulting in the widespread deposition of marine sandstones and shales over East Greenland during the Late Permian to earliest Triassic (Stemmerik *et al*., 1997). These marine sediments are overlain by erosional arkosic fluvial channels (Stemmerik *et al*., 1997) which may represent incision of rivers into shelf deposits during a period of lowered base level toward the end of

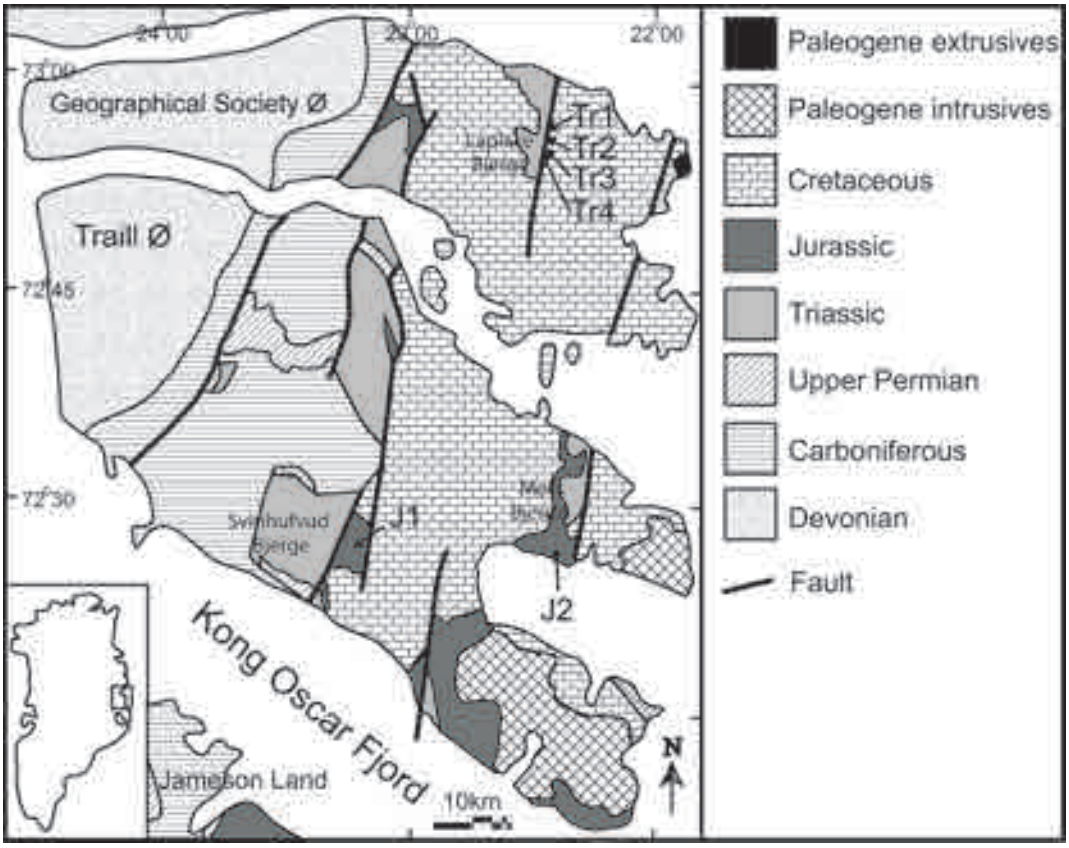

Figure 2. Geological map of the East Greenland study area, with sample localities indicated.

the Permian. A phase of early Triassic rifting is recorded by alluvial fan deposits of probable Scythian age in Jameson Land. This Early Triassic rift event was regionally extensive, and is recognised in many basins on the Atlantic Margin (e.g. Doré *et al*., 1999; Roberts *et al*., 1999).

There is a significant unconformity between the Triassic sediments of East Greenland and the overlying Middle Jurassic, with the Rhaetian-Aalenian section largely missing. The Late Bajocian-Valanginian rift event is characterised by block faulting, depositing predominantly fluvial medium-coarse grained arenitic sandstones with subordinate muds, conglomerates and thin coals (Stemmerik *et al*., 1997). The Jurassic sequence includes the BernBjerge Formation (named the Hareelv Formation in Jameson land (Price *et al*., 1997)), a sequence of marine black shales identified as a major oil source rock in East Greenland (Requejo *et al*., 1989; Larsen *et al*., 1998).

The end of the Middle Jurassic-Lower Cretaceous rift sequence is marked by a peneplanation of the uplifted footwall crests of fault blocks due to the onlap of marine mudstones. This occurred in response to thermal subsidence of the East Greenland margin in Aptian times (Price and Whitham, 1997). The Tertiary saw the onset of seafloor spreading in the North Atlantic during the Eocene, the culmination of a rifting phase which was probably initiated in the Maastrichtian (Price and Whitham, 1997). The period just prior to the creation of oceanic crust saw the intrusion of numerous dykes and sills in East Greenland which probably acted as feeders for the thick lava piles such as those found on Scoresby Sund (Larsen *et al*., 1989). Intrusion of hypabyssal intrusions in the

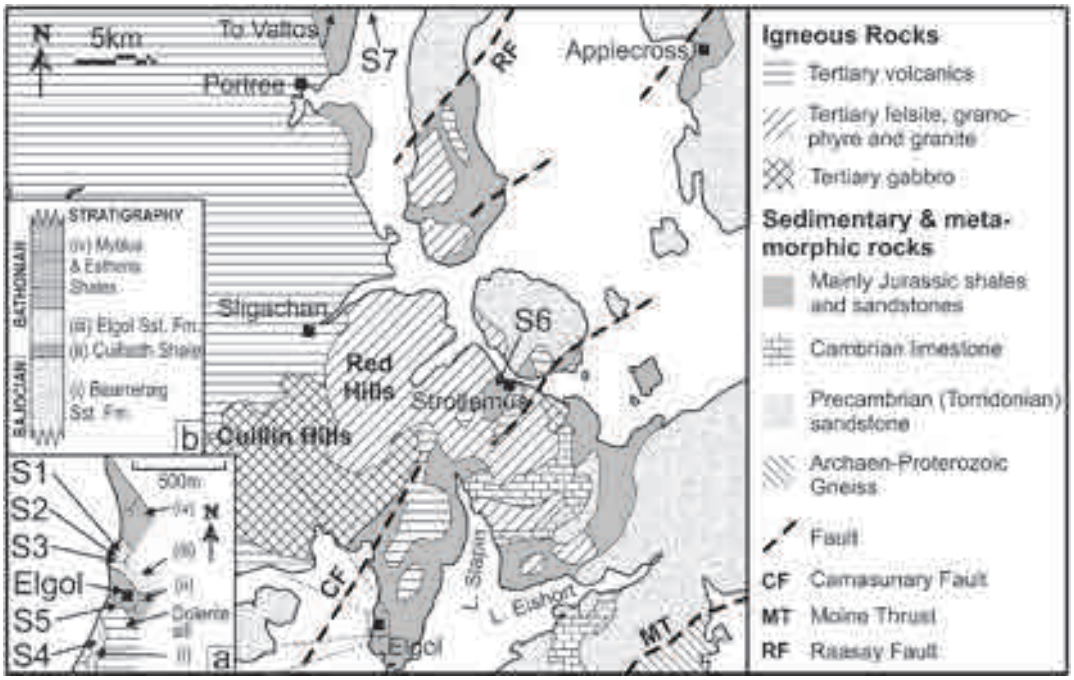

Figure 3. Geological map of the Skye study area, with sample localities indicated. Inset map (a) of Elgol coastal section modified after Hudson (1962). Stratigraphy of Elgol area (inset a) is shown in inset b.

early Tertiary is associated with contemporaneous faulting in the Traill Ø and Geographical Society Ø regions (Haller, 1970), indicating that that upwelling magma may have utilised fracture pathways during emplacement into the sedimentary pile.

Skye

The Skye study area (figure 3) lies within the Sea of Hebrides Basin, an elongate, NNW-SSE oriented half-graben system. The Jurassic section, the subject of this study, is well preserved in the Skye region, and is characterised by the onset of marine sedimentation. During this time, conditions of anoxia existed for long enough to deposit rich source rocks in the Middle to Upper Jurassic, as well as high net:gross sandstone with good reservoir potential. A period of uplift following the Jurassic is marked by an unconformity between the Kimmeridgian and Cenomanian, which is sporadically preserved at the basin margins (Kilyeni and Standley, 1985). Another major exhumation in the Early Tertiary was caused by hotspot activity and associated igneous activity in the Paleocene prior to the onset of seafloor spreading in the North Atlantic (Ebdon *et al*., 1995). The Tertiary section is dominated by large thicknesses of plateau lavas in the Sea of Hebrides Basin.

The Jurassic rocks of Skye have been extensively studied and visited in recent times, partially because they offer potential analogues for Jurassic sequences which are important in hydrocarbon plays in the North Atlantic region. Thus, studies have included sand body geometry (Harris, 1992), regional sequence stratigraphy (Morton, 1993), burial history (Kilyeni and Standley, 1985), cementation (Wilkinson *et al*., 1992) and organic geochemistry (Bishop and Abbott, 1991; Thrasher, 1992).

Skye includes a well-exposed succession of Jurassic sandstones, mudrocks and subordinate limestones, intruded by the plutonic Skye igneous complex and sills/dykes, both of Early Tertiary age. The extent of the plutonic aureole has been recorded by organic geochemical maturation parameters in Jurassic mudrocks (Thrasher, 1992),

oxygen isotopic compositions in igneous rocks (Taylor and Forester, 1971), contact metamorphic mineralogy (Ferry *et al*., 1987) and clay mineralogy in the Jurassic (Andrews, 1987). Beyond the aureole, the Jurassic is thermally immature except in the vicinity of the sills/dykes (Bishop and Abbott, 1991; Farrimond *et al*., 1999). Several shale units may have some source rock potential, but the Cullaidh Shale Formation is particularly rich in organic matter (Thrasher, 1992) and has been described as an oil shale in several parts of the island (Lee, 1920).

Field sampling was focussed at Elgol, where there is an uninterrupted succession of sills, shales and sandstones (figure 3). The Bearreraig Sandstone Formation is a potential regional hydrocarbon reservoir (Morton, 1993). A major dolerite sill has been intruded along the contact between the Bearreraig Sandstone and the overlying Cuilladh Shale Formation oil shale. Higher in the sequence, the shales are succeeded by the Elgol Sandstone Formation (White Sandstone Formation) and the Mytilus and Estheria Shales. At the top of the main sill described above, exposed at Elgol Jetty, quartz-calcite veining at the contact with the host Cuilladh Shale Formation includes solid black bitumens. Two kilometres to the north, fallen blocks from a higher sill have also yielded bitumen in mineral veinlets. Black bitumen staining is, ironically, most evident in the stratigraphic unit known as the white sandstone (Elgol Sandstone Formation). Sandstones were sampled to discriminate the

								T_hC			Sal. (wt.%NaCl)		
No.	**Locality**	**Age**	**n**	**Nature**	**Host**	**P/S**	**Occurrence**	**Mean**	**Min**	**Max**	**Mean**	**Min**	**Max**
J1	Svinhufvud Bjerge	Jur.	11	H_2O/NaCl	Qtz	P	GOB	142,2	117,0	157,0	6,09	4,18	9,34
			6	H_2O/NaCl	Qtz	S	Fracture	185,3	180,6	191,2	6,37	3,39	9,34
			6	CH_4/H_2O	Qtz	S	Fracture	164,2	142,5	184,5	n/a	n/a	n/a
J2	Mols Bjerge	Jur.	4	H_2O/NaCl	Qtz	P	Early OG (GOB1)	78,4	69,4	88,9	1,66	1,57	1,74
			10	H_2O/NaCl	Qtz	P	Late OG (GOB2)	137,4	124,6	158,2	7.50	5,71	9,47
			6	H_2O/NaCl	Qtz	S	Fracture	136,5	127,5	152,1	4.91	3,23	6,59
Tr1	Laplace Bjerge	Trias.	2	Liquid HC	Qtz	S	Pre-OG Fracture	n/a (1P)	n/a	n/a	n/a	n/a	n/a
			8	H_2O/NaCl	Qtz	P	GOB	188,8	175,5	201	3,31	3,06	3,55
			5	H_2O/NaCl	Qtz	S	Fracture	148,0	133,0	169,4	7,94	7,73	8,14
			4	H_2O/NaCl	Cal	P	Cleavage	109,7	86,2	124,6	19,20	18,80	19,60
			2	H_2O/NaCl	Jar	P	Cleavage	88,1	84,6	91,5	13,67	12,16	15,17
Tr2	Laplace Bjerge	Trias.	6	H_2O/NaCl	Qtz	P	Early OG (GOB1)	190,6	182,3	205	7,73	7,31	8,14
			5	H_2O/NaCl	Qtz	P	Late OG (GOB2)	170,1	159,8	184,5	5,56	5,26	5,86
			8	H_2O/NaCl	Qtz	S	Fracture	145,6	138,4	155,2	6,60	5,71	7,89
			6	H_2O/NaCl	Cal	P	Cleavage	108,5	97,6	122,0	20,28	19,13	21,33
			2	H_2O/NaCl	Jar	P	Cleavage	90,3	89,1	91,5	12,27	11,46	13,07
Tr3	Laplace Bjerge	Trias.	9	H_2O/NaCl	Qtz	P	GOB	171,2	155,9	184,2	5,20	1,40	9,08
			11	H_2O/NaCl	Qtz	S	Fracture	159,8	135,9	177,2	5,54	4,80	7,02
Tr4	Laplace Bjerge	Trias.	9	H_2O/NaCl	Qtz	P	GOB	172,3	156,6	182,6	5,55	4,34	6,74
			11	H_2O/NaCl	Qtz	S	Fracture	142,9	127,2	164,7	4,28	1,40	6,59

Table 1. Summary of fluid inclusion microthermometry data from East Greenland. Salinity converted from final ice melting temperature (Bodnar, 1993). 1P=Monophase (liquid) inclusions, Cal=Calcite, GOB1/2=First/second phase grain/overgrowth boundary, HC=Hydrocarbon, Jar=Jarosite, OG=Quartz overgrowth, P=Primary, Qtz=Quartz, S=Secondary, Sal.=Salinity.

possible effects of regional heating by the Skye Igneous Complex and localised heating by sills and dykes. Sample localities include Strollamus, where sandstones are baked by very close proximity to the Skye Igneous Complex. Sampling was also carried out at Valtos, which is beyond the metamorphic aureole of the main batholithic centre, but where sandstones are locally intruded by sills.

Previous studies of diagenesis (Hudson, 1965; Hudson and Andrews, 1987) have shown that the sandstones are predominantly cemented by calcite and to a lesser degree by quartz.

Methodology

Sampling

Samples were collected from the localities identified in Figures 2 and 3, and Table 1 and 2. In East Greenland, the samples are from a region intruded by numerous sills, but not from the immediate contact zones. In Skye, the Bearreraig Sandstone Formation and Elgol Sandstone Formation were sampled about 3 m below, and 3 m above, a sill at Elgol Jetty respectively. At Valtos, the analyzed sample was at least 2 m from contact with a sill.

Scanning Electron Microscopy (SEM) studies

Carbon-coated SEM stubs and polished probe slides were prepared from sandstones from Laplace Bjerge, Mols Bjerge and Svinhufvud Bjerge in East Greenland, and from Elgol on Skye. SEM studies were conducted using an ISI ABT-55 Scanning Electron Microscope and dedicated Energy Dispersive X-ray analyser (EDS). Backscattered SEM (BSEM) examination was performed using a Link Analytical Backscatter Detector. SEM-CL studies were carried out using an Oxford Instruments CL302 Cathodoluminescence system.

Fluid inclusion studies

Fluid inclusions have a great diversity of applications in geology, and are an invaluable tool in the reconstruction of pore fluid histories in reservoir rocks (Goldstein and Reynolds, 1994). The value of fluid inclusions lies in the information which they can yield about temperatures, salinities, pressures and compositions of pore fluids in the geological past. In most studies these data are exclusively based on microthermometric measurements. Homogenization temperature (T_h) is the temperature at which a multi-phase fluid inclusion homogenizes to a single phase (typically liquid+vapour at room temperature, with homogenization to a liquid on heating). The temperature of homogenization records the minimum temperature of pore fluids at the time of inclusion entrapment i.e. during cement precipitation and/or fracture annealing. Measurements were made on calcite first to avoid effects of thermally-induced stretching on the data. Final ice melting temperature (T_m) is the temperature at which the last crystal of ice melts on re-heating the inclusion from frozen, and allows conversion to weight % salinity in simple H_2O-NaCl systems using the equation of Bodnar (1993). Monophase aqueous inclusions do not generally yield useful microthermometric data and so are given less attention. The exception to this is where monophase inclusions contain liquid petroleum (discussed below), as the presence of oil inclusions is significant. Inclusions of solid bitumen are also recorded, as they may represent thermal degradation of originally live, liquid petroleum which was encapsulated within fluid inclusions. All homogenization temperature data represent minimum fluid trapping temperatures, as pressure corrections have been omitted due to inherent uncertainties in modelling the amount of overburden at the time of inclusion entrapment. Fluid inclusions containing liquid petroleum can be readily examined using ultraviolet (UV) fluorescence microscopy (Burruss, 1991).

Wafers for fluid inclusion analysis were produced from sandstone samples from Laplace Bjerge, Mols Bjerge and Svinhufvud Bjerge in East Greenland, and from Elgol, Strollamus and Valtos on Skye. Microthermometry was carried out using a Linkam THM600 heating-freezing stage coupled to an Olympus BH-2 microscope fitted with objectives up to x100. The stage was calibrated using chemicals of known melting point, including naphthalene, urea, benzanilide and distilled water. A Nikon Eclipse E600 with a Y-FL Epi-fluorescence attachment and a UV-2A filter cube (excitation 330 to 380 nm, longpass barrier) was used for UV fluorescence microscopy.

								T_hC			Sal. (wt.%NaCl)		
No.	**Sample**	**Age**	**n**	**Nature**	**Host**	**P/S**	**Occurrence**	**Mean**	**Min**	**Max**	**Mean**	**Min**	**Max**
S1	Elgol- Coarse Elgol Sandstone Formation	Jur.	5	H_2O/NaCl	Qtz	P	GOB1 (pre-def)	191,1	186,2	196,6	3,43	2,24	4,34
			4	H_2O/NaCl	Qtz	P	GOB2 (syn-def)	170,9	165,6	177,3	2,57	1,05	5,26
			7	H_2O/NaCl	Qtz	S	Fracture	114,3	102,6	126,6	5,12	3,06	8,41
			5	CH_4±CO_2	Qtz	P	Late SiO_2 cement	-58,8	-66,7	-52,6	n/a	n/a	n/a
S2	Elgol- Elgol Sandstone Fm. w/ SiO_2 cement	Jur.	7	H_2O/NaCl	Qtz	S	Pre-OG fracture	197,6	184,3	209	6,04	3,87	8,68
			6	H_2O/NaCl	Qtz	P	GOB2 (syn-def)	164,6	155,9	172,3	1,73	0,71	2,74
S3	Elgol- Elgol Sandstone Fm. w/bitumen	Jur.	14	H_2O/NaCl	Qtz	P	Pre-OG fracture	198,8	183,9	212	4,84	3,23	8,14
			10	H_2O/NaCl	Qtz	S	GOB2 (syn-def)	167,0	163,1	174,2	2,10	0,35	3,71
S4	Elgol- Bearreraig Sst Fm., below sill	Jur.	13	H_2O/NaCl	Qtz	P	GOB	175,9	159,3	189,2	5,42	2,74	8,41
			8	H_2O/NaCl	Qtz	S	Fracture	126,5	115,6	137,7	3,14	0,35	6,45
S5	Elgol- Quartz/calcite veining in top of sill	Jur.	13	H_2O/NaCl	Cal1	P?	Vein fill	212	195,6	229	1,19	0	2,9
			12	Liquid HC	Cal1	P?	Vein fill	n/a (1P)	n/a	n/a	n/a	n/a	n/a
			8	H_2O/NaCl	Qtz	P?	Vein fill	172,3	164,5	182,3	5,36	2,74	7,17
			6	H_2O/NaCl	Cal2	P?	Vein fill	80,4	75,6	85,9	18,85	18,30	19,21
S6	Strollamus- Hornfelsed sandstone near Skye Igneous Complex	Jur.	4	H_2O/NaCl?	Qtz	P	GOB	>300	>300	>300	n/a	n/a	n/a
			6	H_2O/NaCl	Qtz	S	Fracture set 1 (early)	194,3	184,2	204	4,94	2,24	8,41
			7	H_2O/NaCl	Qtz	S	Fracture set 2 (late)	125,0	114,4	130,5 -	5,16	3,06	8,55
			2	CH_4±CO_2	Qtz	S	Fracture	-68,5	-70,6	66,4	n/a	n/a	n/a
			5	H_2O/NaCl	Fsp	P?	Dissolved cleavage	110,6	98,5	123,3	3,76	2,90	4,34
S7	Valtos- Valtos Sandstone Fm.	Jur.	4	H_2O/NaCl	Qtz	P	GOB	192,3	187,6	196,0	1,05	1,05	1,05
			9	H_2O/NaCl	Qtz	S	Fracture	137,9	128,6	149,9	6,06	4,34	8,14
			6	H_2O/NaCl	Fsp	P?	Dissolved cleavage	138,0	119,9	155,2	4,19	1,40	6,74
			>20	Liquid HC	Fsp	P?	Dissolved cleavage	n/a (1P)	n/a	n/a	n/a	n/a	n/a

Table 2. Summary of fluid inclusion microthermometry data from Skye. Salinity converted from final ice melting temperature (Bodnar, 1993). 1P=Monophase (liquid) inclusions, Cal1/2=First/second phase calcite, Within deformation band, Fsp=Feldspar, GOB1/2=First/second phase grain/overgrowth boundary, OG=Quartz overgrowth, P=Primary, Qtz=Quartz, S=Secondary, Sal.=Salinity.

Petrography and Diagenesis

East Greenland

Samples of Triassic sandstone from Laplace Bjerge on Geographical Society Ø record the most complete diagenetic sequence in the East Greenland study area, with a number of distinct authigenic cementation and dissolution events documented (figure 4). The earliest recorded diagenetic phase is sporadically developed, volumetrically minor grain-coating illite and mixed-layer illite/smectite. These clays line and bridge pore throats where present (Figure 5a), with resultant reduction in porosity and permeability.

Extensive syntaxial quartz overgrowths (i.e. in optical and crystallographic continuity with nucleating grains) postdate grain-coating clay minerals and are the most volumetrically significant authigenic phase in the East Greenland study area (Figure 5b). Quartz cementation has had a profound detrimental effect on reservoir quality, causing up

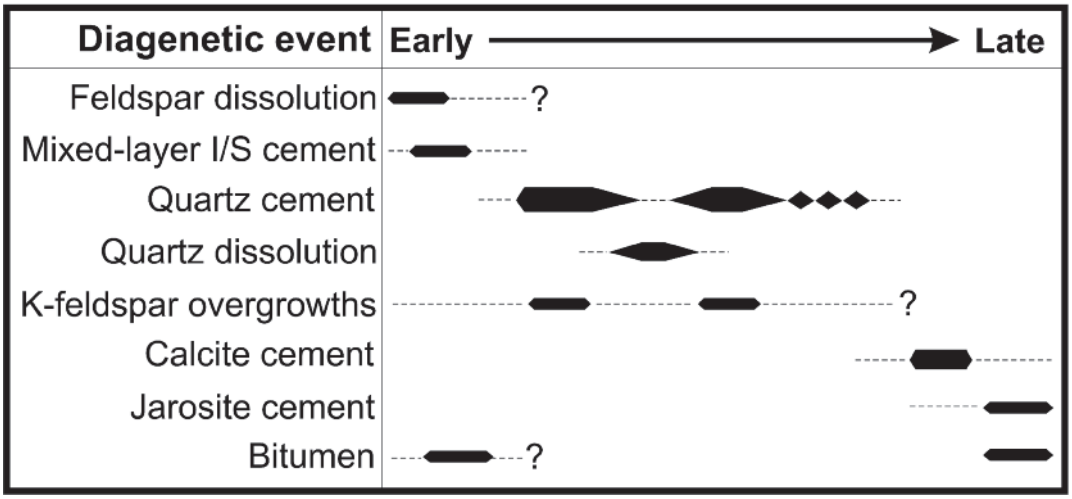

Figure 4. Diagenetic sequence for the East Greenland study area, showing relative ages (progressively labelled as early to late) based on textural evidence. The entire diagenetic history is only recorded in the Triassic sandstones. Bitumen is the latest phase recorded.

to 75% occlusion of porosity and reduction of pore connectivity. In some samples, transmitted light microscopy shows two distinct phases of quartz overgrowth, recorded by populations of fluid inclusions entrained along the interface between the two cement phases. SEM-CL studies have shown that authigenic quartz overgrowths are characterised by several growth zones, distinguished by alternating light and dark CL zones (Figure 6). An early generation of dark-luminescing cement is followed by a later phase which contains distinct growth zones which are often thin and alternate between light and dark luminescence. Most growth zones do not display a transition from dark to light and vice versa, but rather an abrupt change in luminescence character.

Following the cessation of quartz precipitation, a phase of calcite cementation is recorded in some samples. The calcite forms a patchy, poikilitic spar where developed, occluding porosity and resulting in a significant reduction in reservoir quality. Volumetrically minor authigenic jarosite appears to postdate all other cements and fills extant porosity where present. Dissolution of detrital plagioclase and alkali feldspar grain cores has created minor amounts of secondary intragranular porosity (Figure 5c). Rare albite overgrowths occur on detrital alkali feldspar and plagioclase clasts.

Solid bitumen, representing residual liquid petroleum which has been altered by thermal degradation, water washing, aerial exposure, and/or biodegradation, occurs in a number of samples within the East Greenland study area. The Triassic of Laplace Bjerge contains large volumes of bitumen within pore space, indicating an exhumed oil reservoir as described by Price and Whitham (1997), complete with a well-defined palaeo-oil/water contact below a palaeo-oil leg. Where sample localities are in close proximity to a major Tertiary sill, the bitumen has been altered to a highly reflective carbonaceous residue, as what was originally liquid petroleum has cracked to almost pure carbon due to magmatic heating. The bitumen often occurs in association with authigenic jarosite. Bitumen is also recorded at the grain/overgrowth boundary in two samples (samples Tr1 and Tr3) from the same section. A single sample from the Jurassic of Mols Bjerge (sample J2) displays rare residual bitumen in pore space, occurring as volumetrically minor stringers ~100 microns thick. Other Jurassic samples which were not subjected to microthermometry show some evidence for two discrete phases of bitumen. An early bitumen predates quartz overgrowths, occurring

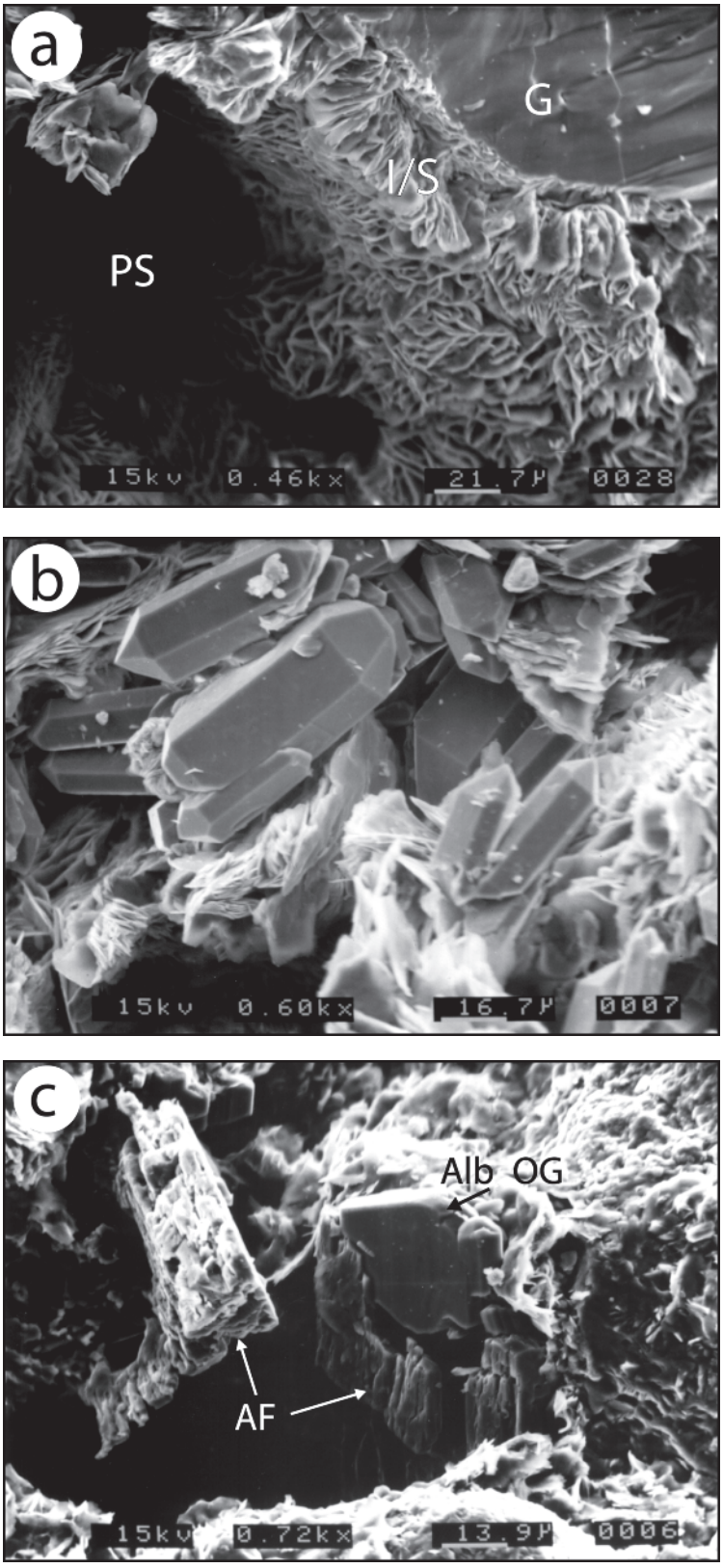

Figure 5. Scanning electron photomicrographs showing typical diagenetic features, East Greenland. (**a**) Grain-coating authigenic mixed-layer illite/smectite, which reduces hydraulic conductivity by lining and bridging pore throats. (**b**) Volumetrically significant authigenic quartz fills extant porosity to the detriment of reservoir quality (**c**) Creation of secondary porosity resulting from feldspar dissolution. Rare albite overgrowths occur on detrital grains of alkali feldspar, distinguished by energy dispersive analysis. AF=Detrital alkali feldspar grain, Alb OG=Albite overgrowth, G=Detrital quartz grain, I/S=Authigenic mixed-layer illite/smectite, PS=Pore space.

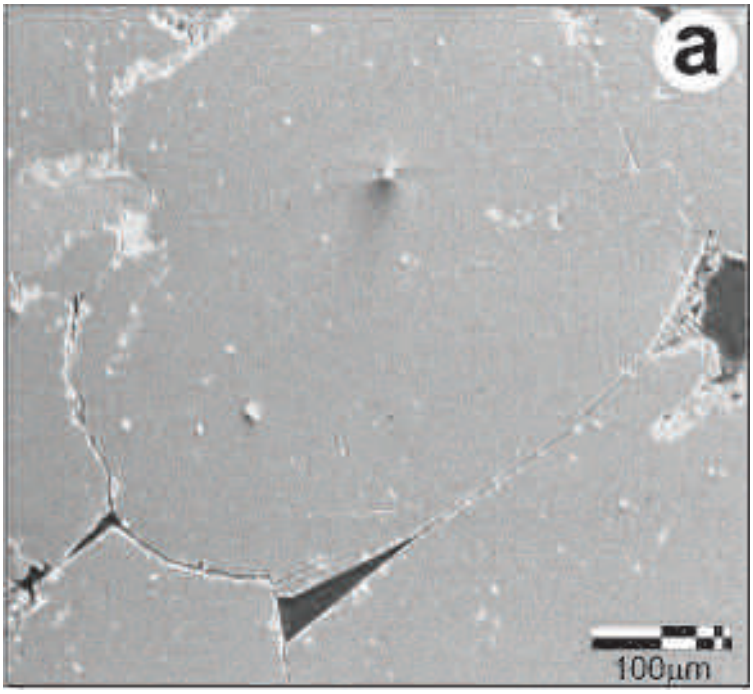

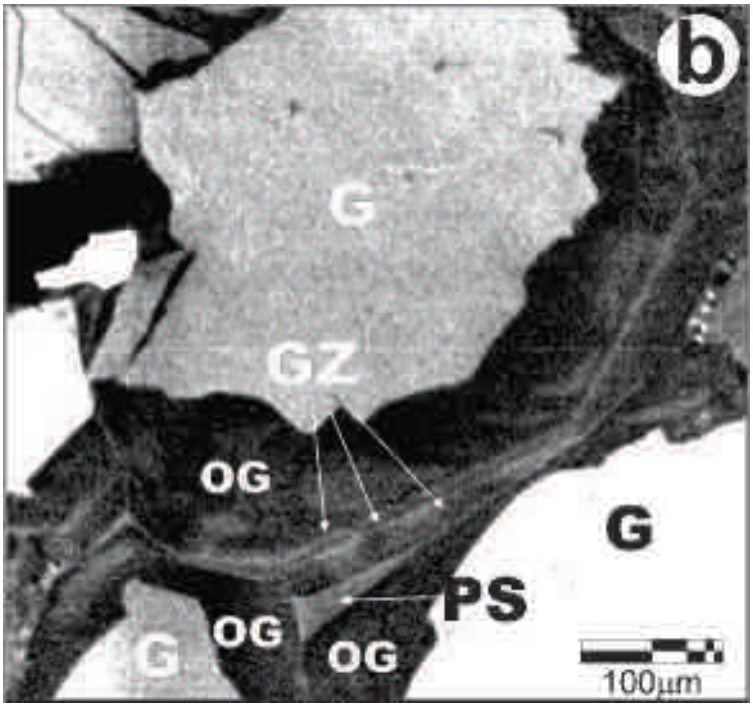

Figure 6. Porosity occlusion due to quartz authigenesis, Jurassic sandstone, East Greenland. Multiple growth zones in quartz cements, which are only recognisable under cathodoluminescence, record complex pore fluid histories. (**a**) Backscattered electron image. (**b**) Scanning electron microscope cathodoluminescence image. G=Detrital quartz grain, OG=Quartz overgrowth, PS=Pore space, GZ=Growth zones in authigenic quartz.

at grain/overgrowth boundaries, while a later stage postdates overgrowths. Evidence for liquid petroleum is also found in petroleum fluid inclusions (see below).

Skye

A generalized diagenetic sequence for the Skye samples is given in figure 7. Pore-lining mixed-layer illite/smectite clays are the earliest authigenic phase, and appear to be randomly distributed throughout the samples. The clays constitute a volumetrically minor cement, and are postdated by authigenic quartz (Figure 8a).

Quartz overgrowths nucleated on detrital quartz grains are well developed, notably in the immediate vicinity of igneous intrusions. Overgrowths have drastically reduced reservoir quality in affected sandstones, causing severe occlusion of porosity (Figure 8b). Integrated BSEM and SEM-CL analyses allow the quantitative assessment of porosity reduction, with up to 75% loss of pre-cement porosity in some areas, notably above a large Tertiary sill at Elgol. In the Elgol area, most notably in the Elgol Sandstone Formation, quartz cementation is sporadically developed, leading to a patchy white appearance of samples in hand specimen. Quartz authigenesis occurred in two phases, evinced by petrographic relationships of overgrowths in the vicinity of deformation bands. These deformation bands are present in the Elgol Sandstone Formation, occurring as anastomosing sets of small-scale faults which have resulted in locally extensive cataclasis and grain comminution (Parnell *et al*., 2004). An early generation of quartz overgrowths appears to be pre-tectonic in origin, as this cement is commonly fractured and broken within the faults. A later phase of quartz occurs exclusively within the deformation bands themselves, and as such appear to be syn-, or less likely post-deformation. This two-phase quartz cementation history is supported by fluid inclusion data from each cement phase, as discussed below.

Carbonate cements are poorly developed in the samples examined in this study, although they are extensively developed at other horizons in the Jurassic of Skye. With the exception of vein calcite which occurs as a fracture-fill at the top of the main sill at Elgol, only the Bearreraig Sandstone just below the intrusion contains significant authigenic calcite. Where present, the calcite cement occurs as a late phase which postdates quartz overgrowths in the paragenetic sequence.

Residual bitumen is recorded in a number of samples from the study area. Samples S1, S3 and S4 from Elgol, and sample S7 from Valtos, contain sporadically developed intergranular bitumen. Two separate bitumen phases are observed in samples S1 and S3, with early bitumen entrained preferentially along deformation bands and a later bitumen, with distinct properties of fluorescence and

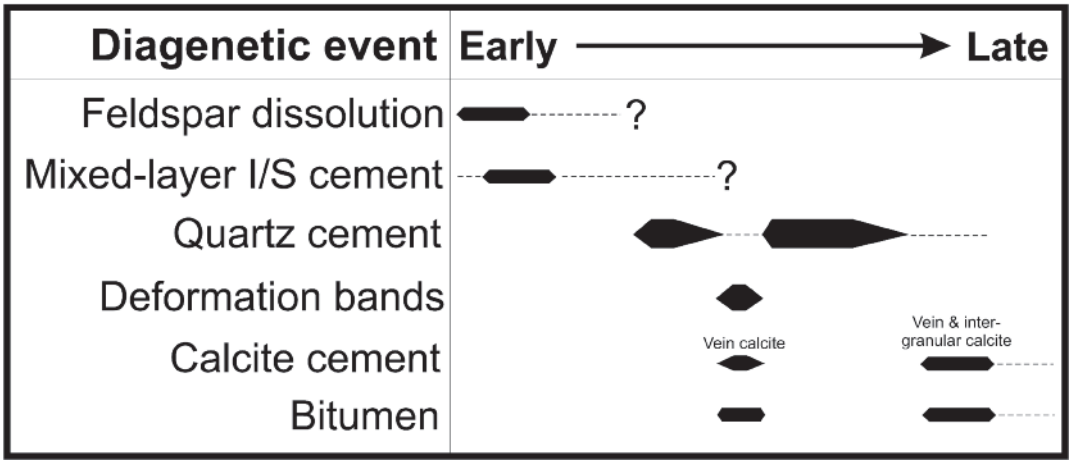

Figure 7. Diagenetic sequence for the Skye study area, showing relative ages (progressively labelled as early to late) based on textural evidence.

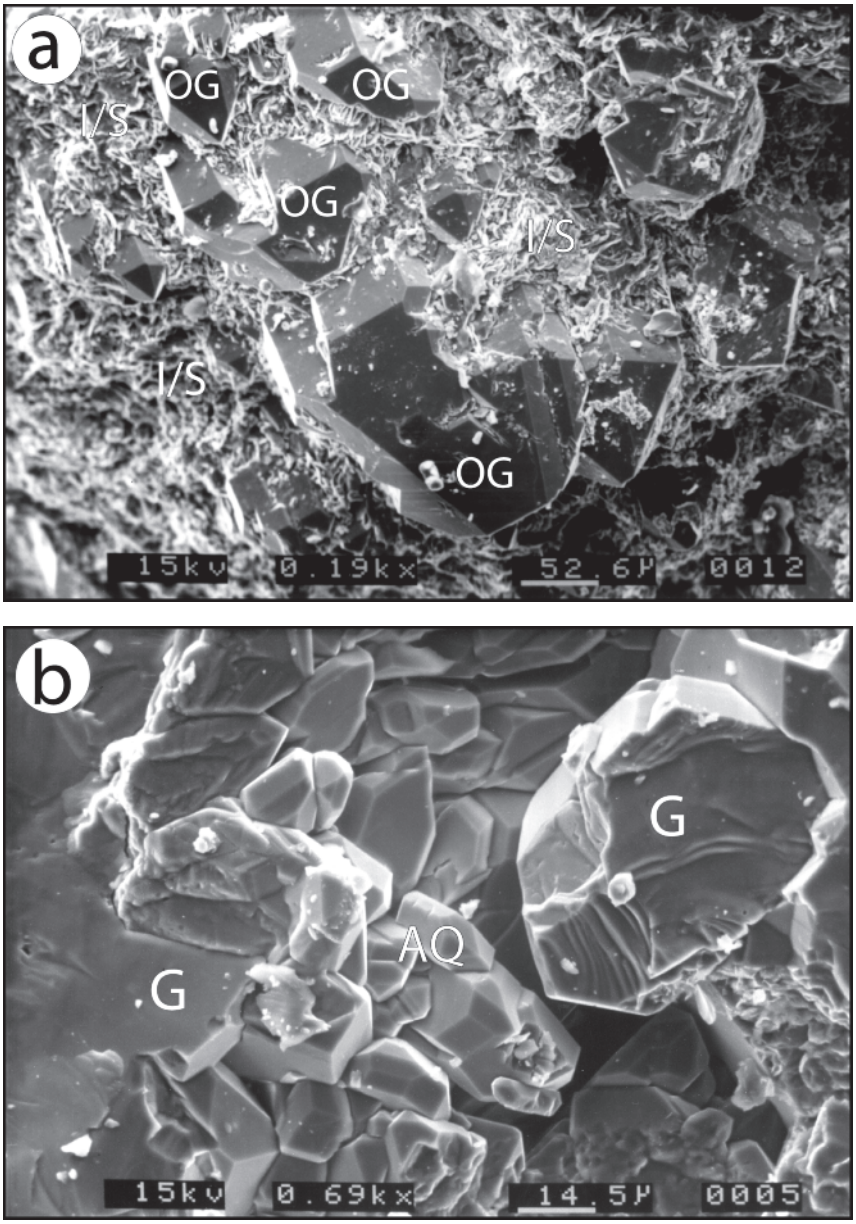

Figure 8. SEM photomicrographs showing typical diagenetic features, Skye. (**a**) Euhedral quartz overgrowths extrude from a grain-coating surface of mixed-layer illite/smectite. (**b**) Occlusion of porosity due to authigenic quartz cement nucleated upon detrital quartz grains, which display conchoidal fractures due to pre-depositional saltation. AQ=Authigenic quartz, G=Detrital quartz grain, I/S=Authigenic mixed-layer illite/smectite, OG=Quartz overgrowth.

reflectance, randomly distributed throughout the samples but excluded from deformation bands. Sample S5, a mineralized fracture within a Tertiary dolerite sill, contains two phases of bitumen entrained within early and late calcite vein fills.

Fluid Inclusion Data

Fluid inclusion data for East Greenland are summarised in table 1 and figure 9. Most notable are monophase liquid petroleum inclusions which have been recorded within annealed microfractures that predate quartz cementation in the Triassic of Laplace Bjerge.

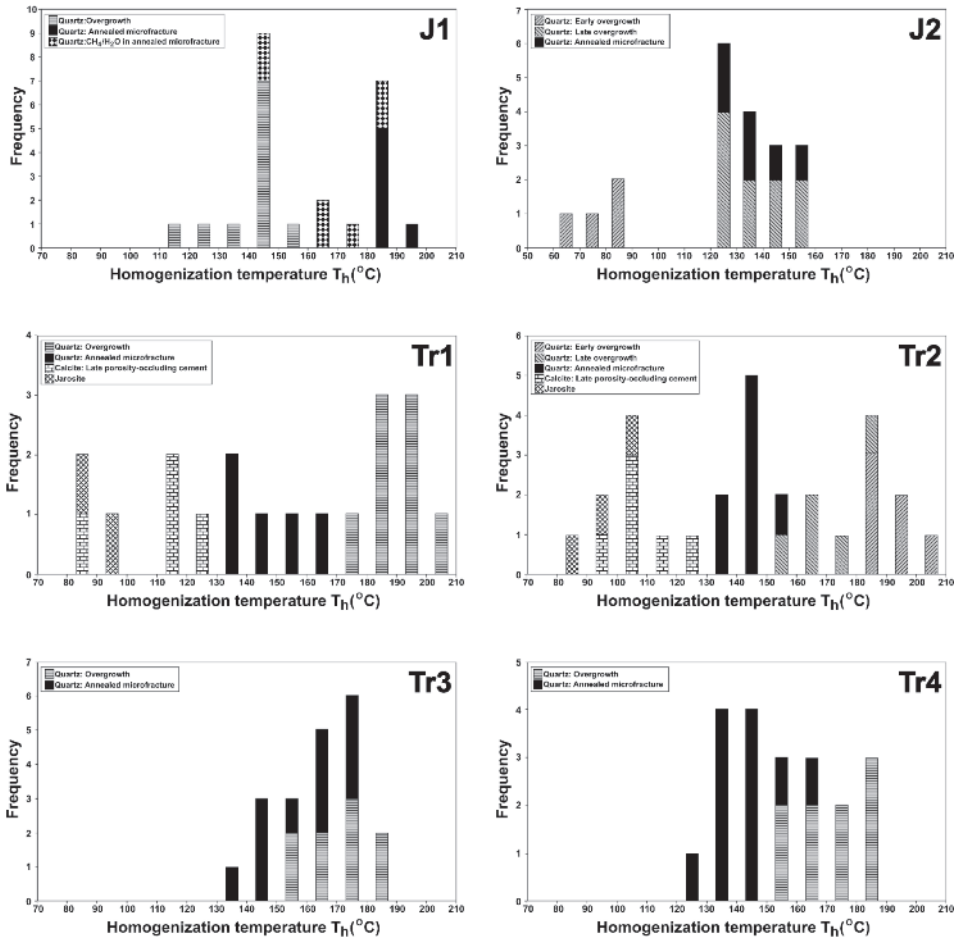

Figure 9. Fluid inclusion histograms, East Greenland study area. Sample localities are shown on Figure 2.

Data were also collected from samples from Elgol, Strollamus and Valtos on Skye. These data are summarised in table 2 and figure 10. Petroleum inclusions in the form of monophase liquid (live oil) and bitumen (degraded oil) are recorded in a calcite vein fill within a Tertiary sill at the contact with the Cuilladh Shale Formation at Elgol (sample S5). Early sparry calcite displays evidence for contemporaneous hydrocarbon generation/migration in the presence of inclusions of liquid oil and solid bitumen. Live oil inclusions are rare, monophase, and of pale green-yellow fluorescence colour. The solid bitumen probably represents a degraded version of the oil inclusions, possibly due to ineffective sealing of the inclusion cavity. A second period of oil charge is recorded by entrained bitumen within a late-stage calcite vein fill. This bitumen is of a different character to that associated with the early calcite, being less reflective, more abundant, and entrapped between crystal interfaces rather than within the crystals themselves. There is a significant time gap between the emplacement of both oils, as the two charge events were separated by a phase of quartz cementation which bears no evidence for associated petroleum migration.

In a sample from Valtos (S7), petroleum is encapsulated at grain/overgrowth boundaries in detrital quartz as solid bitumen, indicating a possible oil-wet reservoir pre- or syn-quartz authigenesis.

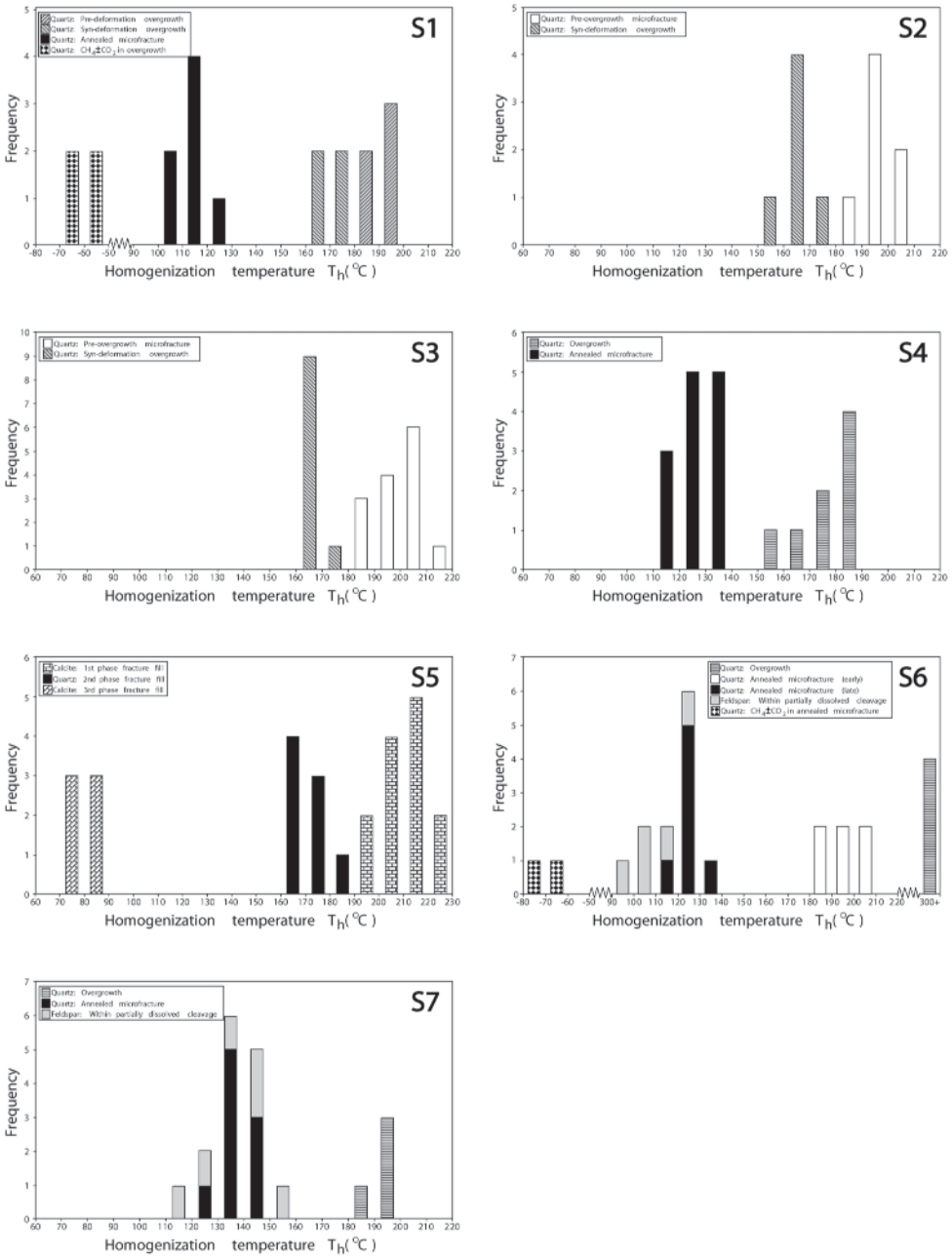

Figure 10. Fluid inclusion histograms, Skye study area. Sample localities are shown on Figure 3.

Furthermore, abundant liquid petroleum inclusions occur within secondary porosity created by the dissolution of detrital feldspar clasts. These inclusions display green fluorescence colour and are monophase, precluding palaeotemperature determination. A later oil charge event is recorded by intergranular bitumen in pore space in the same sample. Samples from both the Elgol Sandstone

Formation (S3) and Bearreraig Sandstone Formation (S4) also record a late, pore-filling oil emplacement event due to the presence of intergranular solid bitumen.

Discussion

Basins on the North Atlantic Margins often include large volumes of basic igneous material as sills and dykes, associated with the formation of oceanic crust during the opening of the North Atlantic. The emplacement of such igneous intrusions into the sedimentary pile has diverse consequences for diagenesis, reservoir heterogeneity, generation and migration of hydrocarbons, thermal degradation of reservoired oil, resolution of seismic imaging, and basal heat flux. An understanding of such processes is essential to the successful modelling of petroleum potential and risk assessment in petroleum systems along the Atlantic Margin.

Fluid flow histories

Research into fluid flow histories in Atlantic Margin basins suggests that pulses of anomalously hot fluids, often around and above 200°C and not spatially related to igneous intrusions, may be a common feature of passive margin basins (Duddy *et al*., 1994; Middleton *et al*., 2001; Wycherley *et al*., 2003; Parnell *et al*., 2005). It is difficult to estimate the duration of heating, but as the heating is not shown by vitrinite reflectance data it must have been short-lived, hence oil in the region has not all been cracked to gas (Parnell *et al*., 2005). Nevertheless, the widespread occurrence of evidence for these high temperatures indicates that large volumes of rock were affected. The implications of such hot fluid flow events for basal heat flux, oil charge and hydrocarbon prospectivity are significant (Green *et al*., 1999). Indeed, intimate links have been found elsewhere on the Atlantic Margin between hydrocarbon migration and hot aqueous fluids (Parnell *et al*., 1999; 2005).

The most immediate observation to be made prior to further discussion is the extent to which the spatially disparate East Greenland and Skye study areas share many similar features with respect to pore fluid histories. This may seem unsurprising considering that the two areas formed part of a largely continuous sequence of basins along the proto-Atlantic rift system prior to the onset of seafloor spreading *sensu stricto* in the Early Tertiary. However, many of the fluid flow events discussed in this section are evidently contemporaneous with, or later than, the intrusion of igneous bodies and associated continental separation. The inference is that aspects of fluid flow histories described below may be applicable to many of the numerous basins on the Atlantic Margin intruded by sills.

East Greenland

Fluid inclusion studies of sandstones in the East Greenland study area have yielded evidence of complex pore fluid histories. Fluid inclusions encapsulated within sandstone of Middle Jurassic age from Svinhufvud Bjerge (sample J1) indicate at least two distinct fluid migration events. Authigenic quartz overgrowths are well developed, forming euhedral syntaxial precipitates nucleated on detrital quartz grain surfaces. The numerous two-phase aqueous fluid inclusions encapsulated along grain/overgrowth boundaries represent palaeo-pore fluids at the time of quartz cementation. This population of fluid inclusions is characterised by moderate homogenization temperatures (mean T_h 142.2°C) and salinities (mean 6.09 wt.% equiv. NaCl). A separate, later fluid migration event is represented by trails of secondary inclusions entrapped within annealed microfractures which crosscut and postdate authigenic overgrowths. These inclusions record a higher temperature aqueous fluid, of mean T_h 185.3°C. Such fluid temperatures are uncommon in diagenetic environments, and may represent formation waters heated by igneous intrusions and undergoing migration after early quartz cementation. Rare, volumetrically minor methane-bearing inclusions associated with this second population are identified by microthermometric analysis, due to the formation of clathrates on freezing and final ice melting temperatures above 0°C.

Sandstone of Jurassic age at Mols Bjerge (sample J2) displays evidence for two separate phases of quartz cementation, with overgrowths having two distinct dust rims defined by fluid inclusions.

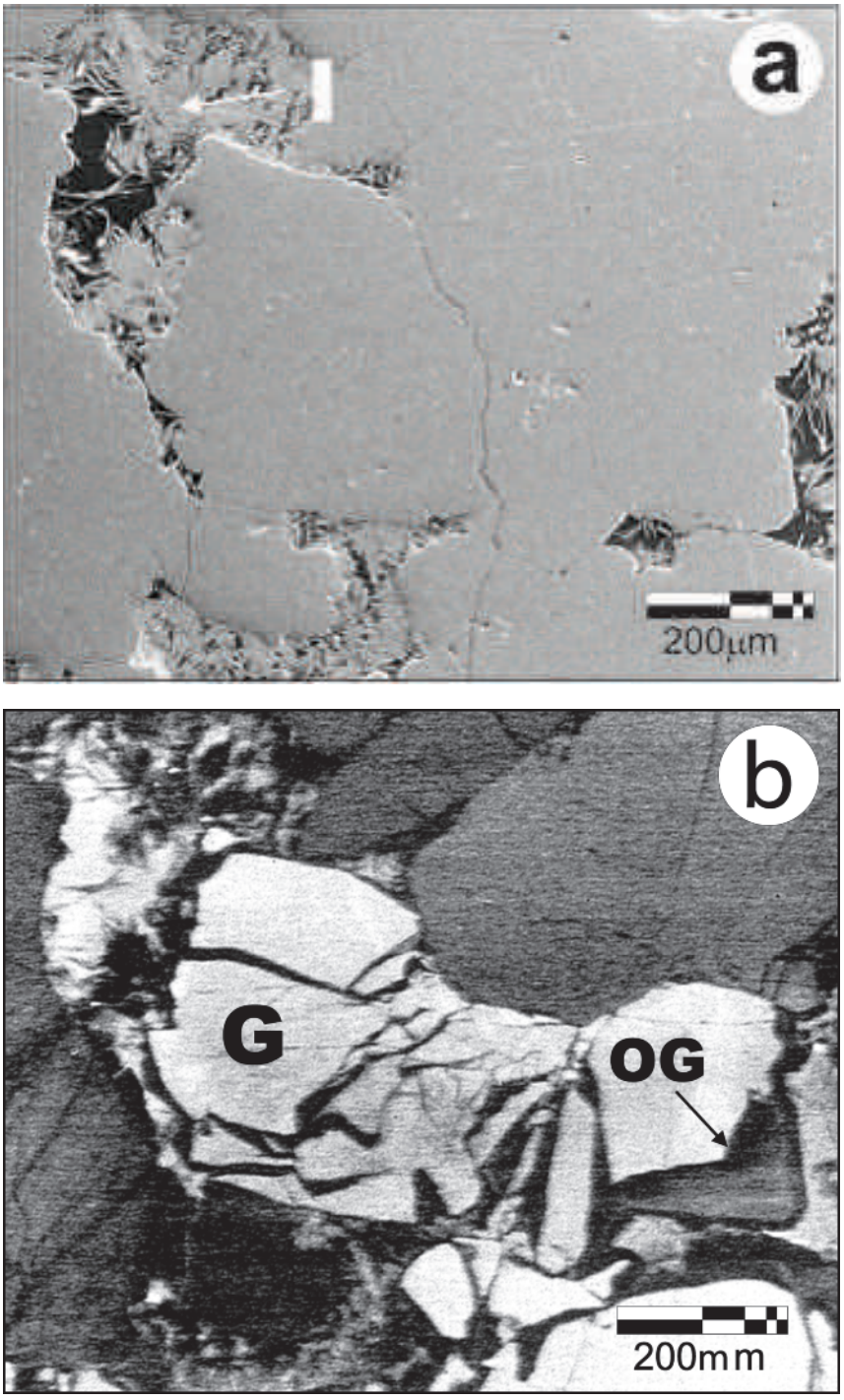

Figure 11. Extensive crushing and dilation of grains prior to annealing of fractures by authigenic quartz (dark under scanning electron microscope cathodoluminescence), Jurassic sandstone, East Greenland. Note that the quartz within the overgrowth (arrowed) appears contiguous with that in fractures. (**a**) Backscattered electron image. (**b**) Scanning electron microscope cathodoluminescence image. G=Detrital quartz grain, I=Pore-filling authigenic illite, OG=overgrowth.

Minimum trapping temperatures of inclusions encapsulated at the grain/overgrowth boundary, representing the earliest diagenetic fluid recorded, are low (mean T_h 78.4ºC). This probably represents an early quartz precipitate from connate pore fluids in thermal equilibrium with ambient formation temperatures, without the heating effect of igneous intrusions. However, inclusions trapped at the interface between the first and second generation of overgrowth are of much higher palaeotemperature (mean T_h 137.4ºC), which may indicate an influx of formation waters heated by the intrusion of sills/dykes into the sedimentary succession. Secondary fluid inclusions along annealed microfractures show pore fluid palaeo-temperatures and salinities similar to this second overgrowth phase, indicating that the two inclusion populations may be contemporaneous. That is to say, this later fluid flow event may have been associated with fracturing as well as diagenetic cementation. SEM-CL studies support this, with quartz within the fractures having a continuous boundary with, and showing identical optical properties to, that in the overgrowths (figure 11).

SEM-CL studies support this multi-stage cementation history. The earliest generation of dark-luminescing quartz appears to be partially dissolved with an anhedral outer surface, and probably represents the correlative of the early, anhedral quartz defined by fluid inclusions described below. The thin, cyclic growth banding apparent in the outer parts of the overgrowths probably indicates an evolving pore fluid chemistry during precipitation of the later quartz cement. The fact that the boundary between growth zones is not gradual indicates a series of sporadic pulses of silica precipitation rather than a continuous process of authigenesis.

The Triassic samples (Tr1-Tr4) show the opposite trend to that of the Jurassic, with evidence for decreasing pore fluid temperatures over time. Fluid inclusions associated with early-formed quartz overgrowths yield palaeofluid homogenization temperatures of up to 205ºC. Rarely (e.g. sample

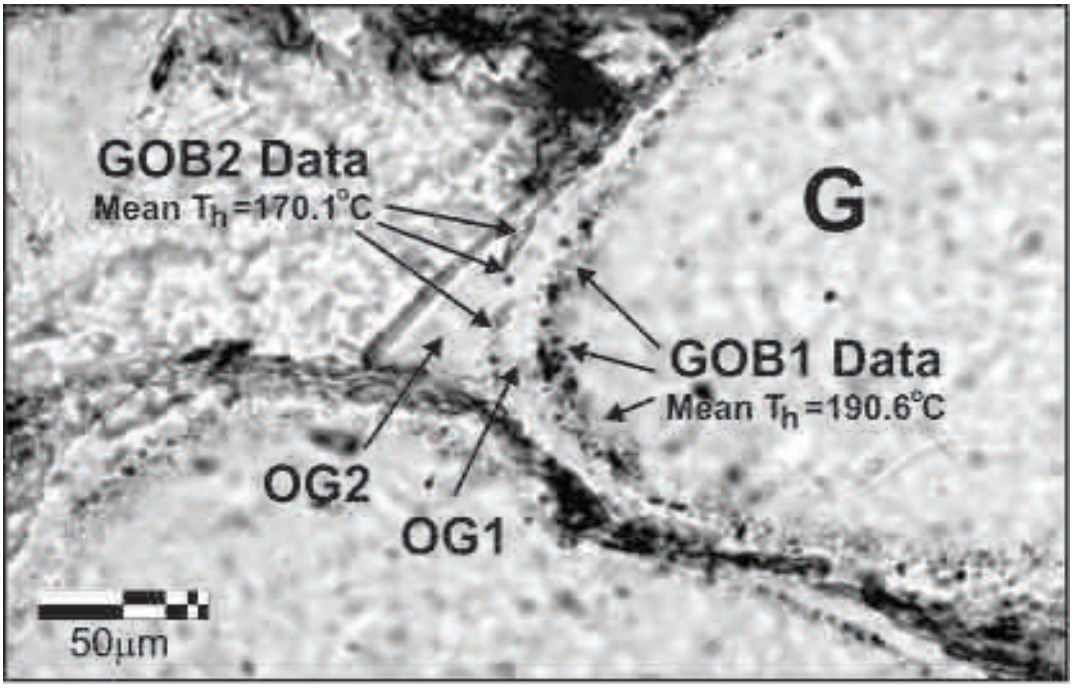

Figure 12. Two distinct episodes of quartz cementation are recorded by multiple "dust rims" at grain/overgrowth boundaries, East Greenland. Fluid inclusions trapped at these interfaces indicate a 20°C decline in pore fluid temperatures during precipitation of the second cement phase. G=Detrital quartz grain, OG1/2= First/second overgrowth phase, GOB=Grain/overgrowth boundary.

Tr2), a subsequent phase of quartz precipitation is recorded by a second, discrete phase of overgrowth cementation, the boundary between the two being defined by a plane of fluid inclusions. The early overgrowth phase typically exhibits an anhedral to subhedral outer surface, while the later phase is euhedral with well-defined crystal terminations. This may be evidence for some dissolution of the early quartz phase, prior to precipitation of the latter. Microthermometric data obtained from this second phase of quartz cement show evidence for a decline in pore fluid temperature (mean T_h 170.1ºC) since the previous generation of quartz overgrowths (mean T_h 190.6ºC), as shown in figure 12. The widespread distribution of the early cement and consistency in fluid inclusion data preclude a recycled origin for these overgrowths. Each of the Triassic samples display evidence for a late fluid flux event, recorded by secondary inclusions which crosscut all overgrowths and can be traced across several detrital grains. Microthermometric analysis indicates that these late fluids had experienced a further decline in pore fluid temperature, with mean T_h values of 148.0ºC, 145.6ºC, 159.8ºC and 142.9ºC in samples Tr1-Tr4 respectively, from the Triassic section.

Where calcite cement is present in Triassic sandstones (samples Tr1, Tr2), fluid inclusion microthermometric data are well constrained, indicating mean homogenization temperatures of 108-110ºC and salinities of 19.2-20.3 wt.% equiv. NaCl. Such high pore fluid salinities are normally indicative of an influx of highly evolved brine (present-day seawater has approximately 3.5 wt. % equiv. NaCl and other salts). Meteoric water is an unlikely source, due to the amount of water-rock interaction which would have to take place to allow the fresh water to achieve such high salinities. The source of the ions for calcite cementation is not constrained by this study. Rare fluid inclusions encapsulated within jarosite in the same samples yield mean pore fluid minimum trapping temperatures of 88.1ºC and 90.3ºC, and salinities of 12.3 and 13.7 wt.% equiv. NaCl. Jarosite is a mineral commonly encountered due to oxidative weathering, but in this case the trapping temperatures indicate a hydrothermal origin. Fluid inclusion studies indicate that the late non-silicate cements of the Laplace Bjerge Triassic section were precipitated from pore fluids of distinctly different compositions to those which resulted in quartz authigenesis. Figure 13 shows a crossplot of T_h vs. salinity data derived from fluid inclusions within

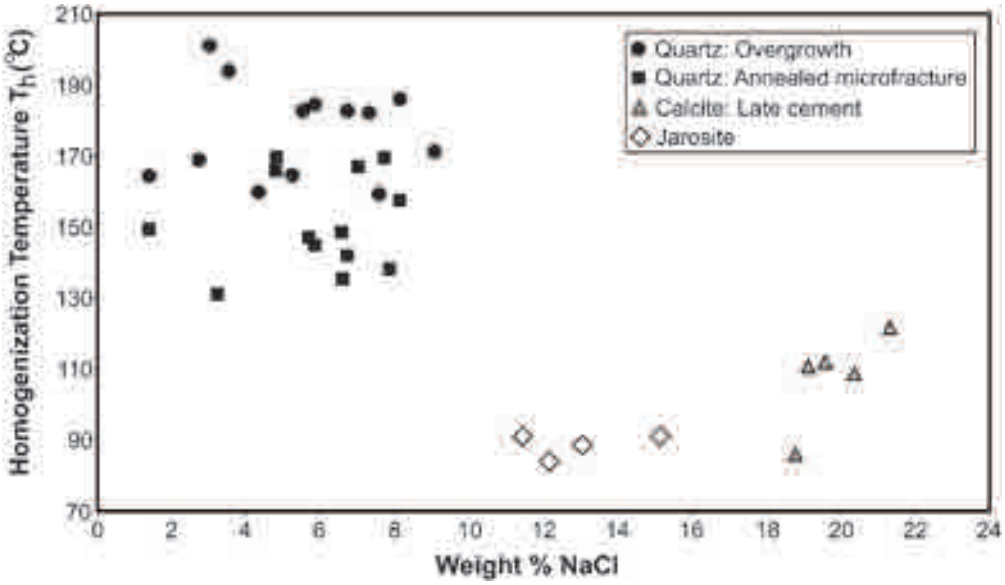

Figure 13. Crossplot of palaeofluid temperature vs. salinity, derived from fluid inclusions, East Greenland Triassic. Each mineral phase was clearly precipitated from different pore fluids with distinct thermal and compositional properties.

the East Greenland Triassic. Clearly, the fluids encapsulated within non-silicates represent discrete pore fluid populations which may be completely unrelated to the earlier silica-saturated formation waters.

Skye

At Elgol, each of three samples from the Elgol Sandstone Formation (samples S1, S2 and S3) display evidence of an early pulse of high-temperature (~200ºC) aqueous fluids contemporaneous with the formation or reactivation of deformation bands. The intimate association of hot fluid flow with fracturing is evident from the numerous trails of high-T_h secondary fluid inclusions encountered in these samples (Parnell *et al*., 2004). These occur almost exclusively subparallel to planes of cataclasis and crosscut numerous detrital grains. This high-temperature fluid pulse probably represents the earliest recorded fluid flow event in the area, as the trails of secondary inclusions often terminate at grain-overgrowth boundaries, which they clearly predate. Such inclusion populations are usually disregarded during fluid inclusion studies due to the possibility that they may be inherited and not representative of true diagenetic fluids. However, the unimodal orientation of the inclusion trails in the Elgol samples, and the fact that individual trails can often be traced across several detrital grains, confirms a diagenetic origin.

Similarly, high-temperature palaeofluids were responsible for a phase of pre-deformation quartz authigenesis. Quartz overgrowths in proximity to the deformation bands have been spalled and fractured where they protrude into the plane of cataclasis. A population of fluid inclusions entrained along these grain/overgrowth boundaries displays a mean T_h of 191.1ºC in sample S1. These early overgrowths are interpreted as being concomitant with the early pulse of high-temperature fluids discussed above, due to the similar T_h values of both fluid inclusion populations.

A later phase of quartz cementation is documented almost exclusively within the deformation bands themselves. Comminuted and dilated grains have been extensively annealed by silica precipitation and by the development of a second generation of quartz overgrowths. Unlike the earlier overgrowths, these are not fractured and as such are interpreted to be syn-, or less likely post-deformation. Microthermometric data from inclusions encapsulated at grain/overgrowth boundaries within the deformation bands have yielded minimum trapping temperatures in the range 155.9-177.3ºC, with a mean of 167.5ºC. This represents a decline in pore fluid temperatures with time, with this second fluid pulse undergoing migration at around 32.5ºC cooler than the earlier event. It is notable that this fluid flow history is very similar to that recorded in the Triassic of East Greenland, with comparable temperatures, relative timings and progressive cooling behaviour.

The dolerite sill at Elgol displays quartz and calcite veining at close to its upper contact with the host Cullaidh Shale Formation, and is heavily stained with bitumen (sample S5). The Cullaidh Shale is oil-prone and would have become mature in immediate proximity to the intrusion (Thrasher, 1992). Petrographic examination of the vein material indicates that three separate paragenetic phases have occurred. Each mineral cement is populated by fluid inclusions with distinctive properties of T_h, salinity and vapour/liquid ratio (figure 14). An early, sparry calcite is the dominant vein mineral, and is followed by subordinate euhedral vein quartz and finally a minor, late calcite. The early calcite contains abundant aqueous fluid inclusions of mean T_h 212ºC, many of which do not homogenise below 300ºC. Such high trapping temperatures do not represent quiescent diagenesis from connate waters, and are interpreted to be the result of precipitation of superheated pore fluids during the emplacement of the intrusion. The additional presence of inclusions of solid bitumen and monophase liquid petroleum inclusions in the early calcite indicates that hydrocarbons were also undergoing generation and migration during precipitation of this cement phase. The bitumen inclusions are equidimensional and may represent thermal degradation of originally live oil inclusions post-entrapment, although oil inclusions have been recorded elsewhere surviving to temperatures of 300ºC (Dutkiewicz *et al*., 2006). No hydrocarbon inclusions are demonstrably coeval with aqueous inclusions. The second mineral

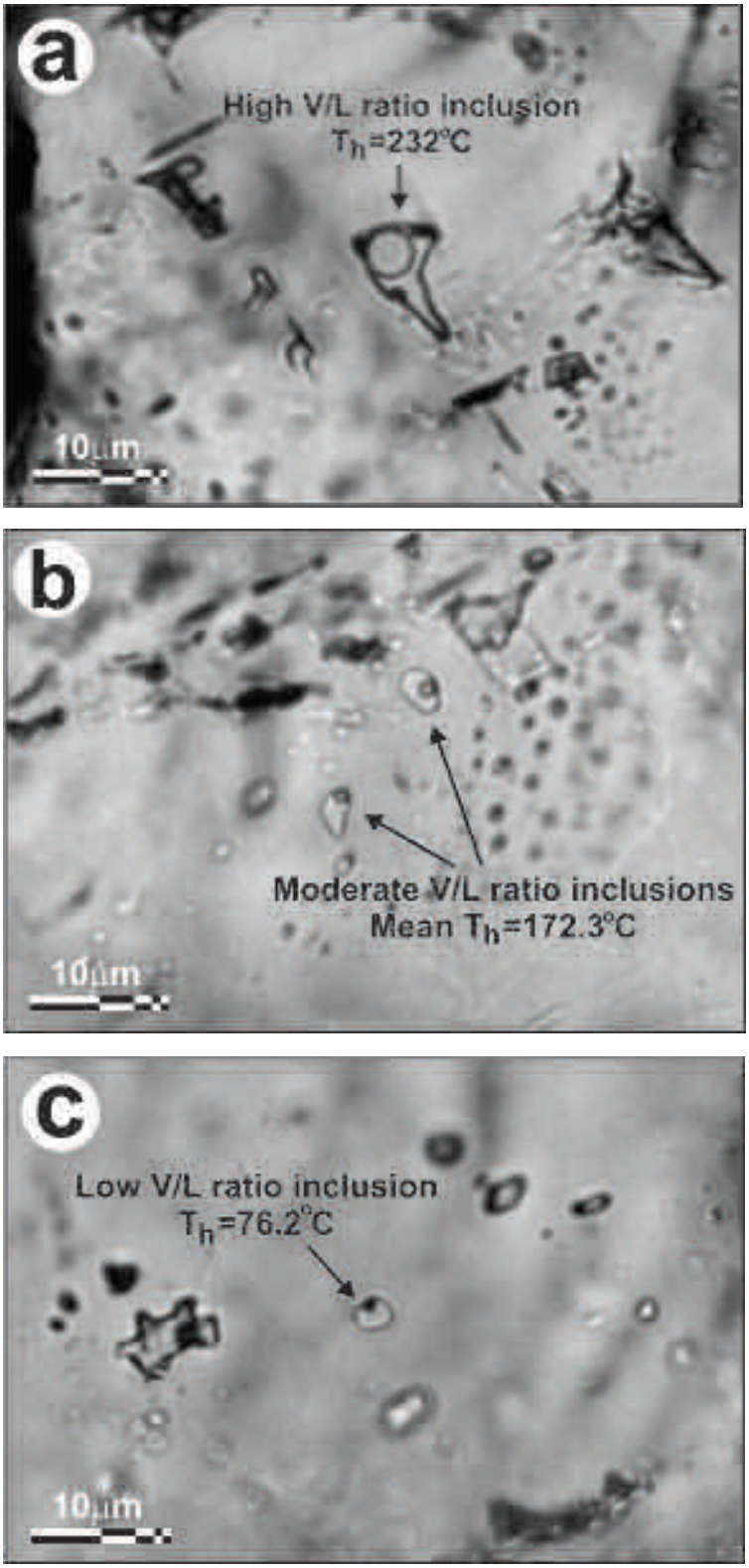

Figure 14. Photomicrographs of typical fluid inclusions recorded within veins in a dolerite sill at Elgol, Skye. Vapour/liquid ratios display a close correlation with homogenization temperatures. (**a**) High-T_h early (first stage) calcite. (**b**) Moderate-T_h quartz. (**c**) Low-T_h late (second stage) calcite.

phase in the sample is euhedral quartz which contains rare aqueous inclusions of mean T_h 172.3ºC. This represents a trend of cooling pore fluids with time and is similar to that observed in the overlying Elgol Sandstone samples discussed above. The third phase is a turbid calcite which is observed to crosscut the quartz vein material in places. This late calcite contains significant amounts of entrained bitumen along the vein margins and between crystal boundaries. The bitumen represents a second phase of oil charge, and may have altered to its current solid state due to thermal or biological degradation, water-washing, or exposure at outcrop. Aqueous fluid inclusions in the late calcite indicate mineral precipitation from a fluid of much lower temperature (mean T_h 80.4ºC) and significantly higher salinity (mean 18.9 wt.% equiv. NaCl) than recorded in other samples in the Skye study.

A sample of Jurassic sandstone taken from the contact with the main granite of the Skye Igneous Complex at Strollamus (S6) displays abundant authigenic quartz cement as overgrowths on detrital quartz grains. Microthermometry carried out on primary aqueous inclusions occurring at grain/overgrowth boundaries and within overgrowths yields palaeofluid temperatures of >300ºC during quartz precipitation. In this case, magmatically-heated pore fluids precipitated a large amount of authigenic quartz cement.

A sample from Valtos (S7), well outside the metamorphic aureole of the Skye Igneous Complex, exhibits sporadically developed quartz overgrowths which contain fluid inclusions. Microthermometry indicates that these overgrowths precipitated from high-temperature palaeofluids (mean T_h 192.3ºC), similar to those in close proximity to the main igneous centre. Inclusions of solid black bitumen and fluorescent liquid oil inclusions occur within partially dissolved cleavage planes in detrital feldspar grains. The oil inclusions are monophase, precluding the assessment of the trapping temperature of the migrant petroleum. Monophase hydrocarbon inclusions within partially dissolved feldspar cleavage planes often occur in coexistence with two-phase aqueous inclusions of mean T_h 138.0ºC at Valtos, indicating that liquid petroleum may have been undergoing migration along with water as two immiscible fluids. The comparable homogenization temperatures and salinities of aqueous fluid inclusions within annealed microfractures and detrital feldspars indicate that the two may be contemporaneous.

There is evidence for a late fluid flow event which was widespread and is ubiquitous in every sample examined from the three localities in Skye. This late fluid pulse is recorded by trails of secondary aqueous fluid inclusions encapsulated along annealed microfractures in detrital quartz grains, which crosscut and hence postdate quartz overgrowths. The inclusions are characterised by relatively low palaeofluid temperatures, with many monophase as well as two-phase inclusions. Monophase inclusions are normally thought to represent inclusion entrapment around or below 60ºC, while two-phase inclusions in this population have a mean T_h of 126.7ºC and a range from 102.6ºC to 149.9ºC across all samples. These data indicate a late, spatially widespread pulse of cooler aqueous fluids, which caused extensive microfracturing and annealing. This is discussed further below.

Igneous intrusions cause rapid, regional quartz cementation

Primary fluid inclusions encapsulated at grain/overgrowth boundaries in quartz grains represent samples of palaeo-pore fluids responsible for precipitation of the cement (Roedder, 1984). In both the East Greenland and Skye study areas, such inclusions often display homogenization temperatures in excess of 200ºC.

Such temperatures are too high to be representative of static connate pore fluids in equilibrium with ambient rock temperatures. Formation waters of such high temperature would only be present at around 6 km depth in a 'normal' geothermal gradient of 30ºC. Even allowing for higher rates of basal heat flux due to crustal attenuation and the emplacement of igneous material, such temperatures are too high to be accounted for by burial alone. In the Skye study area, Jurassic source rocks remain thermally immature where not in the vicinity of igneous intrusions (Thrasher, 1992), and Apatite Fission Track Analysis (AFTA) indicates that

formation temperatures probably never exceeded 50ºC prior to intrusion (Lewis *et al*., 1992). Similarly, maximum burial depths in the East Greenland region are constrained by stratigraphic truncations (Price *et al*., 1997) and mudstone organic maturity indicators (Stemmerik *et al*., 1993) to have been in the range 1.5 to 3 km.

Thus the numerous high-Th (~190 ºC) fluid inclusions observed in both study areas represent rapid, event-driven precipitation of quartz cement from magmatically-heated advecting formation waters. The emplacement of intrusions in the Paleogene would have initiated the flux of large volumes of hot pore fluids through permeable media, notably reservoir intervals and fracture planes. Dissolution of silica from carrier beds would have taken place due to high ambient fluid temperatures, only to be re-precipitated when pore fluids cooled due to thermal equilibration with cold country rocks at distance from intrusions. The tightly constrained spread of data within these high-T_h fluid inclusion populations attests to the rapidity of cementation. If the process was protracted, a much wider distribution of data might be expected as precipitant pore fluids gradually cooled after the cessation of igneous activity.

Other evidence supports the brevity of the hot fluid pulse associated with magmatism. It is commonly accepted that the thermal aureole of a hypabyssal intrusion rarely extends beyond 100% of the thickness of the intrusion itself (e.g. Bostick, 1979; Stewart *et al*., 2005). In Skye, Thrasher (1992) used organic geochemical data to show that Jurassic source rocks without 15km of the Skye Central Igneous Complex are regionally immature. This contrasts with the evidence from fluid inclusions which indicates that fluid-driven advective heating may have been widespread in the region. The apparent discrepancy arises from the fact that many techniques commonly used to determine thermal histories (e.g. vitrinite reflectance, apatite fission track analysis, biomarker ratios) are based on kinetic chemical reactions, i.e. are dependent on time as well as temperature. However, fluid inclusions represent palaeo-pore fluids encapsulated at an instantaneous point in geological time, and as such are not dependent on the duration of the heating event. This means that fluid inclusions have the potential to record very short-lived pulses of hot fluids which may go unrecognised using other techniques. Middleton *et al*. (2001) demonstrated that pulses of hot fluids elsewhere on the Atlantic Margin may have lasted for less than 10 ka. However, in the absence of time markers it is difficult to estimate an approximate time span for the hot fluids event.

The large volumes of authigenic quartz recorded in the study areas are problematic due to the very low solubility of silica in aqueous fluids. Bjørlykke (1994) proposed that high volumes of pore fluids ($10^8 cm^3$ of water passing through each $1cm^2$ of rock) would be required for significant quartz authigenesis by fluid advection. Pore fluid temperatures have a significant effect on the equilibrium thermodynamics and kinetics of silica precipitation (Worden and Morad, 2000), so that high fluid temperatures such as those recorded in the study area greatly enhance the rate of chemical reactions which lead to the liberation and dissolution of silica. Nevertheless, it is likely that most of the silica was locally derived, and thus quartz cementation was largely a function of heating rather than fluid flow.

The absolute pore fluid palaeotemperatures recorded by fluid inclusions are broadly similar in both study areas. This is most apparent on Skye, where samples are taken from spatially disparate parts of the basin. A sample from Valtos shows evidence for very similar pore fluid histories to other samples in the region, despite being well outside the thermal aureole of the main batholithic centre. However, Valtos is affected by the ubiquitous dolerite sills which are found across the basin. The implication is that large numbers of hypabyssal intrusions may be much more significant in terms of regional fluid flow and diagenesis than single large batholithic mass. This is supported by the data from the Triassic of East Greenland, where similar pore fluid histories are recorded in a region with large numbers of sills rather than major igneous centres.

Timing of fluid flow events

The Triassic of East Greenland and the Jurassic of Skye display evidence for two distinct, regionally extensive fluid flow events: an early, high temper-

ature fluid accompanied by major quartz authigenesis, and a late, low-temperature fluid which caused widespread microfracturing on a grain-scale. This study has allowed the assessment of relative and absolute timing of fluid migration and diagenesis in both regions.

High-temperature fluid flow related to Early Tertiary igneous activity

The earliest fluid flow events recorded in the East Greenland and Skye areas are often recorded by aqueous fluid inclusions of high palaeotemperatures. The temperatures involved are consistent and well constrained across both study areas, and were probably directly caused by the emplacement of large volumes of igneous material in the Early Tertiary. Such igneous activity is a common feature of basins on the Atlantic Margin, and can be readily dated by geochemical methods. This allows similar constraints to be placed on the timing of hot fluid migration associated with magmatism.

Igneous activity on Skye included intrusion of granitoid and gabbro batholiths, dolerite sills and dykes, and the widespread extrusion of flood basalts. The dykes and sills which appear to have been chiefly responsible for rapid quartz cementation in the Skye region have been dated at 60.5 Ma to 58.9 Ma (U/Pb dating, Hamilton *et al*., 1998).

A two-stage history of igneous activity has been proven using $^{40}Ar/^{39}Ar$ studies in the Traill Ø region of East Greenland (Noble *et al*., 1988; Price *et al*., 1997), showing evidence for a *c*.54 Ma event and a *c*.36 Ma event. The earlier, Paleocene event was more widespread, producing the large numbers of sills found throughout the study area. The later, Oligocene event was less significant, producing the Kap Parry syenite intrusion in the SE part of Traill Ø. We interpret the high-temperature quartz authigenesis recorded in Triassic sandstones to be associated with the Paleocene event, due to its more regionally extensive nature and the fact that the relevant samples were taken at distance from the Oligocene syenite.

Low-temperature fluid flow related to Late Tertiary uplift

Secondary fluid inclusions encapsulated along annealed microfractures, which postdate Early Tertiary quartz cementation, are ubiquitous throughout the study areas. Minimum trapping temperatures of these inclusion populations are significantly lower (weighted mean T_h 152.4ºC and 126.7ºC for East Greenland and Skye respectively) than those recorded by quartz overgrowths in the majority of samples. This late episode was characterised by extensive microfracturing and annealing of detrital grains and authigenic cements and as such was non-quiescent, involving the widespread expulsion of large volumes of relatively cool formation fluids from basinal areas towards basin flanks. Such a regionally extensive fluid migration episode was probably concomitant with a major post-intrusion tectonic event. The only such significant event was the widespread uplift and exhumation of many basins along the Atlantic Margin in the Late Tertiary. Such regional uplift has been documented in the Tertiary following igneous activity both in Skye (Lewis *et al*., 1992) and in East Greenland (Stemmerik *et al*., 1993; Price *et al*., 1997; Thomson *et al*., 1999). A major exhumation of Britain, including the Skye area, occurred in the Neogene (Roberts, 1999; Japsen, 1997). Similarly, in East Greenland, the timing of late Cenozoic uplift has been constrained by AFTA to be 20 Ma-0 Ma (Thompson *et al*., 1999). If the widespread, relatively cool, post-diagenetic fluid flux indicated by fluid inclusions do indeed represent expulsion of basinal fluids during inversion, then a similar time constraint is also placed on the late fluid migration event.

Deformation bands as fluid migration pathways during tectonism

Deformation bands are a common feature in many high-porosity sandstones, and can have a dramatic effect on reservoir quality and connectivity due to their greatly reduced hydraulic conductivity in relation to their undeformed host rock (Fowles and Burley, 1994; Pittman, 1981). A number of samples from Skye contain deformation bands, characterised by dramatic grain size reduction relative to the undeformed rock on either side of the slip surface. However, there is evidence that, while such cataclastic slip bands undoubtedly act as fluid baffles in the present day, they acted as focii for fluid flow during deformation. Fluid inclusion

studies (Parnell *et al*., 2004) have shown that secondary trails of inclusions, representing pulses of fluids encapsulated within annealed microfractures, are commonly sub-parallel to these faults. Microthermometry indicates that they represent channelling of very hot fluids, probably due to advective heating of pore waters due to igneous intrusions. Combined SEM-CL and fluid inclusion studies indicate that extensive granulation, dilatancy of the resulting breccia, and subsequent annealing by authigenic quartz is a major feature of deformation bands in the Skye study area and elsewhere (Parnell *et al*., 2004).

Role of sills in deformation band formation

It is apparent that fluid migration events and formation/reactivation of deformation bands are intimately associated. However, whether it is the case that the spontaneous channelling of large volumes of pore fluid facilitates fracturing, or conversely that deformation events initiate fluid migration, is difficult to determine. The circumstances under which the Skye deformation bands form favours the former hypothesis. The sudden intrusion of large number of basic igneous bodies would initiate rapid migration of pore fluids, as heating of country rock leads to advection of large volumes of formation water. This would increase pore fluid pressures in aquifers close to intrusions, due to the retarding effects of pore networks with high tortuosity in allowing pre-existing formation waters to migrate away from sites of fluid influx. Sandstones which were under a shear stress, but had not achieved failure stress, would find themselves under transient high pore fluid pressures, thereby facilitating the onset of deformation. As granulation occurred, poroperm characteristics of the embryonic deformation band would decline rapidly, precluding the escape of fluids from planes of deformation and further increasing pore fluid pressures, thus promoting further deformation and cataclasis. This trend would continue until strain hardening due to grain comminution within the slip band had outstripped the effects of high pore fluid pressure, and the fault ceases to be active. However, in the interval between activation and cessation of cataclasis, the deformation band would act as a focus for fluid flow and a site of high pore fluid pressure. This would lead to the precipitation of diagenetic minerals, and hence the annealing of comminuted grains and extensive cementation and porosity occlusion within the fault zone. Further evidence for deformation bands acting as a focus for fluid flow during deformation lies in the fact that entrained bitumen occurs exclusively along faults in some samples, as discussed below.

Supporting evidence for a direct relationship between intrusions and deformation bands is on the adjacent Island of Eigg, where bands are developed parallel to the margins of Tertiary dykes through Jurassic sandstones. Thus deformation bands could be initiated by the intrusion of igneous bodies, with the resultant pulses of formation waters leading to transient high pore fluid pressures in surrounding rocks. Fluid inclusion microthermometric data support this, with palaeofluid temperatures in excess of 200ºC being recorded in association with the onset of fracturing. Cessation of deformation and annealing of deformation bands must have taken place subsequent to magmatic activity, as authigenic cements within the bands record cooler fluid paleotemperatures than those associated with the onset of fracturing.

Hydrocarbon charge histories

Many Atlantic Margin basins are characterised by complex hydrocarbon migration histories characterised by multiple charge events, often involving oils of different compositions (e.g. Parnell *et al*., 1999, 2001; Feely and Parnell, 2003), and remigration of hydrocarbons to new reservoirs at stratigraphically higher levels (e.g. Lamers and Carmichael, 1999). At this stage our interpretation of these oil charge events is based on relative timing and microthermometry of petroleum inclusions, but there is potential to obtain additional information on oil composition using extraction and analysis (e.g. George *et al*., 2004) or by advanced fluorescence studies of the inclusions (Blanchet *et al*., 2003; Ryder *et al*., 2004)

East Greenland

There is evidence for a multi-stage oil charge history in the Triassic-Jurassic section of East Greenland. Inclusions of liquid oil and solid bitumen indicate secondary petroleum migration in the re-

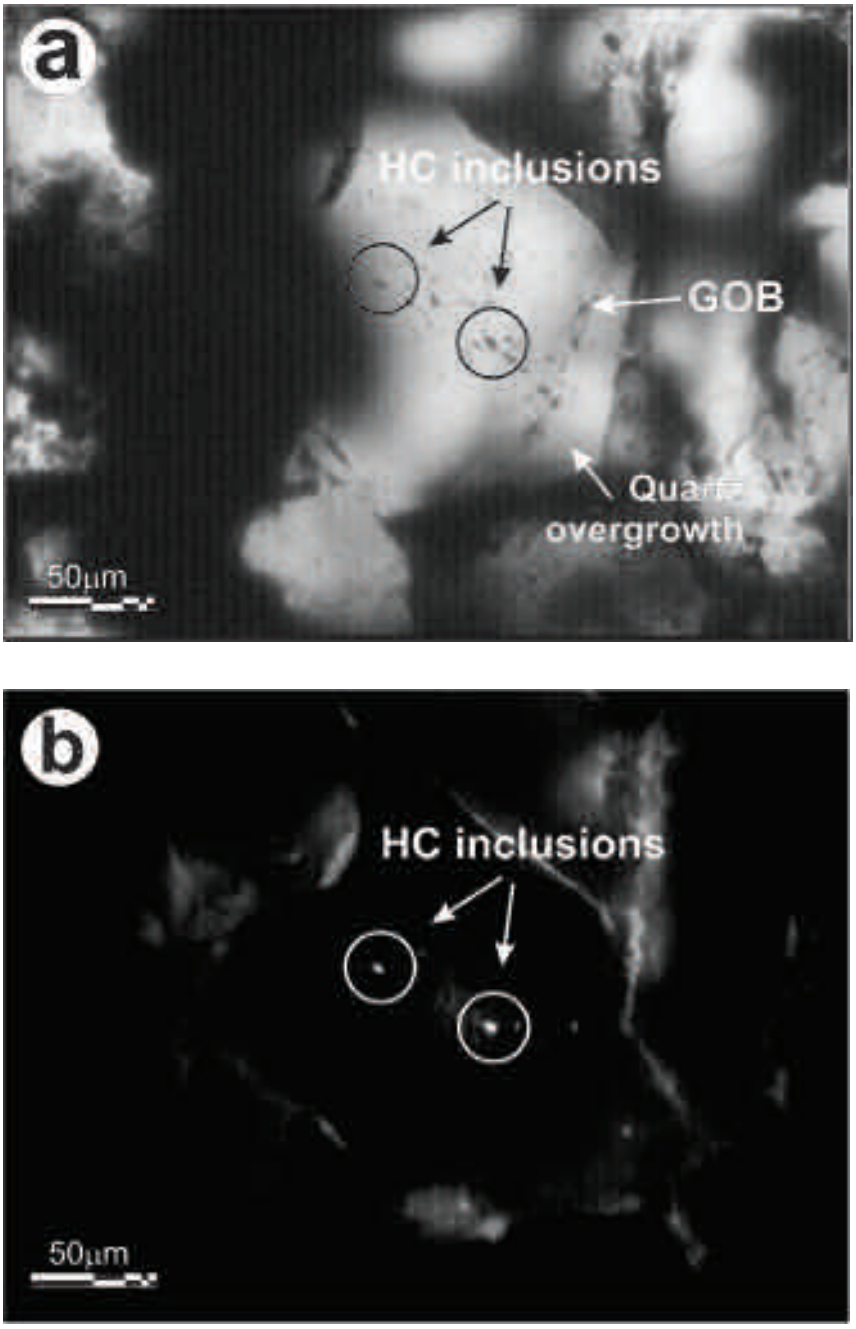

Figure 15. Liquid petroleum inclusions encapsulated within an annealed microfracture which is truncated by a later authigenic quartz overgrowth, East Greenland Triassic. (**a**) Plane polarised light. (**b**) UV light. GOB=Grain/overgrowth boundary. See text for discussion.

gion. Pyrobitumen, representing the solid residue of thermally degraded petroleum, also occurs at grain/overgrowth boundaries and within intragranular and intergranular porosity.

Rare liquid oil, encapsulated as blue-white fluorescent fluid inclusions, is recorded within the Triassic sandstones of Laplace Bjerge. The oil inclusions occur within annealed microfractures in detrital quartz grains, which terminate at and clearly predate quartz overgrowths (figure 15). This is evidence for an early phase of oil charge which preceded quartz cementation. If quartz authigenesis was contemporaneous with Palaeocene magmatism, this oil migration event must have taken place before or during the Palaeocene. Solid bitumen occurs as inclusions within samples of Triassic sandstone from Laplace Bjerge. These probably represent thermal degradation of what were originally liquid petroleum inclusions due to igneous intrusions. The amount of useful information which these inclusions can yield from microthermometry is limited. Two distinct phases of oil charge are recorded from the distribution of bitumen which does not occur within inclusions (figure 16). An early bitumen, which may be the correlative of the oil inclusions described above, occurs exclusively at grain/overgrowth boundaries. A second period of oil emplacement is recorded by large volumes of intergranular bitumen which postdate quartz authigenesis. Price and Whitham (1997) recognised this bitumen as the degraded remnants of palaeo-oil accumulations, with the large Triassic/Jurassic fault blocks (including Svinhufvud Bjerge and Mols Bjerge) representing

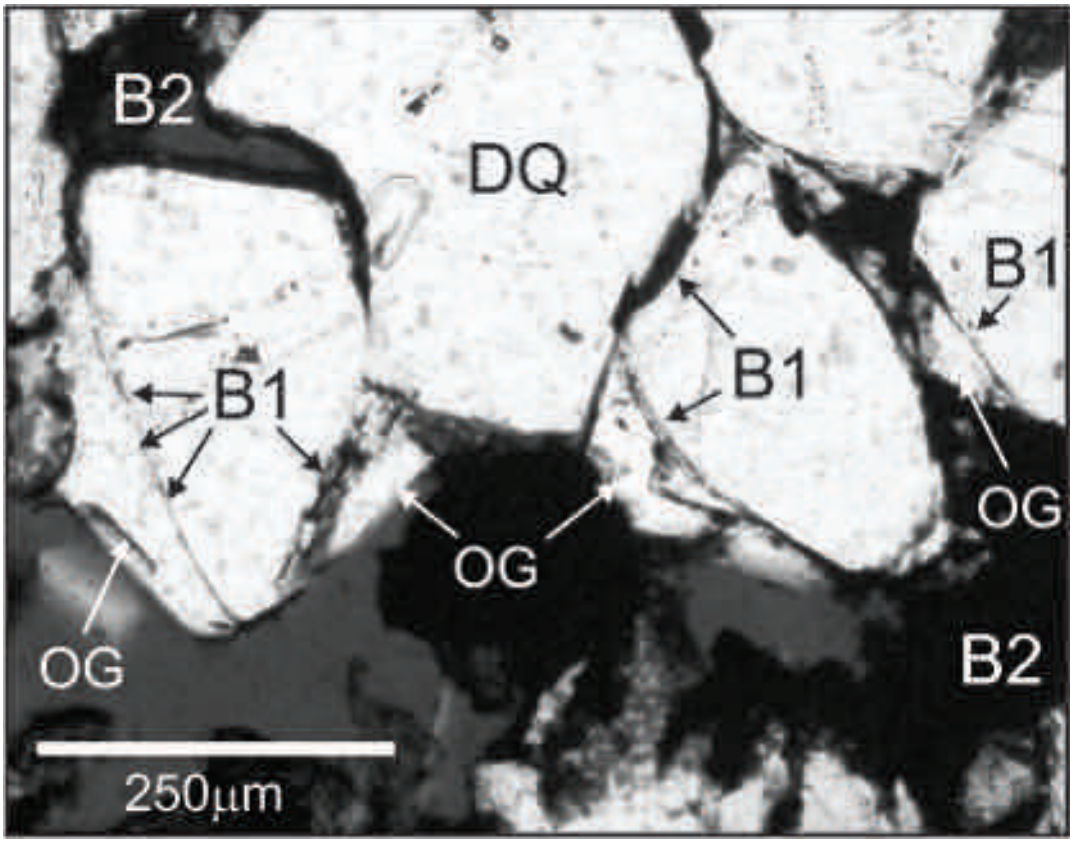

Figure 16. Photomicrograph showing evidence for two phases of oil emplacement, East Greenland Jurassic. An early, pre-quartz bitumen (B1) is entrained along grain/overgrowth boundaries, and is succeeded by a later, post-quartz charge (B2). DQ=Detrital quartz grain, OG=Quartz overgrowth.

exhumed hydrocarbon traps. The timing of oil migration in the East Greenland Triassic can be constrained by combined petrographic and fluid inclusion microthermometric studies. The early, pre-overgrowth charge clearly predates quartz authigenesis of Paleocene age, placing an upper limit on the timing of this migration event. A lower limit is placed on the timing of trap formation of the fault blocks containing the paleoaccumulations, at Albian/Cenomanian. This indicates an early charge of hydrocarbons during the Late Cretaceous to Early Paleocene. The late, post-overgrowth pore-filling bitumen postdates Paleocene magmatism but is thermally altered by intrusions of Oligocene age, allowing the timing of the second charge to be constrained as Paleocene to Oligocene.

Skye

Black sandstones occur in several parts of Skye, including at Rigg, Inver Tote and Holm (Lee, 1920; Anderson and Dunham, 1966), in immediate proximity to the Cullaidh Shale. Petrographic examination shows that the black coloration is due to bitumen (degraded oil) in the pore spaces. The occurrence of black sandstones are so consistently in the immediate vicinity of sills emplaced into black (organic-rich) mudrocks, that a model of local oil generation through intrusion-related heating seems incontrovertible. In particular, sills into the Cuilladh Shale Formation at Inver Tote (Lee, 1920) and Elgol have generated oil.

There is evidence for a two-stage oil charge history in these rocks. Hydrocarbons occur as inclusions of liquid oil and solid bitumen, as well as residual bitumen within pore space and entrained along mineral veins. These bitumens are interpreted as representing the remnant of originally liquid petroleum which has been degraded by thermal alteration, water washing, biodegradation and/or aerial exposure.

In a sample of the Elgol Sandstone Formation (S1), bitumen residue is entrained within deformation bands. These small-scale cataclastic faults are zones of drastically reduced hydraulic conductivity, yet have clearly acted as hydrocarbon migration pathways in the past as they contain bitumen. This could be explained by a syn-tectonic oil charge event in which petroleum preferentially utilised the deformation bands as conduits for migration; any post-tectonic oil charge would have bypassed the deformation bands. This allows the delineation of timing of this early oil charge. As discussed above, fluid inclusion data indicate that cataclasis (and therefore hydrocarbon migration) may have been initiated by (or is at least associated with) igneous activity in the mid to late Palaeocene. In the same sample, a second bitumen occurs with a random distribution in pore space throughout the sandstone, inhabiting 20-30% of the pore volume. This bitumen has a different optical character, being less reflective than that within the deformation bands. Intergranular bitumen of the same type is documented in a number of other samples in the Skye area, and is readily identifiable due to the dark staining of samples in hand specimen. Where deformation bands are present, the second bitumen is absent from the vicinity of the zones of cataclasis. This is probably due to oil emplacement in a sandstone which already contains a structural fabric, i.e. petroleum could not penetrate the low-permeability deformation bands. Thus this second bitumen appears to postdate that found in deformation bands and represents a second charge. A lower limit is therefore placed on migration/accumulation of the second hydrocarbon; a phase of oil charge must have taken place between c.59Ma and the present day, if deformation bands are concomitant with igneous activity as discussed above. Evidence for a two-stage oil charge history is also found in a sample of dyke-hosted vein material from Elgol (sample S5). The presence of bitumen within the vein fill is unsurprising, as the dyke contacts the oil-prone Cullaidh Shale Formation at its upper boundary. The sample from Valtos (S7) similarly displays similar evidence for a two-phase oil charge history.

Thus there are a number of lines of evidence for a two-stage oil charge history in Skye. The early event is recorded in several samples, while the later event appears to postdate all diagenesis and is more widespread. Although no direct microthermometric data were obtainable from oil inclusions representing the early charge, concomitant aqueous inclusions display high temperatures, which indicates an association with igneous emplacement (see above). This indicates that there may have been a time lag between the early oil, gener-

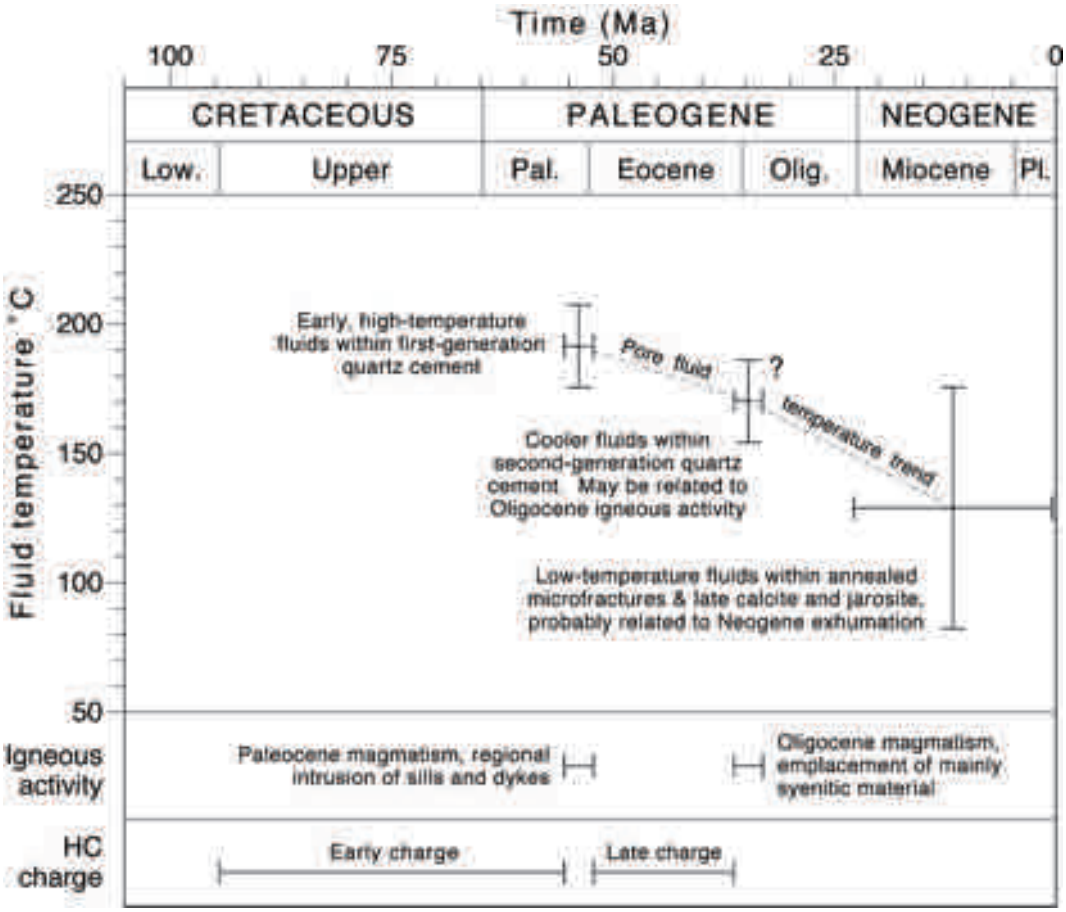

Figure 17. Pore fluid and hydrocarbon migration history for East Greenland region, deduced from petrographic and fluid inclusion data.

ated by flash pyrolysis due to rapid emplacement of igneous bodies, followed by a more volumetrically significant charge caused by conductive heating of source rocks in the immediate vicinity of igneous intrusions.

Conclusions

The East Greenland and Skye study areas represent two Atlantic Margin basins which have been intruded by sills and display evidence for complex histories of fluid flow, diagenesis and hydrocarbon charge, summarized in figure 17 and 18.

A number of conclusions can be drawn:

1. East Greenland and Skye display many similarities in pore fluid histories, including palaeofluid temperature and composition, timing of fluid flow events, and hydrocarbon generation and migration. It is probable that many Atlantic Margin basins affected by sills, including the Faroe-Shetland Basin, exhibit similar features.
2. The emplacement of sills in basins on the Atlantic Margin and elsewhere can have dramatic effects on diagenesis and hence reservoir quality. Igneous intrusions can cause rapid, regionally extensive quartz cementation due to short-lived pulses of hot aqueous fluids.
3. In the Triassic of East Greenland and the Jurassic of Skye, a general trend of declining pore

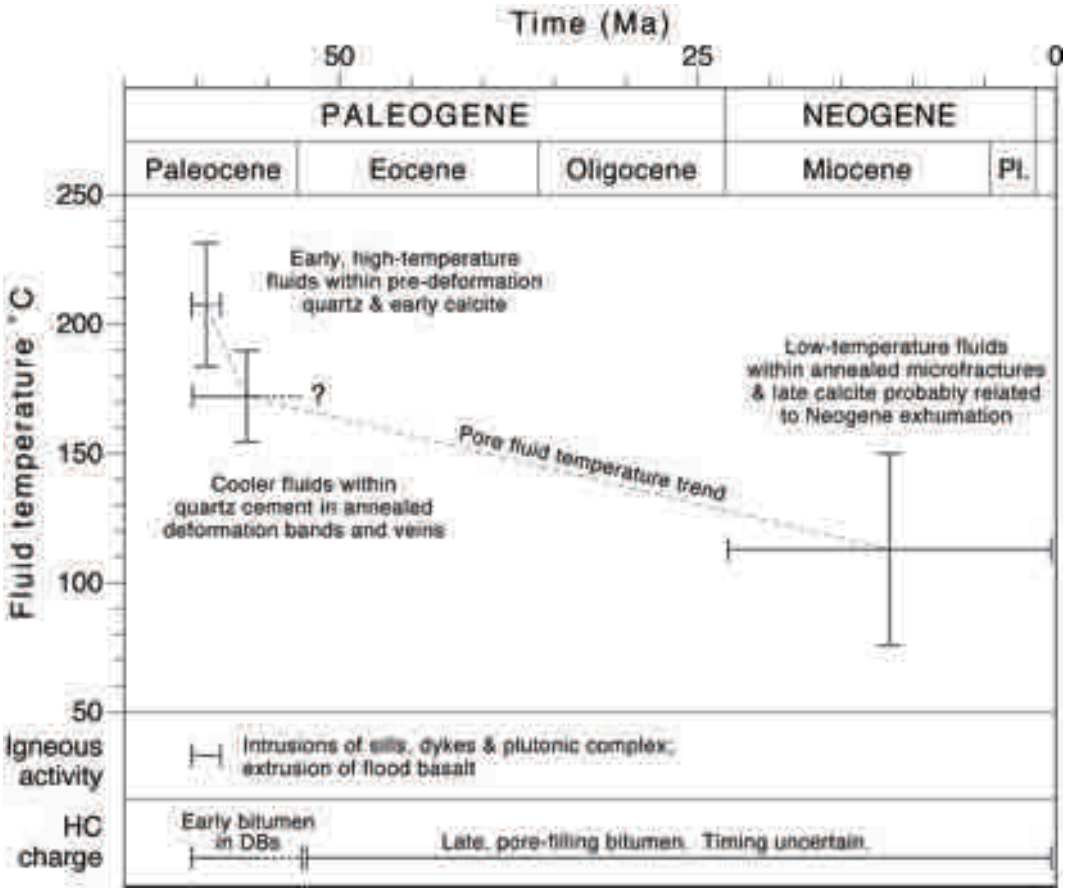

Figure 18. Pore fluid and hydrocarbon migration history for Skye region, deduced from petrographic and fluid inclusion data. DB=Deformation Band.

fluid temperatures with time is observed. Early, high-temperature fluids accompanied by quartz authigenesis are probably contemporaneous with igneous activity during the Paleocene in both regions. A widespread late fluid flow event, recorded by aqueous fluid inclusions in annealed microfractures, may be related to regional basin inversion during the Neogene.

4. In the Skye study area, deformation bands may be initiated by hot fluids due to the emplacement of igneous bodies. While these deformation bands form fluid baffles in the present day, they have acted as migration pathways for aqueous and hydrocarbon fluids during deformation.
5. Both East Greenland and Skye display evidence for complex petroleum charge histories, with at least two discrete phases of oil migration/accumulation. Temporal constraints are placed on oil migration in both regions. In East Greenland, an early charge of oil occurred between the Albian-Cenomanian and Paleocene, with a second charge between Paleocene and Oligocene times. In Skye, an early charge, concomitant with Paleocene magmatism, was succeeded by a later charge of uncertain timing. In both cases, igneous intrusions have not destroyed hydrocarbon potential.

Acknowledgements

The authors are indebted to B. Fulton and J. Still for skilled technical support. DM was supported by a PhD studentship funded by the European Social Fund. We are grateful to Jens Therkelsen (ex-GEUS) for provision of samples from east Greenland. The manuscript was improved by helpful criticism from H. Volk and K. Bjørlykke.

References

Anderson, F.W. and Dunham, K.C. 1966. *The geology of Northern Skye*. Memoirs of the Geological Survey, HMSO, Edinburgh.

Andrews, J.E. 1987. Jurassic clay-mineral assemblages and their post depositional alteration: upper Great Estuarine Group, Scotland. *Geological Magazine* 124: 261-271.

Archer, S.G., Bergman, S.C., Iliffe, J., Murphy, C.M. and Thornton, M. 2005. Palaeogene igneous rocks reveal new insights into the geodynamic evolution and petroleum potential of the Rockall Trough, NE Atlantic Margin. *Basin Research* 17: 171-201.

Bell, B. and Butcher, H. 2002. On the emplacement of sill complexes: evidence from the Faroe-Shetland Basin. *In*: Jolley, D.W. and Bell, B.R. (eds) *The North Atlantic Igneous Province: Stratigraphy, Tectonic, Volcanic and Magmatic Processes*. Geological Society, London, Special Publications 197: 307-329.

Bishop, A.N. and Abbott, G.D. 1991. The effect of minor igneous intrusions on the petroleum potential of Jurassic shales, Isle of Skye, Scotland. *In*: Manning, D.A.C. (ed.). *Organic Geochemistry: Advances and Applications in the Natural Environment*. Manchester University Press, Manchester: 278-280.

Bjørlykke, K. 1994. Pore water flow and mass transfer of solids in solution in sedimentary basins. *In*: Parker, A. and Sellwood, B.W. (eds) *Quantitative Diagenesis: Recent Developments and Applications to Reservoir Geology*: 189-221.

Blanchet, A., Pagel, M., Walgenwitz, F. and Lopez, A. 2003. Microspectrofluorimetric and microthermometric evidence for variability in hydrocarbon fluid inclusions in quartz overgrowths: implications for inclusion trapping in the Alwyn North field, North Sea. *Organic Geochemistry* 34: 1477-1490.

Bodnar, R.J. 1993. Revised equation and table for determining the freezing point depression of H_20-NaCl solution. *Geochimica et Cosmochimica Acta* 57: 683-684.

Bostick, N.H. 1979. Microscopic measurement of the level of catagenesis of solid organic matter in sedimentary rocks to aid exploration for petroleum and to determine former burial temperatures - a review. *In*: Scholle, P.A. and Schluger, P.R. (eds) *Aspects of Diagenesis, SEPM Special Publications* 26: 17-43.

Burruss, R.C. 1991. Practical aspects of fluorescence microscopy of petroleum inclusions. *In*: Barker, C.E. and Kopp, O.C. (eds) *Luminesence Microscopy: Quantitative and Qualitative Aspects.* SEPM (Society for Sedimentary Geology) Short Course. SEPM, Tulsa.

Doré, A.G., Lundin, E.R., Jensen, L.N., Birkeland, Ø, Eliassen, P.E. and Fichler, C. 1999. Principal tectonic events in the evolution of the northwest European Atlantic Margin. *In*: Fleet, A.J. and Boldy, S.A.R. (eds) *Petroleum Geology of Northwest Europe: Proceedings of the 5th Conference*. Geological Society, London: 41-61.

Duddy, I.R., Green, P.F., Bray, R.J. and Hegarty, K.A. 1994. Recognition of the thermal effects of fluid flow in sedimentary basins. *In*: Parnell, J. (ed). *Geofluids: Origin, Migration and Evolution of Fluids in Sedimentary Basins*. Geological Society Special Publications 78: 325-345.

Dutkiewicz, A., Volk, H., George, S.C., Ridley, J. and Buick, R. 2006. Biomarkers sealed in oil-bearing fluid inclusions trapped before the Great Oxidation Event. *Geology* 34: 437-440.

Ebdon, C.C., Granger, P.J., Johnson, H.D. and Evans, A.M. 1995. Early Tertiary evolution and sequence stratigraphy of the Faeroe-Shetland Basin: implications for hydrocarbon prospectivity. *In*: Scrutton, R.A., Stoker, M.S., Shimmield, G.B. and Tudhope, A.W. (eds) *The Tectonics, Sedimentation and Palaeoceanography of the North Atlantic Region,* Geological Society Special Publications 90: 51-69.

Farrimond, P., Bevan, J.C. and Bishop, A.N. 1999. Tricyclic terpane maturity parameters: response to heating by an igneous intrusion. *Organic Geochemistry* 30: 1011-1019.

Ferry, J.M., Mutti, L.J. and Zuccala, G.J. 1987. Contact metamorphism/hydrothermal alteration of Tertiary basalts from the Isle of Skye, northwest Scotland. *Contributions to Mineralogy and Petrology* 95: 166-181.

Feely, M. and Parnell, J. 2003. Fluid inclusion studies of well samples from the hydrocarbon prospective Porcupine Basin, offshore Ireland. *Journal of Geochemical Exploration* 78-79: 55-59.

Fowles, J. and Burley, S. 1994. Textural and permeability characteristics of faulted, high porosity sandstones. *Marine and Petroleum Geology* 11: 608-623.

George, S.C., Ahmed, M., Liu, K. and Volk, H. 2004. The analysis of oil trapped during secondary migration. *Organic Geochemistry* 35: 1293-1317.

Goldstein, R.H. and Reynolds, T.R. 1994. *Systematics of Fluid Inclusions in Diagenetic Minerals*. SEPM (Society for Sedimentary Geology) Short Course 31. SEPM, Tulsa.

Green, P.F., Duddy, I.R., Hegarty, K.A. and Bray, R.J. 1999. Early Tertiary heat flow along the UK continental margin and adjacent areas. *In*: Fleet, A.J. and

Boldy, S.A.R. (eds) *Petroleum Geology of Northwest Europe: Proceedings of the 5th Conference*. Geological Society, London: 349-357.

Haller, J. 1970. Tectonic map of East Greenland: an account of tectonism, plutonism and volcanism in East Greenland. *Meddelelser om Grønland* 171, No. 5: 229-243.

Hamilton, M.A., Pearson, D.G., Thompson, R.N., Kelley, S.P. and Emeleus, C.H. 1998. Rapid eruption of Skye lavas inferred from precise U-Pb and Ar-Ar dating of the Rum and Cuillin plutonic complexes. *Nature* 394: 260-263.

Harris, J.P. 1992. Mid-Jurassic lagoonal delta systems in the Hebridean basins: thickness and facies distribution patterns of potential reservoir sandbodies. *In*: Parnell, J. (ed.) *Basins on the Atlantic Seaboard: Petroleum Geology, Sedimentology and Basin Evolution*. Geological Society Special Publications 62: 111-144.

Hudson, J.D. 1962. The stratigraphy of the Great Estuarine Series (Middle Jurassic) of the Inner Hebrides. *Transactions of the Edinburgh Geological Society* 19: 139-165.

Hudson, J.D. 1965. The petrology of the sandstones of the Great Estuarine Series, and the Jurassic palaeogeography of Scotland. *Proceedings of the Geological Association* 75: 499-528.

Hudson, J.D. and Andrews, J.E. 1987. The diagenesis of the Great Estuarine Group, Middle Jurassic, Inner Hebrides, Scotland. *In*: Marshall, J.D. (ed.) *Diagenesis of Sedimentary Sequences*. Geological Society, Special Publications 36: 259-276.

Japsen, P. 1997. Regional Neogene exhumation of Britain and the Western North Sea. *Journal of the Geological Society, London* 154: 239-247.

Kilyeni, T. and Standley, B. 1985. Petroleum prospects in the northwest seaboard of Scotland. *Oil & Gas Journal* 84: 100-108.

Lamers, E. and Carmichael, S.M.M. 1999. The Paleocene deepwater sandstone play West of Shetland. *In*: Fleet, A.J. and Boldy, S.A.R. (eds) *Petroleum Geology of Northwest Europe: Proceedings of the 5th Conference*. Geological Society, London: 645-659.

Larsen, H.C. 1990. The East Greenland Shelf. *In*: Grantz, A., Johnson, L. and Sweeney, J.F. (eds) *The Arctic Ocean region*. Geological Society of America, v. L., 185-210.

Larsen, L.M., Watt, W.S. and Watt, M. 1989. Geology and petrology of the Lower Tertiary plateau basalts of the Scoresby Sund Region, East Greenland. *Grønlands Geologiske Undersøgelse Bulletin* 157: 1-164.

Larsen, M., Piasecki, S., Preuss, T., Seidler, L., Stemmerik, L., Therkelsen, J. and Vosgerau, H. 1998. Petroleum geological activities in East Greenland in 1997. *Geology of Greenland Survey Bulletin* 180: 35-42.

Lee, G.W. 1920. *The Mesozoic rocks of Applecross, Raasay and North East Skye*. Memoir of the Geological Survey of Great Britain. HMSO, Edinburgh.

Lewis, C.L.E. Carter, A. and Hurford A. J. 1992. Low-temperature effects of the Skye Tertiary intrusions on Mesozoic sediments in the Sea of Hebrides Basin. *In*: Parnell, J. (ed.) *Basins on the Atlantic Seaboard: Petroleum Geology, Sedimentology and Basin Evolution*. Geological Society Special Publication 62: 175-188.

Linnard, S. and Nelson, R. 2005. Effects of Tertiary volcanism and later events upon the Faroese hydrocarbon system. *In*: Ziska, H., Varming, T. and Bloch, D. (eds) *Faroe Islands Exploration Conference: Proceedings of the 1st Conference*. Annales Societatis Scientiarum Færoensis, Tórshavn, Supplementum 43: 44-53.

Middleton, D.W.J., Parnell, J., Green, P.F., McSherry, M. and Xu, G. 2001. Hot fluid flow events in Atlantic Margin basins: an example from the Rathlin Basin. Geological Society Special Publications 188: 91-105.

Morton, N. 1993. Potential reservoir and source rocks in relation to Upper Triassic to Middle Jurassic sequence stratigraphy, Atlantic Margin basins of the British Isles. *In*: Parker, J.R. (ed.) *Petroleum Geology of Northwest Europe: Proceedings of the 4th Conference*. Geological Society, London: 285-298.

Noble, R.H., MacIntyre, R.M. and Brown, P.E. 1988. Age constraints on Atlantic evolution: timing of magmatic activity along the East Greenland continental margin. *In*: Morton, A.C. and Parson, L.M. (eds) *Early Tertiary Volcanism and the Opening of the NE Atlantic.* Geological Society Special Publications 39: 201-214.

Parnell, J., Carey, P.F., Green, P. and Duncan, W. 1999. Hydrocarbon migration history, West of Shetland: Integrated fluid inclusion and fission track studies. *In*: Fleet, A.J. and Boldy, S.A.R. (eds) *Petroleum Geology of Northwest Europe: Proceedings of the 5th Conference*. Geological Society, London: 613-625.

Parnell, J., Green, P.F., Watt, G. and Middleton, D. 2005. Thermal history and oil charge on the UK Atlantic margin. *Petroleum Geoscience* 11: 99-112.

Parnell, J., Middleton, D., Chen, H. and Hall, D. 2001. The use of fluid inclusion studies in constraining oil charge history and reservoir compartmentation: examples from the Jeanne d'Arc Basin, offshore Newfoundland. *Marine and Petroleum Geology* 18: 535-549.

Parnell, J., Watt, G.R., Middleton, D., Kelly, J. and Baron, M. 2004. Deformation band control on hydrocarbon migration. *Journal of Sedimentary Research* 74: 552-560.

Pittman, E.D. 1981. Effect of fault-related granulation on porosity and permeability of quartz sandstones,

Simpson Group (Ordovician), Oklahoma. *American Association of Petroleum Geologists Bulletin* 65: 2381-2387.

Price, S.P., Brodie, J., Whitham. A.G. and Kent, R. 1997. Mid-Tertiary rifting and magmatism in the Traill Ø region, East Greenland. *Journal of the Geological Society, London* 154: 419-434.

Price, S.P. and Whitham, A.G. 1997. Exhumed hydrocarbon traps in East Greenland: Analogs for the Lower-Middle Jurassic play of Northwest Europe. *American Association of Petroleum Geologists Bulletin* 81: 196-221.

Requejo, A.G., Hollywood, J. and Halpern, H.I. 1989. Recognition and source correlation of migrated hydrocarbons in Upper Jurassic Hareelv Formation, Jameson Land, East Greenland. *American Association of Petroleum Geologists Bulletin* 73: 1065-1088.

Ritchie, J.D., Gatliff, R.W. and Richards, P.C. 1999. Early Tertiary magmatism in the offshore NW UK margin and surrounds. *In*: Fleet, A.J. and Boldy, S.A.R. (eds) *Petroleum Geology of Northwest Europe: Proceedings of the 5th Conference*. Geological Society, London: 573-584.

Roberts, D.G., Thompson, M., Mitchener, B., Hossack, J., Carmichael, S. and Bjørnseth, H.-M. 1999. Paleozoic to Tertiary rift and basin dynamics: mid-Norway to the Bay of Biscay- a new context for hydrocarbon prospectivity in the deep water frontier. *In*: Fleet, A.J. and Boldy, S.A.R. (eds) *Petroleum Geology of Northwest Europe: Proceedings of the 5th Conference*. Geological Society, London: 7-40.

Roedder, E. 1984. *Fluid Inclusions*. Reviews in Mineralogy Volume 12. Mineralogical Society of America.

Ryder, A.G., Przyjalgowski, M.A., Feely, M., Szczupak, B. and Glynn, T.J. 2004. Time-resolved fluorescence microspectroscopy for characterizing crude oil in bulk and hydrocarbon-bearing fluid inclusions. *Applied Spectroscopy* 58: 1106-1115.

Smallwood, J.R. and Kirk, W.J. 2005. Paleocene exploration in the Faroe-Shetland Channel: disappointments and discoveries. *In*: Dore, A.G. and Vining, B.A. (eds) *Petroleum Geology: North-West Europe and Global Perspectives - Proceedings of the 6th Petroleum Geology Conference*. Geological Society, London: 977-991.

Smallwood, J.R. and Maresh, J. 2002. *In*: Jolley, D.W. and Bell, B.R. (eds) *The North Atlantic Igneous Province: Stratigraphy, Tectonic, Volcanic and Magmatic Processes*. Geological Society, London, Special Publications 197: 271-306.

Stemmerik, L., Christiansen, F. G., Piasecki, S., Jordt, B., Marcussen, C. and Nøhr-Hansen, H. 1993. Depositional history and petroleum geology of the carboniferous to Cretaceous sediments in the northern part of East Greenland. *In*: Vorren, T.O., Bergsager, E., Dahl-Stamnes, Ø.A., Holter, E. Johansen, B., Lie, E. and Lund, T.B. (eds) *Arctic Geology and Petroleum Potential.* Norwegian Petroleum Society (NPF), Special Publications 2: 67-87.

Stemmerik, L., Clausen, O.R., Korstgård, J., Larsen, M., Piasecki, S., Seidler, L., Surlyk, F. and Therkelsen, J. 1997. Petroleum geological investigations in East Greenland: project 'Resources of the sedimentary basins of North and East Greenland'. *Geology of Greenland Survey Bulletin* 176: 29-38.

Stewart, A.K., Massey, M., Padgett, P.L., Rimmer, S.M., and Hower, J.C. 2005. Influence of a basic intrusion on the vitrinite reflectance and chemistry of the Springfield (No. 5) coal, Harrisburg, Illinois. International Journal of Coal Geology 63: 58-67.

Surlyk, F., Hurst, J.M., Piasecki, S., Rolle, F., Scholle, P. A., Stemmerik, L., and Thomsen, E. 1986. The Permian of the western margin of the Greenland Sea: A future exploration target. *In*: Halibouty, M.T. (ed.) *Future petroleum provinces of the world.* American Association of Petroleum Geologists Memoir 40: 629-659.

Taylor, H.P. and Forester, R.W. 1971. Low-O^{18} igneous rocks from the intrusive complexes of Skye, Mull and Ardnamurchan, Western Scotland. *Journal of Petrology* 12: 465-497.

Thomson, K., Green, P.F., Whitham, A.G., Price, S.P. and Underhill, J.R. 1999. New constraints on the thermal history of Northeast Greenland from apatite fission-track analysis. *Geological Society of America Bulletin* 111: 1054-1068.

Thrasher, J. 1992. Thermal effects of the Tertiary Cuillins Igneous Complex in the Jurassic of the Hebrides: an organic geochemical study. *In*: Parnell, J. (ed.) *Basins on the Atlantic Seaboard: Petroleum Geology, Sedimentology and Basin Evolution*. Geological Society, London, Special Publications 62: 35-49.

Wilkinson, M. 1992. Concretionary cements in Jurassic sandstones, Isle of Eigg, Inner Hebrides. *In*: Parnell, J. (ed.) *Basins on the Atlantic Seaboard: Petroleum Geology, Sedimentology and Basin Evolution*. Geological Society, London, Special Publications 62: 145-159.

Worden, R.H. and Morad, S. 2000. Quartz cementation in oil field sandstones: a review of the key controversies. *In*: Worden, R.H. and Morad, S. (eds) *Quartz Cementation in Oil Field Sandstones.* International Association of Sedimentologists Special Publication 29: 1-21.

Wycherley, H.L., Parnell, J., Watt, G.R., Chen, H. and Boyce, A.J. 2003. Indicators of hot fluid migration in sedimentary basins: evidence from the UK Atlantic Margin. *Petroleum Geoscience* 9: 357-374.

Palynofloral evidence for the onset and cessation of eruption of the Faroe Islands lava field

DAVID W. JOLLEY

Department of Geology and Petroleum Geology, University of Aberdeen, Meston Building, King's College, Aberdeen, AB24 3UE, UK.
Email: d.jolley@abdn.ac.uk; Tel: +44 (0)1224 273450

ABSTRACT

Isotopic dating of the oldest flood basalt sequence of the Faroe Islands has been used alongside lava geochemistry to derive a correlation between the Faroe Islands and East Greenland. Here, this correlation is compared to palynological data from the Faroe Islands, Greenland and offshore flood basalt sequences using a sequence stratigraphical framework. Using a combination of published and new data, it is demonstrated that the eruption ages inferred by the geochemical and isotope correlation (60.1±0.6 to 56.8±0.6 Ma for the oldest lava sequence), do not correspond to those derived from sequence stratigraphical analysis (54.9 Ma to 56.8 Ma for the oldest lava sequence). Similar flood basalt sequences constrained by palynological and sequence stratigraphical data within offshore well sections from the Corona Basin, Corona Ridge, the Erlend Complex and in the Flett Sub-basin. These lava flow packages occur within Sequences T40 and T45, within the Late Paleocene to Early Eocene. Older lavas field are currently only encountered Sequence T36 in well 219/23-1, drilled through the isolated Ben Nevis structure. However, the Faroe-Shetland Basin record of dispersed volcanic ash is more extensive, occurring sporadically from Sequence T10 in the uppermost Early Paleocene to Sequence T36, where extensive re-sedimented ash deposits occur. These data demonstrate that volcanism in the North Atlantic Igneous Province commenced in the Early Paleocene, with the oldest widespread flood basalt eruptions occurring within Sequence T40 in the Late Paleocene, terminating in the Early Eocene (Sequence T45).

This highlights a continuing disparity between the isotopic dating of the lower part of the FIBG lava field, and the ages assigned to the geologic timescale of some 3my.

Introduction

The Faroe Islands lie in the North Atlantic (Figure 1), midway between the Shetland Islands and Iceland at 62°N. In this position, they are marginal to the spreading ocean ridge of the NE Atlantic. The islands have drifted to the SE away from Greenland, a process that began with the eruption of flood basalt lavas over the area now occupied by the Faroe Islands. In the first comprehensive study of Faroe Islands geology, Rasmussen and Noe-Nygaard (1970), established a three - fold division of the lava pile into Lower, Middle and Upper series. These authors also introduced the terms "Coal-bearing sequence" and "Tuff-agglomerate zone" for sedimentary and volcaniclastic rocks between the Lower and Middle series (Figure 2). Currently, the lithostratigraphical classification of the Faroe Islands lavas is under review (Passey and Jolley, submitted), replacing the older nomenclature with a classification that complies with the International Subcommission on Stratigraphy guidelines. In this review, the proposed new lithostratigraphy is utilised.

Age dating of the Faroe Islands Basalt Group (FIBG) was first attempted using K-Ar techniques by Tarling and Gale (1968), these dates being subsequently reviewed by Fitch *et al*. (1978). Since this work, a more extensive study of FIBG dating was undertaken by Waagstein *et al*. (2002), concentrating on the Beinisvørð Formation, which yielded ages between 55.8 ± 0.1 Ma and 58.8 ± 0.5 Ma. The most recent isotopic dates extend the range of these ages (Storey *et al*., 2007), adding a range of 56.8 ± 0.6 Ma to 60.1 ± 0.6 Ma for the

Faroe Islands Exploration Conference: Proceedings of the 2nd Conference.
Annales Societatis Scientiarum Færoensis, Supplementum 50, 2009: 156-173

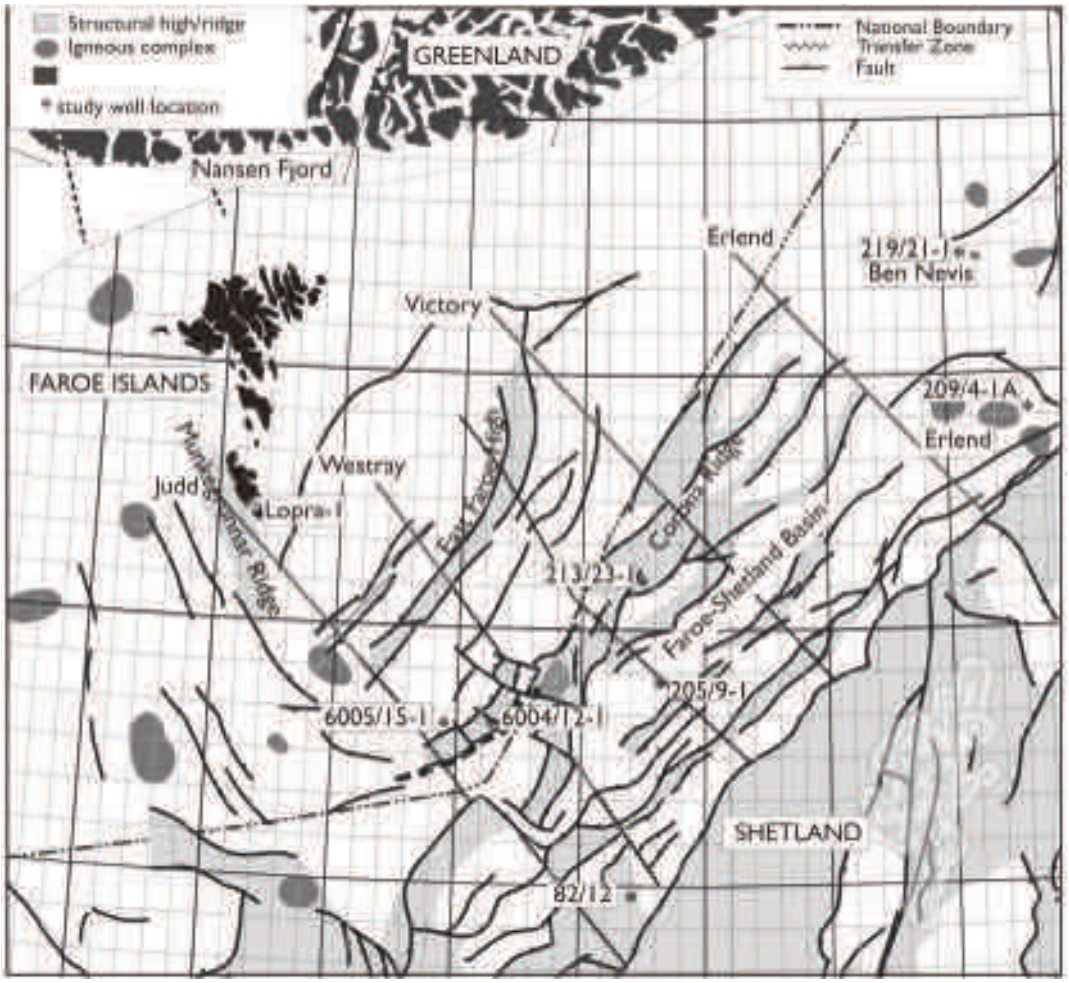

Figure 1. Location and structural map of the northeastern Atlantic prior to the initiation of sea floor spreading in the Early Eocene.

Beinisvørð Formation in the Lopra borehole, and 55.2 + 0.7 Ma to 54.9 + 0.7 Ma for the Malinstindur - Enni formations interval.

Complimentary to the isotopic analysis of the FIBG, Schöenharting and Abrahamsen (1984), Waagstein (1988), and Riisager *et al*. (2002), demonstrated the dominantly reversed polarity of the Enni, Malinstindur and Beinisvørð formations in the exposed section, and that drilled in the Lopra-1/1a borehole. Both Schöenharting and Abrahamsen (1984) and Waagstein (1988) identified two intervals of normal polarity within the Beinisvørð Formation, mostly within the exposed section (Figure 2), which they attributed to Chrons 26n and 25n. This attribution was made by reference to the isotopic ages recorded for the Beinisvørð Formation, and further reinforced by the work of Waagstein *et al*., (2002) using the biomagnetostratigraphical timescale of Cande and Kent (1995). This interpretation was used to suggest a duration of >3my for the eruption of the Beinisvørð Formation.

An alternative approach to the interpretation of Faroese geology was adopted by Ellis *et al*. (2002). These authors compared sedimentary and lava sequences offshore to those of the Faroe Is-

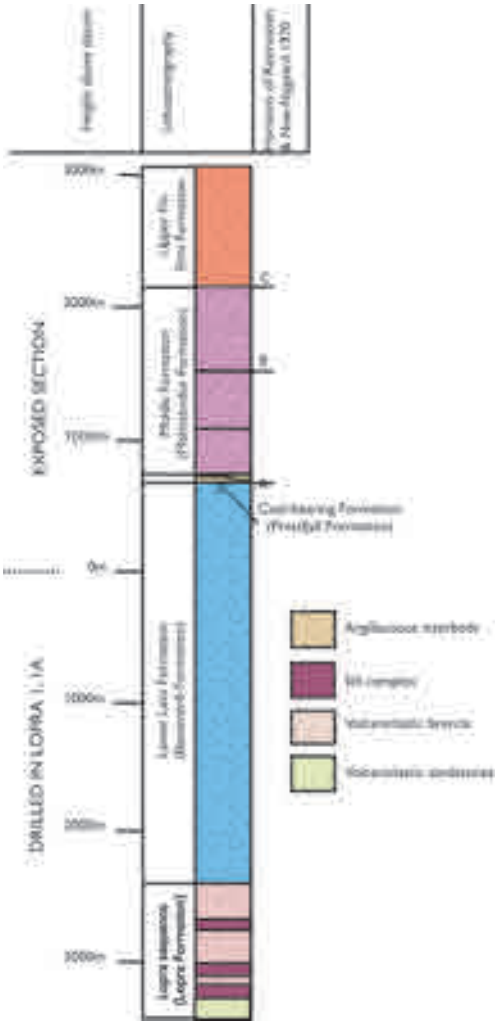

Figure 2. Faroe Islands Basalt Group composite stratigraphical column showing the lithostratigraphy and gross lithology. Datum 0m is taken at the base of the exposed Beinisvørð Formation. The symbology for the Beinisvørð, Malinstindur and Enni formations is notational, but is used throughout the figures herein for lava flow packages of equivalent age where possible.

lands, by means of geophysics and biostratigraphy (Figure 3). Using seismic, wireline log and biostratigraphical correlations, these authors suggested a Late Paleocene to Early Eocene age for the lava field eruption. This was amplified by Jolley and Bell (2002a) and Jolley *et al*. (2002), who presented biostratigraphical evidence attributing the Beinisvørð Formation to depositional sequence T40 (Ebdon *et al*., 1995), to which ages between 54.9 and 56.8 Ma can be assigned (by comparison to the geological timescale of Gradstein *et al*., 2004). This evidence highlighted a disparity between the sequence stratigraphy (which incorporates the biostratigraphy), and the isotopic dating and magnetostratigraphical interpretation.

In a study of the coeval lava field in East Greenland, Larsen *et al*. (1999) presented a correlation between the lava succession north of Nansen Fjord and the Faroe Islands (Figure 4), based on lava geochemistry. Ages were attributed to this geochemical correlation by K/Ar and Ar/Ar isotopes,

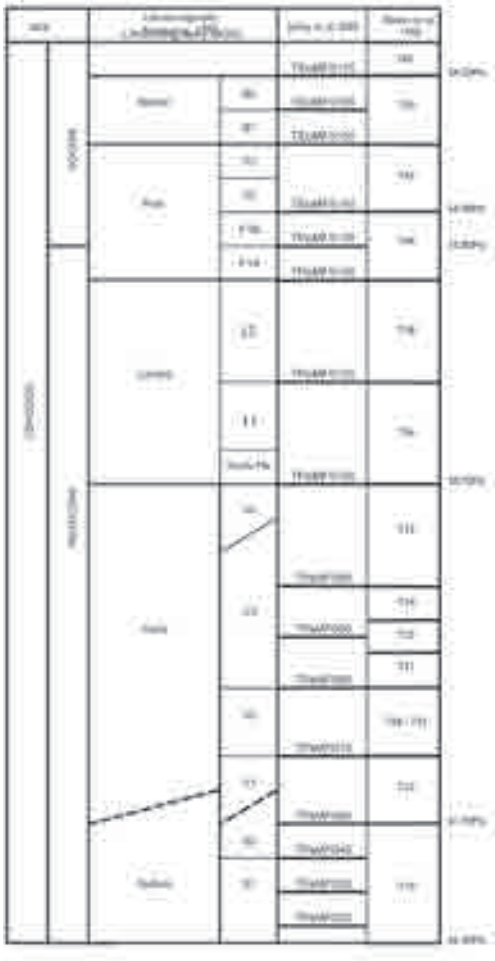

Figure 3. Stratigraphical units of the Paleocene - Early Eocene of the Northeast Atlantic (after Jolley *et al*.,2005).

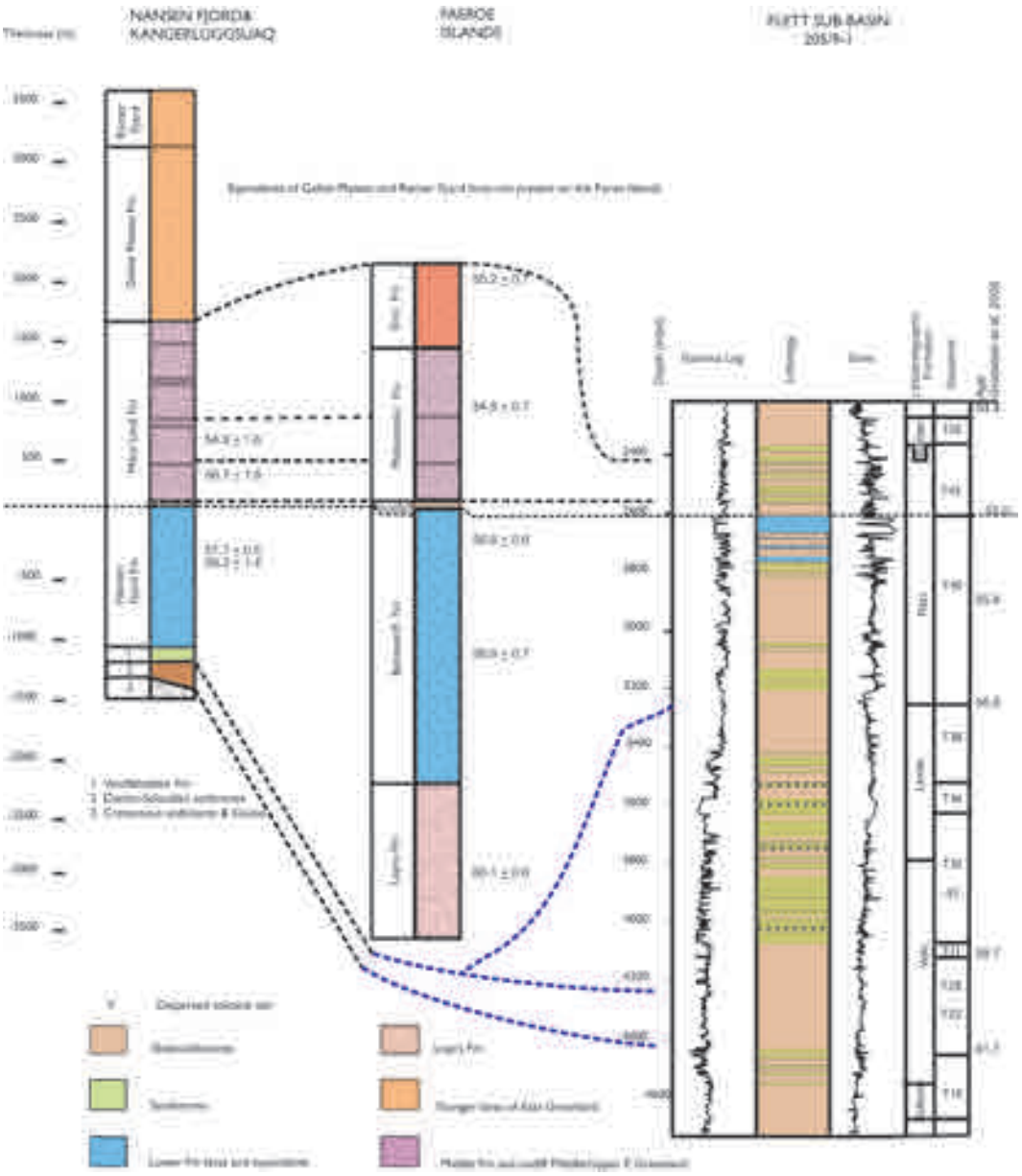

Figure 4. Geochemical and isotopic age correlation of the East Greenland succession with the FIBG after Larsen *et al*. (1999) with dating from Hansen *et al*. (2002) and Storey *et al*. (2007). The geochemical correlation is based on the Nansen Fjord area immediately to the E of the Kangerlussuaq region from which the palynofloras have been obtained. However, the Vandfalsdalen Formation sediments of Kangerlussuaq are either age equivalent or, more probably older than the base of the Nansen Fjord sediments (Nielsen *et al*. 2001). Note the disparity between the isotopic dates and the correlative equivalent dates of the depositional sequences derived from Gradstein et al. (2004).

but the results were provisional and only a broad dating framework was published. In a subsequent publication, Hansen *et al*. (2002) presented Ar/Ar analysis of coeval volcanic rocks of the nearby Prinsen af Wales Bjerge region, allowing more precision in the ages assigned to the earlier geochemical correlation. The ages derived from the dating of the Prinsen af Wales Bjerge volcanic rocks (Hansen *et al*., 2002) are comparable to those derived from the FIBG (Waagstein *et al*., 2002), again supporting the correlation based on igneous geochemistry.

In summary, there is a significant body of isotopic evidence indicating the onset of FIBG eruption during the latest part of the Early Paleocene into the earliest part of the Late Paleocene between 61.6±1.3 Ma to 58.8±0.5 Ma. Here, this age model for the onset of FIBG volcanism is examined in the light of stratigraphical evidence available from the FIBG sedimentary interbeds, wells drilled recently in the Faroe-Shetland Basin, and from exposures in East Greenland.

Palynofloral Evidence

Review of biostratigraphical data

Offshore igneous complexes and lava fields have not presented attractive drilling prospects, limiting the amount of available information on their age and lithologies. Wells drilled on the Erlend centre were examined by Jolley and Bell (2002b), and comprised onlapping tuffaceous marine claystones of the Balder Formation, attributed to Sequence T50 (Ebdon *et al*., 1995 and Figure 3), resting unconformably on a succession of terrestrial Sequence T40 lavas which are in turn overlying marine neritic shales and sandstones attributed to Sequence T36 -T38. Of importance in this record is the influx of *Apectodinium augustum,* in an association of *Apectodinium* species between the uppermost flows of well 209/4-1A (Figure 1). This distinctive dinocyst has a well-defined stratigraphical range, confirming that the Erlend lava field ceased eruption during the upper part of Sequence T40.

The age of the sediments underlying the extensive lavas in East Greenland has been a subject of debate, many of the sections being in non-marine facies. Palynofloras attributable to Sequence T40 have been recovered from sediments at the base of the lava pile in the Vandfalsdalen Formation of Kangerlussuaq, (Hjortkjaer and Jolley, 1999) and in the equivalent sub-lava sediments of central East Greenland (Jolley and Whitham, 2005). Attribution of these palynofloras to Sequence T40 is indicative of an age between 54.9 and 56.2 Ma (Gradstein *et al*., 2004), some 2 my younger than the age derived from isotopic dating of the overlying Nansen Fjord Formation (Larsen *et al*., 1999; Nielsen *et al*., 2001), and the Urbjerget Formation (Hansen *et al*., 2002). It is possible to refine the biostratigraphical dating further, the occurrence of *A. augustum* in the central East Greenland sub-lava sediments indicating that eruption in this area began late in Sequence T40. *Apectodinium augustum* has been recognised as part of the worldwide phytoplankton response to changes in nutrient flux resulting from the greenhouse climate (Crouch *et al*., 2001), associated with the Paleocene - Eocene Thermal Maximum (PETM). Records of the occurrence of these palynofloras in the North East Atlantic, and the dates attributable to them (Gradstein *et al*., 2004), have recently been confirmed by the identification of the PETM and its associated phytoplankton response in the high Artic Ocean (Sluijs *et al*., 2006).

It is clear from the published literature that the nascent North Atlantic Rift was not the only focus for eruption of flood basalt lavas during the Late Paleocene to Early Eocene, in particular the Erlend Complex discussed above, can be cited as an example of a localised volcanic system (Gatliff *et al*., 1984). Lavas with a local, dyke fed source have also been proposed in well 205/9-1 in the Flett Sub-basin (Smallwood and Maresh, 2002). The stratigraphical relationship of these lavas within the Paleogene basin fill is demonstrated by published seismic lines (Smallwood and Maresh, 2002), showing the position of these flows relative to the overlying top Balder Formation and underlying base of the Late Paleocene. Palynofloral analysis of sedimentary rocks from well 205/9-1 (Ellis *et al*., 2002) has recorded that the strata immediately overlying the lavas yielded palynofloras attributable to Sequence T45 (Ebdon *et al*., 1995). The lavas themselves overlie, and are interbedded

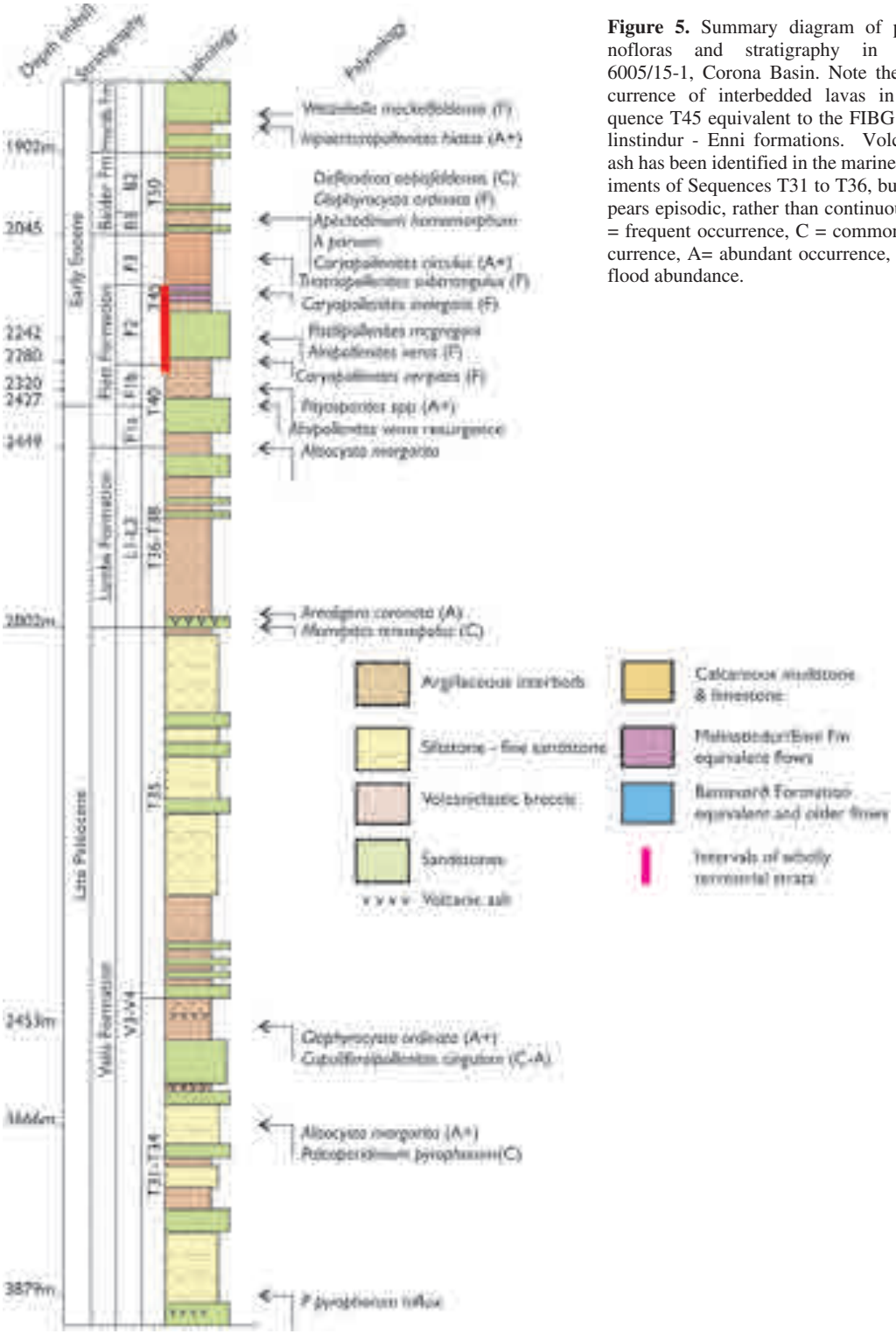

Figure 5. Summary diagram of palynofloras and stratigraphy in well 6005/15-1, Corona Basin. Note the occurrence of interbedded lavas in Sequence T45 equivalent to the FIBG Malinstindur - Enni formations. Volcanic ash has been identified in the marine sediments of Sequences T31 to T36, but appears episodic, rather than continuous. F = frequent occurrence, C = common occurrence, A= abundant occurrence, A+= flood abundance.

with, strata yielding terrigenuous palynofloras attributable to Sequence T40 (Ellis *et al*., 2002). These palynofloras allowed Ellis *et al*. (2002) to demonstrate a correlation with terrigenuous palynofloras recovered from mudstone and coaly interbeds within the exposed FIBG Beinisvørð Formation (Figure 4).

New Palynofloral Evidence from the Corona Basin

Well 6005/15-1 was drilled in the south of the Corona Basin in 2001 (Figure 5) through a Paleocene hydrocarbon prospect. It penetrated two distinct basaltic lava flow units at a depth of 2144 m - 2177 m, within a sequence of sandstones and shales of the Flett Formation Unit F2. Because the majority of the samples available from exploration wells are ditch cuttings, potential caving of rock fragments down the well makes it necessary to discuss the palynofloras recovered in down-hole order.

The age of the sedimentary rocks above the lava flows in 6005/15-1 is confirmed by the influx of *Cerodinium wardenense* at 2060 m, this dinocyst event being recorded in uppermost Flett Formation Unit F3 sediments across the Faroe-Shetland region. Down section from this influx, a flora composed of frequent specimens of the dinocysts *Apectodinium quinquelatum* and *Eocladopyxis peniculata,* and common specimens of *Dinopterygium* cf. *fehmarnense* was recorded. Palynofloras of closely similar character have been recorded by Jolley and Spinner (1989) from the middle of the Nacton Member, a unit equivalent to Sele Formation Unit 3 in the North Sea Basin (Jolley, 1996), and equivalent to the upper part of Flett Formation Unit F2. The lower beds of the Balder Formation yield characteristic palynofloras which include common specimens of *Deflandrea oebisfeldensis* and highly abundant *Caryapollenties circulus* (Figure 5). The majority of the dinocyst components of the flora have their last downhole occurrence in the Flett Formation unit F3, above the top of the lava flow interval. Below these flows, down-section to the base of Sequence T45, only freshwater microplankton and algae occur.

Occurring in the sedimentary interbeds between the two lava flow packages in 6005/15-1 are common specimens of *Caryapollenites inelegans*. This influx has been recorded by the author in a number of wells, derived from sediments attributed to uppermost Flett Formation Unit F2 in the Faroe-Shetland Basin. Beneath this, a significant change in the pollen and spore flora occurs at 2242m, with the occurrence of frequent - common specimens of *Alnipolenites verus* and *Pistilipollenites mcgregorii.* This palynoflora is comparable with the intra-top Sele Formation Unit S2a event seen widely over the North Sea Basin, first published in a study of the Forties field by Schroder (1992). Palynofloras of this character have also been recovered from the Prestfjall Formation sedimentary rocks of the Faroe Islands, where this flora is seen extensively on the island of Suðuroy (Lund, 1989; Ellis *et al*., 2002).

The first palynofloras typical of the upper part of depositional Sequence T40 are seen at 2280 m, where an influx of frequent specimens of *Caryapollenties veripites* and *Alnipollenties verus* occurs in association with consistent specimens of *Platycaryapollenites platycaryoides*. These non-marine floras dominate down-section to 2320m, where a dramatic increase in the frequency of *Pityosporites* spp. occurs. In this depositional setting, *Pityosporites* is a 'facies component' (Boulter and Hubbard, 1982), and is indicative of a marine, or strong fluvial, influence. In these samples this flood of conifer pollen is matched by an influx of freshwater algae and acritarchs characteristic of estuarine or shallow marine arenaceous facies.

An intra Sequence T40 compositional change in the palynofloras at 2427 m is marked by a resurgence in the frequency of *Alnipollenites verus*. This event is widespread across the NE Atlantic margin and has been reported by Schroder (1992), from the Forties Field in the North Sea Basin, where this event is associated with strata beneath the last downhole occurrence of *Apectodinium augustum,* marking pre-PETM assemblages (Crouch *et al*., 2001). Occurring immediately beneath this assemblage, palynofloras derived from Lamba Formation sediments attributable to Sequence T38 include the occurrence of *Alisocysta margarita* (2449 m). Other taxa recovered including common *Spiniferites* species and *Cometodinium coma-*

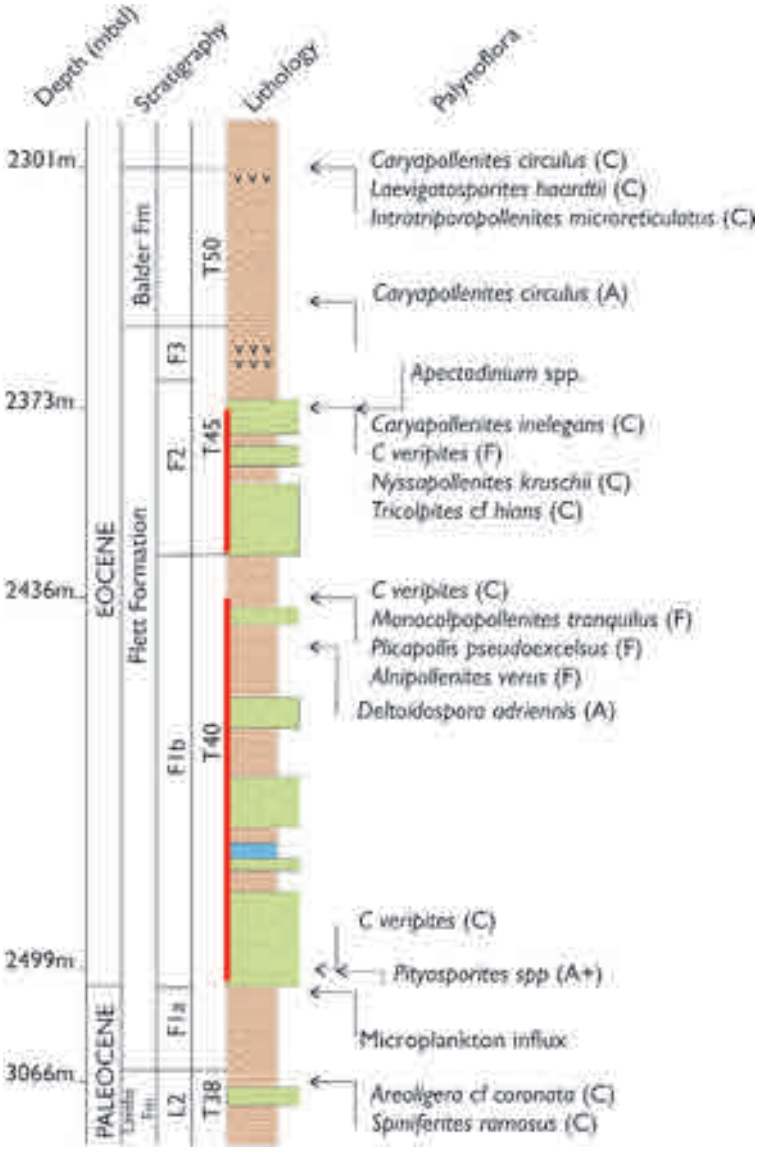

Figure 6. Summary diagram of palynofloras and stratigraphy in the Lamba - Flett Formation of well 6004/12-1, Corona Basin. Note the occurrence of interbedded lavas in the terrestrial sediments of Sequence T40. Key as for figure 5.

tum, both typical of upper Lamba Formation assemblages.

Analysis of the palynofloras from the Balder and Flett formations of another Corona Basin well, 6004/12-1 show comparable results to those derived from 6005/15-1 (Figure 6). Pollen and spores recorded in 6004/12-1 include many species that characterise the extensive flooplains and coal swamps developed during the upper part of Flett Formation Unit 1b and Flett Formation Unit 2 (Sequences T40-T45). These include an influx of *Caryapollenites inelegans* within Sequence T45,

comparable to that recovered from between the lava flows in well 6005/15-1. This species is particularly associated with intra-lava floodplain floras in the Flett Formation Unit 2 interval, and is also recorded in the Malinstindur Formation of the FIBG (author, unpublished data).

Of significance in well 6004/12-1 is the occurrence of a lava flow package within Sequence T40, this is of an age equivalent to those in the FIBG Beinisvørð Formation. This confirms that flood basalt lavas within the drilled part of the Corona Basin are constrained within the interval from Sequence T40 (Ebdon *et al*., 1995) to within uppermost Sequence T45. The microplankton events that are used to define the stratigraphical framework for this interpretation are readily comparable to those presented in the geologic time scale of Gradstein *et al*. (2004), and indicate ages between 56.8 Ma and 54.8 Ma.

Evidence from the Corona Ridge

Evidence for the age of flood basalt volcanism on the Corona Ridge, to the east of the Corona Basin, is provided by one well within the public domain. The volcanic rocks in well 213/23-1 (Figure 7) occur within the upper part of Sequence T40, the underlying rocks yielding consistent occurrences of *Apectodinium* species including *A. augustum*. Occurrences of these dinocysts indicate that the lavas in this well occur within Flett Formation Unit F1b, an interpretation corroborated by the pollen and spore flora. Dominated by *Inaperturopollenites hiatus* and *Pityosporites* spp., sub-dominant taxa in assemblages recovered from these strata are characterised by common specimens of *Caryapollenites veripites*, *Platycaryapollenites platycaryoides*, and by frequent specimens of *Alnipollenites verus*, and *Labrapollis labraferoides*. This is an as-

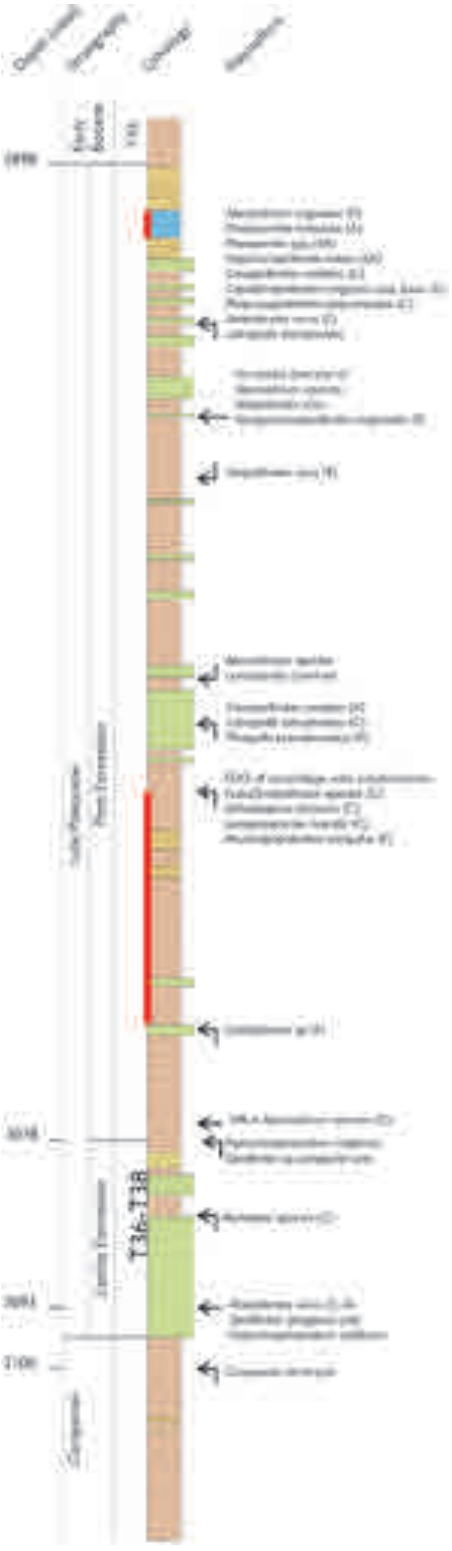

Figure 7. Summary diagram of palynofloras and stratigraphy in well 213/23-1, Corona Ridge: key as for figure 5. Note the lava above the highest occurrence of *Apectodinium* species within uppermost Sequence T40. An unconformity occurs between the T36-T38 neritic marine sediments below 3075m (10090') and the overlying T40 sediments, with a major unconformity separating the Paleocene from the underlying Late Cretaceous. A similar stratigraphical sequence was recorded by Jolley & Bell (2002b) in wells penetrating the Erlend Centre.

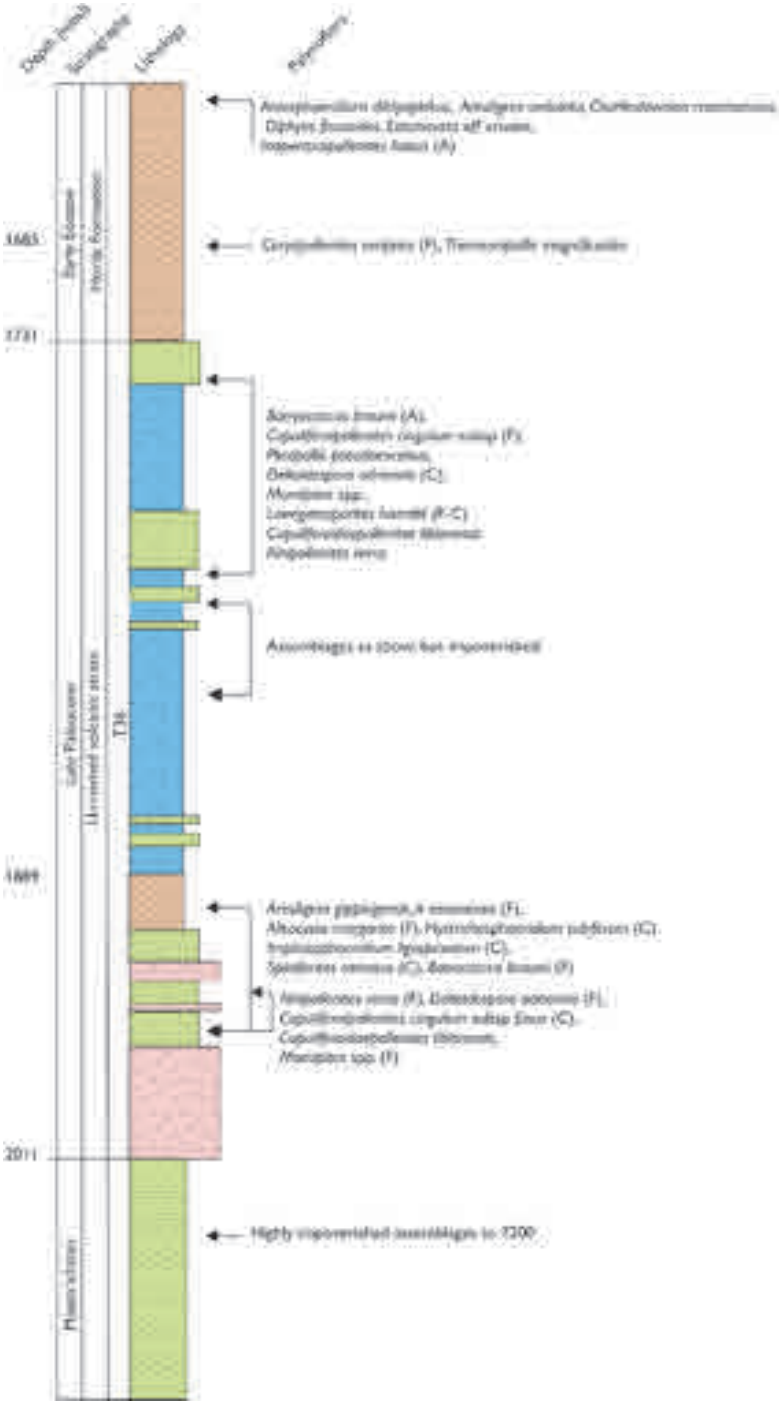

Figure 8. Summary diagram of palynofloras and stratigraphy in well 219/21-1, Ben Nevis structure: key as for figure 5. This mixed volcaniclastic, volcanic and sedimentary sequence shows an overall progradation from hyaloclastite delta with interbedded volcaniclastic sediments, to terrestrial lava field. The mudstone unit between the hyaloclastite - volcaniclastic sandstone and the lava flow units marks the inundation of the hyaloclastite/volcaniclastic prograding system during a maximum flooding event. Rich dinocyst floras are recovered from the interlava mudstones, but have caved downsection into the underlying interval. Their composition is characteristic of assemblages in areas of high nutrient availability, in this case derived from lava field run-off.

semblage characteristic of sediments within the upper part of Sequence T40, having also been recorded from the Faroe-Shetland Basin (Jolley, 1997) and the North Sea Basin (Schroder, 1992) in coeval sedimentary rocks.

Below 2984 m (9790'), only impoverished microplankton palynofloras are recovered, and include low frequency occurrences of *Apectodinium* species and a diversity of acritarch and minor peridinioid dinoflagellate species typical of turbid, low

salinity shallow water assemblages. A significant influx of *Apectodinium* species occurs at 3057 m (10030'), but does not include *A. augustum*. Underlying the Flett Formation in well 213/23-1 an older Late Paleocene succession occurs, resting unconformably on Upper Cretaceous marine sediments. The microplankton flora from the older Paleocene interval is little different from that recorded above. Records of *Apectodinium* species continue to be made in low frequencies, but these may be caved from the overlying interval. Occurrences of *Hystrichosphaeridium tubiferu*m, and the record of a stratigraphically restricted polygonal *Spiniferites sp.* at 3078 m (10100'), suggests that the sediments are attributable to Sequence T36.
Evidence from the pollen flora supports the assignation of these strata to Sequence T36, the pollen flora containing *Momipites* species, which are subdominant in assemblages recovered from within the Lamba and Vaila formations (Jolley and Morton, 2007). Below 3093 m (10150') a resurgence in numbers of *Alnipollenties verus* occurs. This pollen event is characteristic of Hebrides-Shetland 'central flora' associations from Lamba Formation strata (Jolley and Morton, 2007). In summary, the available evidence indicates that Corona Ridge flood basalts are no older than mid Sequence T40, an age comparable to that recorded for the Corona Basin wells.

Evidence from the Ben Nevis structure

To the north of the Sequence T40 flood basalts of the Erlend Complex lies a further succession of flood basalts. These form part of the Ben Nevis structure, the succession being proven by exploration well 219/21-1 drilled by Shell and Statoil (Figure 8). This well penetrated a thick sequence of volcanic rocks and volcaniclastic sediments.

Overlying these strata is a succession of argillaceous marine sedimentary rocks, which yield diverse microplankton assemblages. These contain frequent occurrence of *Homotryblium tenuispinosum with occurrences of Areosphaeridium diktyoplokus, Areoligera undulata, Diphyes ficusoides* and *Eatonicysta* u*rsulae,* all species consistent with an Early Eocene age. This is confirmed by the frequent occurrence of *Caryapollenties veripites* at 1685 m (5530'), which occurs in association with *Thomsonipollis magnificoidus,* the two species being characteristic of the later part of the Early Eocene (Krutzsch, 1966; Gruas-Cavagnetto, 1976).

A major unconformity occurs between these Eocene sediments and the underlying volcanic and volcaniclastic strata. The interval from 2011 m to 1889 m (6600' to 6200'), is composed of beds of volcaniclastic breccia (hyaloclastite) and volcaniclastic sandstone which are interpreted as having been deposited in water, by a prograding lava front. Shortly after its initiation, this breccia delta appears to have been flooded as a consequence of an increase in relative sea level. Extrusion and progradation of volcanic material failed to keep pace with the increasing accommodation space provided by the rise in relative sea level, leading to the deposition of middle neritic marine claystones. These marine claystones contain dinoflagellate cyst dominated palynofloral assemblages, comprising common *Hystrichosphaeridium tubiferum, Areoligera coronata*, *Alisocysta margarita* and the chlorophycean algae, *Botryococcus braunii*.

These species occur in highly abundant, flood proportions, and are part of a phytoplankton response to increased macronutrient availablility (N,P,K,Ca,Mg) in the water draining from the volcaniclastic delta (Uematsu *et al*., 2004). This flooding event and its associated flora, provide a means of dating this prograding volcanic system, as the composition of the dinoflagellate cyst flora is characteristic of Sequence T36, indicating that the section is equivalent to the lower beds of the Lamba Formation. Pollen and spore assemblages from this interval also support the dinocyst-based age determination. Frequent occurrences of specimens of *Momipites* spp. and *Alnipollenites verus*, with common occurrences of *Deltoidospora adriennis* and *Laevigatosporites haardtii* are characterisitic of the lower part of the Lamba Formation in palynofloras from this region (Jolley, 1997; Jolley and Morton, 2007).

Overlying these strata, the interval between 1731 m and 1889 m (5680' to 6200') comprises lava flows and volcaniclastic sandstones with some thin interbedded soil or fluvial sedimentary rocks. There are considerable cavings present in the samples, derived from the unconformably

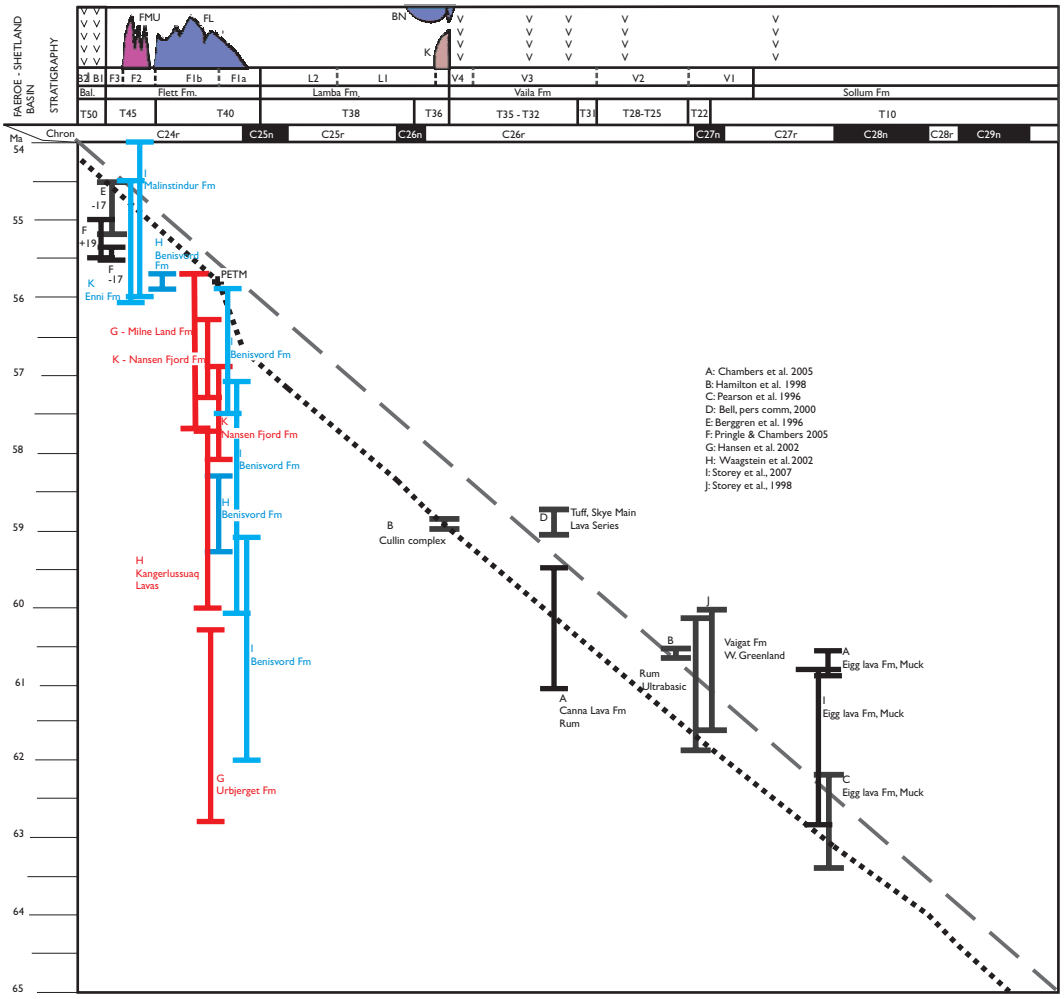

Figure 9. Age - sequence crossplot for the NE Atlantic. Dashed line = Cande and Kent (1995) time scale; dotted line = Gradstein *et al*., (2004) time scale, both fixed relative to the sequence/lithostratigraphy on the X axis by the occurrence of known tie point (e.g. -17 ash), and the polarity record. The Gradstein (2004) line deviates from straight because of non linear disparities in dating of events between this and the Cande & Kent (1995) time scale. The vertical error bars on the graph are isotopic dates, their position relative to the sequence/lithostratigraphy on the X axis is arranged by geological relationship of the strata they are derived from. Blue error bars represent isotopic dates from the FIBG which are positioned with respect to the sequence/lithostratigraphy axis using the work of Ellis *et al*. (2002) and data herein. Error bars in red are isotopic dates from SE Greenland, which are positioned with respect to the sequence/lithostratigraphy axis using the work of Nielsen *et al*. (1981), Hjortkjaer and Jolley (1999), and Jolley and Whitham (2005). Black errors are isotopic dates from other selected NAIP sites positioned using the work of Jolley and Morton (1992), Jolley (1997), Nøhr-Hansen *et al*. (2002) and Jolley *et al*., (2002). Note the disparate dating of the Eigg Lava Formation tuff by different laboratories; all three achieved using the same sample material. This crossplot highlights the disparity between the ages determined for the Faroes-East Greenland lava succession, and the stratigraphy derived from biostratigraphy and sequence stratigraphy.

overlying Early Eocene sediments. There is a variable abundance of *insitu* palynofloras, these being dependant on the presence of interbedded sedimentary rocks in each ditch cuttings sample. Dominated by *Inaperturopollenties hiatus*, the flora is similar to that recovered from the underlying prograding lava delta strata, and can similarly be attributed to Sequence T36. Fern spores occur commonly, indicating wet soils formed over short time periods between successive flows (Jolley *et al*., in press). The co-occurrence of angiosperm pollen from the genera *Cupuliferoipollenties* and *Cupuliferoidaepollenties* indicates that dryer substrates were important (Jolley *et al*., 2005), this dryer environment resulting in the disappearance of pollen from mire plants such as *Momipites* (Hickory types) and *Alnipollenties* (Alders), which are common in the underlying interval. These data confirm that the entire volcanic sequence in 219/23-1 was deposited during one period of eruption; the marine shales do not therefore represent a major hiatus within the lava pile. Ben Nevis remains somewhat atypical in that it is currently the sole example of Sequence T36 extrusive volcanism that has been identified offshore. It is notable that this volcanic centre also lacks any extrusive rocks erupted in sequences T40 to T45, the period of extensive flood basalt eruption.

Dispersed Volcanic Ash

In addition to the results from the wells discussed above, occurrences of volcanic ash have been recorded in Paleocene sediments of the Faroe-Shetland region. The most prominent of these is the occurrence of a unit of volcaniclastic rocks and ash at the base of the Lamba Formation. Termed the Kettla Member (Knox *et al*., 1997), these volcaniclastic sediments have been linked to volcanism on the Munkagrunnur Ridge (Linnard and Nelson, 2005). These volcaniclastic sediments are of the same age as the extrusive lavas of the Ben Nevis lava field discussed above, but there is no evidence that they were sourced from this centre. Instead, the distribution of the Kettla Member (Knox *et al*., 1997) suggests a number of isolated eruptive centres.

Occurrences of volcanic ash within the older Selandian-Thanetian sediments of the Faroe-Shetland Basin has been discussed by Morton *et al*., (1988), who recorded dispersed tephra from BGS borehole 82/12 . Although palynofloral assemblages were reported from this borehole, the details given concentrated on unusual species occurrences rather than the composition of the assemblages. Examination of new sample preparations from this borehole has recovered a palynoflora which includes common specimens of the dinocyst *Palaeocystodinium bulliforme, and Areoligera coronata.* This palynoflora is usually recorded in sedimentary rocks from the Sequence T25 - T28 interval. Occurrences of tephra in other exploration wells (e.g. 6005/15-1) demonstrates that these ashes form part of a series including tephras from uppermost Sequence T10 and sequences T31 - T36 (Figure 9).

Onset of FIBG Eruption

The most direct source of information on the onset of FIBG eruption would be derived from strata underlying the FIBG itself. The Lopra1/1a borehole (Figure 1) did not penetrate the base of the lava pile, although these sub-lava strata are believed to have been drilled by a commercial hydrocarbon exploration well, which is currently held to be confidential. In the light of this lack of direct information, the correlation between East Greenland and the Faroe Islands based on lava geochemistry (Larsen *et al*., 1999) remains of importance. This correlation, and the ages attributed to the strata it encompasses, is examined here by comparison to the biostratigraphical and lithological record derived from East Greenland, the Faroe Islands and offshore wells detailed above.

It is of importance to recognise that the isotopic ages assigned to the basal units of the East Greenland succession (Larsen *et al*., 1999), and the FIBG (Waagstein *et al*., 2002), indicate that volcanism commenced across this area between 61.6 Ma and 58.8 Ma, corresponding to the interval Vaila Formation Unit V1 to the Lamba Formation, Kettla Member (Figure 9). Although dispersed tephra is recorded in Faroe-Shetland Basin wells from uppermost Sequence T10 to Sequence T36 (62 Ma - 58 Ma), flood basalts are only encoun-

tered in the Ben Nevis structure lava field to the N at the youngest period of this age range.

While the lava geochemistry based correlation of the East Greenland succession with the FIBG is seemingly unequivocal, the isotopic dating, and attribution of Chrons to individual normal polarity intervals in the Beinisvørð Formation can be called into question by the sequence stratigraphical data presented above. Palynofloras recorded from the Vandfaldsdalen Formation of Kangerlussuaq by Nielson *et al*. (1981), Hjortkjaer and Jolley (1999) and from equivalent sediments in East Greenland by Jolley and Whitham (2005) all recovered assemblages from within Sequence T40, which by reference to the Gradstein *et al*. (2004) time scale, should proscribe ages between 54.9 and 57 Ma. Accepting the geochemical correlation, these biostratigraphical dates dispute the assignment of the labels Chron 25n and Chron 26n to the short normal polarity intervals identified by Schöenharting and Abrahamsen (1984) and Waagstein *et al*. (2002). This interpretation of these normal polarity events was directed by reference to the Cande and Kent (1995) timescale, and was in accordance with the >3my duration and 55.8 Ma to 58.8 Ma period indicated by isotopic analysis of FIBG lavas. Examination of magnetostratigraphical records from Late Paleocene sedimentary succession in NW Europe, highlights the occurrence of cryptochrons. Multiple short term fluctuations in polarity of this kind have been documented within Chron 24r sedimentary rocks from outcrops and cored boreholes within the London Basin by Ali and Jolley (1996). These short-duration normal polarity events are <1m thick in these condensed sedimentary records from the basin margin, in contrast, the thickness of a cryptochron in a lava field would be dependent on the rate of lava extrusion.

While the short normal polarity flows of the Beinisvørð Formation can be interpreted as cryptochrons, the relationship between the biostratigraphical framework and the published isotopic dates from the base of the East Greenland lava pile and the FIBG exhibit a consistent disparity that is not readily explained. This disparity was originally identified by Jolley *et al*. (2002), but has subsequently been disputed on the grounds of inadequate stratigraphy (Aubry *et al*., 2003; Pringle and Chambers, 2005; Chambers *et al*., 2005). However, as demonstrated above, this disparity remains (Figure 9). Until it is resolved, it remains impractical to relate stratigraphy derived from isotopic analysis, to that derived from sequence stratigraphy, reducing the utility of regional studies in a hydrocarbon exploration context.

It should be noted that lava fields older than Sequence T40 have been identified at both the Ben Nevis structure lava field and from a separate, unidentified source by its volcaniclastic product (the Kettla Member). However, these eruptive centres currently appear to be localised, and possibly related to the position of lines of structural weakness (Ellis *et al*., in press). Outside these local eruptive centres, volcanic rocks are represented across the basin as airfall ashes or within density flow sediments such as the Kettla Member.

Offshore wells confirm that the oldest widespread flood basalt lavas are attributable to Sequence T40. Some of these, particularly in the eastern FSB may be locally sourced, as has been demonstrated for 205/9-1 and the Erlend Centre (Chalmers and Western, 1979). The feather margin of the true FIBG occurs in exploration wells, with the oldest, drilled in 6004/12-1, attributable to Sequence T40. These show a remarkable consistency with the biostratigraphical age attributed to the sediments beneath the oldest lavas of East Greenland and within those of the FIBG, suggesting the onset of widespread flood basalt volcanism within Sequence T40, not within Sequence T21 to Sequence T36 as suggested by the isotopic stratigraphy. This has one significant consequence for hydrocarbon exploration in the Northeast Atlantic; there is accommodation for 8 m.y. of Paleocene sedimentation under the lava flows of the FIBG, rather than the <3 m.y. that is imposed by the current FIBG isotopic dating.

Cessation of FIBG eruption

Cessation of eruption away from the main FIBG lava field shows a considerable degree of variance in age. Intuitively, it is to be expected that isolated local centres such as Erlend will have a restricted stratigraphical extent. These areas cannot assist

in the determination of cessation of FIBG eruption, emphasis must therefore be placed on the exposed FIBG, and from nearby exploration wells.

A major, and consistent change in the palynofloras recovered from Faroe-Shetland Basin wells occurs immediately below the Flett Formation Unit F2-F3 boundary. This is particularly accentuated in coastal plain well locations on the west of the basin, where a transgressive surface resulted from a minor marine incursion (Figures 5 and 6). This marine component persisted to the top of the Flett Sequence, terminating at the flooding surface at the base of the overlying Balder Formation.

The importance of this Flett Formation Unit 2 regional flooding lies in the correlation of the Faroe-Shetland Basin margin to the onshore Faroe Islands Lava Field. As a result of such a relative sea level rise, an environmental change in the lava field to the NW would be anticipated. Accordingly, the transgressive event below the Flett Formation Unit F2-F3 boundary should result in the incursion of estuarine or fluvial facies in the lower-lying areas of the lava field. Such an incursion is recognised within the Enni Formation of the FIBG, as estuarine facies on Sandoy, Nólsoy and Kunoy-Borðoy (Ellis *et al*., 2002; and author unpublished data), suggesting a correlation of this interval with the Flett Formation Unit F2-F3 boundary. The deepening of the marginal Faroe-Shetland Basin environments during deposition of Flett Formation Unit F3 is a possible indication that flood lava activity was waning, accompanied, and perhaps caused by regional thermal subsidence. This represents a prelude to the phreatomagmatic activity at the rift that is represented by the ash bearing Balder Formation (Larsen *et al*., 2003; Jolley and Widdowson, 2005), a deposit not preserved on the Faroe Islands.

Attribution of the FIBG Malinstindur-Enni formations interval to within Sequence T45 also assigns an age of between 54.5 Ma to 54.9 Ma (Gradstein *et al*., 2004). These ages are again younger than those attributed to the correlative succession in East Greenland. This mismatch has been compounded by the recent publication of new analyses for the rhyolitic +19 and nephelinitic -17 ashes from the Fur Formation of Denmark (Pringle and Chambers, 2005). These ashes have a first order correlation to the biostratigraphical and lithostratigraphical record (see Jolley, 1996) of the North Sea Basin, the new ages assigning 55.26$\pm$0.24 Ma to the +19 ash and 55.44$\pm$0.08 Ma to the -17 ash. These are clearly at variance with earlier analyses reported by Berggren *et al*. (1995), which were used as a spline point in the Cande and Kent time scale (1995). These recent dates also demonstrate variance with the Gradstein *et al*. (2004) geologic timescale (Figure 9), under which the age determined for the -17 ash by Pringle and Chambers (2005) would imply that it occurred within Sequence T40, instead of its true position in the uppermost beds of Sequence T45. Clearly, until further research into the integration of isotopic and biostratigraphical dating is undertaken, age determinations from isotopic methods cannot be readily used to indicate age against the sequence stratigraphical framework of the Northeast Atlantic.

Acknowledgements

The author is indebted to Statoil Færøyene A/S for funding research into the offshore sections discussed in this paper and to two anonymous reviewers for their constructive comments.

References

Ali, J.R. and Jolley, D.W. 1996. Biostratigraphically constrained magnetostratigraphy of the Late Paleocene and Early Eocene of the Anglo - Belgium - Paris Basin. *In*: Knox, R.W.O'B. Corfield, R. and Dunay, R.E. (eds) *Correlation of the Early Paleogene in Northwest Europe*. Geological Society of London, Special Publications 101: 129-144.

Aubry, M.-P., Swisher, C.C., Kent, D.V. and Berggren, W.A. 2003. Paleogene time scale miscalibration: Evidence from the dating of the North Atlantic igneous province: Comment. *Geology* 31: 468-469.

Berggren, W.A., Kent, D.V., Swisher, C.C. and Aubry, M.-P. 1995. A revised Cenozoic geochronology and chronostratigraphy. *In*: Berggren, W.A. *et al*. (eds) *Geochronology, time scales and global stratigraphic correlations*. SEPM Special Publication 54: 129-212.

Boulter, M.C. and Hubbard, R.N.L.B. 1982. Objective paleoecological and biostratigraphic interpretation of Tertiary palynological data by multivariate statistics. *Palynology,* 6: 55-68.

Cande, S. and Kent, D.V. 1995. Revised calibration of

the geomagnetic time scale for the Late Cretaceous and Tertiary. *Journal of Geophysical Research* 100: 6093-6095.

Chalmers, J.A. and Western, P.G. 1979. A Tertiary igneous centre north of the Shetland Isles. *Scottish Journal of Geology*, 15: 333-342.

Chambers, L.M., Pringle, M.S. and Parrish, R.R. 2005. Rapid formation of the Small Isles Tertiary centre constrained by precise $^{40}Ar/^{39}Ar$ U-Pb ages. *Lithos* 79: 367-384.

Crouch, E.M., Heilmann-Clausen, C., Brinkhuis, H, Morgans, H.E.G, Rogers, K.M., Egger, H. and Schmitz, B. 2001. Global dinoflagellate event associated with the late Paleocene thermal maximum. *Geology* 29: 315-318.

Ebdon, C.C., Granger, P.J., Johnson, H.D., and Evans A.M. 1995. Early Tertiary evolution and stratigraphy of the Faeroe-Shetland Basin: Implications for hydrocarbon prospectivity. *In*: Scrutton R.A., *et al*. (eds) *Sedimentation and palaeoceanography of the North Atlantic region*. Geological Society of London, Special Publications 90: 51-69.

Ellis, D., Bell, B.R., Jolley, D.W. and O'Callaghan, M. 2002. The stratigraphy, environment of eruption and age of the Faroes Lava Group, NE Atlantic Ocean. *In:* Jolley, D.W. and Bell, B.R. (eds) *The North Atlantic Igneous Province; stratigraphy, tectonic, volcanic and magmatic processes*. Geological Society, London, Special Publications 197: 253-270.

Ellis, D., Jolley, D.W., Passey, S.R. and Bell, B.R. in press. Transfer Zones: The application of new geological information from the Faroe Islands applied to the offshore exploration of intra basalt and sub-basalt exploration. *Faroe Islands Exploration Conference: Proceedings of the 2nd Conference*. Annales Societatis Scientiarum Færoensis (Faroese Society of Sciences and Humanities), Tórshavn. This volume.

Fitch, F.J., Hooker, P.J., Miller, J.A. and Brereton, N.R. 1978. Glauconite dating of Palaeocene - Eocene rocks from east Kent and the timescale of Palaeogene volcanism in the North Atlantic region. *Journal of the Geological Society, London* 135: 499-512.

Gatliff, R.W., Hitchen, K., Ritchie, J.D. and Smythe, D.K. 1984. Internal structure of the Erland Tertiary volcanic complex, north of Shetland, revealed by seismic reflection. *Journal of the Geological Society*, London 141: 555-562.

Gradstein, F.M., Ogg, J.G. and Smith, A.G. 2004. *A geologic time scale 2004*. Cambridge University Press 585pp.

Gruas-Cavagnetto, C. 1976. Étude palynologique du Paléogéne du sud de l'Angleterre. *Cahiers de Micropaleontologie* 1: 5-49.

Hamilton, M.A., Pearson, D.G., Thompson, R.N., Kelley, S.P. and Emeleus, C.H. 1998. Rapid eruption of Skye lavas inferred from precise U-Pb and Ar-Ar dating on the Rum and Cuillin plutonic complexes. *Nature* 394: 260-262.

Hansen, H., Pedersen, A.K., Duncan, R.A. Bird, D.K., Brooks, C.K., Fawcett, J.J., Gittings, J., Gorton, M. and O'Day, P. 2002. Volcanic stratigraphy of the southern Prinsen af Wales Bjerge region, east Greenland. *In*: Jolley, D.W. and Bell, B.R. (eds) *The North Atlantic Igneous Province; stratigraphy, tectonic, volcanic and magmatic processes*. Geological Society, London, Special Publications 197: 183-218.

Hjortkjaer, B.F. and Jolley, D.W. 1999. A spore and pollen assemblage from the Late Paleocene sedimentary section at Kulhøje, East Greenland. Implications for the break-up history of the North Atlantic. Abstracts and Programme, *The North Atlantic Igneous Province: Magmatic controls on sedimentation*, Geological Society, Burlington House, London 1pp.

Jolley, D.W., Widdowson, M. and Self, S. in press. Volcanogenic nutrient fluxes and plant ecosystems in Large Igneous Provinces. An example from the Columbia River Basalt Group. *Journal of the Geological Society, London.*

Jolley, D.W. and Morton, A.C. 2007. Understanding basin sedimentary provenance: evidence from allied phytogeographic and heavy mineral analysis of the Paleocene of the NE Atlantic. *Journal of the Geological Society, London* 164: 553-564.

Jolley, D.W., Morton, A.C. and Prince, I.P. 2005. Volcanogenic impact on phytogeography and sediment dispersal patterns in the NE Atlantic. *In*: Doré A.G. and Vining, B.A. (eds) *Petroleum Geology: NW Europe and Global Perspectives: Proceedings of the 6th Petroleum Geology Conference*. Geological Society, London: 969-975.

Jolley, D.W. and Whitham A.G. 2005. A stratigraphical and palaeoenvironmental analysis of the sub-basaltic Paleogene sediments of East Greenland, *Petroleum Geology* 10: 53-60.

Jolley, D.W. and Widdowson M. 2005. North Atlantic rift eruptions drive Eocene climate cooling, *Lithos* 79: 355-366.

Jolley, D.W. and Bell, B.R. 2002b. Genesis and age of the Erlend Volcano, NE Atlantic Margin. *In*: Jolley, D.W. and Bell, B.R. (eds) *The North Atlantic Igneous Province; stratigraphy, tectonic, volcanic and magmatic processes*. Geological Society, London, Special Publications 197: 95-110.

Jolley, D.W. and Bell, B.R. 2002a. The evolution of the North Atlantic Igneous Province and the opening of the NE Atlantic rift. *In*: Jolley, D.W. and Bell, B.R. (eds) *The North Atlantic Igneous Province; stratigraphy, tectonic, volcanic and magmatic processes*. Geological Society, London, Special Publications197: 1-14.

Jolley, D.W., Clarke, B. and Kelley, S. 2002. Paleogene time scale miscalibration: evidence from the dating

of the North Atlantic Igneous Province. *Geology* 30: 7-10

Jolley, D.W. 1997. Palaeosurface palynofloras of the Skye lava field and the age of the British Tertiary volcanic province. *In*: Widdowson, M. (ed.) *Palaeosurfaces: Recognition, reconstruction and palaeoenvironmental interpretation*. Geological Society of London, Special Publications 120: 67-94.

Jolley, D.W. 1996. The earliest Eocene sediments of eastern England: an ultra-high resolution palynological correlation. *In*: Knox, R.W.O'B., Corfield, R. and Dunay, R.E. (eds) *Correlation of the Early Paleogene in Northwest Europe*. Geological Society of London, Special Publications 101: 219-254.

Jolley, D.W. and Morton, A.C. 1992. Palynological and petrological characterisation of a North Sea volcaniclastic sequence. *Proceedings of the Geologists' Association* 103: 119-127.

Jolley, D.W. and Spinner, E. 1989. Some dinoflagellate cysts from the London Clay (Palaeocene-Eocene) near Ipswich, Suffolk, England. *Review of Palaeobotany and Palynology* 60: 361-373.

Knox, R.W.O'B, Holloway, S., Kirkby, G.A. and Bailey, H.E. 1997. Stratigraphic nomenclature of the UK North West Margin. *2. Early Paleogene Lithostratigraphy and Sequence Stratigraphy*. British Geological Survey.

Krutzsch, W. 1966. Die sporenstratigraphisce des alteren Tertiar im Nordlichen Mittteleuropa (Palaozan-Mitteloligozan) methodisce grundlagen und gegenwartiger stand der untersuchungen. *Abhandlingen des Zentalen geologischen Instituts* 8: 112-149.

Larsen, L.M., Fitton, J.G. and Pedersen, A.K. 2003. Paleogene volcanic ash layers in the Danish Basin: compositions and source areas in the North Atlantic Igneous Province, *Lithos* 71: 47-80.

Larsen, L.M., Waagstein, R., Pedersen, A.K., and Storey, M. 1999. Trans-Atlantic correlation of the Palaeogene volcanic successions in the Faeroe Islands and East Greenland. *Journal of the Geological Society*, *London* 156: 1081-1095.

Linnard, S. and Nelson, R. 2005. Effect of Tertiary volcanism and later events upon the Faroese hydrocarbon system. *In*: Ziska, H., Varming T. and Bloch, D. (eds) *Faroe Islands Exploration Conference: Proceedings of the 1st Exploration Conference*. Annales Societatis Scientiarum Faeroensis, Tórshavn, Supplementum 43: 44-53.

Lund, J. 1989. A late Paleocene non-marine microflora from interbasaltic coals of the Faeroe Islands, North Atlantic. *Bulletin of the Geological Society of Denmark* 37: 181-203.

Morton, A.C. Evans, D., Harland, R., King, C. and Ritchie, D.K. 1988. Volcanic ash in a cored borehole W of the Shetland Islands: evidence for Selandian (Late Palaeocene) volcanism in the Faroes region. *In*: Morton, A.C. and Parson, L.M. (eds) *Early Tertiary opening of the NE Atlantic*. Geological Society London, Special Publications 39: 263-269.

Nielsen, T.F.D, Hansen, H., Brooks K.C. Lesher, C.E. and field parties. 2001. The East Greenland continental margin, the Prinsen af Wales Bjerge and new Skaergaard intusion initiatives. *Geology of Greenland Survey Bulletin* 189: 83-98.

Nielsen, T.F.D, Soper, N.J., Brooks K.C. Faller, A.M., Higgins, A.C. and Matthews, D.W. 1981. The prebasaltic sediments and the Lower Basalts at Kangerlussuaq, East Greenland; their stratigraphy, lithology, paleomagnetism and petrology. *Meddelelser om Grønland, Geoscience* 6: 3-28.

Nøhr-Hansen, H., Sheldon, E. and Dam, G. 2002. A new biostratigraphic scheme for the Paleocene onshore West Greenland and its implications for the timing of the pre-volcanic evolution. *In*: Jolley, D.W. and Bell, B.R. (eds) *The North Atlantic Igneous Province; stratigraphy, tectonic, volcanic and magmatic processes*. Geological Society, London, Special Publications 197: 111-156.

Passey, S.R., Jolley, D.W. and Bell., B.R. in prep. Formalisation of the lithostratigraphic nomenclature for the Faroe Islands Basalt Group, NE Atlantic.

Pearson, D.G., Emeleus, C.H. and Kelley, S.P. 1996. Precise 40Ar/39Ar dating for the initiation of Palaeogene volcanism in the Inner Hebrides and its regional significance. *Journal of the Geological Society, London* 153; 815-818.

Pringle, M.S. and Chambers, L.M. 2005. Paleocene timescale miscalibration: fact or fiction? Collection of Goldschmidt Conference Abstracts 2005. *Geochemica et Cosmochimica Acta* 69 (10): A325-A325

Riisager, P., Riisager, J., Abrahamsen, N., and Waagstein, R. 2002. New paleomagnetic pole and magnetostratigraphy of Faroe Islands flood volcanics, North Atlantic igneous province. *Earth and Planetary Science Letters,* 201: 261-276.

Rasmussen, J. and Noe-Nygaard, A. 1970. *Geology of the Faeroe Islands*. Danmarks Geologiske Undersøgelse 1: 25.

Schroder, T. 1992. A palynological zonation for the Paleocene of the North Sea Basin. *Journal of Micropalaeontology* 11: 113-126.

Sheldon, N. 2003. Pedogenesis and geochemical alteration of the Picture Gorge subgroup, Columbia River basalt, Oregon. *Geological Society of America Bulletin* 115: 1377-1387.

Schöenharting, G and Abrahamsen, N. 1984. Magnetic investigations on cores from the Lopra-1 drillhole, Faroe Islands. *In*: Berthelsen, O., Noe-Nygaard, A., and Rasmussen, J. (eds) *The deep drilling project 1980-1981 in the Faroe Islands.* Føroya Fróðskaparfelag, Tórshavn: 109-114.

Sluijs A., Schouten, S., agani, M., Woltering, M., Brinkhuis, H., Damste, J.S.S., Dickens, G.R., Huber,

M., Reichart, G.J., Stein, R., Matthiessen, J., Lourens, L.J., Pedentchouk, N., Backman, J., Moran. K. and Expedition 302 Scientists 2006. Subtropical arctic ocean temperatures during the Palaeocene/Eocene thermal maximum. *Nature* 441 (7093): 610-613.

Smallwood, J.R. and Maresh, J. 2002. The properties, morphology and distribution of igneous sills: modelling, borehole data and 3D seismic from the Faroe-Shetland area. *In*: Jolley, D.W. and Bell, B.R. (eds) *The North Atlantic Igneous Province; stratigraphy, tectonic, volcanic and magmatic processes*, Geological Society, London, Special Publications 197: 271-306.

Storey , M., Duncan, R.A. and Tegner, C. 2007. Timing and duration of volcanism in the North Atlantic Igneous Province: Implications for geodynamics and links to the Iceland hotspot, *Chemical Geology* in press.

Storey, M., Duncan, R.A., Pedersen, A.K., Larsen, L.M. and Larsen, H.C. 1998. $^{40}Ar/^{39}Ar$ geochronology of the West Greenland Tertiary volcanic province. *Earth and Planetary Science Letters* 160: 569-586.

Tarling, D.H. and Gale, N.H. 1968. Isotopic dating and palaeomagnetic polarity in the Faroe Islands. *Nature* 218: 1043-1044.

Uematsu, M., Toratani, M., Kajino, M., Narita, Y., Senga, Y. and Kimoto, T. 2004. Enhancement of primary productivity in the western North Pacific caused by the eruption of the Miyake-jima volcano, *Geophysical Research Letters* 31: L06106, doi:10.1029/2003GLO18790.

Waagstein, R., Guise, P. and Rex, D., 2002. K/Ar and $^{39}Ar/^{40}Ar$ whole-rock dating of zeolite facies metamorphosed flood basalts; the upper Paleocene basalts of the Faroe Islands, NE Atlantic. *In*: Jolley, D.W. and Bell, B.R. (eds) *The North Atlantic Igneous Province; stratigraphy, tectonic, volcanic and magmatic processes*. Geological Society, London, Special Publications 197: 219-252.

Waagstein, R. 1988. Structure, composition and age of the Faroe basalt plateau. *In*: Morton, A.C. and Parson, L.M. (eds) *Early Tertiary Volcanism and the opening of the NE Atlantic*. Geological Society, London, Special Publications 39: 225-238.

Recognition of a faulted basalt lava flow sequence through the correlation of stratigraphic marker units, Skopunarfjørður, Faroe Islands

SIMON R. PASSEY

Jarðfeingi, Brekkutún 1, P.O. Box 3059, FO-110, Tórshavn, Faroe Islands
Email: simon.passey@jf.fo; Tel: +298 357033; Fax: +298 357001

ABSTRACT

The recognition of three distinctive stratigraphic marker units, the Sneis Formation, the Høvdhamarin Flow and the Argir Beds, has facilitated the correlation of a >300 m thick volcanic interval of the central Faroe Islands, NE Atlantic Ocean. The interval consists of compound lava flows, sheet lobes and various volcaniclastic lithologies of the Malinstindur, Sneis and Enni formations of the Faroe Islands Basalt Group. The construction of planar surfaces and structural contours for the bases of the three stratigraphic marker units in a Geographic Information System (GIS) led to the recognition of a vertical discontinuity of 200-300 m across Skopunarfjørður, which separates the islands of Sandoy and Hestur. This vertical discontinuity is accounted for by an ESE-trending, dextral strike-slip fault aligned parallel to the bathymetry low in Skopunarfjørður. This Skopunarfjørður fault parallels the dominant ESE-trending fractures of southern Hestur, which do not show any vertical displacement. The lateral movement along this strike-slip fault is suggested to be between 4.2 and 6.2 km. This major Skopunarfjørður fault is tentatively extended offshore towards the Faroe-Shetland Channel due to the parallelism defined by offshore bathymetric features.

Introduction

The Faroe Islands, covering an area of *ca.* 1400 km^2, are located *ca.* 280 km to the NW of the British Isles. The Faroe Islands and its insular shelf form the Faroe Platform, which has a roughly triangular shape and is part of the NE Atlantic margin, a passive continental margin that extends from the western Barents Sea to offshore west of Ireland. The Faroe Islands are an exposed remnant of the Faroe Islands Basalt Group (FIBG) which forms the eastern part of an extensive, predominantly subaerial, continental flood basalt (CFB) province that is also exposed in East Greenland (Saunders *et al*., 1997; Larsen *et al*., 1999). The arrival of the putative proto-Iceland plume beneath Greenland led to widespread volcanic activity during the Palaeocene and early Eocene (62-54 Ma). During the same period rifting resulted in the eventual continental break-up between Greenland and Eurasia, culminating with the onset of ocean floor spreading in magnetochron 24r (ca. 55 Ma; Saunders *et al*., 1997; Ritchie *et al*., 1999; Jolley and Bell, 2002). Prior to the commencement of ocean floor spreading, the Faroe Islands and East Greenland were <120 km apart, based on simple plate reconstructions and likely geochemical correlations between the two originally contiguous sequences (Larsen *et al*., 1999).

On the Faroe Islands, the FIBG has a gross stratigraphic thickness of at least 6.6 km and is dominated by tholeiitic basalt lava flows. The volcanic pile is subdivided into seven formations based on the recognition of major disconformity surfaces and changes in lithology (Figure 1; Rasmussen and Noe-Nygaard, 1969; 1970; Passey *et al*., 2006), but also on geochemistry (Waagstein, 1988). The base of the volcanic pile comprises the Lopra Formation, a >1 km thick sequence of volcaniclastic rocks, including hyaloclastites, which have been intruded by basaltic sills/invasive lavas (Ellis *et al*., 2002; Waagstein, 2006). The Lopra Formation is overlain by the laterally extensive,

Faroe Islands Exploration Conference: Proceedings of the 2nd Conference.
Annales Societatis Scientiarum Færoensis, Supplementum 50, 2009: 174-204

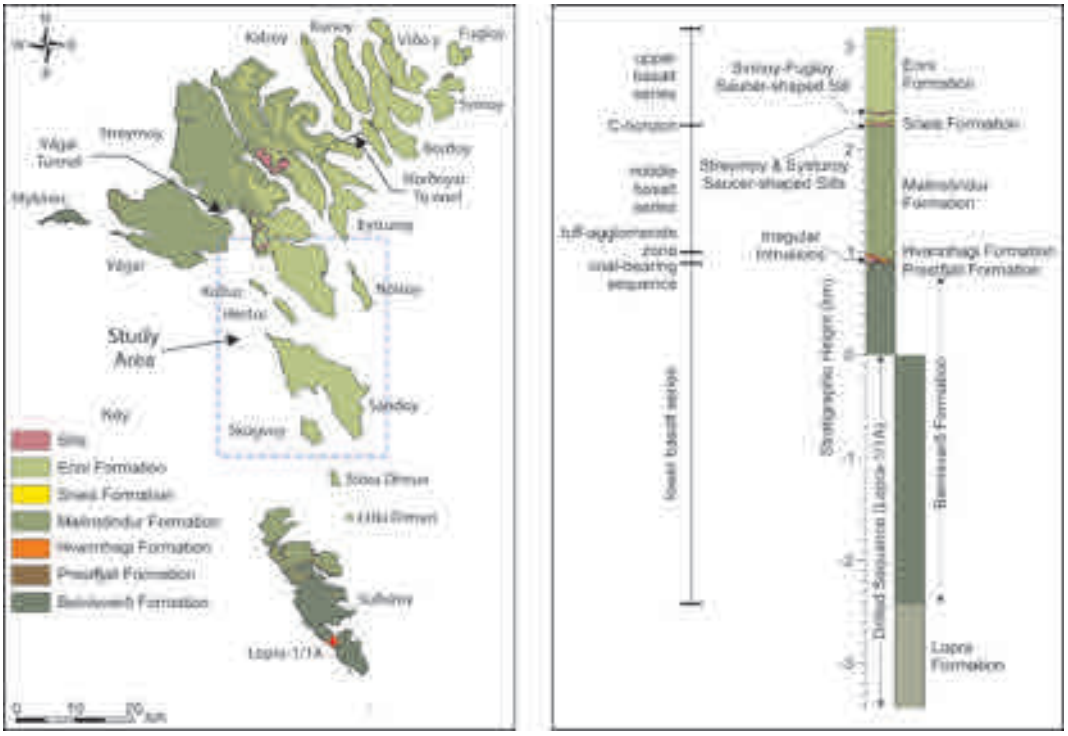

Figure 1. Simplified geological map and gross stratigraphic column for the Faroe Islands Basalt Group, Faroe Islands. The previous stratigraphy of Rasmussen and Noe-Nygaard (1970) is given to the left of the stratigraphic column. The study area is indicated by the dashed blue line on the geological map. The geological map is modified after Rasmussen and Noe-Nygaard (1969; 1970).

predominantly aphyric, sheet lobes (simple flows), with a characteristic layer-cake appearance, of the *ca.* 3.3 km thick Beinisvørð Formation (Noe-Nygaard and Rasmussen, 1968; Rasmussen and Noe-Nygaard, 1969; 1970; Hald and Waagstein, 1984; Waagstein, 1988; Ellis *et al.*, 2002; Waagstein, 2006). The Lopra Formation and the basal *ca.* 2.4 km of the Beinisvørð Formation have only been encountered in the onshore borehole Lopra-1/1A at Lopra on the southernmost island of Suðuroy (Figure 1; Hald and Waagstein, 1984; Waagstein, 2006).

A volcanic hiatus followed the emplacement of the Beinisvørð Formation which allowed for the erosion of the uppermost lava flows and deposition of the 3-15 m thick Prestfjall Formation, consisting of coals, mudstones, sandstones and conglomerates of swamp, lacustrine and fluvial association (Rasmussen and Noe-Nygaard, 1969; 1970; Lund, 1983; 1989). This inter-eruption facies is overlain by the Hvannhagi Formation, consisting of basaltic airfall tuffs, floodplain facies and mass flow deposits, which is up to 50 m thick and has been heavily intruded by irregular intrusions (Passey, 2004).

The <1.4 km thick Malinstindur Formation marks a return to the eruption of subaerial lava flows, predominantly compound flows, which evolve up section, from olivine-phyric through aphyric to plagioclase-phyric basalts (Noe-Nygaard and Rasmussen, 1968; Rasmussen and Noe-Nygaard, 1969; 1970; Waagstein and Hald, 1984; Waagstein, 1988). The top of the Malinstindur Formation commonly exhibits a pronounced weathering surface which marks another significant hiatus in the volcanism (Rasmussen and Noe-Nygaard, 1969; 1970; Passey *et al.*, 2006). This disconformity surface is overlain by the laterally extensive, maximum 30 m thick, Sneis Formation, consisting of a sequence of volcaniclastic sand-

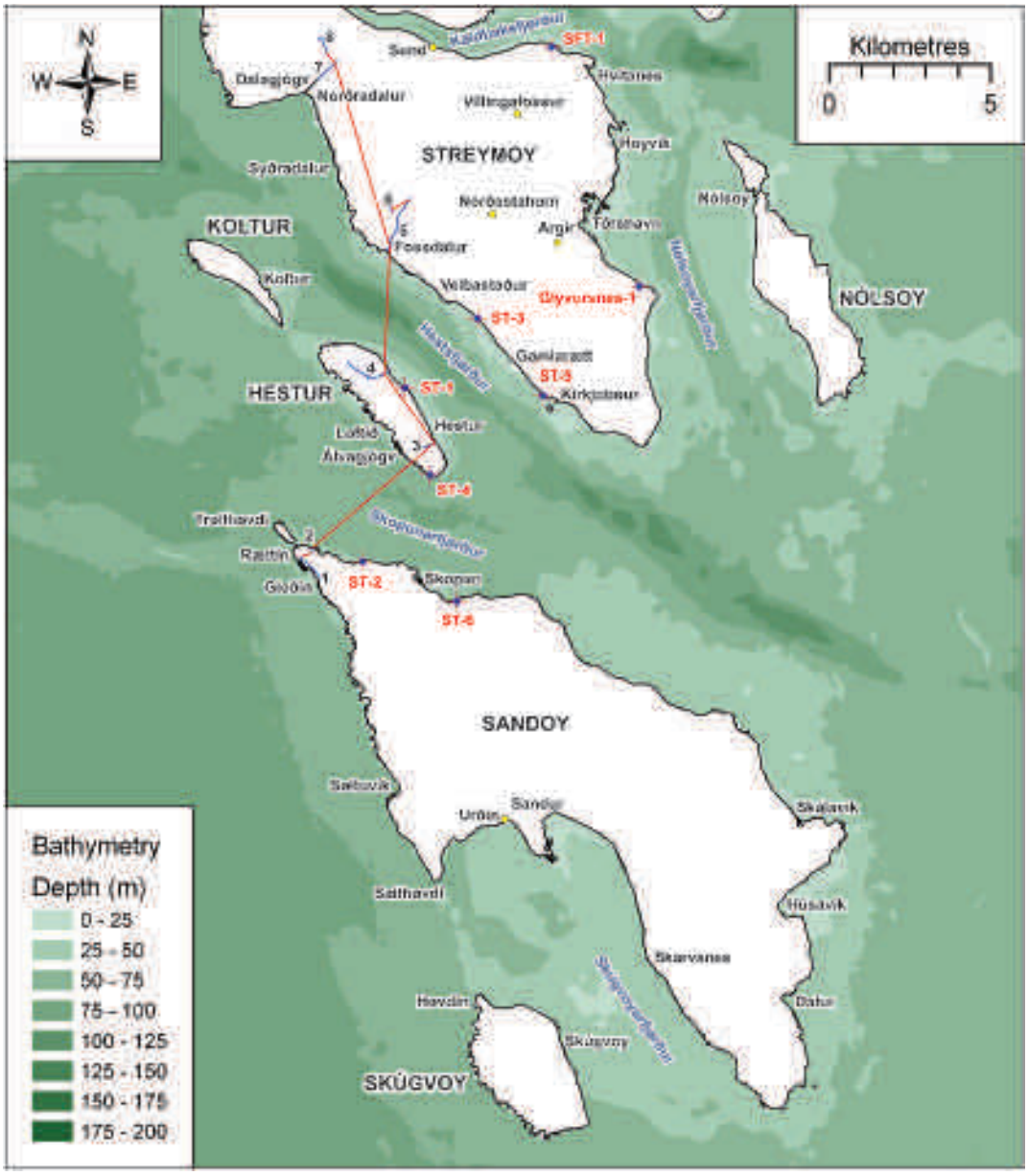

Figure 2. Bathymetry map for the study area, central Faroe Islands. The blue lines and associated numbers delineate the locations of the logged sections for the eight lithostratigraphic columns depicted in Figure 4 and the red lines represent the correlation tie lines between the columns. Notice the strong SE- and ESE-trend of Hestsfjørður and Skopunarfjørður, respectively. The yellow dots refer to key locations mentioned in the text. The locations of the six Sandoyartunnilin (ST-1 to -6) boreholes and the Skálafjarðartunnilin-1 (SFT-1) borehole are indicated on the map.

stones and conglomerates deposited mainly from mass flow events (Passey, 2004; Passey *et al.*, 2006). The base of the Sneis Formation, northeast of Syðradalur, Streymoy, consists of the distinctive and ubiquitous Sund Bed, a typically 50 cm thick, reddened, highly porous volcaniclastic sandstone (Passey *et al.*, 2006). The surface between the Sund Bed and the overlying conglomer-

ates typically marks the appearance of a suite of distinctly brown weathering, flow banded, aphyric basaltic sheets with a low-Ti, MORB-like composition (Waagstein, 1977; 1988), which were referred to as the C-horizon flows by Rasmussen and Noe-Nygaard (1969; 1970). These so-called C-horizon flows are highly invasive within the volcaniclastic strata of the Sneis Formation and are re-interpreted to be intrusions (Passey *et al*., 2006). The lower surface of these invasive sheets corresponds to the C-horizon of Rasmussen and Noe-Nygaard (1969; 1970).

The Sneis Formation is overlain by the Enni Formation, a sequence of interfingering compound and simple (sheet lobes) lava flows, which also comprise a mixture of high- and low-Ti (MORB-like) basalts (Noe-Nygaard and Rasmussen, 1968; Rasmussen and Noe-Nygaard, 1969; 1970; Waagstein, 1988; Passey and Bell, 2007). The Enni Formation has a minimum thickness of at least *ca.* 900 m due to the estimated erosion of a few hundred metres from the top of the volcanic pile (Figure 1; Waagstein *et al*., 2002; Jørgensen, 2006).

Continental break-up, initiation of seafloor spreading and thermal contraction of the proto-Iceland plume in the Eocene led to the magmatism being restricted to the active rift system, which resulted in the subsidence of the Faroe-Shetland region (Saunders *et al*., 1997). This is supported by palynofloral evidence from the Enni Formation on the Faroe Islands, which indicates estuarine and marginal marine settings and implies that the altitude of the formation was at, or near, sea level during the eruption of the lava flows (Ellis *et al*., 2002). Andersen (1988) suggests that this subsidence, most likely, resulted in the general easterly dip of <4° for the lava flows of the Faroe Islands.

The aseismic Faroe Islands comprise 18 main islands which are separated by narrow, elongated fjords with a dominant NW-SE trend (Figure 1). Rasmussen and Noe-Nygaard (1969; 1970) suggested that this trend is determined by a pre-existing tectonic fracture system and that the fjords may be the location of the fissures that fed the volcanism. However, no major fracture zones or dyke swarms have been proven across the fjords, even with the drilling of the two sub-sea tunnels (Figure 1; Madsen, 2006a, T. Madsen 2006 personal communication). Geoffroy *et al*. (1994), through palaeostress analysis of the basalts, identified four tectonic events dominated by transtensional strike-slip faulting and a compressional phase. However, only minor displacements, in the order of several metres have been observed for the fractures of the Faroe Islands, with vertical and lateral displacements rarely attaining offsets of 20 and 100 m, respectively (Rasmussen and Noe-Nygaard, 1969; 1970).

This study provides field evidence for the existence of a major strike-slip fault aligned sub-parallel to the axial trend of one of the fjords with a displacement of a few kilometres. The fault is identified through the logging and correlation of a >300 m thick lava flow interval and the displacement of triangulated structural contours of three stratigraphic marker units, the Sneis Formation, the Høvdhamarin Flow and the Argir Beds. This paper outlines the techniques used in mapping the lava flow sequence and how this data can be modelled in a Geographic Information System (GIS) and extrapolated into areas where direct observations are limited or cannot be made, for example, across a fjord. Descriptions of the lithologies encountered are given but no detailed facies interpretations are discussed as this will be published elsewhere in the broader context of the evolution of the FIBG.

Study Area

The study area extends from the island of Skúgvoy as far north as Kaldbaksfjørður, southern Streymoy but focuses on the area surrounding the SE-trending island of Hestur, which is *ca.* 5 km long by *ca.* 1 km wide (Figs. 1 and 2). Hestur is separated from the island of Sandoy by the ESE-trending Skopunarfjørður, which is *ca.* 9 km long and has a shallow dipping bathymetry obtaining depths of up to *ca.* 75-80 m. This contrasts with the *ca.* 11 km long Hestsfjørður that separates Hestur and Streymoy, which is characterised by a steeply dipping ravine, with a strong SE-trend that reaches maximum depths in the order of *ca.* 115 m. The ravine of Hestsfjørður extends offshore, although curving to the ESE, for a further *ca.* 12 km after merging with Skopunarfjørður to the SE of Hestur. The islands in the study area are characterised by dissected mountainous terrain sculpted by glacial

action during the Quaternary. The western coastlines of Skúgvoy, Sandoy, Hestur and Koltur are characterised by near vertical cliff sections with complete exposures of the geology. This contrasts with the eastern sides of these islands and southern Streymoy which are grass covered and easily accessible, although rock exposures are primarily limited to stream sections. However, rock exposures typically increase as the terrain steepens towards the mountain tops, which are relatively flat-lying and covered in rock boulders.

According to Rasmussen and Noe-Nygaard (1969; 1970) the geology of the study area should straddle the C-horizon level (i.e. *ca.* base of the Sneis Formation), which should be exposed as far south as Lítla Dímun (Figure 1). However, Rasmussen and Noe-Nygaard (1969; 1970) state that there is some uncertainty surrounding the position of the C-horizon and if they had mapped the horizon from east to west instead of west to east it would have been at a somewhat lower position. Moreover, they clearly state that the position of the C-horizon between Streymoy and Lítla Dímun is highly tentative, for example, on Koltur the position of the presumed C-horizon was mainly mapped from a boat and its position on Stóra Dímun and Lítla Dímun was only calculated from these suppositions and not actually observed. As mentioned above, the C-horizon corresponds to the lower surface of the distinctive C-horizon flows, but within the study area these basalts have only been observed as far south as the Breiðá stream, Syðradalur, Streymoy. On Skúgvoy and Sandoy the C-horizon, according to Rasmussen and Noe-Nygaard (1969; 1970), corresponds to the lower surface of a prominent pale (grey) weathering, plagioclase-phyric sheet lobe, which on Skúgvoy overlies a thick reddened sandstone. It shall be demonstrated that the so-called C-horizon on Skúgvoy corresponds to the upper surface of the Argir Beds and on Sandoy correlates to the lower surface of the Høvdhamarin Flow. This discrepancy has arisen due to the absence of the so-called C-horizon flows across the study area and has been resolved through the detailed logging and correlation of sections between Skúgvoy and Streymoy.

Methodology

In order to constrain the geology of the study area and to identify any structural displacements, a number of stream sections were examined (Figure 2) and representative lithostratigraphic columns were produced. The terminology used to produce these columns is outlined below. From the correlation of these columns three key stratigraphic marker units, the Sneis Formation, the Høvdhamarin Flow and the Argir Beds, were identified, which are easily recognisable in the field. The spot heights from the lower surfaces of these stratigraphic marker units were measured in the field to an accuracy of 1 m using a Suunto® Escape 203 altimeter and cross-referenced with topographic maps. Additional spot heights for the bases of the stratigraphic marker units, other than those obtained from the stream sections, were measured from individual exposures that were mapped out in the field. The spot heights were entered into the Geographic Information System, ArcGIS® 9.2, as x, y, and z points in the WGS84 UTM29 map projection. Spot height data for the bases of the Sneis Formation and Høvdhamarin Flow were also incorporated from the boreholes drilled in connection with the proposed Sandoy (boreholes Sandoyartunnilin-2, -3, -5 and -6) and Skálafjørður (borehole Skálafjarðartunnilin-1) sub-sea tunnels (Ólavsdóttir, 2005; Madsen, 2006b; Højgaard, 2007). Spot heights were also obtained for the three stratigraphic marker units from the deep borehole, Glyvursnes-1 which was drilled as part of the SeiFaBa (Seismic and petrophysical properties of Faroes Basalt, 2002-2005) project in 2002 to a depth of 700 m (Japsen *et al*., 2005).

The spot height data for each of the three stratigraphic marker units were entered into ArcGIS® 9.2 as separate point shapefiles for each island, for example, the Argir Beds had four shapefiles, one each for Skúgvoy, Sandoy, Hestur and Streymoy. The spot height data were then used in a number of combinations (e.g. all islands, southern area, northern area) to construct Triangulated Irregular Network (TIN) layers, which produced averaged planar surfaces, at 50 m structural contour intervals, for the lower surfaces of the selected stratigraphic marker units. These TIN layers are limited to the extent of the spot height data and therefore,

the surfaces were extrapolated to fill the geographically defined southern (Skúgvoy and Sandoy) and northern (Hestur and southern Streymoy) areas, respectively. However, caution is advised as the TIN layers are only as accurate as the amount of spot height data that is entered and their extrapolation assumes a constant dip and strike of the surface, but it shall be demonstrated that the dip and strike of the strata is relatively constant across the study area and is essentially replicated by all three stratigraphic marker units. It should be noted that these are "living" data files that are constantly being updated as more information is added to them. The TIN layers are useful predictive tools that suggest where a certain horizon should occur, which can then be checked in the field and then the TIN layer can be updated if necessary. TIN layers were constructed rather than the mathematically determined geostatistical layers in ArcGIS® 9.2 because the amount of height data for each surface is too limited to warrant statistical analysis. The triangulation method is already proven on the Faroe Islands as it was intensively used by Rasmussen and Noe-Nygaard (1969; 1970) when they originally modelled the C-horizon surface by hand.

Terminology

As mentioned above, the geology of the Faroe Islands is composed almost exclusively of subaerial basalt lava flows intercalated with various, minor volcaniclastic lithologies. In order to correlate between sections it is important to have a consistent and to some degree, simple classification scheme for producing the lithostratigraphic columns. Since the classical work of Rasmussen and Noe-Nygaard (1969; 1970) considerable advances have been made in the understanding of lava flow morphology (e.g. Self *et al*., 1998) and the importance of inter-flow sedimentation (e.g. Fisher and Smith, 1991). The following sections outline the descriptive terminology employed in this study for the different lava flows and volcaniclastic units.

Lava Flows

Petrology

For simplicity, the tholeiitic basalt lava flow lobes were subdivided into three broad groups based on their gross, macroscopic petrographic characteristics: (1) *aphyric*, (2) *plagioclase-phyric* and (3) *olivine-phyric*. The aphyric basalts, as the name implies, lack phenocrysts and have a typically aphanitic groundmass. The plagioclase-phyric basalts are a very broad group where the concentration (<10-30 vol.%) and (lath) sizes (<0.5-2 cm) of the plagioclase feldspar phenocrysts vary laterally as well as vertically within individual flow lobes, but these properties are given wherever possible. For example, it is common to see cumulate flow lobes where the plagioclase feldspar phenocrysts are concentrated in the basal section of the flow lobe, whereas the upper crust has a more aphyric texture. In addition, it is not uncommon within individual flow lobes to have alternating horizontal zones (usually <20 cm thick) of plagioclase-phyric and aphyric basalt. The last group consists of olivine-phyric basalts, which commonly consist of very small (<2 mm), typically equant, olivine (typically altered) phenocrysts (<10 vol.%) in a conspicuously aphanitic groundmass.

Morphology

In describing the subaerial lava flows of the FIBG the terminology proposed by Self *et al*. (1997) has been adopted. A *flow lobe* is used to describe an individual package of lava surrounded by a chilled crust and a *lava flow* is the product of a single, more or less continuous outpouring of lava that can be composed of one or more flow lobes. Individual lava flows are typically separated from other flows by weathering surfaces and/or clastic lithologies. If a lava flow consists of a single flow lobe it is referred to as a *simple lava flow* (Walker, 1970) and conversely, a *compound lava flow* (Walker, 1970) is made up of two or more flow lobes of any geometry or size. If an individual lobe has a sheet-like or tabular geometry, where the lobe is considerably wider than it is thick, it is classified as a *sheet lobe* (Self *et al*., 1997). On the Faroe Islands, sheet lobes typically form simple lava flows and these names are regarded as synonymous in this study (Passey and Bell, 2007), although in other provinces, sheet lobes may form compound flows (e.g. Self *et al*., 1997). Sheet lobes in the study area are typically >10 m thick. This contrasts to flow lobes of compound flows

that are usually <2 m thick and rarely attain thicknesses >5 m, although the compound flows are commonly >10 m thick. Passey and Bell (2007) suggest that a'a lava is extremely rare on the Faroe Islands and that both the simple and compound lava flows of the FIBG consist of flow lobes exhibiting features consistent with having been emplaced as inflated pahoehoe lava (Figure 3).

Weathering Attributes

Another feature used to distinguish between the basalt lava flows of the FIBG is their weathering coloration and two qualifiers are used. Firstly, *pale (grey) weathering* (accentuated by whitish-grey lichen) lava flows that are generally composed of plagioclase-phyric to aphyric basalt and secondly, *brown weathering* lava flows which typically consist of olivine-phyric to aphyric basalt. As the majority of the basalt lava flows have a pale (grey) weathering attribute only the qualifying term of 'brown weathering' is usually mentioned.

Other Characteristics

The qualifying term, *kandisgrót*, is used for a 'brecciated' variety of a typically coarse grained (1-2 cm long phenocrysts) plagioclase-phyric basalt, which usually has a sheet lobe geometry. Kandisgrót lobes are characterised by having a distinctly brecciated texture where the loose fragments resemble candy sugar (crystalline sugar). This is why this rock type is locally known as candy rock, i.e. kandisgrót in Faroese. One explanation for this texture is the quenching of the basalt as the lobe flowed over water-saturated terrain (Passey, 2004).

Composite Unit Name

Based on the characteristics described above, the basalt lava flows of the study area are named according to their gross petrology (aphyric, plagioclase-phyric or olivine-phyric) and morphology (sheet lobe (simple) or compound). For example, a lava flow composed of numerous flow lobes which have a predominantly aphyric texture would be named as an *aphyric compound flow*, conversely a lava flow composed of a single flow lobe with a tabular geometry and having a plagioclase-phyric texture would be named as a *plagioclase-phyric sheet lobe*. In addition, if the lava has a distinctive brown weathering attribute then the qualifying term of 'brown weathering' is added to the name, e.g. *brown weathering aphyric to olivine-phyric compound flow*. The following classification, *interbedded compound flow* is used to describe compound flows composed of numerous flow lobes with varying plagioclase-phyric and aphyric textures. These interbedded compound flows typically exhibit a progression upwards from plagioclase-phyric to aphyric lobes, but alternations of the different lobes are also commonly seen (Figure 3).

Volcaniclastic Rocks

A volcaniclastic rock, according to the Shipboard Scientific Party (2002), should contain >60 vol.% volcanic debris and the resulting nongenetic name is based on the rocks clastic textural properties (grain size and grain roundness) following the scheme of Wentworth (1922). For example, a clastic rock containing >60 vol.% rounded volcanic clasts with a grain size of small pebbles would be classified as a pebble-grade volcaniclastic conglomerate irrespective of its mode of formation (e.g. sedimentary vs. pyroclastic). This naming procedure is adopted in this study because it is extremely difficult in the field, unless there is unequivocal evidence, to apply a genetic interpretation without further microscopic analysis. Previous studies on the Faroe Islands have tended to refer to the majority of minor volcaniclastic rocks (sandstones/mudstones) as tuffs (Rasmussen and Noe-Nygaard, 1969; 1970). In this study the term "tuff" shall only be applied where there is explicit evidence to support its usage.

Correlation between Sandoy and Streymoy

Figure 4 is a correlation based on eight lithostratigraphic columns from Gleðin, NW Sandoy to Norðradalur, Streymoy (Figure 2) and covers a near vertical height of *ca.* 350 m from the top of the Malinstindur Formation to *ca.* 330 m above the base of the Enni Formation. The interval is correlated and subdivided into seven alternate sections through the recognition of three distinctive strati-

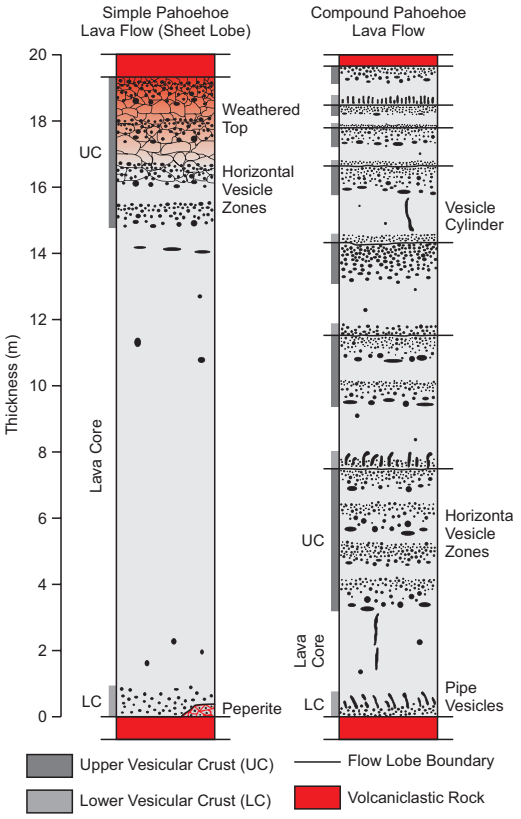

Figure 3. Simplified vertical sections through simple (sheet lobes) and compound lava flows of the Faroe Islands. Modified after Waagstein (1998) and incorporating data from Passey and Bell (2007).

graphic marker units: the Sneis Formation, the Høvdhamarin Flow and the Argir Beds. The units (beds and flows) of the interval have a layer cake appearance defined by their relatively planar bases, which exhibit only minor topographic relief (Figure 5). This is highlighted by the extremely constant vertical thickness between the bases of the Sneis Formation and the Argir Beds which averages *ca.* 252 m (range: 231-276 m). This is based on 20 randomly selected locations between Hestur and southern Streymoy and calculated using TIN layers constructed for each surface, excluding data from the Glyvursnes-1 borehole and before they were extrapolated. The planar bases and the somewhat constant thicknesses between units are due, in part, to the relatively flat-lying terrain over which the lava flows were emplaced (Rasmussen and Noe-Nygaard, 1969; 1970; Passey and Bell, 2007).

Malinstindur Formation

The base of the correlated sections (Figure 4) consists of the uppermost plagioclase-phyric compound lava flows of the Malinstindur Formation (Figure 5b). These compound flows are composed of flow lobes up to 2 m thick, which occasionally exhibit horizontal amygdale zones within the upper crusts (cf. Self *et al*., 1997). The flow lobes contain between 5 and 30 vol.% phenocrysts of plagioclase feldspar, which range in size from <0.5 cm to 2 cm. Occasionally, the phenocrysts form small glomerocrysts with a characteristic stellar arrangement. Across the study area, the upper surface of the Malinstindur Formation is not particularly reddened due to weathering, unlike the sections observed to the NE of Norðradalur, Streymoy. Another marked difference is that the uppermost compound lava flows to the NE typically contain conspicuous laths (<30 vol.%) of plagioclase feldspar up to 2 cm in length, whereas the flows in the south contain smaller laths (<10 vol.%) up to 0.5 cm. The upper surface commonly undulates with a relief of a few metres and this is seen across the study area, but particularly in the area of Rættin, NW Sandoy and within Dalagjógv, Norðradalur and is, most likely, the result of differential erosion.

Sneis Formation

The upper surface of the Malinstindur Formation is overlain by the volcaniclastic lithologies of the Sneis Formation (Figs. 1 and 4). In the area of Norðradalur, Streymoy, the Sneis Formation is up to *ca.* 25 m thick and has a bipartite subdivision. The basal reddened unit is a predominantly, medium grained volcaniclastic sandstone, that is on average 50 cm thick. The sandstone is poorly sorted, clast supported and relatively structureless apart from some minor laminations at the very top of the unit. The sandstone is composed almost entirely of basaltic glass at various stages of palagonitisation. The individual clasts exhibit a high degree of

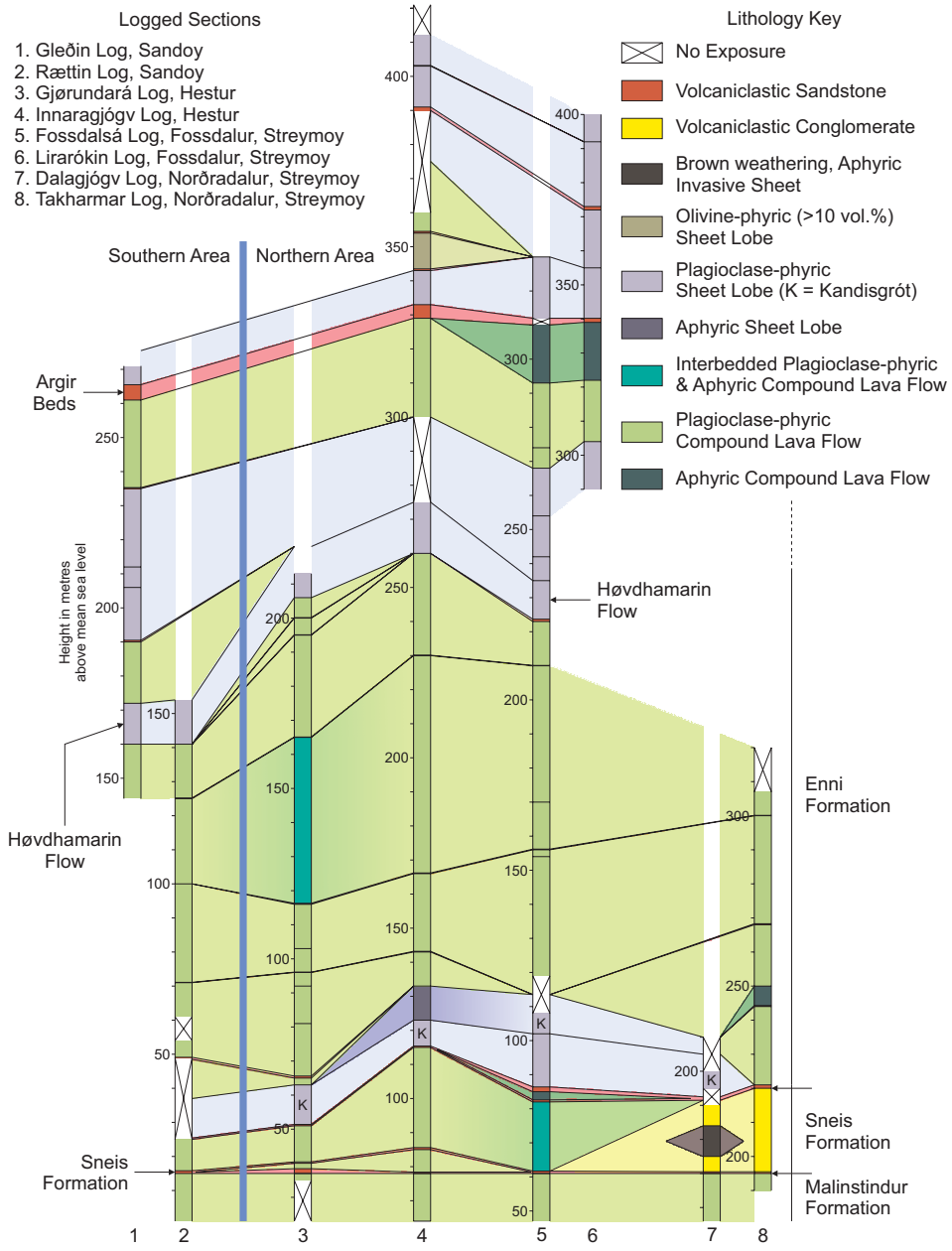

Figure 4. A *ca.* 20 km long, S-N correlation of 8 lithostratigraphic columns from Gleðin, NW Sandoy to Takharmar, Norðradalur, Streymoy. The columns are flattened to the base of the Sneis Formation, expect for column 1 which is flatten to the base of the Høvdhamarin Flow and column 6 which is flatten to the top of the Argir Beds. The correlation tie lines and the location of the logged sections can be seen in Figure 2. The three main stratigraphic marker units (Sneis Formation, Høvdhamarin Flow and Argir Beds) are indicated. It should be noted that these columns are primarily obtained from stream sections and therefore, are not truly vertical and depending on the regional dip of the strata the columns may be effected by foreshortening or stretching, but as the dip is typically <3° and the lateral deviation between the bases and tops of the columns is <2 km this effect is considered negligible.

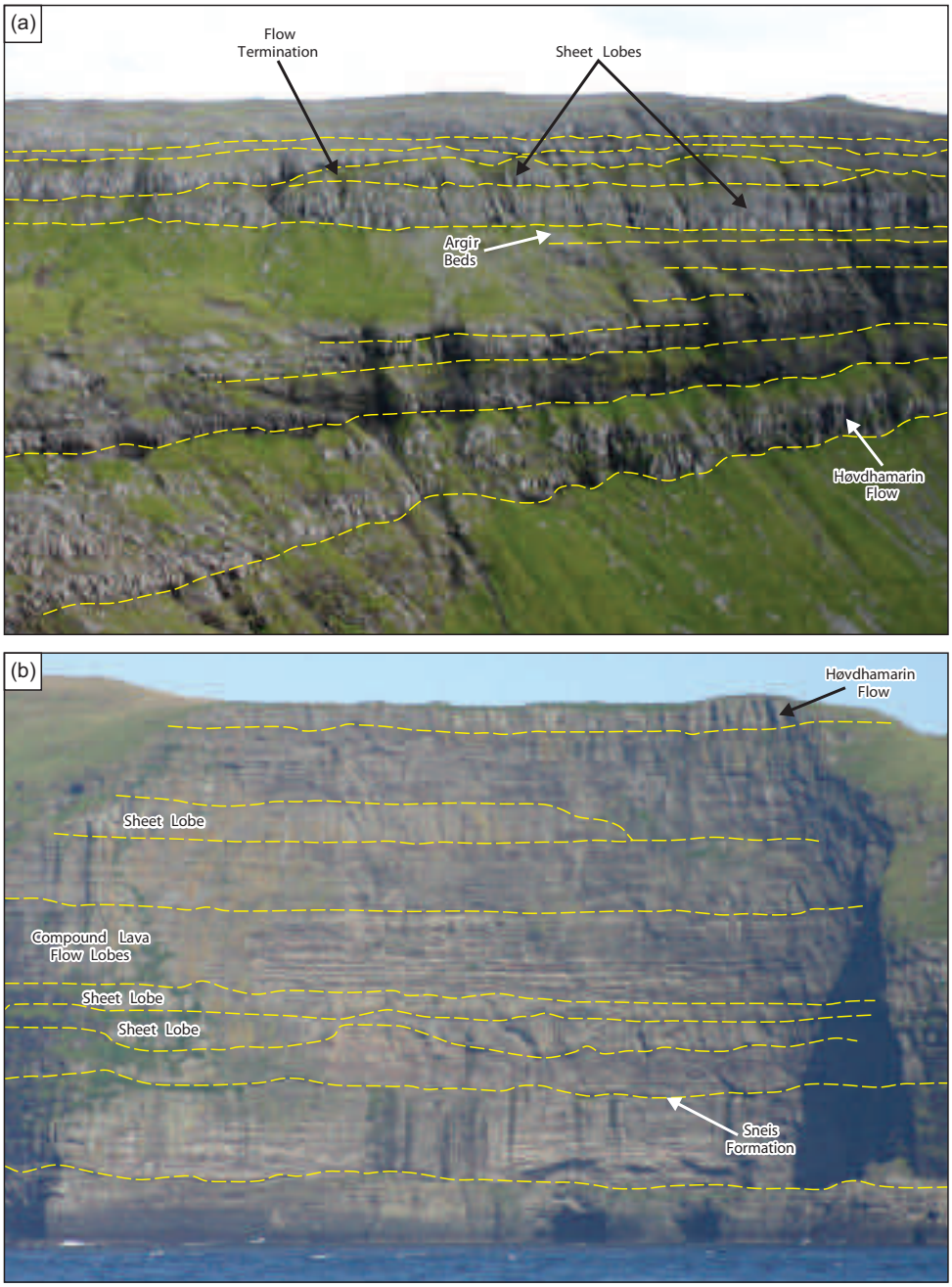

Figure 5. General views of the lava flow sequence depicted in Figure 4. The dashed yellow lines indicate flow boundaries. (a) The southern mountainside of Fossdalur, Streymoy, which covers the *ca.* 150 m thick vertical section above the Høvdhamarin Flow to the sheet lobe dominated sequence above the Argir Beds. This sequence corresponds to the lithostratigraphic columns 5 and 6 from the northern side of Fossdalur depicted in Figure 4. Notice the laterally restricted sheet lobe towards the base of the sequence above the Argir Beds. (b) The *ca.* 240 m high Loftið cliff section, western Hestur, which covers the vertical section from the top of the Malinstindur Formation to the Høvdhamarin Flow, Enni Formation. This section corresponds extremely well to the lithostratigraphic columns from eastern Hestur (columns 3 and 4 in Figure 4). However, the sheet lobe identified below the Høvdhamarin Flow is not observed on the eastern side of Hestur.

rounding, although larger clasts preserve cuspate margins and vesicles. Typically, the sandstone contains abundant creamish, charcoalified branchwood fragments with a 'boxwork' structure, which is a characteristic feature of the upper third of the unit and is clearly seen in the exposures at Sund Quarry, Streymoy, where branchwood fragments up to 4 m in length are preserved. This basal sandstone is the Sund Bed, which is highly distinctive and ubiquitous across the northern Faroe Islands where it retains a relatively constant thickness (Passey *et al*., 2006). The top of the Sund Bed corresponds approximately to the C-horizon of Rasmussen and Noe-Nygaard (1969; 1970).

The Sund Bed is overlain by a greyish-red volcaniclastic conglomerate that forms a prominent bench and associated plateau in the Norðradalur area and in the Niðari Botnur valley, NNE of Syðradalur, Streymoy. The conglomerate sequence thins in a southerly direction from *ca.* 25 m in the vicinity of Takhamar bench, Norðradalur to *ca.* 8 m in the Niðari Botnur valley, *ca.* 2.5 km away. The conglomerate consists of anastomosing and overlapping lobes (<5 m thick) which are generally ungraded, but normal and reverse grading does occur (Figure 6a). The conglomerates are matrix supported, polymodal, poorly sorted and clasts range in size from <1 mm up to large cobbles, although clasts >50 cm across are common. The clasts are generally sub-angular to sub-rounded and are composed primarily of various types of pebble-grade very finely to finely crystalline basalt, which consist of aphyric and plagioclase-phyric (<125 m) textural varieties that can be distinctly amygdaloidal or non-vesicular (Figure 6b). Primary clay is virtually absent from the conglomerates and is only present due to the subsequent alteration of the basalt clasts. In some sections, the conglomerate has been clearly cemented together by brownish green zeolitic material.

Ubiquitously associated with this conglomerate-dominated facies of the Sneis Formation is a distinctly brown weathering, basalt sheet with a noticeable foliation (Figure 4). This massive basalt is typically aphyric with a conspicuously aphanitic groundmass, although occasionally small phenocrysts of olivine, commonly altered, are present. The basalt sheet forms a prominent bench in the landscape, which exhibits poorly developed columnar jointing along some sections. The basal contact is usually sharp and planar which contrasts with the diffuse and highly irregular upper contact. The sheet typically occurs at the interface between the Sund Bed and the overlying conglomerates, although in Dalagjógv the sheet occurs *ca.* 4 m above the base of the conglomerates and is *ca.* 9 m thick (Figure 7). In the Niðari Botnur valley the basalt sheet is *ca.* 6 m thick and there appears to be a slight thinning of the sheet moving away from Dalagjógv, a weathered out NE-trending, 6-7 m wide aphyric dyke. In Dalagjógv, the basalt sheet clearly exhibits internal intrusive contacts, sug-

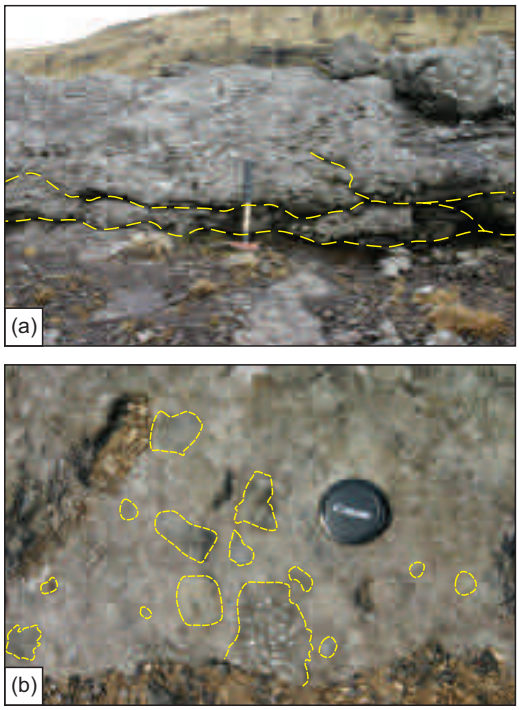

Figure 6. General views of the conglomerate facies from the conglomerate-dominated Sneis Formation, Norðradalur, Streymoy. (a) Thin, anastomosing and overlapping lobes of conglomerate. The bases of some of these lobes exhibit apparent normal grading. The hammer is *ca.* 40 cm long. (b) Matrix-supported conglomerate consisting of various sub-angular to sub-rounded clasts of various intraformational basaltic lithologies. Notice the distinct variability between amygdaloidal and non-vesicular varieties of basalt. The lens cap has a diameter of *ca.* 5 cm.

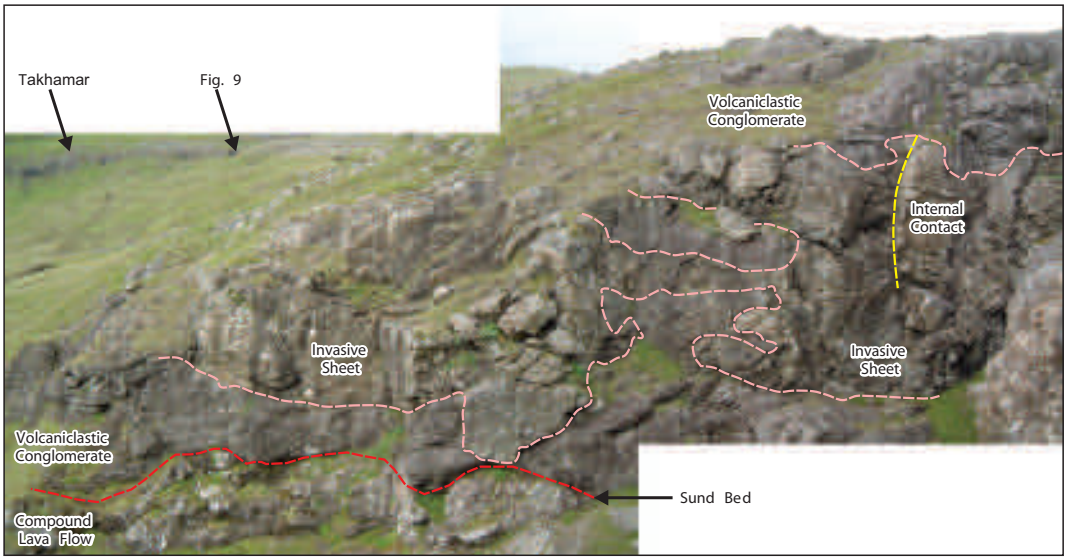

Figure 7. The northern face of Dalagjógv, Norðradalur, Streymoy. The conglomerate-dominated Sneis Formation consisting of the basal Sund Bed and overlying conglomerate, which have been intruded by a noticeably brown weathering, *ca.* 9 m thick aphyric invasive sheet. The pink dashed lines outline the intrusive contacts and the yellow dashed line indicates an internal contact within the invasive sheet.

gesting it may consist of more than one invasive phase (Figure 7) and apophyses are observed invading the conglomerate facies all along the Langareyn bench to the stream at the NE end of the prominent Takhamar bench, *ca.* 500 m to the NW (Figure 8). The edges of these apophyses typically exhibit poorly developed chilled margins and on the eastside of the stream at the NE end of Takhamar the sheet is observed to terminate within the conglomerate as a number of smaller finger-like lobes (Figure 9).

These basalt sheets correspond to the so-called C-horizon flows of Rasmussen and Noe-Nygaard (1969; 1970), which have been shown to have a low-Ti, MORB-like composition (Waagstein, 1977; 1988). However, the highly intrusive contacts and the ubiquitous association with the conglomerate facies, suggest that they are actually sills that have exploited the mechanically weaker rocks of the Sneis Formation. This is supported by the distinctive geochemistry of these basalts which is extremely similar to the low-Ti, MORB-like composition of the Dalagjógv dyke (sample Str.17; Hald and Waagstein, 1991), which terminates at the top of the Sneis Formation and may have been a feeder for the invasive sheet in this area.

The conglomerate-dominated Sneis Formation with the invasive sheets, as described above, is the typical sequence which is observed across the northern islands as far NE as Viðoy, some *ca.* 40 km away. The extent to which the conglomerate-facies can be mapped is only constrained by the lack of exposure (Rasmussen and Noe-Nygaard, 1969; 1970; Passey *et al.*, 2006). However, moving *ca.* 2.5 km in a southerly direction from Norðradalur, the basal Sund Bed is missing from the conglomerate-dominated Sneis Formation in the Breiðá stream, Niðari Botnur valley. In the Syðradalsá stream, a further *ca.* 1.1 km to the south, the conglomerate-dominated Sneis Formation is absent (i.e. no Sund Bed or conglomerates). However, at the same stratigraphic level, a *ca.* 1.4 m thick sequence of green to red volcaniclastic sandstones and mudstones crops out (Figure 4).

This sandstone-dominated sequence is considered to be the lateral facies variation of the conglomerate-dominated sequence of the Sneis For-

mation and is observed as far south and west as Rættin, NW Sandoy (Figure 10) and as far east as the Glyvursnes-1 borehole. In the well exposed section along the coastline to the west of Rættin, the sandstone sequence is seen to thicken and thin over the undulating upper surface of the Malinstindur Formation, where the largest observed trough is *ca.* 1.4 m deep by *ca.* 4 m wide. The sandstone-dominated Sneis Formation ranges in thickness from 0.7 to 2.3 m and is composed of bedded, predominantly medium to coarse grained volcaniclastic sandstones and mudstones (Figure 11). The sandstones are generally clast supported, moderately sorted and the coarser clasts are sub-angular to sub-rounded, some of which exhibit vesicles, suggesting they are reworked volcanic ash. The sandstones are generally greenish but typically consist of a reddened upper section, as a result of subaerial weathering.

Remapping of the Sneis Formation (i.e. base of the C-horizon) has led to the recognition of the sandstone-dominated facies of the formation between the depths of *ca.* 297-299 m in the Glyvursnes-1 borehole. However, the base of this sandstone facies occurs *ca.* 56 m above the surface originally selected as the C-horizon in the borehole (Waagstein and Andersen, 2003; Japsen *et al.*, 2005). The original C-horizon was placed at a depth of *ca.* 355 m at the base of a *ca.* 9 m thick aphyric basalt that occurs in between two reddened volcaniclastic sandstone units (Waagstein and Andersen, 2003). This basalt was described as being morphologically and lithologically similar to the basalts that are associated with the Sneis Formation in the north of Streymoy, which was subsequently supported by the basalt having a similar low-Ti, MORB-like composition (Waagstein and Andersen, 2003; Japsen and Waagstein, 2005). However, similar basalts are common from two-thirds above the base of the Malinstindur Formation and throughout the Enni Formation (Rasmussen and Noe-Nygaard, 1970; Waagstein, 1988). Indeed, a similar basalt has been observed within the Sandoyartunnilin-4 borehole, *ca.* 9 km to the SW on southern Hestur where it occurs *ca.* 48 m below the base of the Sneis Formation and also occurs in between two reddened volcaniclastic sandstone units (Figure 2; Højgaard, 2007). In addition, a similar basalt has also been observed *ca.* 20 m below the Sneis Formation in Dalagjógv, Norðradalur and others have been observed occurring *ca.* 30-40 m below the Sneis Formation from Blábjørg, NE Eysturoy. Therefore, the low-Ti basalt encountered in the Glyvursnes-1 borehole does not necessarily have to correlate to those associated with the C-horizon but most likely correlates to the basalt observed in the Sandoyartunnilin-4 borehole, *ca.* 48 m below the Sneis Formation (i.e. base of the C-horizon; Højgaard, 2007).

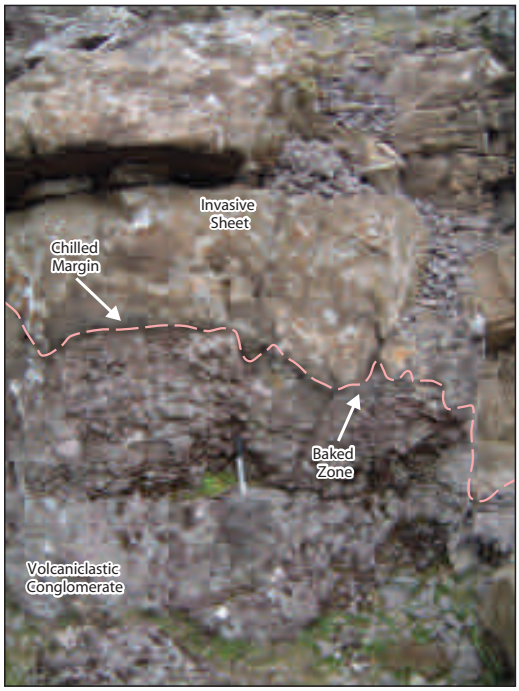

Figure 8. Intrusive contact between the conglomerate facies of the conglomerate-dominated Sneis Formation and a distinctly brown weathering, aphyric invasive sheet, N of Dalagjógv, Norðradalur, Streymoy. Notice the discoloration at the edge of the sheet representing a chilled margin. The top of the conglomerate also exhibits a discoloration as a result of baking effects.

Support for placing the C-horizon at a higher level in the Glyvursnes-1 borehole is also given by Japsen *et al.* (2005) who state that the *ca.* 70 m thick sequence overlying their C-horizon is very similar to what is expected from the middle basalt series (i.e. the Malinstindur Formation). In addition, the relatively constant vertical thickness of

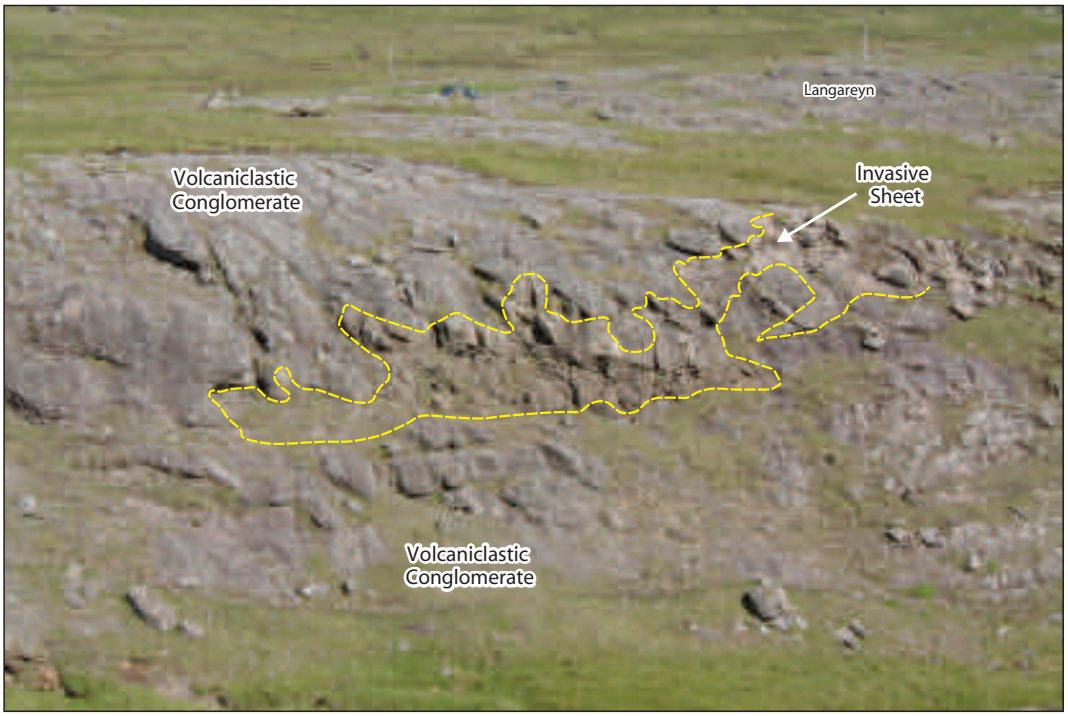

Figure 9. View of the leading edge of the invasive sheet at the NE end of the Takhamar bench, *ca.* 500 m NW of Dalagjógv, Norðradalur, Streymoy. The invasive sheet is *ca.* 2-3 m thick and terminates within the conglomerate of the Sneis Formation as finger-like lobes or apophyses.

ca. 252 m between the Sneis Formation and the Argir Beds, as mentioned above, corresponds extremely well to the 255 m (*ca.* 44-299 m) between the aforementioned units in the Glyvursnes-1 borehole, as defined in this study. Therefore, it is reasonably suggested that the sandstone-dominated Sneis Formation identified in the Glyvursnes-1 borehole corresponds approximately to the C-horizon originally mapped by Rasmussen and Noe-Nygaard (1969; 1970) and consequently, occurs at a depth of *ca.* 299 m (i.e. *ca.* 282 m below mean sea level) rather than *ca.* 355 m.

Facies Interpretation

The conglomerate-dominated facies of the Sneis Formation was originally interpreted as an agglutinate, consisting of loose eruptive products welded together by lava (Rasmussen and Noe-Nygaard, 1969; 1970). However, the lateral conformability and extensiveness, over distances of 25-30 km, of the conglomerate-dominated facies, associated with clast heterogeneity, clast size and textural features of the units indicate that they are sedimentary deposits and not pyroclastic in origin (cf. Smith, 1986; Cas and Wright, 1987; Scott, 1988; Smith, 1991; Smith and Lowe, 1991; Orton, 1996). The lateral variation from N to S of the conglomerate-dominated facies to a crudely stratified sandstone-dominated facies is similar to the lateral facies transitions reported for mass flow (lahar) deposits of volcanic (Pierson and Scott, 1985; Scott, 1988) and non-volcanic settings (Sohn *et al.*, 1999), which suggests that the Sneis Formation was sourced towards the N and transported in a southerly direction.

The bipartite subdivision of the conglomerate-dominated facies, consisting of the thin basal Sund Bed overlain by a thicker conglomerate sequence, is similar in morphology to the debris flow conglomerates underlain by thin sole layers reported

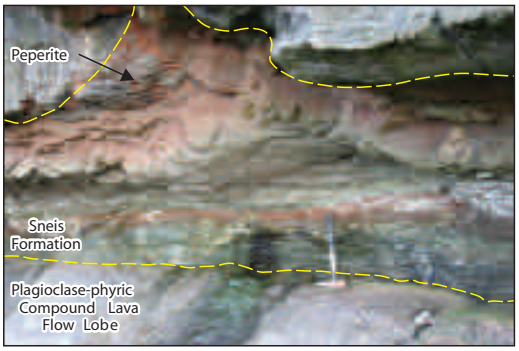

Figure 10. View of the sandstone-dominated facies of the Sneis Formation, coastline section W of Rættin, *ca.* 3.6 km WNW of Skopun, Sandoy. Notice the relatively unweathered upper surface of the underlying compound lava flow. The sandstone sequence is bedded and alternates between green and red sections, where the reddening is due to subaerial weathering. The hammer is *ca.* 40 cm long.

by Scott (1988) for lahars deposited in channel and floodplain environments. The relatively massive texture of the Sund Bed, the lack of basal erosional structures and cross-stratification, and the concentration of the low density organic material within the top of the unit are characteristic features of units deposited from hyperconcentrated flows (cf. Smith, 1986; 1987a; b; 1988; Smith and Lowe, 1991; Sohn *et al*., 1999). The lateral extensiveness of the conglomerate-dominated facies, the dominance of pebble-grade material and the poorly sorted nature of the conglomerate favours deposition from a debris flow in a flood (Scott, 1988) or alluvial (Sohn *et al*., 1999) plain environment. The rapid disappearance of the conglomerate from *ca.* 10 m in thickness to being absent within a lateral distance of <1 km in the Syðradalur area suggests that the conglomerate was deposited *en masse* from a debris flow that terminated abruptly (cf. Smith, 1986; Smith and Lowe, 1991).

The sandstone-dominated facies, which consists of relatively massive strata and lacks erosional bases and cross-stratification implies that these units represent the hyperconcentrated flow runout deposits of the mass flow event(s) (Pierson and Scott, 1985; Smith, 1986; Scott, 1988; Smith and Lowe, 1991; Sohn *et al*., 1999). However, the presence of some tentative ripple structures may suggest the influence of streamflow processes (Pierson and Scott, 1985; Smith, 1986; Scott, 1988; Smith and Lowe, 1991; Sohn *et al*., 1999). A detailed discussion of the flow processes of the Sneis Formation mass flow deposits and their implications for the evolution of the FIBG is beyond the scope of this paper and shall be dealt with elsewhere.

Sneis Formation to Høvdhamarin Flow

In the south of the study area the sandstone-dominated facies of the Sneis Formation is overlain by a predominantly plagioclase-phyric compound lava flow with an average thickness of *ca.* 25 m (Figure 4). The flow lobes are generally <1-2 m thick and typically contain <10 vol.% plagioclase feldspar laths <0.5 cm in length, although on Streymoy the flow lobes are generally aphyric. Some of the flow lobes are distinctly amygdaloidal throughout their entire thickness. The basal flow lobes on Hestur are intercalated with the Sneis Formation separating the strata by between 1.5 and 6.5 m.

The compound lava flow is overlain by a 0.4 to 1.4 m thick volcaniclastic sequence, which thickens in a northerly direction. In the Fossdalsá stream, Fossdalur, Streymoy the volcaniclastic sequence is subdivided into two sections by a *ca.* 2.5 m thick aphyric flow lobe with a reddened upper ropy surface (Figure 4). The predominantly reddened volcaniclastic sequence consists of bedded, fine to coarse grained sandstones, which infill the undulating basal surface. The sandstones are commonly observed infilling cracks in the underlying flow lobes up to a depth of *ca.* 1 m. This bedded sandstone sequence also overlies the undulating upper surface of the conglomerate-dominated Sneis Formation of the Norðradalur area. In the Norðradalur area, the thickest sandstone sequences are found in the troughs on the underlying surface whereas on the highs, the sand-grade material is generally only observed infilling the gaps between the clasts of the conglomerate.

This sandstone sequence is overlain by at least one, possibly two, predominantly plagioclase-

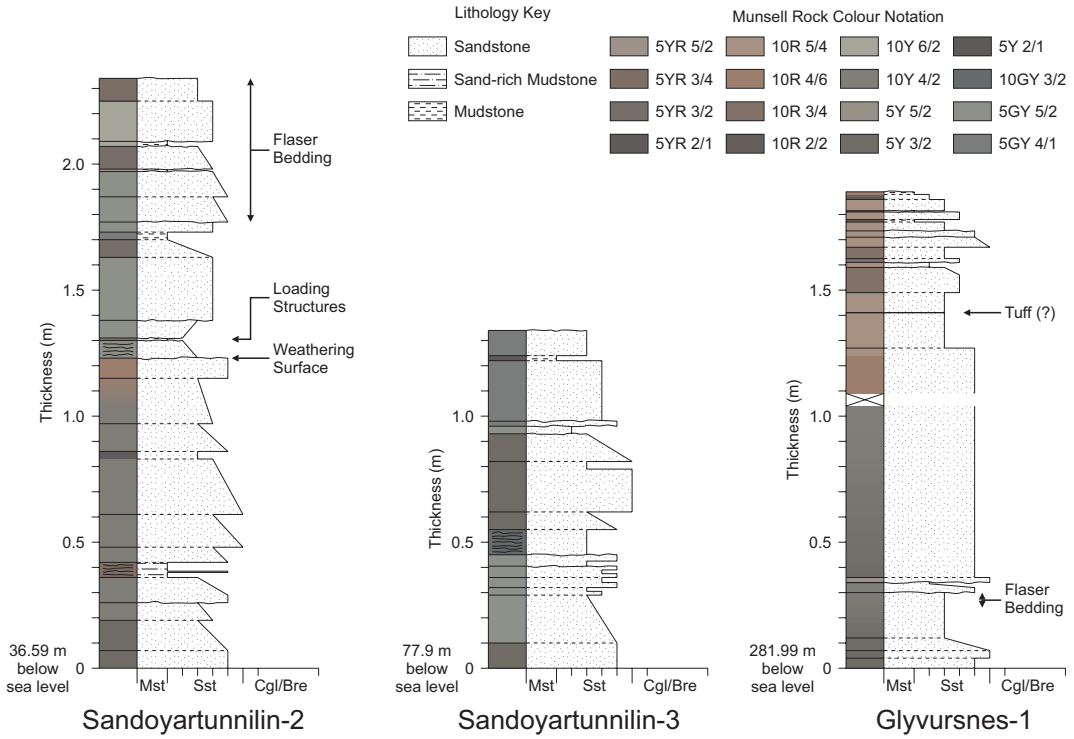

Figure 11. Simplified graphic logs for the sandstone-dominated facies of the Sneis Formation from three boreholes that have encountered the sequence. The units are relatively massive sandstones, some of which exhibit crude normal grading. Cross-stratification where present is very poorly defined. The colours of the units are given to the left of the graphic logs and are based on the Munsell rock colour notation (Rock-Color Chart Committee, 1995). The red shades represent the subaerial weathering of the units.

phyric sheet lobes. The sheet lobes have an average thickness of between 10 and 12 m and rarely exceed 15 m. The sheet lobes typically form small discontinuous benches in the landscape. The sizes of the plagioclase feldspar laths vary from <0.5 cm to 2 cm and the sheet lobes with the larger laths tend to have the texture of kandisgrót.

The sheet lobes are overlain by a dominantly plagioclase-phyric compound lava flow sequence between *ca.* 100 and *ca.* 140 m thick (Figure 4). There are at least 5 compound lava flows separated by minor volcaniclastic lithologies and the thickest compound lava flow is *ca.* 65 m. The compound flows are generally composed of flow lobes <1 to 2 m thick, but occasionally flow lobes up to 5 m thick occur. The lobes are generally plagioclase-phyric with laths occurring between 1 and 2 cm in length and concentrations between 20 and 40 vol.%. The flow lobes towards the top of the Gjørundará stream section on Hestur contain conspicuous plagioclase feldspar laths up to 4 cm long. Some of the flow lobes also exhibit well preserved ropy surfaces and the tops to the lava flows are commonly reddened due to weathering. The volcaniclastic units separating the lava flows are generally <10 to 20 cm thick and usually consist of fine to medium grained sandstones and mudstones. The top of this compound lava flow sequence is on the whole extremely reddened due to weathering and is occasionally overlain by a 40 to 70 cm thick reddened, fine to medium grained volcaniclastic sandstone. In Álvagjógv, Hestur, the uppermost sequence of this compound lava flow sequence has been incised by up to 10 m producing an irregular topography, which has been infilled by the overlying Høvdhamarin Flow.

Høvdhamarin Flow

The Høvdhamarin Flow is a thick, whitish-grey sheet lobe that forms a very prominent bench in the landscape that can be traced over a distance of at least *ca.* 25-30 km (Figure 12). The well exposed Høvdhamarin Flow contrasts with the underlying compound lava flow sequence which is usually poorly exposed and grass covered. This contrast can clearly be seen along the eastern side of Hestur, between Rættin and Skopun, NW Sandoy and along the coastline to the north of the prominent Salthøvdi headland, *ca.* 3 km WSW of Sandur, Sandoy. It is in the area of Salthøvdi that this prominent sheet lobe is locally called Høvdhamarin, literally meaning 'head bench' (Figure 12a). The base of the Høvdhamarin Flow between Rættin and Skopun, Sandoy (Figure 12b) was originally mapped as the C-horizon by Rasmussen and Noe-Nygaard (1969; 1970).

The Høvdhamarin Flow is between 10 and 15 m thick and commonly exhibits weakly-developed columnar jointing. The surfaces defined by the columnar jointing typically display chisel markings. In some sections the Høvdhamarin Flow has a more compound lava flow morphology, appearing to consist of two or three, 5 m thick, lobes. This is prevalent along the western side of Streymoy where the Høvdhamarin Flow has a weathering pattern typically associated with compound lava flows. However, the sheet lobe morphology of the Høvdhamarin Flow dominates and can also be seen along the coastline N of Hvítanes on eastern Streymoy (Figure 12c). The Høvdhamarin Flow is a plagioclase-phyric basalt which contains <10 to *ca.* 20 vol.% plagioclase feldspar laths that range in size from <0.5 to 1 cm in length. The smaller laths typically form glomerocrysts in the finely crystalline groundmass. The lower *ca.* 2 m of the Høvdhamarin Flow is distinctly vesicular compared to the overlying non-vesicular core and the basal contact is usually sharp and planar (Figure 12). The upper surface of the Høvdhamarin Flow is generally poorly exposed due to weathering of a more vesicular upper crust.

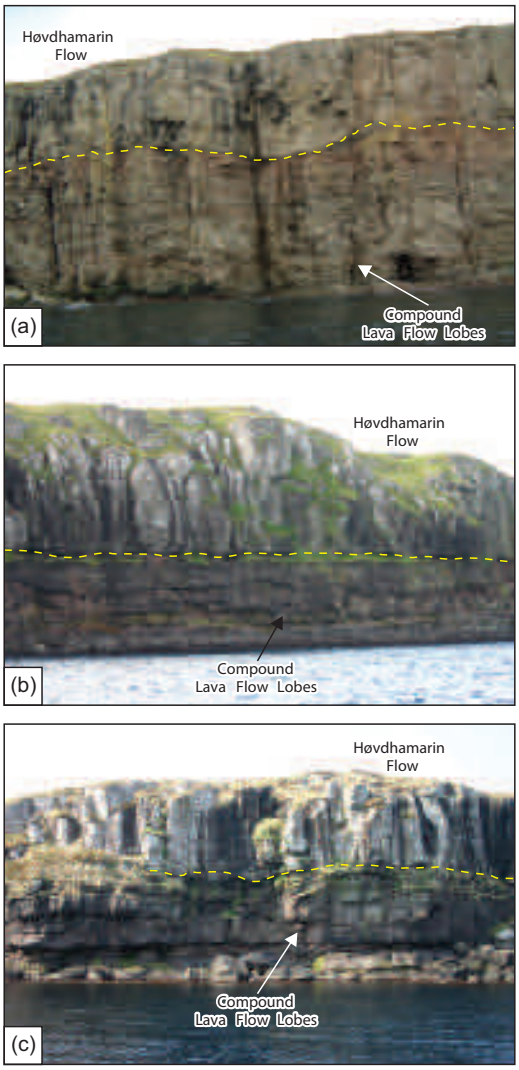

Figure 12. General views of the plagioclase-phyric Høvdhamarin Flow, from localities over a distance of *ca.* 25-30 km, central Faroe Islands. The flow overlies a distinctly reddened compound lava flow. The Høvdhamarin Flow is whitish-grey and exhibits poorly developed columnar jointing. (a) *ca.* 20-30 m high cliff section, *ca.* 1.3 km NNE of Salthøvdi, Sandoy. (b) *ca.* 30 m high cliff section, Hæraberg, *ca.* 600 m NNW of Skopun, Sandoy. (c) *ca.* 15 m high cliff section, *ca.* 300 m NNE of Hvítanes, Streymoy.

Høvdhamarin Flow to Argir Beds

The average vertical thicknesses of *ca.* 92 m (range: 74-115 m) and *ca.* 90 m (range: 52-124 m) between the bases of the Høvdhamarin Flow and the Argir Beds is extremely similar for both the

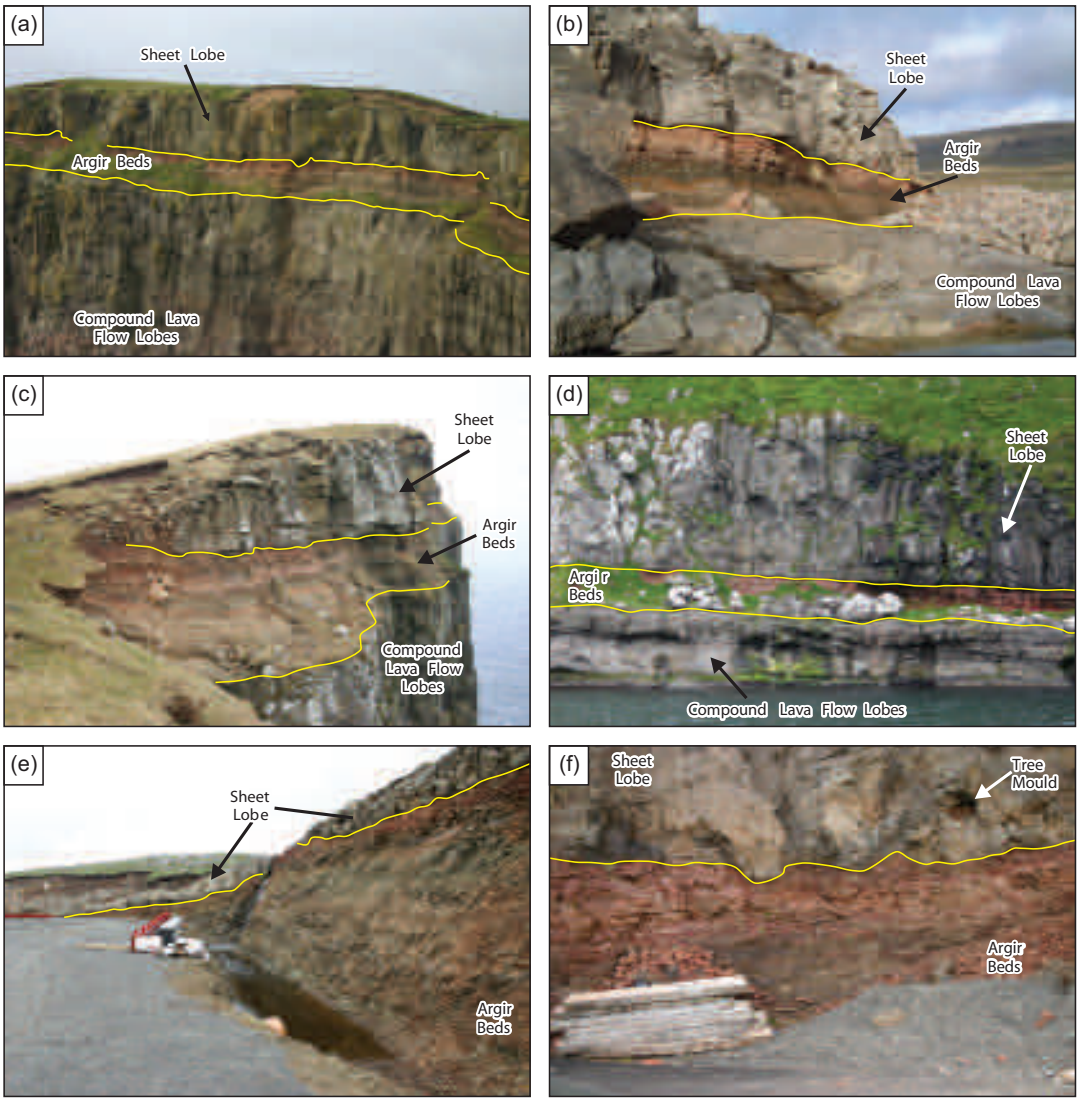

Figure 13. General views of the Argir Beds from Skúgvoy to Streymoy. The Argir Beds range in thickness between 1 and 6 m, but are generally 3-4 m. The Argir Beds are noticeably bedded due to the colour variation between the different units. (a) Høvdin, *ca.* 3 km WNW of Skúgvoy village, Skúgvoy. (b) Urðin, *ca.* 700 m W of Sandur, Sandoy. (c) Gleðin summit, *ca.* 3 km W of Skopun, Sandoy. (d) Cliff section, *ca.* 700 m ESE of Kirkjubøur, Streymoy. (e) Horse stables, Norðastahorn, Streymoy. (f) Reynsgøta 83, Argir, Streymoy.

northern and southern areas, respectively. This reiterates the general conformability of the units across the study area. The interval overlying the Høvdhamarin Flow is composed of a mixture of plagioclase-phyric sheet lobes and compound flows (Figure 4). In the NW of Sandoy the Høvdhamarin Flow is overlain by a <20 m thick plagioclase-phyric compound lava flow, which in turn is overlain by a poorly exposed, *ca.* 50 cm thick, reddened volcaniclastic sandstone. This compound flow and sandstone couplet is not observed in the sections from Hestur or Streymoy suggesting it is laterally constrained to the south. This couplet sequence and the Høvdhamarin Flow

further to the north are overlain by a 30-50 m thick sequence dominated by three or more plagioclase-phyric sheet lobes, similar in character to the Høvdhamarin Flow (Figure 4). This sequence of plagioclase-phyric sheet lobes crop out between Hvítanes and Tórshavn, Streymoy and which, including the Høvdhamarin Flow, were referred to as the "Tórshavn type" by Walker and Davidson (1936). These sheet lobes range in thickness between 5 and 30 m and average *ca.* 15 m. The sheet lobes commonly have slightly reddened tops due to weathering but no overlying sandstones have been observed. In the area of Hvítanes and Hoyvík the sheet lobes are occasionally separated by thin, plagioclase-phyric compound lava flows.

The top of the sheet lobe sequence is distinctly reddened due to weathering and on Sandoy the sheet lobes are overlain by a *ca.* 30 cm thick reddened, fine to medium grained volcaniclastic sandstone, which has not been observed further to the north. This is overlain by a *ca.* 25 m thick plagioclase-phyric compound lava flow comprising <2 m thick flow lobes commonly containing <10 vol.% laths of plagioclase feldspar 1-2 cm long. The top of this lava flow is not reddened. In the Fossdalur sections, Streymoy, the plagioclase-phyric compound lava flow is overlain by an aphyric compound lava flow, consisting of flow lobes <0.5 m thick. These aphyric flow lobes typically have pipe amygdales along their bases and the upper crusts are noticeably amygdaloidal.

Argir Beds

The Argir Beds is a visibly bedded volcaniclastic sequence that is between 1 and 6 m thick, but is generally 3-4 m (Figure 13). The Argir Beds are named after the village where the first exposures were observed and provisionally described (Passey, 2004). In general, the beds coarsen and thicken upwards from a mudstone and fine grained sandstone facies to a facies dominated by coarse to very coarse sandstones, which commonly contain granule-grade material (Figure 14). The coarser beds are normally very poorly sorted and consist primarily of reworked palagonitised basaltic glass at various stages of hydration and exhibit a high degree of rounding. In addition, the beds contain

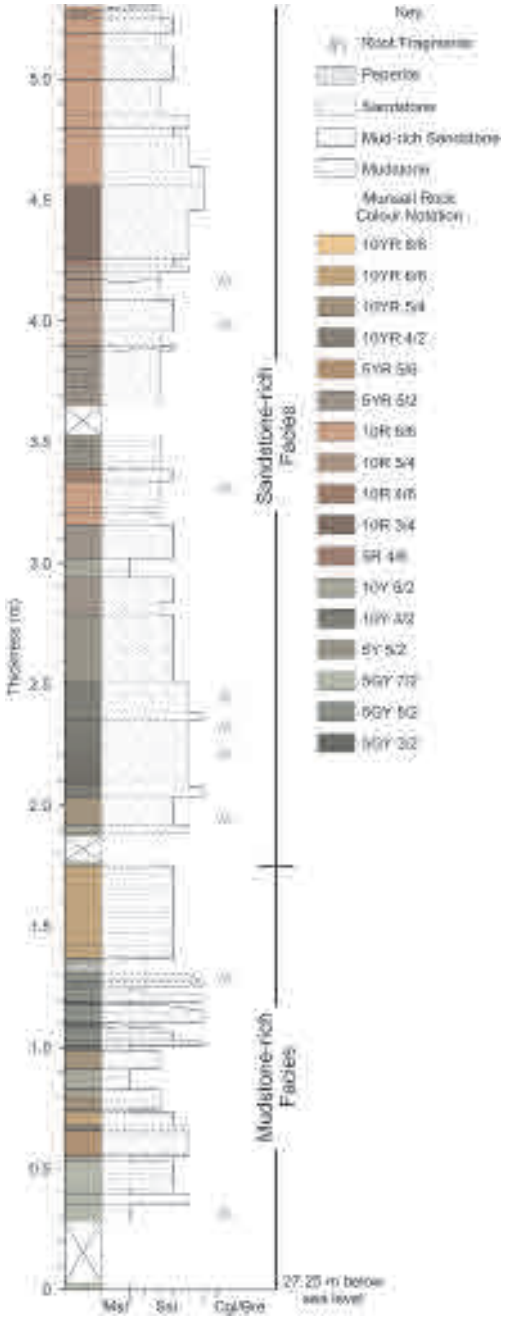

Figure 14. Simplified graphic log for the Argir Beds from the Glyvursnes-1 borehole, Streymoy. In general, the sequence thickens and coarsens upwards from a mud-rich facies to a sand-rich facies dominated by coarse to very coarse sandstones. The contacts between the beds are typically gradational. The colours of the units are given to the left of the graphic logs and are based on the Munsell rock colour notation (Rock-Color Chart Committee, 1995). The red shades represent the subaerial weathering of the units.

sub-rounded, intraformational lithic clasts composed of well sorted volcaniclastic siltstone and finely crystalline, equigranular basalt, most likely, derived from the surrounding lava flows. The coarser beds also contain sub-rounded to rounded grains of, clearly twinned, plagioclase feldspar up to 2 mm in length. These plagioclase feldspar grains are completely liberated and are not contained in a glassy or crystalline selvage.

The upper surface of the Argir Beds is generally sharp and planar. However, at the Norðastahorn section the >50 m long exposure of the Argir Beds is differentially overlain by a sheet lobe that thickens from *ca.* 2 to >6 m in an easterly direction, suggesting an undulating, possibly eroded, upper surface of the Argir Beds (Figure 13e). The upper surface of the Argir Beds on Skúgvoy (Figure 13a) was originally mapped as the C-horizon by Rasmussen and Noe-Nygaard (1969; 1970).

The Argir Beds also contain abundant plant fragments commonly forming linear features on bedding surfaces, which consist of a number of aligned, black tabular fragments. These plant fragments are up to 3 cm long by 1 cm wide and can be tentatively separated into internodal and nodal segments. The Argir Beds, encountered in the Glyvursnes-1 borehole, contains numerous black, near vertical, tabular plant fragments, interpreted to be roots. These roots range in length from *ca.* 1.5 to 4 cm but are dominantly 1-2 mm wide and are found at least nine different levels within the sequence (Figure 14). Further evidence for the development of a vegetated landscape, during the formation of the Argir Beds, is preserved by the underlying and overlying lava flows. The upper surface of the underlying compound lava flow at the western end of the Urðin isthmus, *ca.* 700 m west of Sandur, Sandoy, contains the basal hemicylinders of at least seven tree moulds (Passey and Bell, 2007). Similarly, at the same location, the base of the overlying sheet lobe contains cylindrical tree moulds. Tree moulds have also been observed from the base(s) of the immediately overlying sheet lobe(s) in the sections at Villingafossur, Norðastahorn and Argir (Figure 13f) on Streymoy.

Facies Interpretation

The coarsening and thickening upward succession from a mudstone-dominated to sandstone-dominated facies associated with the abundance of rootlets suggests that at least the Glyvursnes-1 section was, most likely, deposited in an overbank fluvial environment during flooding (cf. Elliott, 1974; Collinson, 1996). A more detailed investigation of the lithofacies variations across the study area is required to constrain the environment(s) of deposition.

Above the Argir Beds

The sequence above the Argir Beds varies from west to east across the study area. On Skúgvoy and western Sandoy the Argir Beds are overlain by a *ca.* 10 m thick plagioclase-phyric sheet lobe which, on Skúgvoy, is overlain by a >100 m thick poorly exposed compound flow sequence mainly composed of aphyric basalt. On Sandoy, to the east of Skopun, the Argir Beds are directly overlain by a *ca.* 100 m thick plagioclase-phyric compound flow sequence which is, in turn, overlain by a *ca.* 22 m thick plagioclase-phyric sheet lobe.

On Hestur the Argir Beds are overlain by a *ca.* 10 m thick plagioclase-phyric sheet lobe that is overlain by a *ca.* 10 m thick, distinctly brown weathering, olivine-phyric sheet lobe containing >10 vol.% equant phenocrysts of olivine 1-2 mm in size. The olivine-phyric sheet lobe is weakly columnar jointed and has a vesiculated upper crust and is also found occurring with the Argir Beds in the Syðradalsá section, western Streymoy where it is *ca.* 6 m thick. The brown weathering sheet lobe on Hestur is overlain by a *ca.* 50 m thick plagioclase-phyric compound flow sequence that is overlain by at least two plagioclase-phyric sheet lobes that are on average 10 m thick.

In the Fossdalur-Syðradalur area, western Streymoy, the Argir Beds are overlain by a >100 m thick sequence of laterally extensive sheet lobes with a characteristic layer-cake appearance (Figs. 4 and 5a). This is also seen in the area of Glyvursreyn to the west of the Glyvursnes-1 borehole, where the Argir Beds are overlain by a *ca.* 150 m thick sequence dominated by plagioclase-phyric sheet lobes that range in thickness between 10 and 30 m. Although, these sheet lobes are intercalated with minor plagioclase-phyric compound

flows and volcaniclastic lithologies. The plagioclase-phyric sheet lobes are composed predominantly of pale (grey) weathering, plagioclase-phyric basalt with <5 vol.% laths of plagioclase feldspar up to 0.5 cm in length. In the Glyvursreyn area, the plagioclase-phyric sheet lobe sequence is overlain by a suite of at least three distinctly brown weathering, flow banded, aphyric sheet lobes between 15 and 30 m thick, which have not been observed elsewhere in the study area, but are common on the islands to the northeast (e.g. Borðoy, Viðoy and Kunoy).

Geological Evolution of the Study Area

For completeness a brief outline of the development of the lava sequence shall be given, but a more comprehensive discussion in the broader context of the evolution of the FIBG shall be published elsewhere. Towards the end of the Malinstindur Formation the eruption frequency began to slow down and the time interval between the emplacement of the compound lava flows increased, resulting in the widespread deposition of volcaniclastic lithologies (Rasmussen and Noe-Nygaard, 1969; 1970). This is supported by the pronounced reddened weathering profile, which is clearly seen at the top of the Malinstindur Formation across the northern Faroe Islands and as far south as Norðradalur, Streymoy. During this volcanic hiatus the hyperconcentrated and debris flows of the Sneis Formation were deposited, implying that there was an abundant source of loose volcanic debris and significant amounts of water available for mobilisation (cf. Smith and Lowe, 1991). The lateral thinning and fining of the Sneis Formation from north to south suggests that the source region was located to the north and therefore, the mass flow travelled in a general southerly direction.

The sandstone-dominated facies of the Sneis Formation, in the south of the study area, is overlain by a plagioclase-phyric compound lava flow that is comparable in thickness to the conglomerate-dominated Sneis Formation (Figure 4). Both the compound lava flow and the conglomerate-dominated Sneis Formation are overlain by a <1.5 m thick sandstone sequence, which implies that the plagioclase-phyric compound lava flow is constrained to the south of area, which in turn, suggests that it may have also been sourced from a southerly direction. The intercalation of the basal flow lobes on Hestur with the Sneis Formation tentatively suggests that the plagioclase-phyric compound lava flow may have been contemporaneous with the deposition of the Sneis Formation.

In simplistic terms, the sequence between the Sneis Formation and Argir Beds, in the study area at least, represents a transitional phase from the compound lava flows similar in type to those of the Malinstindur Formation to a predominance of sheet lobe lavas above the Argir Beds (Figs. 4 and 5). This change implies a switch in volcanic styles from point sourced shield volcanoes to linear fissure systems (Passey and Bell, 2007). As a consequence of this distinct change in lava morphology, it may, with future mapping, necessitate the promotion of the Argir Beds to member or even formational status.

The interfingering nature of the compound and simple (sheet lobes) lava flows of the study area is similar in character to the volcanic landscape of the Snake River Plain, Idaho, USA, which Greeley (1977; 1982) referred to as basaltic plains volcanism. In the Snake River Plain, the landscape is dominated by low shield volcanoes with slopes typically <0.5° but which steepen to *ca.* 5° at the summit region (Greeley, 1977; 1982). The compound lava flows fed from the low shield volcanoes are typically emplaced into the low-lying areas between the volcanoes, maintaining a regionally planar surface (Greeley, 1977; 1982). This may account for the relatively constant thickness of *ca.* 250 m between the bases of the Sneis Formation and the Argir Beds, which suggests that the lava flow sequence of the study area must have been, in part, laterally constrained. The presence of a topographic low in the vicinity of the study area is supported by a number of the compound lava flows above the Sneis Formation dying out in a northerly direction, which in turn implies that these flows at least, may have been sourced from a low shield volcano situated to the south of the area. In addition, the abrupt disappearance of the conglomerate facies in the Syðradalur area may also support the presence of a topographic low. The *en*

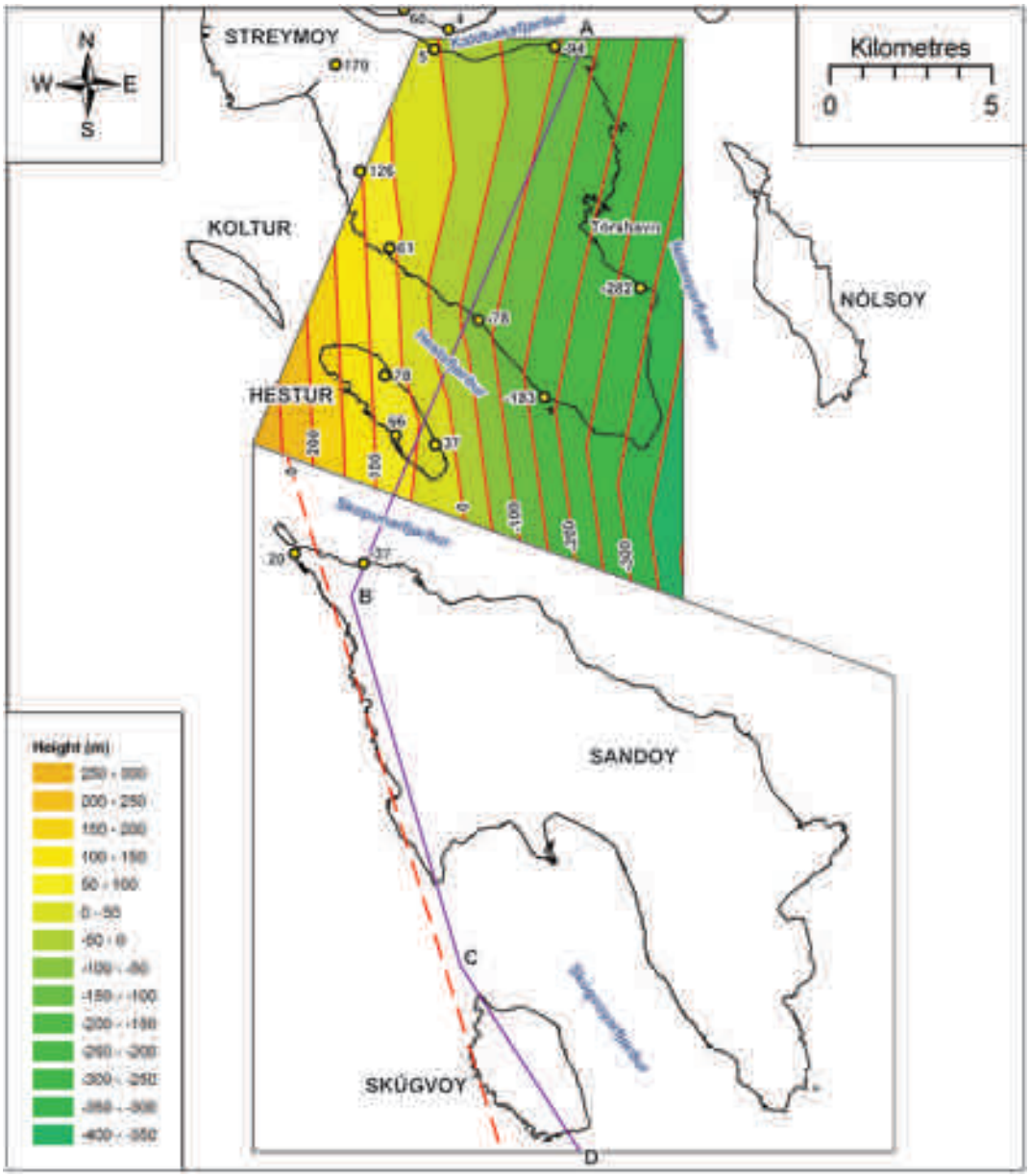

Figure 15. TIN layer for the basal surface of the Sneis Formation, northern area, central Faroe Islands. The surface is contoured at 50 m intervals. The spot heights are given relative to mean sea level. The -183 m spot height on southern Streymoy is suggested to occur *ca.* 10 m below the base of the Sandoyartunnilin-5 borehole based on lithological patterns observed in the borehole, but also conforms to the average vertical thickness between the Sneis Formation and the Argir Beds, which is relatively constant between Hestur and Streymoy. The spot height was required to constrain the dip and strike of the Sneis Formation in this area and conforms to the observed dip and strike of the strata for southern Streymoy. In the southern area the Sneis Formation is only exposed in the NW of Sandoy and therefore, there are currently not enough spot heights to produce a TIN layer for this area. The red dashed line across the southern area is the inferred 0 m structural contour. The strike direction of this structural contour is comparable to the strike directions for the Høvdhamarin Flow and Argir Beds in this area. The Sneis Formation in the northern area dips between 1.3 and 3.6° and the dip direction ranges from ENE to ESE. The lateral displacement of the 0 m structural contour between the northern and southern areas is *ca.* 5.8 km. The purple solid line delineates the cross-section shown in Figure 18.

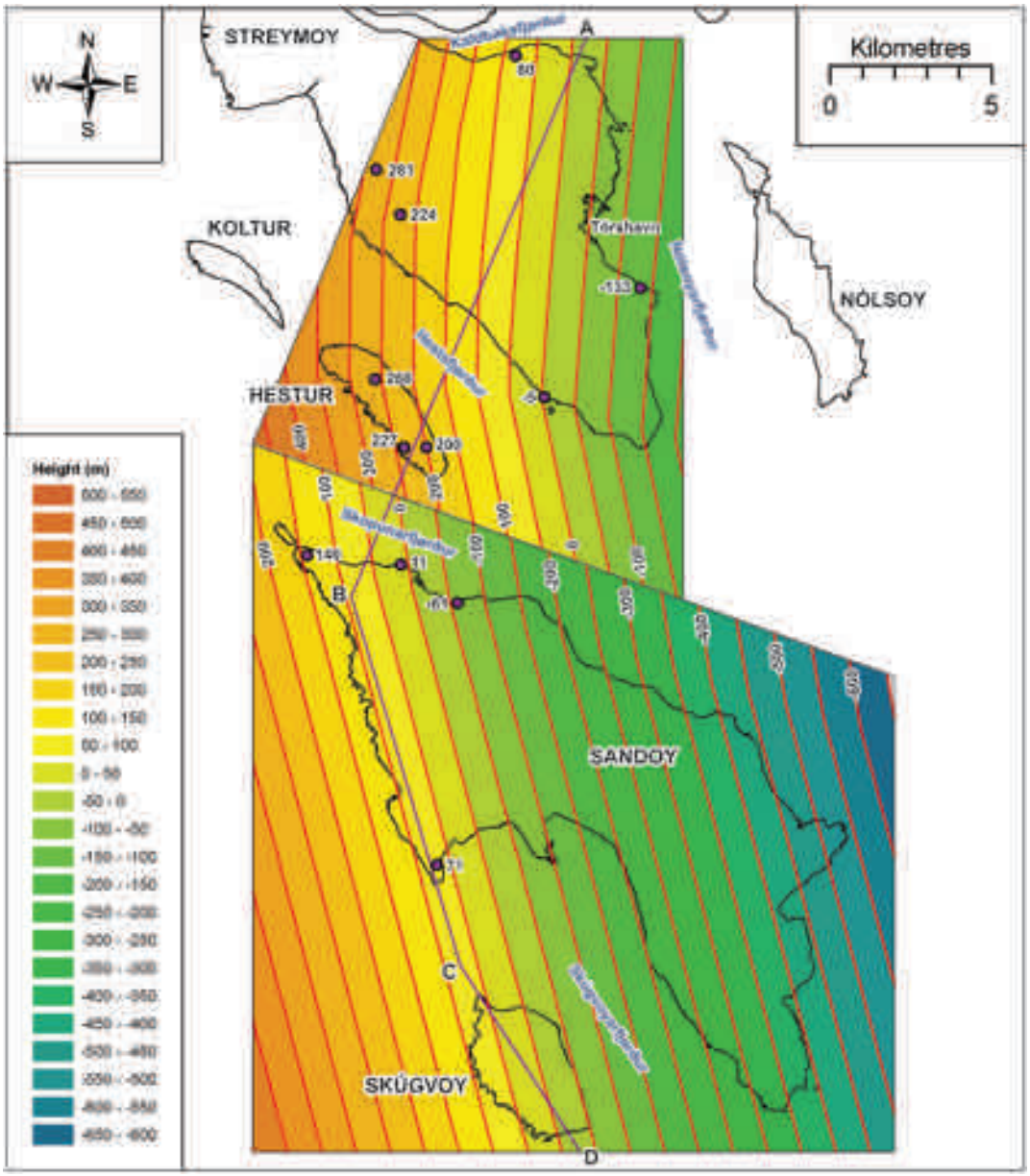

Figure 16. TIN layers for the basal surface of the Høvdhamarin Flow, northern and southern areas, central Faroe Islands. The surfaces are contoured at 50 m intervals. The spot heights are given relative to mean sea level. In the northern area the Høvdhamarin Flow dips between 2.7 and 3.3° and the dip direction ranges from ENE to ESE. In the southern area the Høvdhamarin Flow dips essentially to the ENE by between 2.6 and 2.8°. The lateral displacement of the corresponding structural contours between the northern and southern areas varies between 5.6 and 6.2 km. The purple solid line delineates the cross-section shown in Figure 18.

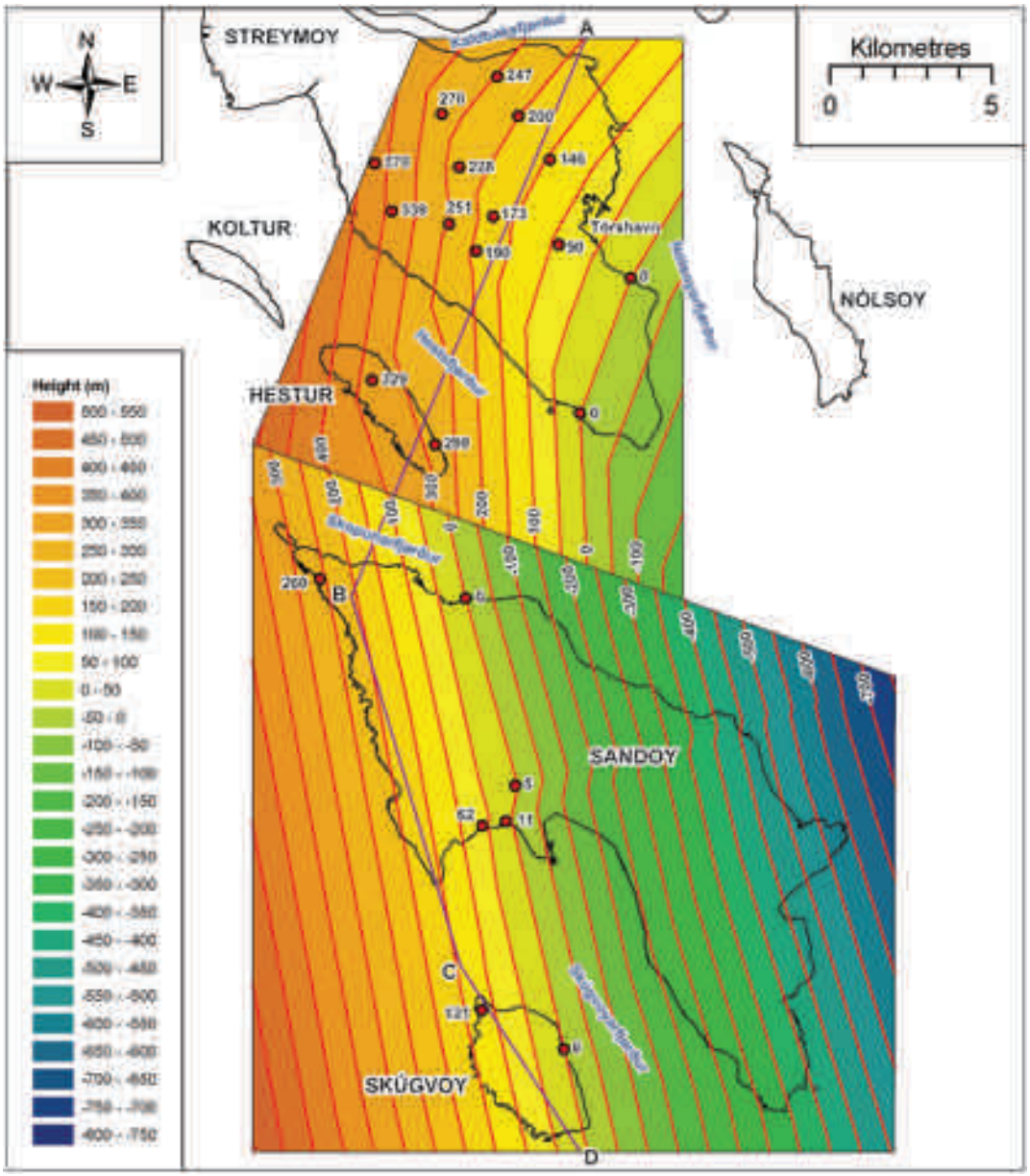

Figure 17. TIN layers for the basal surface of the Argir Beds, northern and southern areas, central Faroe Islands. The surfaces are contoured at 50 m intervals. The spot heights are given relative to mean sea level. The 289 m spot height on southern Hestur is inferred from the average vertical thickness between the Sneis Formation and the Argir Beds, which is relatively constant between Hestur and Streymoy. The spot height was required to constrain the dip and strike of the Argir Beds in this area and conforms to the observed dip and strike of the strata for Hestur. In the northern area the Argir Beds dip between the ENE and SE by between 1.9 and 3.7°. In the southern area the Argir Beds dip between 2.5 and 4.2° towards the ENE and E. The lateral displacement of the corresponding structural contours between the northern and southern areas varies between 4.2 and 5.4 km. The purple solid line delineates the cross-section shown in Figure 18.

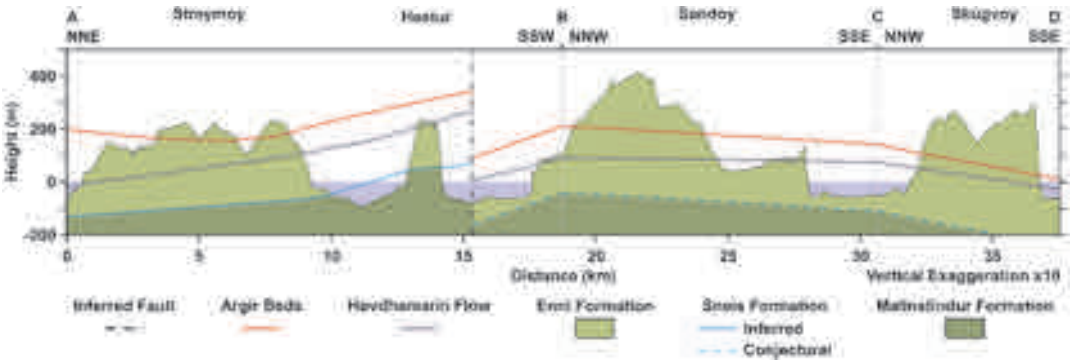

Figure 18. Simplified geological cross-section from Sandvíkatangi, Streymoy to southern Skúgvoy, central Faroe Islands. The cross-section route is depicted in Figs. 15 to 17. The cross-section shows the predicted positions of the basal surfaces of the Sneis Formation, Høvdhamarin Flow and Argir Beds obtained from the TIN layers shown in Figs. 15 to 17. The position of the Sneis Formation to the right of the cross-section (southern area) is conjectural and is based on the relatively constant vertical distance between the Sneis Formation and the Argir Beds. The cross-section shows the relatively conformable vertical thicknesses between the surfaces and the vertical discontinuity due to strike-slip movement along Skopunarfjørður. This vertical discontinuity is between 235 and 265 m. The cross-section also demonstrates how the basal surface of the Sneis Formation (*ca.* C-horizon) from the northern area correlates to the basal surface of the Argir Beds in the southern area and this accounts for the original misplacement of the C-horizon in the southern area by Rasmussen and Noe-Nygaard (1969; 1970).

masse freezing of the debris flow, from which the conglomerates were deposited, may have been caused when the applied shear stress fell below the yield strength of the following debris, which may simply reflect a decrease in gradient on these primarily gravity driven flows (cf. Smith and Lowe, 1991).

Strike-Slip Faulting

The TIN layers produced for the southern and northern areas for the three stratigraphic marker units (Sneis Formation, Høvdhamarin Flow and Argir Beds) show a relatively constant dip and strike across Skopunarfjørður (Figs. 15 to 17). The three stratigraphic marker units have average dips of between 2.4° and 3.4° in an essentially easterly direction, although changing more towards the SE moving northwards. However, there is a vertical discontinuity of 200-300 m between the corresponding structural contours of the northern and southern areas, respectively (Figs. 15 to 18). This discontinuity is suggested to occur along the ESE-trending lineament defined by the bathymetry low in Skopunarfjørður (Figure 19) and can be accounted for by either normal faulting with dip-slip movement to the south, dextral strike-slip faulting or a combination of oblique-slip movement.

This ESE-trending lineament in Skopunarfjørður parallels the fractures of Vítisgjógv and Álvagjógv on southern Hestur which intersect with the ENE-trending Klæmintsgjógv and Húsagjógv forming conjugate fractures. This conjugate configuration occurs across the Faroe Islands and increases in dominance towards the north of the islands (Rasmussen and Noe-Nygaard, 1969; 1970). Geoffroy *et al*. (1994) suggested that these conjugate faults have a strike-slip element with the maximum stress orientated to the ENE to E and are related to a N-S transtensional event. Therefore, dextral strike-slip faulting, in the order of *ca.* 5.8 km for the Sneis Formation, *ca.* 5.9 km for the Høvdhamarin Flow (range: 5.6-6.2 km) and *ca.* 4.8 km for the Argir Beds (range: 4.2-5.4 km) is the preferred explanation for the vertical discontinuity across Skopunarfjørður (Figs. 15 to 17). In addition, dextral strike-slip faulting is supported, in part, by the bedding planes that can be traced across the Vítisgjógv and Álvagjógv fractures without any noticeable vertical movement (Figure 20). This is reiterated by Rasmussen and Noe-Nygaard (1969; 1970) who demonstrated that the majority of fractures on the Faroe Islands have very limited vertical movement, typically, in the order

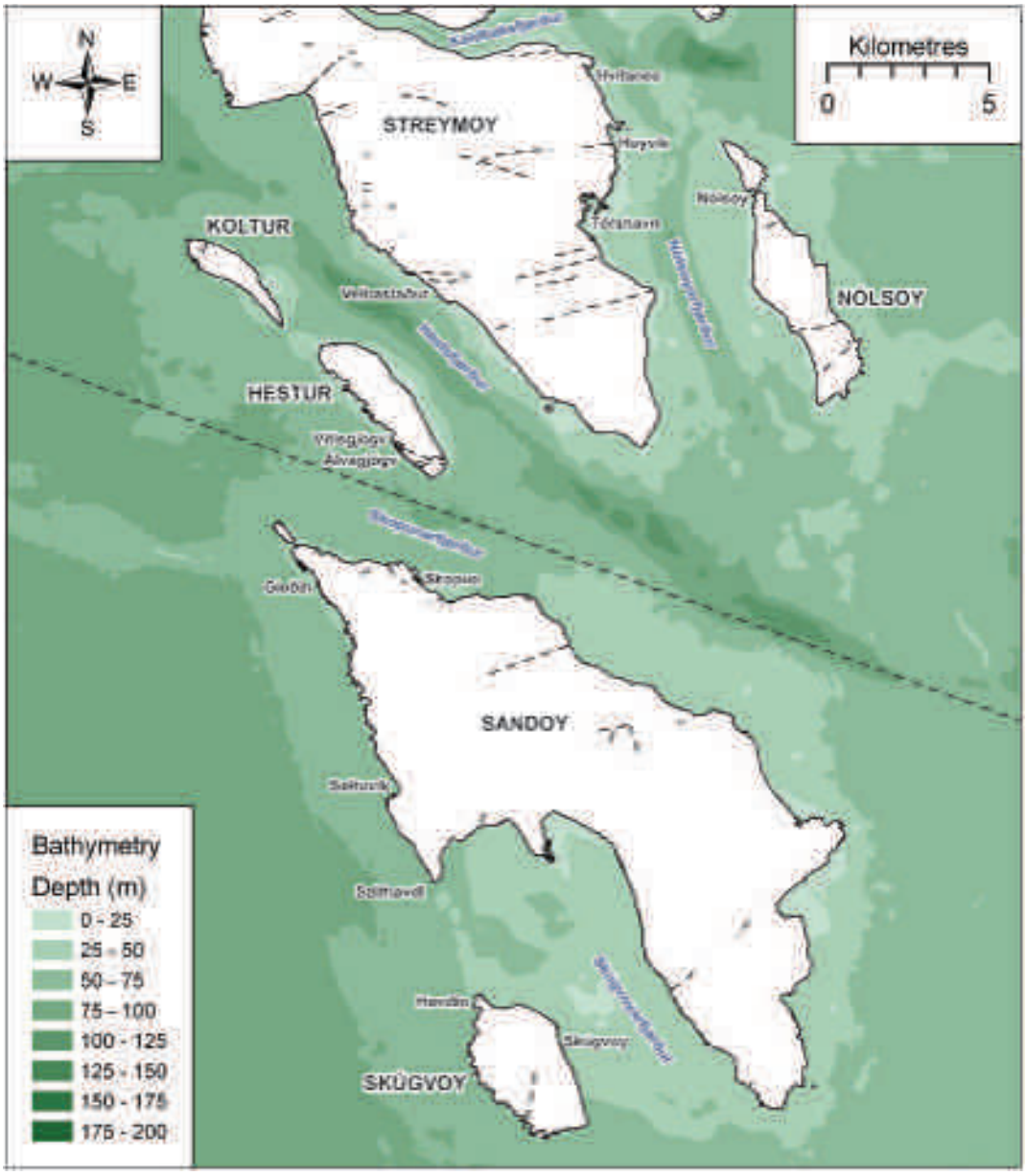

Figure 19. Fracture map for the central Faroe Islands. Fractures are represented by black dashed lines. Onshore fractures are from Rasmussen and Noe-Nygaard (1969; 1970). A major dextral strike-slip fault is inferred along the ESE-trending bathymetry low of Skopunarfjørður, which parallels the Vítisgjógv and Álvagjógv fractures of southern Hestur.

of several metres and rarely exceeding 20 m. However, normal faulting or a component of oblique-slip movement cannot be confidently discounted.

The faulting also implies that the Sneis Formation (*ca.* C-horizon) to the south of Skopunarfjørður, except for the northwest of Sandoy, occurs below sea level (Figure 19). The position of the C-horizon on Sandoy, Skúgvoy, Stóra Dímun and Lítla Dímun was mainly inferred by extending the structural contours of the horizon from southern Streymoy without the consideration of faulting in the area (Rasmussen and Noe-Nygaard, 1969;

Figure 20. N-S view of the ESE-trending Vítisgjógv and Álvagjógv fractures, western Hestur. The dashed lines highlight the boundaries between the lava flows. The red dashed lines are on the SSE and side of Álvagjógv, the yellow dashed lines are on the NNE and SSE sides of Álvagjógv and Vítisgjógv, respectively and the purple dashed lines are on the NNE side of Vítisgjógv. This view demonstrates the conformability of these flow surfaces across these two fractures, implying that there is little or no appreciable vertical movement across them. The height of the cliff is *ca.* 240 m.

1970). As a result, the C-horizon was correlated to the base of the Høvdhamarin Flow in northwest Sandoy and to the top of the Argir Beds on Skúgvoy. Consequently, the new position of the Sneis Formation (*ca.* C-horizon) is *ca.* 200-300 m below the former C-horizon of Rasmussen and Noe-Nygaard (1969; 1970) and it also tentatively implies that the Sneis Formation is not exposed on Stóra Dímun and Lítla Dímun, even if the dip direction does change to the NE, as inferred from northern Suðuroy (Rasmussen and Noe-Nygaard, 1969; 1970). Therefore, this suggests that the thickness of the Malinstindur Formation between Suðuroy and Skúgvoy is much thinner than predicted by Rasmussen and Noe-Nygaard (1969; 1970) and implies that the Malinstindur Formation thins in a southerly direction across the Faroe Islands, as originally suggested by Waagstein (1988). This is supported by seismic imaging in the vicinity of Glyvursnes which predicts a thinning of the Malinstindur Formation by *ca.* 300-400 m from Vestmanna, *ca.* 30 km to the northwest (Petersen *et al*., 2006).

Circumstantial evidence to support the presence of a fault along the axial trend of Skopunarfjørður is the strong parallelism between the coastlines of SW Vágar and NE Sandoy, which have a comparatively ESE-trend (Figure 21). These two coastlines, although *ca.* 25 km apart, also have a similar, dominating zigzag configuration, where the coastline alternates from E-, ESE- and SE-trending segments. The strong ESE-trending lineament can also be tentatively extended offshore by up to *ca.* 100 km towards the Faroe-Shetland Channel and is defined by the parallelism between Sandoyarbanki and Suðuroyarbanki and the small bathymetry low between these two features (Figure 21). However, there is currently no evidence to support a major fault within this area, although Morgan and Murphy (1998) suggest, based on potential field data, the presence of at least two ESE-trending strike-slip faults across the NE of the Faroe Islands which extend towards the Faroe-Shetland Channel.

If the fault does extend offshore then it may have implications for hydrocarbon exploration in the Faroese area. Due to the apparent lack of thinning/thickening of the beds and flows across the Skopunarfjørður fault, it implies that the fault

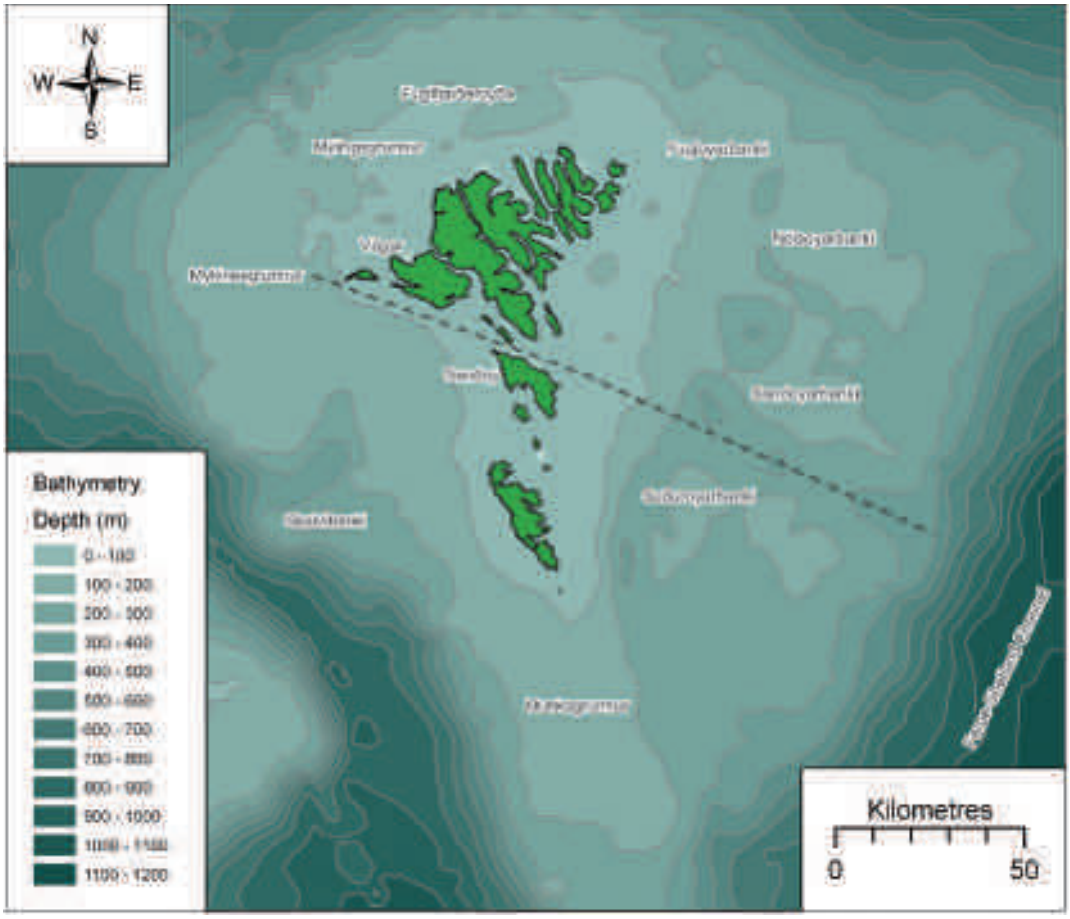

Figure 21. Bathymetry map for the greater Faroe Platform region. The inferred strike-slip fault of Skopunarfjørður (black dashed line) can be tentatively extended to the WNW due to the strong parallelism between the coastlines of SW Vágar and NE Sandoy. Similarly, the fault can be extended by *ca.* 100 km towards the Faroe-Shetland Channel due to the parallelism between the bathymetric features of Suðuroyarbanki and Sandoyarbanki. However, there is currently no evidence to support a major fault within this area. There are a number of other similar trending bathymetric features to the N and S of the inferred Skopunarfjørður fault, which may be related to a pre-existing tectonic system.

post-dates the deposition and emplacement of the units. In addition, the faulting must also post-date the regional tilting of the sequence or the discontinuity would not have been recognised. Therefore, the fault has, most likely, not had an influence on sub-FIBG sedimentation patterns within the Faroe-Shetland Basin, the focus of hydrocarbon exploration in the area (Ziska and Andersen, 2005). However, if the fault is present offshore it may have acted as a hydrocarbon pathway, which may have been beneficial (e.g. migration to reservoirs) or detrimental (e.g. seeps at seafloor) for exploration. Similarly, the movement of rock units may have resulted in a structural trap or conversely, allowed any trapped hydrocarbons to escape. Until the potential of the offshore continuation of the Skopunarfjørður fault is evaluated the affect of the fault on hydrocarbon exploration shall remain speculative.

Synthesis

The refining of the lithostratigraphy and the recognition of stratigraphic marker units has enabled the identification of major structural elements previously only inferred. The following list is some of

the main findings of this study and future aims and objectives.

1. The Sneis Formation was deposited from hyperconcentrated and debris flows that were sourced to the north and travelled in a general southerly direction.
2. A number of the compound lava flows across the study area die out in a northerly direction implying they were sourced from the south.
3. The Argir Beds mark a significant change between contrasting volcanic styles, primarily across southern Streymoy (i.e. compound vs. simple lava flows).
4. The sequence between the Sneis Formation and Argir Beds represents a transition from compound lava flows to sheet lobes.
5. The relatively constant thickness of *ca.* 250 m between the bases of the Sneis Formation and the Argir Beds, most likely, implies the lava flow sequence was laterally restricted.
6. The vertical discrepancy of 200-300 m between corresponding structural contours across Skopunarfjørður is accounted for by a major ESE-trending, dextral strike-slip fault, with a lateral displacement of between 4.2 and 6.2 km.
7. The misplacement of the C-horizon by Rasmussen and Noe-Nygaard (1969; 1970) on Sandoy, Skúgvoy and most likely, Stóra Dímun and Lítla Dímun is accounted for by the presence of the Skopunarfjørður fault and the absence of the conglomerate-dominated Sneis Formation and associated invasive sheets on these islands.
8. The extension of the Skopunarfjørður fault offshore towards the Faroe-Shetland Channel maybe proven by future seismic and potential field investigations.
9. Detailed logging and correlation of sections across other fjords on the Faroe Islands may identify other faulted sequences.
10. A more detailed subdivision of the lithostratigraphy of the FIBG, through logging and mapping, may constrain transport directions and source regions of the lava flows and sedimentary packages.

Acknowledgements

This work has been carried out as part of the ongoing mapping project of the Faroe Islands funded by Statoil (U.K.) Ltd. and ENI (UK) Ltd. Many thanks go to the following for assistance in the field: Thomas Varming, David Jolley, Turid Madsen, Uni Árting and Jana Ólavsdóttir. Grateful appreciation also goes to John Zachariassen for help in producing the TIN layers in ArcGIS® 9.2. The author would also like to thank Jonathan Imber and Morten Sparre Andersen for their constructive and thoughtful reviews.

References

Andersen, M.S. 1988. Late Cretaceous and early Tertiary extension and volcanism around the Faeroe Islands. *In*: Morton, A.C. and Parson, L.M. (eds) *Early Tertiary Volcanism and the Opening of the NE Atlantic*. Geological Society, London, Special Publications 39: 115-122.

Cas, R.A.F. and Wright, J.V. 1987. *Volcanic Successions: Modern and Ancient*. Allen & Unwin, London.

Collinson, J.D. 1996. Alluvial Sediments. *In:* Reading, H.G. (ed.) *Sedimentary Environments: Processes, Facies and Stratigraphy*. 3rd Edition. Blackwell Science, Oxford: 37-82.

Elliott, T. 1974. Interdistributary bay sequences and their genesis. *Sedimentology* 21: 611-622.

Ellis, D., Bell, B.R., Jolley, D.W. and O'Callaghan, M. 2002. The stratigraphy, environment of eruption and age of the Faroes Lava Group, NE Atlantic Ocean. *In*: Jolley, D.W. and Bell, B.R. (eds) *The North Atlantic Igneous Province: Stratigraphy, Tectonic, Volcanic and Magmatic Processes*. Geological Society, London, Special Publications 197: 253-269.

Fisher, R.V. and Smith, G.A. 1991. Volcanism, tectonics and sedimentation. *In*: Fisher, R.V. and Smith, G.A. (eds) *Sedimentation in Volcanic Settings*. SEPM (Society for Sedimentary Geology) Special Publication 45: 1-5.

Geoffroy, L., Bergerat, F. and Angelier, J. 1994. Tectonic evolution of the Greenland-Scotland ridge during the Paleogene: new constraints. *Geology* 22: 653-656.

Greeley, R. 1977. Basaltic 'plains' volcanism. *In*: Greeley, R. and King, J.S. (eds) *Volcanism of the Eastern Snake River Plain, Idaho: A Comparative Planetary Geology Guidebook*. NASA CR-154621: 23-44.

Greeley, R. 1982. The Snake River Plain, Idaho: representative of a new category of volcanism. *Journal of Geophysical Research* 87(B4): 2705-2712.

Hald, N. and Waagstein, R. 1984. Lithology and chem-

istry of a 2-km sequence of Lower Tertiary tholeiitic lavas drilled on Suðuroy, Faeroe Islands (Lopra-1). *In*: Berthelsen, O., Noe-Nygaard, A. and Rasmussen, J. (eds) *The Deep Drilling Project 1980-1981 in the Faeroe Islands*. Annales Societatis Scientiarum Færoensis, Tórshavn Supplementum IX: 15-38.

Hald, N. and Waagstein, R. 1991. The dykes and sills of the Early Tertiary Faeroe Island basalt plateau. *Transactions of the Royal Society of Edinburgh: Earth Sciences* 82: 373-388.

Højgaard, B. 2007. *The Sandoyar Tunnel. Core descriptions. Cores 4-6. Report to Landsverk*. Jarðfeingi, Tórshavn 04.00291-R-7.

Japsen, P., Andersen, C., Andersen, H.L., Andersen, M.S., Boldreel, L.O., Mavko, G., Mohammed, N.G., Pedersen, J.M., Petersen, U.K., Rasmussen, R., Shaw, F., Springer, N., Waagstein, R., White, R.S. and Worthington, M. 2005. Preliminary results from investigations of seismic and petrophysical properties of Faroes basalts in the SeiFaBa project. *In*: Doré, A.G. and Vining, B.A. (eds) *Petroleum Geology: North-West Europe and Global Perspectives - Proceedings of the 6th Petroleum Geology Conference*. Geological Society, London: 1461-1470.

Japsen, P. and Waagstein, R. 2005. *Preliminary analysis of ultrasonic and geochemical properties of core samples from Glyvursnes-1 and Vestmanna-1, Faroe Islands*. Geological Survey of Denmark and Greenland Report, Copenhagen 2005/19.

Jolley, D.W. and Bell, B.R. 2002. The evolution of the North Atlantic Igneous Province and the opening of the NE Atlantic rift. *In*: Jolley, D.W. and Bell, B.R. (eds) *The North Atlantic Igneous Province: Stratigraphy, Tectonic, Volcanic and Magmatic Processes*. Geological Society, London, Special Publications 197: 1-13.

Jørgensen, O. 2006. The regional distribution of zeolites in the basalts of the Faroe Islands and the significance of zeolites as palaeotemperature indicators. *In*: Chalmers, J.A. and Waagstein, R. (eds) *Scientific Results from the Deepened Lopra-1 Borehole, Faroe Islands*. Geological Survey of Denmark and Greenland Bulletin 9: 123-156.

Larsen, L.M., Waagstein, R., Pedersen, A.K. and Storey, M. 1999. Trans-Atlantic correlation of the Palaeogene volcanic successions in the Faeroe Islands and East Greenland. *Journal of the Geological Society, London* 156: 1081-1095.

Lund, J. 1983. Biostratigraphy of interbasaltic coals from the Faeroe Islands. *In*: Bott, M.H.P., Saxov, S., Talwani, M. and Thiede, J. (eds) *Structure and Development of the Greenland-Scotland Ridge. New Methods and Concepts*. Plenum Press, New York: 417-423.

Lund, J. 1989. A late Paleocene non-marine microflora from the interbasaltic coals of the Faeroe Islands, North Atlantic. *Bulletin of the Geological Society of Denmark* 37: 181-203.

Madsen, T. 2006a. *The Vágar Tunnel, Faroe Islands. Geological Profile*. Jarðfeingi, Tórshavn 06.00007-R-1.

Madsen, T. 2006b. *The Skálafjarðar Tunnel. Core Descriptions. Cores 1-4. Report to Skálafjarðartunnilin P/F*. Jarðfeingi, Tórshavn 06.00034-R-3.

Morgan, R. and Murphy, C. 1998. The use of potential fields in the search for potential fields in the Faroe-Shetland area. *SPE Reservoir Evaluation & Engineering* 1: 476-484.

Noe-Nygaard, A. and Rasmussen, J. 1968. Petrology of a 3,000 metre sequence of basaltic lavas in the Faeroe Islands. *Lithos* 1: 286-304.

Ólavsdóttir, J. 2005. *Kjarnalýsingar í sambandi við møguliga gerð av undirsjóvartunli til Sandoyar. Frágreiðing til Landsverk*. Jarðfrøðisavnið, Tórshavn 04.00291-R-2.

Orton, G.J. 1996. Volcanic environments. *In*: Reading, H.G. (ed.) *Sedimentary Environments: Processes, Facies and Stratigraphy*. 3rd Edition. Blackwell Science, Oxford: 485-567.

Passey, S.R. 2004. *The Volcanic and Sedimentary Evolution of the Faeroe Plateau Lava Group, Faeroe Islands and the Faeroe-Shetland Basin, NE Atlantic*. PhD Thesis. University of Glasgow.

Passey, S.R. and Bell, B.R. 2007. Morphologies and emplacement mechanisms of the lava flows of the Faroe Islands Basalt Group, Faroe Islands, NE Atlantic Ocean. *Bulletin of Volcanology* 70: 139-156.

Passey, S.R., Jolley, D.W. and Bell, B.R. 2006. *Lithostratigraphic Framework for the Faroe Islands Basalt Group, NE Atlantic*. A George P.L. Walker Symposium on Advances in Volcanology, 12-17 June, Reykholt, Iceland.

Petersen, U.K., Andersen, M.S., White, R.S. and the SeiFaBa Group. 2006. Seismic imaging of basalts at Glyvursnes, Faroe Islands: hunting for future exploration methods in basalt covered areas. *First Break* 24: 45-52.

Pierson, T.C. and Scott, K.M. 1985. Downstream dilution of a lahar: transition from debris flow to hyperconcentrated streamflow. *Water Resources Research* 21: 1511-1524.

Rasmussen, J. and Noe-Nygaard, A. 1969. *Beskrivelse til Geologisk Kort over Færøerne i Målestok 1:50 000*. Danmarks Geologiske Undersøgelse, København, 1/24.

Rasmussen, J. and Noe-Nygaard, A. 1970 (1969). *Geology of the Faeroe Islands (Pre-Quaternary). Trans:* Henderson, G. Geological Survey of Denmark, Copenhagen 1/25.

Ritchie, J.D., Gatliff, R.W. and Richards, P.C. 1999. Early Tertiary magmatism in the offshore NW UK margin and surrounds. *In*: Fleet, A.J. and Boldy, S.A.R. (eds) *Petroleum Geology of Northwest Europe: Proceedings of the 5th Conference*. Geological Society, London: 573-584.

Rock-Color Chart Committee. 1995. *Rock-Color Chart*.

The Geological Society of America, Boulder, Colorado.

Saunders, A.D., Fitton, J.G., Kerr, A.C., Norry, M.J. and Kent, R.W. 1997. The North Atlantic Igneous Province. *In*: Mahoney, J.J. and Coffin, M.L. (eds) *Large Igneous Provinces: Continental, Oceanic, and Planetary Flood Volcanism*. American Geophysical Union, Geophysical Monographs 100: 45-93.

Scott, K.M. 1988. *Origins, behavior, and sedimentology of lahars and lahar-runout flows in the Toutle-Cowlitz River system: lahars and lahar-runout flows in the Toutle-Cowlitz River system, Mount St. Helens, Washington*. United States Geological Survey Professional Paper, 1447-A.

Self, S., Keszthelyi, L. and Thordarson, T. 1998. The importance of pahoehoe. *Annual Review of Earth and Planetary Sciences* 26: 81-110.

Self, S., Thordarson, T. and Keszthelyi, L. 1997. Emplacement of continental flood basalt lava flows. *In*: Mahoney, J.J. and Coffin, M.L. (eds) *Large Igneous Provinces: Continental, Oceanic, and Planetary Flood Volcanism*. American Geophysical Union, Geophysical Monographs 100: 381-410.

Shipboard Scientific Party. 2002. Explanatory Notes. *In*: Tarduno, J.A., Duncan, R.A. and Scholl, D.W. (eds) *Proceedings of the Ocean Drilling Program, Initial Reports*. College Station, Texas (Ocean Drilling Program) 197: 1-89.

Smith, G.A. 1986. Coarse-grained nonmarine volcaniclastic sediment: terminology and depositional process. *Geological Society of America Bulletin* 97: 1-10.

Smith, G.A. 1987a. The influence of explosive volcanism on fluvial sedimentation: the Deschutes Formation (Neogene) in central Oregon. *Journal of Sedimentary Petrology* 57: 613-629.

Smith, G.A. 1987b. Sedimentology of volcanism-induced aggradation in fluvial basins: examples from the Pacific Northwest, USA. *In*: Ethridge, F.G., Flores, R.M. and Harvey, M.D. (eds) *Recent Developments in Fluvial Sedimentology*. Special Publication of the Society of Economic Palaeontologists and Mineralogists, Tulsa, Oklahoma 39: 217-228.

Smith, G.A. 1988. Sedimentology of proximal to distal volcaniclastics dispersed across an active foldbelt: Ellensburg Formation (late Miocene, central Washington). *Sedimentology* 35: 953-977.

Smith, G.A. 1991. Facies sequences and geometries in continental volcaniclastic sediments. *In*: Fisher, R.V. and Smith, G.A. (eds) *Sedimentation in Volcanic Settings*. SEPM (Society for Sedimentary Geology) Special Publication 45: 109-121.

Smith, G.A. and Lowe, D.R. 1991. Lahars: volcano-hydrologic events and deposition in the debris flow-hyperconcentrated flow continuum. *In*: Fisher, R.V. and Smith, G.A. (eds) *Sedimentation in Volcanic Settings*. SEPM (Society for Sedimentary Geology) Special Publication 45: 59-70.

Sohn, Y.K., Rhee, C.W. and Kim, B.C. 1999. Debris flow and hyperconcentrated flood-flow deposits in an alluvial fan, northwestern part of the Cretaceous Yongdong Basin, Central Korea. *Journal of Geology* 107: 111-132.

Waagstein, R. 1977. *The Geology of the Faeroe Plateau*. PhD Thesis. University of Copenhagen.

Waagstein, R. 1988. Structure, composition and age of the Faeroe basalt plateau. *In*: Morton, A.C. and Parson, L.M. (eds) *Early Tertiary Volcanism and the Opening of the NE Atlantic*. Geological Society, London, Special Publications 39: 225-238.

Waagstein, R. 1998. *A geological field guide to the Palaeogene flood basalts of Suðuroy, Faroe Islands*. Danmarks og Grønlands Geologiske Undersøgelse 1998/130.

Waagstein, R. 2006. Composite log from the Lopra-1/1A well, Faroe Islands. *In*: Chalmers, J.A. and Waagstein, R. (eds) *Scientific Results from the Deepened Lopra-1 Borehole, Faroe Islands*. Geological Survey of Denmark and Greenland Bulletin 9.

Waagstein, R. and Andersen, C. 2003. *Well completion report: Glyvursnes-1 and Vestmanna-1, Faroe Islands*. Geological Survey of Denmark and Greenland 2003/99.

Waagstein, R., Guise, P. and Rex, D. 2002. K/Ar and $^{39}Ar/^{40}Ar$ whole-rock dating of zeolite facies metamorphosed flood basalts: the upper Paleocene basalts of the Faroe Islands, NE Atlantic. *In*: Jolley, D.W. and Bell, B.R. (eds) *The North Atlantic Igneous Province: Stratigraphy, Tectonic, Volcanic and Magmatic Processes*. Geological Society, London, Special Publications 197: 219-252.

Waagstein, R. and Hald, N. 1984. Structure and petrography of a 660 m lava sequence from the Vestmanna-1 drill hole, lower and middle basalt series, Faeroe Islands. *In*: Berthelsen, O., Noe-Nygaard, A. and Rasmussen, J. (eds) *The Deep Drilling Project 1980-1981 in the Faeroe Islands*. Annales Societatis Scientiarum Færoensis, Tórshavn Supplementum IX: 39-70.

Walker, F. and Davidson, C.F. 1936. A contribution to the geology of the Faeroes. *Transactions of the Royal Society of Edinburgh* 58: 869-897.

Walker, G.P.L. 1970. Compound and simple lava flows and flood basalts. *Bulletin Volcanologique* 35: 579-590.

Wentworth, C.K. 1922. A scale of grade and class terms for clastic sediments. *Journal of Geology* 30: 377-392.

Ziska, H. and Andersen, C. 2005. Exploration opportunities in the Faroe Islands. *In*: Ziska, H., Varming, T. and Bloch, D. (eds) *Faroe Islands Exploration Conference: Proceedings of the 1st Conference*. Annales Societatis Scientiarum Færoensis, Tórshavn, Supplementum 43: 146-162.

Transfer zones: The application of new geological information from the Faroe Islands applied to the offshore exploration of intra basalt and sub-basalt strata

DAVE ELLIS[1*], SIMON R. PASSEY[2], DAVID W.JOLLEY[3]
AND BRIAN R.BELL[4]

[1] Statoil UK Ltd, Statoil House, 11a Regent St, London, SW1Y 4ST, UK
* Email: ddael@statoilhydro.com; Tel: +44 2077 667777; Fax: +44 2077 667862
[2] Faroese Earth and Energy Directorate (Jarðfeingi), Brekkutún 1, P.O. Box 3059, FO-110 Tórshavn, Faroe Islands
[3] Department of Geology and Petroleum Geology, University of Aberdeen, Meston Building, King's College, Aberdeen, AB24 3UE, UK.
[4] Department of Geographical and Earth Sciences, University of Glasgow, Gregory Building, Lilybanks Gardens, Glasgow, G12 8QQ, UK

ABSTRACT

Transfer zones are large, linear features interpreted to be geologically very old (600 Ma or older) and linked to deep crustal fractures. Transfer zones in the North Atlantic around the Faroe-Shetland area have a strong NW-SE orientation and sub parallel spacing of up to 20-25km. In the Faroes area, onshore evidence is presented to show the influence of the Judd, the newly identified Brynhild (this paper) and Westray transfer zones on the development of the lava sequences, inter-bedded coals and other sedimentary rocks. Critical linking of transfer zones from the Faroe-Shetland margin across to a palaeo-Greenland hinterland during the geological past would have had great influence on the volumes, location and type of sediments made available for offshore deposition during the Palaeocene.

Introduction

This paper summarises the field and laboratory analysis of the distribution of lavas and inter-lava sedimentary rocks in the Faroe Islands Basalt Group (FIBG). The objective of the study was to examine the variation in the development of the lava, inter-lava sediments and their biofacies to establish the impact of the Judd, Brynhild and Westray transfer zones on the development of the Palaeogene Faroe Islands Basalt Group (the Brynhild is a newly identified transfer zone named after the convention established by Keser Neish, 2004). An initial objective of the study was to establish a stratigraphical framework for the rocks exposed on either side of the prognosed Westray and Brynhild transfer zones where they transect the islands. A datum on which to base this stratigraphy was provided by mapping the Sneis Formation (Passey *et al*., 2006), the base of which equates approximately to the C-horizon of Rasmussen and Noe-Nygaard (1970). This sequence of debris- and hyperconcentrated-flow deposits extends over much of central and southern Streymoy, Eysturoy and the smaller islands in the NE of the Faroe Islands.

Using the base of the Sneis Formation as a datum it was possible to build correlation panels which demonstrate the variation in both lava and sedimentary facies. From these correlation panels the newly identified inter-bedded sediments of the upper Malinstindur and Enni Formations could be demonstrated to be generally thickest or geographical restricted on the NE sides of the predicted transfer zones.

Faroe Islands Exploration Conference: Proceedings of the 2nd Conference.
Annales Societatis Scientiarum Færoensis, Supplementum 50, 2009: 205-226

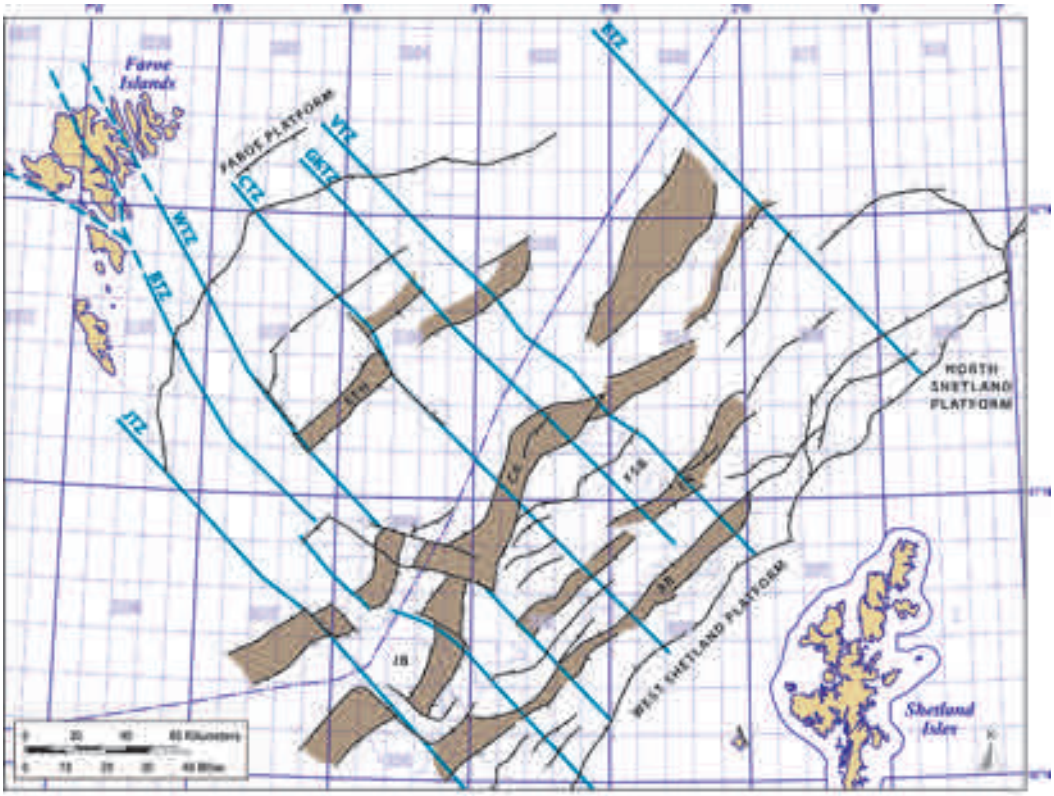

Figure 1. Regional structural elements map of the Faroe-Shetland Basins based on seismic, gravity and magnetic interpretations (RR : Rona Ridge, FR : Flett Ridge, CR : Corona Ridge, EFH : East Faroe High, JB : Judd Basin, FSB : Flett sub-basin, JTZ : Judd Transfer Zone, BTZ : Brynhild Transfer Zone, WTZ : Westray Transfer Zone, CTZ : Clair Transfer Zone, GKTZ : Grimur Kamban Transfer Zone, VTZ : Victory Transfer Zone).

Tectonic Framework

The principal tectonic elements of the Faroe-Shetland area are shown in Figure 1. Two key observations can be made, one the identification of NE-SW trending basins and ridges and two, the NW-SE orientated transfer zones. The latter are exemplified by the Judd, Brynhild, Westray, Clair, Grimur Kamban, Victory and Erlend transfer zones. The concept of transfer zones within the Faroe-Shetland Basin was first proposed by Rumph *et al*. (1993) and a cursory examination of the structure of the Faroe Islands reveals that there is a pronounced structural grain from NW to SE (Rasmussen and Noe-Nygaard, 1970), which is exemplified by the dominant fjord orientations. This direction is directly in parallel with the orientation of inferred transfer zones in the offshore Faroe-Shetland Basin. Previous authors (e.g. Naylor *et al*., 1999; Lamers and Carmichael, 1999; Grant *et al*., 1999; Ellis *et al*., 2002 and Jolley and Morton, 2007) have invoked offshore evidence, directly and indirectly from gravity, magnetic and well penetration data to show the influence of transfer zones on sediment distributions in the offshore Faroe-Shetland Basins (Figure 2).

The Palaeocene onshore and offshore Faroe-Shetland stratigraphy is shown in Figure 3, while Figure 4 shows the exposed and drilled upper Palaeocene-Eocene stratigraphy established in the Faroe Islands (adapted from Rasmussen and Noe-Nygaard, 1970 and Passey *et al*., 2006).

It has been noted that the present day North Atlantic margins roughly coincide geographically with the Ordovician-Devonian Caledonian oro-

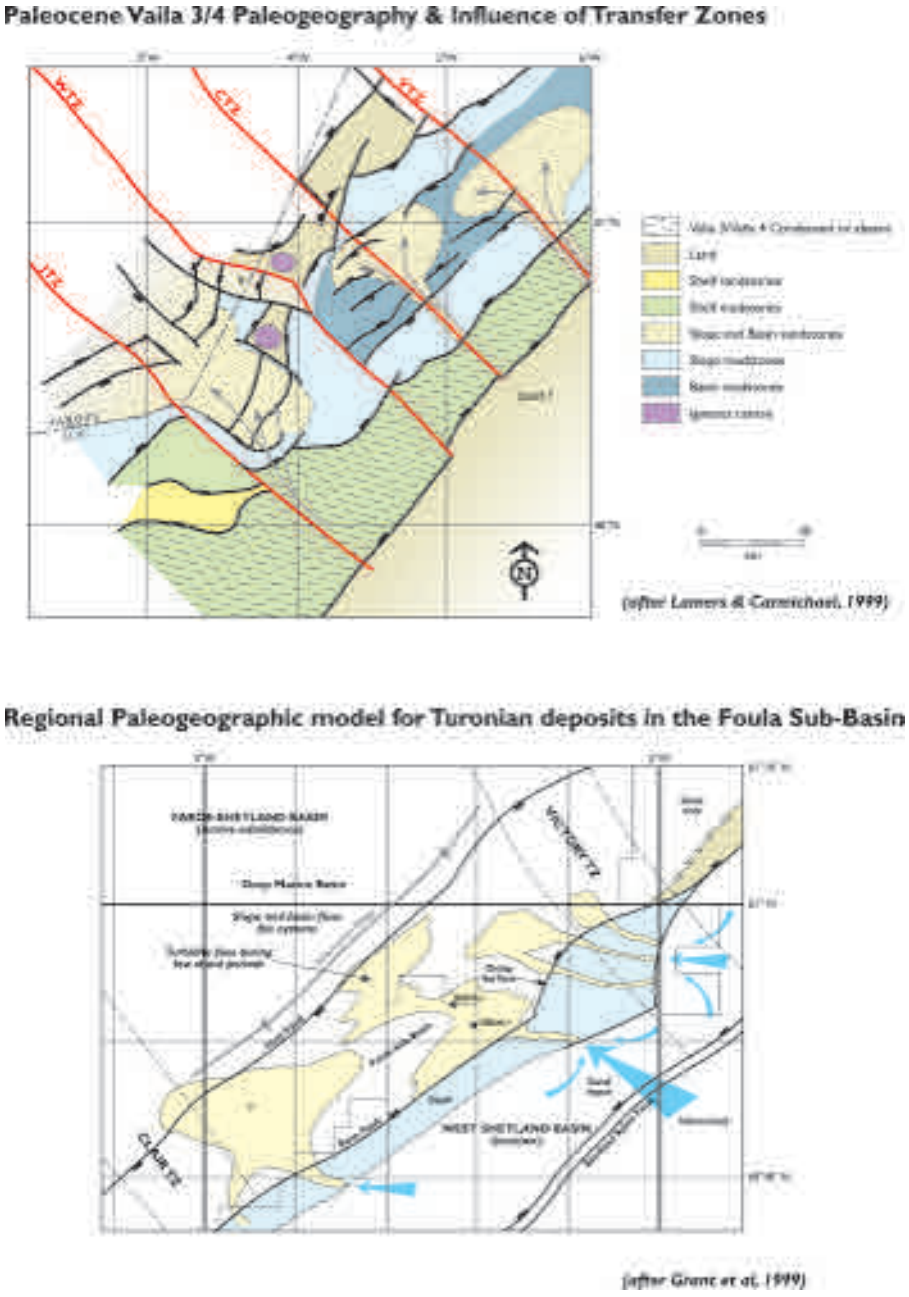

Figure 2. Interpreted effects of transfer zones on sediment distributions in offshore Faroe-Shetland Basins. (a) Palaeocene (after Lamers and Carmichael, 1999) and (b) Cretaceous Turonian (Grant *et al*., 1999).

genic belt (Doré and Gage, 1987; Doré *et al*,. 1999). This implies that during the early Devonian, NW Britain and E Greenland were underlain by thickened continental lithosphere, which, during successive extensional events became thinned until continental failure occurred in the late

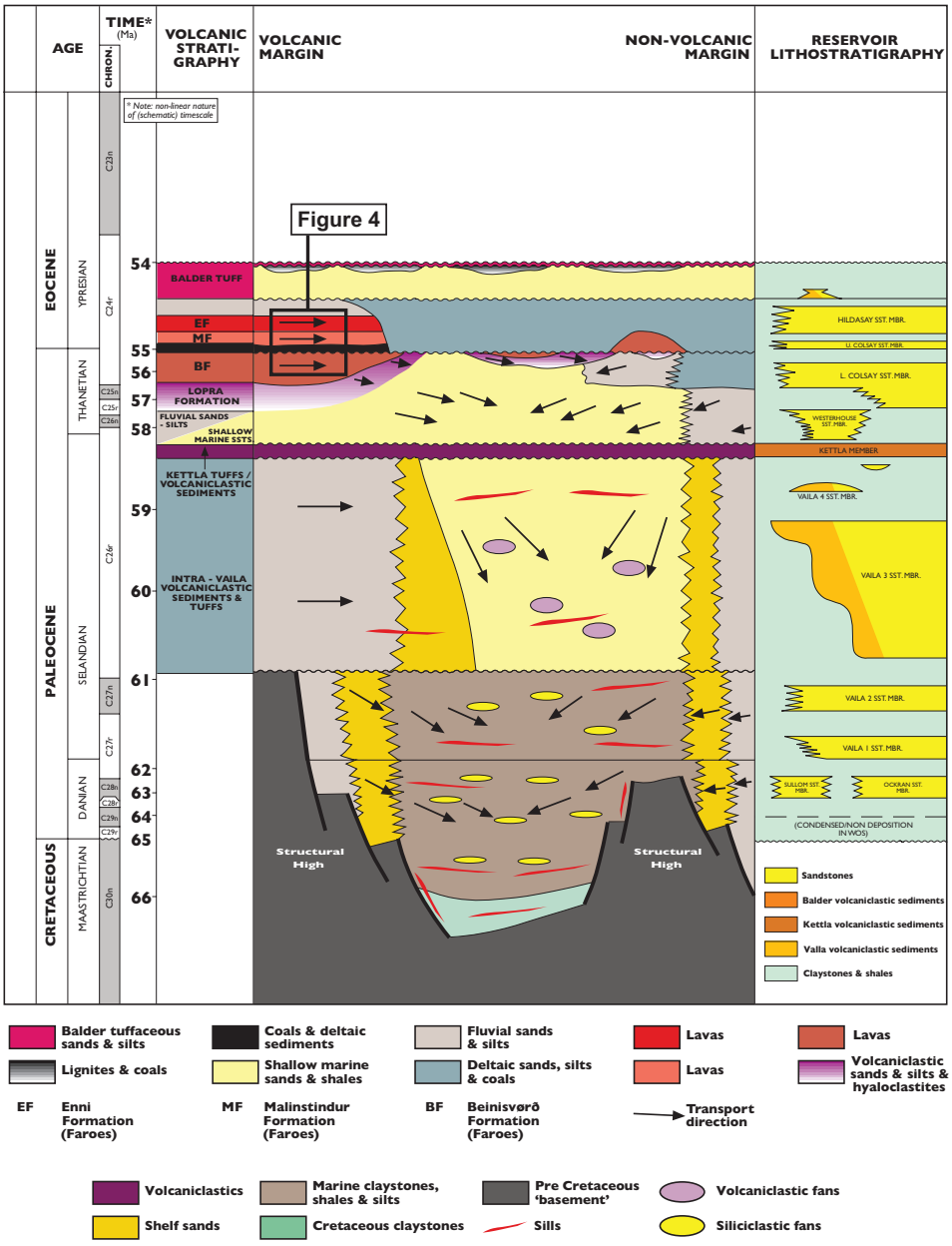

Figure 3. Faroe-Shetland regional Palaeocene stratigraphy.

Palaeocene. Rifting events leading to North Atlantic break-up in the late Palaeocene are documented in the Devono-Carboniferous, the Permo-Triassic and the late Jurassic (Doré *et al.*,1999) The present day basin structure was largely initiated during the early to mid Cretaceous when NW-SE extension produced major structural relief along the entire Norway/U.K. Atlantic Margin.

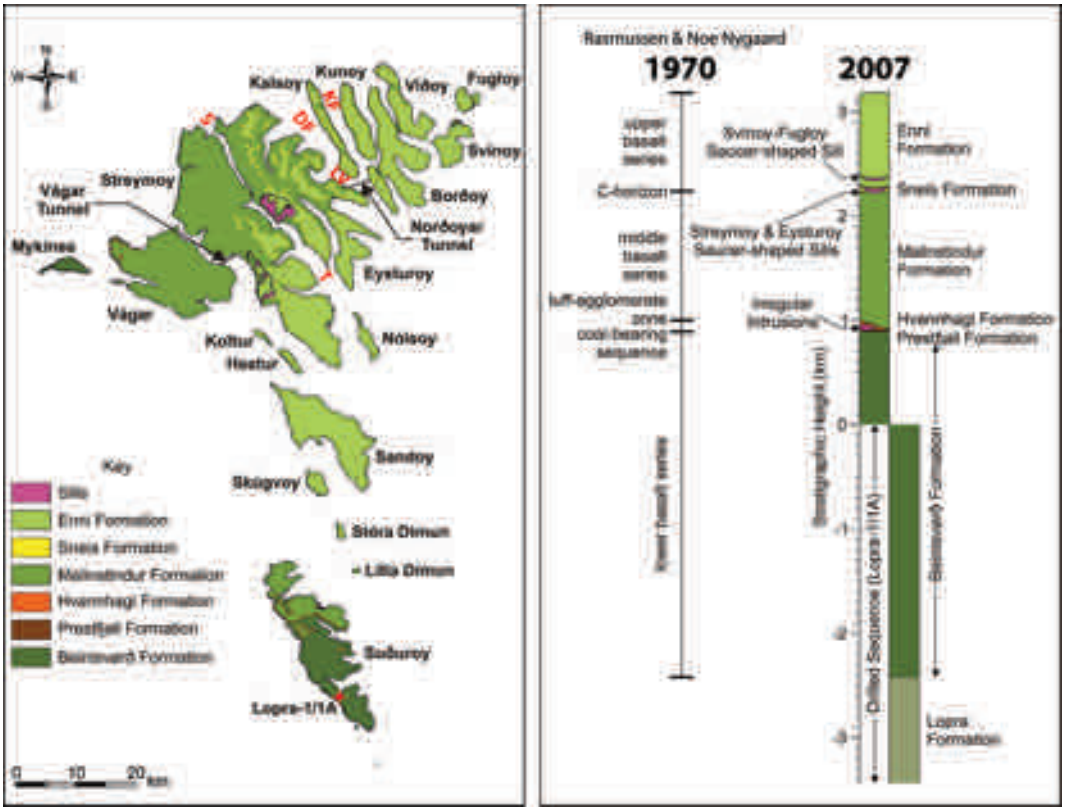

Figure 4. Faroe Islands geology and stratigraphy after Rasmussen and Noe-Nygaard (1970) and Passey et al. 2007. S: Sundini fjord, T: Tangafjørður, LF: Leirvíksfjørður, KF: Kalsoyarfjørður, and DF: Djúpini fjord.

Major tectonism affected the area during the latest Cretaceous-Palaeogene with further NW-SE (slightly oblique) orientated extension along transfer faults. This resulted in lithospheric thinning and focusing of a deep mantle plume close to the coast of East Greenland. The flanks of the Faroe-Shetland Basin (including large areas of East Greenland) were subject to uplift, erosion and removal of the uppermost Cretaceous section. In the mid to late Palaeocene an array of E-W and NE-SW tensional faults developed across the Faroe-Shetland Basin (Figure 5). The faulting affected the Palaeocene section, though in many cases not penetrating the top of this section. Their deeper linkage to pre-Palaeogene faults is enigmatic, but we propose that they are related to Palaeogene right lateral oblique-slip movements on NW-SE orientated transfer faults. Although generally of small throw these faults are important, when combined with transfer zone movements, as they appear to affect sediment and basalt and sub-basalt distribution patterns. Palaeogene tectonism culminated with significant igneous activity, including the FIBG, and the eventual opening of the North Atlantic Ocean in the earliest Eocene.

On the Faroe Islands the projected extension of the Brynhild Transfer Zone through the Sundini and Tangafjørður fjords and the Westray Transfer Zone through the Djúpini, Kalsoyarfjørður and Leirvíksfjørður fjords provides an opportunity to test the impact of the transfer zones on the eruption of the Malinstindur and Enni Formations (formerly the middle and upper basalt series of Rasmussen and Noe-Nygaard, 1970) and assess the likely compartmentalisation of lava eruption and volcaniclastic sediment transfer in the offshore zones.

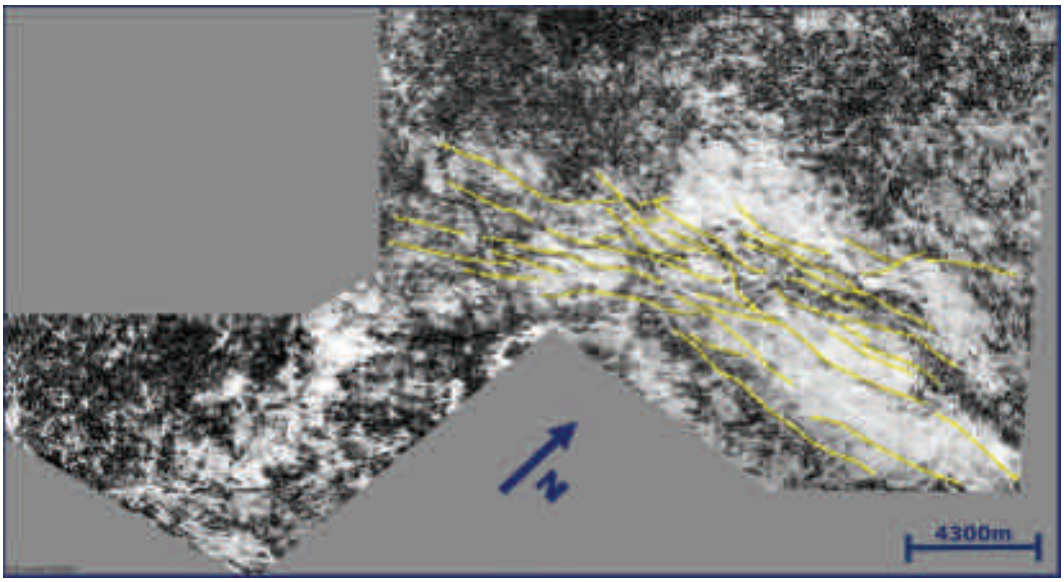

Figure 5. Seismic interpretation of a 3D 'similarity slice' southeast of the Faroes at Palaeocene sub-basalt level. Note the east-west and northeast-southwest faults.

The Faroe Islands Basalt Group

The Faroe Islands lie in the North Atlantic Ocean, midway between the Shetland Islands and Iceland at 62° N. In the reconstructed position at 57 Ma they were marginal to the spreading ocean ridge of the NE Atlantic and to the Iceland plume (Larsen *et al*., 1999; Jolley and Whitham, 2004). Due to their location adjacent to the rift the islands have drifted to the SE away from Greenland, a process that began with the eruption of flood basalt lavas over the area now occupied by the Faroe Islands. The first comprehensive study of Faroe Islands geology was published by Rasmussen and Noe-Nygaard (1970) and established a five-fold division of the lava pile including the lava-dominated lower, middle and upper basalt series (Figure 4). The authors also introduced the coal-bearing sequence and tuff-agglomerate zone for sedimentary and volcaniclastic rocks between the lower and middle basalt series. They also provided descriptions of the different lava units and an interpretation of the main inter lava units. Subsequent published studies of the geology of the islands include those of Waagstein *et al*. (1988), who utilised the presence of short intervals of normal polarity in the exposed lower basalt series to suggest a late Palaeocene age for the Faroe Islands lava pile.

With the rejuvenation of interest in Faroese geology, publications have appeared recently which consider the age of the lava field and its environments of deposition. Isotopic dating has been undertaken by Waagstein *et al*. (2002) and Riisager *et al*. (2002), but the dating has been limited by the availability of suitable material. In particular, the necessity of using whole rock techniques, with consequent experimental errors, has led to imprecision in fine detail dating of the lava field.

An alternative approach to the interpretation of Faroese geology by Ellis *et al*. (2002), compared offshore sedimentary and lava sequences to those of the Faroe Islands utilising biostratigraphy and seismic stratigraphy. Most recently, the Faroese Earth and Energy Directorate (Jarðfeingi) instigated an update of the lithostratigraphy of the Faroe Islands lava field (Passey *et al*., 2006). The review allied to a mapping programme has led to an expanded understanding of the stratigraphy and processes involved in the eruption of the lava flows and deposition of inter lava sediments (see Passey and Bell, 2007).

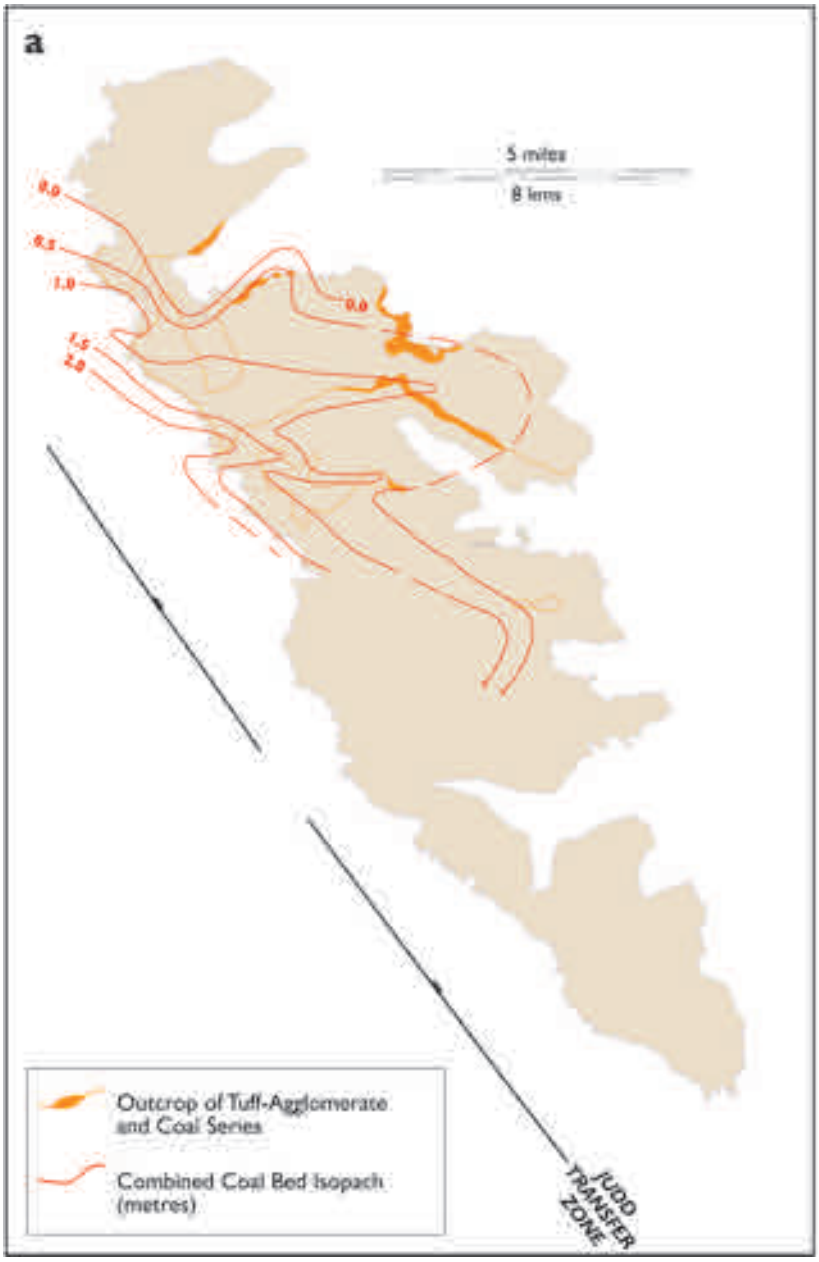

Figure 6. Total coal bed isopach data for the Prestfjall Formation on the island of Suðuroy based on data from Rasmussen and Noe-Nygaard (1970).

The Prestfjall Formation

Examination of data from the Faroese coal-bearing sequence on the island of Suðuroy (Rasmussen and Noe-Nygaard, 1970; now termed the Prestfjall Formation by Passey *et al*., 2006) allows an impact assessment of the effect of the nearby Judd Transfer Zone on the development of this formation. Isopach mapping of the coal beds of the Prestfjall Formation shows that they thicken SW towards the Judd Transfer Zone, but with also secondary development of E-W syn-depositional thins (palaeo-highs) and thicks (palaeo-lows; Figure 6). The maximum development of the coal beds of the Prestfjall Formation in the interpreted palaeo-lows

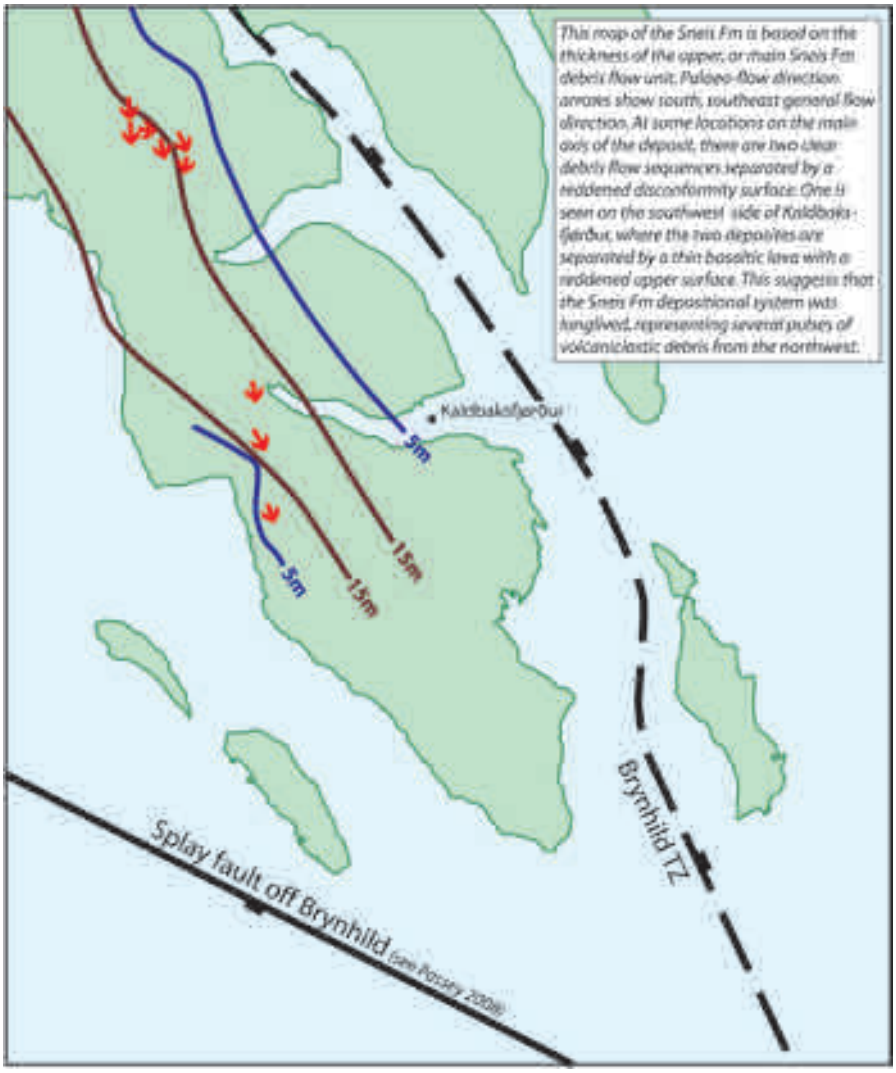

Figure 7. Conglomerate and sandstone isopach map for the Sneis Formation on southern Streymoy.

is in excess of 2 m, while palaeo-highs are defined by non-deposition or thickness development of less than 0.5 m. Discussion of this observation follows later in this paper.

Sneis Formation Mapping

The Sneis Formation, consisting of the C-horizon units of Rasmussen and Noe-Nygaard (1970, Figure 4), has been re-mapped and shown to cover a wide area comprising a complex sequence of volcaniclastic and intrusive rocks. It is composed of volcaniclastic sedimentary units derived from adjacent strata and comprises two distinct lithotypes, volcaniclastic sandstones and basaltic clast conglomerates. Flow directions are consistent to the S-SE, with the coarsest conglomeratic facies found on the slopes of Árnadalstindur (Figure 7). At some locations there are two clear debris flow sequences separated by a reddened disconformity

surface. Laterally and down palaeoflow the formation passes from coarse conglomeratic material into thinner sandstones and siltstones (Passey this volume).

Stratigraphy of the Malinstindur and Enni Formations

By establishing the Sneis Formation as a mappable datum across the Faroe Islands, it has been possible to begin to understand the detailed eruption history of the lava field and the influence of the transfer zones. To establish correlations between sections logged in the field, both volcanic and sedimentary rocks were used. Examination of the lithology and succession of these rocks allowed repeated patterns to be identified and provide the basis for correlations (Figure 8). It was possible to test the validity of these correlations by matching sedimentary inter-bed outcrop location and height to bespoke stratum datum maps produced by Jarðfeingi. In using these maps, any mismatch between the correlation and the expected outcrop height and location indicated either a miss-correlation, or the presence of a structure or fault. The correlations and the data from the stratum maps are further discussed below. The correlations that have been established from this process are most robust in the Enni Formation, and in the Malinstindur Formation immediately below the Sneis Formation (Figures 4 and 8). Older parts of the Malinstindur Formation are less well mapped, as a consequence of the often poor exposure due to their easily eroded compound flow morphology. It should be emphasized that the sedimentary inter-beds are either single events or groupings of sedimentary deposits laid down over a more extended period of time. In some cases there are clear relationships between the eruptive facies, the composition of the lavas and the nature of the sedimentary inter-beds. During the course of this research the authors have identified the following inter-bed units. The heights above and below the Sneis Formation are a guide only, as intervening lava flow thickness can vary considerably.

- Horizon SF+3: ca. 500 m above the Sneis Formation Datum.
- Horizon SF+2.5: ca. 400 m above the Sneis Formation Datum.
- Horizon SF+2: ca. 350 m above the Sneis Formation Datum.
- Horizon SF+1 (Argir Beds sequence): ca. 200-250 m above the Sneis Formation Datum across Sandoy, Hestur and Streymoy; ca. 250-350 m above the Sneis Formation Datum on Eysturoy and ca. 180-250 m above the Sneis Formation Datum across the NE islands (Figure 8).
- Horizon SF+0.5: ca. 25-50 m above the Sneis Formation Datum.
- **Sneis Formation Datum**: Base of the formation
- Horizon SF-1 (Klaksvík Beds): ca. 50-100 m below the Sneis Formation Datum (Figure 8).
- Horizon SF-2: ca. 200-300 m below the Sneis Formation Datum.
- Horizon SF-3: ca. 380 m below the Sneis Formation Datum.
- Kvívík Beds (formerly the B-horizon of Rasmussen and Noe-Nygaard 1970): ca. 600 m below the Sneis Formation Datum.

Malinstindur Formation

Underlying the Sneis Formation is the <1.4 km thick basalt lava sequence referred to as the Malinstindur Formation. Exposures of the Malinstindur Formation are extremely widespread over the Faroe Islands, stretching from Suðuroy in the south, to the north of Streymoy and onto Viðoy in the northeast. The Malinstindur Formation is characterised by thinly bedded compound lava flows composed of thinner inflated pahoehoe flow lobes (Passey and Bell, 2007). Due to the rapid eruption of the Malinstindur Formation, sedimentary deposits are largely absent from the base of the formation with the exception of the volcaniclastic strata referred to as the Kvívík Beds by Passey *et*

al. (2006). Above the Kvívík Beds the lava flows become separated by extensive inter-beds suggesting protracted weathering intervals between flows. This apparent slowing in eruption rate is critical to the understanding of the development of the Faroe Islands lava field. In one location, Lokkafelli on Eysturoy, there is evidence of early mid-successional vegetation. Here a SF-2 interbed yielded the acritarch *Micrystridium* and the pollen grain *Alnipollenites verus*. These fossils indicate a lacustrine or estuarine environment, with wet soils on a marginal floodplain. In addition support for the presence of estuarine facies in the Kalsoyarfjørður area, between the north-eastern islands of Kalsoy and Kunoy, have been recovered from samples taken from this horizon during the cutting of the Norðoyar (Eysturoy-Borðoy) subsea tunnel. Here fragments of *Apectodinium* species were recorded. This dinocyst is characteristic of brackish water facies in the region during the earliest Eocene (Jolley and Spinner, 1989). These remain the only records of this facies at the SF-2 inter-beds level. From this it can be suggested that the Kalsoyarfjørður area experienced estuarine conditions, with the flanking areas to the NE and SW remaining as actively eroding volcanic landscapes (see discussion on estuarine facies distribution in later sections).

Within the Malinstindur Formation there is evidence of control on environments and lithofacies across the Kalsoyarfjørður, Leirvíksfjørður and Djúpini fjord Westray lineament. A thick conglomeratic unit exposed in the quarry above Klaksvík on Borðoy belongs to the SF-1 inter-bed group (Klaksvík Beds), the intrusive rocks associated with the latter have previously being described as the Klaksvík Flow (Hald *et al*., 1969). This sequence is ca. 20 m in thickness on Borðoy and was mapped as a gross unit, incorporating intrusive rocks, by Hald *et al*. (1969). The "Klaksvík Flow" conglomerates are apparently absent or significantly thinner along the north-eastern side of Eysturoy, but conglomerate thicknesses up to 10 m are recorded along the south-western coastline S of Selatrað, Eysturoy (Figure 8). In general, these sedimentary inter-beds are thickest on the north-eastern sides of the presumed Westray and Brynhild transfer zones, respectively. This implies the presence of structural lows immediately adjacent to the aforementioned transfer zones.

Flattening sequences on specific marker horizons and observed bed thickness change suggests the developed 'lows', or palaeo-valleys, were not of great depth and are estimated to have a maximum depth of 80 m, probably closer to 50 m depth (Figures 8 and 9). It remains possible that these lows were caused by downwarping of pre-Sneis Formation strata across the Brynhild and Westray lineaments in response to movement along the transfer zones at depth.

During the eruption of the Malinstindur and Sneis Formations there is evidence that the land surface was relatively flat lying. A slope of $<2^{o}$ based on lava flow morphology is suggested by Passey and Bell (2007), while sedimentary inter-beds sediments similarly suggest a flat lying landscape with regional sediment movement to the S and SE.

Enni Formation

Above the Sneis Formation the lava flows of the Enni Formation show an intermixing of compound and tabular morphologies. In conjunction with this change in eruption style the character of the sedimentary inter-beds change. The sedimentary inter-beds become thicker and more complex resulting from increasing duration of inter-lava flow periods.

In the lower Enni Formation the strata thickness between the base of the Sneis Formation and the base of the SF+1 inter-bed (Argir Beds) on Streymoy is relatively constant between 200 and 250 m. This thickness is comparable to the 180 to 250 m thickness observed across the NE islands for the same interval (Figure 8a). However, from E to W across Eysturoy this interval significantly thickens to *ca.* 350 m (Figure 8a), implying a depocentre immediately adjacent the north-eastern side of the Sundini-Tangafjørður fjords (i.e. Brynhild transfer zone). The relative uplift across north-eastern Eysturoy is also confirmed by the development of finer grained sedimentary deposits of the SF+1 inter-beds (finer grained sandstones, siltstones and mudstones). This corroborates the general picture for sediment facies and thickness development

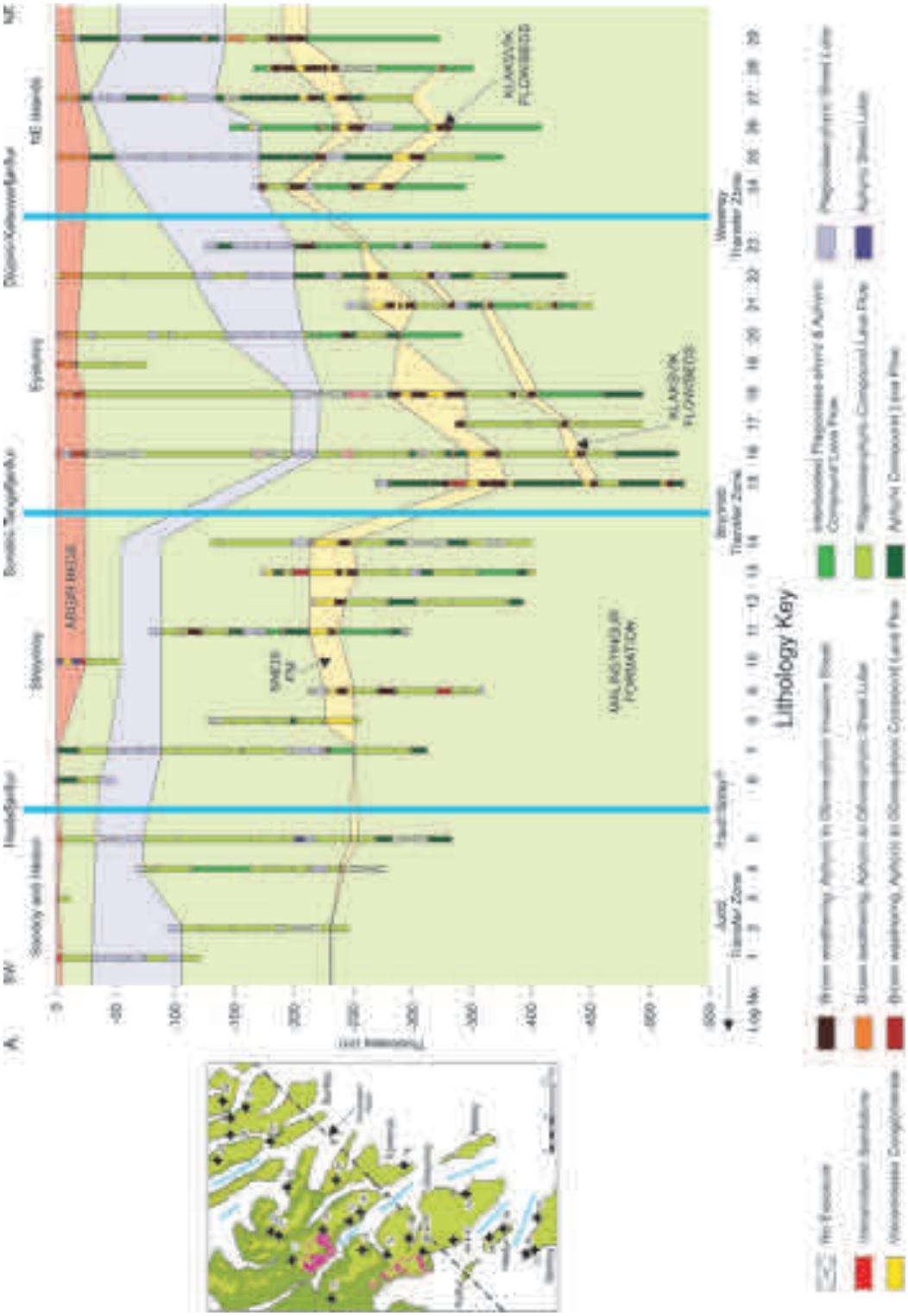
Lithology Key

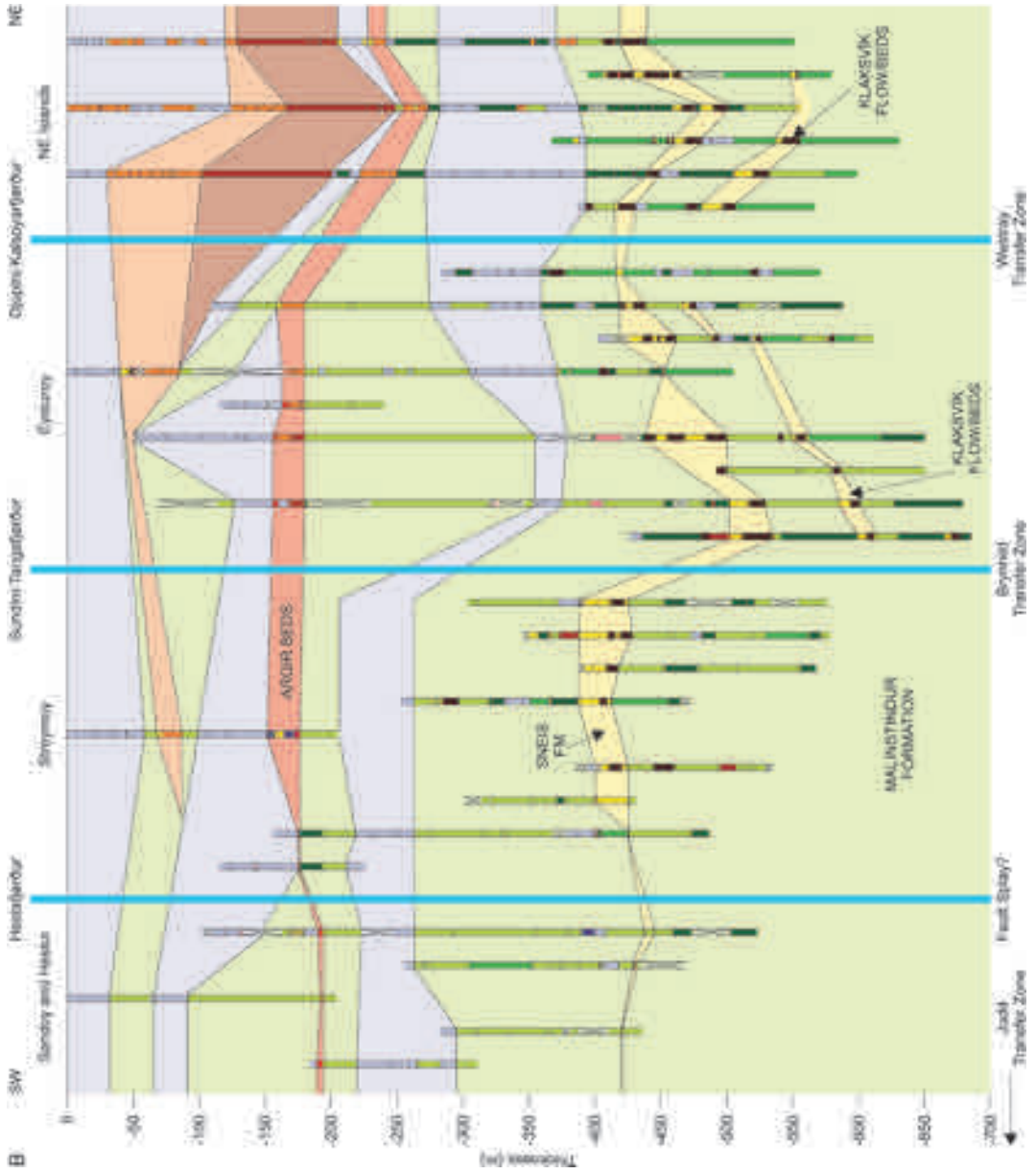

Figure 8. West to east correlation of the Malinstindur, Sneis and Enni Formations across the islands of Sandoy, Streymoy, Eysturoy, Borðoy and Viðoy. Note thickness increase on the NE side of the Brynhild and Westray transfer zones. Correlation also infers variable timing of transfer zone movements between the Judd (off to the W and left of the diagram), the Brynhild and Westray transfer zones. **a**) flattened to the top of the Argir Beds sequence consisting of volcaniclastic units (1-13 m thick; Argir Beds), which become intercalated with brown weathering, olivine-phyric lava flows towards the NE. **b**) flattened to the top of a predominantly plagioclase-phyric sheet lobe sequence. Notice how the brown weathering, olivine-phyric compound flows are restricted to the NE side of the Westray Transfer Zone and that the brown weathering, olivine-phyric sheet lobes thin across this lineament to the SW.

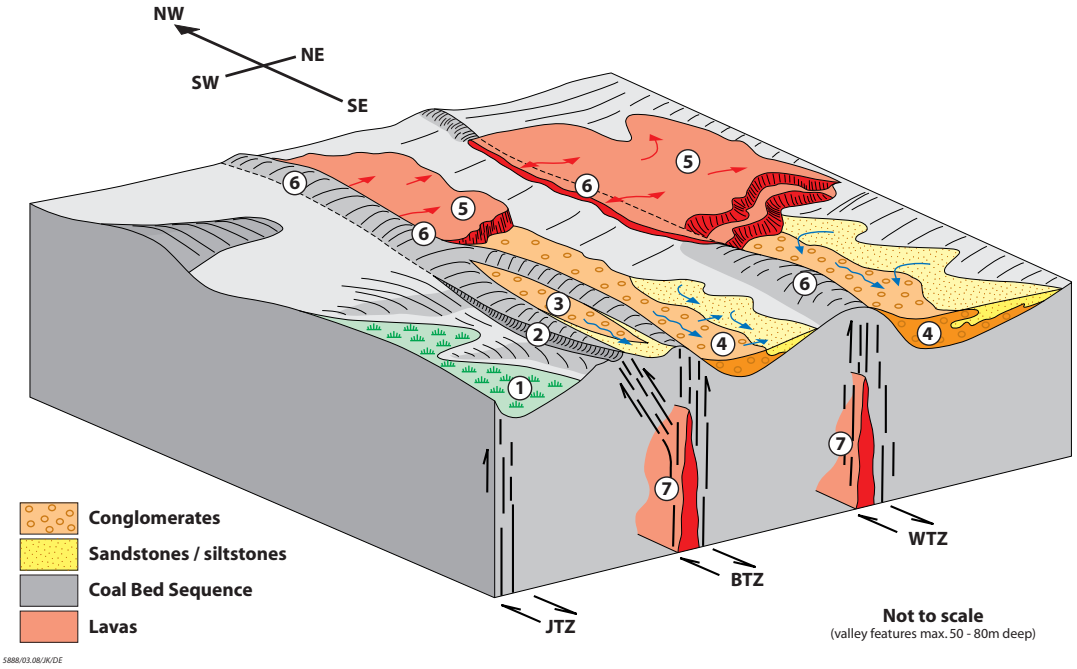

Figure 9. Interpreted effect of transfer zones (movements at depth) on the Faroe Islands Palaeocene sediment deposition and lava emplacement (see Figure 8). Note the interpreted shallow palaeo-valleys developed above the transfer zones (50-80 m deep). Maximum sedimentation and emplacement of sediments and lava is on the NE side of the transfer zones. Subsequent local development of the Sneis Formation on S Streymoy is indicated to relate to inter-action and local uplift of a spur fault off the Brynhild transfer Zone (see text). 1: Coal beds of the Prestfjall Formation thickening towards JTZ, 2: splay fault off BTZ, 3: Sneis Formation developed on southern Streymoy due to local uplift and erosion between a spur fault and the BTZ, 4: Enni Formation sediments more developed on NE side of TZs (see Figure 8), 5: lava flows more developed on NE side of TZs (see Figure 8), 7: Dyke swarms penetrating up TZs to form sills (subsurface) or lava flows (surface).

across transfer zones depicted in Figure 9. Units thicken and contain coarser grained material immediately NE of transfer zones, but thin and become finer grained with increased distance NE of the transfer zones in parallel with reduced accommodation space for sediment deposition. The Sneis Formation to SF+1 interval indicates that during this period of the FIGB development the Brynhild Transfer Zone was more influential in creating accommodation space than the Westray Transfer Zone (Figures 8 and 9).

Above the Argir Beds in the Stórafjall area in SE Eysturoy a thick SF+2 conglomerate unit is developed which is underlain by, and passes laterally eastwards into a thin sandstone (Figure 8b). This channelised conglomerate is unusual in that the foreset bedding indicates a current direction to the W (though E-W palaeo-valley orientations are observed on Suðuroy, see Figure 6). Immediately above the SF+1 (Argir Beds) the lava flows on Viðoy, Borðoy and Kunoy are brown-weathering olivine-phyric compound and tabular flows, but these are thin or absent on Eysturoy at this time (Figure 8b). This provides evidence of a barrier along the Kalsoyarfjørður, Leirvíksfjørður and Djúpini fjords. As this is the optimal route of the Westray Transfer Zone, the SF+2 conglomerates of Stórafjall suggest that the north-eastern edge of Eysturoy was uplifted with respect to the remainder of the island (Figure 9). Thus post SF+1 times the influence of the Brynhild and Judd transfer zones had declined and the Westray Transfer Zone

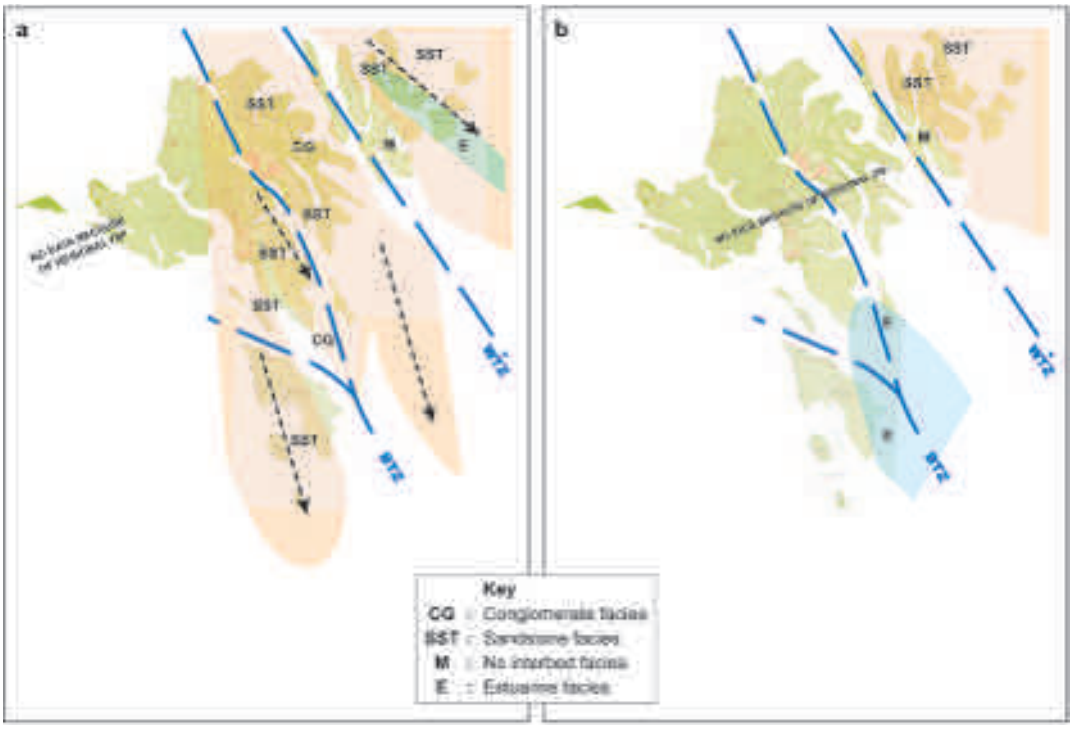

Figure 10. a) Enni Formation SF+2 interpreted facies map. **b**) Enni Formation SF+3 interpreted facies map. Note the development of estuarine facies in the locality of the Brynhild Transfer Zone (Sandoy) and the Westray Transfer Zone (Borðoy).

became dominant (Figure 8b).

Stratigraphically higher are the SF+3 sedimentary inter-bed exposures at Høsmøl on Nólsoy and close to Nólsoyarfjørður. The Nólsoy inter-beds are in two sequences separated by a 3-4 m thick brecciated amygdaloidal flow lobe. A lower sequence of claystone and siltstone with coarse sandstone alternations reaches over 8 m in thickness. The upper sequence is similar, but partly obscured by recent soils. The flora of these relatively coarse sediments is sparse and dominated by Metasequoia pollen. In samples towards the top of the lower sedimentary interval, the recovery of small *Leiosphaera* species (algae), scolecodonts (annelid worm jaws) and *Pediastrum bifidites* (chlorophycean algae) indicates a weak brackish water influence on the site of deposition. This may have been due to an estuary flooding into low-lying parts of the SF+3 lava field, thus confirming the persistence of a low relief landscape. Further to the S on the island of Sandoy, a similar thick (ca. 3.5 m) inter-bedded claystone, siltstone and sandstone inter-bed is exposed at Dalur. Here, a basaltic breccia, most likely of pyroclastic origin, is overlain by coarse sandstones, passing up into claystones and fine sandstones. These sedimentary units have poor palynofloras, although in the finer siltstone lithologies, the repeated presence of the dinocysts *Spiniferites ramosus* and *Impletosphaeridium densicomatum* indicate estuarine conditions. Taken together, the evidence from Nólsoy and Sandoy suggests that estuarine conditions persisted in the Enni Formation in the SW of the Faroe Islands and possibly following structurally controlled features parallel to the Brynhild and Westray transfer zones (Figure 10). The area now forming Streymoy and W Eysturoy may have remained emergent, but the current outcrop does not permit resolution of this issue. In the NE thin sandstones are exposed on Kunoy and Viðoy, but

we are currently lacking palynofloral data to confirm their environment of deposition. It can be suggested, however, that following on from the existence of estuarine facies in the SF+2 interbeds of Kunoy, this area continued to be low lying, with an emergent zone parallel to the Westray Transfer Zone on the eastern flank of Eysturoy.

Correlation with Offshore Wells

During the eruption of the FIBG, clastic sedimentation continued in conjunction with lava eruption over much of the western margin of the Faroe-Shetland Basin. The co-existence of floodplain and estuarine sedimentation with lavas erupted from localised vents has been documented from the Palaeocene Flett Formation (T40; Ellis *et al*., 2002; Smallwood and Maresh, 2002). Although data from exploration wells in Faroese waters is not currently in the public domain, the margin of the upper Palaeocene coastal plain can be seen in wells in UK waters, including the already documented data from well 205/9-1 (Ellis *et al*., 2002). These authors demonstrated the correlation of the palynofloras from the exposed Beinisvørð Formation (lower basalt series of Rasmussen and Noe-Nygaard, 1970) with those of the Flett Formation Unit F1b in well 205/9-1 (although the lavas in the well appear locally sourced). In addition, within this well the Flett Formation Unit 2-3 interval (Sequence T45) is characterised by a stable floodplain marsh flora dominated by *Inaperturopollenites hiatus*, associated with common *Alnipollenites verus*, and common to abundant *Caryapollenites circulus*. In wells to the south of the Corona Ridge common occurrences of *Caryapollenites inelegans* replace *C. circulus* in intra lava sediments, suggesting apparent plant adaptation to a flow top mire environment.

The importance of this Flett Formation Unit 2 regional flooding event lies in the correlation of the Faroe-Shetland Basin margin to the onshore FIBG. As a result of such a relative sea level rise, an environmental change in the FIBG to the NW would be anticipated as a consequence of base-level shift. Accordingly, the transgressive event below the Flett Formation Unit 2-3 boundary should result in the incursion of estuarine or fluvial facies into the lower-lying areas of the lava field. This marine incursion would result in estuarine facies inter-beds being deposited in the Enni Formation on Sandoy and Nólsoy (the SF+3 Interbeds). This event therefore correlates this interval with the Flett Formation Unit 2-3 boundary. The deepening of the marine Faroe-Shetland Basin environments during deposition of Flett Formation Unit 3 is a possible indication that flood lava activity was waning, accompanied by regional thermal subsidence. This represents a prelude to the phreatomagmatic activity at the rift represented by the ash bearing Balder Formation (Larsen *et al*., 2003; Jolley and Widdowson, 2005), a deposit not present in the FIBG. During this later phase of eruption the Faroe Islands area may have been emergent, or a shallow marine shelf.

A low Thermal Alteration Index (TAI) of the recovered organic walled microfossils (evaluated TAI2) suggests that relatively little has been removed from the lava pile by erosion and that burial was not significant. The palynofloras recovered from the FIBG provide a hitherto unavailable source of evidence pertaining to the structural evolution of the area. From the initial progradation of the hyaloclastite delta of the Lopra Formation (Ellis *et al*., 2002), to the intra lava floras of the Enni Formation, the palynofloras provide evidence of a terrain dissected by fluvial channels inundated periodically by marine estuarine incursions geographically controlled by local NW-SE lineaments (transfer zones). Significant palaeo-topography is implied by the presence of mass flow sediments, but the absence of an upland flora mitigates against the presence of high altitude terrain. Changes in relative sea level in the Faroe-Shetland Basin are reflected in the intra lava strata of the Faroe Islands. These introduce estuarine floras into the fluvial systems and provide points of correlation with Faroe-Shetland Basin sequences.

Discussion on the influence of associated transfer zone tectonics on Palaeocene Faroe Islands development onshore and offshore

With completion of the new mapping it is possible to equate the development of the FIBG with re-

gional tectonics and the influence of movements along NW-SE orientated transfer zones.

Detailed mapping and correlation of units within the Sneis, Malinstindur and Enni Formations has established the presence of the Brynhild and Westray transfer zones in the Faroe Islands. The Brynhild Transfer zone is located along the NW-SE line of the Sundini and Tangafjørður fjords and the Westray Transfer Zone NW-SE through the Kalsoyarfjørður, Leirvíksfjørður and Djúpini fjords (Figures 4 and 8). Across these transfer zones units of lavas and sediments can be demonstrated to thicken along the NE side of the transfer zones, though mapping of individual beds indicates only gentle warping and thickening across the transfer zones at any one time (Figures 8 and 9). The depth of palaeo-accommodation space along the NE side of the transfer zones is estimated 50-80 m maximum based on individual bed geometries. Therefore, the increased thickness of units NE across the transfer zones must be the result of continuous and not pronounced vertical and horizontal movements long the transfer zones to give a cumulative effect.

Evidence for the presence of the Judd Transfer Zone is less available as it is prognosed to lie just SW and offshore the island of Suðuroy. However, similar evidence to that observed across the Brynhild and Westray transfer zones is observed for the coal beds of the Prestfjall Formation that thicken towards the fracture zone (i.e. on the transfer zones NE side; Figure 6).

Figure 11 shows the geological map of the island of Suðuroy with the mapped fractures, some containing basaltic dykes, from Rasmussen and Noe-Nygaard (1970). Fractures can be observed NW-SE (parallel the offshore Judd Transfer Zone to the SW), but also E-W and NE-SW. Figure 12a (redrawn from Figure 6) shows the isopach data for the combined coal bed thickness from the Prestfjall Formation, the deposition of which is dictated by the E-W palaeo-highs and lows. Figure 12b shows the interpreted structural control placed on the coal bed isopach by observation of the mapped fractures. Examination of the stress ellipsoid associated with right lateral oblique-slip (transpressional) movements along the Judd and Brynhild transfer zones would create the observed E-W and NE-SW orientated faults and fractures (de Paola *et al*., 2005 and Figure 12b). Spacing and orientation of the fractures is consistent with observed Palaeocene fractures mapped offshore the Faroe Islands (Figure 5).

The interpreted Faroe Islands structural pattern by application of the structural model from Suðuroy (Figure 12b), observation of the mapped fractures (Rasmussen and Noe-Nygaard, 1970), and the stress ellipsoid associated with right lateral oblique-slip (transpressional) movements along NW-SE transfer faults is shown in Figure 13. The resultant tectonic map was tested during the remapping of the Faroe Islands. To date E-W and NE-SW faults at Gjógv and Eiði on N Eysturoy and Leynar on SW Streymoy indicate confirmatory evidence for the tectonic model by demonstrating oblique-slip or strike-slip movements with minimal or no vertical offset (to be the subject of future publications). The faults die out vertically within the volcanic pile and again mirror offshore 3D seismic Palaeocene fault mapping which indicates many intra-Palaeocene faults do not penetrate the upper Palaeocene marker surface.

Observed widths of the transfer zones are variable. The Brynhild Transfer Zone has a very narrow width and equates approximately to the width of the Sundini-Tangafjørður fjords, averaging 1-2 km (Figures 4 and 13). The Westray Transfer Zone appears substantially wider, extending from the NE margins of Eysturoy to Klaksvík on the island of Borðoy (Figures 4 and 13). This equates to an average width of 5 km for the transfer zone. The long and narrow island of Kalsoy, surrounded by the Kalsoyarfjørður, Leirvíksfjørður and Djúpini fjords, is currently interpreted to be sliver of rock units trapped within the NW-SE transfer zone (Figures 4 and 13). Future fieldwork on Kalsoy may constrain its development during the activity of the Westray transfer zone.

An interesting observation is also noted in association with the Brynhild Transfer Zone in the area of Sandoy. Here displacement of the Sneis and Enni strata between Hestur and Sandoy is clearly demonstrated by plotting the elevation of the Sneis Formation, Argir Beds (SF+1 interbeds) and the prominent Høvdhamarin Flow within the underlying Enni Formation (Figure 7; Passey, this vol-

Figure 11. Geological map of Suðuroy with mapped fractures (from Rasmussen and Noe-Nygaard, 1970).

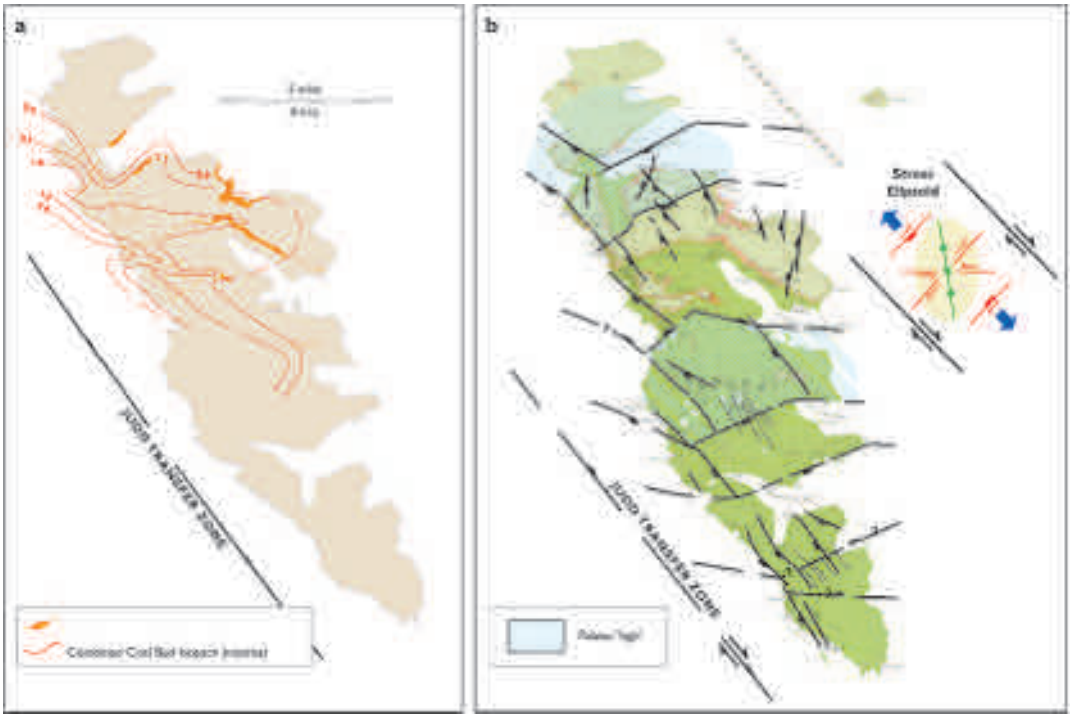

Figure 12. a) Total coal bed isopach data for the Prestfjall Formation on the island of Suðuroy based on data from Rasmussen and Noe-Nygaard (1970). Redrawn from Figure 6. **b**) Syn-sedimentary structural interpretation placed on the coal bed isopach map combined with the mapped fractures and predicted right lateral oblique-slip movements due to NW-SE extension constrained by NW-SE orientated transfer faults.

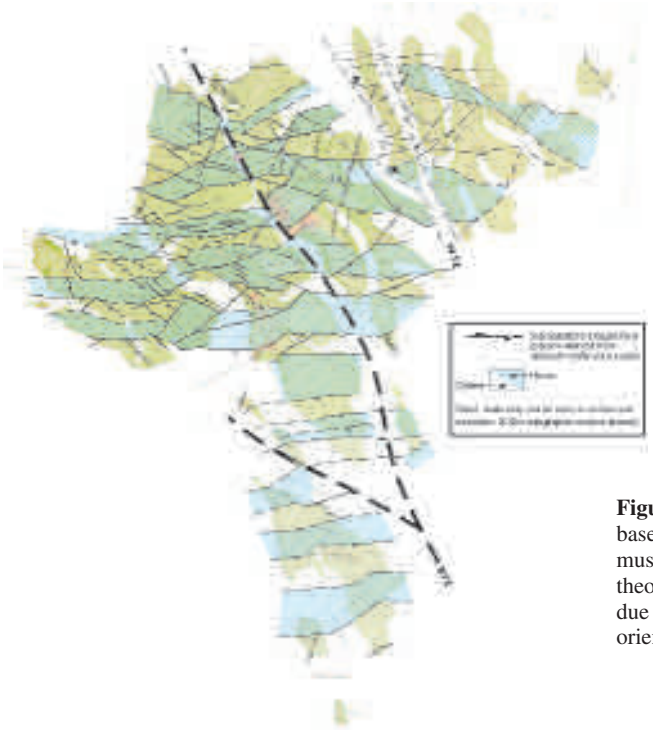

Figure 13. Interpreted Faroe Islands tectonic map based on the mapped fractures and dykes of Rasmussen and Noe-Nygaard (1970) and applying theoretical right lateral oblique-slip movements due to NW-SE extension constrained by NW-SE orientated transfer faults.

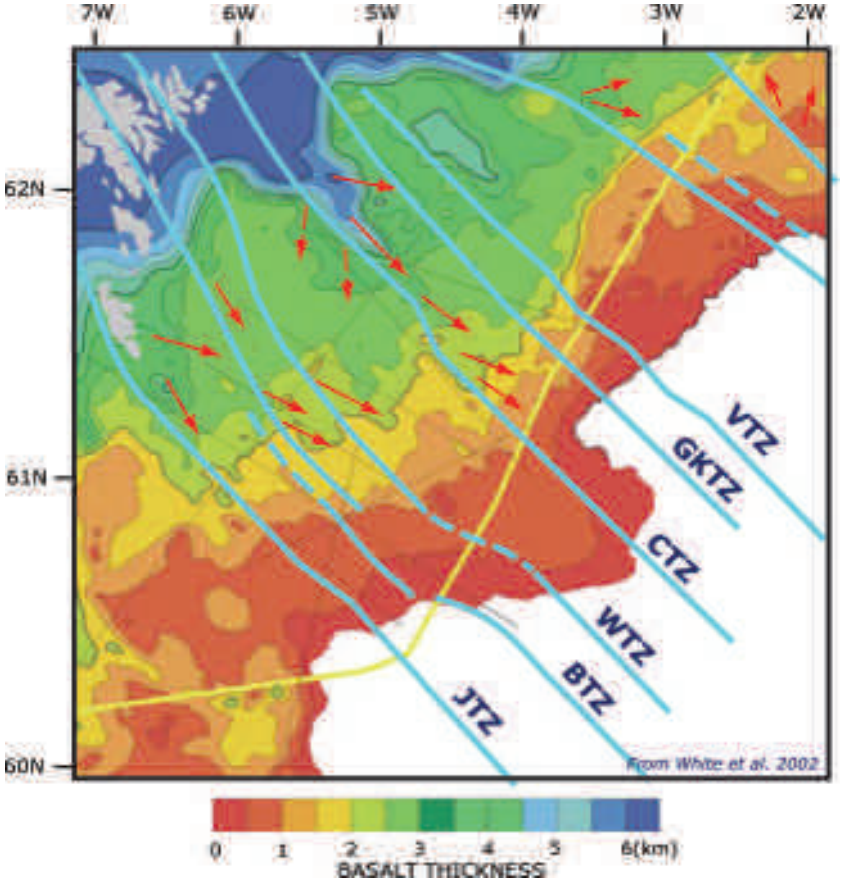

Figure 14. Faroe-Shetland Basin regional basalt isopach map (White *et al*., 2003). Note development of increased thickness adjacent and northeast of several transfer zones.

ume). Thickness and facies within these units does not change between Sandoy and Streymoy indicating that the displacement down to the SW took place after deposition of the Argir Beds. This is currently a rare example of significant fault displacement between islands and the mapped stratigraphy (Passey, this volume). The fault is interpreted to be a splay fault off the Brynhild Transfer Zone (Figures 7 and 9). The presence of this fault at depth and before final failure could also have influenced the deposition of the Sneis Formation on southern Streymoy. Continued transpression along the Brynhild and the spur fracture would have resulted in local compression and uplift between the two fracture systems (de Paola *et al*., 2005). Orientation of the minor anticlinal uplift would be N-S and erosion of the crestal area was later exploited by deposition of the Sneis Formation in this area (Figure 9).

The location of the estuarine facies indicators is of significance. Confirmation of these periods of estuarine facies geographically located along the prognosed and now confirmed transfer zones highlights the role of these lineaments as sediment conduits. These pathways for sediment transfer from the shelf to the Faroe-Shetland Basins would have operated for the duration of the lava field activity. Longevity of these structures would also have resulted in the supply of non-volcanic sediment to the south and southeast into the Faroe-Shetland basins prior to the initiation of lava field activity in the late Palaeocene (Lamers and Carmichael,

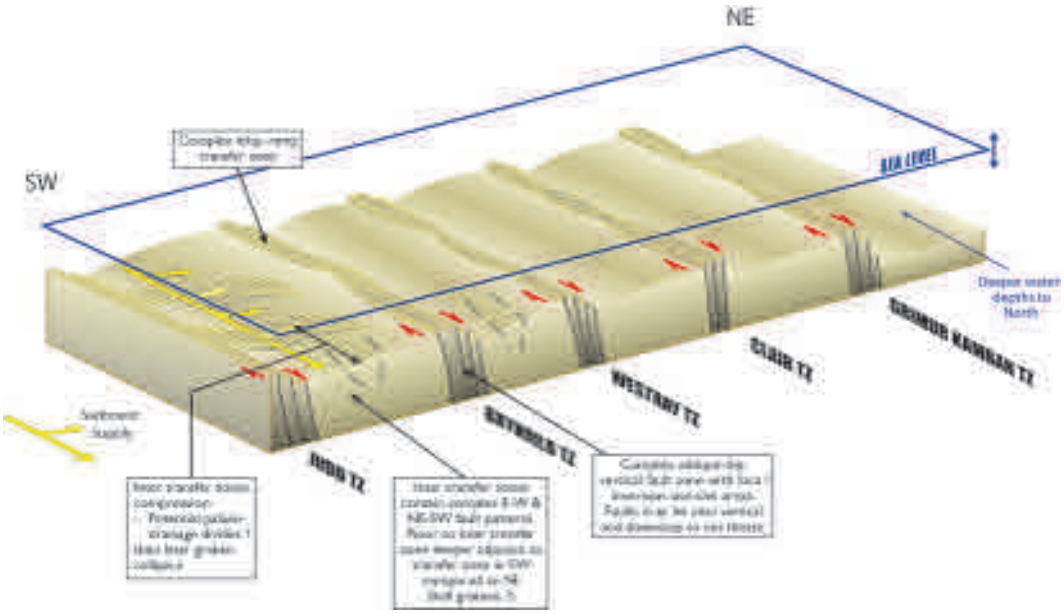

Figure 15. Conceptual model for transfer zone influence on Palaeocene Faroe-Shetland Basin topography. Note the progressive deepening of the basin to the NE across successive transfer zones and increased accommodation space on the NE side of each transfer zone, as implied by onshore Faroe Islands mapping and offshore UK well penetrations.

1999; Grant *et al*., 1999; Ellis *et al*., 2002).

With reference to Figures 4 and 13 it can be observed the Streymoy and Eysturoy sill complexes are bisected by the Brynhild Transfer Zone. The sills have a tendency of flattening out within the conglomerates and sandstones of the Sneis Formation and the conglomerates and sandstones of the Klaksvík Beds are similarly injected by intrusive material in close association with the Brynhild and Westray transfer zones. Taken with the evidence that some lava flows are more developed on one side of the transfer zones than the other (Figures 8 and 9), it can be surmised the transfer zones have acted as major conduits for vertical movement of igneous material as either sills (subsurface) or lava flow development (surface expression). With reference to the gross regional isopach for Palaeocene lava development it can be seen that thicker lava sequences develop predominantly on the north-eastern side of regional transfer zones (Figure 14; after White *et al*., 2003). From the evidence observed on the Faroe Islands and presented in this paper the current authors speculate that Palaeocene subsurface igneous material injected along the transfer zones from a local SE Greenland plume to spread deep into the offshore Faroe-Shetland Basins to create local igneous centres (e.g. the Erlend igneous complex close to the Erlend Transfer Zone, Figure 1), and/or intersect major NE-SW faults bounding intra-basin highs to create major igneous outpourings that spread out laterally to cover much of the Faroe-Shetland area. As Atlantic rifting progressed, the igneous source centres retracted NW towards the developing ocean ridge, thereby denying the outer margins of the area access to igneous activity but allowing the continuing build-up of the Palaeocene lava 'wedge' closer to the main rift as the Atlantic developed (Figure 14).

Based on the results from this study and other offshore observations a conceptual transfer zone model is shown in Figure 15. It also suggests general deepening of the Faroe-Shetland Basin to the northeast across successive transfer zones as observed from Palaeocene well penetrations in the UK sector.

Conclusions

1) New field mapping of the Faroes Islands Basalt Group has provided evidence to support regional extension of the Judd, Brynhild (proposed in this paper) and Westray transfer zones into the Faroe Islands.
2) The lava pile can be demonstrated to thin southeast from onshore the Faroes to the offshore, with the proportion of volcaniclastic sedimentary material in proportion to lava flows expected to increase to the south and southeast.
3) The thickest development of the Faroe Island Basalt Group and its inter-bedded sediments is adjacent to the NE sides of the Judd, Brynhild and Westray transfer zones.
4) A structural model is proposed based on right lateral transpressive oblique-slip movements along the major transfer zones in conjunction with northwest-southeast regional extension during Palaeocene development of the Faroe-Shetland area.
5) Local evidence from the Faroe Islands indicates a close relationship between igneous subsurface (sill) and surface (lava) activity and transfer zones. The authors surmise that offshore transfer zones have played significant roles in the development of the overall Palaeocene igneous activity of the Faroe-Shetland area.

Acknowledgements

This paper is the result of cooperation between the Statoil led Faroes Licence 006 Group, the University of Aberdeen, the University of Glasgow and most importantly the Faroese Earth and Energy Directorate (Jarðfeingi) who did much of the field mapping. Permission to publish is gratefully acknowledged from the Statoil Faroes Licence 006 Group who comprises representatives from Shell, DONG, Faroe Petroleum and Atlantic Petroleum. The manuscript benefited from constructive comments from Dr G. Smith (University of New Mexico). This study was funded under Faroes Licence 006 Annex 2 commitments.

References

Doré, A.G. and Gage, M.S. 1987. Crustal alignments and sedimentary domains in the evolution of the North Sea, Northeast Atlantic margin and the Barents Shelf. *In*: Brooks, J. and Glennie, K.W. (eds) *Petroleum Geology of Northwest Europe*. Graham and Trotman, London: 1131-1148.

Doré, A.G., Lundin, E.R., Jensen, L.N., Birkeland, Ø., Eliassen, P.E., and Fichler, C. 1999. Principal tectonic events in the evolution of the northwest European margin. *In*: Fleet, A.J. and Boldy, S.A.R. (eds) *Petroleum Geology of Northwest Europe: Proceedings of the 5th Conference*. The Geological Society, London: 41-62.

Ellis, D., Bell, B.R., Jolley, D.W. & O'Callaghan, M. 2002. The stratigraphy, environment of eruption and age of the Faroes Lava Group, NE Atlantic Ocean. *In*: Jolley. D.W. and Bell, B.R. (eds) *The North Atlantic Igneous Province: Stratigraphy, Tectonic, Volcanic and Magmatic Processes*. Geological Society of London, Special Publication 197: 253-270.

Grant, N., Bouma A. and McIntyre, A. 1999. The Turonian play in the Faroe-Shetland Basin. *In*: Fleet, A.J. and Boldy, S.A.R. (eds) *Petroleum Geology of Northwest Europe: Proceedings of the 5th Conference*. Geological Society, London: 661-673.

Hald, N., Noe-Nygaard, A. and Waagstein, R. 1969. On extrusion forms in plateau basalts. 2. The Klakksvik flow, Faeroe Islands. *Meddelelser Dansk Geologisk Forening, Kobenhavn* Bind 19: 2-7.

Jolley, D.W. and Morton, A. 2007. Understanding basin sedimentary provenance: evidence from allied phytogeographic and heavy mineral analysis of the Paleocene of the NE Atlantic. *Journal of the Geological Society, London* 164: 553-563.

Jolley, D.W. and Spinner, E.G., 1989. > Some Dinoflagellate Cysts from the London Clay (Palaeocene - Eocene) near Ipswich, Suffolk, England. > *Review of Palaeobotany & Palynology* 60: 361-373.

Jolley, D.W. and Widdowson M. 2005. North Atlantic rift eruptions drive Eocene climate cooling. *Lithos* 79: 355-366.

Jolley, D.W. and Whitham A.G. 2004. A stratigraphical and palaeoenvironmental analysis of the sub-basaltic Paleogene sediments of East Greenland. *Petroleum Geology* 10: 53-60.

Keser Neish, J. 2004. Faroese Region: A Standard Structural Nomenclature System. Jarðfrøðisavnið (Faroese Geological Survey), Tórshavn: p. 66.

Lamers, E. and Carmichael, S.M.M. 1999. The Paleocene deepwater sandstone play West of Shetland. *In*: Fleet, A.J. and Boldy, S.A.R. (eds) *Petroleum Geology of the Northwest Europe: Proceedings of the 5th Conference*. Geological Society, London: 645-660.

Larsen L.M., Fitton, J.G., and Pedersen, A.K. 2003. Pa-

leogene volcanic ash layers in the Danish Basin: compositions and source areas in the North Atlantic Igneous Province. *Lithos* 71: 47-80.

Larsen, M.L., Waagstein, R., Pedersen, A.K.M. and Storey, M. 1999. Trans Atlantic correlation of the Palaeogene volcanic successions in the Faeroe Islands and East Greenland. *Journal of the Geological Society, London* 156: 1081-1095.

Naylor, P.H., Bell, B.R., Jolley, D.W., Durnall, P. and Fredsted, R. 1999. Palaeogene magmatism in the Faeroe-Shetland Basin: influences on uplift history and sedimentation. *In*: Fleet, A.J. and Boldy, S.A.R. (eds) *Petroleum Geology of the Northwest Europe: Proceedings of the 5th Conference*. Geological Society, London: 545-558.

Passey, S.R. 2008. Recognition of a faulted basalt lava flow sequence through the correlation of stratigraphic marker units, Skopunarfjørður, Faroe Islands. *Faroe Islands Exploration Conference: Proceedings of the 2nd Conference*. *Annales Societatis Scientiarum Færoensis* (this volume).

Passey, S.R. and Bell, B.R. 2007. Morphologies and emplacement mechanisms of the lava flows of the Faroe Islands Basalt Group, Faroe Islands, NE Atlantic Ocean. *Bulletin of Volcanology* 70: 139-156.

Passey S.R., Jolley, D.W. and Bell B.R. (2006). Lithostratigraphic framework for the Faroe Islands Basalt Group, NE Atlantic. *A George P.L. Walker symposium on advances in volcanology, 12-17 June*. Reykholt, Iceland

De Paola, N., Holdsworth, R.E., McCaffrey, K.J.W. and Barchi, M.R., 2005. *Journal of Structural Geology* 27 (4): 607-625.

Riisager, P., Riisager, J., Abrahamsen, N., and Waagstein, R. 2002. New paleomagnetic pole and magnetostratigraphy of Faroe Islands flood volcanics, North Atlantic igneous province. *Earth and Planetary Science Letters* 201: 261-276.

Rasmussen, J. and Noe-Nygaard, A. 1970. Geology of the Faeroe Islands. *Danmarks Geologiske Undersøgelse* 1: 25.

Rumph, B., Reaves, C.M., Orange, V.G. and Robinson, D.L. 1993. Structuring and transfer zones in the Faeroe basin in a regional tectonic context. *In*: Parker, J.R. (ed) *Petroleum Geology of Northwest Europe: Proceedings of the 4th Conference*. Geological Society, London: 999-1010.

Waagstein, R., 1988. Structure, composition and age of the Faroe basalt plateau. *In*: Morton, A.C. and Parson, L.M. (eds) *Early Tertiary Volcanism and the Opening of the NE Atlantic*. Geological Society, London, Special Publication 39: 225-238.

Waagstein, R., Guise, P. D Rex, D. 2002. K/Ar and Ar/Ar whole-rock dating of zeolite facies metamorphosed flood basalts; the upper Paleocene basalts of the Faroe Islands, NE Atlantic. *In*: Jolley, D.W. and Bell, B.R. (eds) *The North Atlantic Igneous Province: Stratigraphy, Tectonic, Volcanic and Magmatic Processes*. Geological Society, London, Special Publication 197: 219-252.

White R.S., Smallwood, J.R., Fliedner, M.M., Boslaugh, B., Maresh, J., and Fruehn, J. 2003. Imaging and regional distribution of basalt flows in the Faroe-Shetland Basin. *Geophysical Prospecting* 51: 215-231.

Reservoir quality assessment of the volcaniclastic post-basalt sediments in the Faroese area of the Faroe-Shetland Basin

JANA ÓLAVSDÓTTIR* AND HERI ZISKA

* Jarðfeingi (Faroese Earth and Energy Directorate), Brekkutún 1, Postbox 3059, FO-110 Tórshavn, Faroe Islands – E-mail: jana.olavsdottir@jardfeingi.fo; Tel: +298 357031; Fax +298 357001

ABSTRACT

In the last decade, the Faroese sector of the Faroe-Shetland Basin, northeast Atlantic margin, has been an area of increased interest in terms of hydrocarbon exploration. During this time, the main focus has been on sediments beneath the Palaeocene-Eocene flood basalts, which cover most of the Faroese Continental Shelf. Discoveries have, however, been made in the post-basalt succession in the UK sector of the Faroe-Shetland Basin. Consequently, this study is focused on the predicted reservoir quality of the post-basalt sediments in the Faroese sector of the basin.

The post-basalt sediments in the Faroese area of the Faroe-Shetland Basin are poorly understood, especially in relation to their provenance. Most of the literature that exists about the post-basalt sediments in the basin shows sediment being deposited from the S to SE (the NW British shelf area). These sediments are of siliciclastic origin and have been shown to be of a very good reservoir quality. However, this study shows that sediment has also been derived from the Faroese Platform and the Munkagrunnur Ridge. Both of these structures are wholly made up of basaltic material; this sediment derived from these source areas will be of volcaniclastic composition.

Whereas siliciclastic material is known to have very good reservoir quality at the burial depths of the post-basalt sequence, the reservoir quality of volcaniclastic sediments has been reported to deteriorate faster than in siliciclastic deposits. We will discuss this issue, and show what kind of depths we expect volcaniclastic rocks to be of useful reservoir quality in relation to the burial depths of the post-basalt sequence in the Faroe Shetland Basin. By considering the development of three prograding sediment sequences of Eocene to Miocene age, we highlight the mixed provenance of the post-basalt infill of the Faroe-Shetland Basin, and assess the kind of depths within the basin that we can expect volcaniclastic rocks to be of useful reservoir quality. From this study we conclude that the post-basalt sandstone in the Faroese area of the Faroe-Shetland Basin could be a prospective reservoir in the future.

Introduction

Exploration in the Faroe Shetland Basin was initially focused on structural plays on the south-eastern flank of the basin. This effort resulted in discoveries in Palaeozoic and Mesozoic rocks, with the target stratigraphy becoming increasingly younger into the axis of the basin (Lamers and Carmichael, 1999). The youngest prospective section in the Faroe-Shetland Basin consists of Middle Eocene deep water fans in the central part of the basin (Davies et al., 2004). As exploration moved onto the Faroe Continental Shelf, the focus was primarily on the Paleocene sequence, with sub-Tertiary targets of secondary importance. The post-basalt sequence was not targeted at all in the early phases of exploration. One reason for this might be the expected influence of volcaniclastic rocks, which can have a negative effect on reservoir qualities.

This paper will focus on the reservoir quality of the post-basalt sequence. We firstly describe three Eocene to Miocene age, prograding sedimentary

Faroe Islands Exploration Conference: Proceedings of the 2nd Conference.
Annales Societatis Scientiarum Færoensis, Supplementum 50, 2009: 227-240

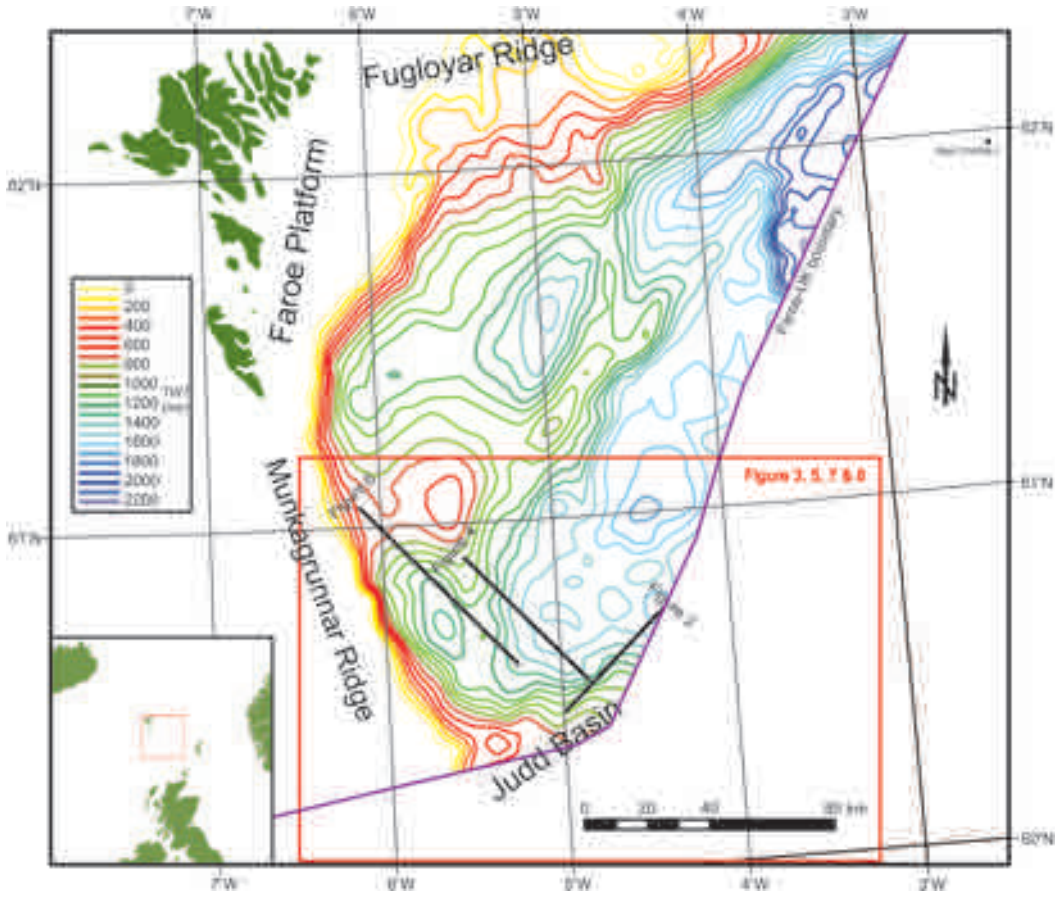

Figure 1. Map showing the thickness (milliseconds, TWT) of the post-basalt succession in the Faroe sector of the Faroe-Shetland Basin. The succession is thickest in the NE part of the area with a maximum thickness of about 2000 ms. Inset map shows the regional location of the study area.

units that we have mapped in order to demonstrate the mixed provenance of the basin fill. We then discuss various the issues relating to reservoir parameters in areas influenced by volcanic detritus, from which we draw same conclusions regarding the potential reservoir quality of the post-basalt volcaniclastic sediment unit in the Faroe-Shetland Basin.

Geological setting

The study area is located between the Shetland and Faroe islands in the Faroe sector of the modern-day Faroe-Shetland Channel (Figure 1). This is an elongate, NE-SW trending basin up to 200 km wide, and deepens from about 1000 m in the SW to about 1700 m in the NE where the Faroe-Shetland Channel enters the Norwegian Basin. The Faroe-Shetland Basin lies beneath the Faroe-Shetland Channel, and has been a major depocentre since the Late Palaeozoic (Doré et al., 1999; Knott et al., 1993; Roberts et al., 1999; Ziegler, 1989).

The most recent development of the Faroe-Shetland Basin is related to processes involved with the separation of Greenland and NW Europe, and the onset of sea-floor spreading and development of the NE Atlantic Ocean in Late Paleocene-Early Eocene time. This was

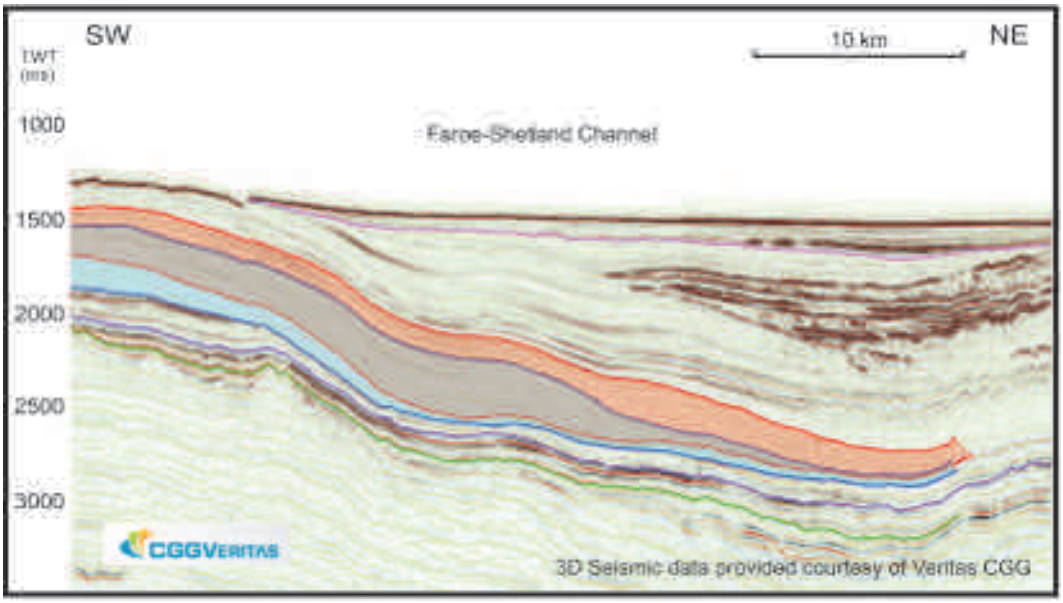

Figure 2. Seismic profile showing a NE aggrading unit. The blue area is interpreted as the NE aggrading unit. The read area is the NW prograding unit. The interpreted green line is the top of the basalt, the dark purple line is the top of Balder Formation and the light purple line is the Miocene unconformity. Profile located in Figures 1 and 3.

accompanied by extensive volcanism that was extruded over a large part of the Faroe-Rockall area, and which forms a significant component of the Faroe Islands and its continental shelf (Boldreel and Andersen, 1995; Boldreel and Andersen, 1993; Passey and Bell, 2007; Waagstein, 1988)

Hot-spot-related uplift of the Faroe-Shetland region immediately prior to break-up gave way to thermal subsidence as sea-floor spreading was initiated. However, compression generated by ridge-push processes in the developing ocean is envisaged to have been responsible for the uplift of the Munkagrunnur, Wyville Thomson and Ymir Ridge between late Paleocene/early Eocene to Miocene time (Boldreel and Andersen, 1995; Boldreel and Andersen, 1993). This is disputed by (Ziska et al., In Press)) who suggest that a transient rifting episode in the early Paleocene was heavily influential in the creation of these mentioned ridges, and that the later compressive phases augmented simply and reorganised these pre-existing features (Ziska and Varming. In Press). The development of the Munkagrunnar and Wyville-Thomson Ridge are especially enhanced during the Miocene (Stoker et al., 2005), with localised uplift in the Faroe-Shetland Basin into the Plio-Pleistocene (Johnson *et al*., 2005).

In terms of sedimentation, the sea transgressed southwestwards into the Faroe-Shetland Basin in the latest Palaeocene – earliest Eocene as the area underwent thermal subsidence (Dean *et al*., 1999). A series of shelf margin prograding systems build out into the Faroe-Shetland Basin through the Eocene, including a numbers of deepwater fans (Andersen *et al*., 2000; Davies *et al*., 2004). A significant deepening of the Faroe-Shetland Basin occurred in late Eocene-early Oligocene time, which was fully accentuated by compression in the early Miocene, that led to the deepwater gateway of the Faroe-Shetland and Faroe Bank Channels, and which provides a deepwater connection between the Norwegian and Iceland basins (Stoker *et al*., 2005). Initially vigorous bottom water circulation in the Faroe-Shetland Basin caused widespread erosion including the formation of the

Munkagrunnar fall (Stoker *et al*., 1993; Stoker *et al*., 2005). However the deep-water current system stabilised, bottom current have played an important role in eroding and depositing sediments throughout the Neogene. Because of this process, the cover of Neogene sediments is of variable thickness. In the central part of the basin, the Neogene deposits are thin or absent due to a very low deposition rate or local erosion of the seafloor (Boldreel and Andersen, 1995). In contrast, Plio-Pleistocene glaciation result in the renewed build-out of the Faroe continental shelf through a series of prograding fans (Nielsen *et al*., 2005).

Post-basalt sediment input directions and provenance areas

The post-basalt sediments in the Faroese sector of the Faroe-Shetland Basin have thus far only been mapped as a single succession; no detailed mapping of the individual sequences has yet been establishes on the regional basis. However detailed mapping in the southwestern part of the basin has revealed several large prograding/aggrading systems from different locations into the basin. These prograding/aggrading systems have different provenance areas, which, by implication, we infer them to have different sediment composition. The Munkagrunnur Ridge, Faroe Platform and Fugloyar Ridge (Figure 1) are covered by the flood basalts of the Faroe Islands Basalt Group, which means that material eroded from these structures will have a volcaniclastic composition. In contrast sediments originating on the NW British shelf area are likely to be of siliciclastic composition.

In the following sections we briefly describe three different prograding and aggrading systems out into the Faroe-Shetland Basin. We have informally named these the NE aggrading unit, the NW and SE prograding units. The aim of having examples is to highlight both the variable sediment in-

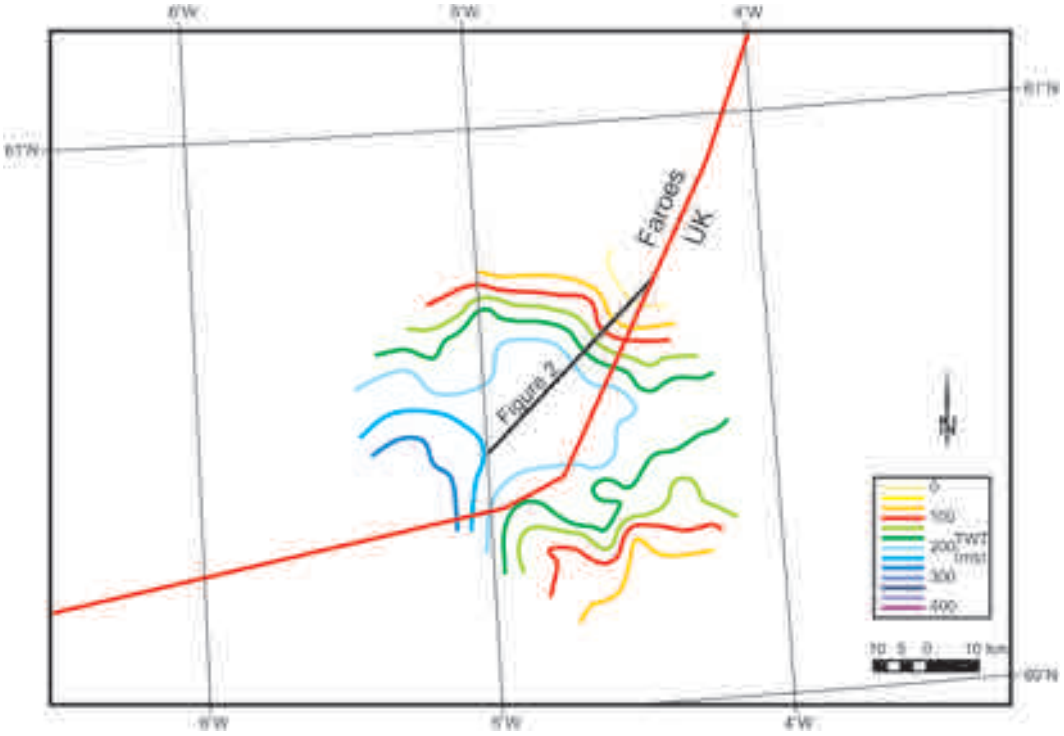

Figure 3. Map showing thickness (milliseconds, TWT) of the NE aggrading unit. Black line shows location of profile in Figure 2.

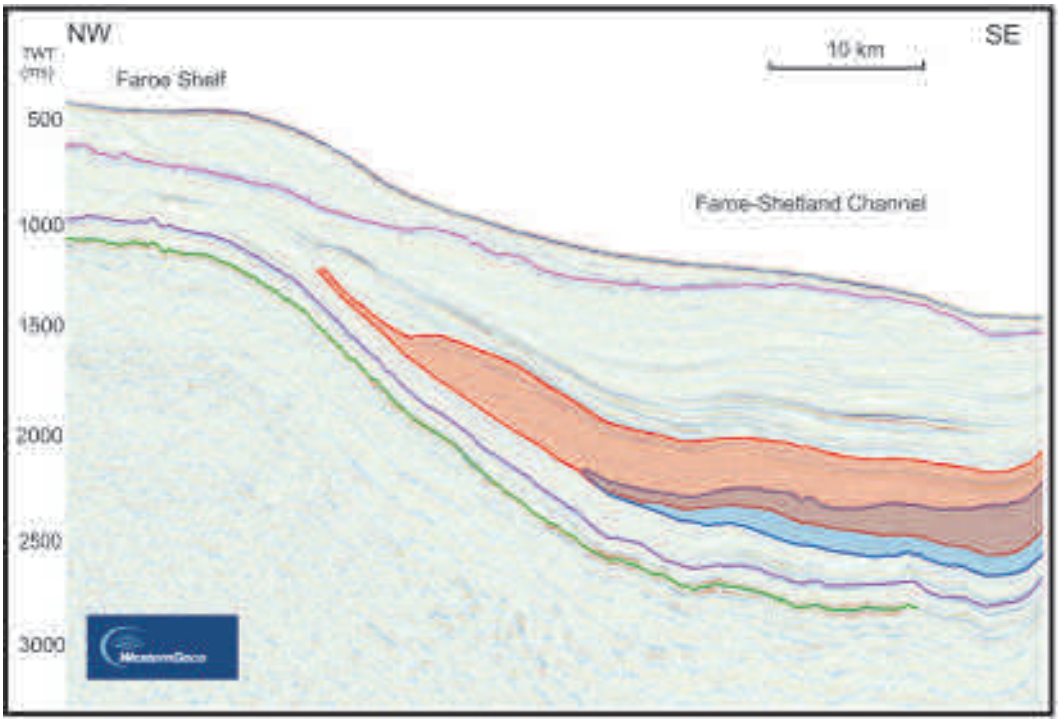

Figure 4. Seismic profile showing a NW prograding unit. The red area is interpreted as the NW prograding unit and the blue area is interpreted as the NE aggrading unit. The interpreted green line is the top of the basalt, the dark purple line is the top of Balder Formation and the light purple line is the Miocene unconformity. Profile located in Figure 1 and 5.

put directions, and the variable depth of the prograding/aggrading system in the post-basalt succession. The later has implications for processes of diagenesis, which we discuss later in the paper.

Thickness and depth of the post-basalt sedimentary units is inferred using average velocity of 2240 m/s (Stoker *et al*., 1993). Since the maximum time thickness of the post-basalt sediments is approximately 2 sec two-way travel time (TWT) the maximum thickness of post-basalt sediments is about 2240 m (Figure 1), so the maximum burial depth of any post-basalt sequence is 2240 m.

NE aggrading unit

The NE aggrading unit has not been dated but it is located immediately above the Balder Formation in the SW part of the Faroe-Shetland Basin (Figure 2 and 3). The Balder Formation is of Early Eocene age (Ebdon *et al*., 1995), this means that the NE aggrading unit is of Early to Middle Eocene age or younger.

The source area for the NE aggrading unit is Munkagrunnar Ridge, which means that it most likely consists of volcaniclastic sediments.

The size of the unit is about 60 km in both length and width and has a maximum thickness between 280 m and 340 m (250-300 ms TWT) (Figure 3). The internal reflectors in the NE aggrading unit show a Sigmoid clinoform type, where the offlap break point trajectory is going upwards. From the offlap break point trajectory the unit is exhibiting an aggrading depositional architecture where the sediment influx, the subsidence and the sea-level rise have been moderate during the deposition/formation of the NE aggrading unit (Emery and Myers, 1996).

The unit is dipping into the basin, with its updip (SW) end being approximately 200 m below

seabed, while the termination of the aggrading unit towards the NW is about 1200 m below seabed (Figure 2). By detailed mapping of the unit it is possible to tell that the unit is a wave/input dominated shelf edge delta, where the slope gradient is approximately 3.0° (found by flattening of the topset).

According Orton and Reading, (1993) a delta front gradient (slope gradient/clinoform) is directly proportional with the grain size of the delta. When a delta has a slope gradient at about 3.0°, as the NE aggrading unit has the expected grain size in the delta will be fine sand.

NW prograding unit

This unit progrades in a northwestward direction from the NW British shelf area (Figure 4 and 5) into the SW part of the Faroe-Shetland Basin, approximately at the place where the NE ward aggrading unit is situated, albeit with the base at a higher stratigraphic level (Figure 2 and 4). This unit is dipping into the basin with the southeastern end being about 200 m under the seabed, while the deepest part towards the northwest is up to 1200 m under the seabed.

The internal reflectors in the NW prograding unit show a Complex Sigmoid-Oblique clinoform type, where the offlap break point trajectory is going in a seaward direction, this depositional architecture is related to a high sediment influx, static sea-level and no subsidence in the area (Emery and Myers, 1996). Andersen et al. (2000) mentioned this same prograding unit and characterised it as a north- to westward prograding delta.

The NW prograding unit is 75 km long and 65 km wide, and with a maximum thickness of around 400 m (350 ms TWT) (Figure 5) and the slope gradient of the unit is calculated to be approximately 1.0°. The slope gradient is found by flattening of the topset of the prograding unit because the angle of the topset is nearly 0º during deposition of a delta. A slope gradient at 1.0° indicates, according to Orton and Reading (1993), a silty to sandy delta.

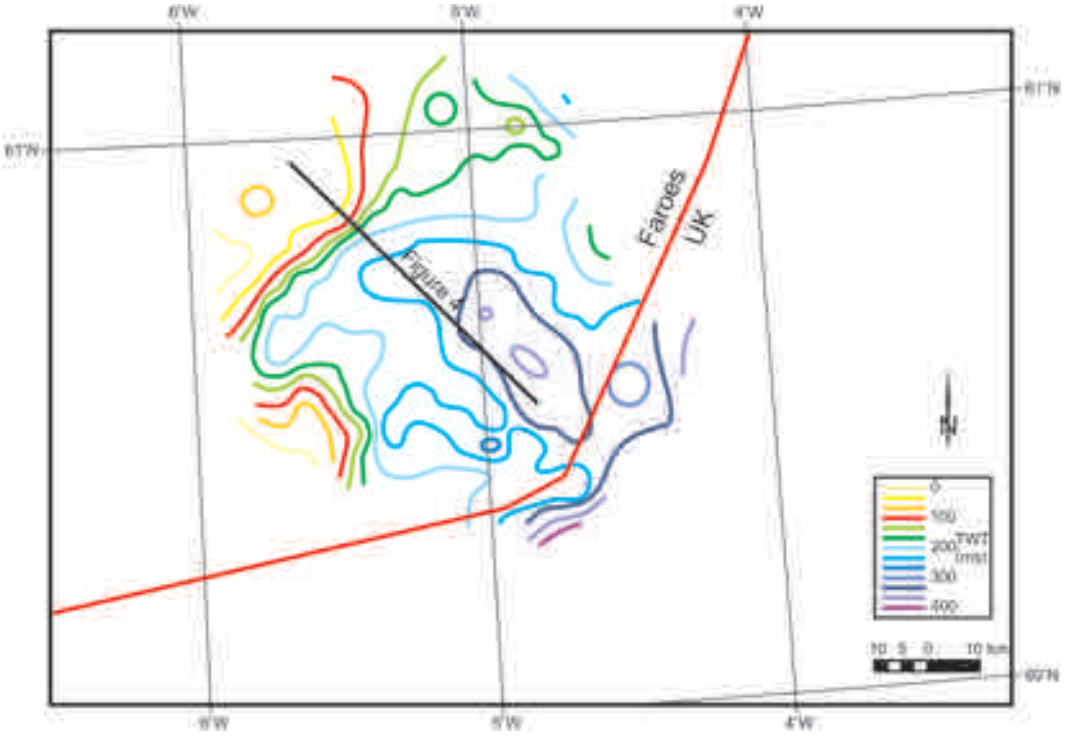

Figure 5. Map showing thickness (milliseconds, TWT) of NW prograding unit. Black line shows location of profile in Figure 4.

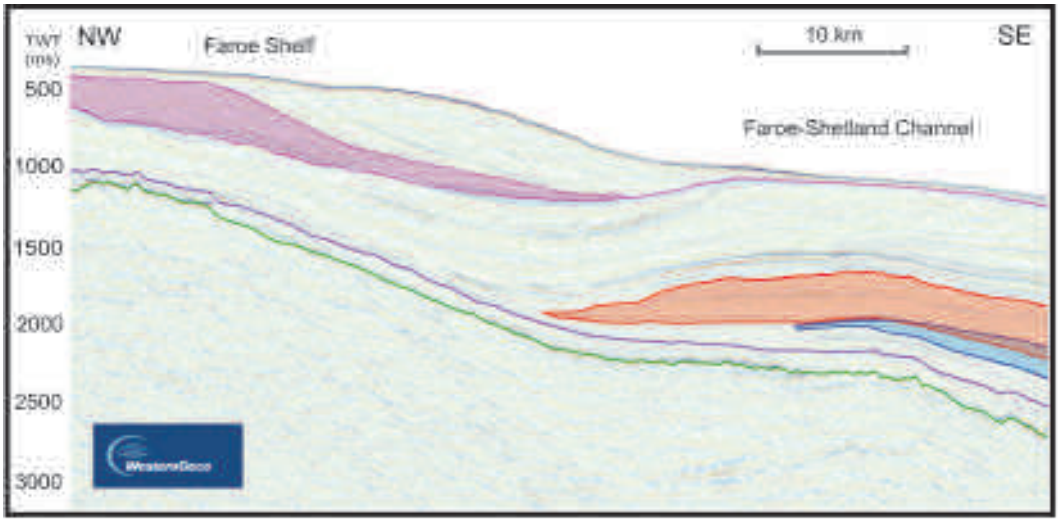

Figure 6. Seismic profile showing a SE prograding unit. The light purple area is interpreted as the SE prograding unit. The read and the blue areas is representatively the NW prograding and the NE aggrading units. The interpreted green line is the top of the basalt, the dark purple line is the top of Balder Formation and the light purple line is the Miocene unconformity. Profile located in Figures 1 and 7.

The lowermost part of this prograding unit is interbedded with the uppermost part of the NE aggrading unit described above. This tells us that these two systems were active at the same time, but with different provenance areas (Figure 2, 4 and 8).

Since the NW British shelf area is a siliciclastic provenance area we can expect the sediments in this NW prograding unit to have a siliciclastic composition. The age of the delta is similar to the NE aggrading unit, i.e. early-mid Eocene or younger.

SE prograding unit

The internal reflectors in the SE going unit show a Oblique Tangential clinoform structure and the offlap break points is going in a seaward direction, which indicates a prograding unit (Figure 6). The structure of the internal reflectors and the offlap break point trajectory indicates a depositional environment where there was a high sediment influx rate, no subsidence and static sea-level rise during the deposition of the unit.

This unit progrades from the Faroese Platform in a southeastwards direction and it terminates to the north of the two previously described units (Figure 6). The prograding unit is about 55 km long, 35 km wide and has a maximum thickness of approximately 400 m (Figure 7). The slope gradient is approximately 4°, which indicates a sandy delta (Orton and Reading, 1993). The prograding unit directly overlies the mid Miocene unconformity, so that indicate that the prograding unit probably is a delta of mid-late Miocene age or younger (Andersen *et al*., 2000; Nielsen *et al*., 2005; Stoker *et al*., 2005).

Since the unit is prograding out from Faroe Platform, the sediment in the unit, most likely consists of volcaniclastic sediments. The prograding unit extends from the seabed to 500 m below the seabed where it is deepest.

Reservoir parameters of Volcaniclastic rocks

We have demonstrated that aggrading/prograding units have built out from volcanic source areas. This introduces the question as to what kind of reservoir parameters can thus be expected from volcaniclastic rocks. Although there was some research into this issue undertaken in the 1980's and

early 1990's (e.g (Mathisen and McPherson, 1991; Vernik, 1990; Willumsen and Schiller, 1994)), it is only in resent years that there has been an increase in research into reservoir quality of volcaniclastic rocks, reflecting the increasing exploration focus in volcanic provinces (e.g. Berger *et al*., 2005; Klarner *et al*., 2008; Lou *et al*., 2005; Wu *et al*., 2006). In this section we briefly discuss some issues relating to this type of reservoir.

Volcaniclastic classes and facies

Volcaniclastic sediments can be divided into four major classes; autoclastic, pyroclastic, hydroclastic and epiclastic (Fisher and Smith, 1991). The post-basalt sediments deposited in the Faroe-Shetland Channel are epiclastic which according to Willumsen and Schiller (1994), usually offer the best reservoir potential of the four volcaniclastic sediment types. Volcaniclastic sediments can be further divided into four general facies (Figure 9), which are based on the distance from the volcanic source. The four facies are core, proximal, medial, and distal facies, with the rate of erosion of the volcanic and volcaniclastic rock being highest in the core and proximal facies, and decreasing in the medial and distal facies (Reading, 1996).

The distal volcaniclastic facies is sub-divided into two groups, marine and non-marine (Figure 9). Volcaniclastic sediments deposited as marine distal facies is better sorted than volcaniclastic sediments deposited in proximal and medial facies because reworking results in reduction of the volcanic component before final deposition. Consequently the marine distal facies has a better initial sorting related reservoir quality, which is further improved by an increase in the relative content of more stable mineral assemblages. The more stable mineralogy may limit the formation of early pore filling cements, and therefore preserving some of the primary porosity (Mathisen and McPherson, 1991). In general, only the two distal groups can be expected to have acceptable reservoir quality (Willumsen and Schiller, 1994).

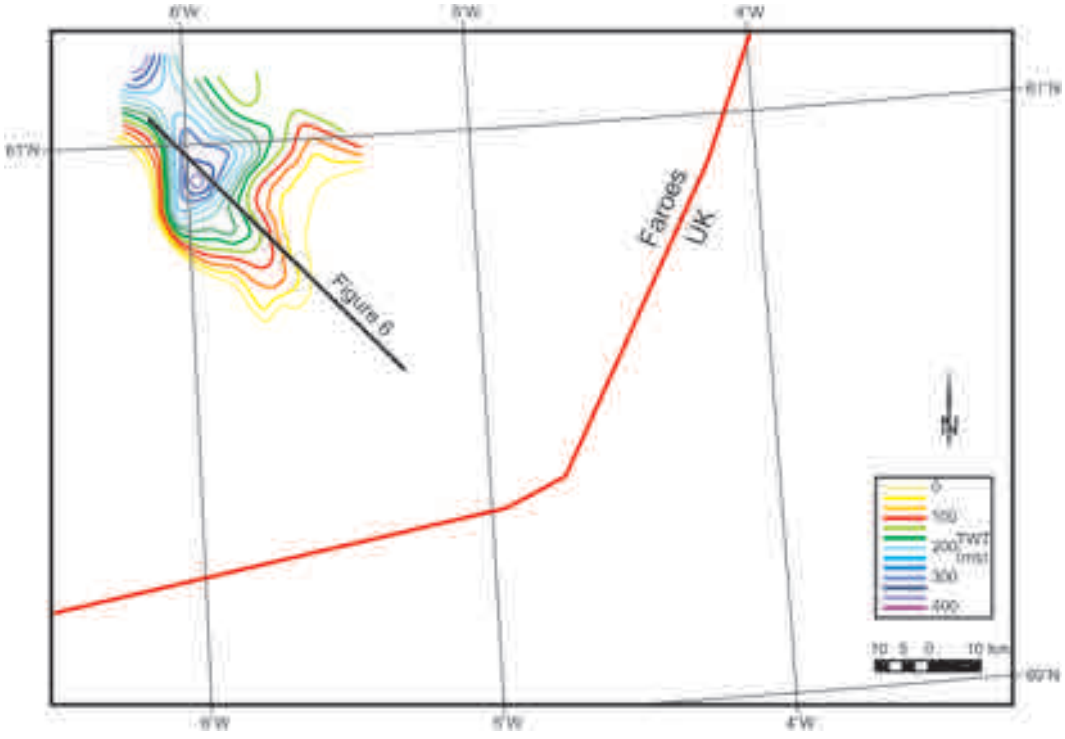

Figure 7. Map showing thickness of SE prograding unit. Black line shows location of profile in Figure 6.

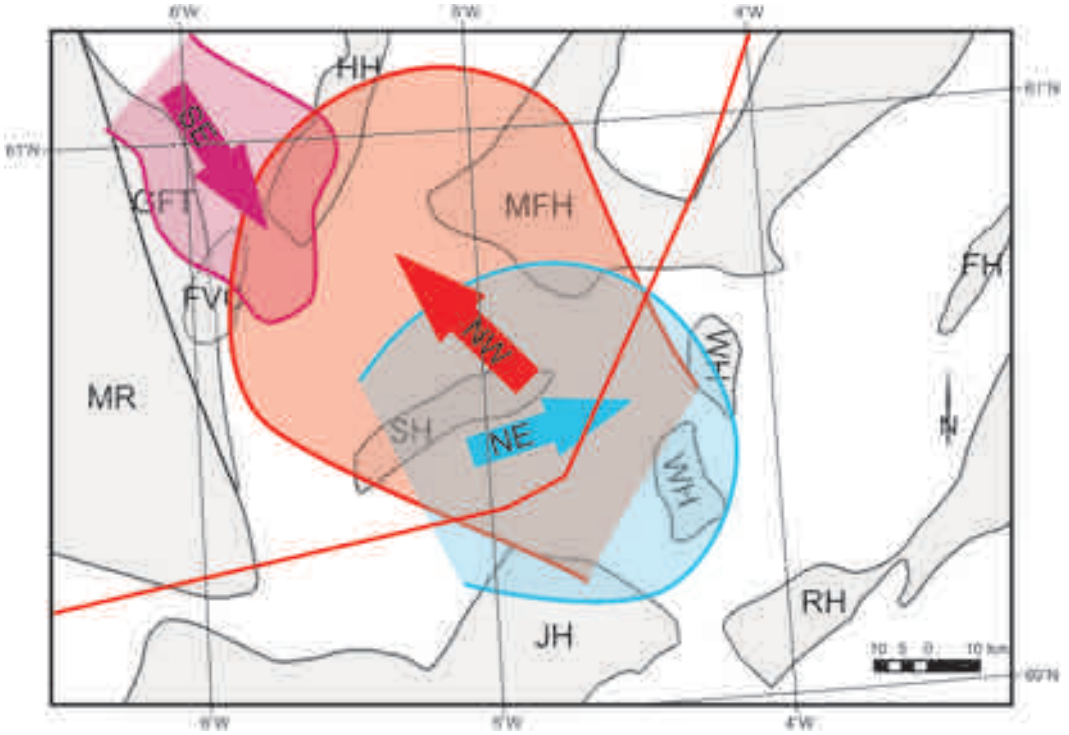

Figure 8. Overview map showing relative spatial setting of the NE, NW and SE prograding/aggrading units. Structural elements on the figure is FH=Flett High, FVC= Frænir Volcanic Centre, GFT= Grani Fault Terrace, HH=Heri High, JH=Judd High, MFH=Midd Faroe High, MR=Munkagrunnar Ridge, RH=Rona High and SH=Sjúrður High and WH=Westary High.

Reservoir quality of volcaniclastic sediments

During burial diagenesis, the sandstone became compacted and cementation begins; both these processes reduce the porosity and permability of the rock. Some of the key controls of sediment diagenesis are fluid flow and fluid composition, along with temperature, depth and pressure. In volcaniclastic sandstone early carbonate cements are commonly created especially in marine environments (Mathisen and McPherson, 1991). During compaction the grains became more closely packed, which reduces the porosity of the sediment with increasing depth of burial. Overpressure can, however, reduce the effect of this process.

The mineral composition of sandstone is a significant control of reservoir quality, because of variations in the stability of minerals. For example, quartz is much more stable than plagioclase, pyroxene and olivine. Thus a sandstone consisting of stable minerals experiences less reduction in reservoir quality compared to sandstones consisting of unstable minerals. Volcaniclastic sandstones, which primarily consists of unstable minerals like feldspar, volcanic rock fragments and heavy minerals, is much more affected by burial diagenesis than siliciclastic sandstone that consists of more stable minerals, such as quartz.

Mathisen and McPherson (1991) have made a schematic diagram of factors controlling the porosity of volcaniclastic sediments with increasing depth (Figure 10).

During shallow burial (not specified in absolute depth) diagentic processes can reduce or preserve porosity (Figure 10). In the first case the development of early carbonate pore-fill will reduce the porosity of the volcaniclastic sediment. The carbonate pore-filling material usually comes from the pore water, but in marine sandstones, much is

probably derived from dissolution of carbonate skeletal grains. If early carbonate precipitated in the post-basalt sediments, the primary porosity may have been significantly reduced. When the sediment is buried to greater depths, dissolution of the unstable fragment grains, primarily carbonate pore fill may occur forming secondary porosity in the sandstone. This is not considered directly relevant for the post-basalt sediments described in this paper, but volcaniclastic rocks have also been found under the basalt (Morton *et al*., 2002) and also within the basalt (Passey and Bell, 2007), which means that secondary porosity might be relevant on other parts of the Faroese Continental Shelf.

The second case of volcaniclastic diagenesis at shallow burial depth, the development of clay rims and coats form around the sediment grains, and is preserving the net porosity until the sediment is buried to depths where zeolite and phyllosilicates will start to fill the pore space and occlude porosity (Figure 10).

Development of the zeolite/phyllosilicate facies depends on burial depth and temperature gradient. Given conditions in Faroe-Shetland Basin with a temperature gradient of 30°C/km (Green *et al*., 1999) the sediments will probably not reach the zeolite facies shallower than 4 km.

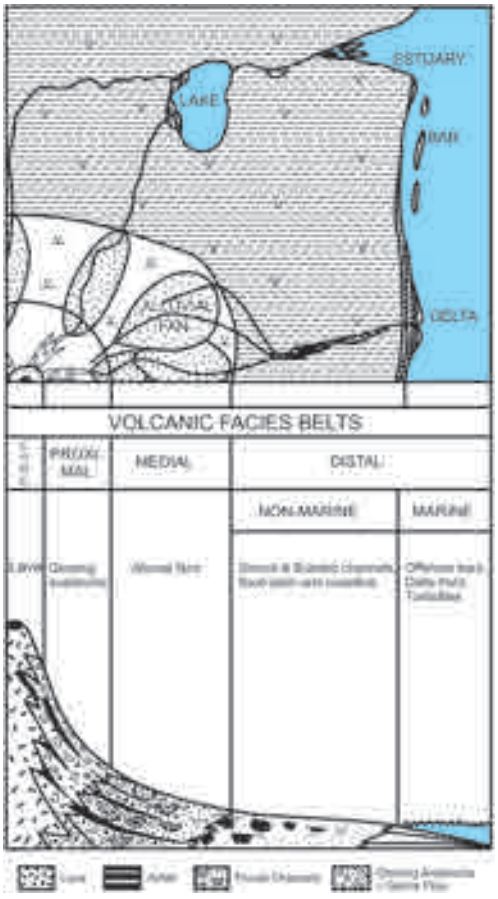

Figure 9. Overview of volcaniclastic facies belts (modified after Willumsen and Schiller 1994). See text for details.

The predicted porosity difference between volcaniclastic and siliciclastic sediments at a given depth is large and increases with depth as plotted by Tucker (1991) (Figure 11).

Epiclastic sediments have been subjected to long distance transport which remove the more unstable elements, do not lose as much porosity with depth as the more unstable volcaniclastic sediments as autoclastic, pyroclastic and hydroclastic (Figure 11). The red curve in Figure 11 is produce out from the porosity of volcaniclastic deltaic sandstones (epiclastic) at a given depth from East Java, Indonesia (Willumsen and Schiller, 1994) and from Santos Basin, Brazil (Klarner *et al*., 2008). The porosity of the volcaniclastic deltaic sandstones is respectively 20% at 2250 m (7500 feet) in East Java, Indonesia and 12-15 % at 3965 m depth in Santos Basin, Brazil. In comparison the porosity for the Paleocene siliciclastic sediments in the Judd Basin (Figure 1) at 2250 m depth, assuming no porosity preserving mechanism, is expected to be about 20 % (Lamers and Carmichael, 1999).

Discussion

Detailed mapping of the post-basalt sediments in the SW part of the Faroe-Shetland Basin has documented three depositional systems building out from the Faroese Platform and NW British shelf area (Figure 8). Although presence of such systems within the basin has been previously documented (Andersen *et al*., 2000; Davies *et al*.,

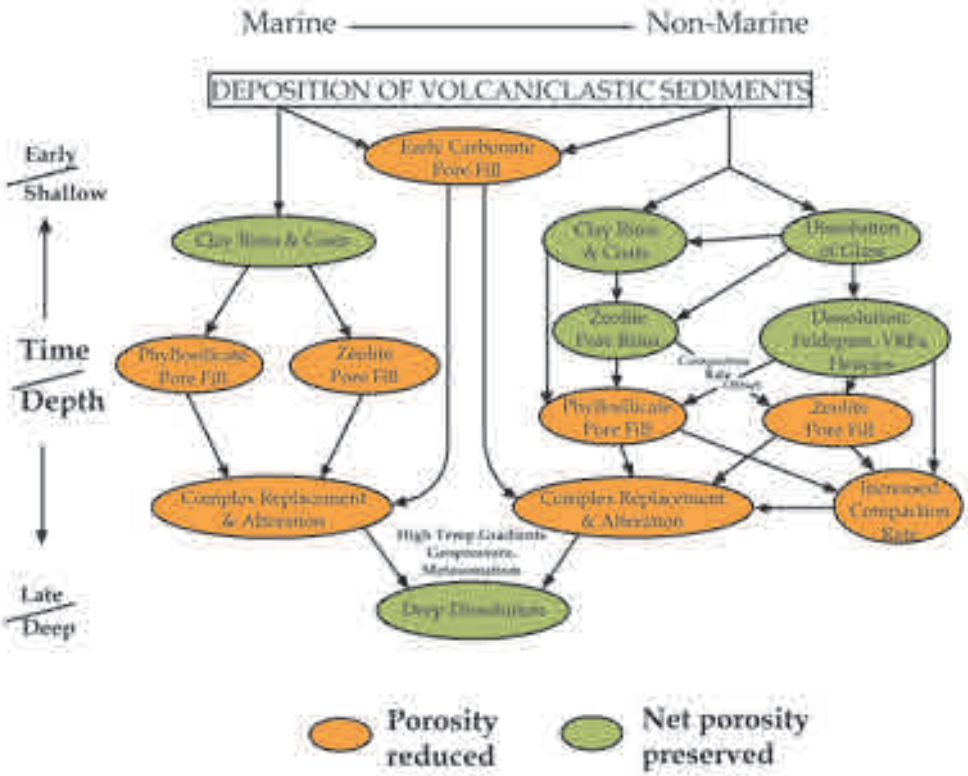

Figure 10. Depositional depth versus diagenesis process (modified after Mathisen and McPherson 1991). See text for details.

2004), this is the first detailed mapping of systems that are derived from the Faroese platform. One fascinating outcome of this study is the interaction between depositional systems originating on opposite sides of the basin. Figure 8 shows how the two older depositional systems (NE aggrading and NW prograding units) overlap in space and time. These two depositional systems are building out into the same basin at the same time but from different areas. The architecture of the two systems is different, one system is aggrading from the Munkagrunnar area and the other system is prograding from the NW British shelf area into the southwestern part of the Faroe-Shetland Basin. The different architecture of the depositional units can indicate that the Munkagrunnar area underwent subsidence during the time of deposit while in the NW British shelf area there was no subsidence. The SE prograding unit was built out towards the two older units.

The complex interaction of sedimentary systems derivate from different provenance areas raises the issue of the potential variation in reservoir quality from different source areas.

The sediments from the Shetland platform, (NW prograding unit in Figure 8), are most likely similar in nature to those which are documented in fan systems of similar age, e.g. in well 214/4-1 (Figure 1) found hydrocarbons in Eocene sandstone. The sandstone was deposited as deep water fans, and the porosity 1100 m below the mudline is about 35 %.

The lithology of the depositional units that originate from the Faroese platform is likely to be volcaniclastic. Consequently, the reservoir quality of the NE and SE prograding unit will be poor due to

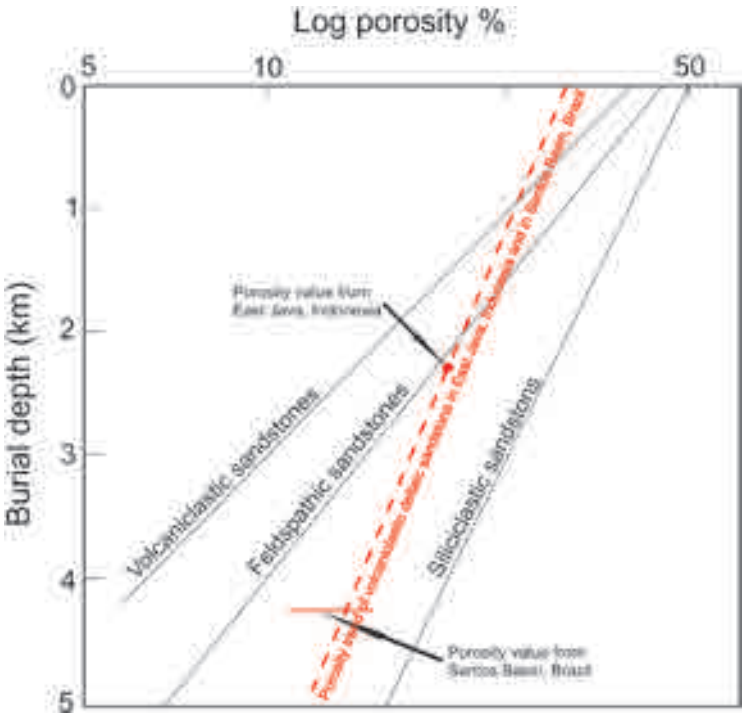

Figure 11. Graph showing general trend of porosity with increasing burial depth for both volcaniclastic and siliciclastic sandstone (black lines) (modifies after (Tucker, 1991). The red line in the figure is derived from porosity values measured from volcaniclastic deltaic sandstones in the Santos Basin, Brasil (horizontal red line) (Klarner *et al*., 2008) and from East Java, Indonesia (red dot) (Willumsen and Schiller, 1994).

a reduction in both the porosity and the permeability of these rock bodies, as outlined above.

The maximum burial depth of the post-basalt sediments in the Faroese area of the Faroe-Shetland Basin is less then 2½ km. This means that the siliciclastic rocks are likely to have a porosity in excess of 25 %, which under most circumstances is adequate when it comes to producing hydrocarbons. In contrast, the reservoir quality of the volcaniclastic rock is, more likely to degrade to such a level that they become unsuitable as hydrocarbon reservoirs. Conventional burial induced porosity reduction in the Faroe-Shetland Basin is unlikely to have resulted in a minimum porosity of less then 15 % (Figure 11, curve for volcaniclastic sandstone) where the deepest burial is found in the NE part of the Faroe Shetland Basin. There are, however, aspects which affect this, both in a positive and negative fashion. These are:

1) The NE aggrading unit and the NW prograding unit practically interfinger with each other. This means that one can expected to find both siliciclastic and volcaniclastic sediments. Such mixing of volcaniclastic and siliciclastic sediments would arguably increase the reservoir quality of the rock, because the larger amount of stable minerals reduce the possibility that early cementation destroy the porosity and permeability.

2) Given the maximum post-basalt sediment burial depth of 2500 m it is unlikely that the diagenetic process has reached the zeolite facies, which can have a very negative effect on the porosity (Mathisen and McPherson, 1991).

3) Early carbonate fill can have a significantly detrimental effect on the reservoir quality. Whether such early carbonate pore-fill has occurred in the Faroe Shetland Basin is not known to these authors.

The volcanic provenance area is the Fugloy Ridge, Faroese Platform and Munkagrunnur Ridge (Figure 1). This means that sediments in the central part of the Faroe Shetland Basin are likely to have been deposited in a distal setting. Such distal epi-

clastic deltaic sediments are known to have the best reservoir quality of the volcaniclastic sediments with an approximate porosity of 20 % at a burial depth of 2500 m (Figure 11, read curve). This is because the longer transport distance of the sediments results in better sorting of the sandstone, and also in the destruction of the less stable minerals, which leaves a well-sorted volcaniclastic sandstone consisting of relatively stable minerals, and where early cementation is less likely to occur.

Conclusions

1) We have shown that depositional systems started building out from the Munkagrunnur Ridge shortly after the extrusion of basalt. This was contemporaneous with similar depositional systems being built out form the West Shetland Platform.
2) Sediments that are derived from the Faroese Platform and Munkagrunnur Ridge are likely to be volcaniclastic in nature. This means that the reservoir quality is likely to degrade faster with depth compared to siliciclastic sediments.
3) The depositional setting in the Faroe-Shetland Basin suggests that potential volcaniclastic reservoirs are deposited in a distal setting, which increases the likelihood of finding post-basalt sandstones with reservoir quality that is suitable for hydrocarbon exploration in deeper parts of the Basin.

Acknowledgements

We would like to thank CGGVeritas for permission to show and use unreleased data in production of maps used in this article. Also we would like to thank Mark Mathisen and Martyn Stoker for reviewing this article.

References

Andersen, M.S., Nielsen, T., Sørensen, A.B., Boldreel, L.O., and Kuijpers, A. 2000. Cenozoic sediment distribution and tectonic movements in the Faroe region: Global and Planetary Change 24: 239-259.

Berger, A., Gier, S., and Tschegg, C. 2005. Porosity-preserving chlorite cementation in volcanoclastic sandstones, Sawan (Pakistan). Geophysical Research Abstracts, v. 7.

Boldreel, L.O., and Andersen, M.A. 1995. The relationship between the distribution of the Tertiary sediments, tectonic processes and deep-water circulation around the Faeroe Islands. *In*: Scrutton, R. A., Stoker, M.S., Shimmield, G.B. and Tudhope, A.W. (eds). ed., *The Tectonics, Sedimentation and Palaeoceanography of the North Atlantic Region*. Geological Society; London, Special Publication 145-158.

Boldreel, L.O. and Andersen, M.S. 1993, Late Paleocene to Miocene compression in the Faeroe-Rockall area. *In*: Parker, J.R. (ed.) *Petroleum Geology of Northwest Europe: Proceedings of the 4th Conference*. Geological Society, London: 1025-1034.

Davies, R., Cloke, I., Cartwright, J., Robinson, A. and Ferrero, C. 2004. Post-breakup compression of a passive margin and its impact on hydrocarbon prospectivity: an example from the Tertiary of the Faeroe-Shetland Basin, United Kingdom. *American Association of Petroleum Geologists Bulletin* 88: 1-20.

Dean, K., McLachlan, K. and Chambers, A. 1999. Rifting and the development of the Faroe-Shetland Basin. *In*: Fleet, A.J. and Boldy, S.A.R. (eds) *Petroleum Geology of Northwest Europe: Proceedings of the 5th Conference*. Geological Society, London: 533-544.

Doré, A.G., Lundin, E.R., Jensen, L.N., Birkeland, Ø., Eliassen, P.E. and Fichler, C. 1999. Principal tectonic events in the evolution of the northwest European Atlantic margin. *In*: Fleet, A.J. and Boldy, S.A.R. (eds) *Petroleum Geology of Northwest Europe: Proceedings of the 5th Conference*. Geological Society, London: 41-61.

Ebdon, C.C., Granger, P.J., Johnson, H.D. and Evans, A.D. 1995. Early Tertiary evolution and sequence stratigraphy of the Faeroe-Shetland Basin: implications for hydrocarbon prospectivity. *In*: Scrutton, R.A., Stoker, M.S., Shimmield, G.B. and Tudhope, A.W. (eds) *The Tectonics, Sedimentation and Palaeoceanography of the North Atlantic Region*. Geological Society, London, Special Publication: 51-69.

Emery, D., and Myers, K. J., 1996, Sequence Statigraphy, Blackwell Science, 297 p.

Fisher, R.V. and Smith, G. A. 1991. Volcanism, Tectonics and Sedimentation. *In*: Fisher, R.V. and Smith, G.A. (eds) *Sedimentation in Volcanic Settings*, SEPM Special Publication 45:. 1-5.

Green, P.F., Duddy, I.R., Hegarty, K.A. and Bray, R. J. 1999. Early Tertiary heat flow along the UK Atlantic margin and adjencent areas. *In*: Fleet, A.J. and Boldy, S.A.R. (eds) *Petroleum Geology of Northwest Europe: Proceedings of the 5th Conference*. Geological Society, London: 349-357.

Johnson, H., Ritchie, J.D., Hitchen, K., McInroy, D.B., and Kimbell, G.S. 2005. Aspects of the Cenozoic deformational history of the Northeast Faroe-Shetland

Basin, Wyville-Thomson Ridge and Hatton Bank areas. *In*: Doré, A.G. and Vining, B.A. (eds) *Petroleum Geology: North-West Europe and Global Perspectives—Proceedings of the 6th Petroleum Geology Conference*. Geological Society, London: 993-1007.

Klarner, S., Bernhardt, U. and Fontana, R.L. 2008. Enhanced depositional and AVO models for lithologically complex sandstones in the Santos Basin, offshore Brazil. *Petroleum Geoscience* 14: 235-243.

Knott, S.D., Burchell, M.T., Jolley, E.J., and Fraser, A.J. 1993. Mesozoic to cenozoic plate reconstructions of the North Atlantic and hydrocarbon plays of the Atlantic margins. *In*: Parker, J.R. (ed.) *Petroleum Geology of Northwest Europe: Proceedings of the 4th Conference*. Geological Society, London: 953-974.

Lamers, E. and Carmichael, S.M.M. 1999. The Paleocene deepwater sandstone play West of Shetland. *In*: Fleet, A.J. and Boldy, S.A.R. (eds) *Petroleum Geology of Northwest Europe: Proceedings of the 5th Conference*. Geological Society, London: 645-659.

Lou, J., Morad, S., Liang, Z. and Zhu, Y. 2005. Control on the quality of Archean volcanic reservoir rocks from the Xinglongtai buried hill, western depression of Liaohe basinm China. *American Association of Petroleum Geologists* 89 (10): 1319-1346.

Mathisen, M.E. and McPherson, J.G. 1991. Volcaniclastic deposits: implications for hydrocarbon exploration. *In*: Fisher, R.V. and Smith, G.A. (eds) *Sedimentation in Volcanic Settings*. SEPM (Society for Sedimentary Geology) Special Publication 45: 27-36.

Morton, A.C., Boyd, J.D. and Ewen, D.F. 2002. Evolution of Paleocene sediment dispersal systems in the Foinaven Sub-basin, west of Shetland. *In*: Jolley, D.W. and Bell, B.R. (eds) *The North Atlantic Igneous Province, Tectonic, Volcanic and Magmatic Processes*. Geological Society, London, Special Publication: 69-93.

Nielsen, T., De Santis, L., Dahlgren, K.I.T., Kuijpers, A., Laberg, J.S., Nygård, A., Praeg, D. and Stoker, M.S. 2005. A compaction of the NW European glaciated margin with other glaciated margins. *Marine and Petroleum Geology* 22 (9-10).

Orton, G.J. and Reading, H.G. 1993. Variability of deltaic processes in terms of sediment supply, with particular emphasis on grain size. *Sedimentology* 40: 475-512.

Passey, S.R., and Bell, B.R. 2007. Morphologies and emplacement mechanisms of the lava flows of the Faroe Islands Basalt group, Faroe Islands, NE Atlantic Ocean. *Bulletin of Volcanology* 70:139-156.

Reading, H.G. 1996. Sedimentary Environments: Processes, Facies and Stratigraphy, Blackwell Science.

Roberts, D.G., Thompson, M., Mitchener, B., Hossack, J., Carmichael, S. and Bjørnseth, H.-M. 1999. Palaeozoic to Tertiary Rift and Basin Dynamics: mid-Norway to the Bay of Biscay – a new context for hydrocarbon prospectivity in the deep water frontier. *In*: Fleet, A.J. and Boldy, S.A.R. (eds) *Petroleum Geology of Northwest Europe: Proceedings of the 5th Conference*.Geological Society, London: 7-40.

Stoker, M.S., Hitchen, K. and Graham, C.C. 1993. The geology of the Hebrides and West Shetland shelves, and adjacent deep-water areas. *HMSO*, London, for the British Geological survey.

Stoker, M.S., Praeg, D., Shannon, P.M., Hjelstuen, B.O., Laberg, J. S., Nielsen, T., van Weering, T.C.E., Sejrup, H.P. and Evand, D. 2005. Neogene evolution of the Atlantic continental margin of NW Europe (Lofoten Islands to SE Ireland): anything but passive. *In*: Doré, A.G. and Vining, B. A. (eds) *Petroleum Geology:North-West Europe and Global Perspectives-Proceedings of the 6th Petroleum Geology Conference*. Geological Society, London: 1057-1076.

Tucker, M.E. 1991 Sedimentary Petrology. An Introduction to the Origin of Sedimentary Rocks, Blackwell Scientific Publications.

Vernik L. 1990, A New Type of Reservoir Rock in Volcaniclastic Sequences. *AAPG Bulletin* 74 (6): 830-836.

Waagstein R. 1988. Structure, composition and age of the Faeroe basalt plateau. *In*: Morton, A.C. and Parson, L.M. (eds) *Early Tertiary Volcanism and the Opening of the NE Atlantic*. Geological Society, London, Special Publications: 225-238.

Willumsen, P. and Schiller, D.M. 1994. High quality volcaniclastic sandstone reservoirs in East Java, Indonesia: 23rd Annual Convention Proceedings.

Wu, C., Gu, L., Zhang, Z., Ren, R., Chen, Z. and Li, L. 2006. Formation mechanism of hydrocarbon reservoirs associated with volcanic and subvolcanic intrusive rocks: Examples in Mesozoic-Cenozoic basins of eastern China. *AAPG Bulletin* 90: 137-147.

Ziegler, P.A. 1989. Evolution of the North Atlantic- An Overview. *In*: Tankard, A.J.B.(ed.) *Extensional Tectonics and Stratigraphy of the North Atlantic Margins*. *AAPG Memoirs*: 111-129.

Ziska, H. and Varming, T. In Press, Palaeogene evolution of the Ymir and Wyville-Thomson Ridge, European North Atlantic Margin.

Rosebank – Challenges to development from a subsurface perspective

DAG HELLAND-HANSEN

Chevron Upstream Europe, Seafield House, Hill of Rubislaw, Aberdeen AB15 6XL, UK
Email: dhhh@chevron.com; Tel: +44 1224 334397

EXTENDED ABSTRACT

In late 2004, Chevron UK Ltd with partners Statoil, OMV and Dong made an oil and gas discovery, in the UK block 213/27 in the Faeroe-Shetland basin, close to the Faeroe boundary.

The discovery well, 213/27-1z drilled the crest of a large anticlinal structure; Rosebank Main, and found an approximately 100 m thick sedimentary unit, with a series of hydrocarbon bearing pay zones interbedded with volcanic rocks within a several 100's of meter thick volcanic sequence of Paleocene age (figure 1).

Rosebank South, Main and North are independent anticline closures on the Corona Ridge. The oil and gas discoveries are in the Colsay sandstones of the Flett Formation, and contain at least 3 reservoir zones with independent oil and gas accumulations. Based upon seismic and sequence stratigraphic correlation with offset wells some 10's of km apart, the Rosebank reservoir sandstones are interpreted to consist of distal equivalents of the Flett delta prograding North-Westward from the South-East. The lower most reservoir zone is interpreted to be deposited in a prograding, shallow marine shore face, shallowing upwards to a delta top environ-

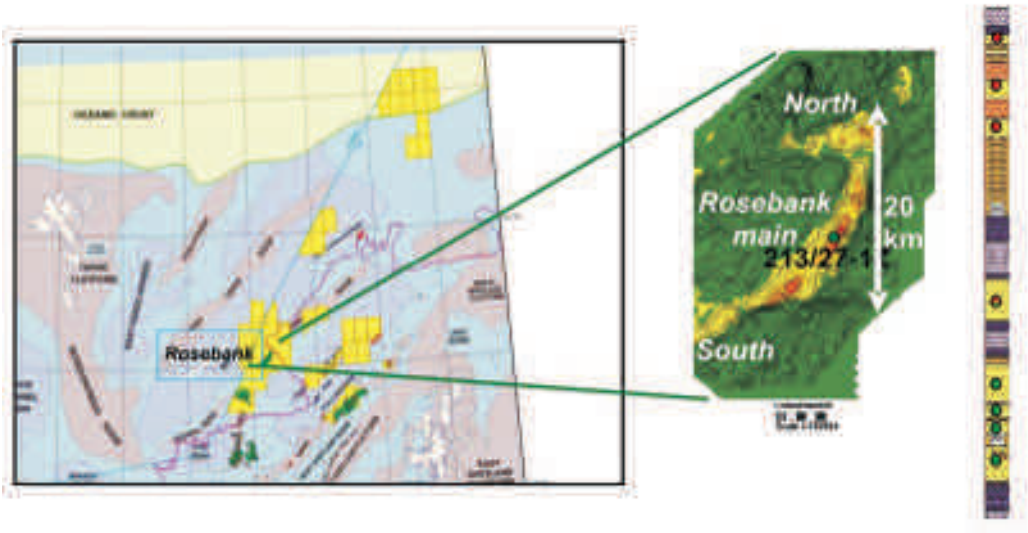

Figure 1. Map- Regional and Field scale, with the lithology log from the Rosebank discovery well.

Faroe Islands Exploration Conference: Proceedings of the 2nd Conference.
Annales Societatis Scientiarum Færoensis, Supplementum 50, 2009: 241-245

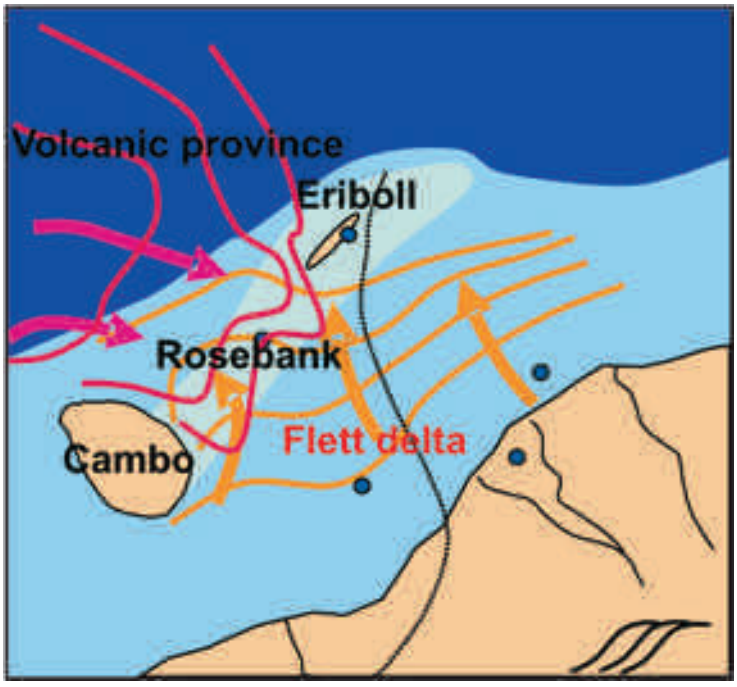

Figure 2. Map view of the depositional nature of the Rosebank siliciclastic and volcaniclastics and basaltic lava flows. Siliciclastic Flett delta prograding NW with provenance Easterly highs (Shetland), synchronous to a Eastward prograding volcanic system with provenance from the westerly rupture zones related to the break-up of the Atlantic margin.

ment in the uppermost Colsay sandstone (figure 2).

Synchronous to the North-westward prograding Flett delta was a long term volcanic eruption associated with the break-up of the Atlantic Ocean ongoing to the west. The basaltic lava flows, hyaloclastites and associated erosion products generated an eastwards prograding system of volcanic rocks which filled up the basin to the west of Rosebank (figure 2). The Rosebank structure was a paleohigh at the time and acted as a barrier between sediments from either side until parts of the Corona structure was drowned in the late Palaeocene. At this stage the area was aggradational with sediments both from the east and west competing for accommodation space, generating a complex vertical sequence of interbedded volcanic and sedimentary rocks (figure 3).

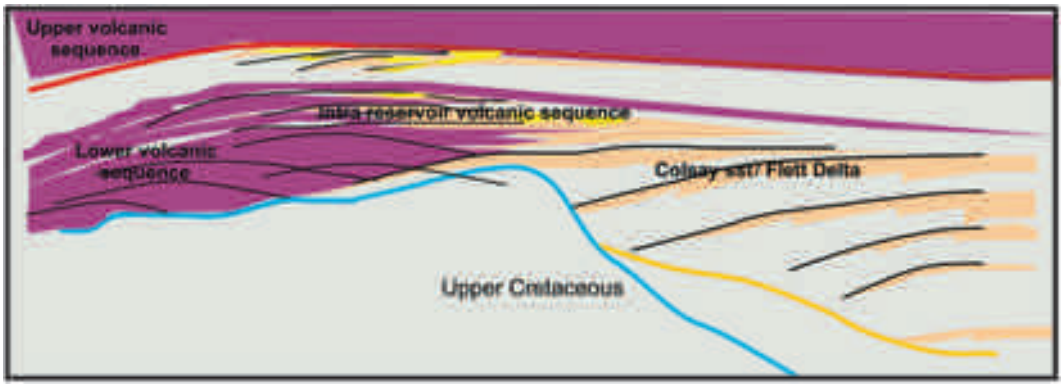

Figure 3. Vertical view of the depositional nature of the Rosebank sediments and volcanic rocks. Note the inter-fingering between the siliciclastic Colsay reservoir sandstones in the Flett Fm and the Volcanic rocks (comprising lava flows, sills, hyaloclastites and volcaniclastics).

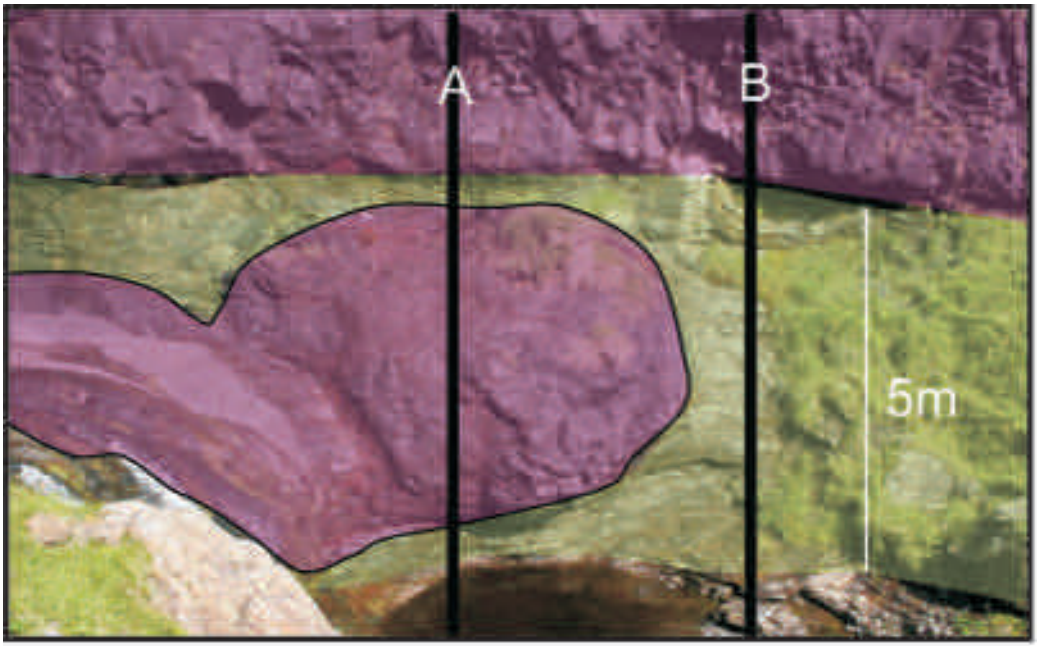

Figure 4. Basaltic lava flow intruded into underlying unconsolidated sandstone. Note the difference in observed reservoir thickness for "wells" A and B and the potential difficulty in correlating, assessing reservoir thickness in this type geologic setting, Skye, Scotland.

Figure 5. Sills cutting through overlying strata, may act as significant baffles / barriers to fluid flow, example of Sill (non reservoir rock) from Skye, Scotland.

The Rosebank appraisal program is designed to address the in-place and recoverable volumes, through vertical wells, sidetracks and production testing. Currently the largest uncertainties are hydrocarbon contacts, lateral extent of sands and their vertical net to gross ratios, the reservoir connectivity, fluid mobility and relative permeability.

In addition to the conventional parameters governing these uncertainties in a delta sequence, the Rosebank discovery is challenging due to the inter-fingering volcanic system, which presents new and old uncertainties in a different fashion. Currently we are expecting a range of possible geologic outcomes, due to the interference of volcanic rocks on a "normal" sedimentary succession, with different impact on both the hydrocarbons in place and the recovery of those. The key uncertainties, described in the following, impact largely 2 factors: Firstly directly on the actual volumetric and recoverable hydrocarbons and secondly on our ability to predict and correlate the reservoir based upon log, seismic and production test data.

- **Hydrocarbons in place:**
  - **Hydrocarbon contacts**
    - Lava flow(s) intersecting reservoir and creating independent and/or isolated hydrocarbon systems
  - **Lateral extent of reservoir sands**
    - Accommodation space filled by volcanic rock as opposed to high reservoir quality siliciclastic sand.
      - The abundance of lava volume and unstable volcanic rock exposed for erosion to the west may drown the sediment rate in the basin arriving from a siliciclastic region in the south-east.
    - Positive topographic highs caused by lava flows deflecting the sands away from "normal" progradational direction over current structural high (figure 4).

- **NTG:**
  - Volcanic low permeable (no-net) sands replace siliciclastic sands
    - I.e. a shore face beach can consist of sand derived from a siliciclastic source and from a more volcanic provenance.
    - Volcanic rocks themselves may act as reservoir, i.e. examples from producing fields
    - Throughout the world and particularly in Argentina there are fields producing from various types of volcanic rocks both from primary and secondary porosity-permeability. This type of reservoir may yield an unconventional upside and is currently not accounted for.

- **Recoverable hydrocarbons**
  - **Connectivity**
    - Faults sealed by mineral precipitation, such as Zeolites due to the volcanic materials
    - Volcanic sills cross cutting the reservoir (figure 5)
    - Lava flow intruding into / down cutting into reservoir rock acting as local barriers and baffles.
  - **Stacking patterns**
    - Sands can be deviated by positive topographic building lava flows, creating un-conventional "sweet spots" (i.e. piling of sand up towards flow and lack of sand in otherwise sand rich areas, figure 6)

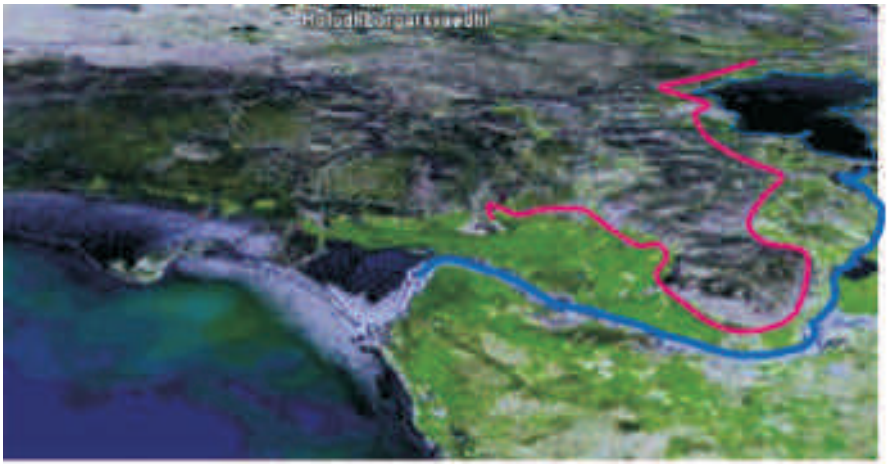

Figure 6. Lava flows can generate positive topography and may deviate "normal" depositional trends, and also cause sweet spot with sands piling up along the lava flow edge, example from Iceland.

- **Reservoir quality**
  - Portion of reservoir sand being volcanic with poorer reservoir quality, particularly permeability reduction
  - Volcanic material seeping into and decreasing reservoir quality through diagenetic processes.
  - Reservoir sands degraded by "cooking" of hot volcanic material (lava flows and sills)

Rosebank has proven crestal hydrocarbons in several separate zones on a large structure. These types of sands are proven in the Greenland to be laterally continuous over 10's of kilometers. However, we recognize significant challenges both conventional and un-conventional caused by volcanic-siliciclastic inter-fingering. Going forward, we are now in the midst of an appraisal program consisting of 3 wells, sidetracks and production testing in 2006/07. In addition we address the challenges through improved sub-surface characterization by re-processing seismic and undertaking field work on intra-basalt plays.

The Anne-Marie Prospect, Licence 005

SIMON BESWETHERICK[1*], GIANPIERO MIGLIO[1], ALWYN ROSS[1] AND SARAH POYNTER[2]

[1] Eni UK Limited, Eni House, 10 Ebury Bridge Road, London, SW1W 8PZ, UK
* Email: simon.beswetherick@eniuk.co.uk; Tel: +44 207 3446024
[2] Eni Australia Limited, Level 3, 40 Kings Park Road, West Perth, WA 6005, Australia

ABSTRACT

Licence 005 comprises parts of blocks 6004/1, 2, 3, 6, 7 and 8 in the Faroese sector of the Faroe-Shetland Basin. The licence is located over an east-west trending structural high (a splay off the Westray-Corona Ridge) which separates the Faroe sub-basin to the north from the Judd sub-basin to the south. The edge of the Faroese Paleocene basalt sheet covers Licence 005 where the basalt is interpreted to be relatively thin and inter-fingered with both volcaniclastic and sedimentary units. Seismic interpretation of the licence area is challenging, the result of seismic imaging problems related to the presence of the basalt and increased structural complexity below the basalt.

One main prospect, Anne-Marie, and several leads have been identified in Licence 005. The Anne-Marie prospect has four-way dip closure, with Paleocene to Eocene reservoirs draped over a large pre-Tertiary fault block. The primary reservoir targets comprise sandstones in the Paleocene T40 and Paleocene T31-T36 intervals. Secondary reservoir targets comprise sandstones in the early Eocene T45-T50, Paleocene T10-T25 and Cretaceous intervals.

To best understand the prospectivity of Licence 005 area and the potential of the Anne-Marie prospect, a technical evaluation has been performed including seismic interpretation, 3D basin modelling, 3D probabilistic petroleum system modelling, common risk segment mapping of plays and seismic amplitude mapping. The evaluation indicates that there is a good chance of the proven petroleum system in the UK sector of the Faroe-Shetland Basin extending into the Faroese sector. The evaluation also highlights the importance of the Westray-Corona Ridge in terms of regional prospectivity. The Westray-Corona Ridge is a focus for hydrocarbon migration, it has the potential to hold early oil generated during Cretaceous and Paleocene times (prior to later re-migration), and faults associated with the ridge are potential gateways for hydrocarbon migration into shallower stratigraphic horizons.

It is concluded that Licence 005 offers good prospectivity, being favourably located within the Faroe-Shetland Basin petroleum system. Furthermore, the Anne-Marie prospect has good reserves potential at low to moderate risk in several plays that have already proven successful in wells along the Westray-Corona Ridge (for example, in the nearby 204/10-1 Cambo and 213/27-1 Rosebank discoveries).

Introduction

This paper describes various aspects of a technical evaluation carried out to assess the prospectivity of Faroese Licence 005 in general and the Anne-Marie prospect in particular. Licence 005 was awarded to Eni (Operator) and partner Faroe Petroleum in August 2000 during the Faroe Islands First Licensing Round. The licence comprises six part blocks (6004/1a, 2a, 3a, 6a, 7a and 8a) and covers an area of 480 square kilometres. Water depth ranges from 960m to 1160m.

Licence 005 is located over an east-west trending splay off the Westray-Corona Ridge, within the greater Faroe-Shetland Basin (Figure 1). The licence also lies within the area of the thick Paleogene basalt sheet that extends over much of the Faroese sector of the basin. Many of the challenges faced in accessing the prospectivity of Licence 005 arise from poor seismic imaging combined with increased structural complexity below

Faroe Islands Exploration Conference: Proceedings of the 2nd Conference.
Annales Societatis Scientiarum Færoensis, Supplementum 50, 2009: 246-266

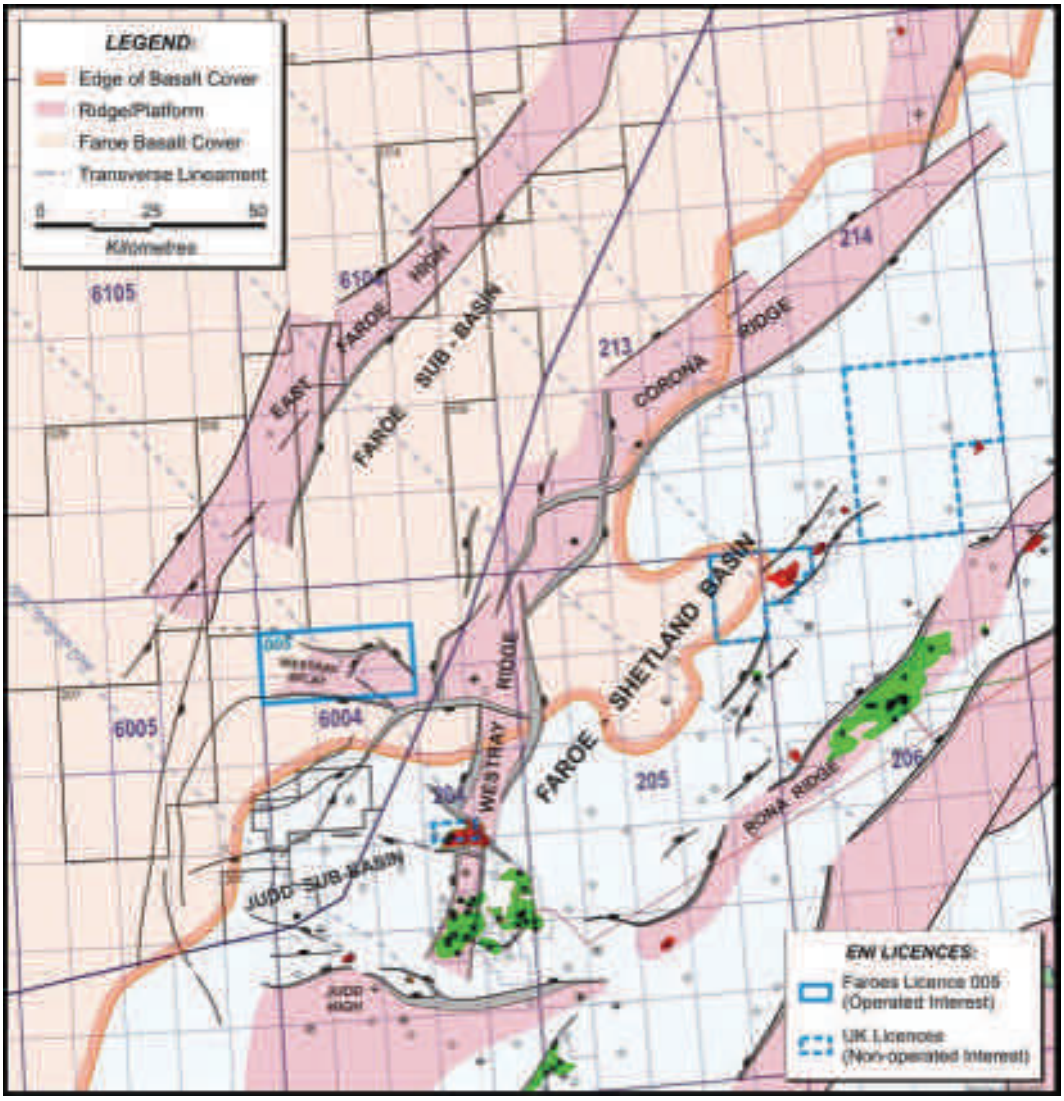

Figure 1. Licence 005 location and setting.

the basalts and limited well control. These challenges are similar to those faced in exploring the Faroese sector of the Faroe-Shetland Basin in general.

One main prospect, Anne-Marie, and several leads have been identified in Licence 005. The Anne-Marie prospect is located in the southeastern part of the licence and has structural closure at several potential reservoir levels related to a deep-seated Mesozoic fault block (Figure 2).

Exploration Overview

Exploration in the greater Faroe-Shetland Basin area began in the early 1970s when drilling was focused along the relatively shallow waters of the Rona Ridge targeting tilted fault block traps analogous to those of the North Sea (Lamers and Carmichael, 1999). This initial phase of exploration led to the discovery of the large Clair oil field in a fractured Devonian and Carboniferous sandstone reservoir and the modest Victory gas

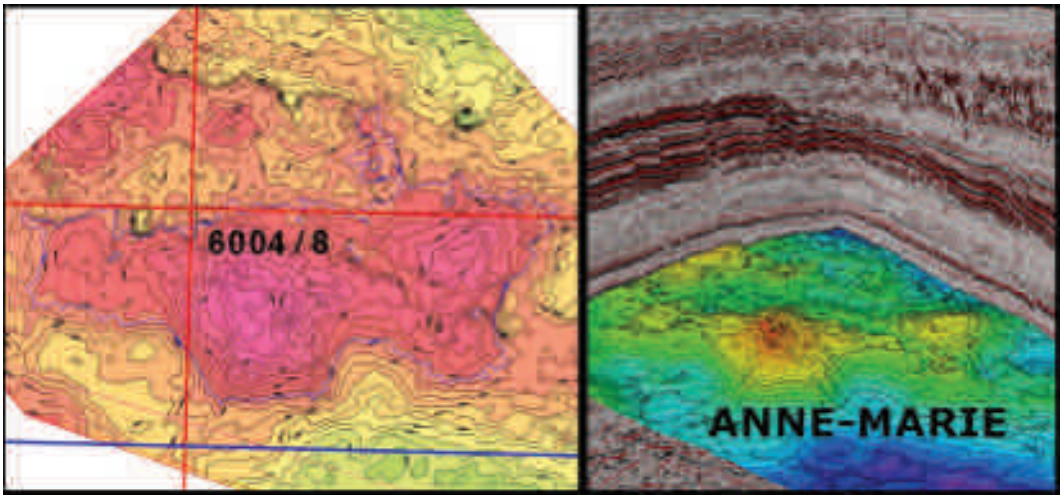

Figure 2. General view of the Anne-Marie prospect in the southeastern part of Licence 005.

discovery in an early Cretaceous sandstone reservoir. Production from the Clair field began in 2005, and the field is estimated to contain in excess of 3 billion barrels of 23 degree API oil in place, of which it is planned that 250 million barrels will be recovered during the first development phase (Clair Asset Portfolio, BP website).

Advances in drilling technology during the 1980s allowed the focus of exploration activity to move out into deeper waters in the pursuit of Paleocene structural-stratigraphic traps in addition to the traditional pre-Tertiary tilted fault blocks (Lamers and Carmichael, 1999). A few modest discoveries were made during this period, but it was not until the early 1990s that the serendipitous discovery of the large Foinaven oil field combined with improved seismic technology led to renewed interest in the area. Exploration during the 1990s was mainly focused on seismic amplitude anomalies in the Paleocene play, which led to the discovery of the Schiehallion, Loyal and Suilven oil fields. Production from the Foinaven field started in 1997 and from the Schiehallion and Loyal fields in 1998. These three fields are estimated to contain reserves in excess of 1 billion barrels of oil (Department of Trade and Industry 'Brown Book' 2001).

Although the use of seismic anomalies as direct indicators of hydrocarbons has led to several successes, it has also led to a number of failures, and a warning about the use and abuse of seismic anomalies in the Faroe-Shetland Basin was sounded by Smallwood and Kirk (2005). The recent focus for exploration has in part swung back to structural high trends such as the Westray-Corona Ridge, both in the Faroese and UK sectors of the basin.

A creaming curve for the Faroe-Shetland Basin shows reserves of approximately 2 billion barrels of oil equivalent discovered from 142 exploration wells, indicating the occurrence of a significant hydrocarbon province (Figure 3). Only five of these wells were drilled in the Faroese sector of the basin, with one small discovery reported. This discovery was made by the 6004/16-1z Marjun well, which encountered a 170 m gross hydrocarbon column in early Paleocene T10 sandstones (Smallwood and Kirk, 2005). The small number of wells drilled in the Faroese sector of the basin mainly reflects technical and practical challenges related to the presence of the Palaeogene basalts, rather than a lack of prospectivity.

Faroe-Shetland Basin Petroleum System and Plays

The significant volume of hydrocarbons discovered in the Faroe-Shetland Basin points to the oc-

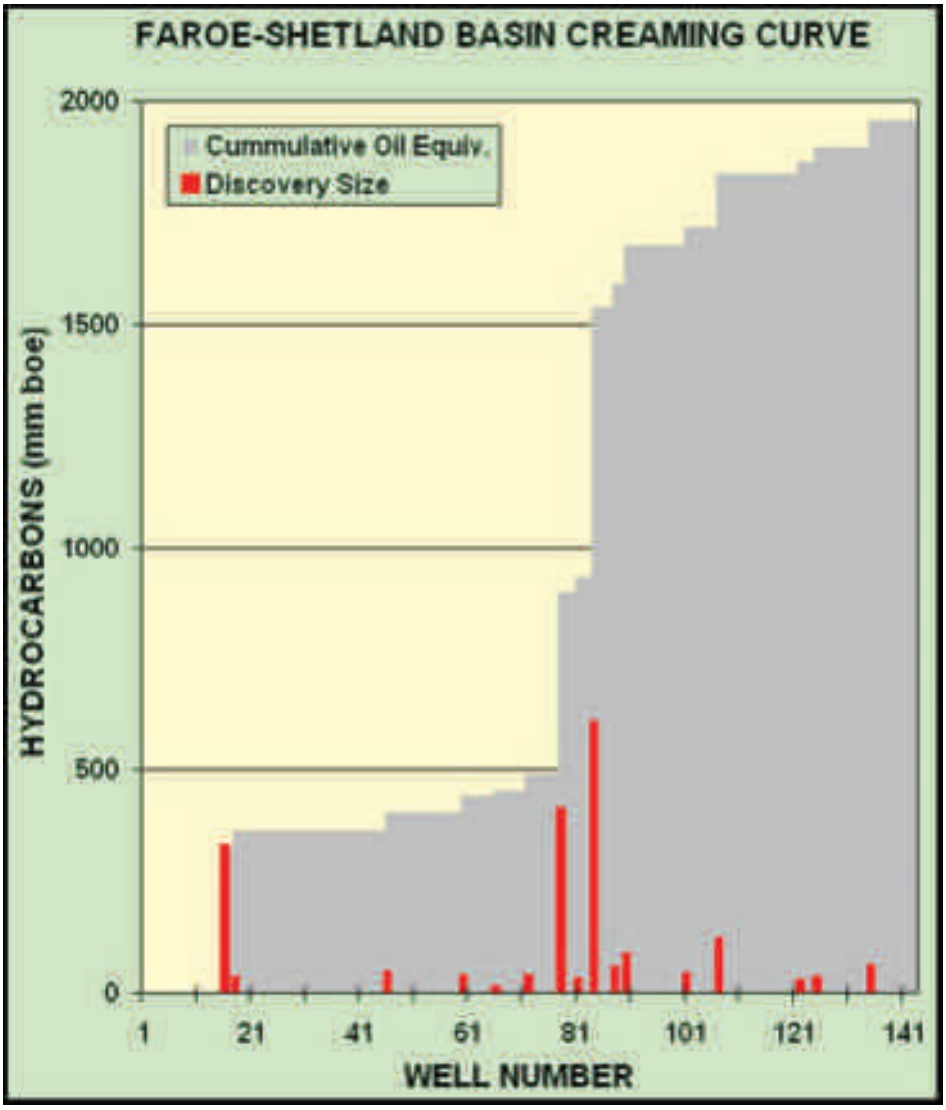

Figure 3. Faroe-Shetland Basin creaming curve (does not include reserves for the recent 213/27-1 Rosebank and 204/10-1 Cambo discoveries).

currence of a prolific petroleum system. Several plays have proven successful in the basin, with reservoirs ranging in age and type from fractured Precambrian basement in the Clair oil field to middle Eocene sandstone in the Tobermory gas discovery (Figures 4 and 5). The potential of a play in a particular part of the basin is in part determined by the complex tectonic evolution of the area, which involved multiple rifting events and periods of inversion (see Dore *et al*., 1999 and Dore *et al*., 2002). This resulted in a series of depocentres and fault-bounded sub-basins within which the fill becomes progressively younger towards the northwest (Lamers and Carmichael, 1999). As a consequence, the main plays in the Faroese sector of the basin in the northwest are likely to be in the Tertiary section. The location of Licence 005 over a splay of the Westray-Corona

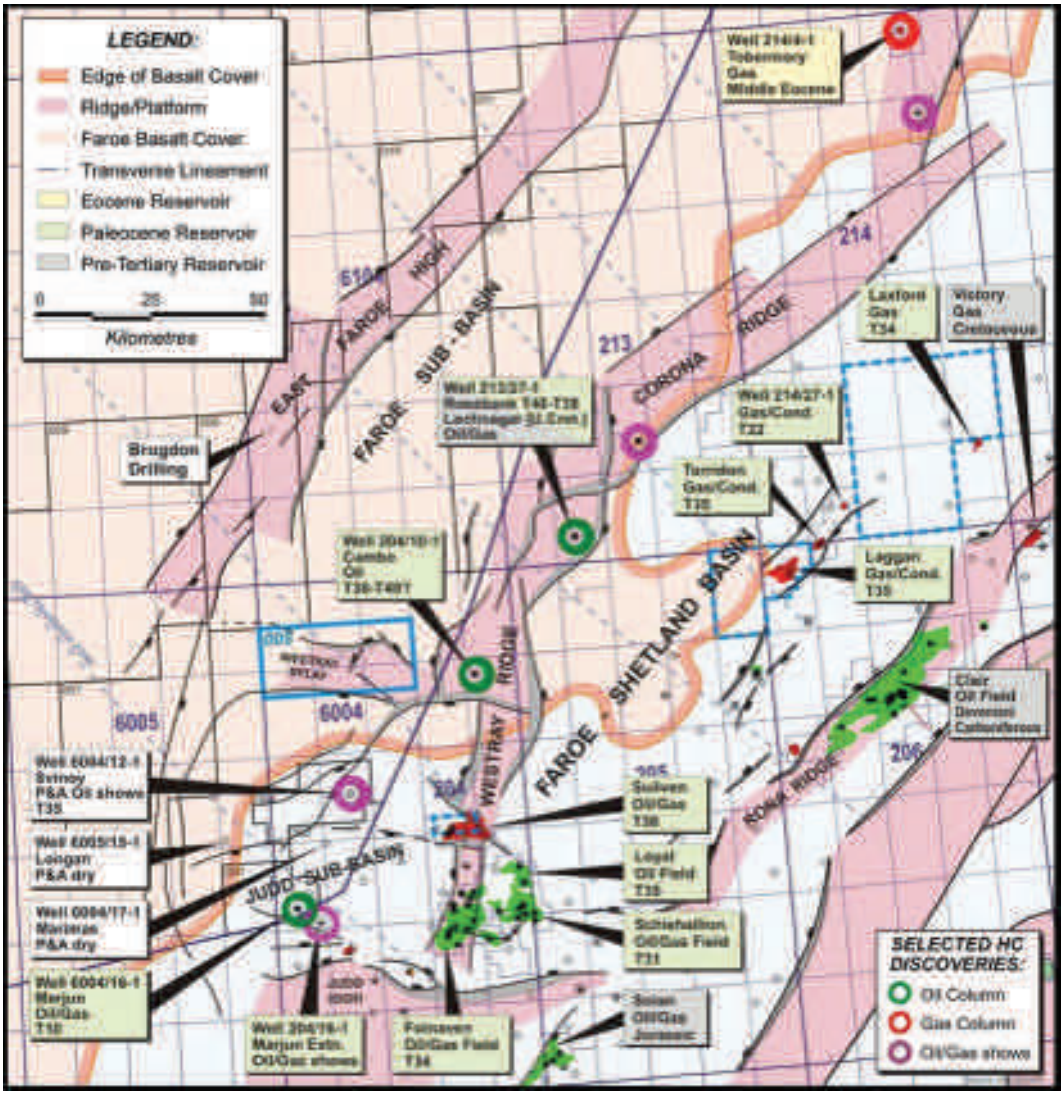

Figure 4. Faroe-Shetland Basin selected hydrocarbon fields and discoveries.

Ridge also means that older Cretaceous plays have potential.

A major factor in the success of the Faroe-Shetland Basin petroleum system is the presence of two rich source rock intervals, one late Jurassic and the other middle Jurassic in age (Cawley *et al*., 2005). The late Jurassic source rock comprises organic-rich, oil-prone shale belonging to the Kimmeridge Clay Formation. This source rock has been penetrated by several wells in the basin, and was deposited in fully marine, outer shelf to bathyal conditions which are likely to have existed on a basin-wide scale. The middle Jurassic source rock also comprises organic-rich, oil-prone shale, but was deposited in restricted marine, nearshore or lagoonal conditions. Only a few wells have penetrated a middle Jurassic section in the basin, with even fewer penetrating source rocks. Al-

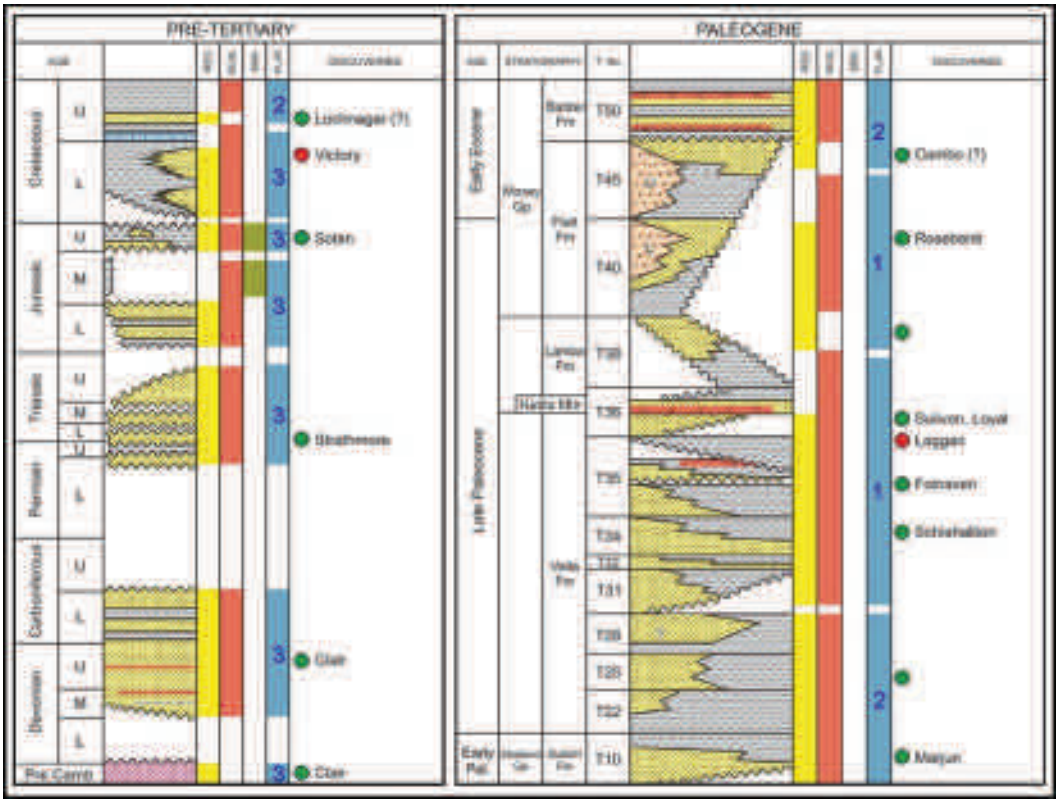

Figure 5. Faroe-Shetland Basin petroleum system showing the primary (1), secondary (2) and tertiary (3) plays for Licence 005 (Paleogene column modified from Smallwood *et al.*, 2004).

though it is possible that the distribution of the middle Jurassic source rock is limited by either deposition or erosion, Cawley *et al*. (2005) used geochemical parameters (particularly 28,30 Bisnorhopane and wax contents) to show that most of the oil accumulations discovered in the Faroe-Shetland Basin comprise a mixture of middle and late Jurassic sourced oils.

Reservoirs in the Faroe-Shetland Basin range from Precambrian to Eocene in age. The most prolific reservoir interval comprises sandstones of Paleocene age. The regional sequence stratigraphic framework for the Paleocene to Eocene section published by Ebdon *et al*. (1995) is used in this paper (the 'T' sequences of BP). Paleocene T31-T36 deepwater sandstones form the main reservoirs in the Judd sub-basin, with discoveries including the large Foinaven and Schiehallion oil fields (Figure 4). Late Paleocene to early Eocene T40-T50 shallow marine and fluvial sandstones form reservoirs on the Westray-Corona Ridge, with discoveries including the 213/27-1 Rosebank oil and gas discovery (Helland-Hansen, D., 2006). Good reservoir sandstones are also developed in the middle Eocene section, although access to a hydrocarbon charge limits the prospectivity of these sandstones to areas where regional Paleocene and early Eocene seals are either poorly developed or breached. Pre-Tertiary reservoirs include sandstones of Cretaceous, Jurassic, Triassic, Carboniferous and Devonian age. These older reservoirs have mainly proved successful along the Rona Ridge where the section has not been too deeply buried.

The main sealing horizons in the Faroe-Shetland Basin comprise shales of Tertiary or Meso-

zoic age (Figure 5). Regional tuff horizons such as the Paleocene T36 Kettla tuff and the Eocene T50 Balder tuff are also important seals for Tertiary reservoirs. Paleocene basalts may also act as local seals.

Two primary and three secondary plays are proposed for the Licence 005 area (Figure 6). The primary plays are: (1) Paleocene T40 sandstone sealed by intra-formational shale or basalt, and (2) Paleocene T31-T36 sandstone sealed by intra-formational shale or the T36 Kettla tuff. The secondary plays are: (1) Eocene T45-T50 sandstone sealed by intra-formational shale or the T50 Balder tuff; (2) Paleocene T10-T25 sandstone sealed by intra-formational shale, and (3) Cretaceous sandstone sealed by intra-formational shale. Plays involving older reservoirs could also be prospective depending on the section preserved in the core of the splay off the Westray-Corona Ridge that crosses Licence 005.

Extension of Petroleum System into Faroese Sector

The extension of the proven petroleum system in the UK sector of the Faroe-Shetland Basin into the Faroese sector will mainly be determined by the distribution of the Jurassic source rocks. None of the wells in the Faroese sector of the basin reached the Jurassic section and seismic data quality below the Paleogene basalt is too poor to confidently identify potential Jurassic source intervals.

Palaeogeographic reconstructions for the middle and late Jurassic intervals indicate the potential for source rocks to have been deposited in the Faroese sector of the Faroe-Shetland Basin. However, the reconstructions are unfortunately poorly constrained in this part of the basin (Figure 7). The outer shelf to bathyal marine depositional environment of the late Jurassic source rock suggests a widespread distribution, which is consistent with the occurrence of rich oil-prone late Jurassic source rocks outcropping along the coast of East Greenland to the northeast (see Strogen *et al.*, 2005). In contrast, the restricted nearshore to lagoonal depositional environment of the middle Jurassic source rock combined with end middle Jurassic erosion suggests it may have a more localised distribution (Lamers and Carmichael, 1999). Surprisingly, geochemical parameters indicate that most of the oil accumulations discovered in the Faroe-Shetland Basin appear to comprise a mixture of middle and late Jurassic sourced oils.

RESERVOIR	SEAL	FIELD/DISCOVERY
Middle Eocene Sst	Eocene or younger shales	Tobermory (214/4-1)
T45-T50 Eocene Sst	T50 Balder Tuff or Eocene shales	Cambo (204/10-1)?
T40 Paleocene Sst	T40 shale or basalt	Rosebank (213/27-1)
T31-T36 Paleocene Sst	T36 Kettla Tuff or T31-T36 shales	Schiehallion, Foinaven, Suilven, Loyal, Corrival, Laggan
T10-T25 Paleocene Sst	T10-T28 shales	Marjun (6004/16-1)
Upper Cretaceous Sst	Upper Cretaceous or younger shales	Lochnagar (213/27-1) ?
Lower Cretaceous Sst	Lower Cretaceous or younger shales	Victory
Upper Jurassic Sst	Upper Jurassic or younger shales	Solan, 205/28-1
Triassic Sst	Upper Triassic or Lower Jurassic marine shales	Strathmore
Devonian-Carboniferous Sst	Mesozoic marine shales	Clair
Fractured basement	Mesozoic marine shales	Clair, Bombadier, 204/23-1

PRIMARY PLAY FOR LICENCE 005 SECONDARY PLAY FOR LICENCE 005

Figure 6. Plays in the Faroe-Shetland Basin and Licence 005.

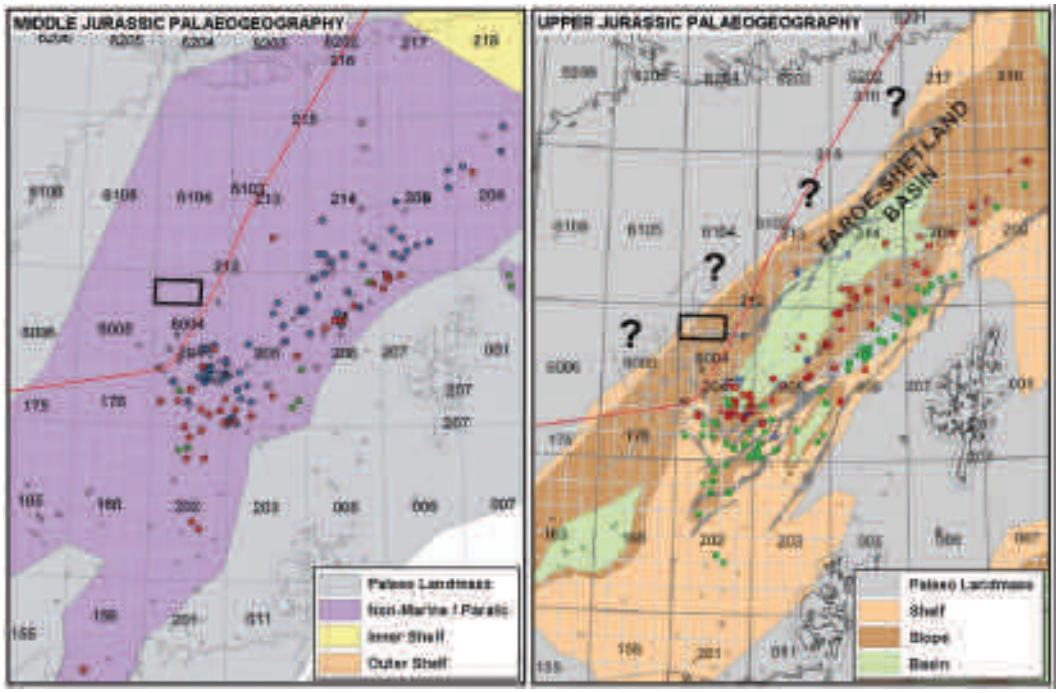

Figure 7. Middle and Late Jurassic palaeogeography reconstructions.

Based on the palaeogeographic reconstructions and the likely depositional environments, there appears to be a good chance that one or both of the Jurassic source rocks will extend into the Faroese sector of the Faroe-Shetland Basin. The occurrence of an active source rock is consistent with satellite and airborne slick data and geochemical data from seabed cores (Ziska and Andersen, 2005).

Regional Basin Modelling

The petroleum system in the Faroe-Shetland Basin was modelled in two ways; regionally using an in-house 3D basin modelling program and locally using an in-house 3D probabilistic petroleum system modelling program. The results of the regional basin modelling are used in the probabilistic petroleum system modelling to evaluate the likelihood of a hydrocarbon charge occurring to the potential reservoir intervals of the Anne-Marie prospect.

The basin modelling used regional depth maps for the sea bed, top T50 Balder tuff, top basalt, base basalt, top T36 Kettla tuff, base Tertiary, base Cretaceous and a basement defined by gravity and magnetic data. Temperature data from key wells were used to define a present day heat flow map, and a heat flow history model based on the basin evolution and calibrated to maturity data was used. The base Cretaceous depth map (Figure 8) was used for the top of the late Jurassic source interval, with the top of the middle Jurassic source interval assumed to occur 400m deeper. Following a review of regional geochemical data, the late Jurassic source rock was modelled with Type II kerogen, an average thickness of 100m, an average TOC of 5% and an average HI of 500 mg HC/g TOC. The middle Jurassic source rock was modelled with Type I kerogen, an average thickness of 50m, an average TOC of 4.5% and an average HI of 650 mg HC/g TOC.

The results of the regional basin modelling broadly indicate that through to end Eocene T50 (Balder) times the sub-basins within the greater Faroe-Shetland Basin are characterised by high cumulative oil expulsion from both the middle and

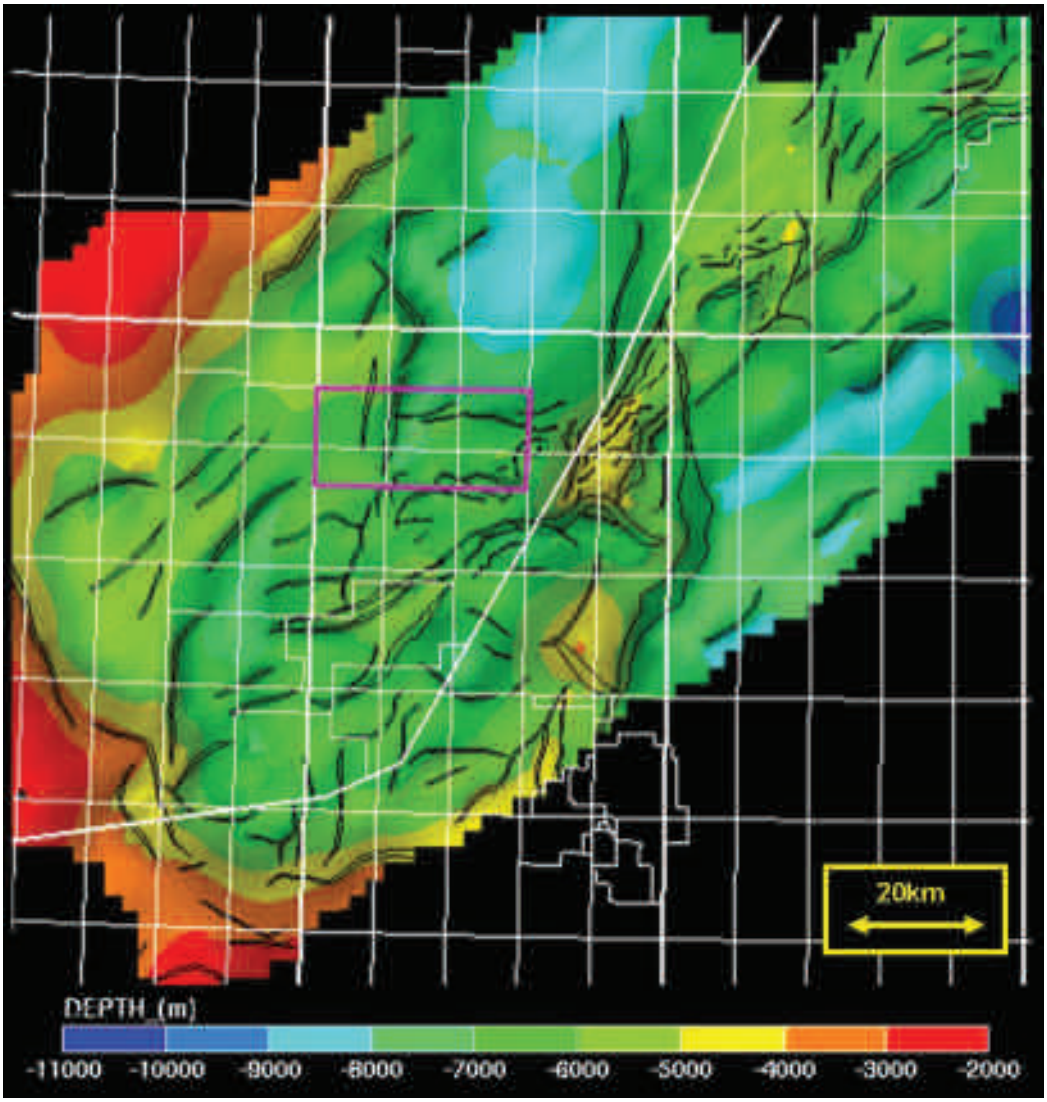

Figure 8. Regional base Cretaceous (top late Jurassic source rock) depth map.

late Jurassic source intervals, whereas the ridges and margins of the sub-basins are areas of minimal oil expulsion (Figure 9). In contrast, from end Eocene T50 times to the present day (when the main Paleogene reservoir intervals were present), it is the ridges and margins of the sub-basins that are characterised by high cumulative oil expulsion, whereas the sub-basins where the oil potential is mainly exhausted and the immature platforms are areas of minimal oil expulsion (Figure 10).

Various sensitivities were run in the regional basin modelling for the source rock parameters (distribution, thickness and richness) and for the thermal history (heat pulses related to stretching and igneous events). In general terms it appears that the depth and burial model has a greater influence on the timing and degree of hydrocarbon generation and expulsion from the source rocks in the Faroe-Shetland Basin than the thermal model used.

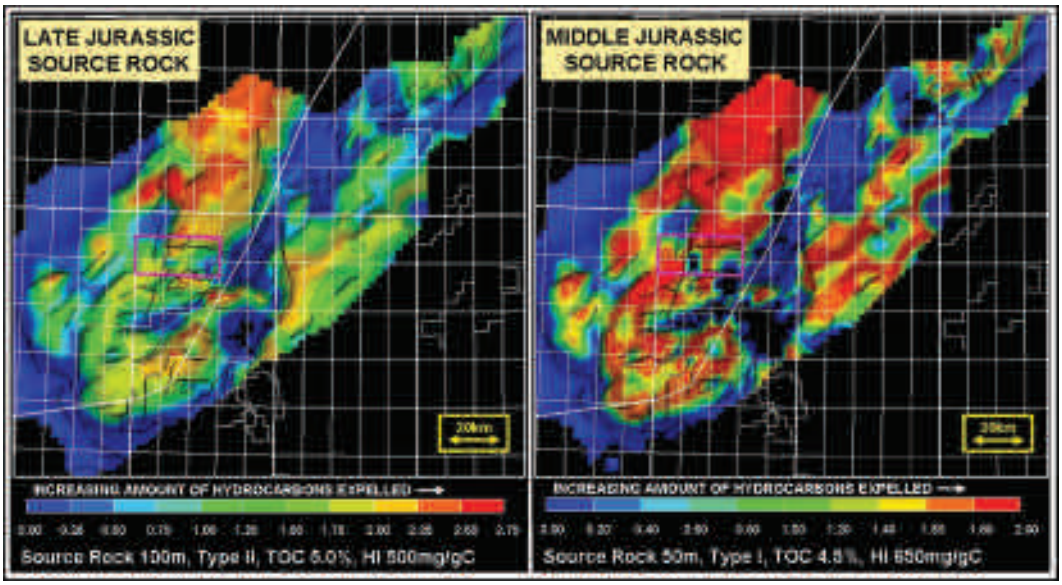

Figure 9. Jurassic source rock oil expulsion through to end Eocene T50 (Balder) times. Palaeo-lows are characterised by high cumulative oil expulsion (warm colours) whereas palaeo-highs and basin margins are areas of minimal oil expulsion (cold colours).

Petroleum System Modelling for the Anne-Marie Prospect

A probabilistic approach to 3D petroleum system modelling can have an advantage over a traditional deterministic approach in studies characterised by uncertainties, either in the geological model or in some of the parameters used for the numerical simulation of the processes. The probabilistic program developed by Eni is described by Corradi *et al*. (2003), and is based on a Monte Carlo sampling

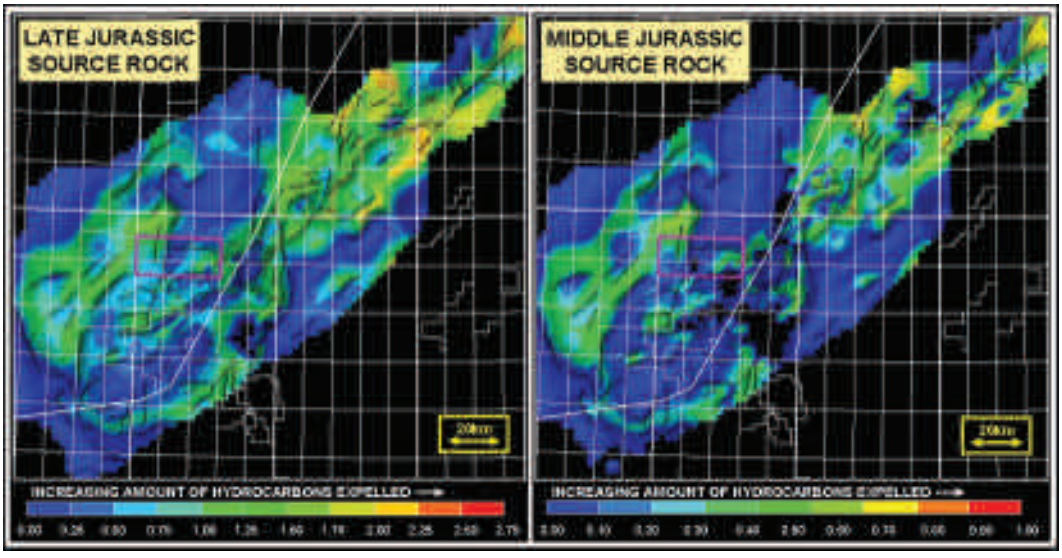

Figure 10. Jurassic source rock oil expulsion from end Eocene T50 (Balder) times to present day. Palaeo-highs are characterised by high cumulative oil expulsion (warm colours). Palaeo-lows where the source potential is mainly exhausted and immature basin margins are areas of minimal oil expulsion (cold colours).

technique, with probability distributions for the uncertain input parameters randomly sampled and a large number of (deterministic) secondary migration simulations performed. The results from the simulations are combined to provide probability distributions for the output data (for example, the hydrocarbon volume in a prospect). These output distributions can provide useful information for prospect evaluation and risk assessment.

The conceptual charging model for the Anne-Marie prospect allows both for migration of hydrocarbons generated from the Jurassic source rocks after end Eocene T50 (Balder) times, and for re-migration of earlier hydrocarbons trapped in a Mesozoic reservoir on old highs (the 'motel' model of Lamers and Carmichael, 1999). Secondary migration simulations (1000 in total) were carried out sampling permeability input distributions for vertical migration up fault planes and through potential sealing intervals. Additional simulations were run for basin modelling runs using alternative source rock distribution, thickness and richness scenarios.

The results of the probabilistic petroleum system modelling can be used to indicate the likelihood of a particular reservoir interval in a prospect having received and retained a hydrocarbon charge. For the potential Paleogene reservoir intervals of the Anne-Marie prospect, the Eocene T45-T50 and Paleocene T31-T36 reservoirs appear to have a moderate to high chance of containing hydrocarbons, the Paleocene T40 reservoir a moderate chance, and the T10-T25 reservoir a low chance (Figure 11). The likelihood of a particular reservoir interval containing hydrocarbons is strongly influenced by the presence or absence of the two main regional seals; the Eocene T50 Balder tuff and the Paleocene T36 Kettla tuff. The Balder tuff appears to be well developed in the Licence 005 area and forms the ultimate top seal for the Anne-Marie prospect. If the Kettla tuff is well developed in Licence 005, then there will be a higher chance of hydrocarbons occurring in the underlying Paleocene T31-T36 reservoir than in the overlying reservoir intervals. If the Kettla tuff is poorly developed in the licence area, then there will be a higher chance of hydrocarbons occurring in the overlying reservoir intervals.

The probabilistic petroleum system modelling for Anne-Marie indicated that there was a better chance of hydrocarbons occurring in the Eocene T45-T50 reservoir interval than in the underlying Paleocene T40 reservoir interval. However, results from the recent 213/27-1 Rosebank oil and gas discovery indicate that shale and basalt in the T40-T45 interval can act as effective seals for both oil and gas (Helland-Hansen, D., 2006).

RESERVOIR INTERVAL	CHANCE OF HYDROCARBONS
T45-T50[A]	High
T45-T50[B]	Moderate
T40	Moderate
T31-T36[A]	Moderate
T31-T36[B]	High
T10-T25	Low

[A] Assumes poor Kettla tuff developed in Licence 005.
[B] Assumes moderate Kettla tuff developed in Licence 005.

Figure 11. Chance of hydrocarbons occurring in the potential Paleogene reservoir intervals of the Anne-Marie prospect, as indicated by the probabilistic petroleum system modelling.

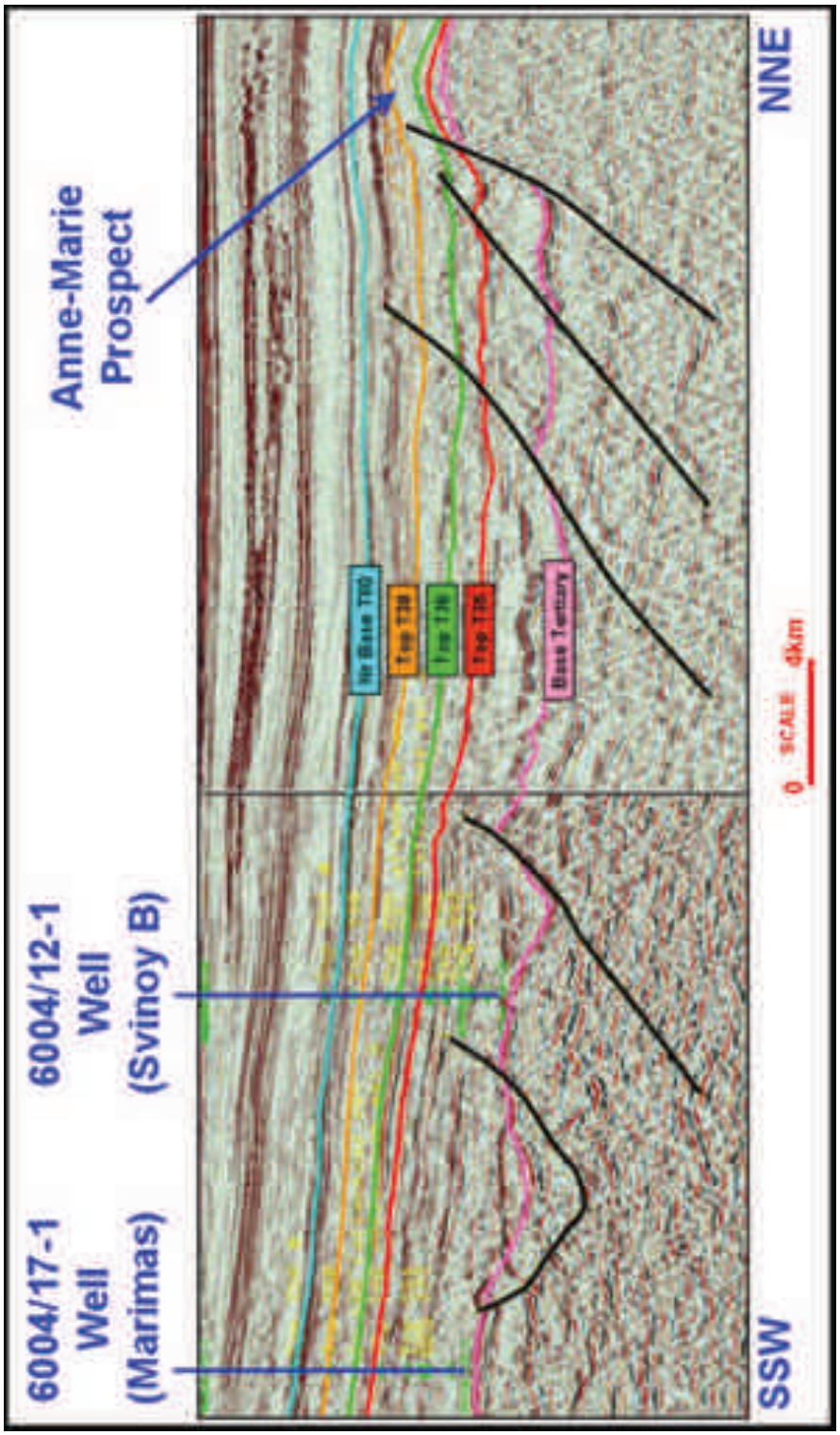

Figure 12. Seismic tie between the Marimas and Svinoy B wells, and the Anne-Marie prospect.

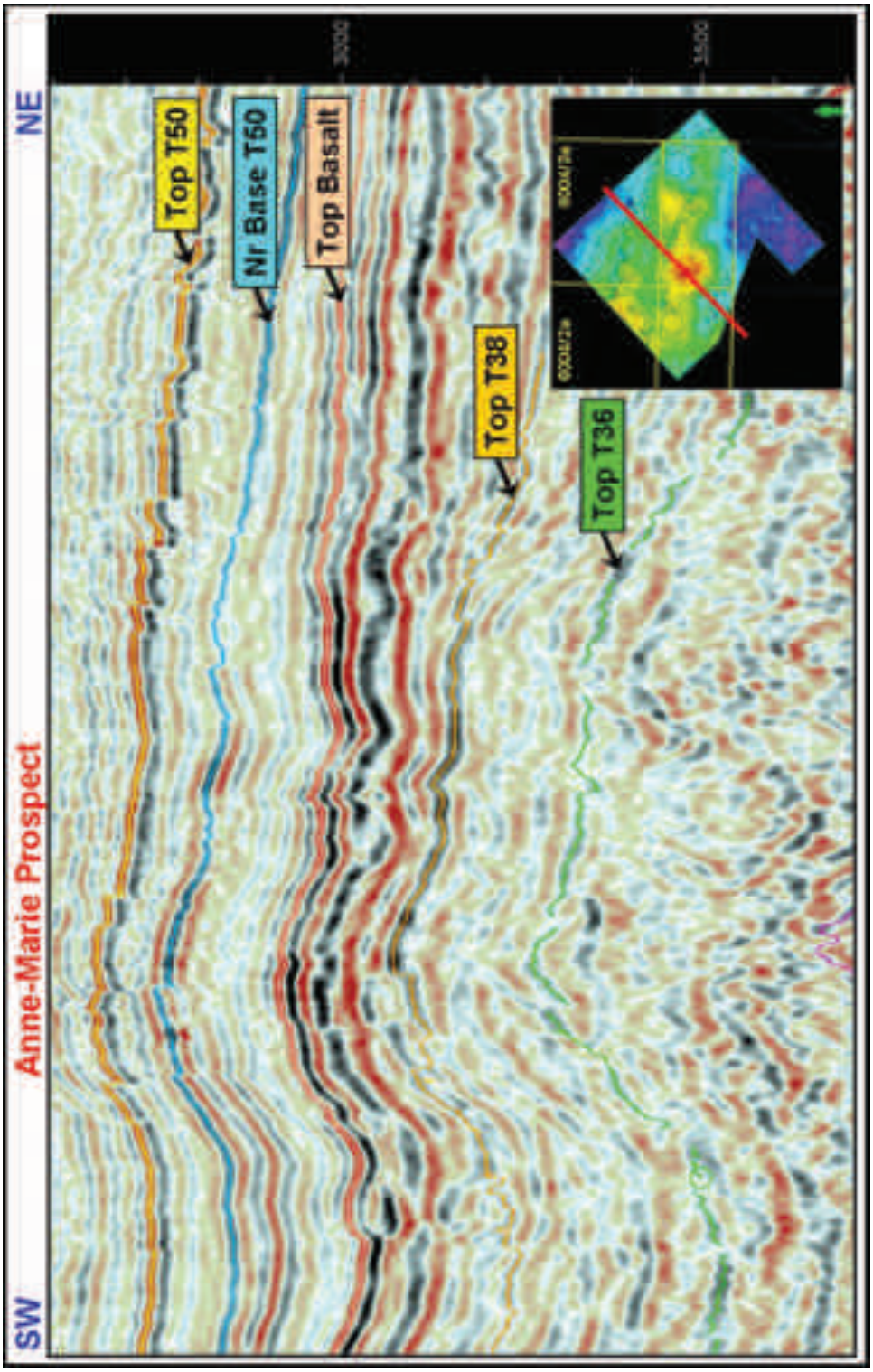

Figure 13. SW-NE seismic line across the Anne-Marie structure highlighting the Paleogene section.

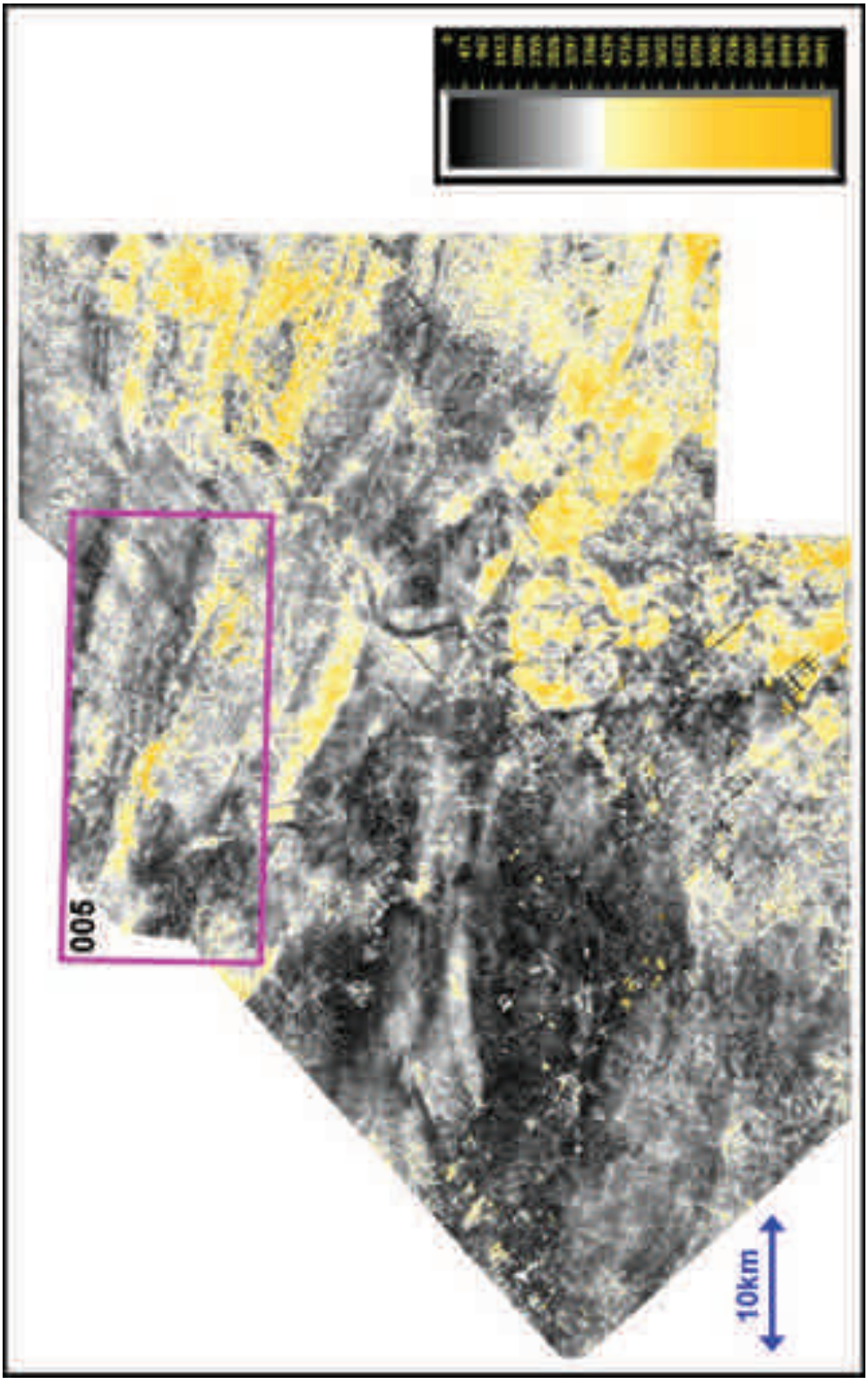

Figure 14. Seismic amplitude map for an early Eocene near base T50 pick.

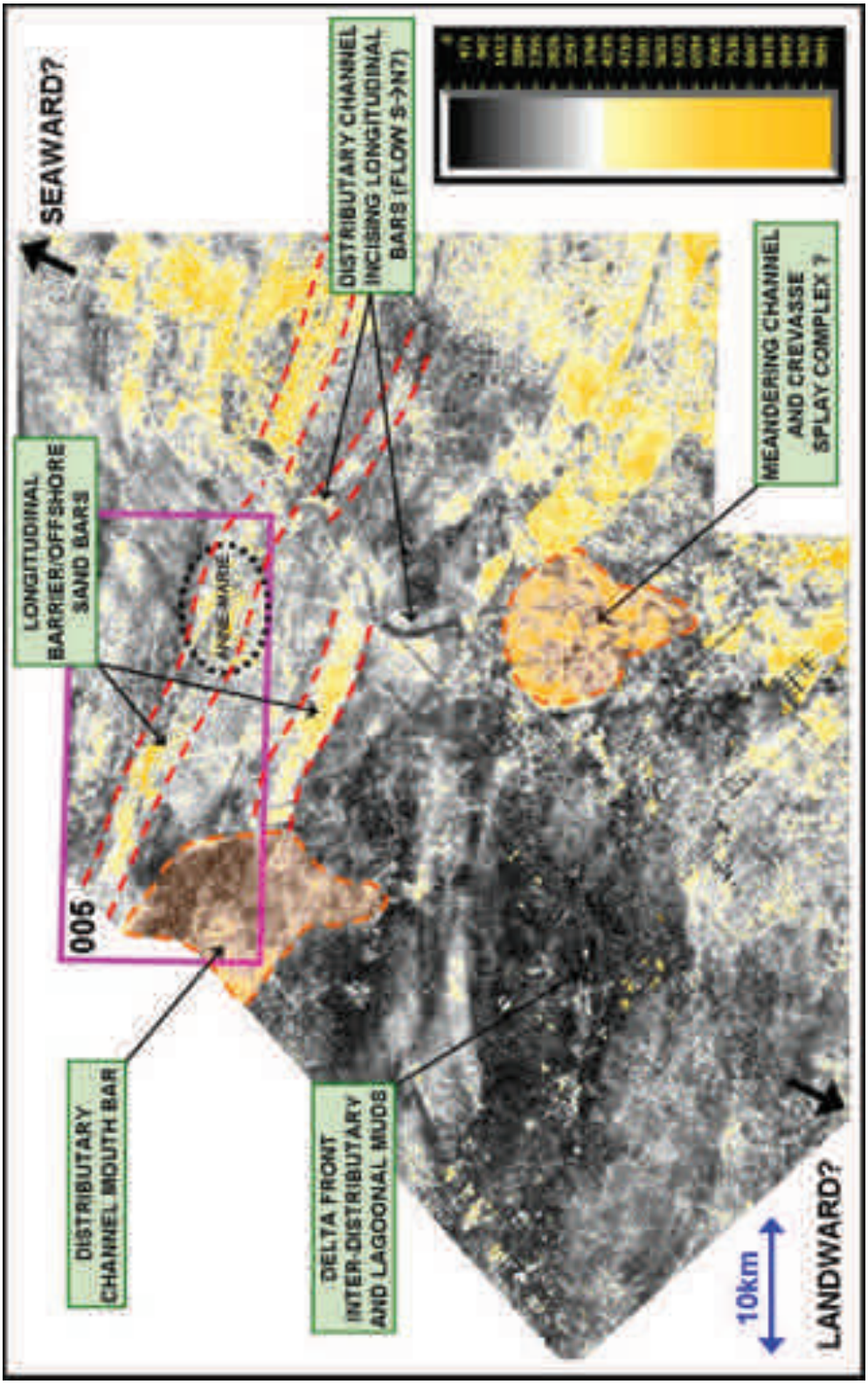

Figure 15. Possible depositional interpretation for the early Eocene near base T50 seismic amplitude map.

Licence 005 and Anne-Marie Prospect Seismic Interpretation

The main challenge to seismic interpretation in the Licence 005 arises from poor seismic imaging below the Paleocene T40-T45 basalts combined with increased structural complexity in the poorly imaged section. A lack of nearby available well control and the occurrence of igneous sills provide additional challenges in interpretation.

The nearest seismic-well tie available to Eni for the Anne-Marie prospect is the 6004/12-1 Svinoy well located approximately 26 km to the south. The seismic correlation between this well, the 6004/17-1 Marimas well to the south and Anne-Marie prospect to the north is very good down to the Paleocene top T45 basalt level, then moderate down to the Paleocene top T36 level and poor below this interval (Figure 12). Correlation of the deeper Paleocene seismic horizons is especially difficult across the faults bounding the Anne-Marie structure (a better correlation is anticipated when the results of the 204/10-1 Cambo well are released early in 2007).

Seismic imaging of the early Eocene top T50 Balder to Paleocene top T45 basalt section over

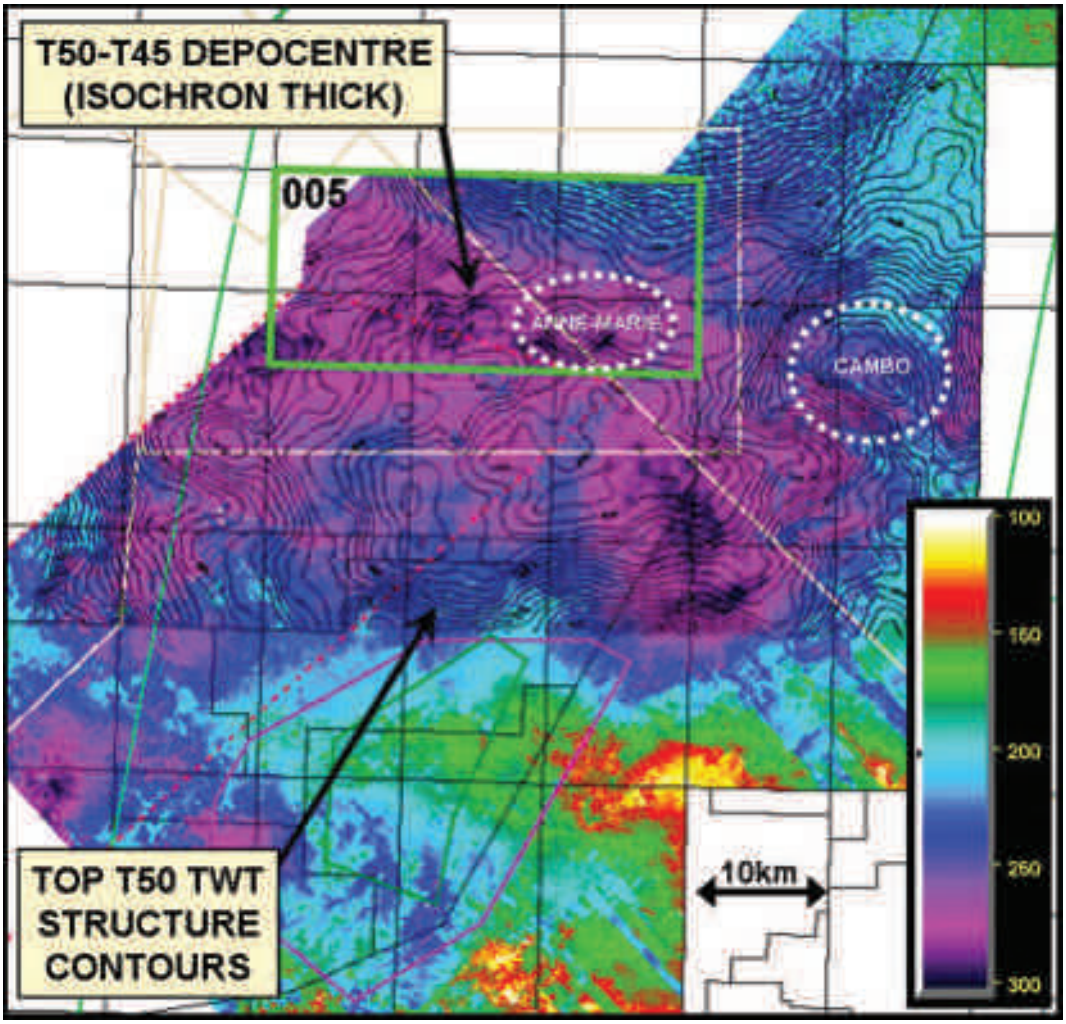

Figure 16. Eocene top T50 (Balder) to Paleocene top T45 basalt isochron map (msec).

the Anne-Marie prospect is fairly good (Figure 13). Several small faults cut the top T50 seismic pick and are probably related to compaction driven polygonal faulting. These faults do not typically extend down into the underlying basalt. The Paleocene T40-T45 basalt interval is moderately well imaged in the seismic data. This interval is interpreted as a stacked sequence of basalt lava flows, volcaniclastics and sediments. Sandstones within the T40-T45 basalt interval are important as they form the reservoir for the 213/27-1 Rosebank oil and gas discovery (Helland-Hansen, D., 2006).

Seismic amplitude extractions were made for several horizons in order to search for any trends that could provide information on likely depositional environments. Interpretations for two seismic amplitude maps are presented; one for an early Eocene near base T50 pick and the other for the Paleocene top basalt pick within the T40-T45 interval (Figure 13).

The early Eocene near base T50 seismic amplitude map shows several ENE-WSW trending linear features together with a meandering channel-like feature (Figure 14). The linear features, one of which passes through the Anne-Marie prospect, are interpreted as sand bars deposited in either a marginal or shallow marine environment (Figure 15). Possible modern day analogues are the beach barrier sand bars that occur along the Texan coast of North America (see Penland *et al*., 1988) or the offshore tidal sand bars that occur parallel to the coast off the eastern seaboard of North America (see Swift *et al*., 1973). At the near base T50 time, the area to the south of Licence 005 is interpreted to be sub-aerially exposed.

An isochron map for the early Eocene top T50 (Balder) to Paleocene top T45 basalt interval shows a thick located over the Licence 005 area (Figure 16). This thick indicates that a depocentre could have existed in early Eocene times, with possible ponding of the marginal to shallow marine sandstones that form one of the potential reservoir targets for the Anne-Marie prospect.

A seismic amplitude extraction map for the Paleocene top T45 basalt pick shows variations which are interpreted to represent changes in the nature of the section preserved at the top of the T40-T45 basalt interval (Figure 17). Areas of high seismic amplitude such as that crossing the southwest corner of Licence 005 are interpreted to be thick basalt lava flows, whereas areas of low seismic amplitude are interpreted to be sediments. Areas of intermediate seismic amplitude are interpreted to be thin basalt lava flows or volcaniclastic sediments. The thick basalts appear to have flowed from the northwest. The top T45 basalt seismic amplitude map also shows what appears to be a fluvial channel that can be traced for over 50km (Figure 17). This channel appears to flow from northeast to southwest, with a meandering form across Licence 005 and a linear form where it crosses the area of thick basalt lava flows in the southwest corner of the licence. In modern fluvial systems, linear channel morphology is commonly observed in areas with competent bedrock. The channel also appears to be offset by a possible fault or fracture within the area of thick basalt flows (Figure 17). To the southwest, the channel dies out, possible as it enters a deltaic system at the coast.

In order to further investigate possible sedimentary systems at the top T45 basalt level, the scale colour bar for the seismic amplitude map was adjusted in order to highlight the lower amplitudes (Figure 18). This map appears to show a fluvial or shallow marine channel-fan system that extends southwards from the southeast corner of Licence 005. It can also be seen that the channel is deflected around the flanks of the Anne-Marie prospect (Figure 18). Interpretation of the sedimentary systems in the Paleocene T40-T45 basalt interval is important as sandstone units within the interval form the reservoir for the recent 213/27-1 Rosebank oil and gas discovery (Helland-Hansen, D., 2006) and are a potential reservoir target for the Anne-Marie prospect.

Conclusions

Some of the main conclusions arising from the technical evaluation carried out to assess the prospectivity of Licence 005 and the Anne-Marie prospect are:

- There is a good chance that the proven petroleum system in the UK sector of the Faroe-Shetland Basin extends into the Faroese sector.

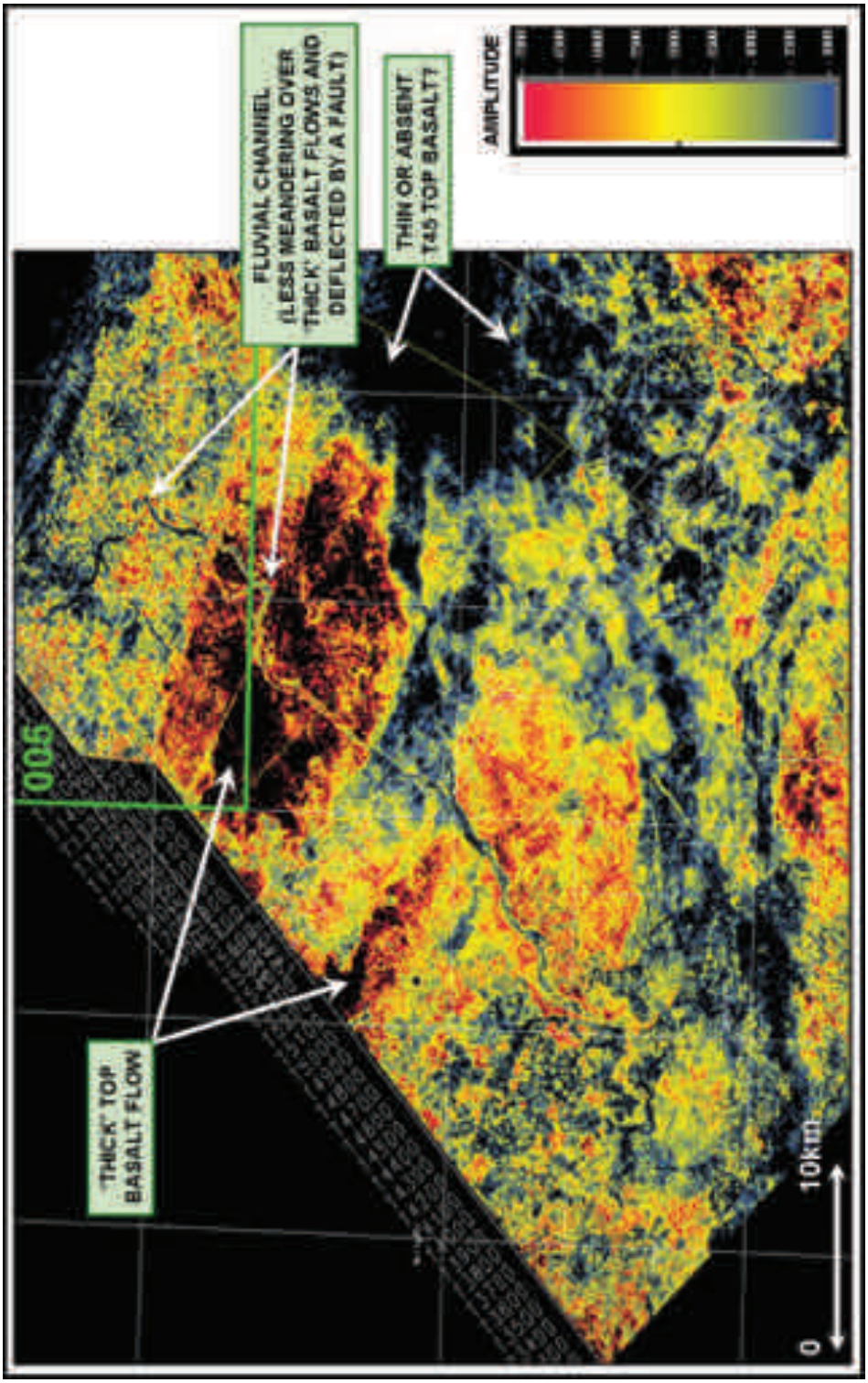

Figure 17. Seismic amplitude map for the Paleocene top T45 basalt pick. Dark red areas are interpreted as thick basalt lava flows, grey to black areas as sediments and intermediate yellow areas as thin basalt lava flows or volcaniclastics.

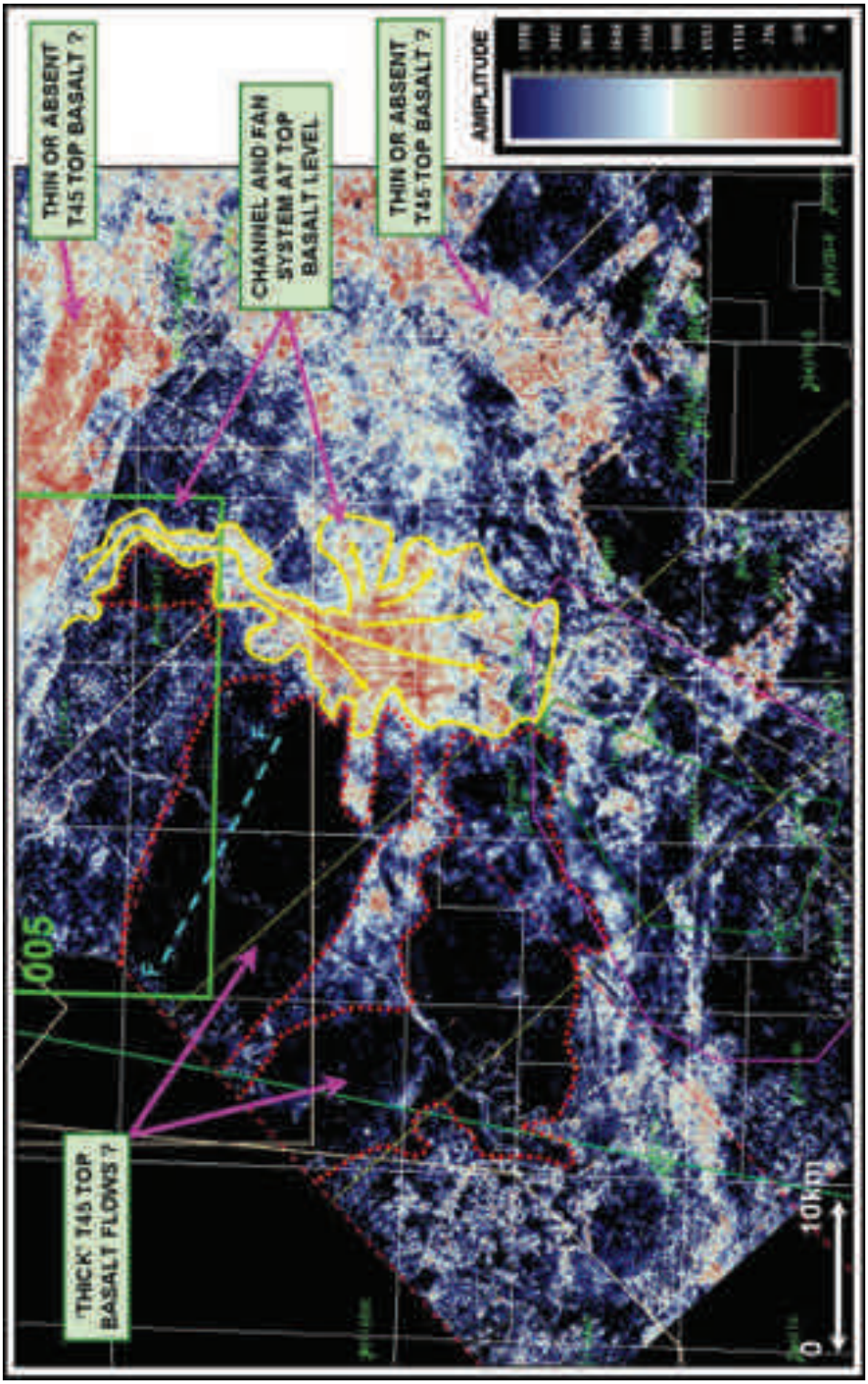

Figure 18. Seismic amplitude map for the Paleocene top T45 basalt pick highlighting the weaker amplitudes.

- Regional basin modelling for the Faroe-Shetland Basin indicates that much of the middle and late Jurassic source potential in the deeper sub-basins was realised prior to end Paleocene times, with post Paleocene oil generation mainly restricted to the margins of the sub-basin and the structural highs.
- The Westray-Corona Ridge is important in terms of regional prospectivity as it acts as a focus for hydrocarbon migration, it has the potential to hold early oil generated during Cretaceous and Paleocene times (prior to later re-migration), and the faults associated with the ridge are potential gateways for hydrocarbon migration up into shallower stratigraphic horizons.
- Licence 005 is located over a splay off the Westray-Corona Ridge. The Anne-Marie prospect in the southeastern part of the licence is a structural trap with the primary reservoir targets comprising sandstones in the Paleocene T40 and T31-T36 intervals. Secondary reservoir targets comprise sandstones in the Eocene T45-T50, Paleocene T10-T25 and Cretaceous intervals.
- Probabilistic petroleum system modelling for the Anne-Marie prospect indicates moderate to good potential for an oil charge to the primary reservoir intervals.
- Licence 005 appears to be located close to the edge of the thick Paleocene T40-T45 Faroese basalt sheet, where a few thin basalt lava flows may occur inter fingered with volcaniclastic and sedimentary units (the basalt section in the nearby UK 204/10-1 Cambo well to the east is approximately 100 m thick).
- Seismic amplitude mapping can be used to indicate depositional settings for potential reservoir units in the early Eocene (T45-T50) interval and, to a lesser degree, the Paleocene intrabasalt (T40) interval.

Eni and Faroe Petroleum believe that Licence 005 offers good prospectivity, being favourably located within the Faroe-Shetland Basin petroleum system. The Anne-Marie prospect offers good reserves potential at low to moderate risk in several plays that have already proven successful in wells along the Westray-Corona Ridge.

Acknowledgements

The authors would like to thank Eni UK Limited and Faroe Petroleum Plc for supporting the publication of this work.

References

Cawley, S., Matheson, H. and Stalker, G. 2005. An updated view of the Faroes-Shetland Petroleum System. *In*: Ziska, H., Varming, T. and Bloch, D. (eds) *Faroe Islands Exploration Conference: Proceedings of the 1st Conference*. Annales Societatis Scientiarum Faeroensis, Supplementum 43, Torshavn: 109-130.

Corradi, A., Ponti, D., Ruffo, P. and Spadini, G. 2003. A methodology for prospect evaluation by probabilistic basin modeling. In: Duppenbecker, S. and Marzi, R. (eds) *Multidimensional basin modeling.* AAPG Datapages Discovery Series 7: 283-293.

Doré, A.G., Lundin, E.R., Jensen, L.N., Birkeland, O., Eliassen, P.E. and Fichler, C. 1999. Principal tectonic events in the evolution of the northwest European Atlantic margin. *In*: Fleet, A.J. and Boldy, S.A.R. (eds) *Petroleum Geology of Northwest Europe: Proceedings of the 5th Conference*. Geological Society, London: 41-61.

Doré, A.G., Corcoran, D.V. and Scotchman, I.C. 2002. Prediction of the hydrocarbon system in exhumed basins, and application to the NW European margin. *In*: Doré, A.G., Cartwright, J.A., Stoker, M.S., Turner, J.P. and White, N. (eds) *Exhumation of the North Atlantic Margin: Timing, Mechanisms and Implications for Petroleum Exploration.* Geological Society, London, Special Publications 196: 401-429.

Ebdon, C.C., Granger, P.J., Johnson, H.D. and Evans, A.M. 1995. Early Tertiary evolution and sequence stratigraphy of the Faeroe-Shetland Basin: implications for hydrocarbon prospectivity. *In*: Scrutton, R.A., Stoker, M.S., Shimmield, G.B. and Tudhope, A.W. (eds) *The Tectonics, Sedimentation and Palaeoceanography of the North Atlantic Region*. Geological Society, London, Special Publications 90: 51-69.

Helland-Hansen, D. 2006. Rosebank - Challenges to development from a subsurface perspective. *Faroe Islands Exploration Conference 2006 (presentation)*, Torshavn.

Lamers, E. and Carmichael, S.M.M. 1999. The Paleocene deepwater sandstone play West of Shetland. *In*: Fleet, A.J. and Boldy, S.A.R. (eds) *Petroleum Geology of Northwest Europe: Proceedings of the 5th Conference.* Geological Society, London: 645-659.

Penland, S., Suter, J.R. and Boyd, R. 1988. The transgressive depositional systems of the Mississippi Riv-

er delta plain: A model for barrier shoreline and shelf sand development. *Journal of Sedimentary Petrology* 58: 932-949.

Smallwood, J.R. and Kirk, W.J. 2005. Paleocene exploration in the Faroe-Shetland Channel: disappointments and discoveries. *In*: Dore, A.G. and Vining, B.A. (eds) *Petroleum Geology: North-West Europe and Global Perspectives: Proceedings of the 6th Petroleum Geology Conference.* Geological Society, London: 977-991.

Smallwood, J.R., Prescott, D. and Kirk, W.J. 2004. Alternatives in Paleocene exploration West of Shetland: a case study. *Scottish Journal of Geology* 40 (2): 131-143.

Strogen, D.P., Burwood, R. and Whitham, A.G. 2005. Sedimentology and geochemistry of Late Jurassic organic-rich shelfal mudstones from East Greenland: regional and stratigraphic variations in source-rock quality. *In*: Doré, A.G. and Vining, B.A. (eds) *Petroleum Geology: North-West Europe and Global Perspectives: Proceedings of the 6th Petroleum Geology Conference*. Geological Society, London: 903-912.

Swift, D.J.P., Duane, D.B. and McKinney, T.F. 1973. Ridge and swale topography of the Middle Atlantic Bight, North America: Secular response to the Holocene hydraulic regime. *Marine Geology* 15: 228-247.

Ziska, H. and Andersen, C. 2005. Exploration Opportunities in the Faroe Islands. *In*: Ziska, H., Varming, T. and Bloch, D. (eds) *Faroe Islands Exploration Conference: Proceedings of the 1st Conference*. Annales Societatis Scientiarum Faeroensis, Tórshavn, Supplementum 43: 146-162.

Paleocene Sedimentary Models in the Sub-basalt around the Munkegrunnar - East Faroes Ridge

TIM GOODWIN[1], DAVID COX[2] AND JONATHON TRUEMAN[2]

[1] BP Exploration Operating Company Limited, Building C, 2nd Floor, Chertsey Road, Sunbury on Thames, Middlesex, TW16

[2] BP Exploration Operating Co Ltd., Burnside Road, Farburn Industrial Estate, Dyce, Aberdeen, AB21 7PB

ABSTRACT

Following disappointing results of exploration drilling in the Faroese extension of the Foinaven sub-basin in 2001, BP reviewed their exploration strategy in the region and identified an area of contrasting prospectivity. This prospectivity was targeted for drilling in 2007.

Exploration in the late 1990's focused on an extension of the play successfully developed in the Paleocene Foinaven and Schiehallion discoveries on the UKCS, targeting an area where Paleocene basalts were largely absent. Significant amplitudes were identified in the Paleocene T30 sequences and related to Direct Hydrocarbon Indicators (DHI) at nearby productive fields. Following drilling, failure was attributed to the absence of a seal linked to an increased volume of sandstone and an amplitude driven strategy without proven rock property support. Several anomalous lithologies were encountered which gave false hydrocarbon Amplitude versus Offset (AVO) signatures on seismic.

Our current area of interest (Faroes Exploration Licence 007) has targeted intervals within the Paleocene which exhibit evidence of northwest - southeast shelf progradation. These are correlated to the T20 and T30 section and can be linked to the tectonic development of the Munkegrunnar - East Faroes Ridge intersection. The interpretation has been clarified by selective re-processing in 2005 of long offset 2D seismic lines acquired in 2001. Correlation with the Paleocene of the Kangerlussuaq region of southwest Greenland can be made from outcrop to seismic. A series of gross depositional environment (GDE) maps are presented and discussed to analyse the potential for Paleocene prospectivity in the License 007 area and beyond.

Introduction

The initial phase of exploration on the Faroese Continental Shelf (FCS) concentrated on the northwestward extension of the successful Paleocene plays of the UKCS Judd Basin/Westray Ridge area beyond the extent of significant late Paleocene basalts (Figure 1a). This phase resulted in an oil and gas discovery at 6004/16-1Z (Marjun), a dry hole at 6005/15-1 (Longan) and oil and gas shows at 6004/12-1 (Svinoy) in 2001. A further dry hole was completed at 6004/17-1 (Marimas) in 2003 (Figure 1b). The results of this first phase have been well documented in the Proceedings of the 1st Faroe Islands Exploration Conference (Ziska *et al*., 2005).

Failure of this first exploration phase resulted largely from the presence of a significantly increased sandstone volume within the objective Paleocene T30's Vaila Formation (Ebdon *et al,*. 1995) and the presence of anomalous tuffaceous lithologies at the T35/36 level above the objective interval. This combination of lithologies resulted in anomalous seismic amplitudes and an AVO response consistent with hydrocarbons. However, the observed AVO response was found to be representative of lithology rather than trapped hydrocarbons. The increased volume of sandstones in the basin effectively decreases the potential for fault bounded traps. The discovery of oil in 6004/16-1Z (Marjun) within the T10 interval (Sullom Formation) and the lack of shows above it illustrates that the thermogenic front has not progressed above the earliest Paleocene sandstones in the basin centre. There the T10 (Sullom Forma-

Faroe Islands Exploration Conference: Proceedings of the 2nd Conference.
Annales Societatis Scientiarum Færoensis, Supplementum 50, 2009: 267-285

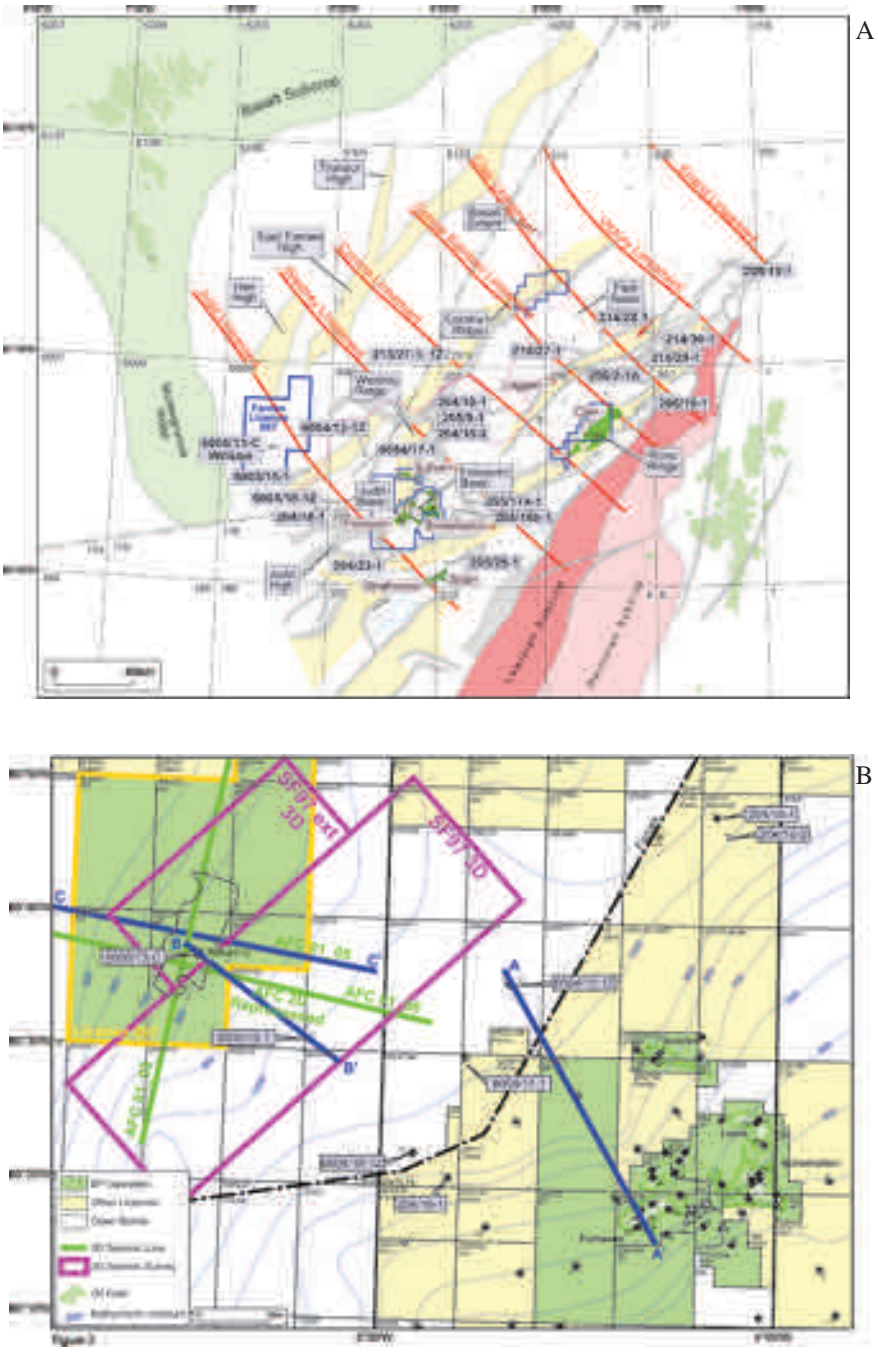

Figure 1a. Location of major tectonic elements in the Faroe-Shetland Basin. Yellow shading indicates basinal highs and the green shaded are indicates the extent of the Basalt outcrop (from Neish, 2005).
Figure 1b. Location map for Faroese Exploration License 007 and the William 6005/13-C well. BP operated licenses is shown in green, other licenses are shown in yellow and unlicensed areas shown as white. The William prospect is outlined (black). 3D seismic areal extent is outlined in purple and 2D seismic data shown in red. Key lines of section are shown in blue. Key exploration and appraisal wells in the Faroe-Shetland Basin discussed in the text.

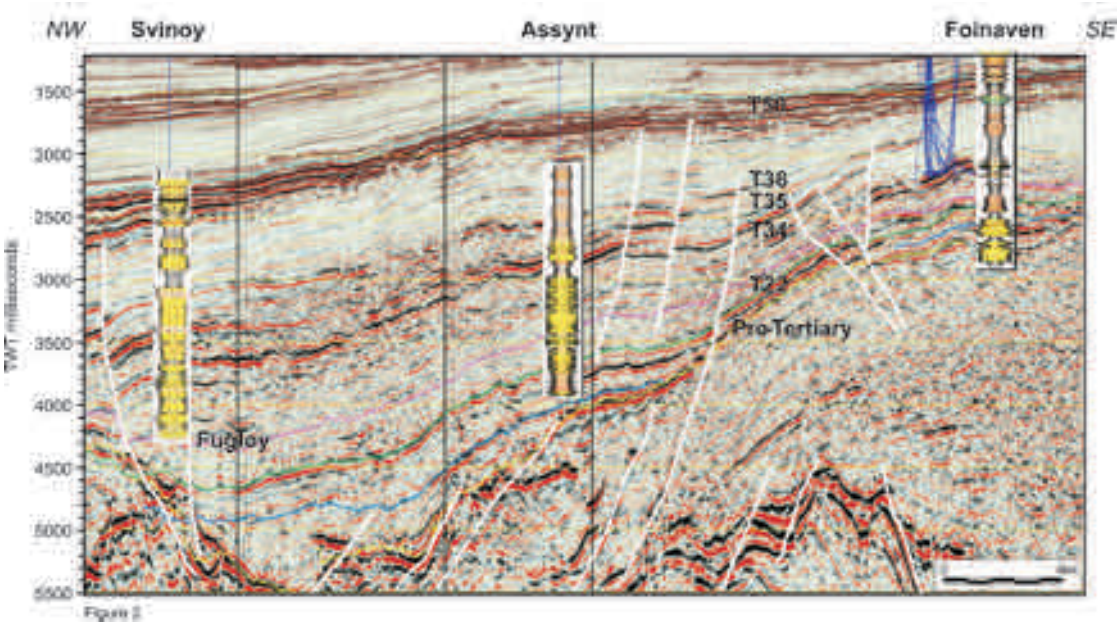

Figure 2. Arbitrary semi-regional seismic line NW-SE (location indicated in Figure 1b A-A') from the Foinaven field (204/24a-2) to the Svinoy (6004/12-1Z) exploration well via the Assynt (204/18-1) exploration well. The two-way time (TWT) interval between the T50 (light blue) and the T22 (green) horizon shows thickening of the unit into deeper water areas. Representative well sticks show the increase in sand proportion basinward (sand, yellow, mudstone and shale brown and grey and volcanics pink).

tion) mudstones are acting as a regional pressure and capillary seal. Review of the region post 2003 indicated lateral hydrocarbon migration from the basin centre rising stratigraphically via the T10's through the T20's and T30's (Vaila Formation). The traps in the UKCS Foinaven and Schiehallion fields forming through decreasing sandstone volumes and hence increased cross fault trapping potential (Figure 2). The phenomenon of vertical versus lateral migration within the Tertiary was described in detail by Cawley *et al*. (2005).

Following this initial phase of exploration a reassessment of prospectivity was undertaken, particularly in light of the exploration commitments that had been made in the first Faroese licence round. This re-evaluation determined that present, remaining prospectivity would most likely be restricted to high-risk, poorly-imaged sub-basalt targets. These opportunities would also be limited by a poor understanding of reservoir and source rock systems in the area.

This paper describes the integration of tectonic, seismic, outcrop, well data and regional knowledge to frame prospectivity around the Munkegrunnar-East Faroe Ridge and in particular, on the possibility of defining shallow and deep marine reservoir systems in the early-mid Palaeocene.

Area of Interest

The area of interest is Faroese Licence 007 and surrounding area (Figure 1b). It is currently operated by BP (50%) on behalf of Shell (25%) and Anadarko Petroleum Corporation (25%). The area lies in 500m - 800m water depth and is located 175km southeast of Torshavn, Faroes and 230km west of Sullom Voe, Shetland. It is 77 km northwest of the Foinaven production vessel. The nearest fixed pipeline is the Schiehallion to Sullom Voe gas pipeline.

Database

BP and Shell have been actively exploring the

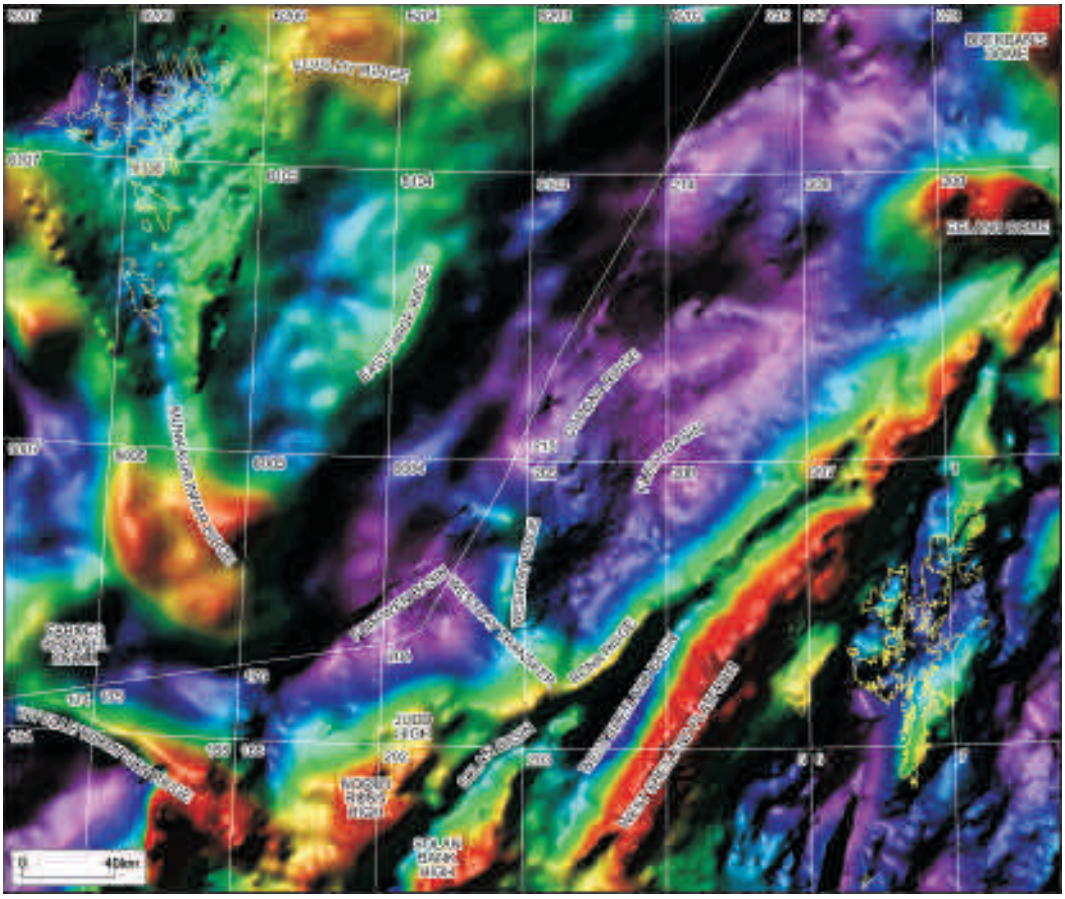

Figure 3. Regional crustal corrected gravity magnetic data for the Faroe-Shetland Basin area of interest (courtesy of Geological Survey of Canada and the British Geological Survey; Verhoef et al., (1996)).

Faroese continental shelf and adjacent UK continental shelf in partnership since the mid 1990's. The area is covered by almost contiguous 3D seismic and several significant regional 2D surveys, largely acquired over the last 10 years. In addition to this seismic database an almost complete set of well data is available for the region in addition to the invaluable field based studies produced as a result of the Sindri consortium over the past five years. The collaboration of BP and Shell with Anadarko in Licence 007 importantly included a recent vintage 2001 2D long offset seismic survey. This survey revealed several features of potentially significant stratigraphic interest.

Seismic Interpretation

The workflow utilised in the evaluation of the area included building an integrated 2D dataset, merging and enhancing the existing 3D survey and reprocessing the long offset 2D data. Reprocessing of the long offset AFC01 2D data brought out some significant features which may represent sedimentary architecture.

Structural interpretation relied heavily on the tie to the offset well 6005/15-1 (Longan) where the late Paleocene basalts are 32 m thick (Figure 4a and 4b). The basalt tie is the most critical issue in the area given its impact on understanding prospectivity. Above the basalt the top Eocene and top Oligocene are clear reflectors, whilst below the

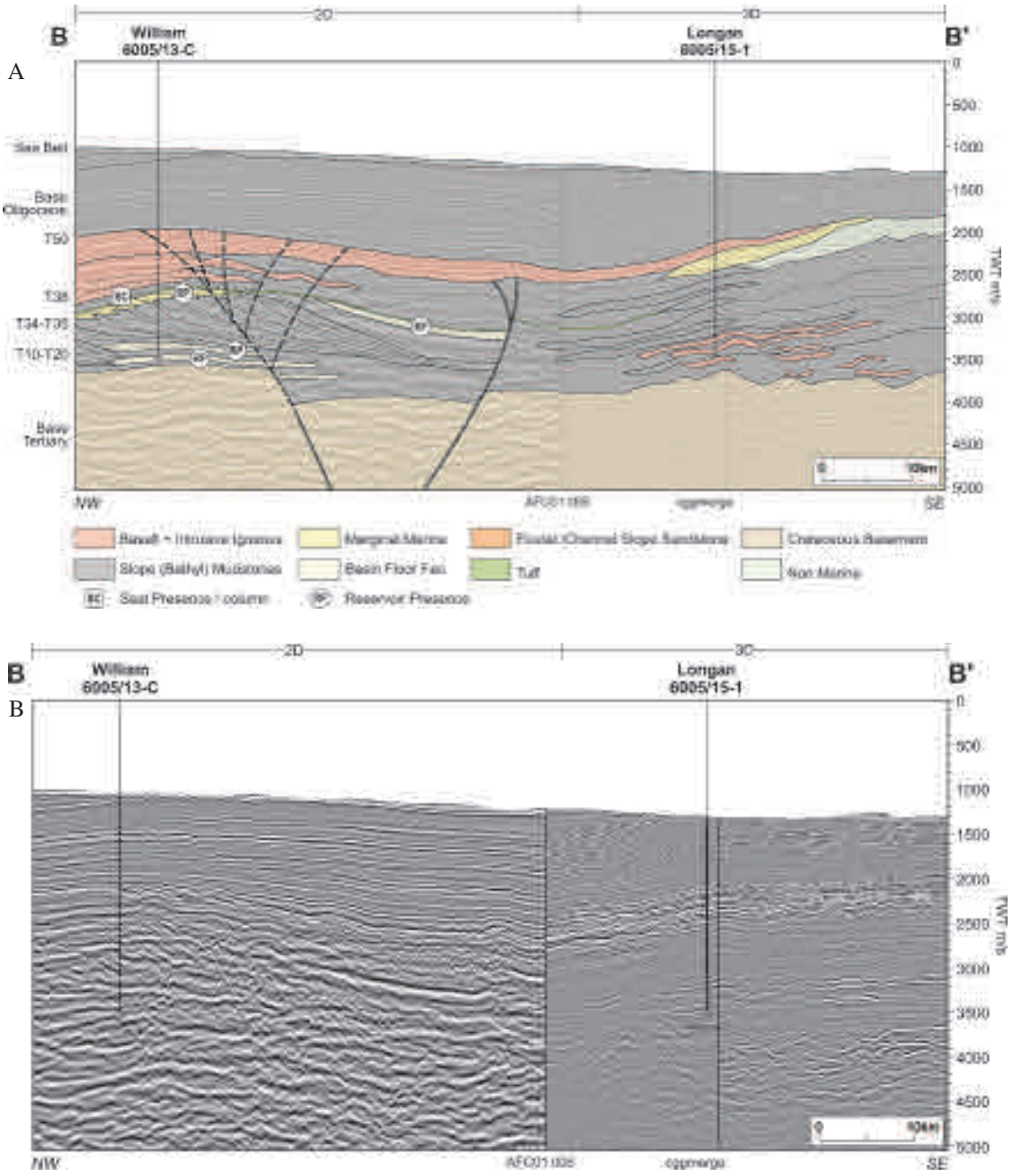

Figure 4a. A NW-SE seismic line (location indicated in Figure 1b B -B') between the 6005/15-1 (Longan) well and 6005/13-C (William) showing the idealised interpretation of the seismic packages between the wells. The William well is located on the AFC01_005 long offset 2D seismic line and the Longan well is located on the cggmerge 3D seismic dataset. **Figure 4b** A NW-SE seismic line (location indicated in Figure 1b B -B') between the 6005/15-1 (Longan) well and 6005/13-C (William) showing the uninterpreted line of section.

basalt significant challenges are encountered making meaningful picks and correlations.

Interpretation Philosophy

The first phase of exploration in the Faroes offshore over-emphasised the seismic analysis approach based strongly on the identification of DHI and AVO effects. The approach relied heavily on an understanding of rock properties which were not calibrated from proximal to distal facies or proven to unproven stratigraphy. The current approach is led by the traditional exploration processes of mapping structure, mapping and modeling reservoir distribution and facies, and regional understanding of source rock and charge systems. Here we have linked seismic observations to onshore outcrops on the tectonically reconstructed conjugate margin, in particular to allow interpretations of the Paleocene sub-basalt sedimentary systems.

Regional Structural Setting

Faroes Exploration Licence 007 lies to the northeast of the Judd Basin and is traversed by two significant structural features, the north-south trending Munkegrunnar Ridge and the northeast-southwest trending East Faroes Ridge (Figure 1a and Figure 3). The Judd transfer zone which delineates significant provinces to the south in the UKCS, is interpreted to transect the area.

The Munkegrunnar Ridge

The origin and expression of the Munkegrunnar Ridge itself is problematic and described in detail by Linnard and Nelson (2005). These authors related the feature to a regional Vaila Plume Belt linking the Lundy Granite, regional Palaeogene uplift and Hebridean volcanism. They proposed the ridge as originating from this early T20 - 30 'Vailian' phase of plume activity and contrasted its nature and size with other significant post-Eocene inversions on the NW-SE trend regionally. From the seismic expression we considered the ridge as a potentially inverted north-south Jurassic rift between the Judd and Inner Hebridean Basins. In the Munkegrunnar Ridge region, the plume event 'hijacked' the precursor rift, growing through the Cretaceous and progressing through eruption and successive extrusion associated with the continental break-up event. The orientation of the feature can be compared to the Hebridean, North Viking Graben and East Greenland Jurassic rift features. Whatever its pre-Tertiary origin, the growth of the feature significantly influences Tertiary deposition and post-Paleoecene sedimentary deposition.

Chronostratigraphic Framework

Our understanding of the region is based on recent interpretation of new seismic, palaeontological, wireline and core data gathered since 2001. This has been integrated with the fieldwork carried out by members of CASP and GEUS under the auspices of the SINDRI consortium through the period. This work has provided the basis for an interpreted Paleocene choronostratigraphy which is based on the widely recognised BP sequence scheme applied in the Judd Basin (Ebdon *et al.,* 1995). The major sequences have been refined and subdivided considerably in the area around Foinaven and Schiehallion but are referred to here by the original coarse classification. Stratigraphic relationships of these plays are illustrated in the regional chronostratigraphic chart (Figure 5).

Sequence T10 - Sullom Fm

The T10 Sequence (Figure 6) is the oldest Paleocene sequence in the region. It was penetrated in wells 6004/16-1Z and UK 204/16-1 where it lies unconformably on the late Cretaceous (Campanian-late Maastrictian). In well 6004/16-1z, a 138m section of grey claystones, siltstones and local thin limestones overlay a 168m+ section of poorly-sorted and well-cemented sandstone interbedded with minor claystones and siltstones. This sandstone was hydrocarbon bearing. Poor quality Modular Formation Dynamics Tester (MDT) samples indicated single phase waxy crude of about 44°API. In UK 204/16-1 well 104m of grey claystones, siltstones and thin limestones were encountered overlying 201m of fine to medium-grained well-cemented sandstones with interbedded medium to dark grey claystones. Some gas

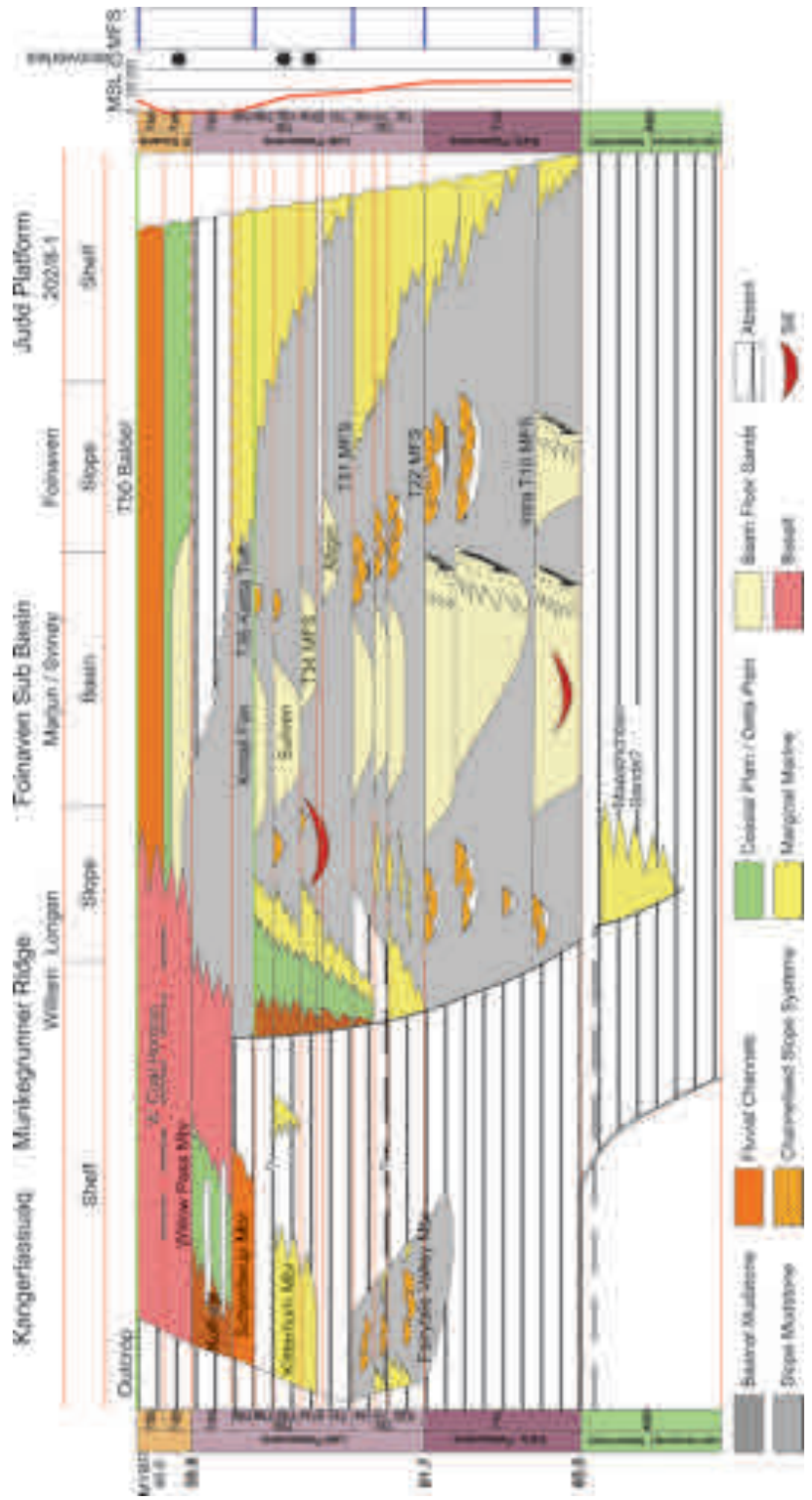

Figure 5. Schematic chronostratigraphic summary correlating the early Paleogene successions West of Shetland, the Faroes and the Kangerlussuaq Basin of southern East Greenland (adapted from Larsen & Whitham 2005). The schematic sea level curve from well 205/9-1 has been added to indicate palaeo-water depth for each depositional sequence.

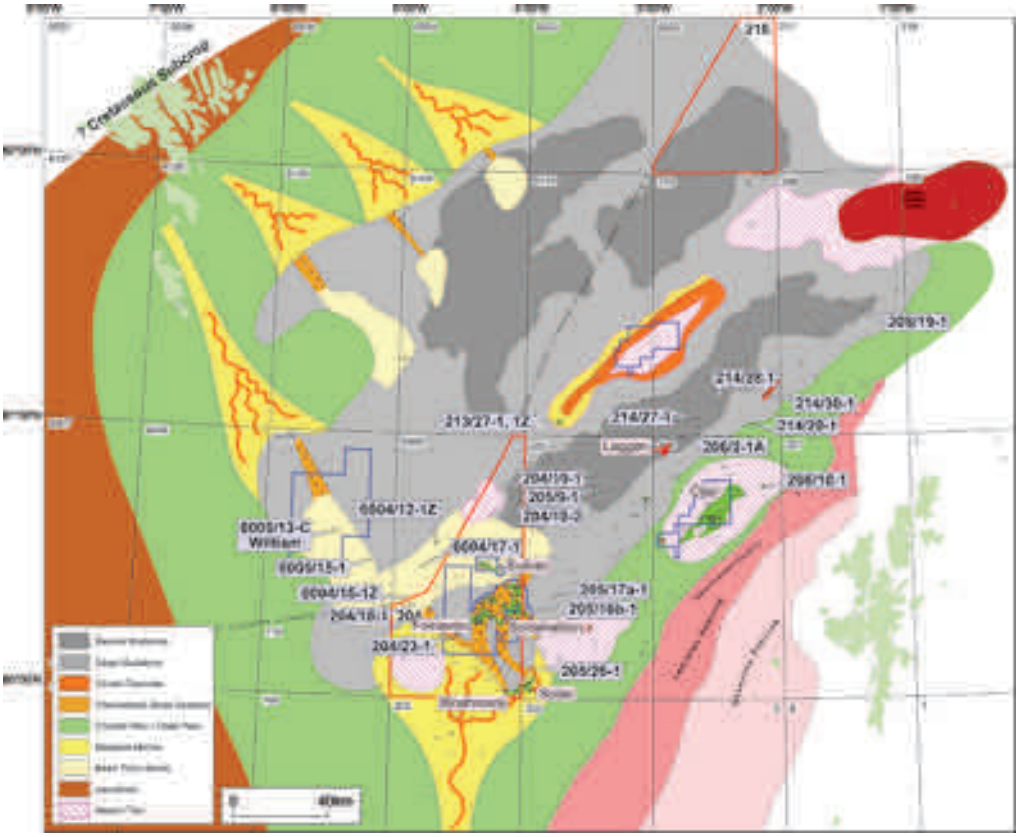

Figure 6. T10 gross depositional environment (GDE) map.

shows were observed in this section.

In the Munkegrunnar Ridge the degraded seismic response and poor biostratigraphic control masks the temporal equivalent of the T10. Measured sections (Larsen and Whitham 2005) at Watkins North End, Watkins Fjord and Sill City in Kangerlussuaq (Figure 7) describe 10-90 m sections of dominantly marine claystones ('deep basin floor,' Larsen *et al.,* 2005). These contain *Spiniferites 'magnificus'* and *Palaeocystdinim bulliforme* indicating late Danian strata.

Plate reconstructions indicate the proximity of the Kangerlussuaq region during early Paleocene times. Possibly condensed (or absent) T10 claystones are interpreted at Kangerlussuaq. On the eastern flank of the Munkegrunnar Ridge current interpretation also anticipates condensed T10 Sullom Formation. This condensation onto and possibly across the Munkegrunnar Ridge to Kangerlussuaq presumes a precursor structure. In the Kangerlussuaq area, both a significant Campanian - Santonian unconformity and a late Maastrictian - early Danian unconformity are described (Christian IV Formation and 204/16-1).

In the Judd Sub-Basin area, the sequence represents deposition from significant aggradational basin floor fans and their abandonment. Towards the southeast they may be locally fault controlled (Ebdon *et al.,* 1995) and heavy mineral analysis supports its provenance largely from the UKCS (Morton *et al*., 2002).

Sequence T20 - Vaila Fm

The T20 sequence (Figure 8) is recognised across the Judd sub-basin where it has been encountered by numerous commercial wells. In the area of in-

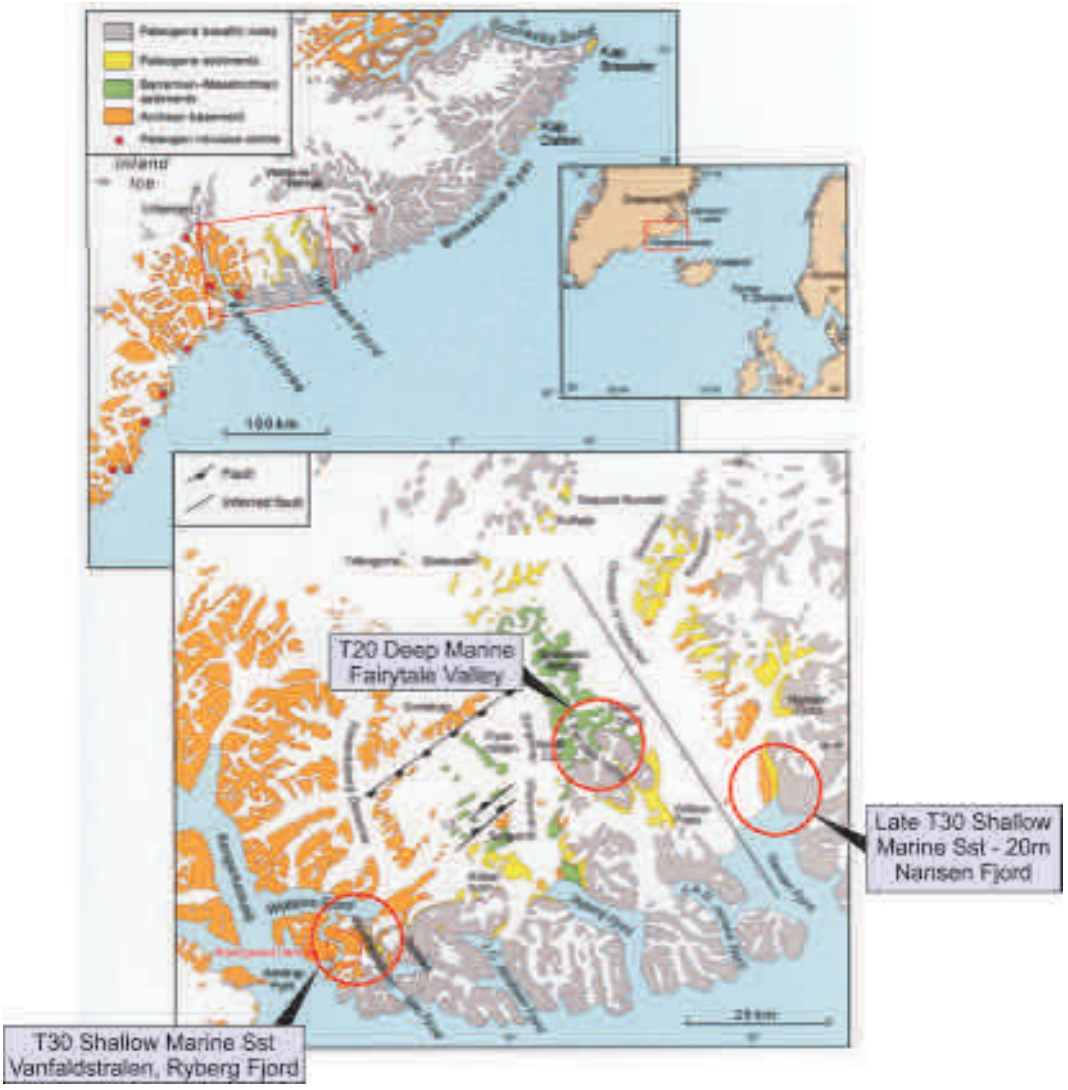

Figure 7. Geological map of the Kangerlussuaq area in southern East Greenland showing the distribution of Cretaceous-Paleogene sediments and Paleogene basaltic rocks. Modified from Larsen & Whitham 2005. interpretation.

terest however it has not been penetrated. The closest penetrations are the 6004/16-1z (463m gross T20 section) and UK 204/16-1 (453m gross T20 section) wells to the south of the area of interest. The definition of top T20 is indistinct given the basin central correlative conformity between T28 and T31 sandstones. The sections encountered comprise an overall coarsening upward cycle from grey claystones and siltstones with minor limestones into massive fine to medium and coarse-grained sandstones. Several thin carbonate-rich intervals are identified throughout on wireline logs.

In the Kangerlussuaq area possible temporal correlative sequences have been identified (Larsen and Whitham, 2005) (Fairytale Valley Member of the Sediment Berge Formation) (Figure 7). In Fairytale Valley the sequence contained stacked sequences of 10-20m fine to medium-grained

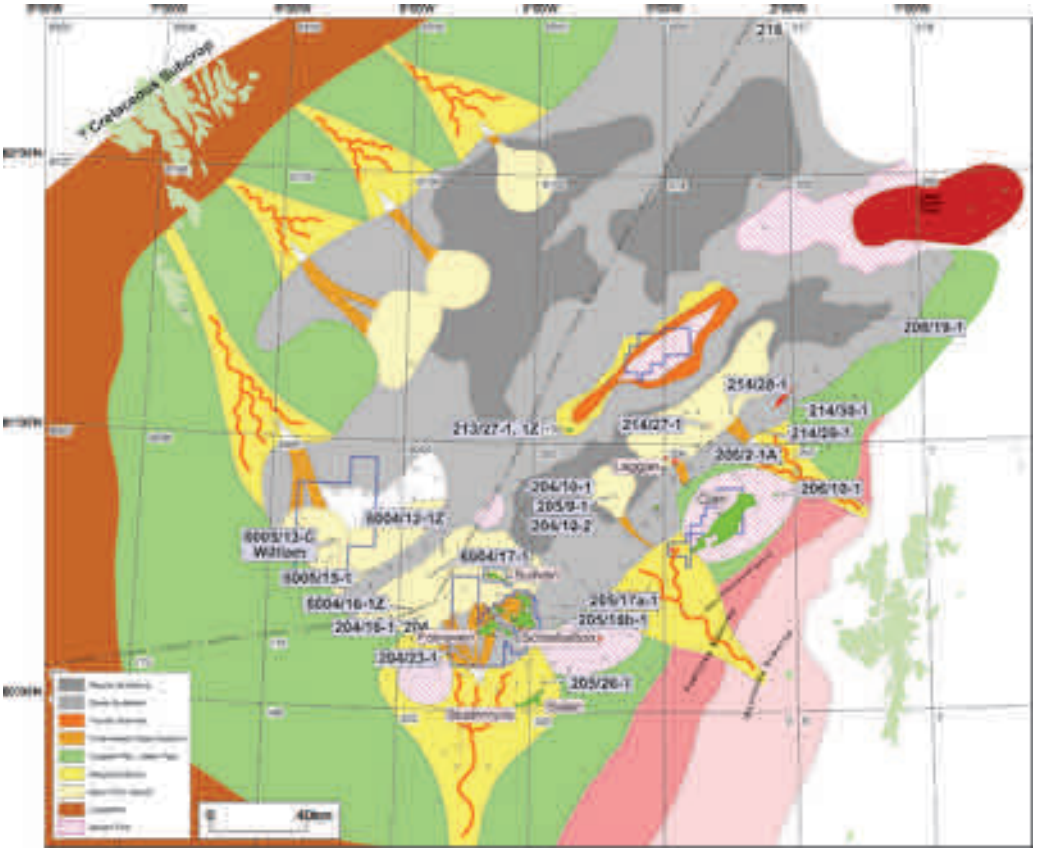

Figure 8. T20 gross depositional environment (GDE) map.

sandstones with interbedded 5-10m mudstones. The sandstones were described containing common *Planolite*s and local *Diplocraterion* traces.

In the area of interest around the Munkegrunnar Ridge (Figure 1a), correlation to the broad T20 sequence has focussed on a thin unit exhibiting a clinoform package as observed on long offset seismic 2D line AFC01_005 (Figures 9a & 9b). This interval of some 200-300 ms two-way time illustrates a simple possible progradational seismic motif trending northwest to southeast.

Review of data along the Faroes escarpment by Naylor *et al.,* (1999) and Kiørboe (1999) clearly describe clinoforms resulting from basaltic flows, albeit from younger Paleocene sequences. The formation of such clinoforms is well established with respect to the Faroe-Shetland escarpment. Several authors (Smythe 1983; Smythe *et al*., 1983 Andersen, 1988; Boldreel and Andersen, 1993) describe the escarpment forming as a result of terrestrially erupted basalts being abruptly halted at the contemporary shoreline bordering a restricted shallow water shelf (Kiørboe, 1999). See below for an explanation of the nature of the observed clinoform package.

Sequence T30 - Vaila Fm & Lamba Fm

The generic T30's sequence (Figure 10) incorporates the T32, T34, T36 and T38 sequences and has been encountered by numerous commercial wells in the Faroe-Shetland basin. The T30's marks a significant change in the position of the palaeo-shelf edge and basin floor topography and encompasses a series of sea level fluctuations and associ-

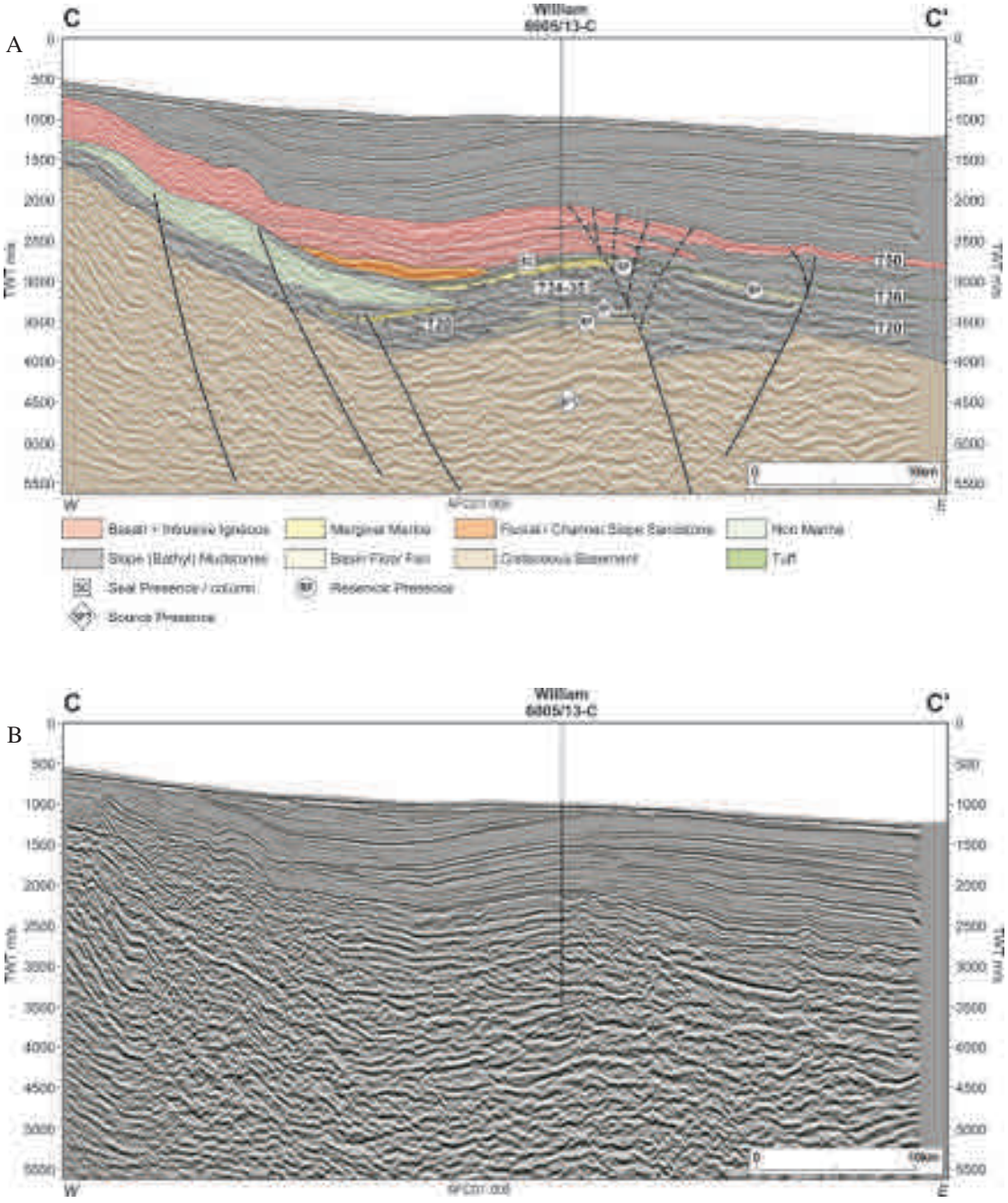

Figure 9a. A West/East seismic line on 2D long offset AFC01_005 (location indicated in Figure 1b, C-C') across the 6005/13-C (William) location showing the idealized geoseismic interpretation. **Figure 9b.** A West/East seismic line on 2D long offset AFC01_005 (location indicated in Figure 1b, C-C') across the 6005/13-C (William) location showing the uninterpreted line of section.

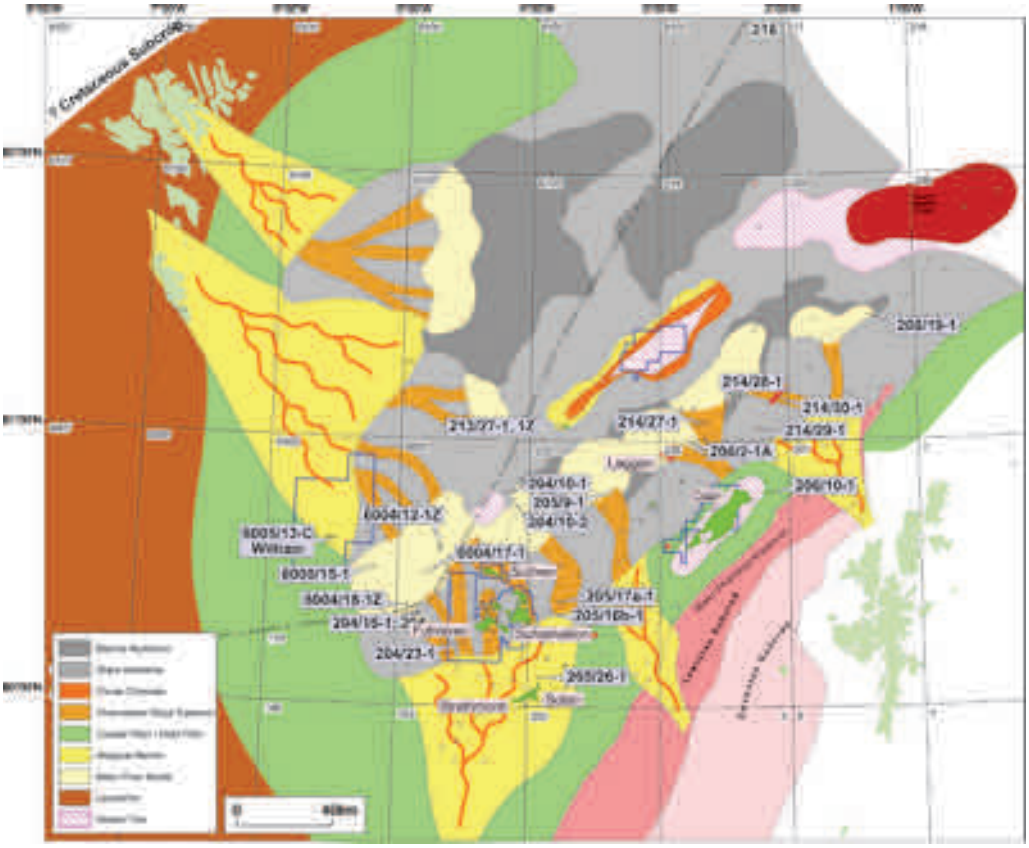

Figure 10. T30 gross depositional environment (GDE) map.

ated pulses of sedimentation.

In the earliest T30's (T32) in the Faroe-Shetland Basin, the sequence progrades to the north-west from the position of the T20 shelf edge. The progradation is associated with an increase in sediment supply fed through existing sediment entry points as a result of shelfal erosion during a lowstand event.

Progradation continues through the middle T30's (T34) with the focal point of progradation now shifting towards the north, although the pattern of the facies distribution is consistent with the preceeding Paleocene depositional sequences (Ebdon *et al*., 1995). Coarse channel fill sandstones are encountered in the 204/23-1 well and form the feeder channels for the extensive T30's fan sandstones encountered in the 6004/16-1Z, 6004/12-1Z and 6005/15-1 wells in the Faroese sector of the Faroe-Shetland Basin. The significant increase in sediment supply and subsequent progradation of the T30's sequence is the result of uplift associated with the mantle plume prior to the opening of the North Atlantic (White and McKenzie, 1989; Nadin *et al*., 1997; White and Lovell, 1997; Champion *et al*., 2008).

The associated fall in relative sea level at this time and incision and erosion of the palao-shelf and recycling of sediment is supported by the heavy mineral assemblages which are depleted (Morton *et al*., 2004) and indicative of recycled sedimentary material. A significant unconformity and regional change in relative sea level is also observed in the outcrops of eastern Greenland (Larsen and Whitham 2005), which could support a basinward shift of sedimentary depositional environments into the licence 007 area. Cored sec-

tions of the T30's also show gravity slide and slump sedimentary structures associated with tectonic instability and regional uplift (Knox *et al*., 1992).

The late T30's (T36) marks a continuation of the large scale progradation basinward with high rates of deposition in a major lowstand event culminating in the formation of the Cuillin and Kintail fans sourced from the south of the Faroe-Shetland Basin and axially from the north-east.

Sequence T40 - Flett Fm

The T40 sequence (Figure 11) reflects the final fill of the available accommodation space at the end of the Paleocene in the Faroe-Shetland Basin. The sequence is characterised by high amplitude seismic reflectors and prograding clinoforms and is interpreted to represent the lowstand prograding wedge of the transgressive systems tract. The depositional environments incorporated into the T40's sequence are delta top coastal plain sandstones capped by coals, which in some instances are interdigitated with extrusive igneous basalts which are the result of the opening of the North Atlantic.

Gross Depositional Environment Mapping

Stratigraphic Framework

The sequence stratigraphic understanding of the Faroe-Shetland Basin is based on the interpretation of 75 2D seismic lines, 1800sq km of 3D seismic, and wireline log and biostratigraphic data from 90 exploration and appraisal wells in the basin. The recent work has provided the basis for the refinement of the gross depositional environment (GDE) maps for the key Tertiary 'T' se-

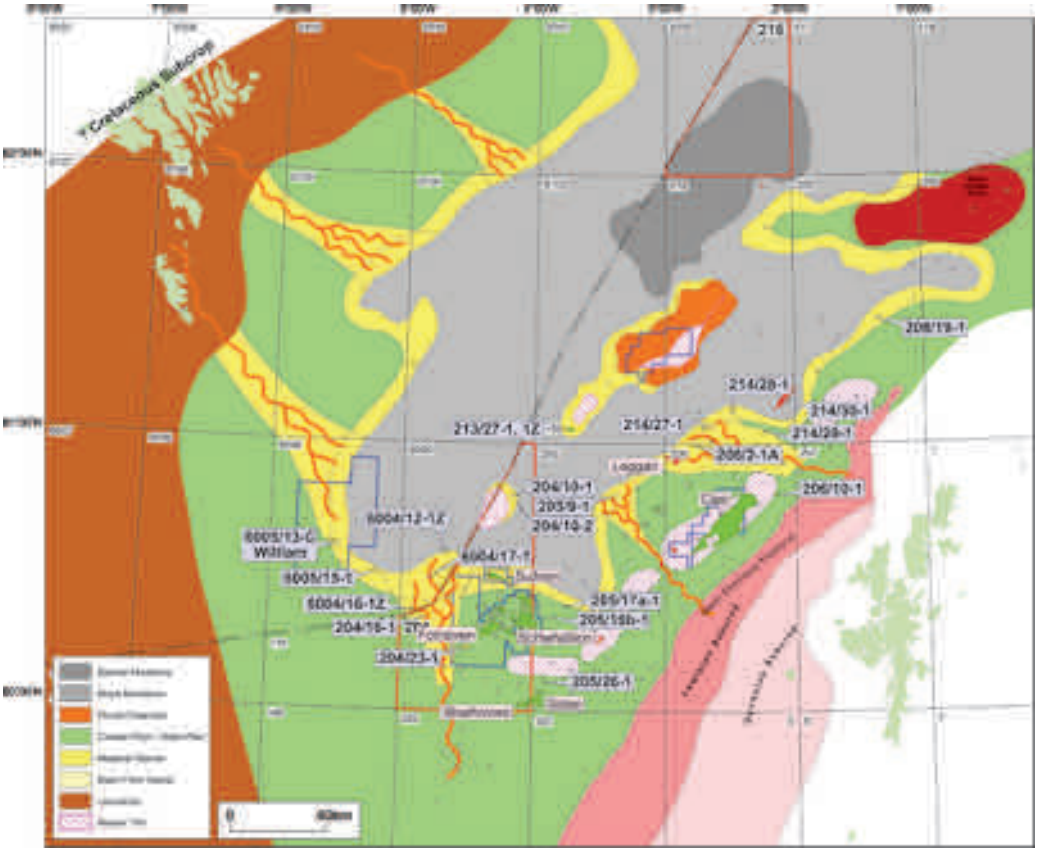

Figure 11. T40 gross depositional environment (GDE) map.

quences. The characteristics of each of the sequences are summarised below.

Sequence T10 GDE (Sullom S1-S2, Danian)
The T10 GDE sequence illustrates the incipient stages of the basin fill in the earliest Paleocene in the accommodation space created by the onset of the Cretaceous rifting events. The T10 sequence incorporates the Sullom Formation of the Shetland Group and represents the sequence stratigraphic high stand. The Sullom Formation is dominated by mudstone which is generally calcareous and is the equivalent to the Ekofisk Formation of the lower part of the Maureen Formation of the Central North Sea. The T10 sequence encompasses shelf, slope and basin depositional environments (Figure 6).

Figure 6 shows that the southwest part of the Faroe-Shetland Basin, around Quadrants 204 and 216 forms the primary depocentre and was the focal point for sedimentary deposition. The sediments deposited at this time were primarily basin floor sands. The major sedimentary entry point is interpreted to be from the south-west coming through Quadrant 204 in the Foinaven/Schiehallion field areas. This entry point provides a means of bringing sediment derived from the Palaeogene uplift of the Orkney-Shetland platform on the UK side of the basin.

To the northwest of the Faroe-Shetland Basin on the Faroe side, sediments are interpreted to have been sourced from Greenland where it has been estimated that some 30% of sediment could have been derived (Smallwood *et al., in press*). Heavy mineral analysis from some of the wells drilled in the Faroes sector undertaken by GEUS (Frei *et al*., 2005) also support a Greenland derived sediment source. These sediments are thought to be the temporal equivalent of the Fairytale Valley Member of the Sediment Berge Formation of the Kangerlussuaq area (Figure 7). The interpreted GDE for the T10 sequence assumes that the sediment entered the basin in the northwest through the transfer fault systems that were in existence at the time and may have acted as conduits for sediment transport. Direct evidence from wells indicates that the focal point for deposition would be to the southwest around Quadrant 6004 on the Faroe side of the median line and Quadrants 204 and 216 on the UK side of the median line.

Sequence T10 (Sullom S1-S2, Danian) Sub-environments
The shelf environments of the T10 sequence can be observed in the 205/26-1 well where the sequence is characterised by fine to medium-grained, sub-rounded to rounded, frosted, locally iron-stained sandstone with abundant shell fragments interbedded with minor shales. The slope depositional environment is characterised by the 205/17a-1 well where the T10 sequence is dominated by dark-grey to green grey, silty calcareous claystone with finely disseminated carbonaceous fragments. The basinal depositional environment is characterised by the 204/16-1 (Marjun appraisal) well, which is located in the deepest part of the Faroe-Shetland Basin and what was the focal point for sedimentation in the earliest Paleocene. The T10 sequence in the well is dominated by dark grey, calcareous claystone and medium grey moderately calcareous siltstone interdigitated with fine to very fine-grained, well -sorted, turbidite sandstones.

Sequence T20 (Vaila T22-T28, Selandian)
The T20 GDE sequence comprises the Vaila Formation of the Faroe Group and incorporates the V1 and V2 informal subdivisions. The Vaila units (V1-V4) are defined by the gamma ray signature of the constituent mudstones in conjunction with microfossil associations. The T20 GDE sequence represents the onset of the sequence stratigraphic lowstand and infill of the Faroe-Shetland Basin through the aggradation and progradation of the T20 sequence. The Vaila Formation comprises medium to dark grey, variably silty mudstones with thick sandstone units present in basin floor sections. The Vaila Formation represents deposition in environments ranging from outer shelf to basin (Figure 8).

Figure 8 shows the continuation of sedimentation following on from the previous T10 sequence. The focal point for sedimentation of the T20 sequence was again in the south-west around Quadrants 204 and 216 where there was greater accommodation space and conduits for sediment input.

From the well database it is evident that there are greater number of potential sedimentary entry points in the T20 sequence and that the supply of sediment was more significant, all other things being equal. Figure 8 shows that on the UK side of the median line the dominant entry point for sediment is still to the south west, however there is evidence to indicate that there are additional entry points developed in the areas of Quadrants 205 & 214 for the T20 sequence, which may reflect increased sediment supply and/or increased basin subsidence.

Sequence T20 (Vaila T22-T28, Selandian) Sub-environments

The shelfal depositional environment of the T20 sequence is not always well preserved because the later T30 and T40 sequences have often eroded the structural highs and, removed the T20 sequence. This leaves later sequences lying unconformably on the Maastrichtian of the late Cretaceous. The slope depositional environment is characterised by the 214/30-1 well where the T20 sequence is dominated by dark brown, non calcareous claystones interbedded with occasional siltstones.

The T20 sequence (V1/T22) in the basinal depositional environment is typified by the sediments in the 214/27-1 gas discovery well where the sequence is characterised by grey to dark grey, occasionally brown and slightly calcareous shales with thinly interbedded siltstones. The T20 sequence (V1/T25) is characterised by grey to grey brown, very fine to fine-grained, moderately-sorted, thick (280m, 80% net to gross) turbidite sandstones interbedded with grey to dark grey, occasionally brown claystones. The T20 (V2/T28) sequence in the basinal depositional environment is characterised by the 208/19-1 well and light grey, slightly calcareous claystones. The T20 (V2/T28) sequence in well 205/9-1 is comprised of a medium to dark grey siltstones, which grades to sandstones in places.

Sequence T30 (Vaila T31-T36 / Lamba T36-T38, Selandian)

The T30 GDE sequence comprises the Vaila Formation of the Faroe Group and incorporates the V3 and V4 informal subdivisions as described in the previous section and includes the T31-T36 sequences. The Lamba Formation constitutes the upper part of the Faroe Group and comprises the T36-T38 sequences including the T36 Kettla Tuff Member. The T30 sequence represents the sequence stratigraphic lowstand and the continued infill of the Faroe-Shetland Basin. The T30 sequence defines deposition in environments ranging from outer shelf to basin (Figure 10).

The division between the Vaila and the Lamba Formations is marked by the Kettla Tuff Member which consists of dark grey-green tuffaceous siltstone. The Kettla Member is presumed to be the result of debris flow deposition (debrites) but in places it does appear to rest directly on the sequence boundary as a condensed section.

The T30 GDE sequence is the key prospective interval for Paleocene reservoirs and represents the continuation of the sequence stratigraphic lowstand. The T30's GDE shows the incision and recycling of the paleoshelf sediments and subsequent infill of the Faroe-Shetland Basin with significant thicknesses of potential reservoir quality sandstones. The T30 GDE shows the progradation of the T30 sequence, as a result of a fall in relative sea level and increase in sediment supply, from already established conduits for sediment input discussed in the context of earlier Paleocene sequences.

The model for the GDE sequence on the Faroese side of the median line utilises outcrop analogue evidence form eastern Greenland (Larsen & Whitham 2005). In the sediments of eastern Greenland there is evidence to support a large scale base level shift in the T30's sequence, which culminates in the basinward migration of the established sedimentary depositional environments. The result of the basinward migration of the depositional environments are the presence of potential reservoir quality sandstones in the Faroes Exploration License 007, William area.

Corresponding evidence for this comes from the reprocessed AFC01, long offset 2D seismic which shows clinoform features which have been interpreted to have a sedimentary origin (Figures 9a and 9b). However, it must be stressed that the same clinoforms could have an extrusive igneous origin. Two clinoform packages have been inter-

preted in the area as candidate T20 and T34/35 sequences. The lower, weakly defined clinoform package is interpreted as a candidate southeasterly prograding T20 shelf edge with condensed slope and toe of slope deposits. This sequence is correlated with potential slope channel deposits in Kangerlussuaq and the Foinaven - Schiehallion area of UK Quadrant 204, where progradation is west and north westerly. The description of clinoforms in the Faroese channel gives rise to two end-member alternate interpretations:

1. Sedimentary clinoforms derived from a north-west to south-easterly drainage basin. This orientation would source sediments from the proto-Faroese and Munkegrunnar Ridge area uplifting in response to mantle underplating or plume activity ahead of continental break up. These are tentatively interpreted as inverted Jurassic-Cretaceous sediments, with shallow marine Cretaceous deposits providing a significant potential second cycle clastic provenance and thick source rock potential

2. Early Paleocene extrusive igneous clinoforms derived from terrestrially erupted basalts being abruptly halted at the contemporary shoreline bordering a restricted shallow water shelf. The extrusive basalts being generated in response to the early emplacement of the Munkegrunnar Ridge associated with plume activity ahead of continental break-up.

The angle of repose of the clinoforms has been considered as a means of differentiating between the end member interpretations. However, measurements of clinoforms observed on the Faroes Escarpment (OF94-55, 40°), the ISiMM line (16°) and the William structure (14°) prove inconclusive (Figure 12).

Sequence T30 (Vaila T31-T36 / Lamba T36-T38, Selandian) Sub-environments

The T30 shelf depositional environments can be observed in well 206/10-1 where the T30 sequence lies unconformably on the Upper Cretaceous. The sandstones in the well are grey-white, well-sorted and angular to sub-rounded with frosted grains. The sandstones are often glauconitic, micaceous and are interbedded with thin coals and limestone stringers. The slope depositional environments are characterised in well 205/16b-1 in which they comprise medium grey-brown, argillaceous and calcareous siltstones occasionally interbedded with thin (2m-5m) very fine to medium-grained, moderately-sorted sandstones. The basinal depositional environment of the T30 sequence is characterised by the basin floor turbidite sandstones of the 6004/12-1 &1Z (Svinoy) well. The sandstones are very fine to medium-grained, transparent, very spherical with moderate sorting, interdigitated with thin, grey, very argillaceous siltstones and grey mudstones.

Sequence T40 (Flett T40-T45, Selandian-Thanetian)

The Flett Formation constitutes the lower part of the Moray Group in the Faroe-Shetland Basin. The T40 GDE sequence was deposited in shallow to intermediate water depths in a ramp margin like setting. The facies exhibited are progradational shallow marine facies, ranging from paralic delta-top facies in proximal sections to pro-delta facies in more distal sections (Figure 11). The T40 sequence represents the final stages of the filling in of the Faroe-Shetland Basin depocentre (Figure 11). Significantly, basaltic lavas are observed to interdigitate with the sedimentary sequences in the 205/9-1 well which would have been extruded at or near sea level.

The paralic delta-top facies of the T40 sequence encountered in 206/2-1a show a coarsening upward gamma array profile indicative of a progradational sequence. Cores were acquired in the T40 sequence of wells 206/2-1a, 214/28-1 and 214/29-1. The cored T40 sequence in the 206/2-1a shows cross-bedding, laminations and is bioturbated. There is also evidence of plant debris, fish scales, gastropods and lamellibranchs. The T40 sequence cored in the 214/29-1 well has coals and lignite in addition to traces of glauconite. The delta-top facies of the T40 sequence cored in the 214/28-1 well shows graded bedding in places, traces of glauconite and carbonaceous material.

The pro-delta sequences of the T40 are characterised by successions consisting of grey, occasionally silty mudstones and claystones which commonly contain carbonaceous material.

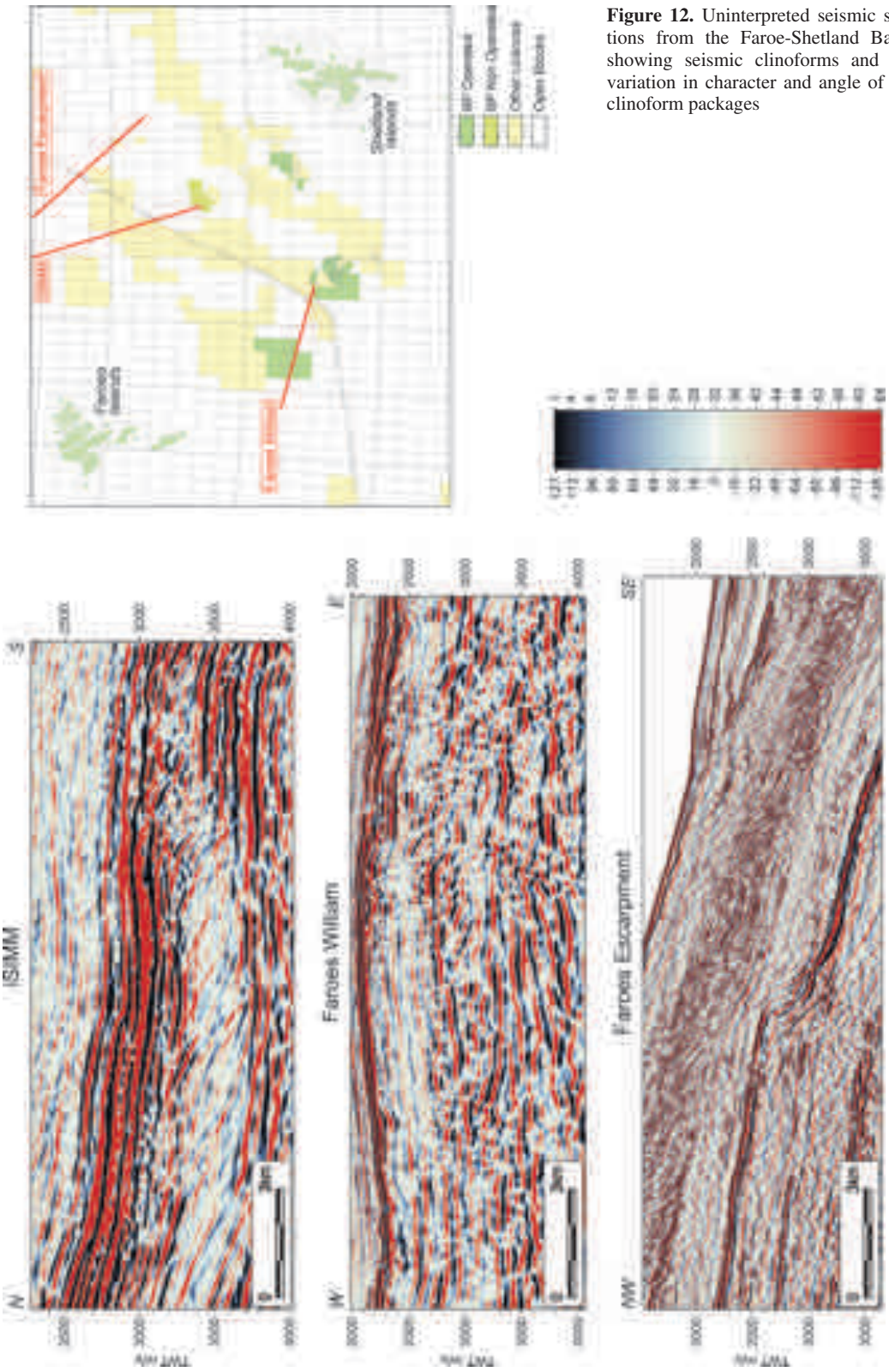

Figure 12. Uninterpreted seismic sections from the Faroe-Shetland Basin showing seismic clinoforms and the variation in character and angle of the clinoform packages

Summary

Following a largely unsuccessful phase of exploration in the Faroese offshore, BP and its co-venturers Shell reviewed there exploration strategy in the region. This revised strategy identified the sub-basalt of licence L007 as an area of hydrocarbon prospectivity. One of the key risks identified in the area was the potential for encountering reservoir quality sandstones below the Tertiary basalts. Considerable effort was therefore made to understand the potential gross depositional environments of the Palaeocene of the region.

Gross depositional environment (GDE) maps were constructed from the earliest Paleocene to the late Paleocene (Sullom S1 - Thanetian) to document the progressive fill of the Faroe-Shetland Basin through time. Outcrop analogues, biostratigraphic, well, 2D and 3D seismic data have provided a detailed framework for this basin fill, particularly on the UK side of the median line. The GDE sequence shows that the main sedimentary depocentre originated in the south-west of the Faroe-Shetland Basin around Quadrants 204, 216 and 6004 and through time moved to the north-east around Quadrants 214, 216 and 217 as the available accommodation space was progressively infilled. The sedimentary fill was capped by extrusive igneous basalts in the latest Paleocene.

Although data are more numerous in the UK, sedimentary models and GDE maps derived from limited well data, in association with the regional evidence from eastern Greenland indicates the potential for reservoir quality sandstones in the sub basalt province of the Faroes continental shelf

Given the potential presence of reservoir quality sandstones in the Paleocene sequence it still remains whether adequate hydrocarbon source and charge potential exist in the region. The validity of this prospectivity was due to be tested by an exploration well in 2007.

Acknowledgements

BP would like to thank its co-venturers Shell and Anadarko for allowing us to publish the results of this regional evaluation. We would also like to particularly thank the efforts of CASP whose extensive fieldwork and analysis on the outcrops of south eastern Greenland proved invaluable in this work. Acknowledgement is also made to Laura Mackay for review and editing and the Henri Ziska and Thomas Varming at Jarðfeingi for their contribution to technical discussions on the area.

References

Boldreel, L.O. and Andersen, M.S. 1993. Late Paleocene to Miocene compression in the Faeroe-Rockall Area. *In*: Parker, J.R. (ed.) *Petroleum Geology of Northwest Europe: Proceedings of the 4th Conference*, 1025-1034. The Geological Society, London: 1025-1034.

Andersen, M.S. 1988. Late Cretaceous and early Tertiary extension and subsidence around the Faeroe Islands. *In*: Parson, L.M. and Morton, A.C. (eds) *Early Tertiary Volcanism and the Opening of the NE Atlantic,* Geological Society, London, Special Publication, 39: 115-122.

Cawley, S., Matheson H., and Stalker, G. 2005. An updated view of the Faroes-Shetland petroleum system. *In*: Ziska, H., Varming T. and Bloch, D. (eds) *Faroe Islands Exploration Conference: Proceedings of the 1st Exploration Conference*. Annales Societatis Scientiarum Faeroensis Supplementum 43: 109 - 130.

Champion, M.E.S., White, N.J., Jones, S.M. and Lovell, J.P.B. 2008. Quantifying transient mantle convective uplift: An example from the Faroe-Shetland basin. *Tectonics* 27: TC1002.

Ebdon, C.C., Granger, P.G., Johnson, H. and Evans, A.M. 1995. Early Tertiary evolution and sequence stratigraphy of the Faeroe-Shetland Basin: implications for hydrocarbon prospectivity. *In*: Scrutton, R.A., Stoker, M.S., Shimmield, G.B., and Tudhope, A.W. (eds) (1995) T*he Tectonics, Sedimentation and Palaeoceanography of the North Atlantic Region*. Geological Society, London, Special Publications 90: 51-69.

Frei, D., Rasmussen T., Knudsen, C., Larsen, M., Whitham, A.G. and Morton, A.C.

2005. New methods and techniques for innovative, integrated provenance studies.

In: Ziska, H., Varming T. and Bloch, D. (eds) *Faroe Islands Exploration*

Conference: Proceedings of the 1st Exploration Conference. Annales Societatis

Scientiarum Faeroensis, Tórshavn, Supplementum 43: 96-108.

Frei, D., Frei, M., and Knudsen, C. (eds) 2005b. Linking the Faroese area and Greenland: an innovative, integrated provenance study. *Danmarks og Gronlands Geologiske Undersogelse Rapport* 2005/54.

Kiørboe, L. 1999. Stratigraphic relationships of the Lower Tertiaty of the Faeroe Basalt Plateau and the Faroe-Shetland Basin. *In*: Fleet, A.J. and Boldy,

S.A.R. (eds) *Petroleum Geology of North West Europe, Proceedings of the 5th Conference*. The Geological Society, London: 559-572.

Knox, R.W.O'B. and Holloway, S. 1992. 1. Paleogene of the Central and Northern North Sea. In: Knox, R.W.O'B. and Cordey, W.G. (eds) *Lithostratigraphic nomenclature of the UK North Sea*. British Geological Survey, Nottingham: 5 - 127.

Larsen, M., Hamberg, L., Olaussen, S., Norgaard-Pedersen, N. and Stemmerik, L. 1999a. Basin evolution in southern East Greenland: an outcrop analogue for the Cretaceous-Palaeogene basins on the North Atlantic volcanic margin. *AAPG Bulletin* 83: 1236-1261.

Larsen, M., Hamberg, L., Olaussen, S., Preuss, T. and Stemmerik, L. 1999b. Sandstone wedges of the Cretaceous-Lower Tertiary Kangerlussuaq basin, East Greenland - outcrop analogues to the offshore North Atlantic. *In*: Fleet, A.J. and Boldy, S.A.R. (eds) *Petroleum Geology of North West Europe, Proceedings of the 5th Conferenc*e. The Geological Society, London: 337-348.

Larsen, M. and Whitham, A.G. 2005. Evidence for a major sediment input point into the Faroe-Shetland Basin from the Kangerlussuaq region of southern East Greenland. *In*: Dore, A.G. and Vinning, B.A. (eds) *Petroleum Geology: North-West Europe and Global perspectives -proceedings of the 6th Petroleum Geology Conference*. Geological Society, London: 913-922.

Linnard, S., and Nelson, R. (2005). Effects of Tertiary volcanism and later events upon the Faroese hydrocarbon system. *In*: Ziska, H., Varming T. and Bloch, D. (eds) *Faroe Islands Exploration Conference: Proceedings of the 1st Exploration Conference*. Annales Societatis Scientiarum Faeroensis, Tórshavn, Supplementum 43: 44-53.

Mitchell, S.M., Beamish, G.W.J., Wood, M.V., Malacek, S.J., Armentrout, M.J., Damuth, J.E. and Olson, H.C. 1992. Paleogene sequence stratigraphic framework of the Faroe Basin. In: Parker, J.R. (ed) *Petroleum Geology of Northwest Europe: proceddings of the 4th conference*. The Geological Society, London: 1011-1023.

Morton, A.C., Whitham, A.G., Fanning, C.M. and Claoue-Long, J. 2004. The role of East Greenland as a source of sediment to the Voring Basin during the Late Cretaceous. *In*: Wandas, B.T.G., Eide, E.A., Gradstein, F and Nystuen, J.P. (eds) *Onshore-offshore relationships on the North Atlantic Margin.* Norske Petroleums forening Special Publication, Elsevier, Amsterdam.

Nadin P.A., Kusznir N.J. and Cheadle M.J. 1997. Early Tertiary plume uplift of the North Sea and Faeroe-Shetland Basins. *Earth and Planetary Science Letters* 148: 109-127.

Naylor, P.H., Bell, B.R., Jolley, D.W., Durnall, P. and Fredsted, R. 1999. Palaeogene magmatism in the Faeroe-Shetland Basin: influences on uplift history and sedimentation. *In*: Fleet, A.J. and Boldy, S.A.R. (eds) *Petroleum Geology of North West Europe, Proceedings of the 5th Conference*. The Geological Society, London: 545-558.

Neish, J.K. 2005. Faroese Area: Structural Interpretation of Seismic Data in a Basalt Environment. *In*: Ziska, H., Varming T. and Bloch, D. (eds) 2005. *Faroe Islands Exploration Conference: Proceedings of the 1st Exploration Conference*. Annales Societatis Scientiarum Faeroensis Supplementum 43: 131 - 145.

Ritchie, J.D., Gatliff, R.W. and Riding, J.B. 1996. *Stratigraphic nomenclature of the UK North West Margin.* 1. Pre-Tertiary lithostratigraphy. British Geological Survey, Nottingham: 3 -193.

Shanmugam, G., Bloch, R.B., Mitchell, S.M., Beamish, G.W.J., Hodgkinson, R.J., Damuth, J.E., Straume, T., Syversten, S.E. and Shields, K.E. 1995. Basin-floor fans in the North Sea: sequence stratigraphic models vs. sedimentary facies. *AAPG Bulletin* 79: 477-512.

Smythe, D.K. 1983. Faeroe-Shetland escarpment and continental margin north of the Faeroes. *In*: Bott, M.H. P., Saxov, S., Talwani, M. and Thiede, J. (eds) *Structure and development of the Greenland-Scotland Ridge*. Plenum Press, New York: 109-119.

Smythe, D.K., Chalmers, J.A., Skuce, A.G., Dobinson, A. and Mould, A.S. 1983. Early opening of the North Atlantic - I. structure and origin of the Faeroe-Shetland Escarpment. *Geophysical Journal of the Royal Astronomical Society* 72: 373-398.

Verhoef, J., Roest, W.R., MacNab, R., Arkani-Hamed, J., *et al* 1996. Magnetic anomalies of the Atlantic & North Atlantic Oceans and adjacent land areas. *Geological Survey of Canada Open File Report* 3125a. Geological Survey of Canada, Dartmouth.

White N. and Lovell B. 1997. Measuring the pulse of a plume with the sedimentary record. *Nature* 387: 888-891.

White R. and McKenzie D. (1989) Magmatism at rift zones: the generation of volcanic continental margins and flood basalts. *Journal of Geophysical Research* 94: 7685-7729.

Ziska, H., Varming T. & Bloch, D. (eds) (2005). *Faroe Islands Exploration Conference : Proceedings of the 1st Exploration Conference*. Annales Societatis Scientiarum Faeroensis, Tórshavn, Supplementum 43.

Enhancing the prospectivity of the Wyville Thomson Ridge

KEVIN SMITH[1*], PATRICK WHITLEY[2], GEOFFREY S. KIMBELL[3], MARTIN KUBALA[2] AND HOWARD JOHNSON[1]

[1] British Geological Survey, Murchison House, West Mains Road, Edinburgh EH9 3LA, UK
* Email: ksm@bgs.ac.uk; Tel: +44 131 667 1000; Fax: +44 131 668 4140
[2] Faroe Petroleum Plc, 24 Carden Place, Aberdeen AB10 1UQ, UK
[3] British Geological Survey, Kingsley Dunham Centre, Keyworth, Nottingham NG12 5GG, UK

ABSTRACT

Føroya Kolvetni (Faroe Petroleum) was awarded Licence 012, covering part of the Wyville Thomson Ridge, in the second Faroese Licensing Round (2005) and this paper summarises some initial results from their work programme. Interest in the prospectivity of the Wyville Thomson Ridge was stimulated in the 1990s by a proposal that it forms an Eocene-Miocene compressional anticline with a thin carapace of Paleogene lavas, overlying an inverted sedimentary basin. Gravity interpretation confirms that the ridge can be modelled as an inverted basin, although uncertainties inherent in the method limit the accuracy of the thickness estimates. Seismic reflection data shot in 2005 provide improved resolution of the pre-lava succession, with some reflector packages resembling seismic facies from the prospective Paleocene succession in the Faroe-Shetland Basin. The *Rannvá* exploration lead consists of an extremely large four-way dip closure beneath thin lavas at the crest of the Wyville Thomson Ridge. Source rock presence and maturity, hydrocarbon migration, and reservoir development in the Licence 012 area are discussed on the basis of regional observations.

Introduction

This paper describes an interpretation of licensed acreage in the Faroese sector of the north-east Atlantic margin, focusing upon the Wyville Thomson Ridge, a linear bathymetric high mantled by volcanic rocks, which forms a physical barrier between the Rockall Trough and the Faroe-Shetland Channel (Morton *et al*., 1988b; Stoker *et al*., 1988; Earle *et al*., 1989) (Figure1).

An early interpretation of the Wyville Thomson Ridge as a 12 km thick pile of basalt overlying Cretaceous oceanic crust was based on gravity modelling together with flexural considerations (Roberts *et al*., 1983). Subsequently, Boldreel and Andersen (1993; 1994; 1995; 1998) made the alternative proposal, partly based on seismic data, that the bathymetric high originated as an inverted sedimentary basin, capped by volcanic rocks. Others have used gravity and magnetic data in conjunction to support an inverted basin model (Tate *et al*., 1999; Waddams and Cordingley, 1999). However, the actual thickness of the concealed sedimentary succession in these interpretations remains poorly constrained. Waddams and Cordingley (1999) show a pre-Cretaceous sedimentary succession more than 8 km thick, with the top of the metamorphic basement lying at a depth of more than 10 km beneath the centre of the ridge. In contrast, the model of Tate *et al*. (1999) for a similar profile shows basement no deeper than 4 - 6.5 km, rising northwards towards the Munkagrunnur Ridge.

In the vicinity of the median line, a buried transfer zone probably underlies Wyville Thomson Ridge (Rumph *et al*., 1993; Stoker *et al*., 1993; Tate *et al*., 1999; Waddams and Cordingley, 1999). To the east, the same transfer zone may control the boundary between the Stack Skerry and

Faroe Islands Exploration Conference: Proceedings of the 2nd Conference.
Annales Societatis Scientiarum Færoensis, Supplementum 50, 2009: 286-302

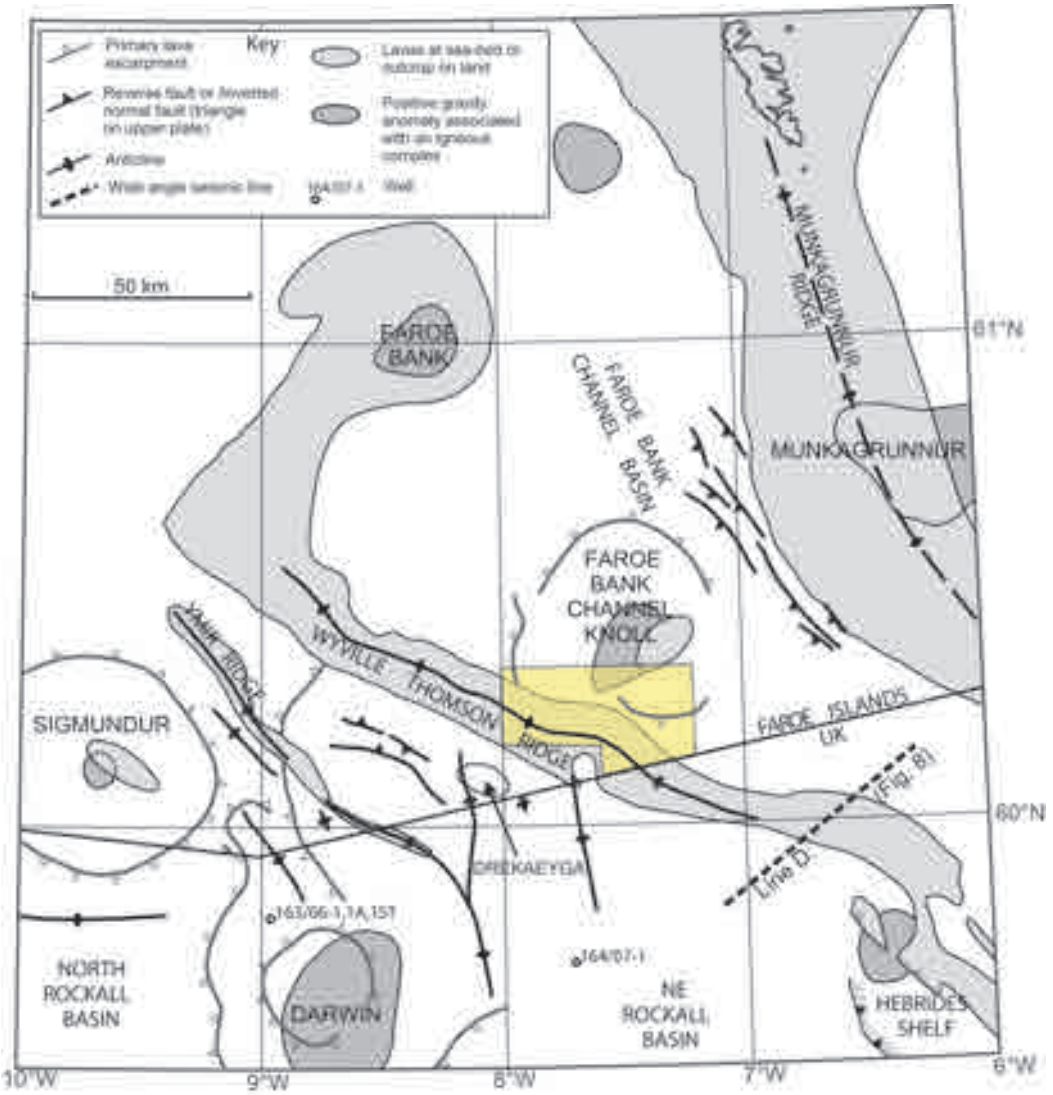

Figure 1. Structural setting of the Wyville Thomson Ridge (modified from Johnson *et al.,* 2005), with the area of Faroese Licence 012 in yellow. The dashed line marks the location of part of a regional wide-angle seismic profile (Line D from Klingelhöfer *et al.,* 2005) (see Figure 8). The location of the Drekaeyga igneous complex is shown, but this is not associated with a positive free-air gravity anomaly.

West Shetland basins (Duindam and Van Hoorn, 1987), or form a part of a broader complex of geophysically defined lineaments, which act together to control the polarity of basins on the Hebridean Platform (Kimbell *et al*., 2005). In either case, it is likely that reactivation of these pre-existing basement structures accommodated the displacement of the main axis of Cretaceous extension between the Faroe-Shetland and Rockall basins. To the north, the Rona Ridge marks the eastern boundary of the Faroe-Shetland Basin, while to the south, the analogues of these structures (the West Lewis Ridge and Rockall Basin) are offset westwards.

The presence of widespread energy-absorbent

volcanic sequences largely accounts for the poor response of the seismic reflection method to the deeper structure of the Faroes continental shelf (White *et al*., 2003), but recently acquired wide-angle seismic data and improved acquisition parameters have helped to establish that some pre-volcanic sediments are preserved locally (Richardson *et al*., 1999; Raum *et al*., 2005; Spitzer *et al*., 2005).

Well data

The well database used in the regional prospectivity assessment consisted mainly of selected hydrocarbon exploration wells from the UK sector, including 154/3-1, 163/6-1A, 164/7-1, 164/25-1Z and 164/25-2. These were supplemented with geological data obtained from relevant shallow boreholes drilled in the West of Shetland area by the British Geological Survey.

The UK well 164/7-1 (Figure 1), which was drilled in the NE Rockall Basin in 1997 by Conoco (U.K.) Limited, tested a large, apparently domal closure that was interpreted by the operators as an anticlinal feature with potential reservoirs and source rocks in the Mesozoic section (Archer *et al*., 2005). However, after penetrating 1166 m of Paleogene volcanic rocks, the well was terminated within a predominantly argillaceous, basinal Cretaceous sequence, without establishing the presence of potential reservoirs or source rocks in the pre-volcanic interval. In the well, Maastrichtian and Campanian rocks are absent and the Paleogene lavas are proven to rest unconformably on a deeply eroded Cretaceous section possibly of Coniacian to Albian age. In the absence of reservoirs and hydrocarbon shows, the well was not tested. Subsequent analysis revealed that the formation of the structural dome was associated with the intrusion of more than 40 basic igneous sills within the Cretaceous section. Interpretation of 3D seismic data across the structure showed that the sills are disposed concentrically around a central uplifted area and have radial outward dips. Potential field data suggest that this whole structure is probably of igneous origin and may be compared with the classic laccolithic intrusions of the Henry Mountains, USA (Jackson and Pollard, 1990). The presence in this area of a large volume, deep-seated igneous body associated with sill intrusion is partly confirmed by the locally enhanced levels of thermal maturity within the Cretaceous succession, as indicated by extremely high values of vitrinite reflectance. Radiometric age dates obtained by the $^{40}Ar/^{39}Ar$ method from the sills have given early Paleocene ages of 63-64 ± 0.5 Ma. These observations combine to suggest that basic sill intrusion in this area was accompanied by local uplift and erosion of the Cretaceous succession, preceding the growth of the lava shield (Archer *et al*., 2005).

The nearby well 163/6-1A, which was drilled in the Rockall Trough as a stratigraphic test, also proved a thick succession of Paleocene basic extrusive rocks, before terminating in a volcanic interval of dacitic composition (Morton *et al*., 1988a) (Figure 1). The interpretation of seismic and potential field data indicates that these rocks form part of the Darwin volcanic centre (Abrahams and Ritchie, 1991). The presence of a Mesozoic section around Darwin remains unproven, but discontinuous high amplitude reflectors observed on seismic data are interpreted as an indication of pervasive sill intrusion at depth (Tate *et al*., 1999).

Most of the exploration effort in the adjoining part of the UK sector has focused upon the eastern flank of the NE Rockall Basin, where several wells have tested potential structures. Well 164/25-2 on the crest of the West Lewis Ridge, and nearby well 154/3-1, both penetrated Paleocene volcanic successions before terminating in metamorphic basement. In 164/25-2, a partly arenaceous clastic interval of Thanetian age separates a thinly bedded upper series of volcanic rocks from a lower volcanic succession that rests directly upon Lewisian basement. In 154/3-1, thin sediments of Campanian age, underlain by thick undated conglomerates, separate an undivided Paleocene volcanic succession from Lewisian basement at terminal depth. With their lack of source rocks and poor development of potential reservoirs, these wells have downgraded hydrocarbon prospectivity in the area of the West Lewis Ridge.

Immediately to the east of the West Lewis Ridge, well 164/25-1Z drilled an anticlinal closure formed by the structural inversion of the West Lewis Basin during the Cenozoic. In this well, the

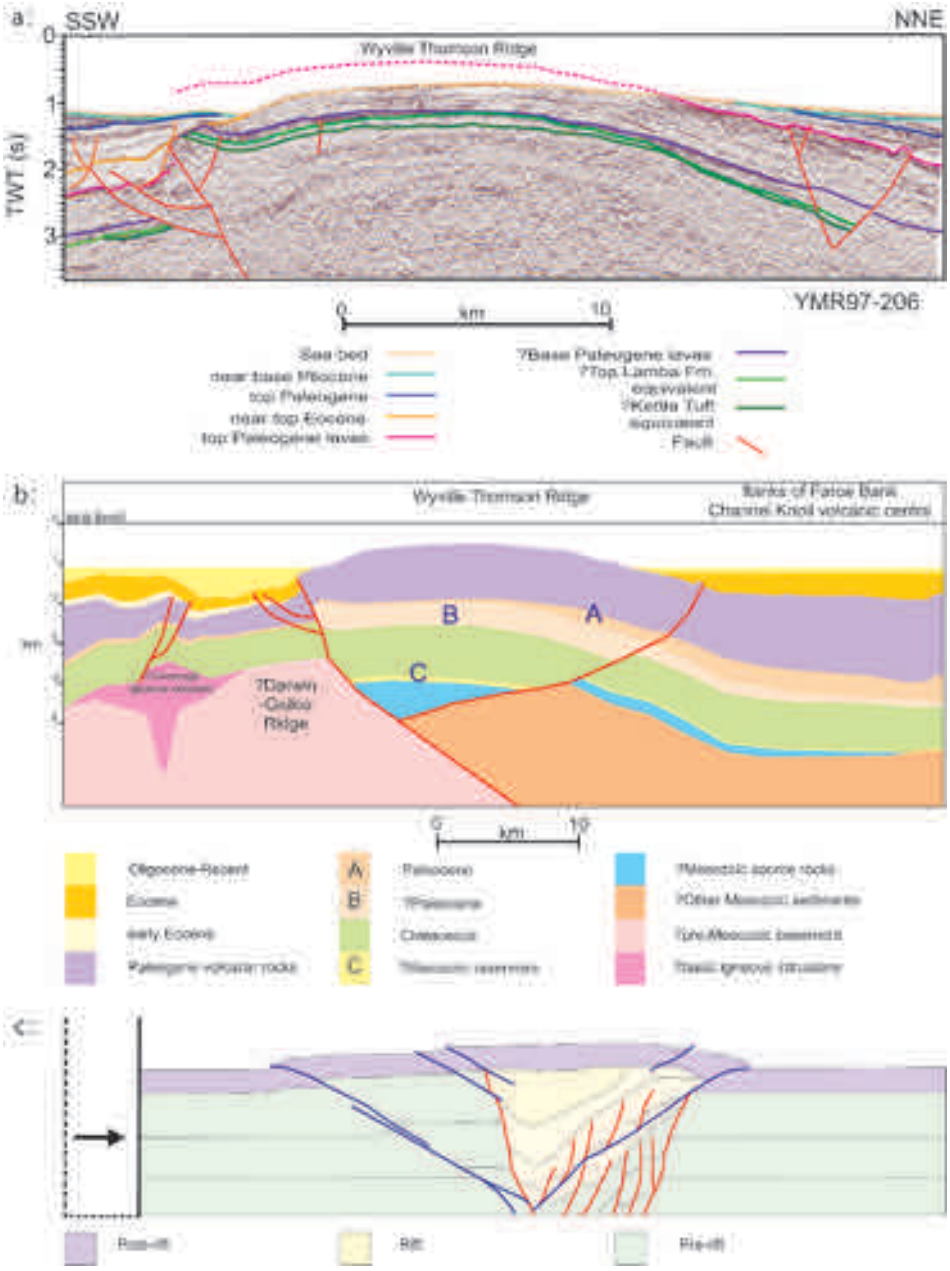

Figure 2. (a) Interpretation of part of seismic line YMR97-206 across the Wyville Thomson Ridge: The dashed reflector was used in the process of horizon flattening and represents the conjectural restored top of the Paleogene volcanic succession before erosion (for location, see Figure 3). (b) A play concept diagram for the Wyville Thomson Ridge partly based on seismic line YMR97-206, showing a speculative schematic reconstruction of an underlying Mesozoic-Paleocene basin. The Darwin-Geikie Ridge was first recognised by Waddams and Cordingley (1999). (c) A cross-section showing a possible structural analogue of the Wyville Thomson Ridge based on sandbox experiments into the process of basin inversion (modified from Panien *et al.,* 2005; their Figure 8d). Syn-rift faults are shown in red; inversion-related faults in blue.

volcanic interval is thin and occurs near the top of a thickly developed Paleocene clastic succession, which includes abundant sandstones. The succession is predominantly of Thanetian age, but a thinly bedded basal interval of Danian sandstones is also present. The Danian rocks overlie Cretaceous mudstones, which rest unconformably on the varied succession of Triassic sediments in which the well terminated. Basic igneous sills, up to 185 m thick, intrude much of the Cretaceous and some of the Paleocene interval in the well. Although the 164/25-1Z well shows that Jurassic rocks are absent locally, shallow boreholes drilled by the British Geological Survey have established the presence of potential hydrocarbon source rocks of Jurassic age elsewhere in the West Lewis Basin (Isaksen *et al*., 2000).

Seismic interpretation

The initial appraisal of the proposed licence area was supported by a detailed interpretation of the seismic profile YMR97-206 (Figure 2). Beginning in the UK sector, this line trends SW-NE across the Wyville Thomson Ridge to provide a complete geological section through the licence blocks 6007/17, 21 and 22 (Figure 3). Seismic interpretation was aided by reference to regional profiles from adjoining blocks (Boldreel and Andersen, 1993, 1994, 1998; Tate *et al*., 1999; Waddams and Cordingley, 1999; Sørensen, 2003; Archer *et al*., 2005; Keser Neish and Ziska, 2005; Johnson *et al*., 2005). In addition, published structural contour maps of the top Paleogene lava surface (Tate *et al*., 1999; Keser Neish and Ziska, 2005) were used to relate the interpreted seismic profile to the regional structure. Eight picked horizons (sea bed; near base Pliocene; top Paleogene; near top Eocene; near top Lower Eocene (Ypresian); top Paleogene lavas; base Paleogene lavas and intra-Paleocene) were provisionally correlated with the regional event stratigraphy of Johnson *et al*. (2005). Identification and dating of events below the top of the lavas remains speculative.

Following the award of the blocks, Føroya Kolvetni purchased additional selected profiles from a non-exclusive seismic survey acquired across the ridge by Fugro-Geoteam in 1997 (Figure 3). A single regional line (SW84-091) was used to tie this seismic grid to well 164/7-1 (Figure 3). A provisional structural contour map showed where the top lava reflector was truncated at the sea bed on the flanks of the high. Since the identification of the true base of the volcanic succession often remains uncertain on seismic data from the Atlantic margin, it is clearly beneficial that the thickness of the lava pile has been reduced by post-volcanic erosion above a potential sub-volcanic target at the crest of the Wyville Thomson Ridge. Extending the interpretation of the presumed base of the volcanic succession throughout the seismic grid defined two separate structural culminations along the ridge axis. The western culmination, which lies entirely within the Faroese sector, forms the basis of the *Rannvá* exploration lead.

Re-examination of the original line YMR97-206 (Figure 2), in the light of the additional profiles led to the recognition of a discontinuous low amplitude reflector beneath the inferred base of the volcanic succession. This reflector is parallel to the lavas and appears to define the base of a mounded seismically transparent interval below the centre of the ridge. Horizon-flattening software was used to restore a reconstructed top lava event to its approximate pre-inversion position to reveal the original depositional geometry of the deeper, possibly pre-volcanic, reflectors. The wedging packages of high amplitude events previously identified on the flanks of the structure appeared on this display to onlap an axial mound-like feature.

In 2005, Føroya Kolvetni shot a set of seismic profiles infilling the original grid (Figure 3) (for details of acquisition and processing parameters, see Holden *et al*., *this volume*). These lines included one profile (FP2005-002) that was planned specifically to transect the crest of the previously identified *Rannvá* structural closure. This line established that the base of the lavas was even shallower than predicted, while the improved acquisition parameters and processing sequence revealed a deeper set of reflectors below the centre of the ridge (Figure 4). Most of these are short high amplitude events probably related to basic intrusions

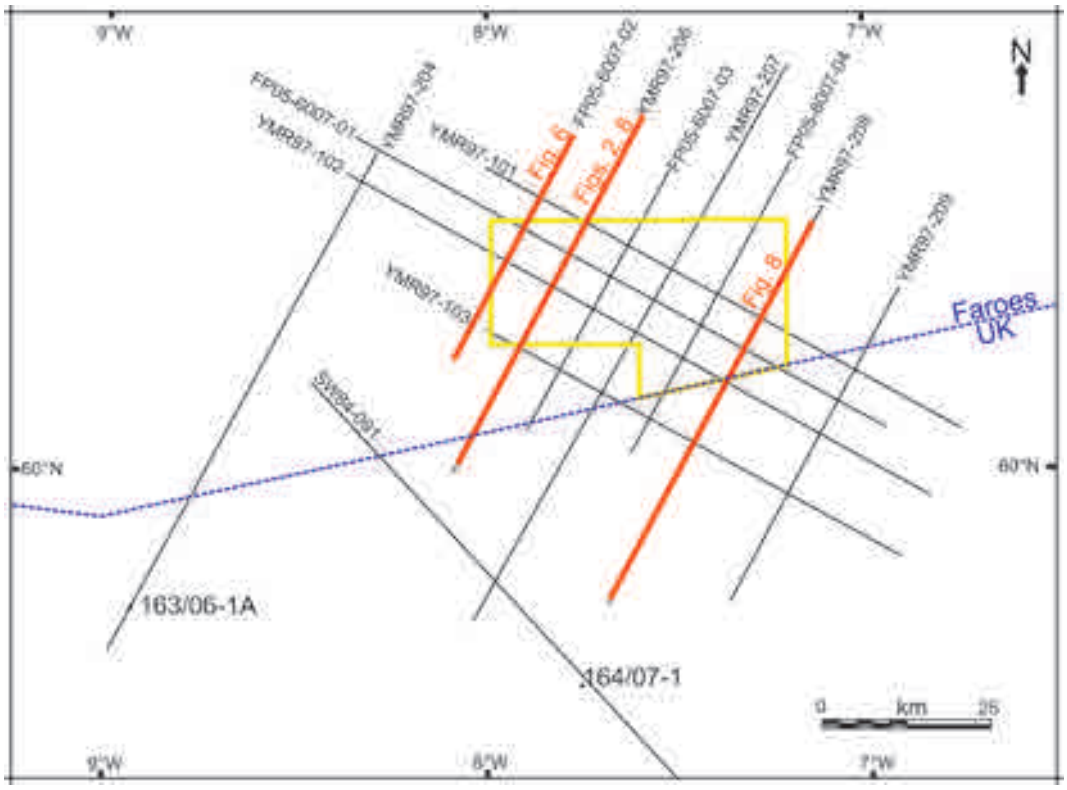

Figure 3. Wyville Thomson Ridge area: Location map of well ties and interpreted seismic reflection profiles (with figure illustrations highlighted in red). The boundary of the Licence 012 area is outlined in yellow.

and possibly affected by faults striking parallel to the ridge and throwing down towards the ridge axis. In the Faroe-Shetland and Rockall basins, reflections related to basic sills occur predominantly within the Cretaceous succession. To assess the tectonic implications of these observations, a palaeogeographic map of structural elements in the vicinity of the UK-Faroes median line was modified to include a Mesozoic basin at the site of the Wyville Thomson Ridge (Figure 5).

Improved imaging of the Wyville Thomson Ridge allows the seismic facies directly below the volcanic layer to be compared with Paleogene reflectivity in the Faroe-Shetland Basin. Comparison with published seismic profiles (for example, Smallwood and Gill, 2002, their Figure 2; Smallwood *et al*., 2004, their Figure 13) reveals a particular correspondence between the seismic character of the interval that pinches out beneath the flanks of the ridge and that of the Upper Flett and Balder formations (Figure 4). Both of these units consist of a thin package of laterally continuous, high amplitude, high frequency reflections. It follows that the mounded seismically transparent interval onlapped by these reflectors, which occurs beneath the axis of the ridge, may be equivalent to the prograding wedge of Lamba Formation sediments in the UK sector (Figs. 2, 4). If this is the case, then the single high amplitude event previously recognised at the base of the transparent interval probably corresponds to the Kettla Tuff Member, which is already known to be a regionally extensive seismic marker (Figs. 2, 4). Elsewhere along the Atlantic margin, a thin shale interval underlying the Kettla Tuff acts as a local seal to the thick turbidite sequences of the Vaila Formation, which form the main Paleocene reservoir in the UK sector. Based on this analogy, a seismic inter-

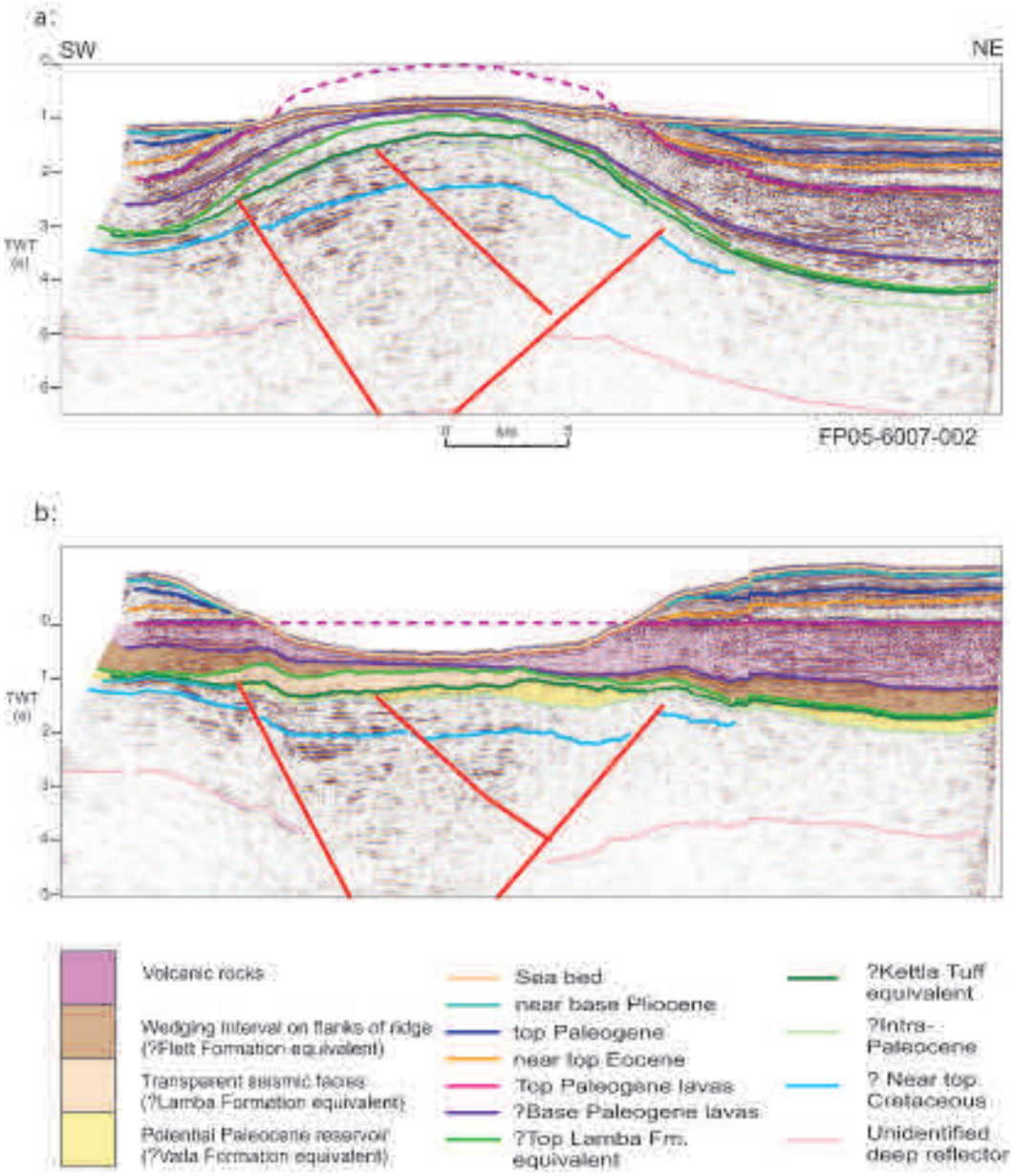

Figure 4. (a) Wyville Thomson Ridge: Interpreted seismic line FP05-6007-02 (for location, see Figure 3). (b) Seismic line FP05-6007-02, flattened at top lava level, including the dashed segment of reflector, which represents the conjectural restored top of the volcanic succession before erosion at the crest of the ridge. Coloured seismic facies below the inferred base of the volcanic succession are interpreted by comparison with seismic data from the SW Faroe-Shetland Basin (Smallwood and Gill, 2002; Smallwood *et al.,* 2004).

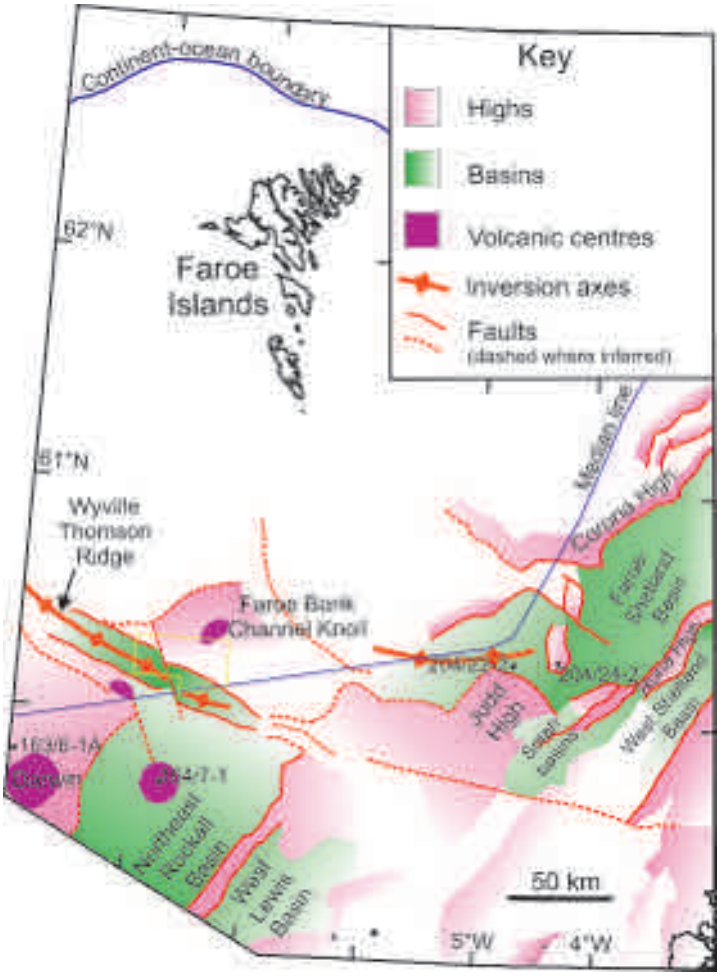

Figure 5. Simplified map showing structural elements of the Atlantic margin in the vicinity of the UK-Faroes median line. Tonal variation is used diagrammatically to indicate the comparative structural relief of the Cretaceous-Paleocene basins (green) and highs (pink) before Eocene-Miocene uplift and inversion. The axis of inversion to the north of the Judd High is taken from Smallwood and Gill (2004).

val corresponding to potential Vaila Formation turbidites beneath the Wyville Thomson Ridge is indicated on Figure 4. The absence of equivalent sediments from the nearby well 164/7-1 can be attributed to non-deposition or erosion at the pre-lava unconformity surface above a structural high (Archer *et al*., 2005).

Biostratigraphic ages obtained from side-wall cores in well 164/7-1 show that the local volcanic succession must have been extruded rapidly, possibly from the Faroe Bank Channel Knoll volcanic centre, during the latest Paleocene and earliest Eocene (Archer *et al*., 2005). The lavas, which may be penecontemporaneous with the Balder Formation, buried the inferred Paleocene sedimentary succession at the Wyville Thomson Ridge as they thinned southwards towards the Rockall Basin. After the formation of the lava shield, local erosion during the earliest Eocene was followed by marine transgression across the Faroes Shelf (Waagstein and Heilmann-Clausen, 1995). Subsequent Middle Eocene deposition in the Faroe-Shetland Basin shows thinning towards the rising axes of basin inversion anticlines (Smallwood, 2004). Seismic evidence of Middle and Upper Eocene chaotic facies from adjoining basins suggests that the Wyville Thomson Ridge was also affected by basin inversion at this time, with folding and uplifting of lavas at the ridge, while a new depocentre developed above the former structural high on its southern flank. The margins of the Drekaeyga intrusive centre (Keser Neish and

Ziska, 2005) were deformed and the Ymir Ridge evolved as a series of transpressional anticlines, possibly buttressed against the Darwin-Geikie Ridge and its associated igneous intrusions (Boldreel and Andersen, 1993, 1994, 1998; Tate *et al*., 1999). A similar pattern of footwall deformation has been observed in sandbox experiments of inverted half graben (Figure 2c; Panien *et al*., 2005). If the tectonic model developed by Imber *et al*. (2005) for the Vøring Basin can be applied to this part of the Atlantic Margin, it is possible that an episode of localised basin inversion was initiated by the effect of sinistral transpression on a restraining right-stepping offset of basement blocks across the Wyville Thomson transfer zone (Figure 5). Potential regional driving mechanisms of north-east Atlantic Cenozoic basin inversion are reviewed by Doré and Lundin (1996).

Uplift of the Wyville Thomson Ridge contributed to a change in oceanic circulation in the evolving Atlantic Ocean. A major submarine unconformity surface developed locally near the end of the late Eocene (= C30 event of Stoker, 1999) and this was onlapped as the Rockall Basin continued to deepen during the Oligocene. A further major episode of uplift and erosion generated another regionally significant unconformity, marking the top of the Paleogene. This was formerly described as the latest Oligocene/early Miocene unconformity (LOEMU) or C20 event by Stoker *et al*. (2002) and may be equivalent to the TPU event of Smallwood (2004) in the Faroe-Shetland Basin. The interval between these late Eocene and top Paleogene unconformities is characterised by a set of small-displacement, compaction-related normal faults that developed in semi-consolidated sediments of predominantly Oligocene age, on the flanks of rising anticlines, including the Wyville Thomson Ridge (Johnson *et al*., 2005). The next regionally significant unconformity is interpreted as the base of the Pliocene-Pleistocene succession on the Atlantic margin and probably corresponds to the C10 reflector of Stoker *et al*. (2002, 2005).

Seismic interpretation concluded with the preparation of revised structural contour maps incorporating the new seismic data. Maps of top Paleogene lava, base Paleogene lava and possible top Paleocene reservoir horizons improved the structural resolution of the *Rannvá* lead and helped to define the depth to a potential target (Figure 6).

Potential field interpretation

Despite the improved resolution of the recent seismic reflection data, there is still little firm evidence for the early geological history and thickness of any precursor basin beneath the Wyville Thomson Ridge. Potential field data provide an independent means of assessing the deep structure of the area.

The large differences between previous gravity interpretations (Roberts *et al*., 1983; Tate *et al*., 1999; Waddams and Cordingley, 1999) illustrate the non-uniqueness inherent in gravity modelling where independent constraints are limited. Comparison with magnetic data does help to reduce the uncertainty. Borehole sampling (Archer *et al*., 2005) and the characteristics of the observed magnetic anomalies indicate that the lavas are reversely magnetised. On the basis of rock property measurements (e.g. Shoenharting and Abrahamsen, 1984; Abrahamsen *et al*., 1984; Sharma, 1994) they are estimated to have a net intensity of magnetisation of 3 - 4 A/m in a direction approximately opposite to the Earth's present field. When magnetisations of this order are adopted in the alternative models for the Wyville Thomson Ridge, the results prove diagnostic. The thick lava pile modelled by Roberts *et al*. (1983) generates a much larger magnetic anomaly than is observed, whereas the thin, folded lava layer in the interpretations of Tate *et al*. (1999), Waddams and Cordingley (1999) and the present study produce a response of appropriate amplitude.

New gravity modelling was undertaken using the results of the seismic interpretation described above. The aim was to remove the gravity effect of the seismically resolved sedimentary and volcanic rocks and interpret the residual anomalies in terms of underlying structure. The modelling focused on seismic lines YMR97-206 and YMR97-208 (Figs. 3, 7). Positive features over the Wyville Thomson and Ymir ridges dominate the free-air gravity anomaly pattern (Figure 7), and another positive anomaly is associated with the Faroe Bank Channel Knoll volcanic centre (Roberts *et al*., 1983; Boldreel and Andersen, 1999; Keser Neish and

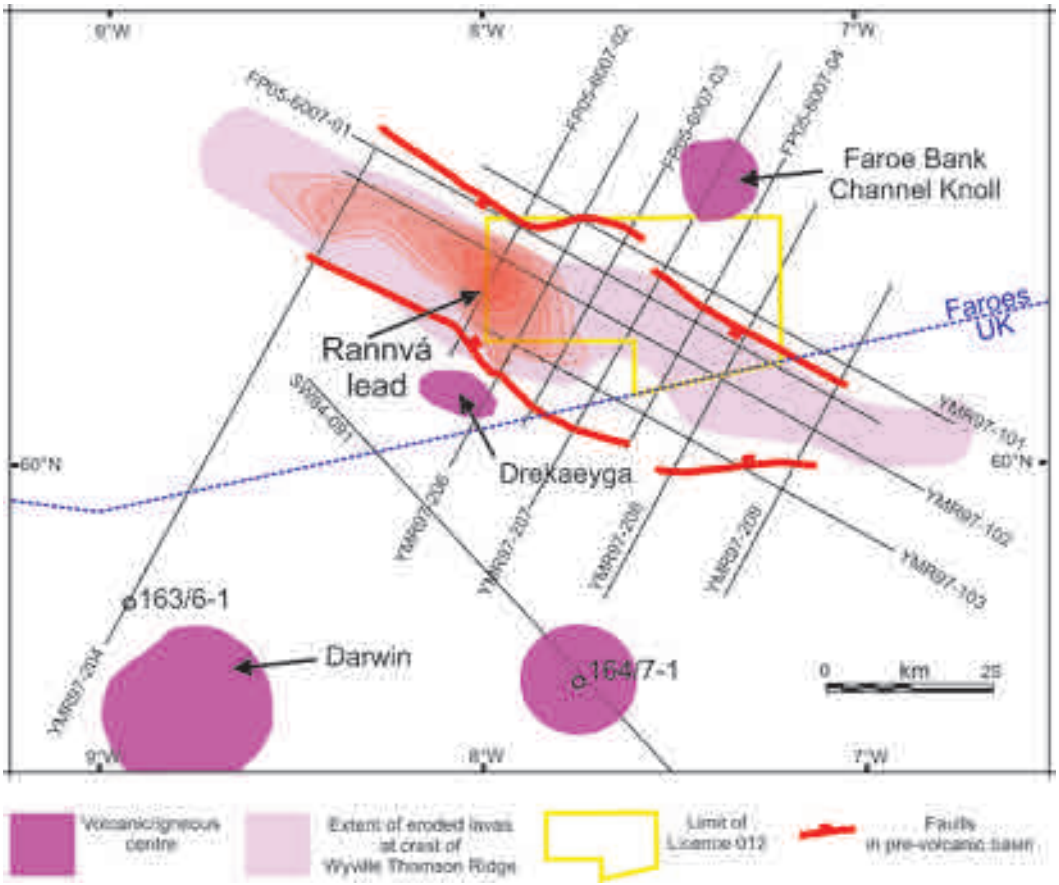

Figure 6. *Rannvá* exploration lead summary map: *Rannvá* lead consists of a pre-volcanic four-way dip closure beneath the axis of the Wyville Thomson Ridge. Provisional structural contours within the closure, colour shaded at intervals of 100 metres, are based on a seismic reflector possibly corresponding to the Kettla Tuff (Smallwood and Gill, 2002; Smallwood *et al.,* 2004).

Ziska, 2005). The Drekaeyga volcanic centre (Figure 7), which has been identified on seismic and magnetic data between the Wyville Thomson and Ymir ridges does not generate a strong free-air gravity feature (Keser Neish, 2004; Keser Neish and Ziska, 2005). Densities of 2.00 Mg/m^3 and 2.55 Mg/m^3 were assumed for post lava sediments and lavas respectively. The relatively low density assumed for the latter reflects the very heterogeneous nature of the volcanic sequence, as revealed by well 164/7-1. Although high densities (2.55-2.85 Mg/m^3) do occur in the interiors of individual flows, values decrease to 2.15-2.55 Mg/m^3 at flow margins (Archer *et al*., 2005). Initial whole-crustal 2D models were constructed assuming that crustal thickness varied such that the bathymetric and cover sequence features identified by seismic surveys (down to the base of the lavas) were in isostatic equilibrium. A two-layer crust was assumed to underlie the lavas, with densities in its upper and lower parts of 2.75 Mg/m^3 and 2.95 Mg/m^3 respectively, and the mantle density was 3.3 Mg/m^3.

The gravity responses predicted by these initial models differed significantly from the observed field, and the next stage was to investigate the extent to which the sub-lava sedimentary rocks could contribute to these differences. Such rocks have been proven at well 164/7-1, about 14 km SSW of

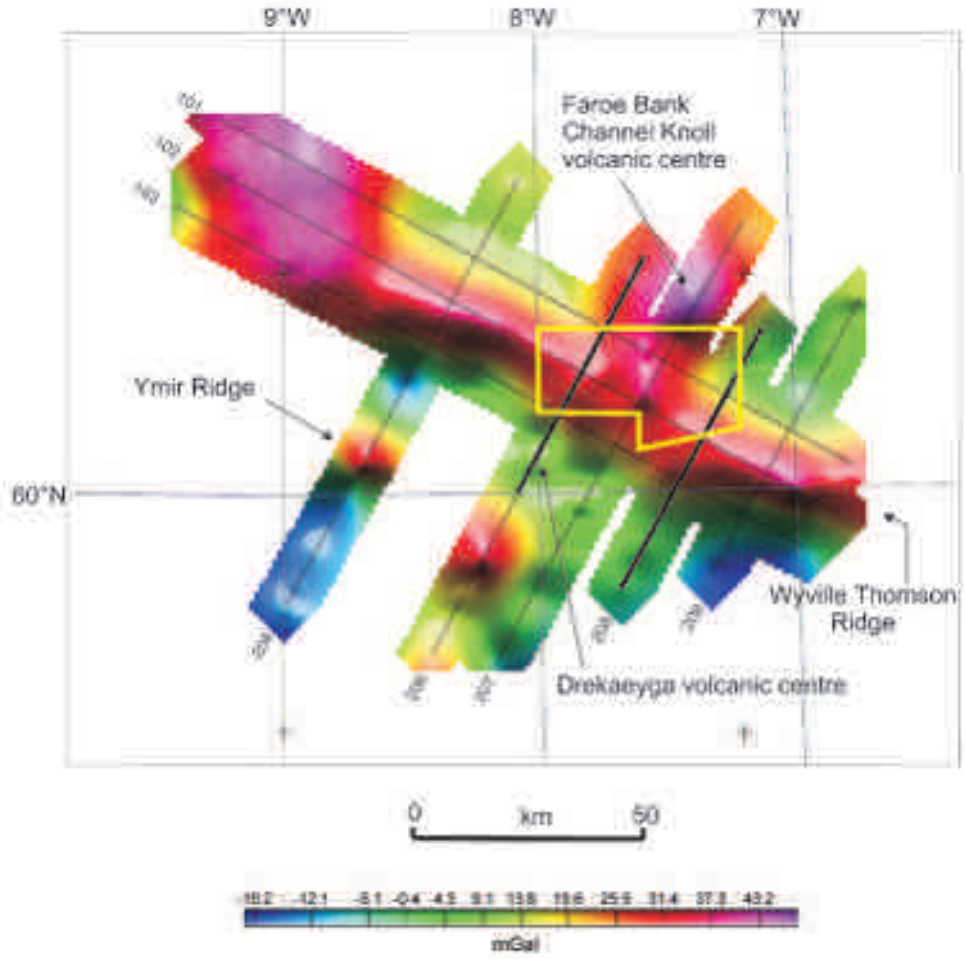

Figure 7. Colour shaded-relief image of the free-air gravity anomalies from the YMR97 survey. Illumination is from the north. Heavy lines indicate the location of the model profiles.

the southern end of line 208 (Figure 6), where a 1.3 km section comprising Paleogene lavas and tuffs underlain by heavily intruded Cretaceous claystones was intersected (Archer *et al*., 2005). The geoseismic interpretation of Archer *et al*. (2005, their Figure 19) suggests that the top of the acoustic basement lies less than 1 km below the bottom of 164/7-1, but at considerably greater depths away from the dome that was drilled by this well. On the basis of the limited available evidence it has been assumed that about 3 km of pre-Cretaceous sedimentary rocks underlie the southern end of line 208. This was used as reference against which pre-lava sedimentary thicknesses variations elsewhere were modelled, as it is not possible to predict absolute thicknesses from the available data in this modelling context. The gravity model presented by Archer *et al*. (2005; their Figure 16) assumed a high density (2.79 Mg/m^3) for the intruded Cretaceous section. While this might be appropriate for the inferred laccolith drilled by 164/7-1, densities are almost certainly significantly lower away from this local intrusive feature. In the present modelling, the pre-lava unit has been divided into upper and lower parts and these assigned average densities (2.50 Mg/m^3 and 2.62 Mg/m^3 respectively) that are closer to those predicted from consideration of the effect of com-

paction on normal mudrocks. The use of the same density for the uppermost part of the pre-lava sequence, regardless of its depth of burial, is compatible with an interpretation in which these rocks originally lay at similar depths but were subsequently affected by different degrees of structural inversion. The effects of inversion were not extended to deeper density structure, and the interface between the 2.50 Mg/m^3 and 2.62 Mg/m^3 components in the pre-lava sedimentary sequence is a modelling approximation with no structural or stratigraphic significance.

Starting at the nominal reference point at the southern end of line 208, the model for this line does not require large changes in the thickness of the pre-lava sedimentary rocks on the southern side of the Wyville Thomson Ridge (Figure 8). A reduction in pre-lava sediment thickness to the north of the ridge is, however, suggested by the modelling. Offline effects from the Faroe Channel Knoll volcanic centre affect this part of the section, and are only crudely simulated in the model. Changes in basement density across the Wyville Thomson Ridge may also have an influence (assuming that it overlies a reactivated basement structure), but have not been incorporated into the current models.

It was necessary to introduce the Faroe Bank Channel Knoll and Drekaeyga volcanic centres into the model for line 206 to produce a satisfactory match between observed and calculated gravity fields. There is latitude in the way the gravity response is partitioned between the volcanic centres and the sediment thickness variations, but it does appear likely that there is a relatively thick pre-lava sedimentary section beneath the Wyville Thomson Ridge on this line (Figure 8).

Comparison of these models with the (subsequently published) results of a wide-angle seismic profile across the Wyville Thomson Ridge in the UK sector (Klingelhöfer *et al*., 2005) reveals significant similarities in the thicknesses and depths obtained by these different methods (Figure 8). In each case, the greatest pre-lava sedimentary thickness occurs beneath the axis of the ridge. However, the apparent indication from the three profiles that this sequence thickens north-westwards towards the Faroese sector should be treated with caution, given the limitations and assumptions of the gravity interpretations. Significant uncertainties remain with regard to control points for the pre-lava sequence and the influence of variations in the thickness and properties of the underlying basement. For example, the gravity modelling adopted an initial assumption of isostatic equilibrium, but the seismic model for profile D does not indicate such equilibrium (implying that the ridge topography is supported by lithospheric strength). The consequences of this were tested by flattening the Moho beneath the ridge in the gravity models and investigating the influence on modelled upper crustal structure. The broad geometries were similar, but an increase in sedimentary thickness beneath the ridge of up to 2 km was required. The conclusion is that the gravity modelling supports the presence of a thick sedimentary sequence beneath the Wyville Thomson Ridge but that the details of its geometry are currently not accurately quantified.

Rannvá lead

The major lead in the licence application area is named *Rannvá* and consists of an anticlinal, four-way dip closure formed during Eocene to Miocene times (Johnson *et al*., 2005) by the compressional inversion of a sedimentary basin inferred to underlie the Wyville Thomson Ridge (Figure 6). The geological history of this basin remains largely unknown and, at present, its hydrocarbon potential can only be assessed on the basis of regional observations.

Source rocks

To the south of the Wyville Thomson Ridge, well 164/7-1 did not penetrate any hydrocarbon source rocks (Archer *et al*., 2005). The Cretaceous succession in which the well terminated had low total organic carbon content and was shown to be thermally metamorphosed and over-mature. This metamorphism is not regional in extent, but was caused by the location of the well above a major plutonic intrusion and its associated shallower complex of basic sills. Potential source rocks are more likely to be developed within deeper Jurassic sequences, but sediments of this age remain un-

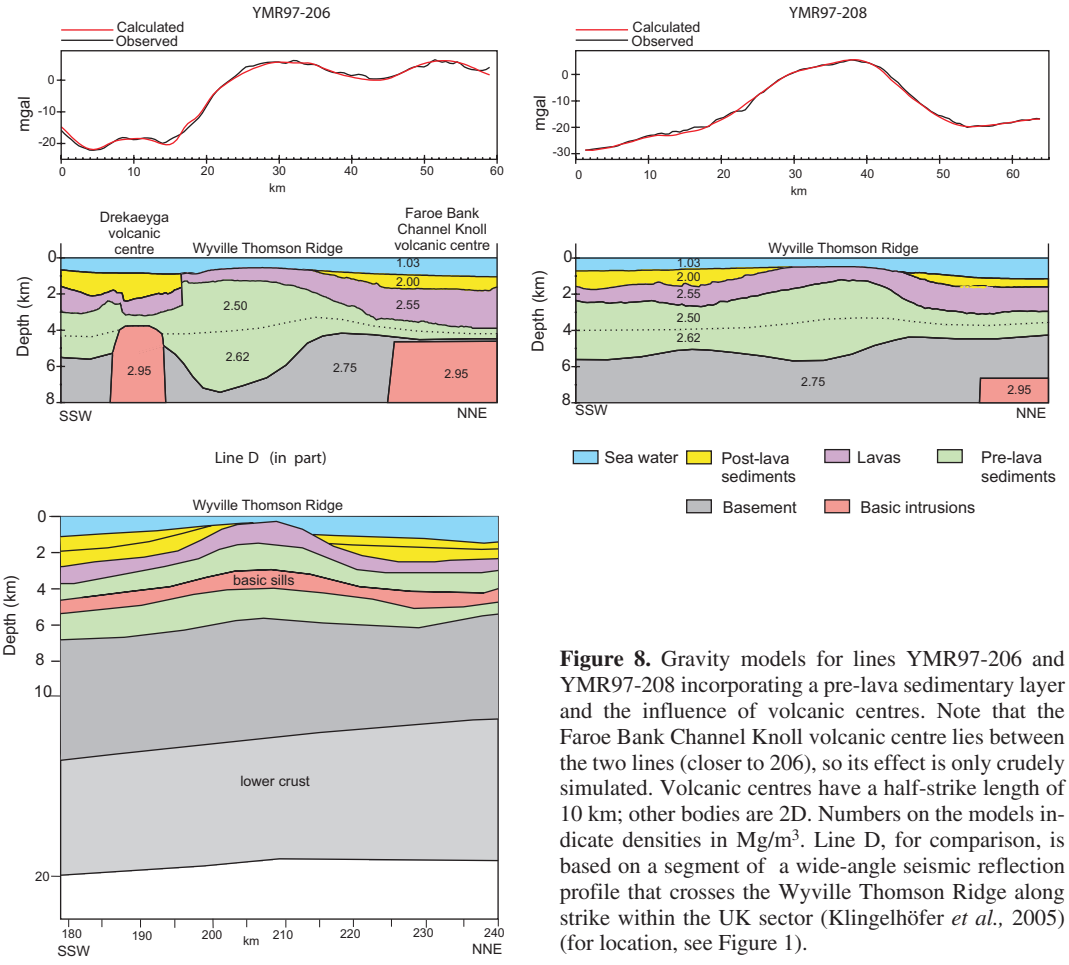

Figure 8. Gravity models for lines YMR97-206 and YMR97-208 incorporating a pre-lava sedimentary layer and the influence of volcanic centres. Note that the Faroe Bank Channel Knoll volcanic centre lies between the two lines (closer to 206), so its effect is only crudely simulated. Volcanic centres have a half-strike length of 10 km; other bodies are 2D. Numbers on the models indicate densities in Mg/m^3. Line D, for comparison, is based on a segment of a wide-angle seismic reflection profile that crosses the Wyville Thomson Ridge along strike within the UK sector (Klingelhöfer *et al.,* 2005) (for location, see Figure 1).

proven, not only beneath the Wyville Thomson Ridge, but also in the NE Rockall Basin. However, some core material recovered from BGS shallow boreholes at the margin of the nearby West Lewis Basin does consist of potential source rocks, including oil-prone Middle Jurassic (Bathonian) sediments and Kimmeridge Clay Formation mudstones of Lower Cretaceous (Ryazanian) age (Isaksen *et al*., 2000). These rocks reflect the varied nature of the hydrocarbon sources that have contributed to the Foinaven and Schiehallion oilfields in the adjoining Faroe-Shetland Basin (Bailey *et al*., 1987; Spencer *et al*., 1999). They also provide an indication that similar source material may be more extensively preserved elsewhere in the separate marginal basins of the Rockall Basin area. Previous interpretations of the Rockall Basin, which implied that it was largely of early Cretaceous origin and possibly lacked Jurassic source rocks, did much to downgrade the prospectivity of the area (Musgrove and Mitchener, 1996). Although the early structural and stratigraphic evolution of the basin remains poorly understood, the recent Doolish discovery by Irish well 12/2-1 casts significant doubt on this pessimistic view of the region and increases the likelihood that an effective petroleum system will also be developed in the area between the Faroe-Shetland and Rockall basins. Similarly, the presence of Devono-Carboniferous strata, including traces of coal, close to

the median line in UK well 213/23-1 means that older Palaeozoic sources may also be capable of generating hydrocarbons in parts of the Atlantic margin, even if Mesozoic source rocks are absent.

Reservoirs

The 164/25-1Z exploration well in the West Lewis Basin previously established that potential Paleocene reservoirs are preserved locally beneath volcanic rocks. However, the expectation that a similar succession may be developed in a comparable basinal setting in the NE Rockall Basin was not confirmed by the 164/7-1 well, which proved a kilometre-thick pile of thinly bedded lavas and pyroclastic rocks completely devoid of potential reservoirs (Archer *et al*., 2005). This well showed that, even in a predominantly basinal area, Paleocene reservoir distribution depends partly on the pattern of pre-volcanic uplift. The lack of a reservoir interval in the 164/7-1 well is attributed to development of a local structural high during the episode of basic sill intrusion that preceded the growth of the lava shield. Better Paleocene reservoirs are likely to be found away from areas of pre-volcanic uplift. Similarities between seismic facies from the pre-volcanic interval beneath the Wyville Thomson Ridge and late Paleocene-early Eocene reflectivity patterns in the Faroe-Shetland Basin increase the possibility that late Paleocene turbidite reservoirs might be preserved in a contemporaneous basin currently concealed by the lava shield. These potential reservoirs could be distal equivalents of the pre-Kettla Tuff Vaila Sandstones of the Foinaven-Schiehallion area, which typically have porosities of more than 20%, or older Paleocene sandstones like those of the Marjun discovery in the Faroese sector, which may have reduced porosities of about 12% (Lamers and Carmichael, 1999; Smallwood *et al*., 2002). Such sandstones need not be derived from the eastern margin of the basin; an origin on the Faroes Shelf, or more local provenance from the block underlying the Faroe Bank Channel Knoll volcanic centre, cannot be ruled out. Regional considerations suggest that older potential reservoirs may exist at Turonian and Cenomanian levels, but sandstones of these ages were not present in the nearby 164/7-1 well. Currently, the deeper stratigraphy of the basin underlying the Wyville Thomson Ridge remains unknown, but basins of similar scale on adjoining parts of the margin commonly originated as sandstone-dominated Permo-Triassic half graben.

Seals

In the Faroe-Shetland Basin, Vaila Formation mudstones underlying the Kettla Tuff provide a widespread seal for reservoirs consisting of overlapping basin floor turbidites. The sealing horizon in the Wyville Thomson Ridge area may consist of fine-grained volcaniclastic sediments at the base of a kilometre-thick pile of interbedded basic lavas and tuffs. Intra-formational seals may also be present in the pre-volcanic succession.

Trap

An analysis of the exploration history of the West of Shetland area has shown that most failed wells were explained by the invalidity of the trap (Loizou, 2005). The unexpected failure of drilling targets defined by amplitude analysis has helped to restore interest in simpler structural plays in this area. The *Rannvá* lead is a robust four-way dip closure (Figure 6). Based on the available seismic grid, the dimensions of the closure (possibly more than 400 km^2) are similar in scale to those of the bathymetrically-defined ridge itself. The anticlinal trap formed by Eocene-Miocene basin inversion (Johnson *et al*., 2005) and is closed along strike by variation in the preserved thickness of the partially eroded volcanic shield that caps the structure. A provisional set of contours at 100 m intervals shows the form of the trap and has an estimated closing contour at 2700 m (Figure 6). The actual height of closure depends upon an accurate depth conversion of the overlying volcanic succession. Thinning of the volcanic carapace at the culmination of the trap increases the risk of breaching, and means that the deleterious effects of flushing and biodegradation present additional risks.

Migration

The complex structural history of the Wyville Thomson Ridge area, combined with the uncertainty about the present depth of burial and maturity of potential source rocks makes it difficult to

reconstruct regional hydrocarbon migration paths. However the juxtaposition of a structural high and an inverted basin means that the remigration ('motel') model of Doré and Lundin (1996) could be applied to this area. This model suggests that early-formed hydrocarbons can be stored temporarily in traps formed by horsts or tilted blocks, before remigrating into a different structure as new traps are created by basin inversion. By this means, previously mobilised oil may still be available to fill late developing structures by remigration, even as the original source rocks themselves become over-mature. Recent reappraisals of the thermal history of the Faroe-Shetland Basin have suggested that such models may no longer be required to maintain prospectivity of the area, with source rock maturity being inhibited instead by the development of overpressure in basinal successions. This process might sufficiently postpone oil generation to allow late forming structures to be filled, without the need for remigration (Carr and Scotchman, 2003).

Conclusions

Føroya Kolvetni have carried out an initial assessment of the hydrocarbon prospectivity of Licence 012 acreage in the Faroese sector of the Atlantic margin. Their *Rannvá* exploration lead consists of a major sub-volcanic anticlinal closure beneath the crest of the Wyville Thomson Ridge. Comparison of Paleocene seismic facies with those of the productive Faroe-Shetland Basin suggests that a correlative of the Kettla Tuff Member may be present beneath the ridge axis, and turbidite sandstone reservoirs are possibly developed immediately below this level. Although there is a robust structural closure, the possible absence of a reservoir interval is a major risk; source presence and maturity and the deeper structure of the area also remain uncertain. However, evidence obtained from regional geological analogues, sandbox experiments into basin inversion, and modelling of potential field data, is consistent with the development of an inverted Mesozoic half graben at depth.

Acknowledgements

We thank Zyg Sarnowski (Fugro Multi Client Services), Robin Holden (Monarch Geophysical Services) and Brian Richardson (Faroe Petroleum) for supervising the acquisition and reprocessing of seismic data from the Licence 012 area, and J.D. Ritchie (BGS), Stuart Archer, Thomas Varming and an anonymous reviewer for their incisive comments. By sharing some of the results of their recent work on velocity variation in lava successions, L.O. Boldreel and M.S. Andersen showed how we might refine our provisional depth conversion in this area. This paper is published with the permission of the Executive Director, British Geological Survey (NERC).

References

Abraham, D.A. and Ritchie, J.D. 1991. The Darwin complex, a Tertiary igneous centre in the Northern Rockall Trough. *Scottish Journal of Geology* 27: 113-125.

Abrahamsen, N, Schoenharting, G., and Heinesen, M. 1984. Palaeomagnetism of the Vestmanna core and magnetic age and evolution of the Faeroe Islands. *In*: Berthelsen, O., Noe-Nygaard, A. and Rasmussen, J. (eds) *The Deep Drilling Project 1980 -1981 in the Faeroe Islands.* Annales Societatis Scientiarium Faeroensis 9: 93-108.

Archer, S.G., Bergman, S.C., Iliffe, J., Murphy, C.M. and Thornton, M. 2005. Palaeogene igneous rocks reveal new insights into the geodynamic evolution and petroleum potential of the Rockall Trough, NE Atlantic Margin. *Basin Research* 17: 171-201.

Bailey, N.J.L., Walko, P. and Sauer, M.J. 1987. Geochemistry and source rock potential of the west of Shetlands. *In*: Brooks, J. and Glennie, K. (eds) *Petroleum Geology of North West Europe*. Graham and Trotman: 711-721.

Boldreel, L.O. and Andersen, M.S. 1993. Late Pliocene to Miocene compression in the Faeroe-Rockall area. *In*: Parker, J.R. (ed) *Petroleum Geology of Northwest Europe: Proceedings of the 4th Conference*, Geological Society, London: 1025-1034.

Boldreel, L.O. and Andersen, M.S. 1994. Tertiary development of the Faeroe-Rockall Plateau based on reflection seismic data. *Bulletin of the Geological Society of Denmark* 41: 162-180.

Boldreel, L.O. and Andersen, M.S. 1995. The relationship between the distribution of Tertiary sediments, tectonic processes and deep-water circulation around the Faroe Islands. *In*: Scrutton, R. A., Stoker, M. S., Shimmield, G.B. and Tudhope, A.W. (eds) *The Tec-*

tonics, Sedimentation and Palaeooceanography of the North Atlantic Region, Geological Society, London, Special Publications 90: 145-158.

Boldreel, L.O. and Andersen, M.S. 1998. Tertiary compressional structures on the Faroe-Rockall Plateau in relation to northeast Atlantic ridge-push and Alpine foreland stresses. *Tectonophysics* 30: 13-28.

Carr, A.D. and Scotchman, I.C. 2003. Thermal history modelling in the southern Faroe-Shetland Basin. *Petroleum Geoscience* 9: 333-345.

Doré, A.G. and Lundin, E.R. 1996. Cenozoic compressional structures on the NE Atlantic margin: nature, origin and potential significance for hydrocarbon exploration. *Petroleum Geoscience* 2: 299-311.

Duindam, P. and van Hoorn, B. 1987. Structural evolution of the West Shetland continental margin. *In*: Brooks, J. and Glennie, K.W. (eds) *Petroleum Geology of NorthWest Europe, Proceedings of the 3rd Conference*. Graham and Trotman, London, 765-773.

Earle, M.M., Jankowski, E.J. and Vann, I.R. 1989. Structural and stratigraphic evolution of the Faeroe-Shetland Channel and Northern Rockall Trough. *In*: Tankard, A.J. and Balkwill, H.R. (eds) *Memoir of the American Association of Petroleum Geologists* 46: 461-469.

Holden, R., Richardson, B. and Northmore, P. in press. Sub-basalt imaging beneath the Wyville Thomson Ridge. *this volume.*

Imber, J., Holdsworth, R.E., McCaffrey, K.J.W., Wilson, R.W., Jones, R.R., England, R.W. and Gjeldvik, G. 2005. Early Tertiary sinistral transpression and fault reactivation in the western Vøring Basin, Norwegian Sea: Implications for hydrocarbon exploration and pre-breakup deformation in ocean margin basins. *American Association of Petroleum Geologists Bulletin* 89: 1043-1069.

Isaksen, G.H., Wilkinson, D.R. and Hitchen, K. 2000. Geochemistry of organic-rich Cretaceous and Jurassic mudstones in the West Lewis and West Flannan basins, Offshore north-west Scotland: implications for source rock presence in the north-east Rockall Trough. *Marine and Petroleum Geology* 17: 27-42.

Jackson, M.D. and Pollard, D.D. 1990. Flexure and faulting of sedimentary host rocks during growth of igneous domes, Henry Mountains, Utah. *Journal of Structural Geology* 12: 185-206.

Johnson, H., Ritchie, J.D., Hitchen, K., McInroy, D.B. and Kimbell, G.S. 2005. Aspects of the Cenozoic deformational history of the northeast Faroe-Shetland Basin, Wyville Thomson Ridge and Hatton Bank areas. *In*: Doré, A.G. and Vining, B. (eds) *Petroleum Geology: NW Europe and Global Perspectives: Proceedings of the 6th Conference*. Geological Society, London: 993-1007.

Keser Neish, J.C. 2004. *Faroese Region: A Standard Structural Nomenclature System*. Faroese Geological Survey, Tórshavn.

Keser Neish, J. and Ziska, H. 2005. Structure of the Faroe Bank Channel Basin. *In*: Doré, A.G. and Vining, B. (eds) *Petroleum Geology: NW Europe and Global Perspectives: Proceedings of the 6th Conference*. Geological Society, London: 873-885.

Kimbell, G.S., Ritchie, J.D., Johnson, H., and Gatliff, R.W. 2005. Controls on the structure and evolution of the NE Atlantic margin revealed by regional 3D gravity modelling. *In*: Doré, A. G. and Vining, B. (eds) *Petroleum Geology: NW Europe and Global Perspectives: Proceedings of the 6th Conference*. Geological Society, London: 933-945.

Klingelhöfer, F., Edwards, R.A. and Hobbs, R.W. 2005. Crustal structure of the NE Rockall Trough from wide-angle seismic data modelling. *Journal of Geophysical Research* 110: B11105.

Lamers, E. and Carmichael, S.M.M. 1999. The Paleocene deepwater sandstone play West of Shetland. *In*: Fleet, A.J. and Boldy, S.A.R. (eds) *Petroleum Geology of Northwest Europe: Proceedings of the 5th Conference*. Geological Society, London: 645-659.

Loizou, N. 2005. West of Shetland exploration unravelled - an indication of what the future may hold. *First Break* 23: 53-59.

Morton, A.C., Dixon, J.E., Fitton, J.G., MacIntyre, R.M., Smythe, D.K. and Taylor, P.N. 1988a. Early Tertiary volcanic rocks in well 163/6-1A, Rockall Trough. *In*: Morton, A.C. and Parson, L.M. (eds) *Early Tertiary Volcanism and the Opening of the NE Atlantic*. Geological Society, London, Special Publications 39: 293-308.

Morton, A.C., Evans, D., Harland, R., King, C. and Ritchie, J.D. 1988b. Volcanic ash in a cored borehole W of the Shetland Islands: evidence for Selandian (late Palaeocene) volcanism in the Faroes region. *In*: Morton, A.C. and Parson, L.M. (eds) *Early Tertiary Volcanism and the Opening of the NE Atlantic*. Geological Society Special Publication 39: 263-269.

Musgrove, F.W. and Mitchener, B. 1996. Analysis of the pre-Tertiary history of the Rockall Trough. *Petroleum Geoscience* 2: 353-360.

Panien, M., Schreurs, G. and Pfiffner, A. 2005. Sandbox experiments on basin inversion: testing the influence of basin orientation and basin fill. *Journal of Structural Geology* 27: 433-445.

Raum, T., Mjelde, R., Berge, A.M., Paulsen, J.T., Digranes, P., Shimamura, H., Shiobara, H., Kodaira, S., Larsen, V.B., Fredsted, R., Harrison, D.J. and Johnson, M. 2005. Sub-basalt structures east of the Faroe Islands revealed from wide-angle seismic and gravity data. *Petroleum Geoscience* 11: 291-308.

Richardson, K.R., White, R.S., England, R.W. and Fruehn, J. 1999. Crustal structure east of the Faroe

Islands: mapping sub-basalt sediments using wide-angle seismic data. *Petroleum Geoscience* 5: 161-172.

Roberts, D.G., Bott, M.H.P. and Uruski, C. 1983. Structure and origin of the Wyville Thomson Ridge. *In*: Bott, M.H.P., Saxov, S., Talwani, M. and Thiede, J. (eds) *Structure and development of the Greenland-Scotland Ridge: new methods and concepts*. Plenum Press, New York: 133-158.

Rumph, B., Reaves, C.M., Orange, V.G. and Robinson, D.L. 1993. Structuring and transfer zones in the Faeroe Basin in a regional context. *In*: Parker, J.R. (ed.) *Petroleum Geology of Northwest Europe: Proceedings of the 4th Conference.* Geological Society, London: 999-1009.

Schoenharting, G, and Abrahamsen, N. 1984. Magnetic investigations on cores from the Lopra-1 drillhole, Faeroe Islands. *In*: Berthelsen, O., Noe-Nygaard, A. and Rasmussen, J. (eds) *The Deep Drilling Project 1980 -1981 in the Faeroe Islands.* Annales Societatis Scientiarium Faeroensis 9: 109-114.

Sharma, P.V. 1994. Late Palaeocene geomagnetic polarity transition in the Vestmanna core of the Lower Basalt sequence on the Faeroe Islands. *In*: Subbarao, K.V. (ed.) *Magnetism: rocks to superconductors*. Memoir of the Geological Society of India 29: 117-135.

Smallwood, J.R. 2004. Tertiary inversion in the Faroe-Shetland Channel and the development of major erosional scarps. *In*: Davies, R.J., Cartwright, S.A. Lappin, M. and Underhill, J.R. (eds) *3D Seismic Technology: Application to the Exploration of Sedimentary Basins*. Geological Society, London, Memoirs 29: 187-198.

Smallwood, J.R., Harding, A. and Kirk, W. 2002. The Marjun Discovery: First Oil in the Faroes. *Conference on Frontier Exploration of Volcanic Continental Margins, Geological Society of London, September 2002*. (Abstract)

Smallwood, J.R., and Gill, C.E. 2002. The rise and fall of the Faroe-Shetland Basin: evidence from seismic mapping of the Balder Formation. *Journal of the Geological Society*, *London* 159: 627-630.

Smallwood, J.R., Prescott, D. and Kirk, W. 2004. Alternatives in Paleocene exploration West of Shetland: a case study. *Scottish Journal of Geology* 40: 131-143.

Sørensen, A.B. 2003. Cenozoic basin development and stratigraphy of the Faroes area. *Petroleum Geoscience* 9: 189-207.

Spencer, A.M., Birkeland, Ø., Knag, G. Ø. and Fredsted, R. 1999. Petroleum systems of the Atlantic margin and NW Europe. *In*: Fleet, A.J. and Boldy, S.A.R. (eds) *Petroleum Geology of Northwest Europe: Proceedings of the 5th Conference*, Geological Society, London, 231-246.

Spitzer, R., White, R.S. and iSIMM Team. 2005. Advances in seismic imaging through basalts: a case study from the Faroe-Shetland Basin. *Petroleum Geoscience* 11: 147-156.

Stoker, M.S. 1999. Stratigraphic Nomenclature of the UK North West Margin, 3. Mid- to Late Cenozoic Stratigraphy. British Geological Survey.

Stoker, M.S., Morton, A.C., Evans, D., Hughes, M.J., Harland, R. and Graham, D.K. 1988. Early Tertiary basalts and tuffaceous sandstones from the Hebrides Shelf and Wyville Thomson Ridge. *In*: Morton, A.C. and Parson, L.M. (eds) *Early Tertiary Volcanism and the Opening of the NE Atlantic*. Geological Society Special Publication 39: 271-282.

Stoker, M.S., Hitchen, K., Graham, C.G. 1993. *The geology of the Hebrides and West Shetland shelves, and adjacent deep water areas*. United Kingdom offshore regional report. HMSO for the British Geological Survey, London.

Stoker, M.S., Nielsen, T., van Weeriing, T.C.E. and Kuijpers, A. 2002. Towards an understanding of the Neogene tectonostratigraphic framework of the NE Atlantic margin between Ireland and the Faroe Islands. *Marine Geology* 188: 233-248.

Stoker, M.S., Praeg, D. Shannon, P.M., Hjelstuen, B.O., Laberg, J.S., van Weering, T.C.E., Sejrup, H.P. and Evans, D. 2005. Neogene evolution of the Atlantic continental margin of NW Europe (Lofoten Islands to SW Ireland): anything but passive. *In*: Doré, A.G. and Vining, B. (eds) *Petroleum Geology: NW Europe and Global Perspectives: Proceedings of the 6th Conference*. Geological Society, London: 1057-1076.

Tate, M.P., Dodd, C.D. and Grant, N.T. 1999. The Northeast Rockall Basin and its significance in the evolution of the Rockall - Faeroes / East Greenland rift system. *In*: Fleet, A.J. and Boldy, S.A.R. (eds) *Petroleum Geology of Northwest Europe: Proceedings of the 5th Conference*, Geological Society, London: 391- 406.

Waagstein, R. and Heilmann-Clausen, C. 1995. Petrography and biostratigraphy of Paleogene volcaniclastic sediments dredged from the Faroes shelf. *In*: Scrutton, R.A., Stoker, M.S., Shimmield, G.B. and Tudhope, A.W. (eds) *The Tectonics, Sedimentation and Palaeoceanography of the North Atlantic Region*. Geological Society, London, Special Publication 90: 179-197.

Waddams, P., and Cordingley, T. 1999. The regional geology and exploration potential of the NE Rockall Basin. *In*: Fleet, A.J. and Boldy, S.A.R. (eds) *Petroleum Geology of Northwest Europe: Proceedings of the 5th Conference*. Geological Society, London: 379-390.

White, R.S. Smallwood, J.R., Fliedner, M.M., Boslaugh, B., Maresh, J. and Fruehn, J. 2003. Imaging and regional distribution of basalt flows in the Faroe-Shetland Basin. *Geophysical Prospecting* 51: 215-231.

The Faroe Shetland Basin: A MegaSurvey Perspective

ADRIAN BURROWS,[1*] ADRIAN P. BESTWICK[2],
ANDREW M. ROBINSON[3] AND STUART D. HARKER[1].

[1] PGS Reservoir, Amicable House, 252 Union Street, Aberdeen, AB10 1TN, UK.
[*] Email: adrian.burrows@pgs.com ; Tel: +44 1224 627795, Fax +44 1224 644293
[2] Senergy Ltd., 15 Bon Accord Crescent, Aberdeen, AB11 6DE, UK.
[3] Statoil ASA., N4035, Stavanger, Norway

ABSTRACT

The interpretation of the Faroe Shetland Basin (FSB) MegaSurvey was completed in two phases, the results of the first phase were presented at FIEC 1st Conference in 2004. We can now illustrate some of the findings over the whole 23,000 sq kms of the combined phases, these include conventional interpretations, visualisation, and potential prospects. These are based on 150 wells, drilled over 4 decades, which have only sampled a small part of the rich variety of structure and stratigraphy in the FSB. MegaSurveys not only give a fascinating and invaluable view of the geology on a basinal scale, but also maintain the resolution capable of defining prospects, or field extension opportunities. They are truly a "clearer image" of the geological framework, and within that the petroleum potential, of the areas they cover.

Introduction

Following on from the paper by Terrell et al in the FIEC 1st Conference Proceedings, a wider understanding of the Faroes Shetland Basin (FSB) has been developed since that work, particularly on the UK side of the international boundary. The interpreted 3D seismic area (Figure 1 in red) has more than doubled to 23,000 sq kms, the number of well ties increased several fold to 150, and a series of new attributes help to provide insight into the geology of this area. These studies have relevance to the Faroes waters as regional geological setting, direct analogues, and for exploration statistics.

The presentation in Torshavn gave an update on the merged 3D seismic dataset (MegaSurvey) itself and placed it in the context of the exploration history of the basin. It also showed some illustrations of the interpretation work, and addressed the issue of scale. The way that the MegaSurvey allows a combination of views at different scales to put even minor features into their regional context and enhance the understanding of both basinal trends and details and genesis of those features was clearly demonstrated. It illustrated the style of prospect seen in the relatively small area of overlap into Faroes waters, and finally looked at the future for the MegaSurvey. Working with a MegaSurvey is a little like the famous Forth Railway Bridge near Edinburgh which is often quoted as the unending task, once the painters have finished at one end, they must be ready to start again at the other! There is always more to do with the MegaSurvey, either adding newly available surveys at the edges (See Figure 18 below), or integrating and analysing more well ties, or working to refine stratigraphic detail.

MegaSurveys are no longer new, but are becoming an accepted facet of the regional understanding of mature or maturing basins. PGS MegaSurveys are aggregations of large numbers of 3D surveys of various vintages, interpolated and merged into a common grid. Following an initial navigation data QC, the migrated trace data are subject to a stringent quality control prior to merg-

Faroe Islands Exploration Conference: Proceedings of the 2nd Conference.
Annales Societatis Scientiarum Færoensis, Supplementum 50, 2009: 303-318

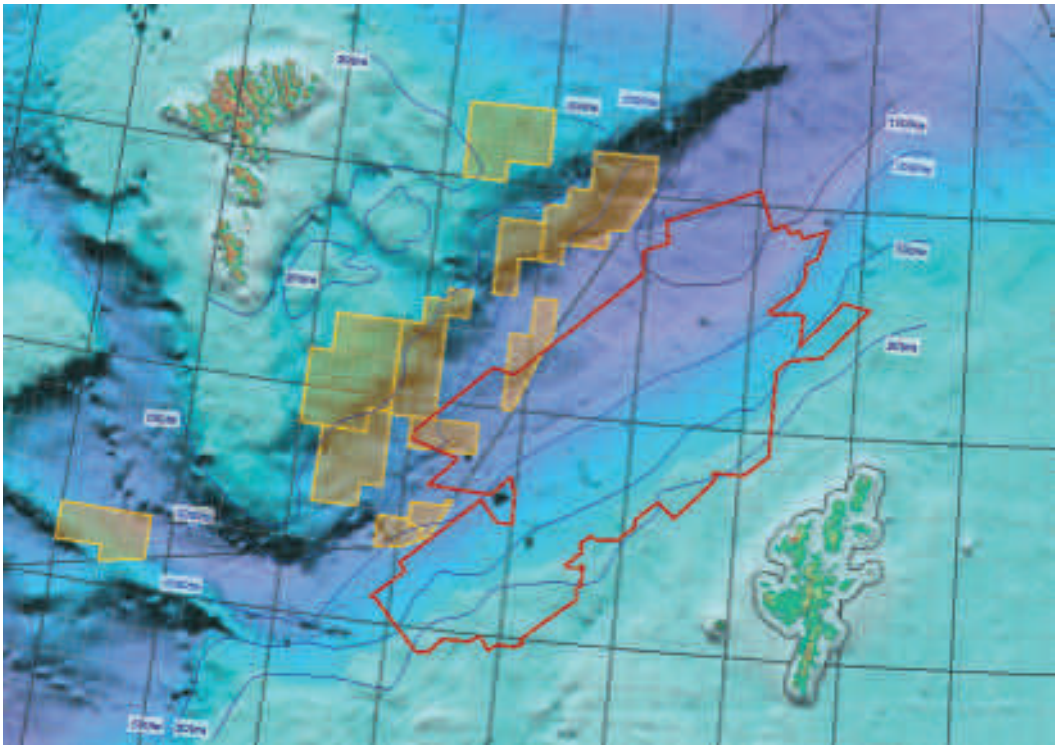

Figure 1. Survey Location and Faroes Licences.

ing. Merge parameters are derived by inline/crossline analysis of frequency, amplitude, phase, and time alignment in an interactive data visualisation environment, and are applied on a survey-by-survey basis to achieve the optimal merge, thereby creating a regional post-stack migration dataset of consistent orientation and line / trace numbering. Despite the different processing vintages, target objectives and record lengths of the individual component surveys, there are surprisingly few artefacts at the boundaries, and the regional interpretation show only minor evidence of sub-optimal joins.

The FSB MegaSurvey has been compiled from 32 individual surveys comprising all available proprietary released 3D data combined with PGS' own 3D multi-client library in the area (> 10,000 sq kms).

Figure 2 shows an inset of the Base Tertiary surface for the MegaSurvey area over the current sea floor bathymetry.

This overview of the basin at high resolution allows everything to be put into context, including the significance of the Corona Ridge and the many wells drilled to date. It also highlights the offset between the present topography and the paleo-topography.

Taking the exploration by decade (Figures 3 to 6), the wells in the 1970's were confined to the shallower water depths, and the basin edges. A variety of stratigraphic targets from Eocene to Carboniferous / Devonian were investigated, and resulted in a major oil find – Clair – now coming on to full production, and the Victory Gas Field.

In the 1980's the exploration reached deeper water, and was unrewarded commercially for a period of 12 years.

In the early 1990's the Foinaven field was discovered, and the ensuing seismically-driven search became focussed on the Paleocene sands. Further successes were made at Schiehallion, Suilven, etc., and at the same time Jurassic successes

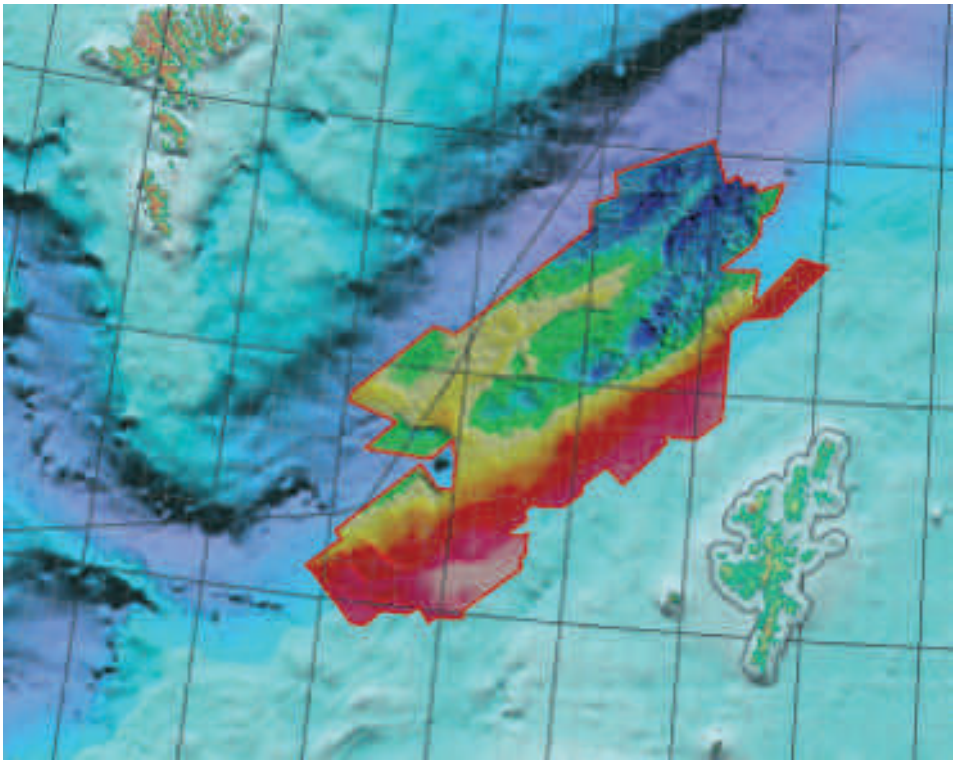

Figure 2. Base Tertiary Horizon and Sea Bed.

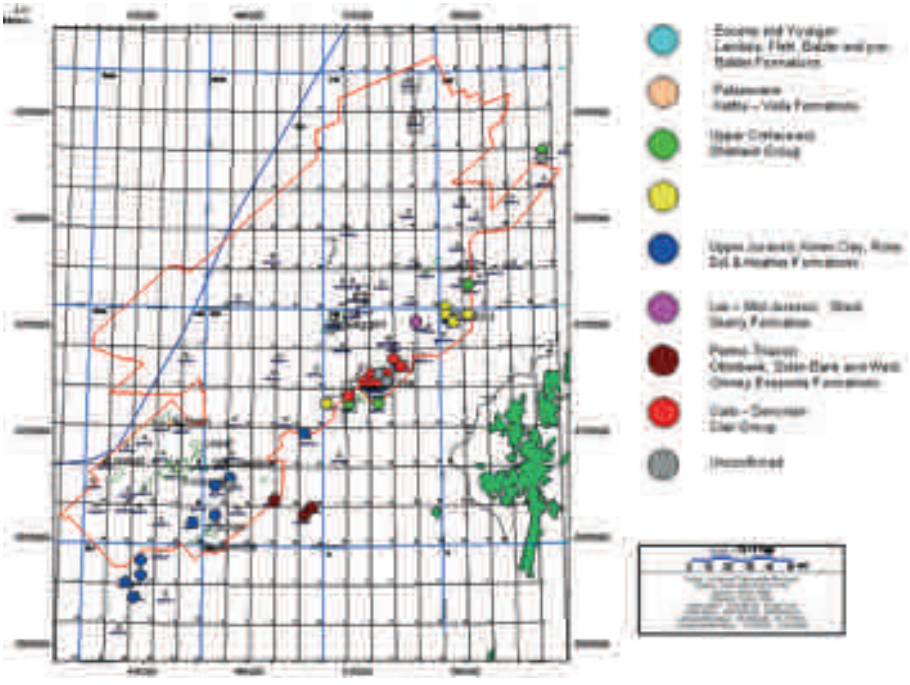

Figure 3. Wells drilled in the 1970's decade.

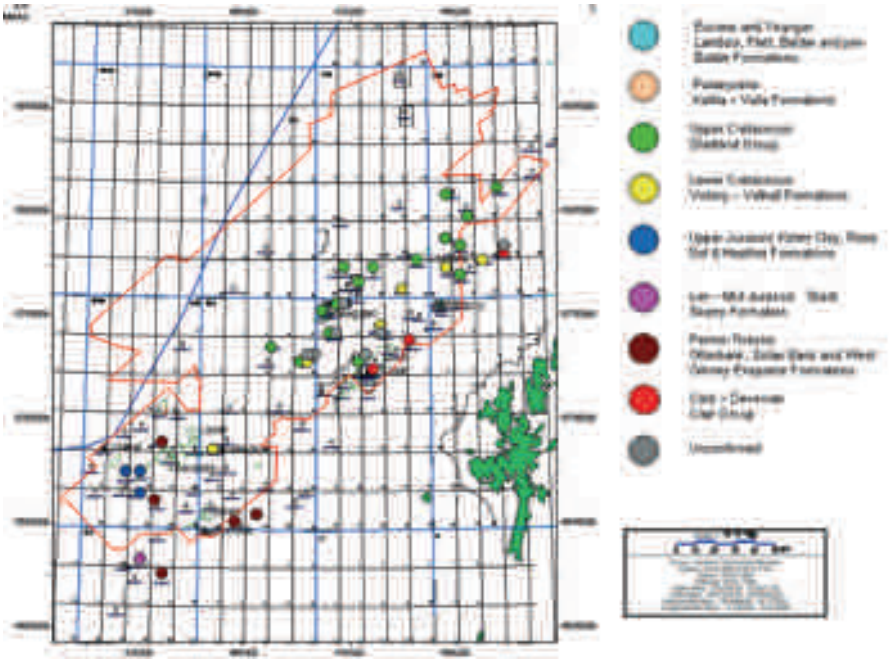

Figure 4. Wells drilled in the 1980's decade.

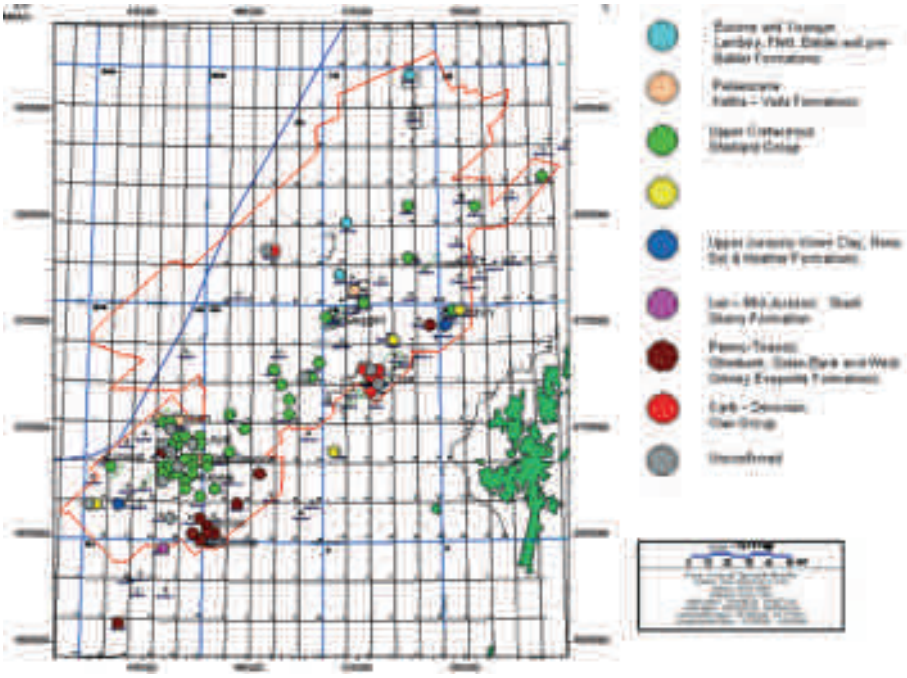

Figure 5. Wells drilled in the 1990's decade.

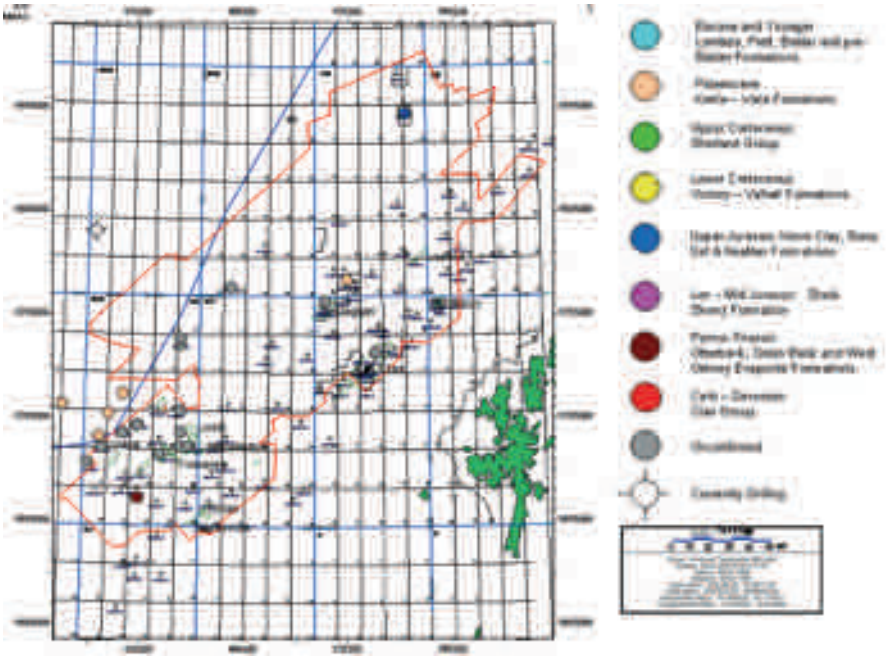

Figure 6. Wells drilled in the 2000's decade.

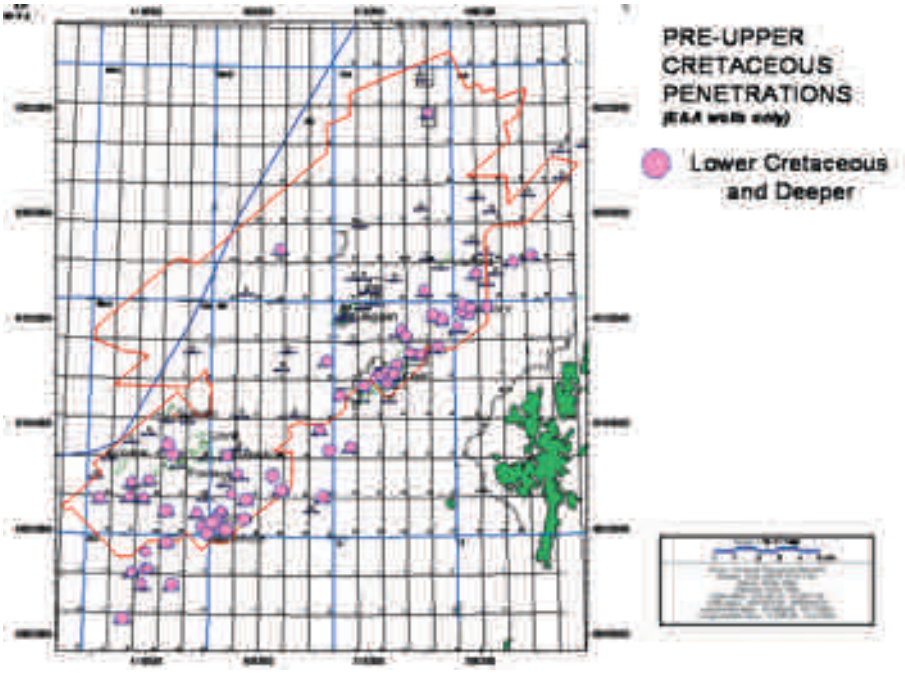

Figure 7. Pre-Cretaceous well penetrations.

Figure 8. FSB Drilling and Discovery Chart.

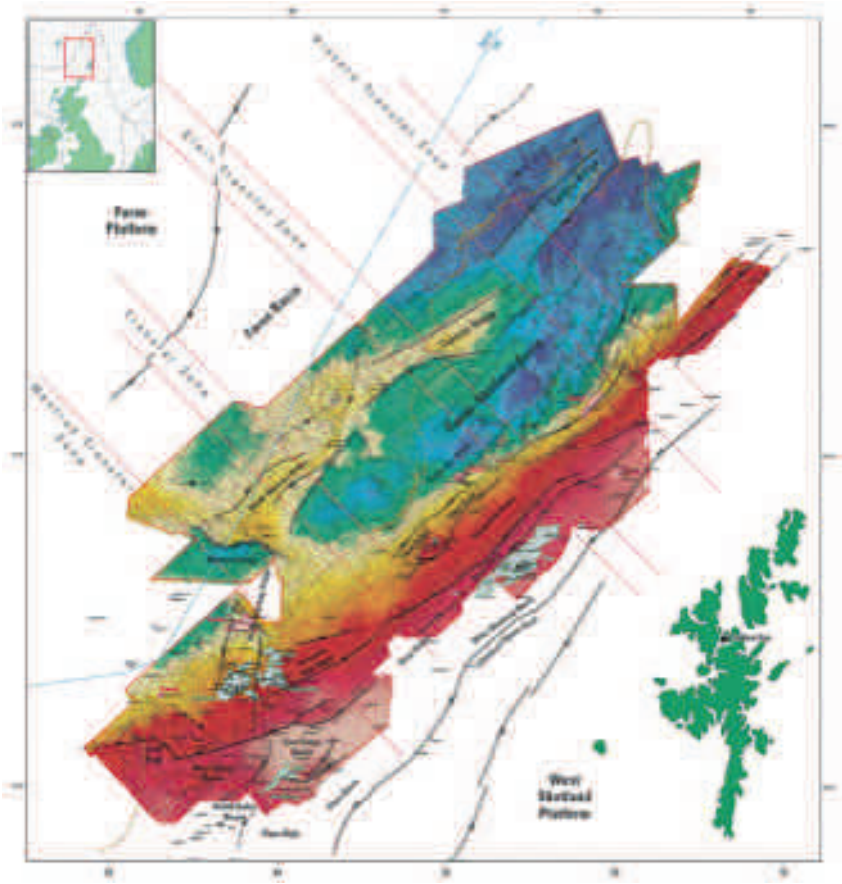

Figure 9. Structural Elements Map.

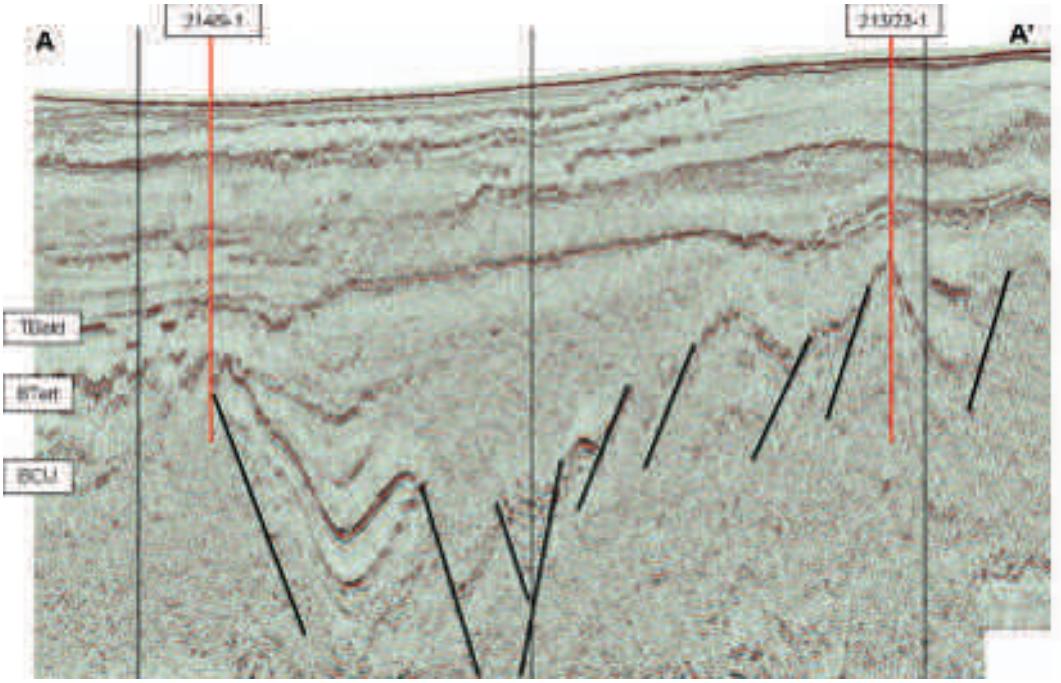

Figure 10. Arbitrary Line along Corona Ridge.

occurred at Solan and Strathmore in Triassic and Jurassic Reservoirs.

Since 2000 we have seen a marked decline in the number of wells (and less is known of those that have not yet been released).

The Judd basin has seen significant interest since the licensing of the White Zone, elsewhere significant successes, as yet singular, have been made at Cambo, Rosebank, and Tobermory in Mesozoic and Tertiary strata.

Taking a quick look at how our knowledge of the full Cretaceous and earlier section is informed (Figure 7) we can see that there are very few penetrations in the north and northwest of the area – something that is vital when constructing and assessing the interpreted regional surfaces in our studies.

In figure 8 we have the exploration time line with E&A wells only. The acceleration after Schiehallion is the most notable feature. This also coincided with a period of intense 3D seismic data gathering.

If we look at the "Exploration rate" (blue curve, right hand scale) the good years have seen around 10 wells drilled – with a maximum of 26 while the poor years have 0 to 5. Since 1998 the years have been "poor". With the current oil price, and recent relative success, one should hope for a resurgence in drilling activity soon. There is certainly no lack of unexplored section in deeper water with a proven petroleum system.

In terms of the updated interpretation, the enlarged area gives an informative structural elements map (Figure 9)

Again this is based on the Base Tertiary, but includes the fields and major fault trends. Both newcomers to FSB and those familiar with the detail can use such maps to put studies in context, and to muse on the existence and impact of the transfer zones shown as overlay here.

The ability to depict the surfaces in 3D from any angle with appropriate lighting can throw into relief specific (e.g. north facing) features such as significant faults and ridges. These highlight the fact that there are many local culminations on the major features only the first of which have been drilled in many cases. 2D lines along the Corona Ridge indicate the complex subcrop at Base Creta-

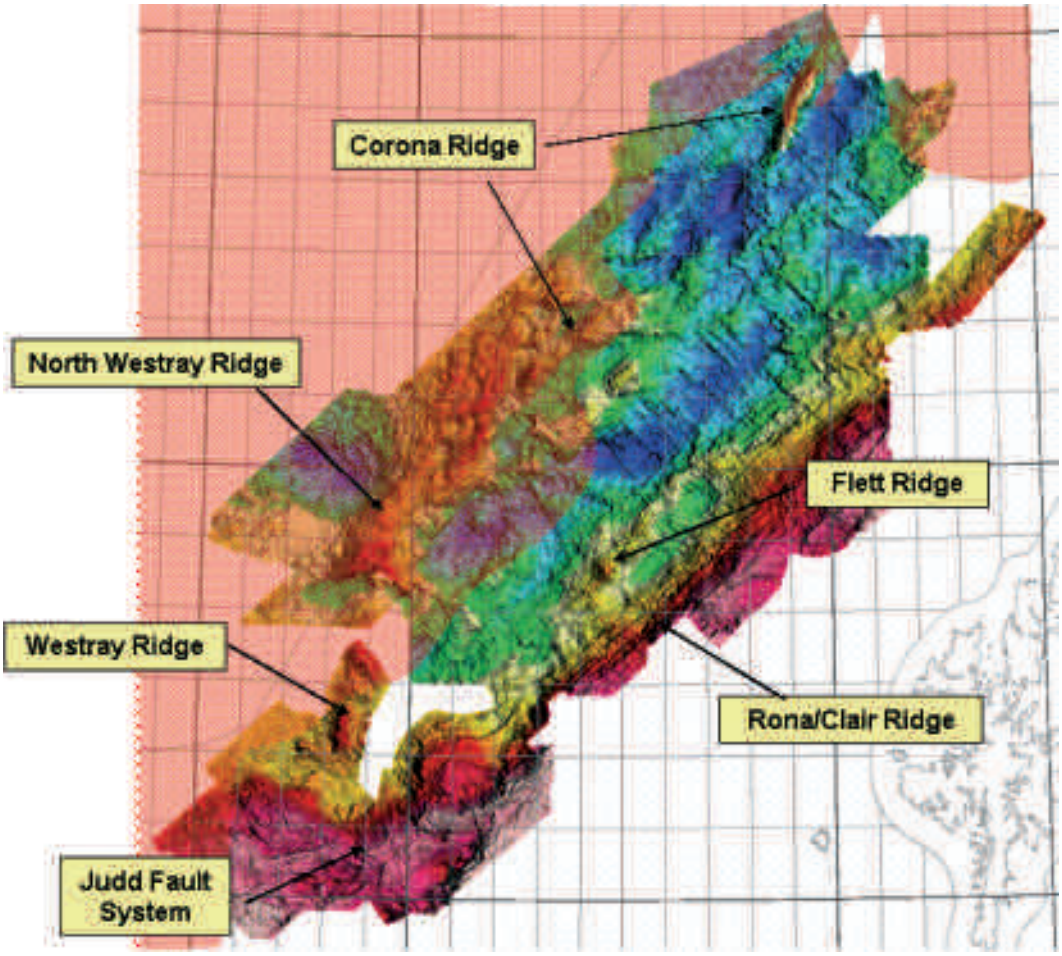

Figure 11. BCU Shaded Relief Surface.

ceous (e.g. Figure 10), and the many potential stratigraphic variations with indeterminate lithology.

The BCU surface involves more subjective interpretation both due to the variable (generally poor) data quality, and the lack of well control to "seed" the horizon with confidence. However, by using the full power of the 3D images it is possible to construct a consistent and coherent map (Figure 11), though this will undoubtedly change with future wells (at least in detail).

Note the area of missing data on the east flank of the Westray ridge where a survey did not have sufficient record length to cover the BCU surface.

There are many potentially valid structures here, the majority not yet touched by the drill bit.

The complexity and richness of structure below Base Tertiary in all probability continues to the northwest under the partial or complete obscurity of the basalts.

In addition to the simple surfaces, a full suite of isopach maps allows the depositional history to be understood in more detail.

In the isochron of Figure 12 pink is thick and green is thin.

There would appear to be some more north northeasterly trends at this level. Other than the Flett basin and inshore areas on trend, the general

tendency is for thinning towards the Faroes, except for the area immediately north of the main Westray Ridge.

There is more to say regarding scale below, but there is a wealth of detail just visible on this isochron on the main basinal trends.

The potential to review the geology at different scales is one of the strongest features of the full MegaSurvey. Within one workstation session we can look at a constant time-slice of the whole basin, giving a snapshot intersecting Eocene to Tertiary strata, then zoom in to an intermediate scale richer in detail, but larger than most 3D surveys, or a Block or small prospect size view (Figure 13).

Although we may be looking at less than a quarter of a UK Block, we still have sufficient detail to define unpixellated fault, horizon or feature lines. Small features jump out and demand investigation. With the MegaSurvey there is never a question of

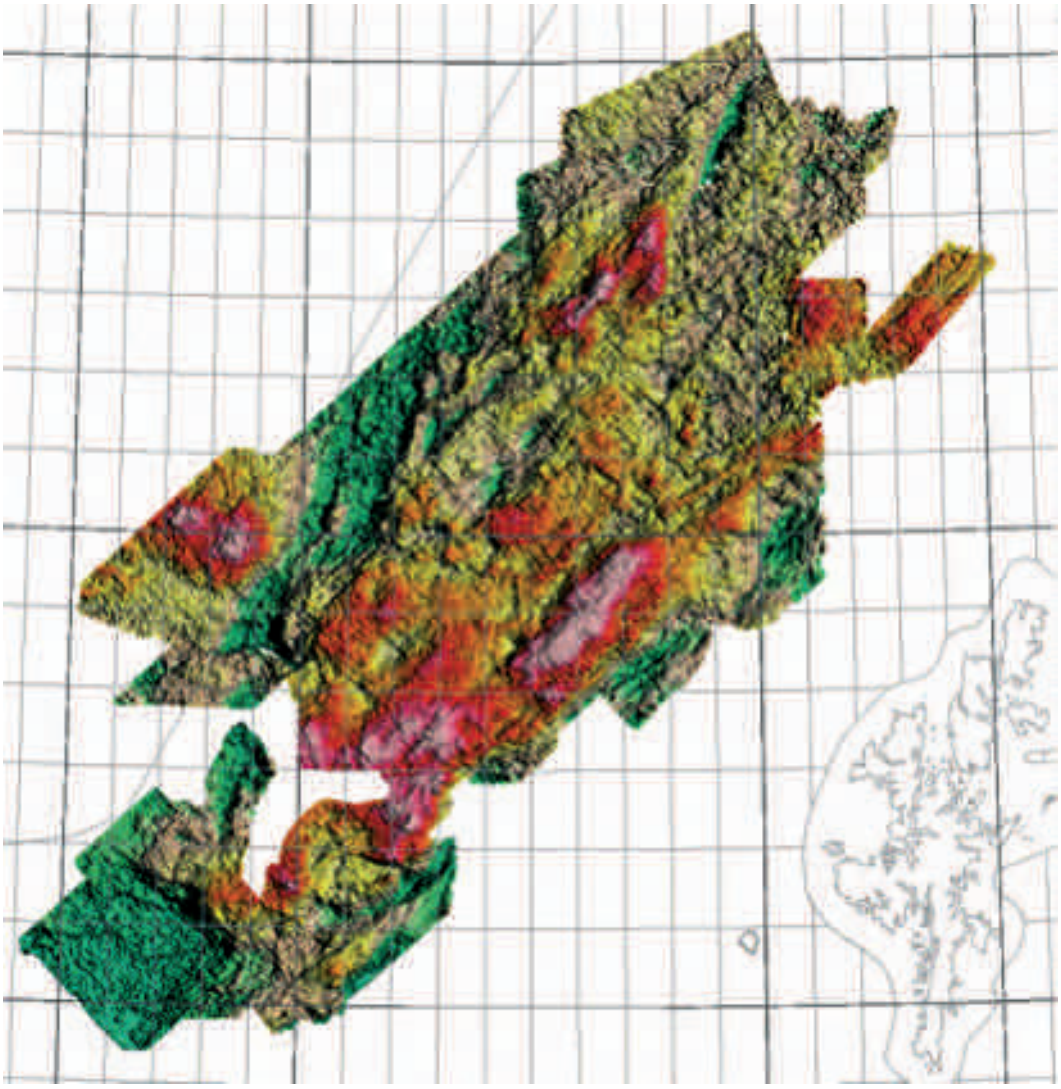

Figure 12. Isochron B Tertiary to B. Cretaceous.

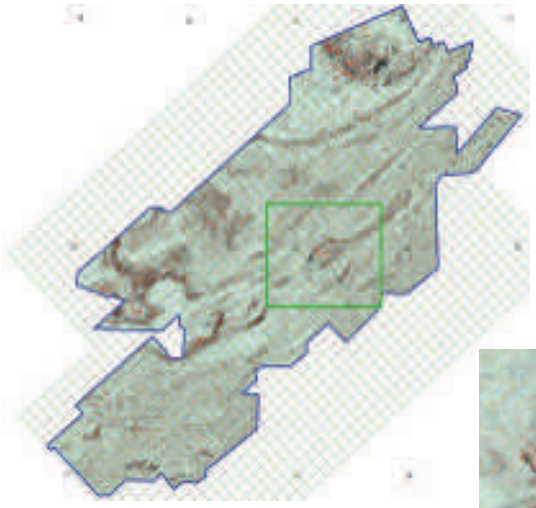

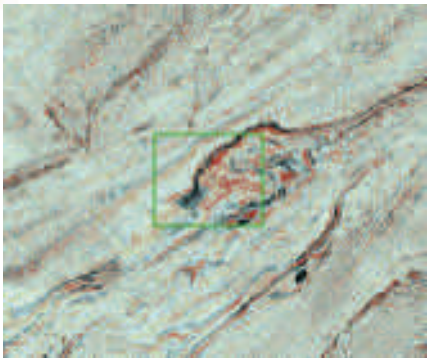

Figure 13. Time Slices at 2400 ms zooming in on a small feature, probably of volcanic origin.

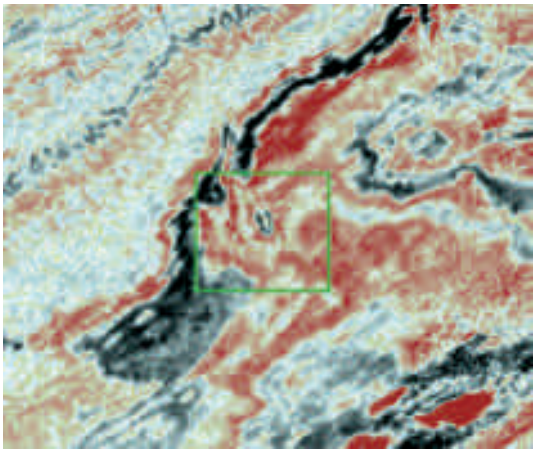

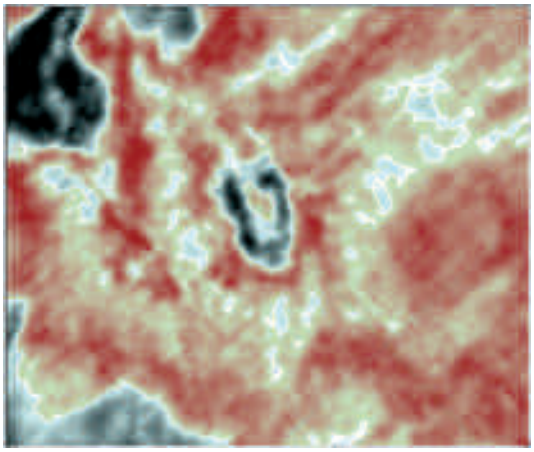

falling between 2D lines, or not being able to look in a specific direction, or tie to a nearby well directly.

The feature identified in Figure 13 is a small volcanic vent. At a fairly large scale in section view it stands out clearly against the regional dip (Figure 14 upper left). The underlying stratigraphy is anomalous in this direction, and there are indications of other anomalies in the overburden – but at this scale the full relationships cannot be understood. If we have limited data available (or loaded to the workstation) it may be tempting to ignore this if it cannot generate a prospect. But it is always worthwhile trying to look at the full context to get a more informed view.

By zooming out a little the regional strike becomes obvious and a strike line through the anomaly covering several blocks shows us the restricted width of the anomaly below the roughly circular vent, and the upward opening flute of the overburden anomaly (Figure 14 lower right). At this vertical scale we can also interpret a relatively long lived feature, with episodic positive "eruptions" and a late stage "collapse", or fluidized crater above.

By zooming out in the strike direction (Figure

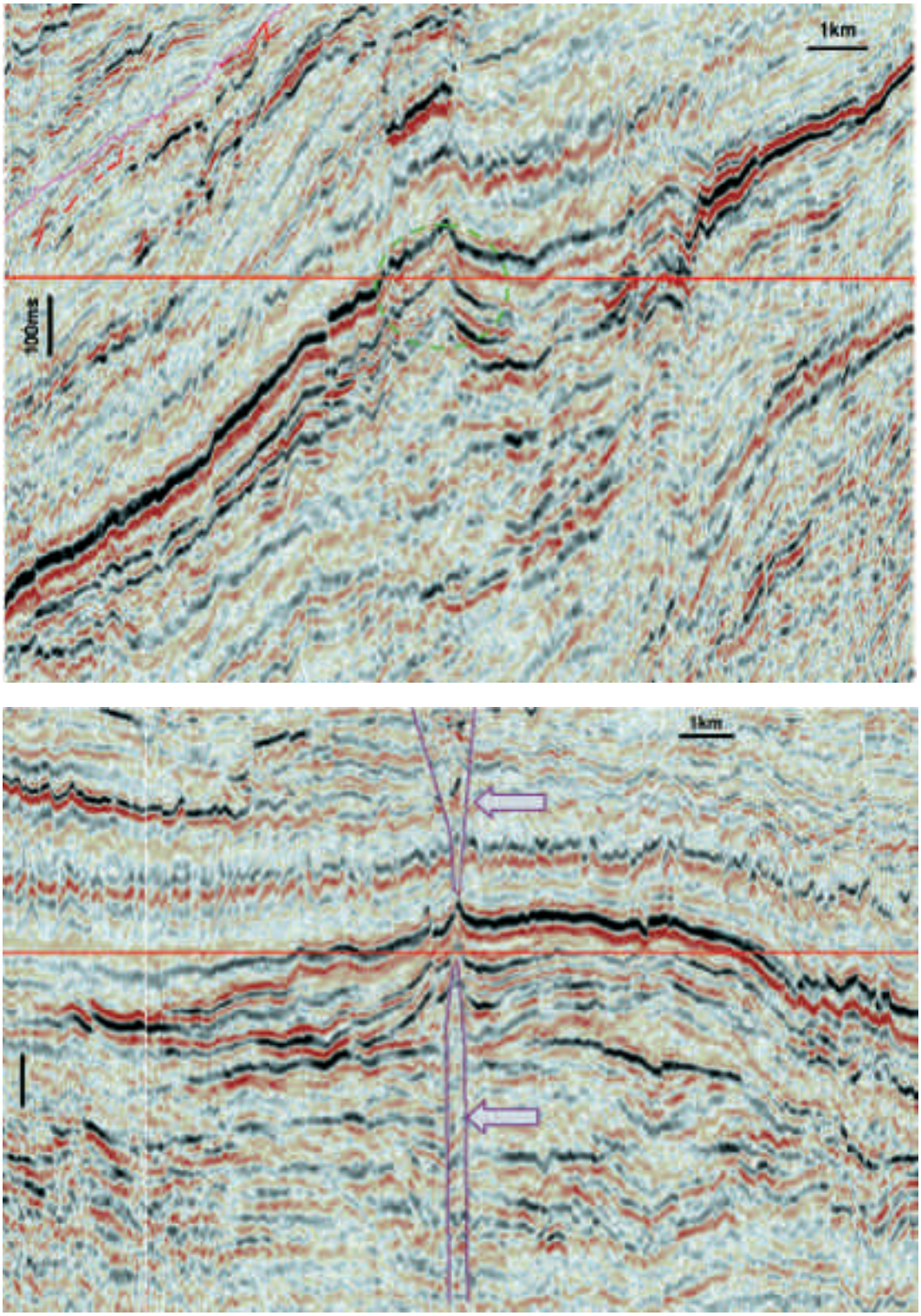

Figure 14. Dip and Strike Line through vent anomaly.

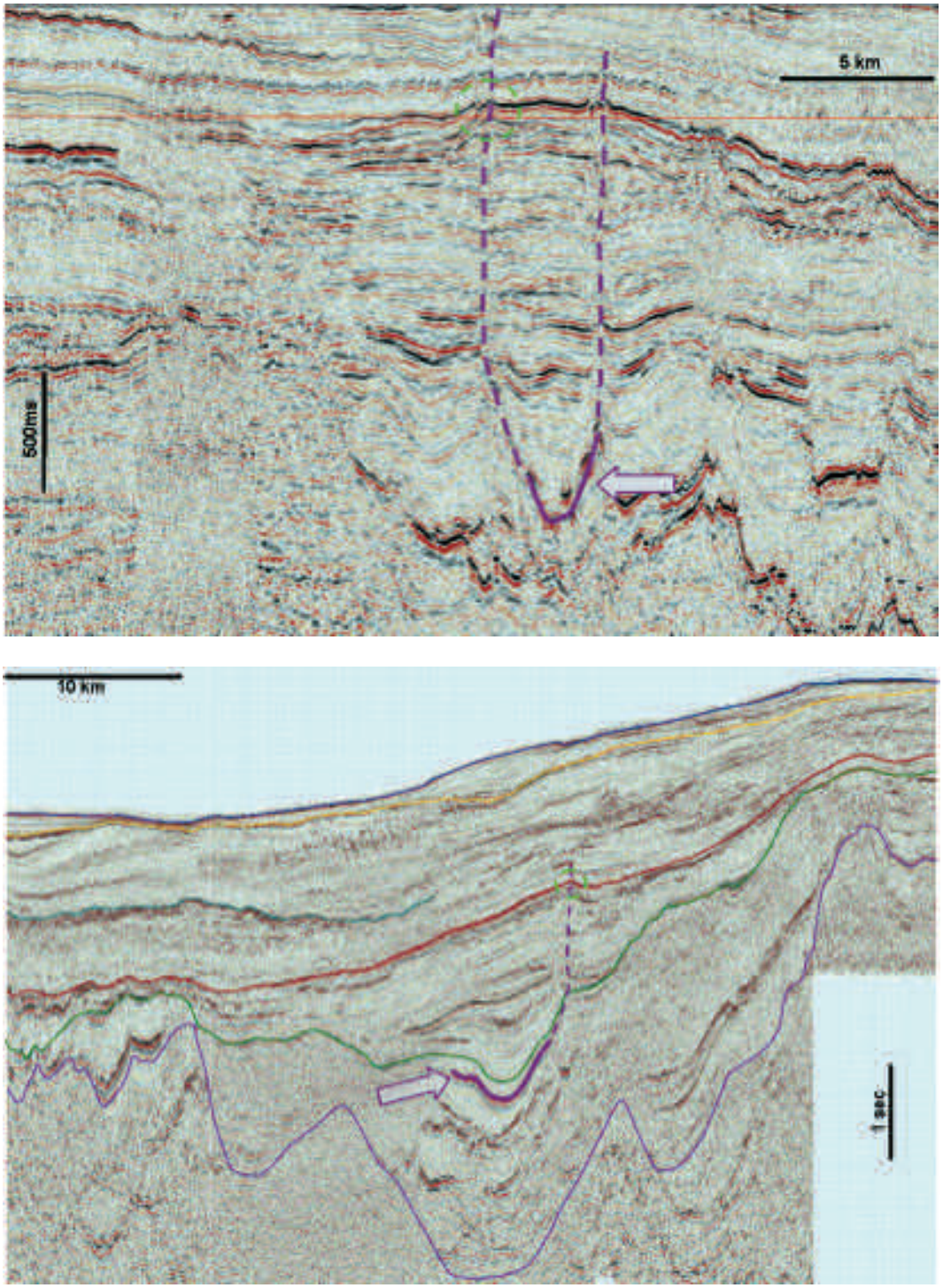

Figure 15. Zoomed out Dip and Strike Lines over the volcanic features.

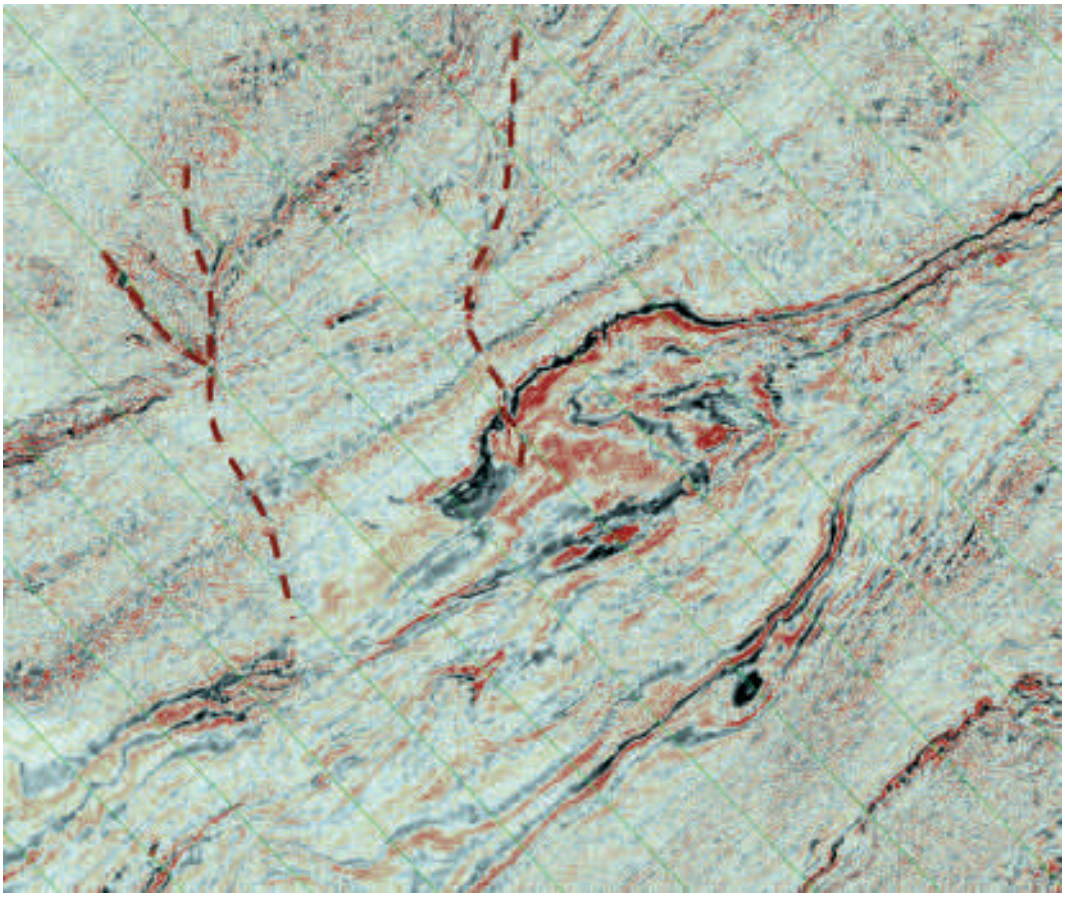

Figure 16. Semi-Regional Time Slice with sinuous linear features related to volcanic vents.

15 upper left) we can see a possible origin of the volcanic eruptions from the tip of an intrusion at depth. We can also see at least one similar feature and others can be interpreted too. They can be interpreted as having semi-vertical feeders, and being of similar age, but not all have the late stage overburden features – are these just related to semi-circular vents, and are all the features related to a similar structural origin?

On a semi-regional view of the time slice (Figure 16) the collapse feature can be traced for some distance to the north in a sinuous line. To the west a similar series of lines exists – but not all the "vents" have such lines associated. A late stage event related to a change in stress field can be postulated to explain this.

Finally by zooming out in the dip line right across the MegaSurvey (Figure 15, lower right) we can see that the deep seated sills which appear to be the source of the volcanic features are injected into the deepest part of the sedimentary package, and the vents come off the up-dip tips of the sills. – All very logical and in keeping with observations in other parts of the Tertiary igneous province further west and south towards Irish waters. (Plus from a recent publication, similar features are also seen on the Norwegian shelf further north). None of this is obvious without the ability to look at both local detail, and regional context of these (small) features.

Note that the dip line actually crosses 7 different 3D surveys – but at this scale the joins are ir-

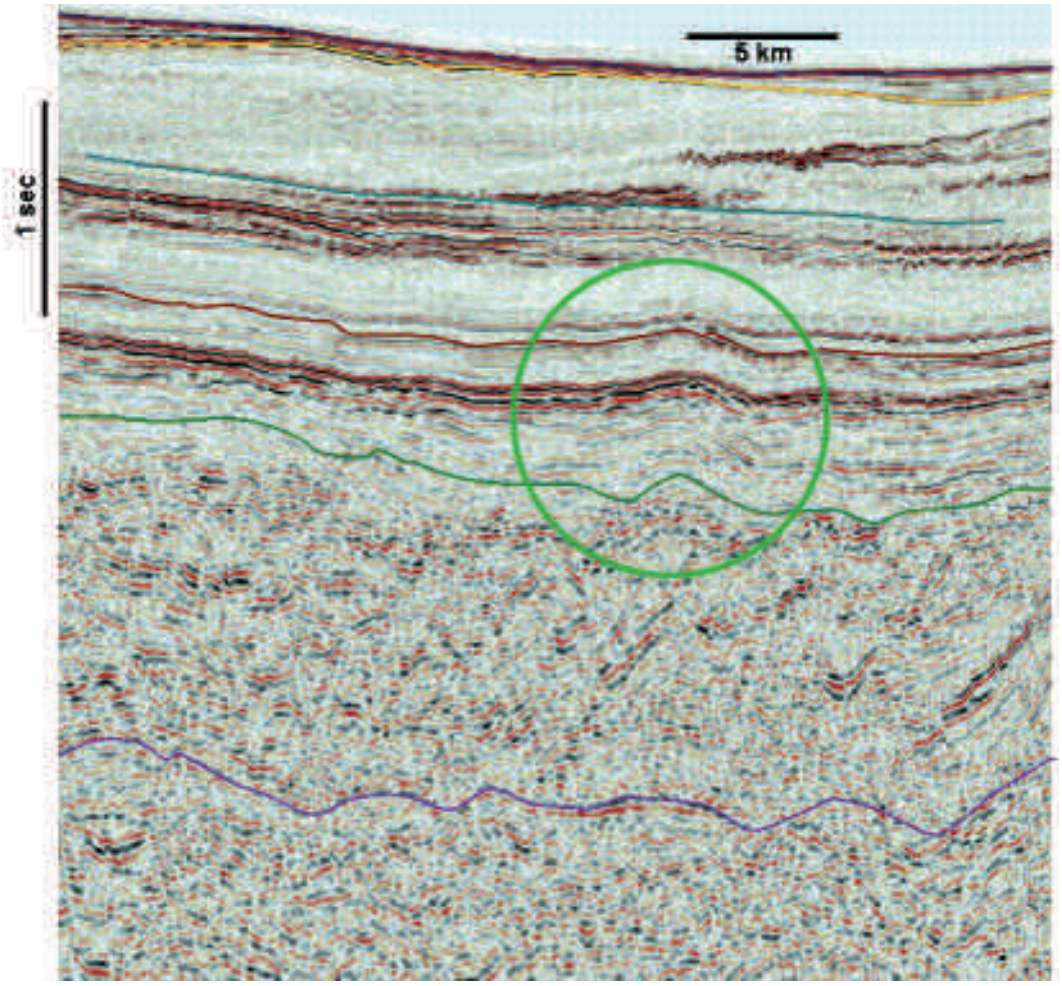

Figure 17. Faroes Waters Prospect.

relevant to the understanding we need.

With specific reference to the Faroes sector, there are several potential prospects, and we can illustrate one of these which exemplifies the somewhat lower relief typical of the shallow section here, and difficulty in picking deeper horizons (Figure 17). Another paper at the conference has more detail on this area and indicated that such prospects may be drilled in the near future.

This Paleocene feature has four-way dip, and a possible deep-seated underlying structure. The shallow overburden has interesting lithological (or other) contrasts in the toes of prograding wedges. There are potentially interesting stratigraphic features in the Eocene, but the deep structure is obscured by the inferred thick basaltic layers. There are angularly discordant reflectors – possible dykes – within this sequence.

For the future PGS will be looking to opportunities to extend the coverage of this MegaSurvey. Figure 18 shows the most obvious opportunities with 3D datasets that might be released in 2007. We believe that with the techniques presented in other talks at the conference the time may soon be right to develop a fuller coverage in Faroes waters which could be much better than the images available when Phase 1 of our work was presented in 2004.

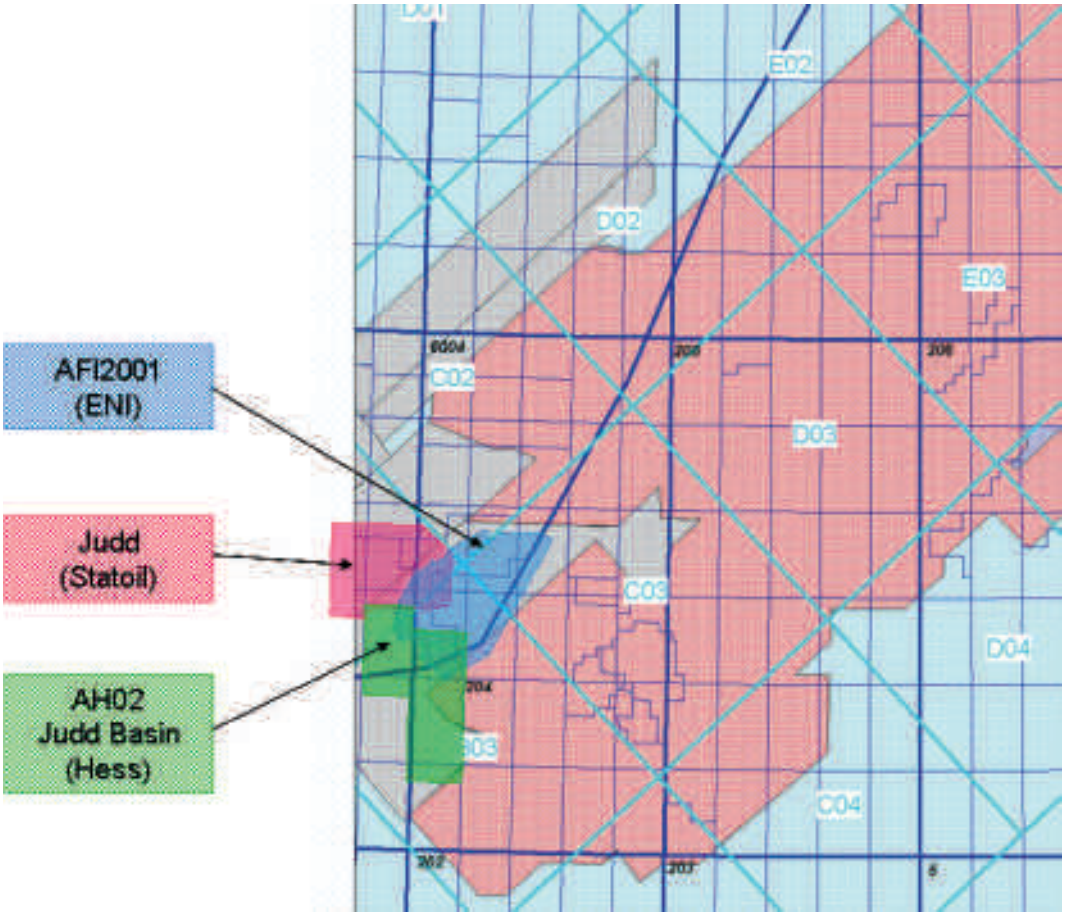

Figure 18. Possible Additional surveys for 2007.

Conclusion

In conclusion we believe that this basin is still relatively under-explored, but has considerable stratigraphic complexity left to evaluate. This is particularly true in the northern portion adjacent to Faroes waters, and is probably true of the sub-basalt portion in those waters if technology can begin to allow base basalt and underlying form to be detected. Notwithstanding this, under the edges of the basalt the 3D is frequently good enough to provide indicative structural interpretations on a regional basis and projecting in 3D across the worst areas.

It would seem to the authors that there are structures which are either analogous to existing discoveries, or sufficiently distinct from unsuccessful tests, that can be mapped well enough to form drillable prospects in the current commercial environment. Combination structural-stratigraphic traps can be interpreted with significant potential, although past history suggests these must be treated as higher risk opportunities.

Much of the MegaSurvey currently covers open acreage, and it should provide the means to understand and reduce the risk of exploring in these areas, and those round-about, to unlock the remaining petroleum potential of this part of the Atlantic Margin, It can also provide a wealth of scientifically interesting detail at various scales. This paper just shows a starting point in regional evalua-

tion, and a number of further studies are under discussion including added-value geological input to improve seismic calibration and the understanding of the petroleum system, potential field modelling, and further seismic attribute analyses. We fully believe that such studies, in increasing detail through time, can provide a stream of opportunities for future drilling – with a significant likelihood of success.

References

Terrell, N., Edwards, H, Scoffield, P. and Martin, M. 2004. PGS Faroe Shetland Basin MegaSurvey – the Key to New Discoveries in a Maturing Frontier Area. *In*: Ziska H., Varming T., and Bloch D. (eds) *Faroe islands Exploration Conference, Proceedings of the First Conference,* Annales Societatis Scientiarum Færoensis, Supplementum 43, Tórshavn: 51-69.

Hansen D.M. 2006. The morphology of intrusion-related vent structures and their implications for constraining the timing of intrusive events along the NE Atlantic margin. *Journal of the Geological society of London* 163: 789-800.

Loizou, N., Andrews, I.J., Stoker, S.J., Cameron, D. 2006. West of Scotland revisited: the search for stratigraphic traps. *In*: Allen, M.R., Goffey, G.P., Morgan, R.K., and Walker, I.M. (eds) *The Deliberate Search for the Stratigraphic Trap.* Geological Society, London Special Publications 254: 225-245.

Lamers, E., and Carmichael S.M.M., 1999. The Paleocene deepwater sandstone play of West Shetland. *In*: Fleet, A.J. and Boldy, S.A.R. (eds) *Petroleum geology of Northwest Europe: Proceedings of the 5th Conference*. Geological Society, London: 645-659.

Sub-basalt seismic imaging – offshore Faroes

JOSEPH W GALLAGHER* AND PETER W DROMGOOLE

StatoilHydro (UK) Limited, Statoil House 11a Regent Street, London, SW1Y 4ST, +44 207 766 7777
* Email: jwg@statoilhydro.com

ABSTRACT

Discoveries in the Faroes-Shetland basin to date have been made in the areas covered by thin or no basalt flows as the presence of these flows has, in the past, seismically obscured the geology and structure of the underlying section. The industry has been tackling this problem for many years and it is known that high frequencies penetrate only a short way into the basalt before being scattered, generating high frequency noise. Recently, Statoil and its partners in FL006, have made a dramatic improvement in sub-basalt imaging in this problem area. The improvement comes primarily from the processing of the data, using careful multiple removal at all stages of the processing and removing high frequencies (dominantly noise) early in the processing to concentrate on the low frequency data. Velocity analysis must be performed as an iterative process and take into account the geological model. Deep towing the source and cable also improves the data by helping to avoid those higher frequencies which generally cause noise and focusing on the lower frequency data. Applying these processing techniques to older 2D surveys also shows significant improvement in imaging the sub-basalt structure. Data examples show that the complex sub-basalt structure can now be mapped on the improved data and sub-basalt prospects defined.

More recently, over/under seismic data has been acquired in this area. However, results to date have failed to match the expectations of this technique.

Introduction

This paper shows how Statoil and partners have made significant progress in seismically imaging stratigraphy below a thick basalt layer in Licence 006, offshore Faroes (Figure 1).

A basalt layer covers much of the Faroes continental shelf varying in thickness from many hundreds of metres in the northwest to just a few me-

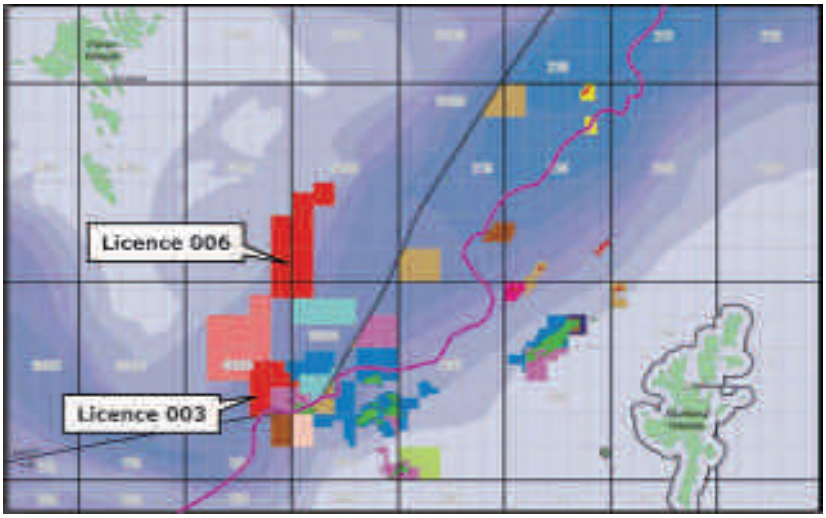

Figure 1. Faroe-Shetland Basin - After First Faroes Licensing Round - The Statoil licences 003 and 006 are indicated

Faroe Islands Exploration Conference: Proceedings of the 2nd Conference.
Annales Societatis Scientiarum Færoensis, Supplementum 50, 2009: 319-332

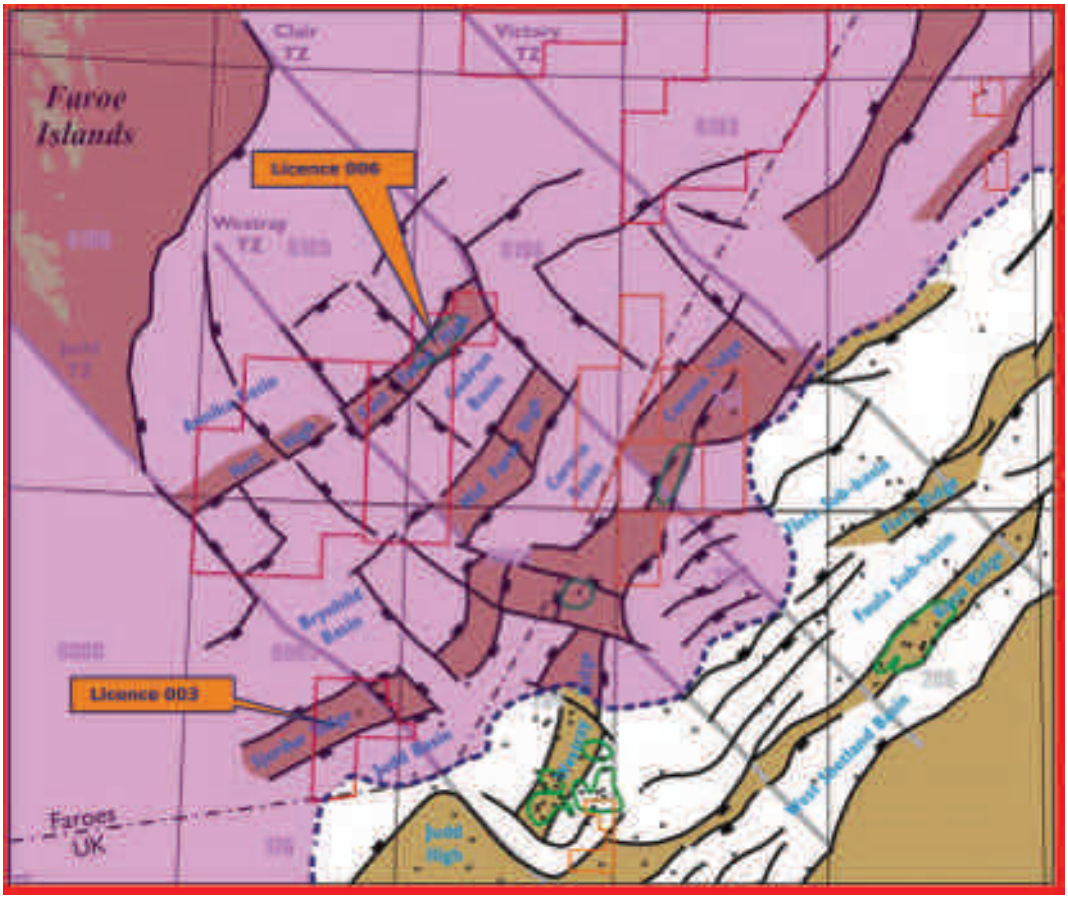

Figure 2. Faroe-Shetland Basin - Structural Elements Map with the Basalt covered area shown in purple

tres in the south-east, see Figure 2. Initially exploration drilling offshore Faroes focussed on the first round licences in the south-eastern area of the Faroes shelf where there is only a very thin or no basalt cover and good quality seismic data. This area is close to the Foinaven and Schiehallion producing oilfields on the UK side and the first Faroes exploration wells in this area were targetting play types similar to the Foinaven and Schiehallion fields but unfortunately the results were not successful. Statoil then moved its exploration focus from Licence 003 to Licence 006.

The Problem

In Licence 006 the basalt cover is significantly thicker than in Licence 003 and this obscures any sub-basalt reflectors. As seen in Figure 3, a 1996 seismic line over Licence 006, there are no primary events seen below the top basalt reflector (red horizon). The challenge in areas of thick basalt is to image the underlying geology. Various consortia addressed the problem over recent years using very long offset data and very large sources as summarised by Roberts *et al.* (2005). However, the main conclusion to date is that low frequencies are required to penetrate the basalt sequence (Pujol and Smithson, 1991). Hobbs (2002) suggested that the high frequencies penetrate only a short way into the basalt before being scattered, generating high frequency noise and Dancer and Pillar (2001) suggested that improved seismic penetration can be achieved when focussing on the low frequency end of the frequency spectrum.

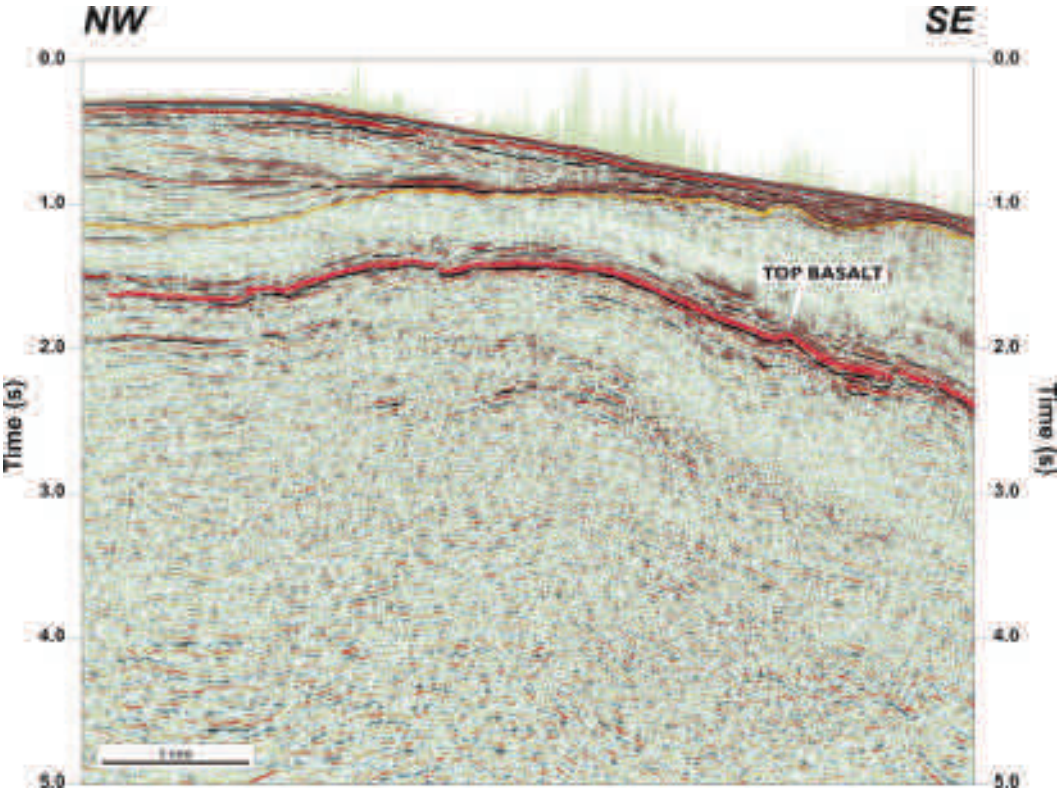

Figure 3. NW-SE 2D seismic line across Licence 006 from the 2D AMG96 seismic survey. All subsequent seismic lines shown are from the same area. The top basalt reflector is the red horizon shown on this and all subsequent seismic sections.

Method – Key acquisition and processing steps

The improvement comes by adapting processing parameters to address the specific problem, benefiting in part from the experiences of the above mentioned previous work. As low frequency seismic energy has better penetrative power than high frequency conventionally acquired seismic, our new offshore seismic acquisition and processing in the Faroes basalt-covered areas is geared towards low frequency acquisition. Deep towing of the source and cables reduces the high frequencies acquired, putting more of the available energy into the low frequencies and hence represents the first step in minimising high frequency noise in the data.

Table 1 lists various speculative and proprietary surveys acquired between 1994 and 2003. Note

Faroes Seismic Acquisition Parameters

Survey	Year	array size (l)	maximum offset (m)	cable depth (m)	gun depth (m)
OF94	1994	5280	5280	10	6
OF95	1995	6000	8150	9	8
AMG96	1996	4736	6600/8100	11	9
GFA99	1999	4960	11550	14	10
ST0107	2001	5025	12150	15	10
ST0112	2001	7610*	12150	15	15
ISIMM	2002	10170*	12000	18	18
ST0308 -3D	2003	5360*	8x7950	20	15

b Bubble Tuned * 'BLAST' (extra large) source

Table 1 Acquisition parameters overview

that ST0107 & ST0112 surveys of 2001 (2D) and the ST0308 survey of 2003 (3D) were acquired with deep-towed cables (15 and 20 m respectively) and for the ST0112 2D and ST0308 3D surveys, a deep-towed source (15 m). The normalised amplitude spectra for the surveys are shown in Figure 4. This figure is designed to show the amplitude/frequency distribution for the source for each

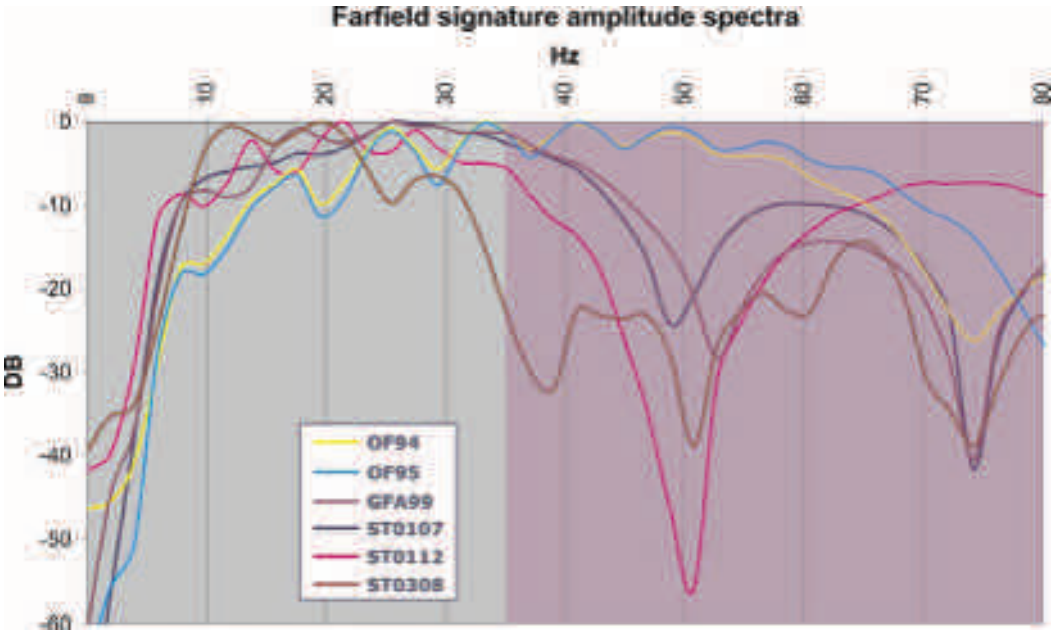

Figure 4. Farfield signature amplitude spectra (normalised with respect to max amp at 0 dB) Purple area dominated by noise. This figure is designed to show the amplitude/frequency distribution for each source and to show the frequencies at which the cable and source notches occur. The figure does not allow comparison of the absolute energy of the individual sources.

survey and to show the frequencies at which cable and source notches occur. It does not allow comparison of the absolute energy of the individual sources. Cable length should be long enough to enable a confident approach to demultiple and accurate velocity analysis and this calculation depends on the depth to top basalt, basalt thickness and target depth.

A bubble-tuned source (described in Avedik *et al*., 1996; White *et al*., 2002) was used to acquire the 2003 test 3D data. However, a comparison test with a conventional peak-tuned source showed little was gained by using the bubble-tuned source (Gallagher and Dromgoole, in press). This 3D survey contains least noise of any of the surveys in the basalt area, acquired with a seismic source at 15 m and cables at 20 m depth. Figure 4 shows the notch in the frequency spectrum for this survey at approximately 38 Hz. No frequencies above this were processed and a 35 Hz high-cut filter became the standard used in all subsequent processing and reprocessing in the area. The area of higher frequencies coloured purple in Figure 4 is dominated by noise and these frequencies should be cut from the seismic data early in the processing.

It is important to acquire data which is optimum for sub-basalt imaging but this has to be matched by good processing. This is where the interpreter's input is vital. The thick basalt interval velocities were not honoured in the initial stages of picking the ST0107 and ST0112 survey velocity analyses but this was spotted by the company QC representative and the stacking velocities were re-picked based on a geological model and with the interpreter's input (Figure 5). This was an iterative process which led to a gradual improvement of the seismic section below top basalt and allowed interpretation of the deeper seismic events with greater confidence (Figure 6).

Demultiple is important to get the best velocity analyses. Surface-Related Multiple Elimination (SRME) and Radon Transform demultiple techniques are combined in a series of passes - each progressively harsher as confidence in the primary velocity trend increases. This is where a choice of longer cable may be of benefit. An open mute - ap-

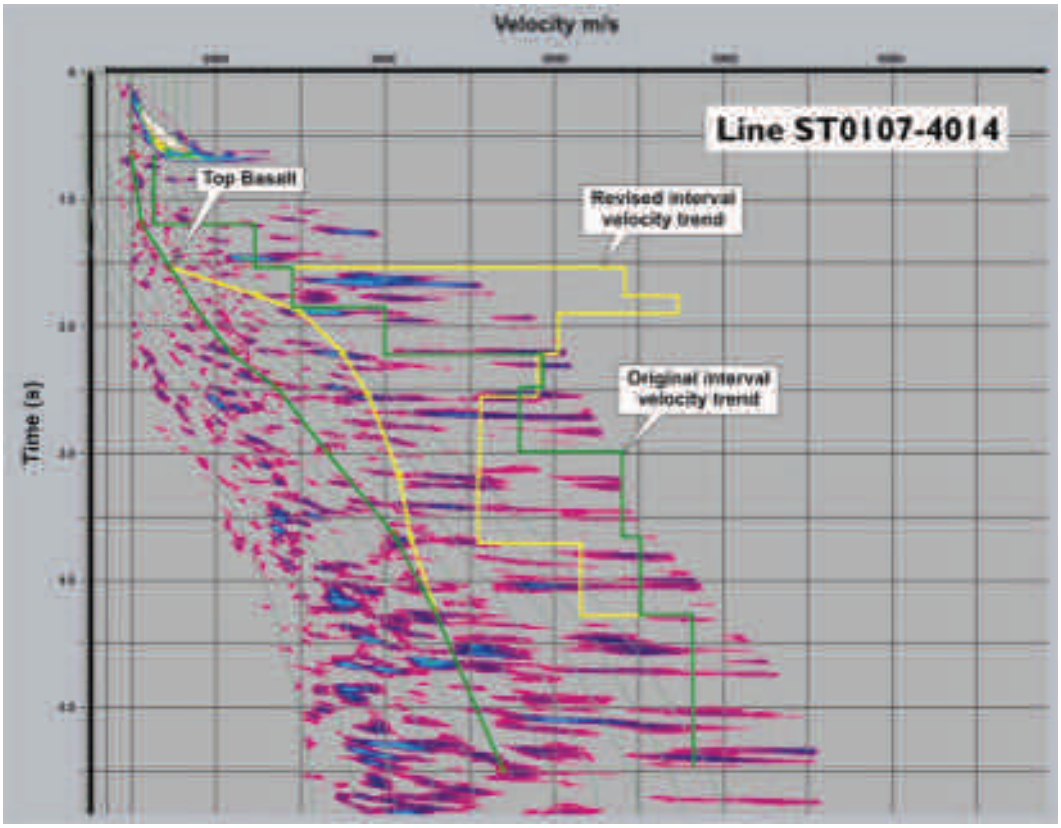

Figure 5. Velocity spectra showing the original velocity trend and the revised velocity trend which takes into account the high velocity basalt layer

proximately 40 degrees here - is preferred. The ST0107 & ST0112 surveys used a 12 km cable which was found to be excessive. The choice of 8 km cables for the ST0308 3D was more than adequate for the basalt depths and interpreted underlying sedimentary section over Licence 006 (see below).

'FX decon' (Canales, 1984) on offset planes was a particularly useful technique to reduce noise. The velocity analysis is one of the most critical steps and everything else is designed to make this as effective as possible and several iterations of velocity analysis should be expected, one after each pass of Radon demultiple.

The ST0308 3D seismic acquisition of 2003 was a test survey in Licence 006. It measures 24 km by 12 km and crosses the East Faroes High within an area of the top basalt structural closure. As shown in Table 1 it was acquired with six 8 km cables towed at 20 m and a bubble-tuned source towed at 15 m.

This survey has been processed extensively, including both pre-stack time and depth migration. The latest dataset, an example of which is shown in Figure 7, is a pre-stack beam-steering depth migration and is a considerable improvement on the data available for interpretation pre-2001, see Figure 3.

Method – Reprocessing of Speculative and Proprietary Data

The improvement in the data quality of recent proprietary surveys resulted from both a systematic approach to the processing and acquisition. In the acquisition, the use of long cables - at least 6 km - has given offsets at target levels sufficient for accurate velocity analysis. Also, the high frequencies

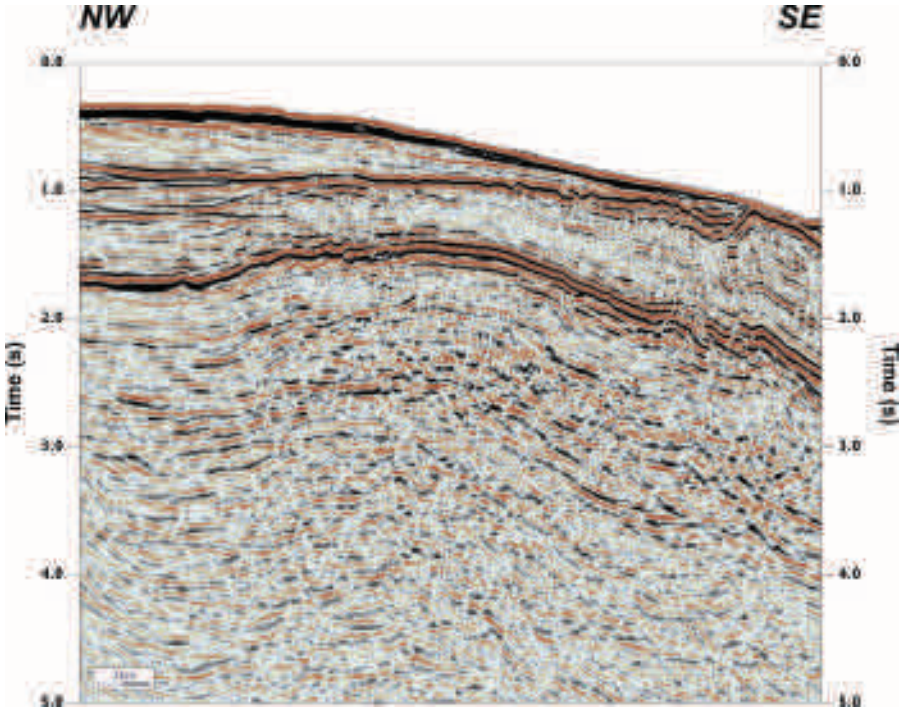

Figure 6. ST0107 2D survey original pre-stack time migration processing

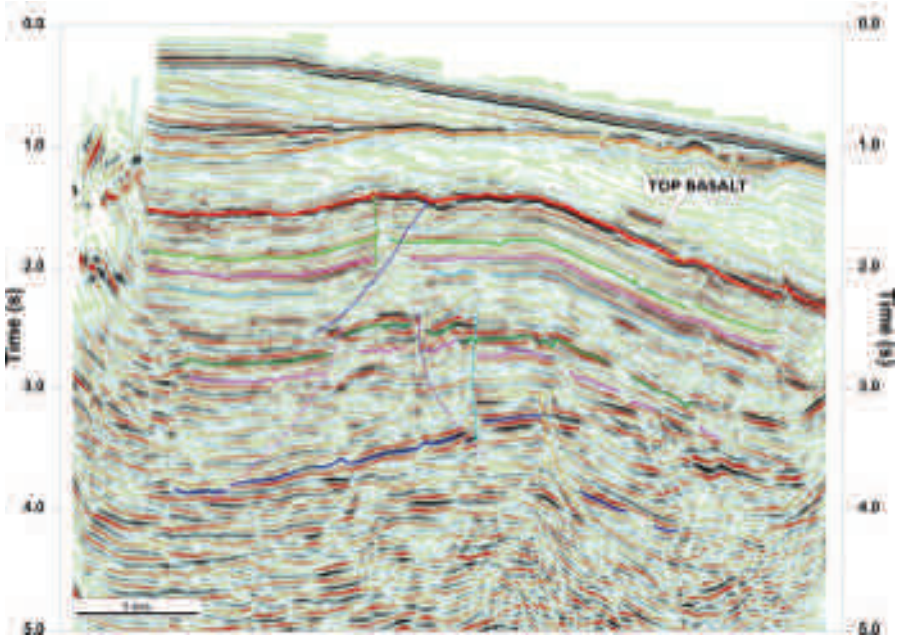

Figure 7. ST0308 3D survey final pre-stack depth migration using a beam migration algorithm

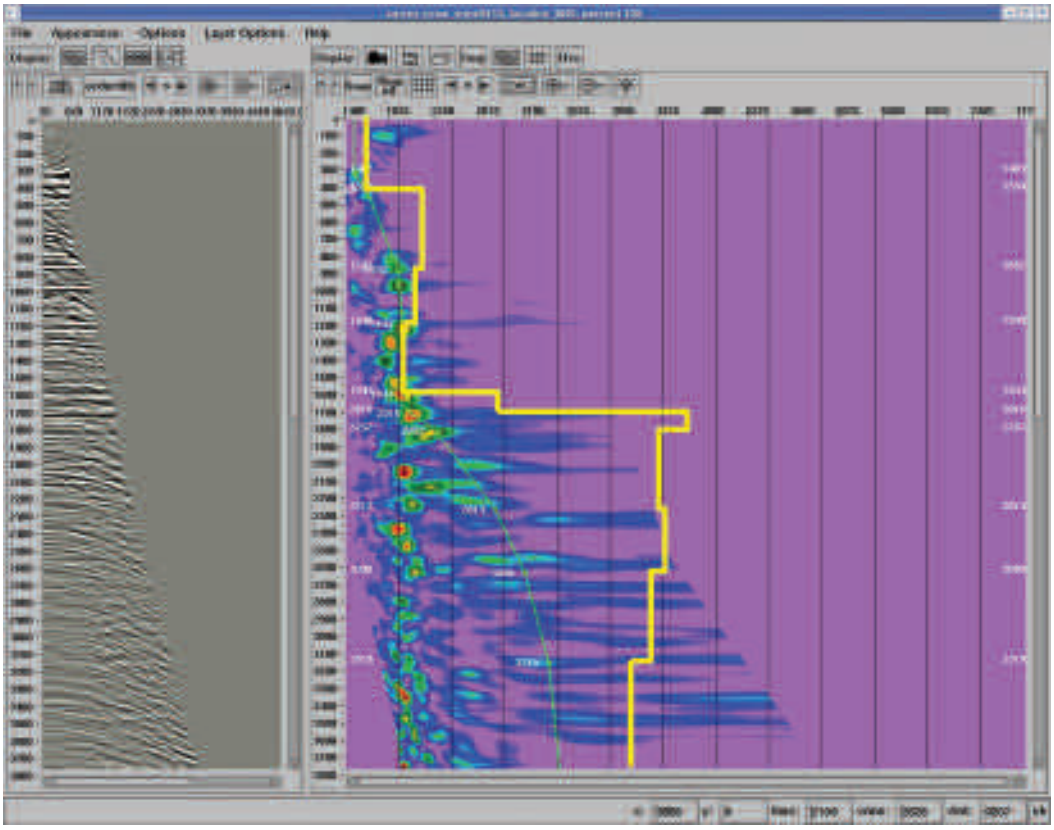

Figure 8. Velocity semblance OF94 2D survey reprocessing - pre demultiple

have been attenuated in the data gathering by deep towing the source and cables which results in less noise to remove in processing.

If these are the more important aspects of optimum acquisition, looking back at Table 1 would suggest the majority of the older surveys were acquired with long enough offsets to satisfy the velocity analysis requirement and from Figure 4 have sufficient low frequencies in the 10-35 Hz band. With shallower, 'conventional' towing, the high frequencies (above 35 Hz in this case) should be removed very early in the processing.

A thorough reprocessing from field tapes of the pre-2001 speculative data and proprietary data was carried out, drawing on the experience gained from the processing of the proprietary 2D and 3D surveys. Figures 8 and 9 show an example of velocity analysis displays before and after the SRME and Radon demultiple passes have been applied. The demultiple process should be taken in small steps as it is important not to remove primary data along with the multiples.

So by focusing very closely at every stage of the reprocessing on low frequencies, noise attenuation, demultiple and velocity analysis it has been possible to extract previously hidden primary data from below top basalt. Figure 10 (original processing) and Figure 11 (reprocessed) show examples from one of the earliest speculative surveys from 1994 and Figure 12 (original processing) and Figure 13 (reprocessed) show an early proprietary survey from 1996. Both examples show a quite dramatic uplift in data quality.

The first general improvement in data quality came with the processing of the proprietary ST0107 & ST0112 2001 2D surveys (Figure 6). When the results of this were seen there was a sense of great achievement as primary events ap-

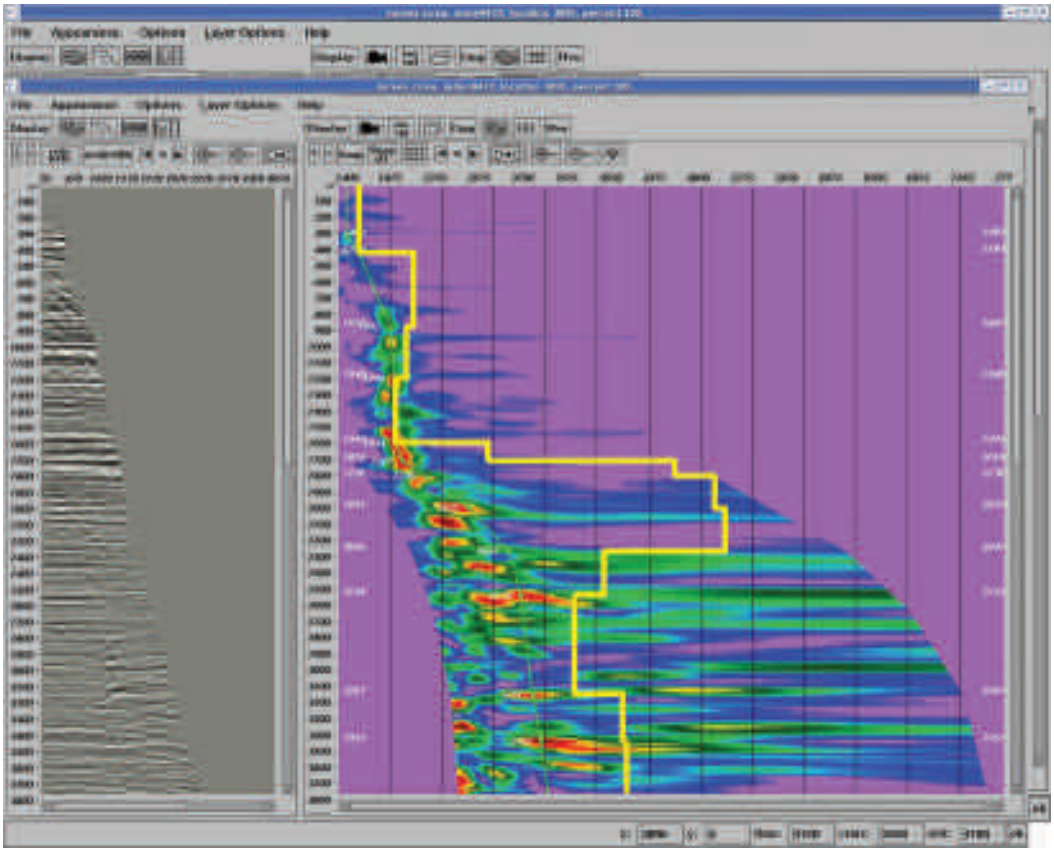

Figure 9. Velocity semblance OF94 2D survey reprocessing - post demultiple

peared in seismic below the basalt and could be interpreted with a reasonable degree of confidence for the first time. This improvement continued as lessons learnt were incorporated into the 2003 3D survey processing. As improvements were seen with each processing and reprocessing phase it was decided to reprocess the proprietary 2001 ST0107 & ST0112 2D. The improvement was significant. Figure 6 (original processing) and Figure 14 (reprocessed) show a line from the ST0107 survey. Coherency has improved at all levels below top basalt (1.5 to 2.0s). Noise has been further reduced compared to the original processing which itself had been seen as a leap forward.

Over/Under data Comparison

Over-under seismic acquisition consists of towing two sources at different depths and two cables at different depths and vertically aligned (Leathard et al. 2007). The example discussed here was acquired by Chevron with sources at 12.5 m and 20 m and cables at 20 m and 30 m.

The present study has shown that processing is more important than acquisition techniques and that surveys from as long ago as 1994 can be reprocessed to give good results when adopting a low-frequency processing approach. Over-under is designed to extend the bandwidth of the data towards both the high and low frequencies by lessening or removing source and receiver ghosts from the frequency spectra. In our opinion extending the bandwidth towards the high frequencies in basalt covered areas only contributes to increasing the noise content. We are not convinced the improvement at the low frequency end is significant and have performed our own comparison of the techniques.

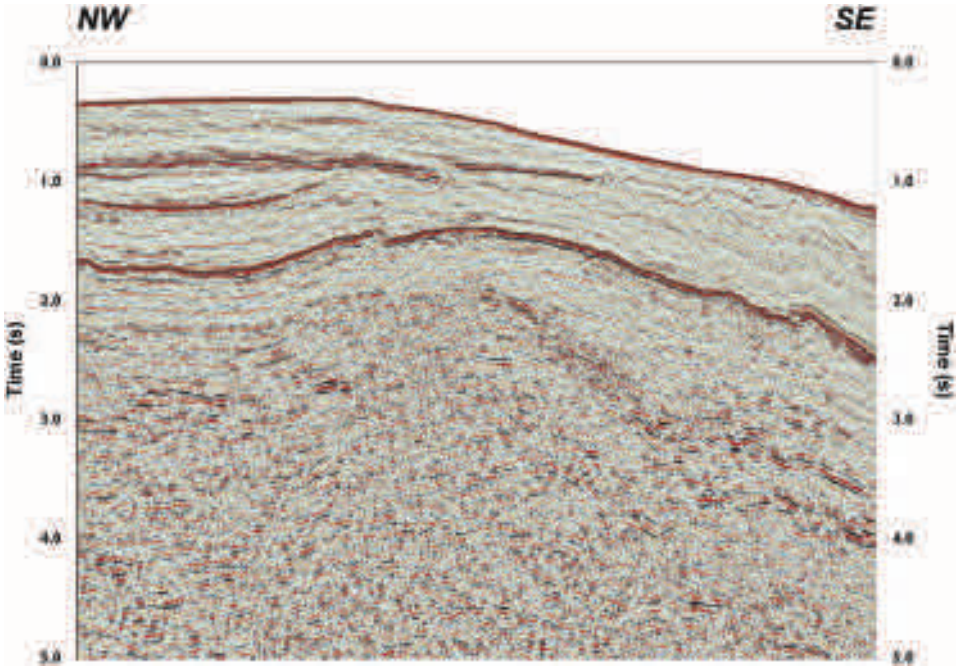

Figure 10. OF94 2D survey original post-stack time migrated processing

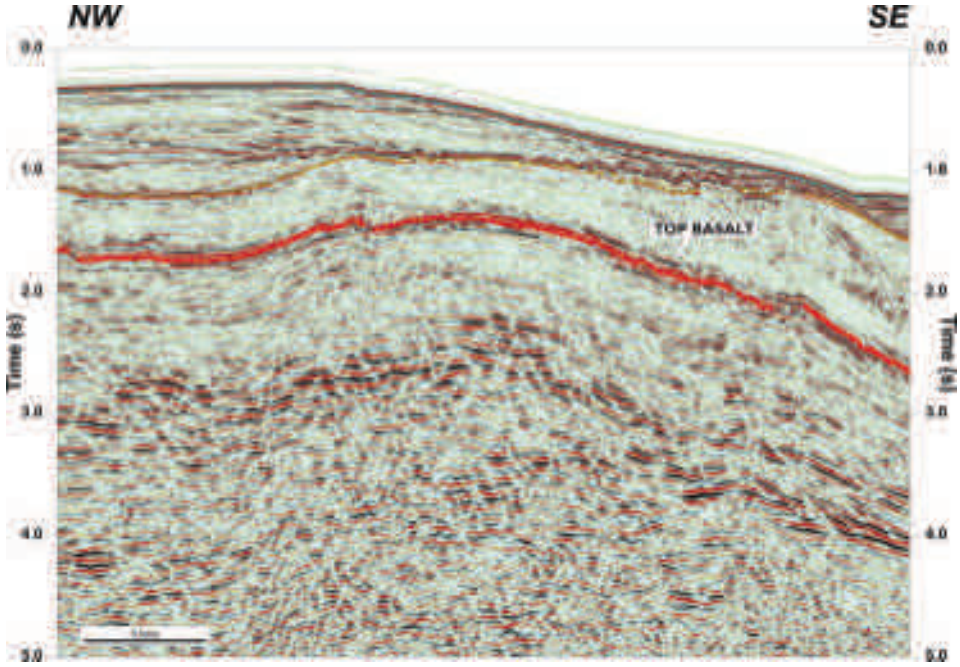

Figure 11. OF94 2D survey pre-stack time migrated reprocessing

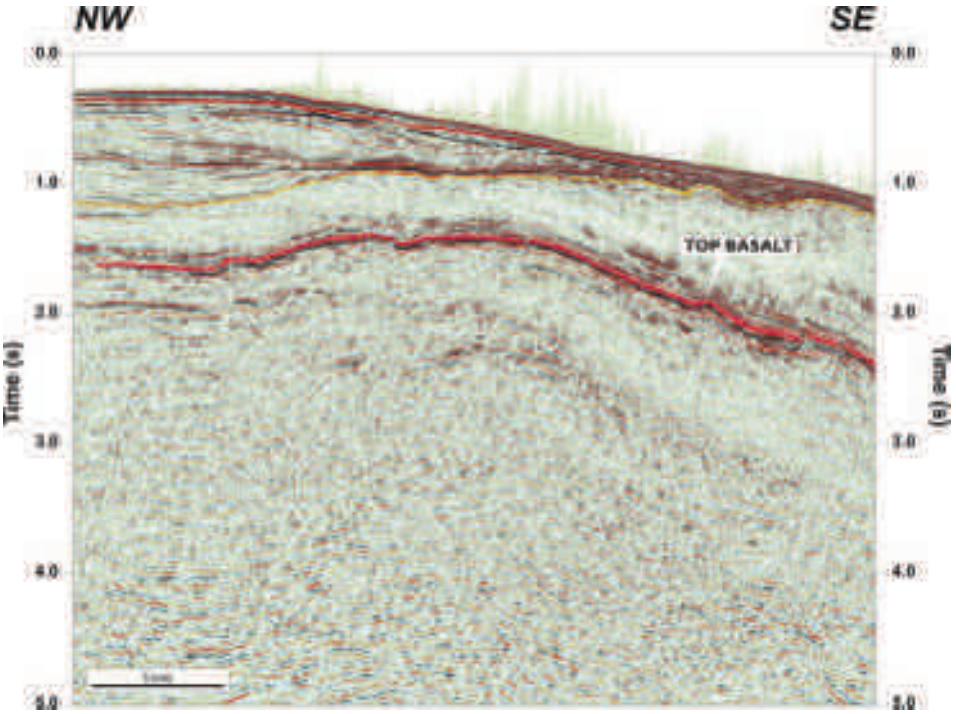

Figure 12. AMG96 2D survey post-stack time migration original processing

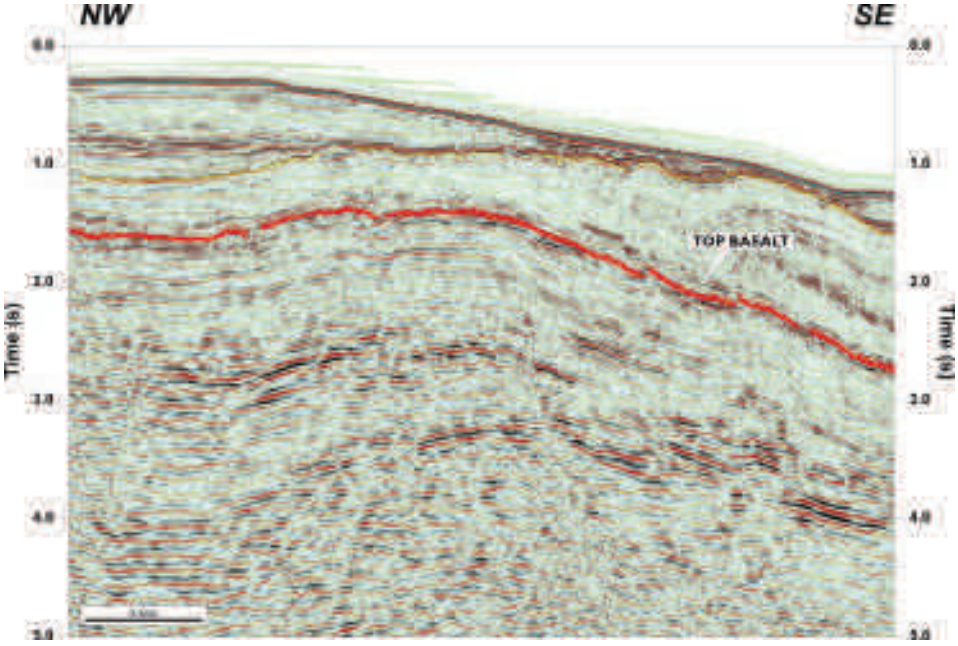

Figure 13. AMG96 2D survey pre-stack time migrated reprocessing

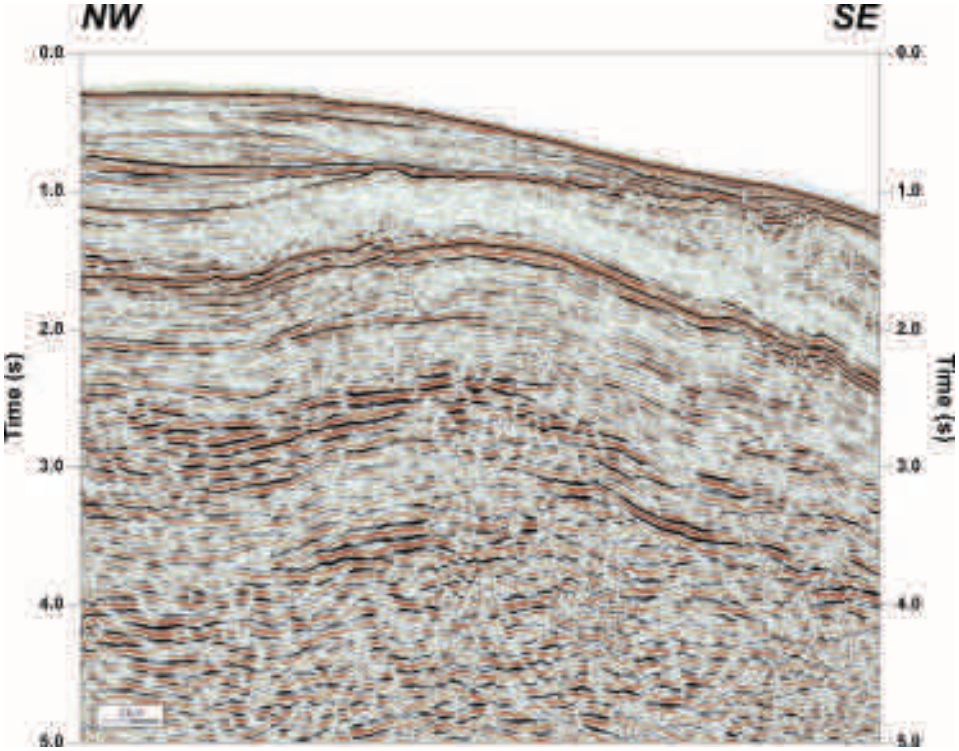

Figure 14. ST0107 2D survey pre-stack time migration reprocessing

The upper source (12.5 m tow depth) and the upper cable (20 m tow depth) were singled out for processing according to the techniques we discuss here. The location of one of the over-under lines was chosen to cross the Faroes Licence 006 area to tie in the Brugdan well and allow for a comparison of the data quality. The final over-under combined line, processed relative amplitude, is shown in Figure 15. Our reprocessing based on only the upper source and upper cable is shown in Figure 16. A further example for comparison is a 2D processing of a line extracted from our 2003 3D dataset (Figure 17). This along with all other reprocessed 2D examples from the area shown in this paper are superior to the combined over/under example in Figure15, Our 3D beem steering prestack depth data (Figure 7) is by far the best image.

We still have a long way to go before over-under seismic can help us with imaging below the basalt.

Conclusions

Seismic data acquired and processed prior to 2000 show very few coherent seismic events below the top basalt reflection. Statoil has acquired proprietary 2D and 3D seismic surveys in the basalt-covered Faroes offshore area from 2001 onwards. We have worked closely with partners and contractors to resolve the sub-basalt imaging problem analysing most aspects of seismic acquisition and processing. A good uplift in data quality was first achieved with the 2001 2D. The 2003 3D acquisition parameters were selected based on the 2001 2D results. Cables were shortened from 12 km used for this 2D to 8 km for the 3D as the outer part of the 12km cable used had played no part in the processing at the target depth. The cables and source were again deep-towed to attenuate high frequency noise and ensure predominantly low frequencies in the data. This improves processing by reducing the high frequency noise in the key zone below the basalt. The final 3D processing re-

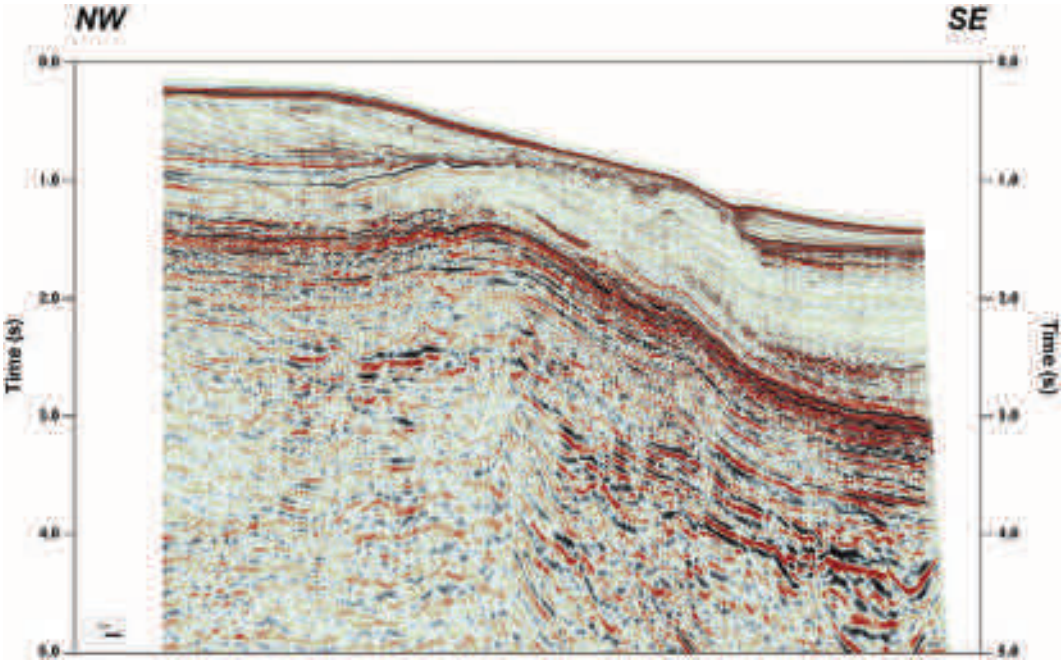

Figure 15. Final results from the over-under line processed relative amplitude. This line is located over the 3D survey area and is in a similar location to all the other lines shown here

sults are very impressive (Figures 7).

For pre- 2000 seismic data, poor imaging below the basalt was attributed to the acquisition parameters chosen for these surveys. The current work shows that seismic data acquired with a wide range of acquisition parameters (Table 1) and re-processed using the techniques described in this paper produce a significantly better sub-basalt image.

Data quality is primarily dependent on processing, although large source arrays and deep-towed cable and source are definitely beneficial as a method of bandlimiting the data in acquisition. Even the earliest speculative data from 1994, acquired with relatively long cables and large source arrays, contained primary data below the top basalt but not imaged correctly, partly due to the dominance of high frequency noise in the data, less-efficient processing routines being available at the time and the lack of a geological input model to the velocity analysis. If a thick basalt is expected it is important to stack with basalt velocities and not clastic rock velocities. Close cooperation between the processing expert and the geoscientists is essential.

The high frequency component of the seismic energy is scattered producing noise when passing through basalt. Therefore attenuate these high frequencies, in acquisition by deep towing cable and source and early in the processing sequence using a high-cut filter.

The 'over-under' seismic acquisition technique theoretically can help increase the bandwidth of the seismic data. Extending the bandwidth at the high frequency end of the frequency spectrum goes against all the principles when it comes to imaging below the basalt and is considered detrimental here. The apparent extra energy at the low end of the frequency spectrum appears to have not given any uplift in data quality when compared to conventional processing of the same dataset or earlier speculative and proprietary data. No argument can be made here in favour of spending the significant extra time and cost involved in such a survey.

The Brugdan well drilled in Licence 006 in the summer of 2006 gives us new information on the

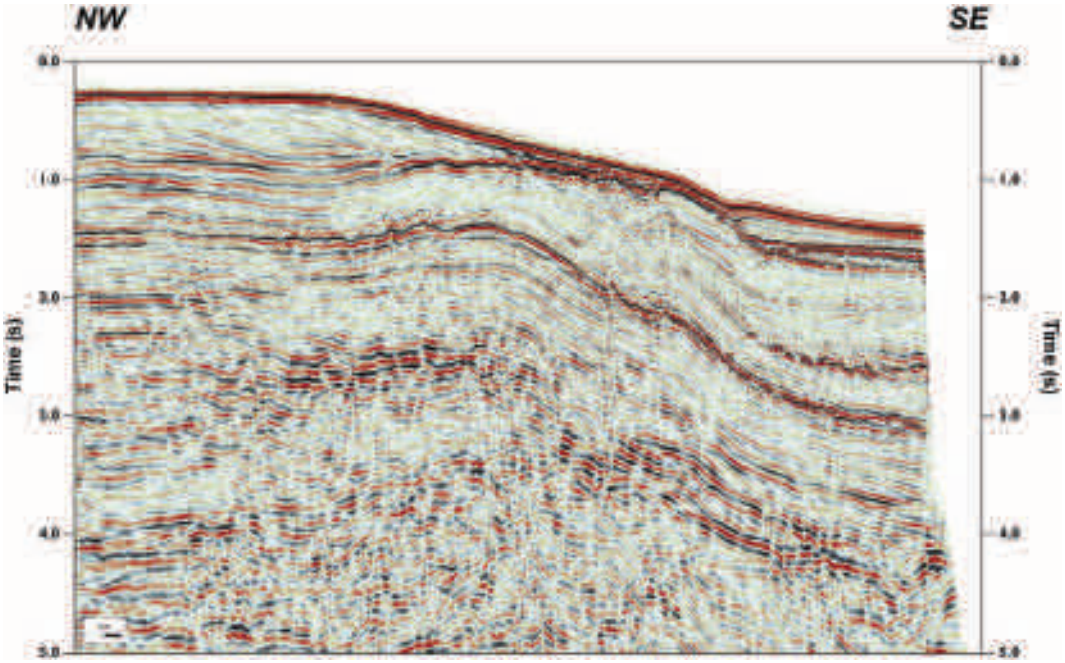

Figure 16. The over-under line shown in figure 15, but processed using only the upper source and upper cable and the processing flow described in this paper

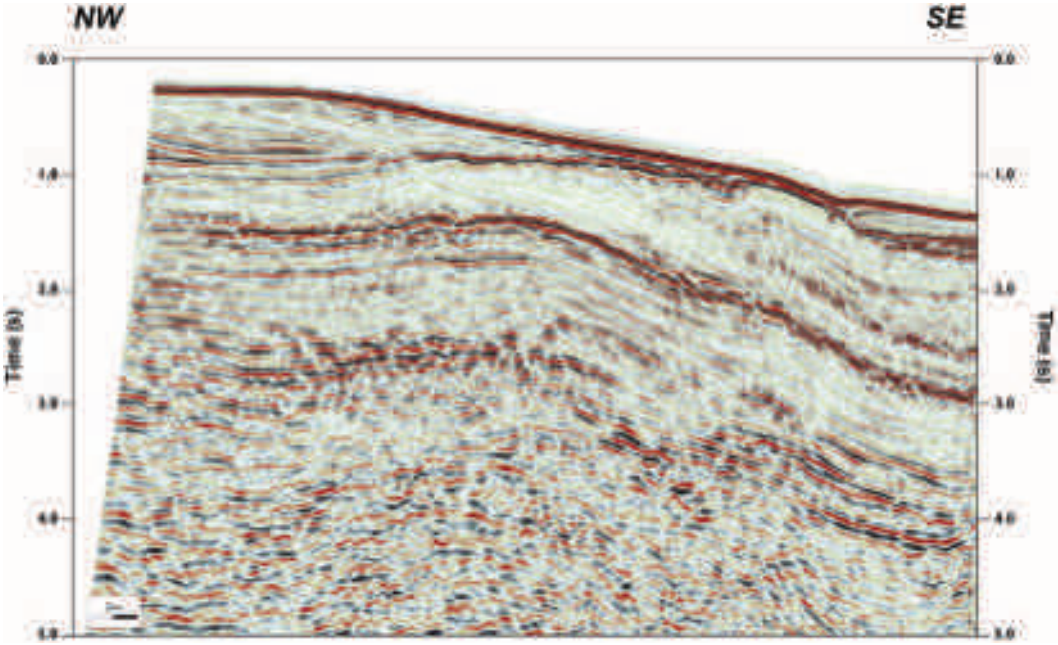

Figure 17. A 2D line processed from our 3D survey in the same location as the over-under line; using a single cable and the processing flow described in this paper.

geology and seismic velocities and will allow a further fine-tuning of seismic processing and may lead to even better imaging below the basalt.

Acknowledgements

The authors would like to thank the contributions of seismic modellers and processors in Statoil, in particular Even O Brenne, Anders Sollid, Anne Svardal, Espen Erlandsen and Paul Meldahl. Thanks also to Tony Doré, Dave Ellis and Steve Kleppa, Statoil, for their geological input and the reviewers of the paper for their constructive comments.

The contributions of the contractors - AGS, CGG, GDC, SIP, VeritasDGC, WesternGeco, is also much appreciated for either allowing us to show their data or for actual processing of the data.

The technical input of Statoil's partners in Faroes Licence 006 - Anadarko, DONG and Shell, is also much appreciated.

Finally the authors wish to thank Statoil and Partners for allowing us to publish this work.

References

Avedik, F., Hirn, A., Renard, V., Nicolich, R., Olivet, J.L., and Sachpazi, M. 1996. 'Single-bubble' marine source offers new perspectives for lithospheric exploration. *Tectonophysics* 267: 57-71.

Canales, L.L. 1984. Random noise reduction. 54th Annual International Mtg., SEG, Expanded Abstracts, Session S10.1.

Dancer, P.N. and Pillar, N.W. 2001. Exploring in the Slyne Basin: a geophysical challenge. *In*: Shannon, P.M., Haughton, P.D.W. and Corcoran, D.V. (eds) *The Petroleum Exploration of Ireland's Offshore Basins*. Geological Society, London, Special Publications 188: 209-222.

Hobbs, R. 2002. Sub-basalt imaging using low frequencies. Sub-basalt imaging 9-11th April, 2002 Cambridge, UK. *Journal of Conference Abstracts Volume* 7(2): 152-153

Leathard, M., McHugo, S. and Hoare, R. 2007. Imaging below Faroese basalts using over/under acquisition. *In*: Varming, T. and Ziska, H. (eds) *Faroe Islands Exploration Conference: Proceedings of the 2nd Conference*. Annales Societatis Scientiarum Færoensis, Tórshavn, this volume.

Pujol, J. and Smithson, S. 1991. Seismic wave attenuation in volcanic rocks from VSP experiments. *Geophysics* 56: 1441-1455

Roberts, A.W., White, R.S., Lunnon, Z.C., Christie, P.A.F., Spitzer, R. and iSIMM Team 2005. Imaging magmatic rocks on the Faroes Margin. *In*: Dore, A.G. and Vinning, B.A. (eds) *Petroleum Geology: North-West Europe and Global Perspectives - Proceedings of the 6th Petroleum Geology Conference*. Geological Society, London: 755-766.

White, R.S., Christie, P.A.F., Kusznir, N.J., Roberts, A., Davies, A., Hurst, N., Lunnon, Z., Parkin, C.J., Roberts, A.W., Smith, L.K., Spitzer, R., Surendra, A. and Tymms, V. 2002. iSIMM pushes frontiers of marine seismic acquisition. *First Break* 20: 782-786.

Does size matter?

RICHARD W. HOBBS[1*], ISAAC FLECHA[2], RAMON CARBONELL[2] AND SCOTT PEARSE[1]

[1] Department of Earth Sciences, University of Durham, South Road, Durham DH1 3LE, UK

* E-mail: r.w.hobbs@durham.ac.uk.

[2] Dept. Geofísica i Tectònica, Institut de Ciències de la Terra "Jaume Almera" (CSIC), Lluís Solé i Sabarís s/n, 08028 Barcelona, ES.

ABSTRACT

Successful seismic reflection imaging of basin structure beneath a layer of extrusive basalts is a major challenge for the exploration and exploitation of potential hydrocarbon reserves on the north western margin of Europe. Over the past decade numerous attempts have been made using a variety of source and receiver configurations. By detailed examination of this legacy data we have identified key parameters in acquisition and processing that may increase the likelihood of success. The source should be rich in low frequency and of sufficient energy to ensure primary reflectivity is above the ambient noise. Though the use of high energy sources may not be necessary. The receiver cable should be towed at a depth to optimise the reception of low frequency energy and of sufficient length to capture the backscattered signal from the sub-basalt interfaces. For pre-critical energy, apertures >6 km are normally sufficient. This gives good discrimination for multiples generated above the basalt layer and can be operated from a single vessel. Longer offset data with high spatial sampling (synthetic aperture) have limited benefit and are primarily of use for determination of the velocity model. The key processing step is to avoid conventional deconvolution based on statistics as this normally degrades low frequency content of the seismogram. We propose an approach where we estimate the low-frequency source function from the data and use that as the deconvolution operator to suppress the source coda. The use of surface related multiple suppression algorithms were effective for the supra-basalt multiples coupled with a slowness based filter to remove coherent late-arriving low velocity events.

Introduction

On examination of the database of seismic data acquired around the Faroe Islands over the past decade one quickly realises that there is a potential problem. Why, for such a limited area are there so many different acquisition geometries and increasing source sizes? Surely, this points to the issue that the processed data are unsatisfactory and not yielding robust interpretations that reduce the exploration risk to an acceptable level. Seismic contractors are struggling to find an acquisition and processing strategy that fulfils their client's expectations. To such an extent that the Faroe's margin has become a test-bed for the development of novel seismic and non-seismic methods that once proven will have world-wide applications for similar challenging areas (Fruehn *et al*., 1998; White *et al*. 2002; Ziolkowski *et al*., 2003; Crawford, 2004; Jegen-Kulcsar *et al*., 2005; Heincke *et al*., 2006). The Faroe-Shetland trough is seen as a key frontier region. Significant proven hydrocarbon reserves are being exploited on the eastern UK margin and it is likely that similar reserves maybe present on the western margin. The issue is the seismic image acquired using conventional strategies is hardly interpretable at the expected target depths. The reason is well known, the presence of a significant thickness of extrusive basalt.

Faroe Islands Exploration Conference: Proceedings of the 2nd Conference.
Annales Societatis Scientiarum Færoensis, Supplementum 50, 2009: 333-345

Energy propagation through basalt is a subject of ongoing active research (Maresh *et al*., 2006). The interfaces between the overlaying sediments and the basalts are highly irregular and may present a high impedance contrast. If the basalts are thin this can be addressed (Martini and Bean, 2002). However, when combined with a significant thickness of extrusive basalts which in themselves are highly heterogeneous, the seismic energy is scattered and attenuated so only a small fraction of the source energy eventually propagates into the underlying sediments. Backscattered energy from these sediments has to pass back through the basalts again to reach the surface and maybe so weak that it is swamped by the scattered noise from the basalt reverberating in the supra-basalt layers.

As part of the SINDRI research initiative we examined this diverse database to see what lessons could be learnt as to what works and to make recommendations for the future exploration of the region. In this paper we examine normal incidence imaging, in other papers (Flecha *et al*., 2008a; Flecha *et al*., 2008b) we appraise the use of long offset data for velocity models and their uncertainty.

Data

The example data presented in this paper come from the western margin of the Faroe-Shetland trough (Table 1). This represents only part of the data analysed but they demonstrate the key findings of the research project. Where possible comparisons are made on profiles that are close to each other to minimise the effects of changes in geology. The key survey characteristics are listed in Table 1 and show data with sources using Marine Vibroseis® and large conventional air-gun arrays, receiver cable lengths also range from 6 km to 11.4 km. We also processed some synthetic aperture two-ship data (Fruehn *et al*., 1998), though only data from the first pass for near-normal incidence imaging (Flecha *et al*., 2007b).

Processing

Examination of the stacked data produced by contractors for each survey at the time of acquisition revealed that the adopted processing strategy had a fundamental effect on the perceived final stack. So the only way to make quantifiable comparisons of the effect of acquisition strategy was to remove this processing footprint. Hence for each survey used, the data had to be reprocessed from the original field tapes with, as near as possible, a common processing flow. This was not simple, as some of the data had preconditioning applied, e.g. the Marine Vibroseis was already correlated to a zero-phase wavelet, and the geometry could be unusual, as in the case of the ship-ship synthetic aperture. Visual inspection of the previous stacked data identified aggressive deconvolution filters as a key culprit in the degradation of the final stack. Previous work (Hobbs and Martini, 2002; Druzhinin *et al*., 2004) had developed a processing strategy that optimised the low-frequency content of the data and avoided statistically based filters. So this was developed for these data. The key steps are listed in Table 2. We will examine the critical steps: (1) source deconvolution filter; (6 & 7) surface related multiple suppression; (8) tau-p filter; (11) mute; and (13) de-ghost filter.

Source deconvolution

The various configurations gave very varied source functions; also as the objective of the project was to identify optimum acquisition strategy we needed to isolate the source wavelet from the

Survey Name	***Source***	***Receiver***
OF94	5280 cu in airgun	6000 m
FAST	9324 cu in airgun	6000 m
WOSMV97	4040 cu in airgun Marine Vibrator®	6000 m
GFA-99	4986 cu in airgun	11400 m

Table 1. List of surveys with data examples in this paper (source: www.sindri.fo)

a)

b)

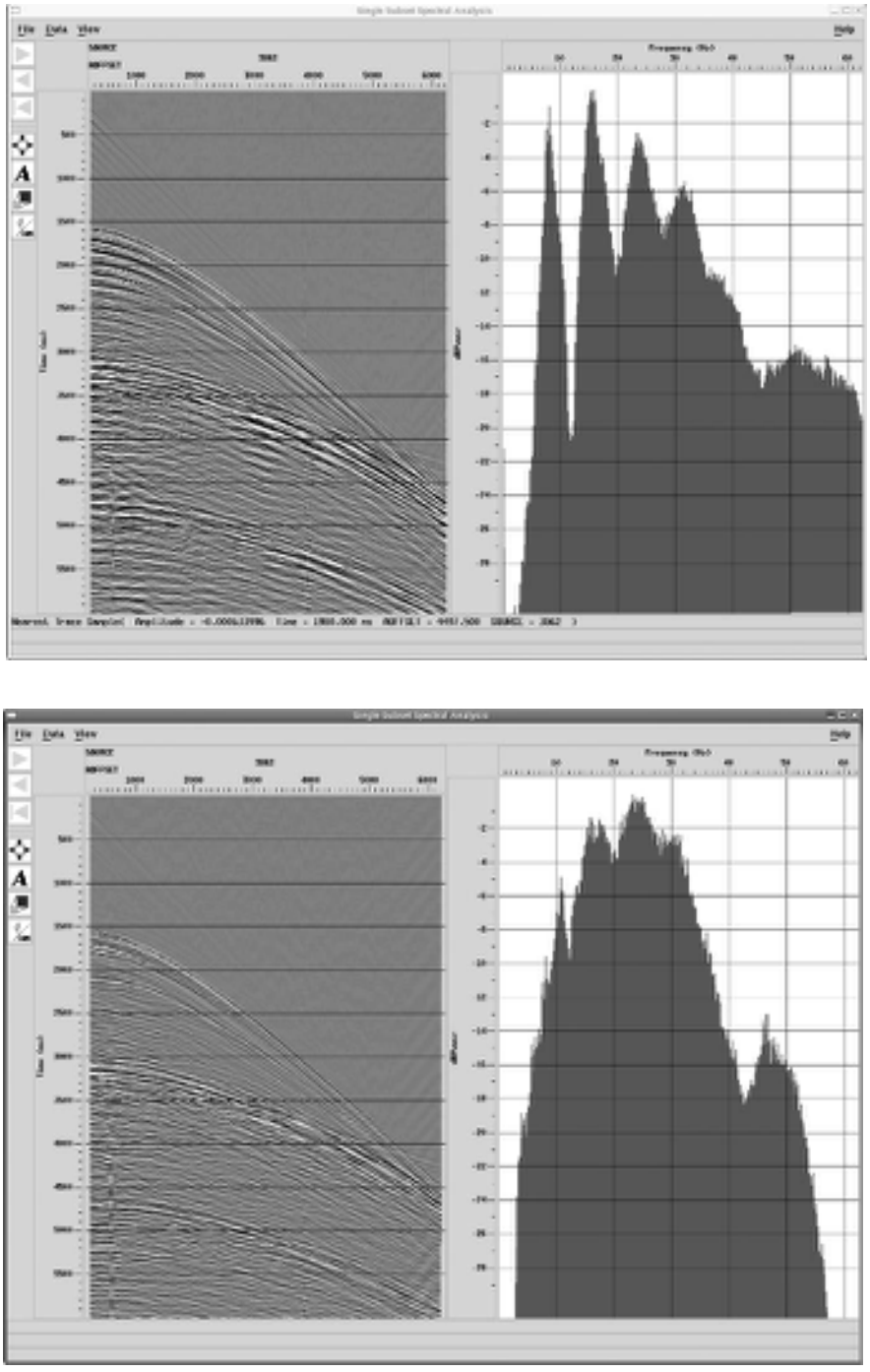

Figure 1. A shot gather taken from the FAST survey **a**) before and **b**) after deconvolution using a filter computed from a source derived from the data after removal of the effects of the source and receiver ghost. The change in the amplitude spectrum shows the suppression of the energy in the low frequency bubble pulse coda. Example of stacked data before and after filtering is shown in figure 5.

	Processing Step	*Parameters*
1	Source matching and deconvolution filter	
2	Assign geometry	
3	Bandpass filter	Ormsby: high-cut 48-64 Hz
4	Resample	8 ms
5	Bin	50 m receiver group/25 m CMP spacing
6	Create Split Spread	extend offsets to -1 km
7	Surface Related Multiple Suppression (SRMS)	multiple model based on sea-bed inter-sediment horizon and top-basalt picked from near-offset stack
8	Tau-p filter applied to both common shot and	Gaussian weighted filter with mean slowness of
	common receiver domains or CMP domain	0.075 ms/m and variance of 0.064 ms/m
9	Velocity analysis	Semblance, function gather and function stacks
10	NMO	
11	Mute	Outer and Inner mute
12	Stack	
13	De-ghost filter	not applied to Marine Vibrator® source
15	Amplitude recovery	$t^{1.8}$
15	Display	includes spatial resampling and long window AGC with minimum and maximum gain clipped at a factor of ¼ and 4 respectively.

Table 2. Processing steps used to minimise variation between stacked sections.

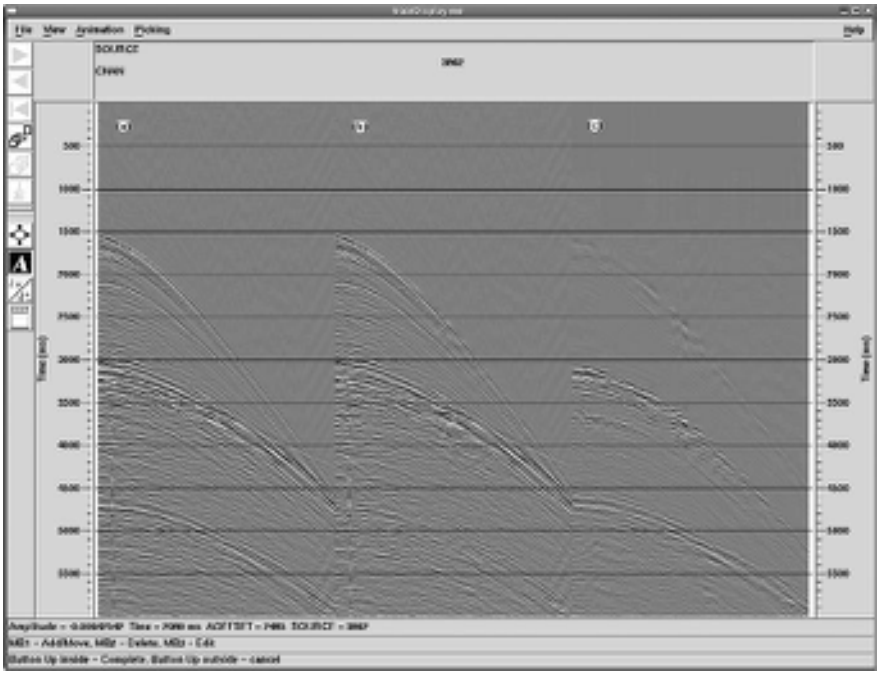

Figure 2. The same shot gather as used in figure 1 with surface related multiple suppression applied. **a**) before multiple suppression, **b**) after multiple suppression and **c**) the difference. Though the process has worked well identifying and removing coherent events, it has left significant low velocity energy with short coherence lengths particularly at longer offsets and the matched filter has mistakenly fitted and removed some energy from the 'top basalt' reflection which is coincident with the first multiple of the sea-bed.

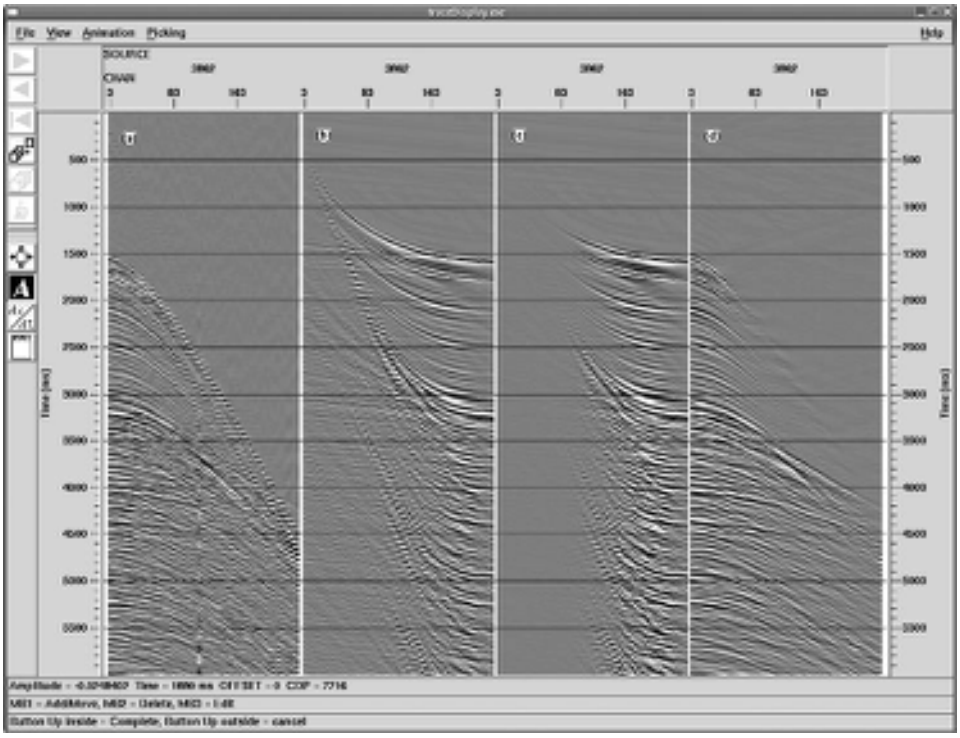

Figure 3. a) Input CMP gather after surface related multiple suppression. **b**) The same gather in the Tau-p domain. **c**) After Gaussian weights in the tau-p domain. **d**) The filtered gather transformed back into the t-x domain. Comparison with panel **a**) shows the low-velocity noise has been successfully attenuated. Example of stacked data before and after filtering is shown in figure 5.

data. To extract the exact source function from the seismic data is not possible (Ziolkowski *et al*., 1982). However, as our primary concern is the low frequency component of the spectrum which mainly constitutes the bubble pulse coda of an air-gun (sleevegun) source we believe that this can be reliably extracted for our special case. Our method is to select a seismic trace from the shot gathers, close to near-offset but avoiding the noisiest near-offset traces themselves. The selected shot gathers, typically more than 500 shots, were taken from where the profile was acquired over deep water (>800 m). By choosing shots in deep water the effects of the sea-surface multiples on the amplitude spectrum is minimised. The source and receiver depths are estimated from the major notches in the average amplitude spectrum, this provided a check on the parameters stated on the observer logs, which maybe imprecise. Inverse filters are applied to back-off the effects of the source and receiver ghost with parameters set by observing the effect on the amplitude spectrum. Typically the required sea-surface reflection coefficient is 0.7 to 0.9, and the period is determined by the notch position. The low reflection coefficients are caused by the averaging of the spectra, spectra from single traces gave larger coefficients but vary shot-to-shot and trace-to-trace (Kragh and Laws, 2006). However, as the resultant filter from this exercise is going to be applied to the whole profile, we opt to take values from the average spectrum. The corrected spectrum is then inverted using the Hilbert transform to impose a minimum phase condition. The resultant wavelet is then used to compute a band-limited inverse filter (Ormsby: low-cut 2-4 Hz; high-cut 44-64 Hz). We feel justified in this approach as the target of the filter was to predict the bubble coda rather than the high-frequency initial

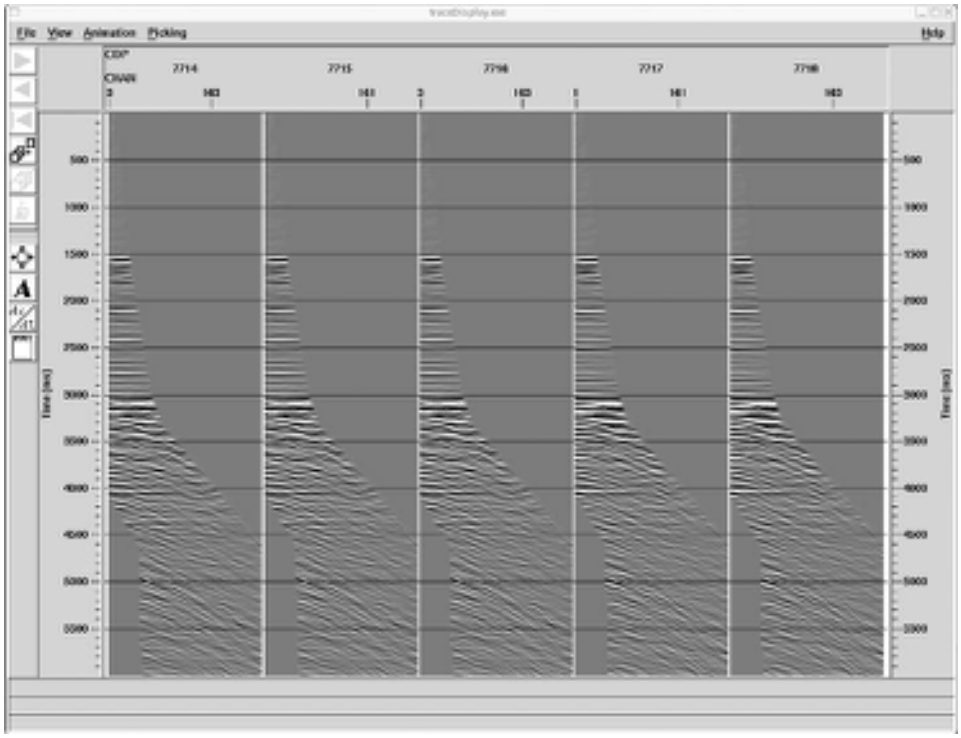

Figure 4. CMP gathers prior to ensemble stacking. Normal moveout applied: with an outer mute to remove distorted, critical angle and post critical angle data; and an inner mute to remove residual multiple energy at near offset where there is little suppression through the stack process.

explosive release of the air, and the minimum phase assumption is a good approximation for a damped oscillatory signal. The effectiveness of the filter is tested for each profile by careful examination of the effects on the sea-bed reflection and the direct wave (Figure 1).

Surface related multiple suppression

Over the shelf margin and into deep water of the trough the most dominant events on the raw stacked data are the sea-bed and top-basalt primary reflections and their sea-surface multiples. Surface related multiple suppression (Verschuur *et al*., 1992.) has proven to be very effective in predicting and removing this class of multiple as is the case for these data. The method we followed involves picking the multiple generating horizons on a stack of near-offset traces, to minimise the effect of uncertainty in the velocity model. Extending the near-offset data through zero-offset by extrapolation using the tau-p transform. Generating the predicted multiple for the picked horizons and optimising the predicted wavelet using a matching filter constrained by least-squares. The predicted and adapted seismogram of the multiples are then subtracted from the real data and the extrapolated near-offset traces removed (Figure 2).

Tau-p filter

The surface related multiple suppression method works well for near-offset data but fails to adequately suppress low velocity noise at long offsets generated in the supra-basalt layers. The arrival time of these high-amplitude events crosses the expected travel-time of the sub-basalt primaries. In the tau-p domain there is a significant velocity difference between the accept and reject regions, so a simple filter can be designed that suppresses this type of noise. Rather than designing a filter on a survey-by-survey basis we opt to apply a common

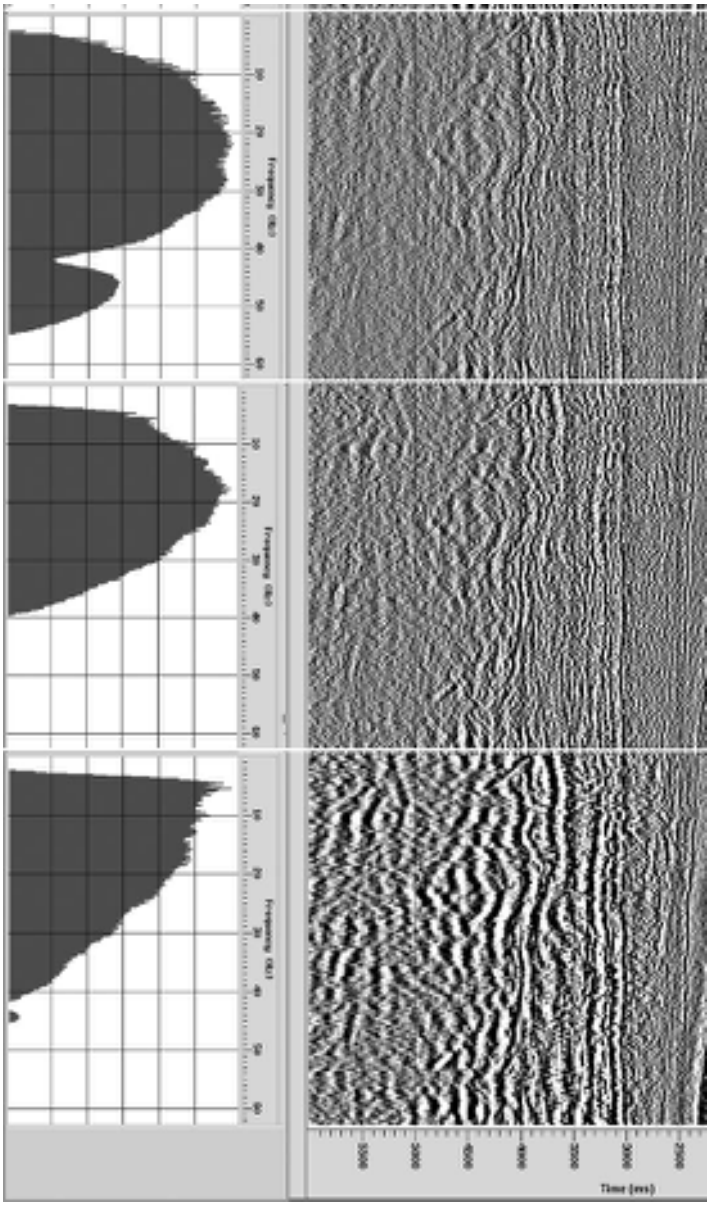

Figure 5. Examples of stacked data, with associated frequency spectra, at key stages through the processing sequence. **a**) stack of unprocessed data: the time section shows the reverberation of the bubble pulse coda of the source function, this can also be seen in the spectrum with a strong dominant peak at 7 Hz and its harmonics. **b**) following deconvolution with a filter derived from the data the reverberation is suppressed and the spectrum has the characteristic shape of the impulse response of the source and receiver ghost functions. Though the first sea-bed multiple is obscured by the 'top basalt' reflection, the second multiple can be seen at around 4.7 s. **c**) the coherent multiple energy is removed by surface related multiple suppression and residual low velocity energy is suppressed by a filter in the tau-p domain. The effect of the tau-p filter can be seen on both the stack and the amplitude spectrum as a marked reduction in high-frequency content, though this might not be generally desirable it is accepted here as the target is the low frequency energy from beneath the basalt. **d**) Final section after application of a post stack de-ghosting filter. This filter recovers the energy suppressed by the ghost notches. The loss of high frequency is partly due to the effect of the preceding tau-p filter but also the effect of the scattering and attenuation Q that has not been compensated by the processing sequence. In particular note the improved image 'beneath basalt' (4.0-5.0 s) with good lateral continuity of primary reflection events.

filter by transforming the data into the tau-p domain and applying a slowness based Gaussian weighted filter that passes energy with a low slowness value (high apparent velocity across the receiver array) and suppresses energy with a high slowness value (low apparent velocity). The filter is applied either as a single pass in the CMP domain or, for data with sparse fold (e.g. synthetic aperture), the filter is applied in both the common shot and common receiver domains (Figure 3).

Mute

Despite best efforts to remove multiples and low velocity energy using the processes above, significant levels of noise still persist in the data (e.g. at near offset and critical energy reflections from the top-basalt). To minimise its effects on the stack both outer and inner trace mutes are used. Wherever possible the same mute functions are used for profiles in the same region (Figure 4).

De-ghost filter

As the sea-surface and tow depths of the source and receiver are continually vary, it is not possible to find a single de-ghosting filter that can be applied for each trace in the pre-stack domain. Each CMP gather takes shot/receiver pairs from a sequence of common shot gathers. When stacked these short term variations, like waves, are averaged so it is now possible to estimate a robust deghosting filters that can be applied to the stacked data. The benefit of the filter is it removes the effects of the source and receiver ghost notches in the amplitude spectrum which increases the gain particularly at low-frequencies where both the receiver and source ghost functions roll off to zero amplitude at D.C.. The parameters used to model the ghost effects are taken from the computed source and receiver depths estimated when computing the inverse source function. This has a dramatic effect on stack section and significantly increases the likelihood of detecting the high impedance contrasts in the sub-basalt section (Figure 5).

Results

Source Comparison

The three profiles compared here are the WOS-

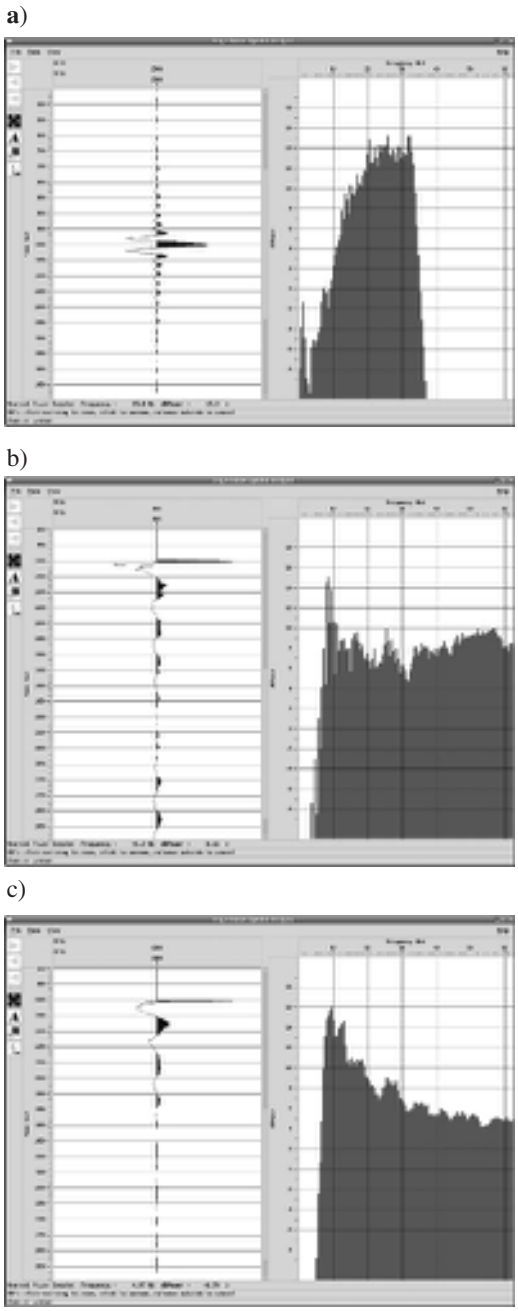

Figure 6. Three source functions used for comparison of the effect of source on the seismic data. **a**) Marine Vibroseis® after correlation. **b**) WOSMV97 airgun source 4040 cu in. **c**) OF94 airgun source 5280 cu in. The dB scales have been approximately corrected so comparisons between plots can be made. For frequencies below 10 Hz the Marine Vibroseis® source is over 10 dB weaker.

a)

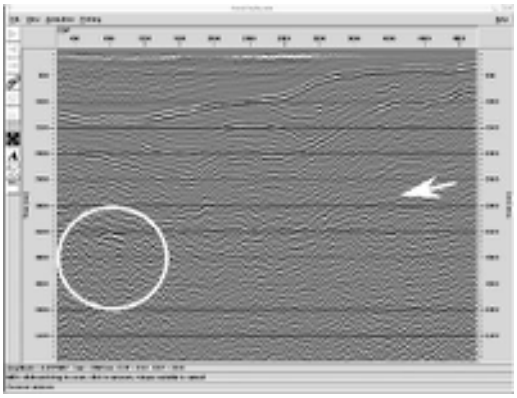

b)

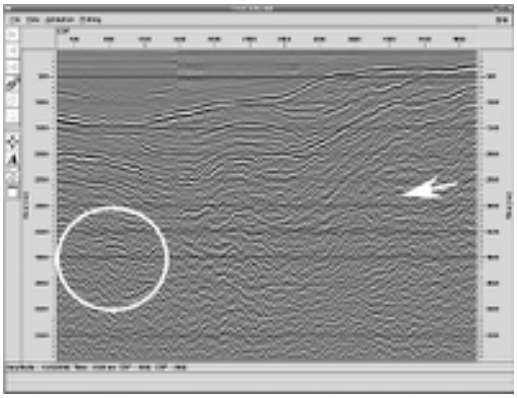

c)

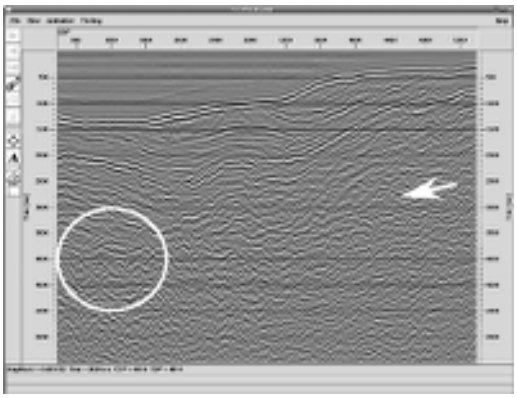

Figure 7. The same profile acquired with 3 different sources. **a**) Marine Vibroseis®, **b**) WOSMV97 airgun array and **c**) OF94 airgun array with source spectra as shown in figure 6. The possible sub-basalt reflection (arrow) is arguably best seen in the **a**) and **b**) but the deeper part of the basin (circle) is best seen in **c**).

MV97 Marine Vibroseis® and Airgun, and OF94-21A. Figure 6 shows the derived source functions for each profile. The Marine Vibroseis® source is a zero-phase wavelet with a high level of side-lobe energy the cause can be seen in the unusual amplitude spectrum which shows the frequency sweep was abruptly cut at 32 Hz. The WOSMV97 airgun source has a pronounced spike at 8 Hz which, as expected, produces a long bubble coda. The OF94 airgun source is well tuned with a short bubble coda. Though absolute amplitude comparisons cannot be made because there was no cross calibration of the two data recording systems. Even though Marine Vibroseis® was recorded on the same system as the MOSMV97 airgun source, there is an unknown scaling factor in the correlation with the input sweep. Using primary to multiple ratios it is possible to compute a scaling coefficient (Warner, 1990) which has been used to scale the power amplitude (dB) so that the spectral content of the three sources can be compared. The Marine Vibroseis® source has a similar energy to the airgun sources at frequencies greater than 16 Hz, it is deficient in low frequency content and is over 10 dB down at 10 Hz.

Figure 7 shows the comparison of the three stacked sections. The data were acquired along the same profile with the same receiver aperture, 6 km, so the processing flow, velocity model and mutes was identical for each section. For the displays here a high cut filter set at 16-32 Hz roll off is applied to remove the effect of the sharp cut in the Marine Vibroseis® source and a 5 trace-mix is used prior to sub-sampling in the spatial domain and a long window AGC is applied for display purposes. What is surprising is the Marine Vibroseis® section is as good as the airgun sections except in the deeper section below 3.5 s probably due to the signal falling below the ambient noise level, an indication of a weaker source at the low frequencies. A possible sub-basalt interface is indicated on all three sections and is arguably better on the Marine Vibroseis® section than the OF94 airgun section.

Receiver aperture

To compare the effect of receiver aperture the profile GFA99-105 is selected as this survey had the longest cable operated from a single ship. The

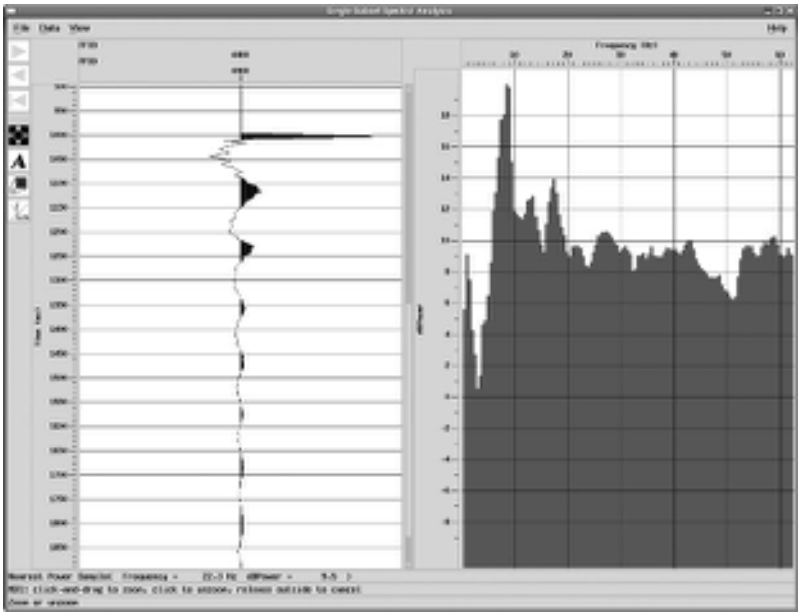

Figure 8. Source function derived for the GFA99-105 profile. Again the dB scale has been calibrated to the same scale as used in figure 6.

source function is similar to the OF94 and WOS-MV97 surveys discussed above, the 4986 cu in array has been detuned slightly to augment the low-frequency content which produces a significant bubble pulse coda (Figure 8).

Three stacks were performed with the maximum aperture of 3000 m, 6000 m and 11400 m (gathers shown in Figure 9), with the sections after mixing, and AGC (as above) for display are shown in figure 10.

The top basalt and supra-basalt sediments are the same irrespective of the maximum aperture as the maximum offset used in the stack is dictated by the outer mute. There is a marked difference in the sub-basalt section between the 3000 m and 6000 m aperture with the longer cable giving a higher fold of stack in this region so weak events are more visible and there is improved discrimination against residual multiple energy. The benefit of the longest cable is questionable. It increases the signal to noise ratio slightly in the region between 4 and 5 s and it does bring out a possible event at 6.5s beneath the shelf (CDP 3000-3500) however robust interpretation is no easier.

Discussion and recommendations

Unfortunately there is no magic bullet through acquisition strategy for surface near-normal seismic reflection data that will address the sub-basalt imaging issue for the western margin of the Faroe-Shetland trough. However, the examination of legacy data shows what gives the best chance to obtain an optimum image in this challenging area. In short we recommend a single ship operation with a source rich in low frequencies and a receiver aperture > 6 km towed at a reasonable depth >15 m to boost the overall low-frequency response and to minimise ambient noise. Though these recommendations in themselves don't appear to offer anything new they do open up possible new areas for testing. The low-frequency spectral content of the source, though dominated by the ghost, can be manipulated by altering chamber size or introducing clusters. This is not true for a single receiver cable where the roll-off towards D.C in the amplitude spectrum is purely a ghost issue. Singh *et al.* (1996) and more recently Moldoveanu *et al.* (2006) have showed how over/under operation of 2 cables can significantly enhance the low fre-

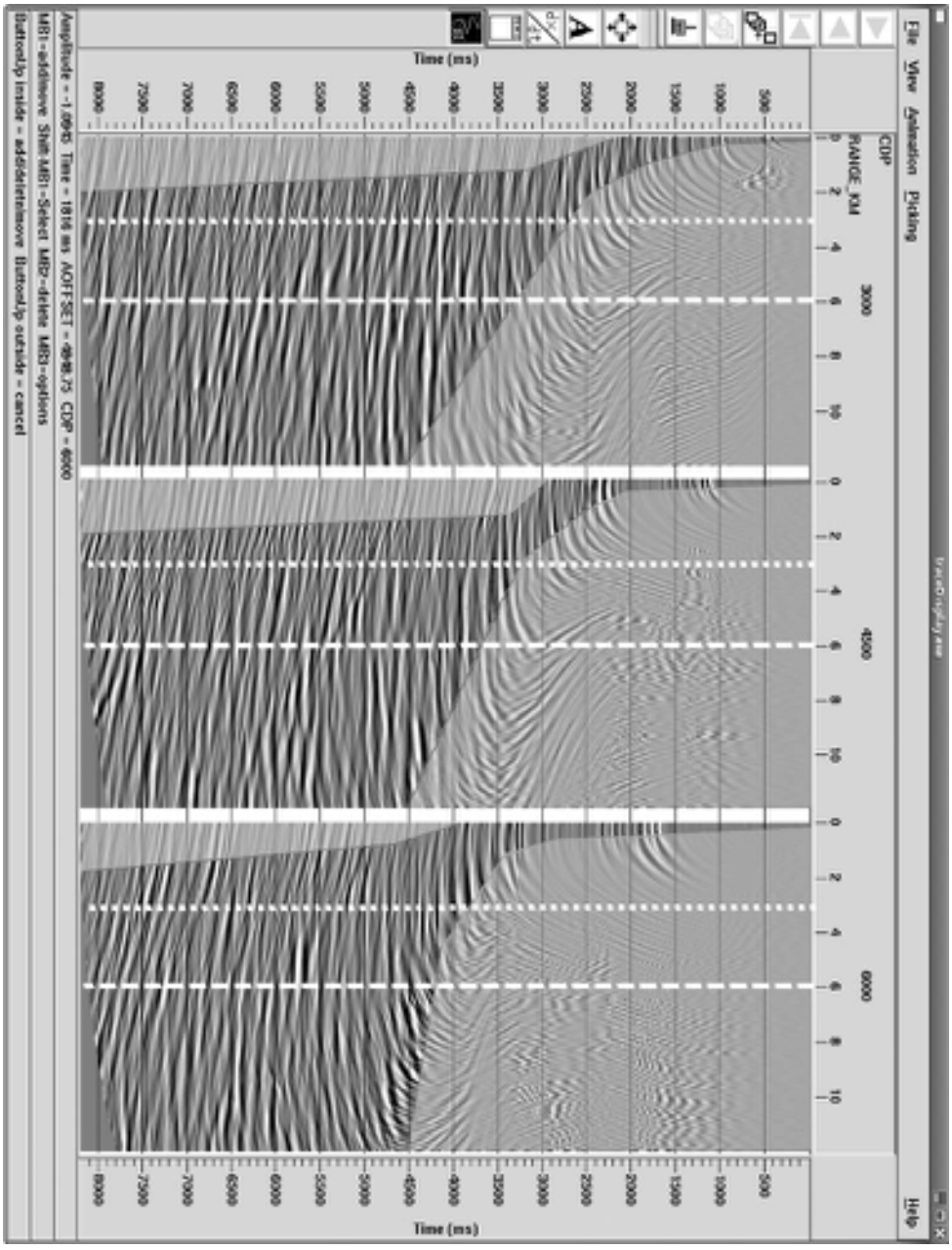

Figure 9. Three CMP gathers from the GFA99-105 profile with NMO applied and outer and inner mutes marked (shaded). The vertical dotted and dashed lines are located at 3 and 6 km offset respectively. These show the stacking aperture used in figures 10**a** (3 km) and 10**b** (6 km); figure 10**c** uses the full offset range of nearly 12 km.

quency response without the need for sophisticated processing. The source function could also be further explored. The major finding that a Marine Vibroseis® source that is weak in low frequencies can match and possibly out-perform a 5000 cu in airgun array raises some interesting questions. The assumption that we require a powerful source to overcome the high impedance contrast at the top basalt surface may not be true and should be restated as we require a source that is powerful enough so that the target primary reflections are above the ambient noise. Increasing source energy once we reach that threshold does not improve matters as we are then shot generated noise limited, i.e. any increase in source energy to increase the amplitude of the reflections is nullified by a corresponding increase in the scattered noise. What is important is maintaining a broad source spectrum that extends the low frequency content. Towing the gun array deep may not help, yes it does increase the energy at low frequencies by moving the constructive interference peak towards lower frequencies but the increased hydrostatic pressure shortens the bubble pulse period hence moves this peak toward higher frequencies, this can be offset by increasing chamber sizes (Ziolkowski *et al*., 2003) or using gun clusters but if the final low-frequency spectrum is the same as a smaller source towed more shallowly then there is no advantage. In fact we are arguing that there is a case to use the large volume arrays currently being using over the margin but towed even shallower. The total energy will be reduced, but that does not appear to be a problem, and the bubble pulse period will be extended which may enhance the overall low-frequency content. However to maximise any potential advantage, improved source estimation with bubble coda estimated to more than 1 s and a robust measure of the low-frequency roll-off caused by the free-surface ghosts will be required.

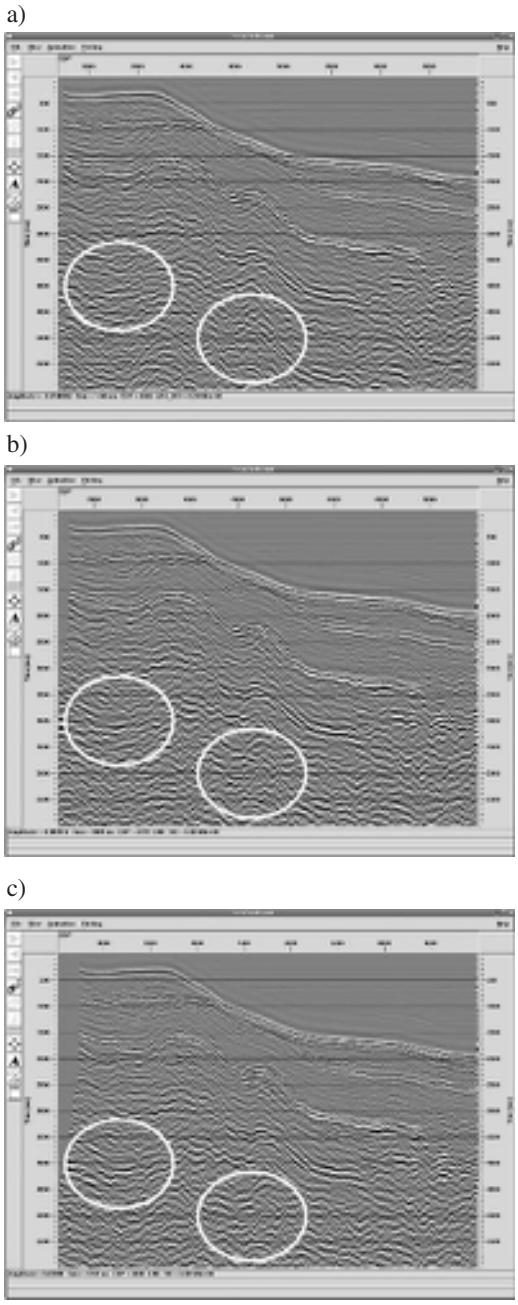

Figure 10. The same profile stacked using different maximum offsets. **a**) 3 km; **b**) 6 km and **c**) 11.4 km. The ellipses highlight areas where there is a marked improvement in the sub-basalt section between **a**) and **b**) with improved suppression of residual multiple energy. There is little improvement between **b**) and **c**) showing that a minimum offset of 6 km is required for effective residual multiple suppression even with surface related multiple suppression, filtering in the tau-p domain and inner trace muting.

Acknowledgements

The authors wish to thank the SINDRI consortium for funding this project. RWH is a NERC Advanced Research Fellow. Processing presented here used the Landmark Promax software.

References

Crawford, W.C. 2004. The sensitivity of seafloor compliance measurements to sub-basalt sediments. *Geophysical Journal International* 157 (3): 1130-1145. doi:10.1111/j.1365-246X.2004.02264.x

Druzhinin, A., Hobbs, R.W. and Li X-Y. 2004. THE IMPACT OF DATA PRE-PROCESSING ON SUB-BASALT SEISMIC IMAGING. Presented at the 66th Annual International Conference and Exhibition, EAGE.

Flecha, I., Carbonell, R. and Hobbs, RW. 2008a. Limitations of wide-angle reflection/refractionmethods in subbasalt imaging: quantifying and investigating null space in refraction data. *Geophysical Prospecting* (submitted)

Flecha, I., Carbonell, R., Hobbs, R.W. and Zeyen, H. 2008b. Some improvements in subbasalt imaging using pre-stack depth migration. *Tectonophysics* (submitted).

Fruehn, J., White, R.S., Richardson, K. R., Fliedner, M., Cullen, E., Latkiewicz, C., Kirk, W. and Smallwood, J.R. 1998. FLARE — A two-ship experiment designed for sub-basalt imaging *SEG Technical Program Expanded Abstracts*: 94-97.

Heincke, B., Jegen, J. and Hobbs, R. 2006. Joint inversion of MT, gravity and seismic data applied to subbasalt imaging. *SEG Technical Program Expanded Abstracts*: 784-789.

Hobbs, R.W. and Martini, F. 2002. Sub-basalt imaging from a wave propagation point of view. AAPG HEDBERG CONFERENCE "Hydrocarbon Habitat of Volcanic Rifted Passive Margins", September 8-11, 2002, Stavanger, Norway

Jegen-Kulcsar, M. and Hobbs, R.W. 2005. Outline of a joint inversion of Gravity, MT and Seismic Data. *In*: Ziska, H., Varming, T. and Bloch, D. (eds.) *Faroe Islands Exploration Conference: Proceedings of the 1st Conference, Annales Societatis Scientiarum Færoensis*, Supplementum 43, Tórshavn: 163-167.

Kragh, E. and Laws, R. 2006. Rough seas and statistical deconvolution. *Geophysical Prospecting* 54(4): 475-485.

Maresh, J., White, R.S., Hobbs, RW. and John R. Smallwood, J.R. 2006. Seismic attenuation of Atlantic margin basalts: Observations and modeling. *Geophysics* 71(6): B211-B221

Martini, F. and Bean, C.J., 2002, Interface scattering versus body scattering in subbasalt imaging and application of prestack wave equation datuming. *Geophysics* 67: 1593-1601.

Moldoveanu, N., Combee, L., Egan, M., Abriel, W. and Hampson, G. 2006. Over/under towed-streamer acquisition: A method to extend the seismic bandwidth to both, higher and lower frequencies. *SEG Expanded Abstracts* 25: 10.

Singh, S.C., Hobbs, R.W. and Snyder, D.B. 1996. Broadband receiver response from dual-streamer data and applications in deep reflection seismology. *Geophysics* 61(1): 232-243.

Verschuur, D.J., Berkhout, A.J. and Wapenaar, C.P.A. 1992. Adaptive surface-related multiple elimination. *Geophysics* 57(9): 1166-1177.

Warner, M. 1990. Absolute reflection coefficients from deep seismic reflections. *Tectonophysics* 173: 15-23.

White, R.S., Christie, P.A.F., Kusznir, N.J., Roberts, A., Hurst, N., Lunnon, Z., Parkin, C.J., Roberts, A.W., Smith, L.K., Spitzer, R., Surendra, A. and Tymms, V. 2002. ISIMM pushes frontiers of marine seismic acquisition. *First Break* 20: 782-786.

Ziolkowski, A., Hanssen, P., Gatliff, R., Jakubowicz, H., Dobson, A., Hampson, G., Xiang-Yang Li, and Enru Liu 2003. Use of low frequencies for sub-basalt imaging. *Geophysical Prospecting* 51 (3), 169-182. doi:10.1046/j.1365-2478.2003.00363.x

Ziolkowski, A., Parkes, G., Hatton, L. and Haugland, T. 1982. The signature of an air-gun array - Computation from near-field measurements including interactions. *Geophysics* 47(10): 1413-1421.

Results from the drilling of the 1st license round wells in the Faroese part of the Judd Basin

THOMAS VARMING

Faroese Earth and Energy Directorate, Brekkutún 1, P.O. Box 3059, FO-110 Tórshavn, Faroe Islands; Email: thomas.varming@jf.fo; Tel: 298 357009 Fax: +298 357001

ABSTRACT

Prior to initial exploration drilling in the Faroese part of the Judd Basin, the combined structural/stratigraphic play type analogue of the producing oil fields, Foinaven/Schiehallion in the UK part of the Judd Basin, was the focal point of hydrocarbon exploration and the four Faroese wells, 6005/15-1 (2001), 6004/12-1z (2001), 6004/16-1z (2001) and 6004/17-1 (2003) were all drilled on this concept.

Seismic data to the west of the Judd High and in to the Faroese area has shown a thickening of the Cenozoic section, but the high net to gross sand ratio of 0.6-0.7 encountered in the Faroese wells in the T28-T36 section (Vaila and Lamba sections) was not expected. The high sand content in the basin has changed the attention from establishing reservoir intervals to locating competent sealing lithologies.

Of the three wells discussed here, only Marjun penetrated Early Paleocene (T10-T22) sands; displaying only marginal reservoir properties for these sands at the well location. Interpretation and mapping of seismic data and well data have identified several igneous intrusive complexes. These comprise basic igneous rocks, intruding into Paleocene sediments. These are most prevalent around to the SE extent of the extrusive basalts. These intrusives have resulted in hydrothermal flux through reservoir sands, causing diagenesis, which blocks the pore throats and decrease permeability.

Introduction.

The Faroese continental shelf is located on the North Atlantic Margin of Europe and forms one of the principal components of the North Atlantic Igneous Province (insert in figure 1), which covers a total of approximately 120.000 km^2 (Saunders *et al*., 1997).

The results discussed in this manuscript rely on released well data analysis and seismic data acquired by the licensee oil companies and acquisition companies. The author of this manuscript is solely responsible for the conclusions put forward in this manuscript and does not necessarily reflect the conclusions of the relevant oil companies.

The first seven hydrocarbon exploration licenses in the Faroese area were awarded in 2000, primarily within the NW part of the Judd Basin, and the first drilling activity commenced in 2001. Four wells have been drilled in the Faroese part of the Judd Basin, targeting Paleocene prospects, in an area characterised by either insignificant or absence of Palaeogene basaltic cover and with water depths of about 1000 m. The rational behind focussing the first exploration activity in this area was the closeness to the successful Paleocene deep-water play types in UK waters, which in the early 90's led to the discovery of the producing fields of Schiehallion and Foinaven (figure 1). In relation to the success of the Paleocene deep-water plays in the neighbouring UK waters, the area experienced an intensive data acquisition activity. In the period between 1992 and 2000, both 2D (almost 50,000 line km) and 3D (8,000 km^2) seismic data were acquired (small figure insert in figure 1), mainly outside the basalt covered area and were the seismic imaging quality is better than within the basalt covered areas to the west.

The first well, 6005/15-1, was drilled by Statoil

Faroe Islands Exploration Conference: Proceedings of the 2nd Conference.
Annales Societatis Scientiarum Færoensis, Supplementum 50, 2009: 346-363

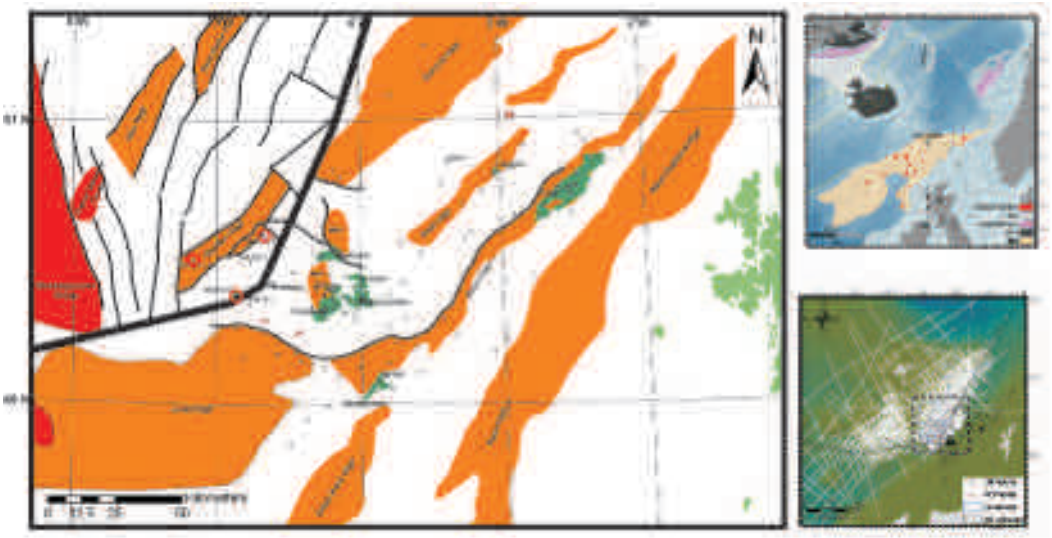

Figure 1. Overview map showing the main structural elements and main discoveries and fields within the southern part of the Faroe-Shetland Channel, also included as grey overlay is the 3D seismic data coverage prior to drilling.

in 2001 on the Sjúrður High (well marked with red circle, figure 1), targeting what was believed to consist of two stacked turbidity sand sections in the older part of the Vaila Formation. Later the same year BP drilled 6004/12-1/1Z, targeting an Upper T35 stacked turbidity sand section, located directly below the T36 (Lamba shale), prognosed as a possible regional seal in the area. This Lamba shale is also seen in the Flett and Judd basins on the UK side (Lamers and Carmichael, 1999). A deeper secondary target, within the T31, was tested with the 6004/12-1Z sidetrack.

Both wells encountered, contrary to pre-drill optimism, hydrocarbons but in non-commercial quantities. They did confirm that an active hydrocarbon system exists within the Faroese part of the Judd Basin. The mode of failure will be discussed in further detail in a later section.

The third exploration well 6004/16-1/1Z (well marked with red circle in figure 1) drilled by Amerada Hess, targeted a structural high of a Tertiary inversion anticline. The well was deepened below a sand dominated Upper Paleocene section through the underlying shales/siltstones. The deepening resulted in the Marjun discovery, consisting of a 170 m gross hydrocarbon column (with a net pay of 66 m using a cut-off of 11.5 % porosity, AHL values) in the T10 Lower Palaeocene interval (Smallwood and Kirk, 2005), with T20 shales acting as seal.

Following the Marjun discovery, Amerada Hess drilled an appraisal well (204/16-1) in 2002 in the UK block 204/16, approximately 6 km south east of 6004/16-1Z, to establish the extent of the discovery. The appraisal well reached total depth in the Late Cretaceous Jorsalfare Formation, and was classified as a gas discovery with the highest gas concentrations occurring below the igneous capped Cretaceous section (from composite log). Only hydrocarbon shows were reported in the Early Paleocene T10 section. A further detailed description of the Marjun discovery and its appraisal will be given in a later section.

In the summer of 2003, ENI UK, drilled 6004/17-1 and targeted the stratigraphic play of the Vaila Formation and a shallower Upper Lamba/Lower Balder target, related to shallow marine, shelfal and pro-delta gravity flows deposited basinward of prograding deltas (Woodfin *et al.*, 2005). The targets were mainly identified from elastic impedance inversion volumes. Since this well was not released at the time of the exploration

conference in 2006, this well will not be included in this paper, but information and some results from the well can be found in Woodfin *et al.* (2005).

Pre-drill Exploration Concepts.

With the successful discoveries of the producing fields of Foinaven/Schiehallion in the SE part of the Judd Basin, exploration in the deeper NW part of the basin had seen a good start and it was initially expected that the same strategy could be applied crossing the boundary into Faroese waters, it was therefore expected that same deepwater Paleocene play models for the SE part of the Judd Basin, also extend into the NW part of the basin. On a basin scale, shallow marine shelfal settings are found in the SE end of the Judd Basin with deepening water to the NW. During the Paleocene a slope system linked the shelf area to the deepwater basin, with turbidites triggered by sediment instability on the shelf supplying sediments to the deep parts of the basin, with thermal uplift related to volcanism in the area as a possible driving mechanism for the sediment instability (Naylor *et al.*, 1999).

The deepwater Paleocene sandstone play in the UK, West of Shetland area has been located within the Judd Basin and Flett Basin and on the Westray and Flett Highs. The traps are formed from a combination of structural and stratigraphic elements, with the Paleocene sandstone reservoir either pinching out or shaleing out updip (Lamers and Carmichael, 1999). The reservoir sands are interbedded with frequently laterally continuous mudstone providing competent top seals if not fault breached. The reservoir section consists of upper slope traps, toe of slope traps and basin floor fans (Lamers and Carmichael, 1999; Naylor *et al.*, 1999), with the Schiehallion and Loyal discoveries being situated on an upper slope terrace and the reservoir appear to have been deposited within or associated with a series of channelised submarine slope systems, of T31-T34 age (see figure 2 for stratigraphic scheme used), and affected by slumping and faulting (Leach *et al.*, 1999; Lamers and Carmichael, 1999). An important part of the Schiehallion/Loyal combined stratigraphic/structural play is the presence of an E-W trending sealing fault system acting as the up-dip structural component to the south (Leach *et al.*, 1999).

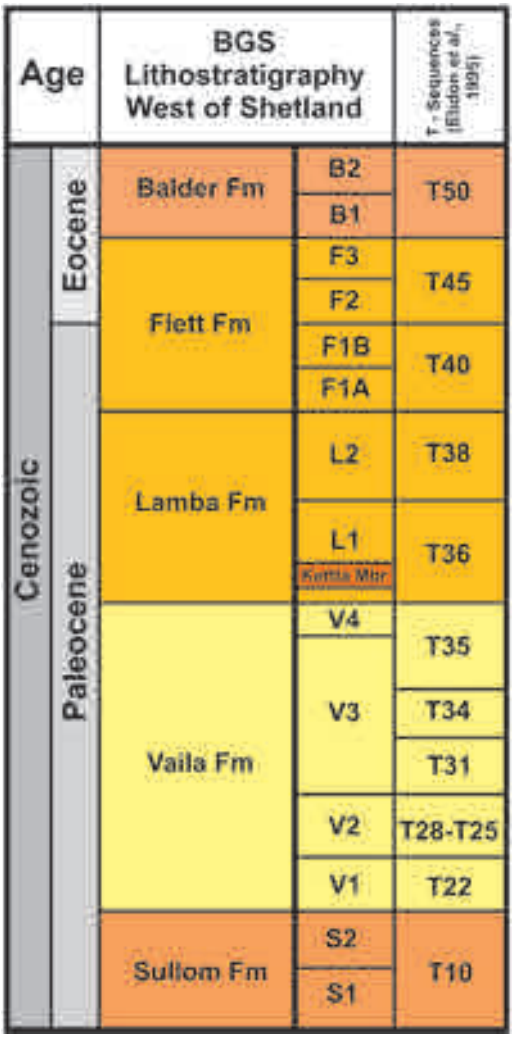

Figure 2. The stratigraphic scheme used within this paper (Ebdon *et al.*, 1995; Knox and Holloway, 1992).

The trap constituting the Foinaven discovery is partly structural and partly stratigraphical. The discovery is located on a faulted anticline structure overlying the Westray Ridge and is the result of compaction and inversion during Late Eocene to Miocene times (Cooper, 1999; Carruth, 2003). Along its western, northern and eastern edges it is dip-closed, with stratigraphic pinchout in the

south-eastern and fault closure at its southern limit (Cooper, 1999; Carruth, 2003). The Foinaven Field is segmented by a WNW-ESE fault system and by stratigraphic boundaries (Cooper, 1999; Carruth, 2003).

The Foinaven reservoir interval comprises channelised, siliciclastic turbidites with T31, T32 and T34 sequence sandstones being the main oil-bearing intervals (Cooper, 1999). They consist of a complex series of stacked slope and basin floor submarine fan sands. Mudstones at the top T34/base T35 acts as regional top seal to the system.

Further out, on the basin floor, is the Suilven discovery; consisting of basin floor fans, with internal sandstone geometry or up-dip pinchouts controlling the trap. The identified prospects were mainly seismic amplitude driven with a various degree of AVO support and relied to a high degree on a stratigraphic component.

Source rock in both the Foinaven and Schiehallion fields is the marine Late Jurassic Kimmeridge Clay Formation with a minor influence from a non-marine Mid Jurassic source (Cawley *et al*., 2005). Charge of the Foinaven field took place in three stages; seen as a mixture of heavy biodegraded oil in the first two phases and a later charged live medium gravity oil (Scotchman *et al*., 1998).

It was on these premises that the first two wells were drilled, 6005/15-1 and 6004/12-1-1Z and also the later 6004/17-1 (2003). The following chapter will deal with the two first wells in more detail. All depth references in this paper are given as measured depth below rotary table in meters (MDRT).

However the closeness of the Faroese part of the Judd Basin to the featheredge of the basaltic Faroese Platform poses an added complexity, with the possible addition of volcanic material to the expected siliciclastic lithologies. This is envisaged on amplitude extracts from a pre-drill semi-regional seismic data set of the T22 sequence. Two examples of amplitude extracts around the T22 reflector are shown in figure 3. Figure 3a illustrates amplitude extracts +/- 40 ms max trough amplitude and figure 3b shows an amplitude extract with the larger window, +/- 150 ms max trough amplitude. Some features seen on the +/- 40 max trough amplitude extract are further emphasized on the extract with the larger window (figure 3b), but new features also appear, in particular the circular features (dashed yellow lines) in the western and south-western area, features that would suggest sill

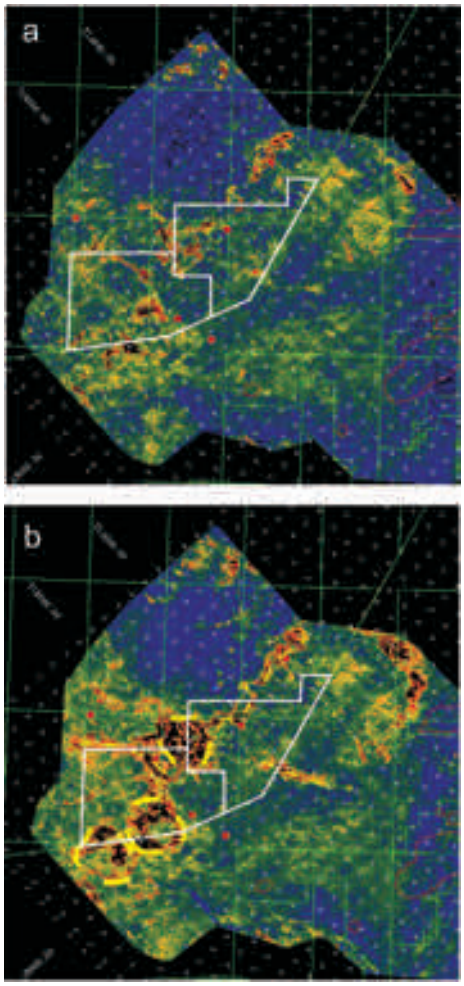

Figure 3. **a**) Semi-regional amplitude extract of the T22 reflector (+/- 40 ms max trough amplitude).Red dots mark the three Faroese wells mentioned and the Marjun appraisal well, 204/16-1. **b**) Larger window (+/- 150 ms max trough) semi-regional amplitude extract around the T22 reflector. Note the circular features outlined by dashed yellow lines in the western and south-western area possibly representing sills and also the linear features (yellow dashed lines), which seem to exploit pre-existing weaknesses.

complexes being present at that interval, but also the linear features likely to be intrusive material exploiting pre-existing weaknesses/faults.

Post-drill evaluation of the combined stratigraphic/structural Paleocene plays in Faroese waters.

6005/15-1.
The first offshore well to be drilled in the Faroese waters was 6005/15-1. It was drilled on the crestal part of the Sjúrður High (figure 1 for location) and consisted of a three-way dip closure with a stratigraphic element of seal along its eastern and western margins. The prospect was supported by an amplitude anomaly/AVO response.

The well targeted two Paleocene intervals in the deeper Vaila Formation section (T25 and T22, figure 5) comprising stacked deep marine turbidite fan sandstone sections encased in shale.

The target intervals proved to consist of dolerite sills encased in interbedded sand and shales (figure 5) with various amounts of volcaniclastic material (Aase, 2002). The section from the base of the Kettla Tuff Member to total depth was sandier than expected and the drilled section only penetrated sediments of the Upper Vaila Formation part (V4 and V3, figure 2 and 5) and not the expected Lower Vaila Formation (V1 and V2). Biostratigraphic analyses (Ichron, 2001) indicate a possible hiatus between the Lower Flett Formation (F1a) and the Upper Lamba Formation (L2-3).

The sandstones within the target section have calculated porosities of 10-18 % in the shallower T34 section and 7-12 % in the deepest reservoir T28 section. These porosity values are derived from wireline logs. No oil or gas shows were observed when drilling through, but in the interval between 3936 m to 3993 m MD RT weak oil shows were reported from well cemented sandstones. Also within the dolerite/volcaniclastic section, slight traces of oil were observed, but the lack of side wall cores from this section leaves the nature of the shows unexamined. The well reached total depth in a dolerite sill at 4026 m MD RT.
In the sandstones close to the sills an increase in quartz cementation is seen, but only locally, suggesting that in this incidence heating from sills has not had a detrimental effect on reservoir properties (Aase, 2002).

6004/12-1,1Z.
The 6004/12-1 and 1Z wells were drilled in the northern end of the Judd Basin, close to the eastern flank of the Sjurður High and the Westray fault on the northern flank of an inversion anticline. Palynological analysis indicates a stratigraphical break at the base of the Moray Group (T45) and the Faroe Group (T38) with no biostratigraphical evidence of the upper part of the Flett Formation (F1a-1b, T40).

The wells primary reservoir targets were thought to consist of stacked T34-T35 deep marine turbidite sandstones. The T36 shale was expected to act as seal and with the presence of local intra sequence seals was thought to be capable of providing effective seals on prospect level (figure 5).

Amplitude extracts of the T35-T36 interval (figure 4a and 4b) of the prospect (outlined by the red square) displays some of the same features that are also recognised in the Foinaven/Schiehallion fields. In particular the E-W trending faults, which in the Foinaven and Schiehallion areas, act as sealing faults. The amplitude anomaly conforms to structure in the north-south trending direction while in the east-west direction it would have to rely on a stratigraphic pinch out. The large NE-SW trending (dashed yellow line, figure 4b) fault is the southeastern bounding fault of the Sjurður High.
On the amplitude extract in figure 4c (T35 sequence reflector, +/- 40 ms, max trough amplitude) an anomaly can be seen to the southeast of the Sjurður High bounding fault. Another noticeable attribute is the circular feature (dashed red circle) in the northwestern part of the area, believed to be a saucer shaped intrusive igneous sill.

The amplitude anomaly in the T35-T36 sequence was initially believed to consist of a stacked set of Upper T35 deep marine turbidite sands lying directly below a thick T36 Lamba shale section acting as the top seal. However the post-drilling evaluation has shown that the amplitude anomaly most likely arose from a basal T36 tuff directly overlying T35 sand, a tuff that had not been encountered in any UK wells.

After having experienced operational difficul-

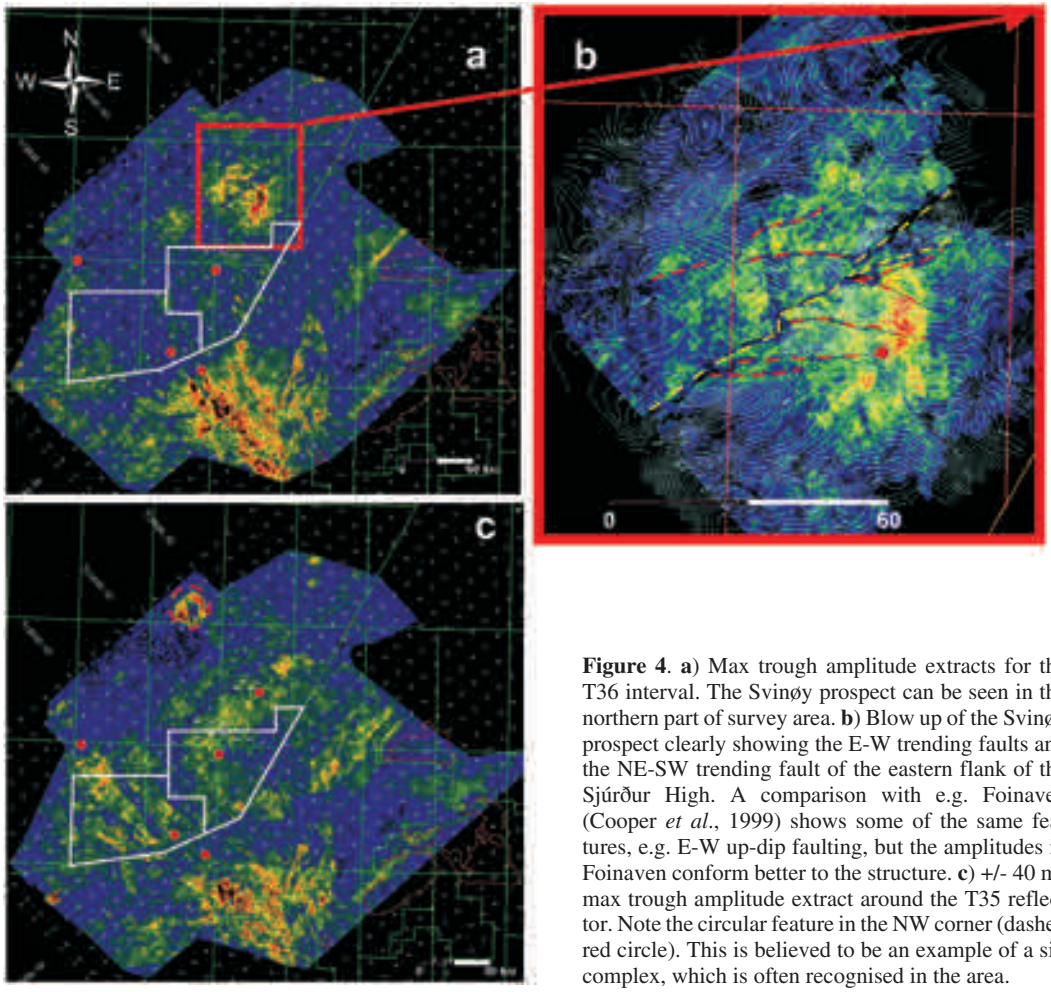

Figure 4. **a**) Max trough amplitude extracts for the T36 interval. The Svinøy prospect can be seen in the northern part of survey area. **b**) Blow up of the Svinøy prospect clearly showing the E-W trending faults and the NE-SW trending fault of the eastern flank of the Sjúrður High. A comparison with e.g. Foinaven (Cooper *et al*., 1999) shows some of the same features, e.g. E-W up-dip faulting, but the amplitudes in Foinaven conform better to the structure. **c**) +/- 40 ms max trough amplitude extract around the T35 reflector. Note the circular feature in the NW corner (dashed red circle). This is believed to be an example of a sill complex, which is often recognised in the area.

ties the well was side tracked and targeted a deeper target within the Vaila Formation (T31). The target however turned out to be water wet.

Results from the combined stratigraphic/structural Paleocene plays.

Although the disappointing results of 6005/15-1 and 6004/12-1Z, in respect to encountering commercially producible volumes of hydrocarbons, the post drilling analysis did show some encouraging results and answered some questions that had existed prior to the first spud.

One of the main issues prior to the first spud was the uncertainty in the presence of reservoirs. The wells demonstrated that the Faroese part of the Judd Basin was more sand prone than anticipated (figure 5). Furthermore the wells showed that the lithologies encountered in the UK part of the Judd Basin were not representative of the lithologies found in the Faroese wells. An example of this is the basal T36 tuff. Also the Longan prospect was influenced by differing lithologies; here an intrusive igneous sill complex gave rise to the amplitude anomaly observed.

Another question that the wells answered was the confirmation of the existence of a hydrocarbon charge system in the Faroese part of the Judd Basin, with biomarker results (28,30 Bis-

norhopane to C_{30} Hopane ratio) demonstrating that the same mechanism of hydrocarbon mixing from marine Late Jurassic, Kimmeridge Clay Formation and lacustrine Mid - Late Jurassic, Heather Formation equivalent source rocks, documented from the fields on the UK side, is also working in Faroese waters (Cawley *et al*., 2005).

Modes of failure.

The modes of failure for the two wells indicates the difficulties that lack of well penetrations and the problem that lack of well to seismic calibration poses in a frontier area. The success the amplitude anomaly and AVO anomaly studies had proven in the Foinaven/Schiehallion area lead to a quite un-

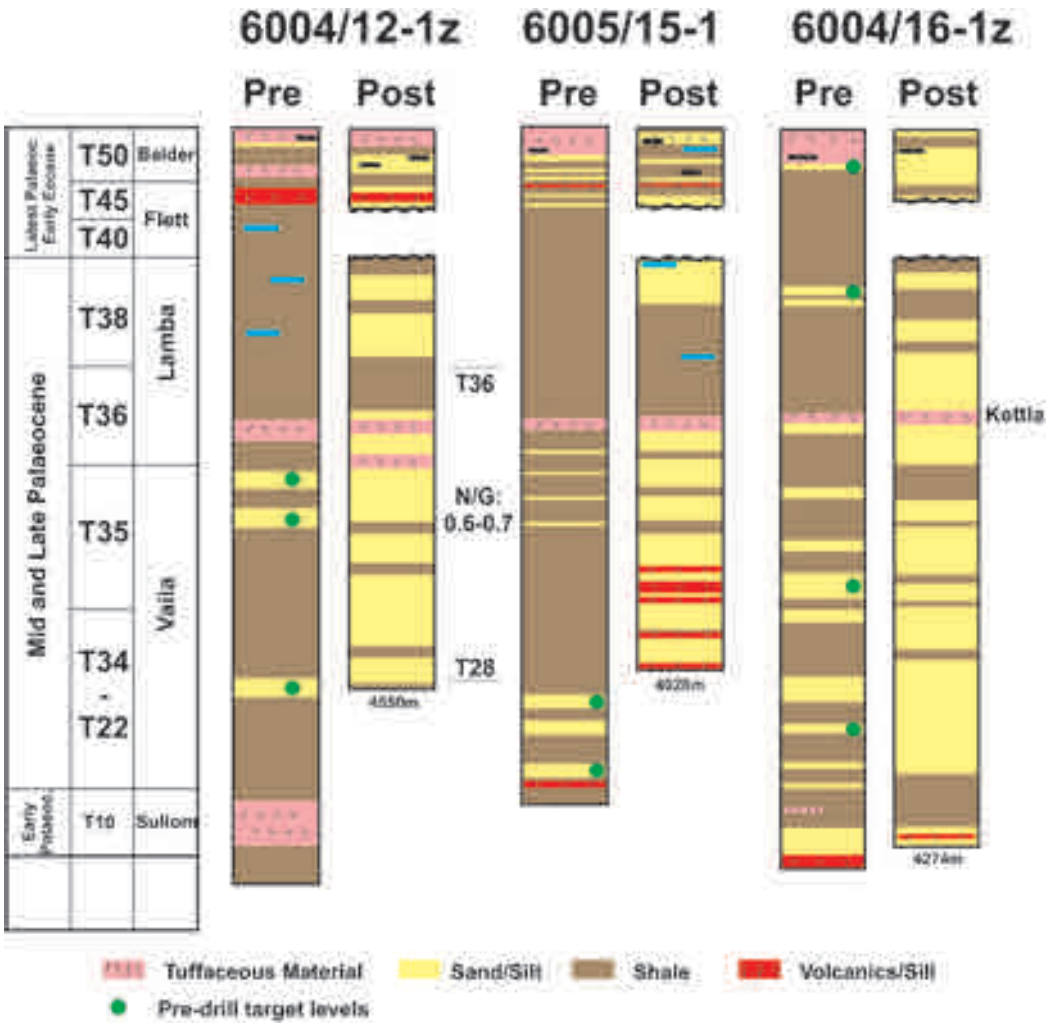

Figure 5. Generalised lithology logs of the three Faroese wells discussed here, levelled on the Kettla Tuff. The sand/shale lithologies are evaluated mainly from gamma-ray log and resistivity log responses and less from the lithology description on the final composite logs. Though a simplistic way of lithology discrimination it was chosen since these data are present through the full drilled sections in the wells. The pre-drill predictions were primarily based on analogues from the UK side of the Judd Basin (Schiehallion/Foinaven) and the post-drilling results clearly show a marked increase in sand content in all of the wells, exemplified with an estimated net to gross of 0.6 - 0.7 in the T28 to T36 interval.

usual start-up strategy entering the Faroese area, applying the same seismic attribute exploration strategies in the Faroese side of the Judd basin, in contrary to an exploration strategy for a frontier area, where the structural play types are usually targeted in the first stages and the more subtle stratigraphic and combined play types being targeted later in the exploration phase.

In the 6004/12-1z well the lack of competent sealing lithologies in the T36 sequence is regarded as the failure component. A pressure drop within the T35-T36 sequence was not observed, suggesting that the detected hydrocarbons might be a result of a paleo-migration path or to seal breakage, but data is non-conclusive. In well 6005/15-1 the expected reservoir section consisted of dolerite sills and the failure mode was lack of both a reservoir section and appropriate seal.

The nature of the amplitude anomalies were initially believed to be caused by differences in pore fluids and both wells were drilled on amplitude and AVO anomaly studies. The anomalies were however instead due to differences in lithologies and the pre-drill conclusions of amplitude and AVO analyses were clearly related to the lack of well calibrations and the misconception that, even though the step out into the deeper parts of the basin from the UK side was considerable, the encountered lithologies would be reflected in the UK well findings.

A subsequent attempt to incorporate knowledge of the differing lithologies, in an elastic impedance inversion study for lithology predictions, was attempted by license 002 holders prior to their drilling of 6004/17-1, when access to 6004/12-1/1Z and 6004/16-1/1Z well results was granted in late 2001 and 2002 (Woodfin *et al*., 2005). The main objective was to discriminate sandstones from shales and predict adequate shale seals and tuffaceous sandstones and investigate any AVO effect of hydrocarbon accumulations.

Their results showed that the use of seismic attributes proved useful as a sand/shale predictor in sections that were correlated to offset wells, but less good outside the calibrated intervals and inefficient as an indicator of pore fluids (Woodfin *et al*., 2005).

The generally very sand-prone basin, compared to what has been observed on the UK side within the same stratigraphic interval, is clearly seen by the results from the Faroese wells, with net/gross ratio of 0.6 - 0.7 in the T28 - T36 section. The cause of this sand-prone nature of the basin has been speculated by several authors, suggesting an influx of westerly sourced sediments during the Paleocene being a possibility (Larsen and Whitham, 2005; Jolley *et al*., 2005; Smallwood, 2006; Ziska, 2006). Analyses of heavy minerals and palynological data have shed some light on this issue and will be discussed later.

The structural play – The Marjun Discovery.

6004/16-1,1z.

As the third well 6004/16-1/1Z was drilled on a Cenozoic inversion anticline, close to the Faroes - UK border (figure 1). In contrast to the 6005/15-1 and 6004/12-1Z wells, 6004/16-1 targeted a four-way dip closure with structural closure on several levels (though 4-way closure at T20-T10 level is dependant on the depth conversion method used) and without a noticeable seismic amplitude anomaly below the Kettla Tuff (Smallwood and Kirk, 2005).

Having reached its pre-determined TD only encountering hydrocarbons in the form of oil shows in a sandy Upper Paleocene section, the well was deepened to target the Early Paleocene T10 sequence.

The T28-T36 interval showed a very sandy section with a net/gross of 0.6-0.7, with poor development of sealing lithologies (figure 5), indicating that the lack of a competent top seal between T28 and T36 was the mode of failure for the lack of significant hydrocarbon accumulations.

The deepening of the well met a siltstone/shale section in the T20's and an overpressured sandy reservoir section in the T10 sequence. A hydrocarbon column of 170 m was encountered within the T10 sequence with a net pay of 66 m (using a 12 % porosity cut-off) and an oil water contact was observed at 4225.4 m MD RT. The reservoir zone, with a net/gross of 0.6 and porosities of 11-16 %, however showed low permeabilities of 0.3-4.0 mD (values from cored sections). The well has not

been flow tested, leaving reservoir deliverability unknown.

Different datasets, vitrinite reflectance data, AFTA (Apatite Fission Track Analysis) and spore colour index (Caslin, 2002; Green, 2002) suggests that erosion of post-Paleocene sediments has occurred, e.g. does AFTA and Vitrinite Reflectance data suggest the removal of 0.5-1 km of post-Paleocene overburden depending on what paleogeothermal gradient is used. Also upwards extrapolation of spore colour index trend suggests erosion of the same amount (Caslin, 2002; Smallwood and Harding, this issue), results which are comparable with estimates from lithology predictions from sonic-log velocity data and porosity-depth trend from wells (Smallwood and Harding, this issue; Smallwood, 2004).

The palynological data suggest no evidence for the presence of the lower part of the Flett Formation (Flett 1a and Flett 1b) in the 6004/16-1Z well (Mahdi, 2002).

The presence of intrusives, observed on seismic data to the west of the 6004/16-1Z as well as encountered in the well as a 6 m thick sill, suggests the possibility of a thermal influence on the reservoir section. This is seen in highly elevated vitrinite reflectance values and spore colours within the T10 section (Green, 2002; Caslin, 2002; Smallwood and Harding, this issue). The increase in these paleotemperature indicators are seen to be confined to the T10 sequence with the above lying thick T20 shale being virtually unaffected (Green, 2002; Smallwood and Harding, this issue), this could suggest that the thermal disturbance is unlikely to have originated from the encountered 6 m sill only and is more likely to have been caused by the thermal flushing of water through the section, with the overlying thick T20 shales acting as a barrier for vertical fluid dissipation and focusing it towards a more lateral fluid movement. Comparisons of sandstones from the cored T10 interval of 6004/16-1Z and 204/22-2Z suggests different diagenesis for the sandstones, with the main differences being preservation of unstable garnet grains in 204/22-2Z; high temperature authigenic phases including rhodrochrosite, high temperature calcite and sericite present in 6004/16-1Z, but haven't been identified in 204/22-2Z; intergranular porosities found to be lower in well 6004/16-1Z (Lucas and Metters, 2002a).

Comparison of the porosity-depth trend with the regional Quad 204 porosity-depth trend shows no marked decrease in porosity in the T10 section, except what is accounted for by 0.5-1 km added burial, suggesting that the thermal event has not affected the porosity in the T10 section. The thermal flushing event has, however, affected the permeability of the section (figure 7b).

Subsequent to the Marjun discovery and drilling of its UK appraisal, the license holders acquired a new 3D seismic data set (with an offset of 6 km) as part of the prospectivity evaluation.

204/16-1 – The Marjun Appraisal well.

Shortly after (2002) the drilling of the Marjun prospect, the L001 licence-holders drilled an appraisal well (204/16-1) on the UK side close to the median line, approximately 6 km south east of 6004/16-1Z (figure 1). The results from this well showed some interesting differences between the two areas, unfortunately differences that did not enhance the discovery.

The 204/16-1 well reached TD in the Late Cretaceous Jorsalfare Formation and was plugged and abandoned as a gas discovery with oil shows within the Paleocene T10 sequence. In the lower T31 sequence, a section with minor gas readings was observed. A thin (4 m) sandstone stringer was observed within the claystone dominated Jorsalfare Formation, indicating that Late Cretaceous sands do exist close to the Faroese area.

The Paleocene and Late Cretaceous sections are divided by approximately 40 meters of igneous intrusive doleritic sills and with the highest gas readings (total gas 20%, value from composite log) observed in the section directly underlying the intrusives.

The overpressure observed in the T10 section of 6004/16-1Z was not present to the same degree in 204/16-1 and combined with the difference in hydrocarbon findings between the two wells indicates that there is a likely pressure barrier between the two wells. The mapping of the T10-T22 sequences on a 3D seismic dataset, acquired by license holders after drilling, does not give any clear indication as to how far the Marjun discovery ex-

tends, since mapping of the faults is difficult and the lateral extent of the fault sets is difficult to map and hence connectivity between the fault sets is difficult to establish. Figure 6 shows a general two way travel time contour map of the T10 sequence with inferred faults.

These two fault sets, the main E-W trending fault set and the more N-S trending fault set could be an important component in the structure, but it is presently still unknown to what degree these fault are acting as impermeable barriers.

The increase in water depth towards the west in the license tilts the western part of the structure towards the east on depth converted data, leading to shallower closure towards the west.

Other data, analysis and some implications.

The results from the conducted analyses from the three wells have shed light on the provenance area of the encountered sands and organic geochemical analyses of solvent extracts from core, side wall cores and oil stained sediments have confirmed the presence of a dual source rock system within the Faroese part of the Judd Basin. These results will be discussed in the following section.

Provenance area.

With the sand prone T28-T36 section found in all three wells, the obvious question is where has this sand been derived from? Volume estimates of offshore Cenozoic sediments and British onshore denudation estimated from missing-post rift subsidence and thermal indicators have been undertaken by several authors (e.g. Clarke, 2002; Jones *et al*., 2002; Smallwood, 2005) and the results range from being in balance between offshore sediment volume in the basin and onshore denudation volume (Clarke, 2002) to being a factor of two to four in the volume of sediments in the basin compared to denudation volume (Jones *et al*., 2002; Smallwood, 2005). This suggests the need for alternative provenance areas compared to the Orkney-Shetland platform suggested by e.g. Lamers and Carmichael (1999).

Both heavy minerals analysis (Morton and

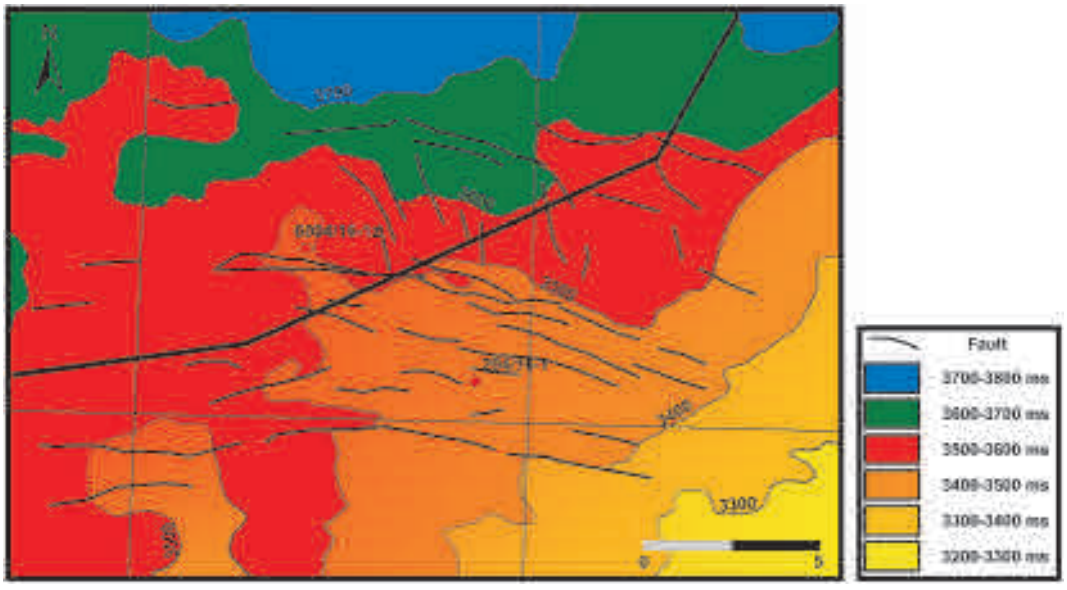

Figure 6. Generalised two-way-travel time (in ms) contour map of the T10 horizon. The main fault direction is East-West but a set of short NNW-SSW faults are also seen. The difficulty in mapping the extent of these hampers the confidence with which connectivity between the two fault sets can be established. Closure at T10 level is difficult and does depend on the chosen depth conversion method.

Hallsworth, 2002a; 2002b; 2002c and 2002d) and pollen and spore flora analysis (Jolley, 2002; Jolley *et al*., 2005) have been conducted on the three wells and results from the heavy minerals analysis suggests a complex picture of provenance areas and source directions during the T10 to T38 interval.

Four sand types have been identified in the pre-Kettla section attributable to different provenance areas. A sand type (sand 1 in table 1) with low RuZi and similar to the T36 in 205/9-1, considered to have a western source, occurs in all three wells. Two sand types (sand 2 and sand 3 in table 1) with similar high RuZi, but with differences in garnet compositions and comparable to those identified in the Foinaven-Schiehallion areas and are therefore attributed to have sourced from the Orkney-Shetland platform. The difference in garnet composition is believed to reflect differences in provenance area within the Orkney-Shetland platform, with one being more northerly than the other. The final sand type (sand 4 in table 1) represents the volcaniclastic component of the sandstones. It is believed to have been predominantly derived from a basaltic terrain and occurs in all three wells, 6004/12-1Z, 6004/16-1Z and 6005/15-1, in association with the first, westerly derived sand type. The provenance area from this sand is also considered to be to the west. The results in table form are shown in table 1.

The occurrence of the different sand types, in the pre-Kettla section within the wells suggests that changes in provenance area identified in individual wells were not synchronous.

In 6005/15-1 the lower parts (T31 to T34) are dominated by westerly sourced sands, which gradually disappears and in the younger section (T35 and younger) where the eastern heavy mineral population dominates. The composition in well 6005/15-1 is generally less diverse as observed in the two other wells.

In the T31-T32 section of 6004/12-1Z a mixture of westerly source with minor contributions of an easterly source is present. In the T34 section particular large concentrations of westerly sourced material is observed, but up-hole the eastern source is seen to dominate. The picture in 6004/16-1Z is very like 6004/12-1Z with the addition that

Provenance Area from Heavy Mineral Analysis for the T10-T50 interval.

Stratigraphy	T - sequences	6005/15-1	6004/16-1z	6004/12-1z
Post Kettla	T50 - T38			Not Evaluated
Kettla Mbr	T36			
Vaila Fm	T36 - T35			
	T34			
	T31 - T33		Upper / Lower	
	T28		Upper / Lower	
Sullom Fm	T10			

Sand 1 Sand 2 Sand 3 Sand 4

Table 1. Reservoir provenance area from heavy mineral analysis. The population of sand found in the wells consists of four sand types, Sand 1 akin to T36 sand in 205/9-1, which is interpreted to have a western source. Sand 2 derived from the SE part of the Shetland Platform, Sand 3 derived from the NE part of the Shetland Platform and Sand 4 which is a volcaniclastic component sourced from basaltic terrain to the West.
In all three wells this volcaniclastic component is observed, but the time of the influx appears not to be synchronous. Also the presence of the third sand type is not observed in the westernmost well (6005/15-1) and influx of the western source (sand 1) appears not to be as pronounced in this well as in the two others.

the oldest sections in the well (T10 to T28) also show sands with a western source (both sand 1 and sand 4).

Palynological data from the wells have shown the presence of a Greenlandic flora in the Upper Sullom Formation (T10) and within the Vaila Formation (T31-T34). The repeated occurrences of this Greenlandic flora within the Sullom Fm and Vaila Fm made Jolley *et al*. (2005) suggest a western influx of argillaceous material with a pulsed nature, possibly correlated to increased volcanic activity in the Hebrides and West Greenland and

with transfer zones possibly impacting the dispersal pattern (Jolley *et al*., 2005). In the 6005/15-1 well the palynological data suggests an influx of a Greenlandic flora from the Kettla Tuff Member and downwards, with this flora being almost absent in the Upper Vaila Formation but becoming common to abundant in the lower part of the penetrated Vaila section. This could suggest that although the heavy mineral analysis doesn't propose an influx of westerly sourced sediments, the palynological data imply it to be the case. This discrepancy can however be explained by the different grain size fractions, the two types of analysis are sampling, with the heavy mineral analysis analysing the sand fraction while the palynological analysis being associated with the clay fraction.
One possible sediment input provenance has been identified in the Kangerlussuaq area of Southern East Greenland (Larsen *et al*., 1999; Larsen and Whitham, 2005; Jolley *et al*., 2005) where the Late Cretaceous/Early Paleocene section is missing but also the Faroese Platform itself, Munkagrunnur Ridge and the Wyville-Thomson Ridge (Waddams and Cordingley, 1999) have been proposed as possible provenance area candidates (Smallwood, 2006; Ziska and Andersen, 2005) in particular for nearby areas.

Reservoir properties.

The influence on reservoir properties given the sandy section encountered in the three wells along with the indications of a western source from heavy mineral analysis might be two fold. At first, the higher proportion of sand in the T28 to T36 section result in higher seismic velocities than expected and the estimated depths to the seismic tops came in deeper than anticipated. The increased depth influences the burial depth the potential reservoir section has experienced and hence with a potential for additional compaction. In figure 7a is the porosity versus depth (in meters below seabed) for the three wells shown. The porosity data have not been averaged and shows considerable scatter in the cored target zones. Figure 7b displays the air permeability versus depth (from seabed) and also here does the data show considerable scatter due to no averaging of data points. In well 6005/15-1, one core was acquired in the interval 3508 - 3514.5 m (2546 - 2552.5 mbml) within the Vaila Formation. The porosity range is 3.8 - 15.6 % with an average of 10 % and a permeability range of 0.144 - 3.75 mD and an arithmetic mean permeability of 1.4 mD. In well 6004/12-1Z one core was obtained in the interval 3576 - 3606 m (2466 - 2496 mbml) in the upper part of T35 within the Upper Vaila Formation. In the cored interval, several levels showed very low porosities (down to 4.1 %) and permeabilities (0.07 mD, minimum value) but with average values of 21 % porosity and average permeability of 97 mD over the cored interval.

In the last of the discussed wells, 6004/16-1Z, three cores were acquired, with the first core obtained in the interval between 3452 - 3462 m (2451.4 - 2461.4 mbml; comprising the uppermost part of T28 and basal part of T31), showing a porosity range 8.1 - 18.1 % and an average value of 15.4 % and a permeability range of 0.21 - 28.6 mD with an average of 9.8 mD. The two lower most cores obtained in the deepened T10 interval, between 4181 - 4203 m (3180.4 - 3202.4 mbml) and 4203 - 4214 m (3202.4 - 3213.4 mbml) with an observed porosity range 5.6 - 8.8 % and an average of 7.8 % and permeability range of 0.01 - 0.24 mD with an average of 0.09 mD.

Comparisons with regional porosity/depth studies (Smallwood, 2005; Smallwood and Harding, this issue) from other UK Judd Basin wells of the T10 to T50 section suggest that porosities are lower in the Faroese wells, indicating that the section has been buried deeper in the Faroese part of the Judd Basin. Estimates of erosion of 500 - 1000 m from different paleothermal indicators have been proposed (Caslin, 2002; Smallwood and Harding, this issue). Trend lines for porosity/permeability data for the three individual wells (figure 7c, red, dark blue and green) and a trend line for all the wells (in yellow) is compared with the results for the T31 to T36 section from other West of Shetland wells (in light blue, Cawley *et al*., 2005) indicating that porosity/permeability is lower in the Faroese wells.

The low permeabilities in the T10 section of 6004/16-1z are likely to have been caused by a combination of intrusion related diagenetic effects arising from one or more thermal flushing events of the reservoir section and deep burial. The high

temperature is seen as development of pore filling authigenic clays and high temperature Mg-rich carbonate cement and complete removal of garnet (Lucas and Metters, 2002a).

Seals.

The three wells confirmed the presence of ample potential reservoir sections within the drilled stratigraphy (figure 5), but raised the issue of locating appropriate sealing lithologies.

For example, results demonstrate that the T36 sequence sealing lithologies found on the UK and which constitutes a regional seal in the Flett and Judd Basins on the UK side (Lamers and Carmichael, 1999), on the Faroese side instead displayed a more sandy section, which in places e.g. 6004/16-1Z have been unable to have acted as competent seal. The challenge then shifted from focusing on reservoir distribution to predicting the areal distribution and vertical extent of potential sealing lithologies especially within the T28 to T36 section. As Woodfin *et al* (2005) showed, the use of elastic impedance Inversion could be a useful tool, but caution is still to be made since careful calibration of the seismic attributes (P and S impedances and Poisson's Ratio) is restricted by the limited number of wells and interpolation over significant distances away from well control still remains an issue.

The T20 shales encountered in 6004/16-1Z did show that a competent sealing lithology are present within the Faroese part of the Judd Basin, but since it has not been penetrated by other Faroese wells, its sealing capacity in other parts of the basin has not been confirmed. The well 204/16-1 did however display the same sealing lithologies in the T20 shales, indicating that at least to the south east are the T20 shales capable of acting as a competent seal.

With the high sand to shale ratio, it could indicate that the wells drilled on the Faroese side of the Judd Basin were located in the middle of a sandy fairway, and drilling on the flanks, either further north or further south could potentially decrease the sand to shale ratio, giving the opportunity for thick shale sequences acting as the necessary seals.

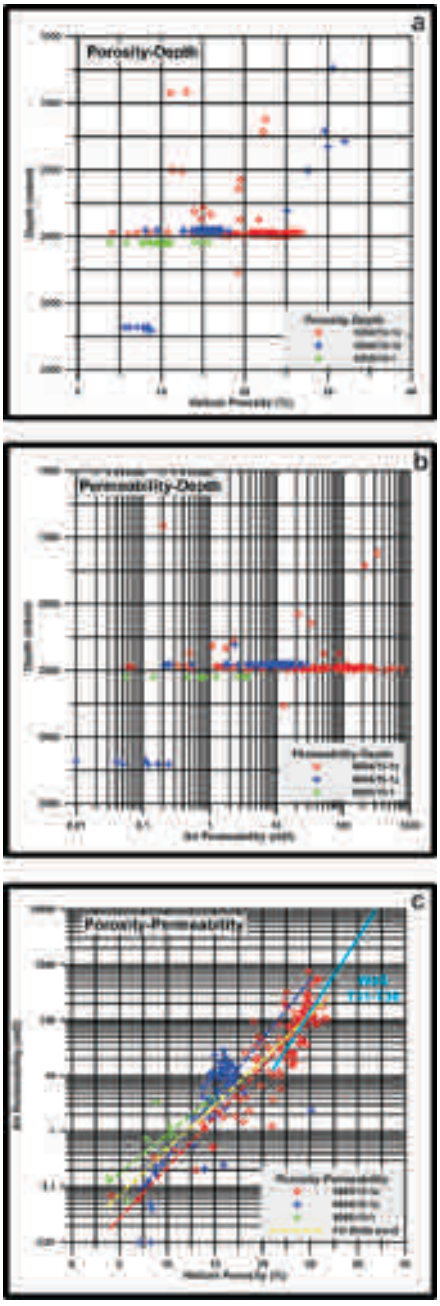

Figure 7. Porosity-Depth **a**) and Permeability-Depth **b**) data from the three wells. All data are shown with no averaging of close spaced data points (in cored sections). Also shown is the Porosity-Permeability data set **c**) with trend lines (in green, red and dark blue) for the individual wells and a trend line for the combined data set (in yellow) and compared to a general West of Shetland T31-T36 poro-perm trend (in light blue, Cawley *et al*., 2005).

Hydrocarbon system and organic geochemistry.

Geochemical analysis of solvent extracts from cores, side wall cores and oil stained sediments on the three wells have confirmed the western extent of the same source rock system that is observed in the Foinaven area. Furthermore, as in the Foinaven area, episodic charging is observed, with the first charge being heavily biodegraded and a later charging episode being only moderately biodegraded, indicating that the temperature at which the second pulse was charged was higher than in the incidence of the first pulse. Gas chromatographic data shows an unresolved complex hump in the saturated fraction, which is also evident from soluble extracts from wells within Q204.

Analysis of biomarker data, specifically the 28,30 Bisnorhopane, which occurs in the Kimmeridge Clay Formation but is not observed in the Middle Jurassic source rock and attributed to euxinic depositional environments (Peters *et al*., 2005), have been used to estimate the relative contribution of the Kimmeridge Clay Formation and Middle Jurassic source rock (Scotchman *et al*., 1998; Cawley *et al*., 2005). These analyses suggest that for both 6004/12-1Z and 6004/16-1Z contributions from both source rock systems can be observed in the hydrocarbons.

This evidence suggests that, although seismic mapping of the Jurassic section is questionable on the current seismic data, presence of source rock and its maturity within the Faroese part of the Judd Basin can be considered low risk.

Other examples of amplitude anomalies.

One of the issues remaining in the Faroese part of the Judd Basin is what prospectivity lies yet within the area and what is its nature?

From the previous sections, the drilled sections proved to be sandier than initially expected and competent sealing lithologies being more prominent in their absence than presence. This clearly reduces the chance for a successful stratigraphic (or combined stratigraphic/structural) play within the Faroese part of the Judd Basin area. However screening of amplitude extracts and AVO anomalies on a 3D seismic data set (DGSF-96, DGSF-97, MC3D and two proprietary 3D data sets in Quad 204, reprocessed by BP/Amoco) obtained prior to drilling has shown that minor amplitude/AVO anomalies do exist within the T25 to T36 section. Just as exemplification of these observed amplitude anomalies, an amplitude extract on the interpreted T25 horizon from block 6005/16 is shown in figure 8. The amplitude extract was performed on the full stack data set and performed on the interpreted horizon only (1 sample = 4 ms). Also insert are two representative seismic sections through the lead. The lead is a simple structure, dipping towards the North and East. The updip edge is faulted, invoking fault sealing to be present in order to work, but the small offset could be a big risk and the faulting could have acted as conduits for hydrothermal fluids from the sills seen in the bottom of the seismic sections, causing an alteration in reservoir sections as has been observed in well 6004/16-1Z, where the low permeability of the T10 reservoir section has been linked with one or more thermal water flushing events.

Though several smaller amplitude anomalies have been mapped within the basin on several levels, it is likely, that some of the afore-mentioned difficulties with reservoir properties e.g. provenance area, thermal effect on reservoir, amplitude anomaly relating to lithology and lack of sealing lithologies could also affect these. But given the variability and seemingly restricted nature of the westerly sourced sandy material, it would be too early to conclude that the basin as a whole is exposed to the same mechanisms.

Conclusions.

What initially was thought to be a problem of locating good quality reservoir sections, instead turned out to be a question of locating competent sealing lithologies, evidenced by the general high net to gross values (0.6-0.7) of the T28 to T36 interval revealed in the wells 6005/15-1, 6004/12-1Z and 6004/16-1Z. Though no commercial discovery has yet been discovered from the wells drilled in Farose waters, results from organic geochemistry reveal that the same mature source rock sys-

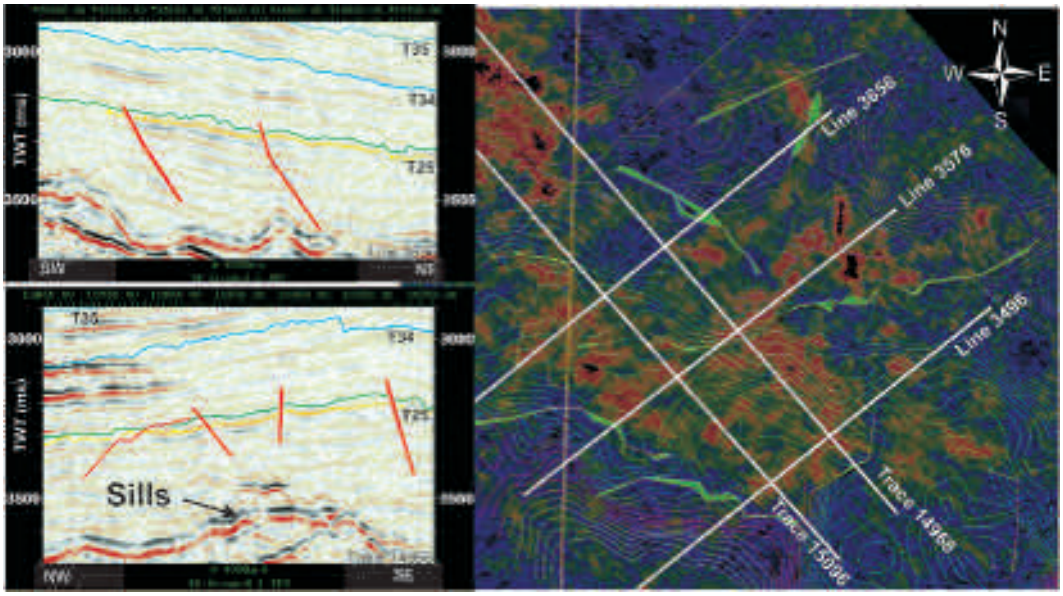

Figure 8. Lead within block 6005/16 exemplified on an amplitude extract map and a two-way time contour map of the T25 equivalent reflector. The amplitudes were extracted on the full stack data set. The contour interval is 5 ms, between 3150 ms to 3350 ms, white being shallow and purple being deep. The amplitude extraction is done on the interpreted T25 horizon only (1 sample = 4 ms). Also insert are two representative seismic displays through the lead. The structure is simple and dipping towards the north and east. The updip edge is fault controlled and the faults towards the south and west are connected. There seems not to be a clear depth dependant amplitude cut-off, indicating that the anomaly is less likely to be a hydrocarbon effect, but could still be a positive lithology indicator. The lack of a clear updip sealing fault is however a major risk component.

tem is present on the Faroese side. In addition, the same dual hydrocarbon migration history, seen in the Q204 wells, also seems to have been present in the Faroese area.

In terms of provenance area for the reservoir sections, heavy mineral analysis suggests that the pre-Kettla section in all three wells have experienced a contribution from westerly sourced material of both siliciclastic and volcaniclastic nature, but to a different degree, with the eastern (6004/12-1Z and 6004/16-1Z) wells having a more prolonged influx of these westerly sources than the westernmost well (6005/15-1). This could suggest a restricted distribution for this source direction. Furthermore, does the volcaniclastic component always seem to occur in association with the westerly sourced siliciclastic component, the implications, if any, of this is not fully understood.

The reservoir properties found in the three Faroese wells have indicated that porosities are slightly lower compared to time equivalent sections found in UK wells West of Shetland and especially permeability occurs to be generally lower than offset wells in West of Shetland, UK, and two mechanisms have been proposed (Aase, 2002; Lucas and Metters, 2002a, 2002b) for this, one being the presence of instable volcanic glass and local effects of thermal flushing from igneous intrusives.

Generally, the sandy sections show variable reservoir parameters and the occurrence of both a volcaniclastic sand component and the influence of thermal flushing events add to the risk of degrading reservoir properties. Therefore future exploration efforts should not only focus on locating competent sealing lithologies, but also consider the potential provenance area for the reservoir section, since this have been seen to have had an influence on the reservoir properties in the wells.

Although a thin Cretaceous sandstone was found in well 204/16-1, the very thick Cenozoic section in the Faroese part of the Judd Basin makes

it unlikely that exploring older pre-rift sediments in the basin will constitute a focus point in near the future. However the very sandy nature of the Cenozoic section could indicate that the wells were drilled in a sandy fairway and that stepping away to the basin edge could give the needed sealing lithologies. These areas are however covered with basalts in various thicknesses and the difficulty that traditional geophysical techniques have in these settings would make the stratigraphic or combined stratigraphic/structural play type a major challenge. Therefore a return to the traditional structural play types in these areas and the recent discoveries in basalt covered areas on the UK side, with the discovery of Cambo in the post-basalt section and the intra-basalt discovery of Rosebank on structural highs is promising for the basalt covered highs (e.g. East Faroe High) in the Faroese area. Until now, two wells have drilled sub-basalt plays within the Faroese area. These wells are however still confidential.

Though advancements in seismic imaging have been achieved, mapping of these volcanics covered areas are problematic and new geophysical methods have still not been tested in this demanding area. A promising technique, which could prove helpful in discriminating whether amplitude anomalies relates to lithology or pore fluids, is the CSEM method. This technique has not yet been used, but hopefully the next couple of years will see it application within Faroese waters.

Acknowledgements

The author would like to extend a big thank you for constructive comments to Jon Seedhouse and Mark Woodfin, any shortcomings or unresolved questions purely rely with this author.

References.

Aase, N.E. 2002. Petrographic composition, diagenesis and reservoir quality of sandstones from well 6005/15-1, Longan well, Faeroe Islands. *Statoil report*: 1-53.

Carruth, A.G. 2003. The Foinaven Field, Blocks 204/19 and 204/24a, UK North Sea. *In*: Gluyas, J.G. and Hichens, H.M. (eds.) *United Kingdom Oil and Gas Fields, Commemorative Millennium Volume*. Geological Society, London, Memoir 20:121-130.

Caslin, E. 2002. Maturity evaluation of the interval 1519m-4271m in the 6004/16-1,1z well, offshore Faroe Islands. *Robertson Report* # 8577/Ic: 1-45.

Cawley, S., Matheson, H. and Stalker, G. 2005. An Updated View of the Faroe-Shetland Petroleum System. *In*: Ziska, Varming and Bloch (eds.) *Faroe Islands Exploration Conference: Proceedings of the 1st Conference*. Annales Societatis Scientiarum Færoensis, Supplementum 43, Tórshavn: 109-130.

Clarke, B.J. 2002. Early Cenozoic denudation of the British Isles: a quantitative stratigraphic approach. Ph.D dissertation, University of Cambridge, UK.

Cooper, M.M., Evans, A.C., Lynch, D.J., Neville, G. and Newley, T. 1999. The Foinaven Field: managing reservoir development uncertainty prior to start-up. *In*: Fleet, A.J. and Boldy, S.A.R. (eds.) *Petroleum Geology of Northwest Europe: Proceedings of the 5th Conference*, Geological Society, London: 675-682.

Ebdon, C.C., Granger, P.G., Johnson, H. and Evans, A.M. 1995. Early Tertiary evolution and sequence stratigraphy of the Faeroe-Shetland Basin: implications for hydrocarbon prospectivity. *In*: Scrutton, R.A., Stoker, M.S., Shimmield, G.B., and Tudhope, A.W. (eds) (1995) T*he Tectonics, Sedimentation and Palaeoceanography of the North Atlantic Region*. Geological Society, London, Special Publications 90: 51-69.

Green, P.F. 2002. Thermal history reconstruction in offshore Faroes well 6004/16-1, using AFTA and Vitrinite Reflectance. *Geotrack Report* #832: 1-131.

Ichron Limited. 2001. A Biostratigraphical Evaluation of the Statoil 6005/15-1. Longan well, East of the Faroe Islands. Ref: 01/407/B: 1-23.

Jolley, D.W. 2002. Biostratigraphy, ecology and phytogeographic evidence for sediment provenance. A Palynological study of the late Palaeocene to early Eocene interval in Statoil 6005/15-1 well, Faroe-Shetland Basin. Report: 1-80.

Jolley, D.W., Morton, A. and Prince, I. 2005. Volcanogenic impact on phytogeography and sediment dispersal patterns in the NE Atlantic. *In*: Doré, A.G. and Vining, B.A.(eds.) *Petroleum Geology: North-West Europe and Global Perspectives – Proceedings of the 6th Petroleum Conference*. Geological Society, London: 969-975.

Jones, S.M., White, N., Clarke, B.J., Rowley, E. and

Gallagher, K. 2002. Present and past influence of the Iceland Plume on sedimentation. *In*: Doré, A.G., Cartwright, J.A., Stoker, M.S., Turner, J.P. and White, N. (eds.) *Exhumation of the North Atlantic Margin: Timing, Mechanisms and Implications for Petroleum Exploration*. Geological Society, London, Special Publications 196: 13-25.

Knox, R.W.O'B. and Holloway, S. 1992. 1. Paleogene of the Central and Northern North Sea. *In*: Knox, R.W.O'B. and Cordey, W.G. (eds) *Lithostratigraphic nomenclature of the UK North Sea*. British Geological Survey, Nottingham: 5 - 127.

Lamers, E., and Carmichael, S.M.M. 1999. The Paleocene deepwater sandstone play West of Shetland. *In*: Fleet, A.J. and Boldy, S.A.R. (eds.) *Petroleum Geology of Northwest Europe: Proceedings of the 5th Conference*, Geological Society, London: 645-659.

Larsen, M., Hamberg, L., Olaussen, S., Preuss, T. and Stemmerik, L. 1999. Sandstone wedges of the Cretaceous-Lower Tertiary Kangerlussuaq Basin, East Greenland – outcrop analogues to the offshore North Atlantic. *In*: Fleet, A.J. and Boldy, S.A.R. (eds.) *Petroleum Geology of Northwest Europe: Proceedings of the 5th Conference*, Geological Society, London: 337-348.

Larsen, M. and Whitham, A.G. 2005. Evidence for a major sediment input point into the Faroe-Shetland Basin from the Kangerlussuaq region of southern East Greenland. *In*: Doré, A.G. and Vining, B.A. (eds.) *Petroleum Geology: North West Europe and Global Perspectives: Proceedings of the 6th Petroleum Geology Conference*. Geological Society, London: 913-922.

Leach, H.M., Herbert, N., Los, A. and Smith, R.L. 1999. The Schiehallion development. *In*: Fleet, A.J. and Boldy, S.A.R. (eds.) *Petroleum Geology of Northwest Europe: Proceedings of the 5th Conference*, Geological Society, London: 683-692.

Linnard, S. and Nelson, R. 2005. Effects of Tertiary Volcanism and later Events upon the Faroese Hydrocarbon System. *In*: Ziska, Varming and Bloch (eds.) *Faroe Islands Exploration Conference: Proceedings of the 1st Conference*. Annales Societatis Scientiarum Færoensis, Supplementum 43, Tórshavn: 44-53.

Lucas, P.M. and Metters, S.J. 2002a. Well 6004/16-1z offshore Faroes, core and spectral gamma correlation study, Paleocene T10-T22. *Robertson Report* # 8537/Id: 1-153.

Lucas, P.M. and Metters, S.J. 2002b. Well 6004/16-1z offshore Faroes, core and spectral gamma correlation study, Paleocene T25-T36. *Robertson Report* # 8522/Id: 1-99.

Mahdi, S.A. 2002. Well 6004/16-1 & 1Z: Biostratigraphy of the intervals (1) 1492m-2259m TD and (1Z) 2354m-4274m TD. *Robertson Report* #B-671: 1-29.

Morton, A.C. and Hallsworth, C. 2002a. Heavy mineral data from Well 6005/15-1, Faeroes sector, Faeroe-Shetland Basin. HM Research Associates Report HMRA/02/07: 1-7.

Morton, A.C. and Hallsworth, C. 2002b. Heavy mineral data from Well 6004/12-1 and 1Z, Faeroes sector, Faeroe-Shetland Basin. HM Research Associates Report HMRA/02/11: 1-13.

Morton, A.C. and Hallsworth, C. 2002c. Heavy mineral data from Well 6004/16-1 and .1Z, Faeroes sector, Faeroe-Shetland Basin. HM Research Associates Report HMRA/02/19: 1-11.

Morton, A.C. and Hallsworth, C. 2002d. Provenance of Paleocene sandstones in the Faroes sector and adjacent areas of the NE Atlantic: heavy mineral constraints. HM Research Associates Report HMRA/02/24: 1-15.

Naylor, P.H., Bell, B.R., Jolley, D.W., Durnall, P. and Fredsted, R. 1999. Palaeogene magmatism in the Faeroe-Shetland Basin: influences on uplift history and sedimentation. *In*: Fleet, A.J. and Boldy, S.A.R. (eds.) *Petroleum Geology of Northwest Europe: Proceedings of the 5th Conference*, Geological Society, London: 545-558.

Peters, K.E., Walters, C.C. and Moldowan, J.M**.** 2005. The Biomarker Guide. Cambridge University Press, New York: 1-1132.

Saunders, A.D., Fitton, J.G., Kerr, A.C., Norry, M.J. and Kent, R.W. 1997. The North Atlantic Igneous Province. *In*: Mahoney, J.J. and Coffin, M.F. (eds.) Large Igneous Provinces: Continental, Oceanic and Planetary Flood Volcanism. *Geophys. Monogr*. 100: 45-93

Scotchman, I.C., Griffith, C.E., Holmes, A.J. and Jones, D.M. 1998. The Jurassic petroleum system north and west of Britain: a geochemical oil-source correlation study. *Organic Geochemistry* 29: 671-700.

Smallwood, J.R. 2005. Quality, Distribution and Provenance of Paleocene Sediments in the Faroe-Shetland Area. *In*: Ziska, Varming and Bloch (eds.) *Faroe Islands Exploration Conference: Proceedings of the 1st Conference*. Annales Societatis Scientiarum Færoensis, Supplementum 43, Tórshavn: 82-95.

Smallwood, J.R. and Kirk, W.J. 2005. Exploration in the Faroe-Shetland Channel: Disappointments and Discoveries. *In*: Doré, A.G. and Vining, B. (eds.) *Petroleum Geology: North West Europe and Global Perspectives: Proceedings of the 6th Petroleum Geology Conference*. Geological Society, London: 977-991.

Smallwood, J.R. and Harding, A. This issue. New seismic imaging methods, dating, intrusion style and effects of sills: A drilled example from the Faroe Islands. *In*: Varming, T. and Ziska, H. (eds.) *Faroe Islands Exploration Conference: Proceedings from the 2nd Conference*.

Turner, J.D. and Scrutton, R.A. 1993. Subsidence patterns in western margin basins: evidence from the

Faroe-Shetland Basin. *In*: Parker, J.R. (ed.) *Petroleum Geology of Northwest Europe: Proceedings of the 4th Conference*. Geological Society, London: 975-983.

Waddams, P. and Cordingley, T. 1999. The regional geology and exploration potential of the NE Rockall Basin. *In*: Fleet, A.J. and Boldy, S.A.R. (eds.) *Petroleum Geology of Northwest Europe: Proceedings of the 5th Conference*, Geological Society, London: 379-390.

Woodfin, M, Seedhouse, J, Spadini, G. and Cardamone, M. 2005. Elastic Impedance Inversion to aid Lithology Prediction in the Palaeocene of the Judd Sub-Basin. *In*: Ziska, Varming and Bloch (eds.) *Faroe Islands Exploration Conference: Proceedings of the 1st Conference*. Annales Societatis Scientiarum Færoensis, Supplementum 43, Tórshavn: 54-69.

Ziska, H. and Andersen, C. 2005. Exploration Opportunities in the Faroe Islands. *In*: Ziska, Varming and Bloch (eds.) *Faroe Islands Exploration Conference: Proceedings of the 1st Conference*. Annales Societatis Scientiarum Færoensis, Supplementum 43, Tórshavn: 146-162.

Log responses in basalt successions in 8 wells from the Faroe-Shetland Channel – a classification scheme for interpretation of geophysical logs and case studies

MORTEN SPARRE ANDERSEN[1, 2 *], LARS OLE BOLDREEL[3] AND THE SEIFABA GROUP[4]

[1] Faculty of Science and Technology, University of Faroe Islands, Noatún 3, Box 2159, FO-165
[2] Geological Survey of Denmark and Greenland, Østervold Gade 10, DK-1350 (e-mail msa@geus.dk)
[3] University of Copenhagen, Department of Geography & Geology, Østervold Gade 10, DK-1350
[4] See Acknowledgements for full list of members
Robert S. White, Giovanni Bais (Cambridge University), Michael Worthington, Felicia Shaw (Oxford University) Uni K. Petersen (University of the Faroe Islands) Peter Japsen, Regin Waagstein (GEUS) Lars Gommesen (ØDS), Garry Mavko (Stanford)

ABSTRACT

Sub-basalt petroleum plays are becoming significant in the Faroe Region and even effort are put on recognizing basaltic successions with intervals of reservoir quality. However, only few studies have been made of wireline data from exploration wells penetrating basalt successions although detailed understanding of the physical properties of basalt successions are important for seismic processing and imaging, interpretation of the geological evolution and well planning. Basaltic successions of various thicknesses and characters have been penetrated in exploration wells in the British sector of the Faroe-Shetland Channel and around the Northeast Rockall Basin. The wireline logs through basaltic successions in eight released wells were selected for a systematic study of the log-response of basaltic rocks in this region. Physical properties recorded by wireline logs show pronounced variation of similar or broader ranges than in most sediment systems. Based on overall log character five distinct classes of basaltic units are distinguished: *simple lava beds*, *compound lava units*, *volcaniclastic units*, *hyaloclastic units* and *hypabyssal intrusives*.

Further characterisation of the individual basaltic unit is carried out using a characteristic trend/pattern or value found on one or more log traces throughout a unit, within a part of a unit or across the boundary between two units. In general terms log characteristics in basaltic successions may be thought of as equivalent to intrafacies components.

The log characteristics used in this study are selected in such a way that they are as far as possible considered diagnostic of typical lava morphological features of basaltic eruptives.

In the studied wells, the classification and characterisation of log responses allow a description of the eruptive style and the environment of lava emplacement, which is in good agreement with descriptions based on palynological and petrological investigations of the successions.

Introduction

In situ properties of basalt measured by downhole logging tools vary in a complex manner. The normal ranges for many commonly logged properties (e.g. neutron porosity, sonic transit time, and resistivity) are as wide in basalts as in sediments. To illustrate this, the variation of sonic velocity in basaltic rocks from the eight wells studied in this paper is presented in Table 1. Using log data, distinction can be made between hypabyssal intrusions, deep-water pillow basalt successions, volcaniclastic successions and flood basalt succes-

Faroe Islands Exploration Conference: Proceedings of the 2nd Conference.
Annales Societatis Scientiarum Færoensis, Supplementum 50, 2009: 364-391

sions; and within flood basalt successions, individual lava flows (or flow units) have been recognised (e.g. Planke, 1994; Boldreel, 2006). However, only few attempts have been made utilising log data to study the geological character of basalt successions (e.g. Planke, 1994; Helm-Clark *et al*., 2004; Boldreel, 2006). Until now, log data have not been used for detailed analysis of emplacement mode and the physical environment of emplacement. However, in recent years sub-basalt plays have become of interest to the petroleum-industry in the Faeroe-Shetland region, and in this region several wells have already been drilled through basaltic succession of various thickness (e.g. Archer *et al*., 2005), and more are expected in the future.

In this paper, we review aspects of lava morphology of possible significance for interpretation of wireline logs available to the present study. Following this, we propose an interpretation scheme by which the mode of emplacements and the physical environments of basalts encountered in boreholes may be analysed efficiently using log data. The database used to derive this classification comprises wireline logs from eight boreholes through basaltic succession in the Faroe-Shetland region (Fig. 1). Completion reports with mud-loggers' descriptions of cuttings and sidewall cores were available for seven of the boreholes. Finally case stories are presented illustrating the application of the interpretation scheme using the same eight wells.

Regional setting

The Faeroe-Shetland Region is situated in the central segment of the North Atlantic Igneous Province (Fig. 1). The province comprises a volume of at least 1.8 x 10^6 km^3 of Cenozoic flood basalts spread over an area of ca. 1.3 x 10^6 km^2. Added to this is an even larger volume of deep-seated and hypabyssal intrusions (White and McKenzie, 1989; Eldholm and Grue, 1994). Large constructive escarpments (i.e. Faroe-Shetland and Geikie escarpments) with associated progradational reflector packages are thought to have formed when sub-aerial basalt flows entered into water (e.g. Smythe *et al*., 1983; Andersen, 1988; Kiørboe, 1999). On the landward side of the escarpment, successions of parallel reflectors and transparent successions are suggested to represent sub-aerial basalt flows (e.g. Andersen, 1988). Wide-angle seismic experiments indicate that the thickness of flood basalts under the Faroe Islands is ca. 5-6 km which decreases eastward (Richardson *et al*., 1998). Below the eastern part of the Faeroes shelf about 1-2 km of basalt is present above a low velocity layer, possibly 2 km thick, presumably composed of a sediment succession (Richardson *et al*., 1999). This sediment succession can be traced into the eastern part of the Faroe-Shetland Channel, where basalts are absent. Here the sediments is comprised by a thick succession of late Palaeozoic, early Mesozoic and Cretaceous sediments deposited in response to several Mesozoic rift phases (Hitchen and Ritchie, 1987) and of Lower Paleocene sediments including deep-water fans deposited in response to uplift of Shetland and Scotland (e.g. White and Lowell, 1997). Especially the Lower Paleocene is prospective with relation to hydrocarbon (e.g. Lamers and Carmichael, 1999). Interpretation of seismic reflection profiles

	N	N*	Mean	Median	St.d.	Min.	Max.
Simple lava beds	5309	5309	5135	5349	707	3198	6063
Compound lava units	4690	4332	3902	3840	964	1698	6026
Volcaniclastic units	31792	31654	3542	3633	392	1273	4623
Hyaloclastic units	906	906	4066	3991	367	3412	5120
Hypabyssal intrusive units	2662	2110	5624	5877	732	3321	7327
All data	45697	44649	3882	3655	842	1273	7327

Table 1. Some statistical parameters for distribution of sonic velocities (m/s) in basaltic rocks from 8 wells in the Faeroe-Shetland Channel. N is the total number of log samples (spaced by 15.24 cm), N* refers to the number of samples after exclusion of samples in well sections with excessive caving that is where caliper (CAL) more than 50 mm larger than bitsize (BSZ).

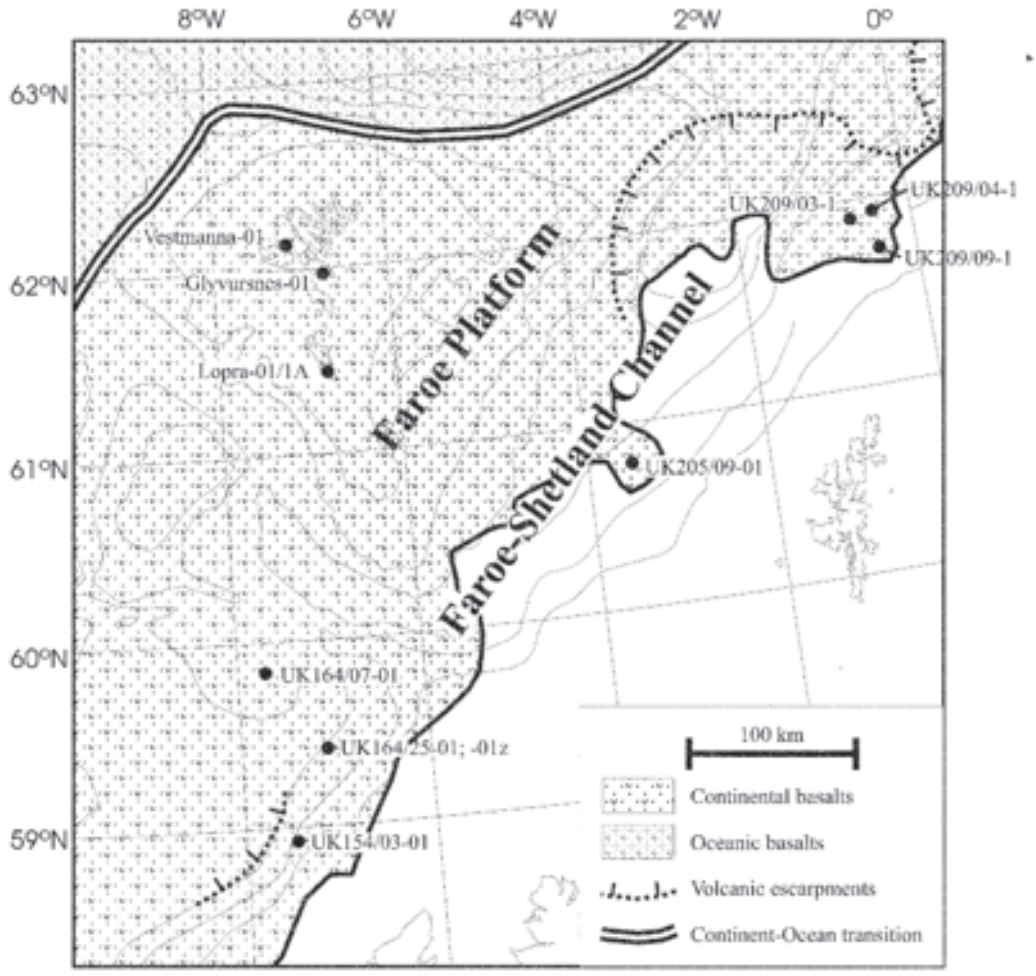

Figure 1. The approximate extent of early Paleogene basalt around the Faeroe-Shetland Channel. The location of wells used in this study and three research wells on the Faeroe Islands are shown as black dots (modified from White and McKenzie 1989; Andersen *et al*., 2002).

indicates lateral and vertical facies changes within the flood basalts (Gatliff *et al*., 1984; Andersen, 1988; Kiørboe, 1999). Sediments covered by less than 2 km of basalt are found within a ca. 100 km wide zone east of the edge of the basalt. This area covers approximately 20 000 km^2. The downhole logging data used for this study are all from exploration wells drilled within this zone, where the petroleum industry for some years have been engaged in exploration for sub-basalt petroleum accumulations.

Lava morphology and log interpretation of basaltic rocks

Studies of lava morphology in active volcanic provinces and fossil flood basalt provinces have provided a wealth of data relating to properties of basaltic lava flows and how these properties are influenced by the environment in which the lava is emplaced (e.g. Keszthelyi *et al*., 1999). It is possible to characterise fossil basaltic flows and interbedded volcaniclastic material using a number of distinguishing features, which on surface mapping can be observed on exposures of lava flows.

Unit class:	phh	aa	slphh	rphh	scale
Characteristic:					
Breccia flow top	-1	1	1	1	~0.5-5m
Breccia flow base	-1	1	1	0	~0.1-0.5m
Spinose aa clinker	-1	1	1	-1	<0.1m
Angular vesicles	-1	1	0	1	N.A.
Entrained clasts	-1	1	1	1	N.A.
Core pushing into breccia	0	1	1	1	~0.1-0.5m
Slabs in breccia	0	-1	1	1	~0.1-0.5m
Welding in basal breccia	0	-1	0	0	<0.1
Intact pahoehoe lobes in breccia	0	-1	-1	1	N.A.
Fragmented pahoehoe lobes	0	-1	-1	1	N.A.
Jigsaw-fit clasts in breccia	0	-1	0	0	N.A.
Sediment infill in breccia	0	0	0	0	<0.1m
Pseudopeperite texture	0	0	0	0	N.A.
Pahoehoe flow top	0	0	0	0	N.A.
Pahoehoe flow base	0	0	0	0	N.A.
Pahoehoe lobes (intact)	1	-1	0	1	N.A.
Glassy chill crust	1	-1	1	1	N.A.
Coherent upper vesicular crust	1	-1	-1	1	~0.5-5m
Coherent lower vesicular crust	1	-1	-1	1	~0.1-0.5m
Round vesicles	1	-1	0	1	N.A.
Horizontal vesicle sheet	1	0	0	0	<0.1m

Table 2. Idealised lava classification scheme (modified from Keszthelyi, 2002). The possible presence or absence of a characteristic in the four classes of flow units is indicated by 1 or -1 respectively. A null indicates the characteristic may or may not be observed in the flow class.aa = a'a, phh = pahoehoe, slphh = slab pahoehoe, rphh = rubbly pahoehoe, scale = approximate vertical scale of feature if applicable to well logs.

From these observations the mode of emplacement and the physical environment of emplacement may be estimated, at least qualitatively (e.g. Lyle, 2000; Single and Jerram, 2004). Distinguishing characteristics observed on surface exposures are generally two or three dimensional, and their lateral size are frequently in the decimetre scale or larger. Many features of significance during surface mapping are therefore generally difficult to observe in drill cores (that are of limited lateral extent), sidewall cores or cuttings. However, using a few selected criteria (Table 2) cores may be interpreted in a way that provides information comparable to that obtained on surface mapping (Keszthelyi, 2002).

In exploration wells, cores are generally recovered in potential reservoir intervals only, and penetrated basaltic successions are generally not cored. Cuttings and sidewall cores may provide lithological information about the intervals of exploration wells, where no cores are retrieved, but description of these intervals rely to a large extent on interpretation of downhole logs. As mentioned above the characteristic features used in surface mapping and core description (e.g. Table 2) are seldom of a scale suitable to study by conventional downhole logs. In addition some features of basaltic rocks, which are of a scale suitable to study by logs, may not all be distinguished

Logging in boreholes offers systematic closely spaced measurements of a number of properties throughout all of the penetrated succession. The close spacing of measurements throughout the succession compensates, to some degree, for the lack of resolution and the one-dimensionality of the observations. In boreholes drilled for petroleum exploration properties like neutron porosity (NPHI), sonic velocity (VP), bulk density (RHOB), various resistivity logs (MSFL, LLS, LLD, SFLU, ILM, ILD), natural gamma radiation (GR) and frequently spectral gamma radiation (providing measurements on the concentration of K, Th and U) are acquired on a routine basis. Usually the sample interval is 15.24 cm (6 inches). However, the actual readings of the logging tools represent weighted averages of the properties

Parameter	Acronymn	Symbol	Units	Application	Res. [1m	DoP[2m
Porosity	NPHI[3	ΦN	LPU[4	Porosit	0.5	0.2
Sonic velocity	VP (DT[5])	VP	m/s	and	0.5	0.1
Bulk density	RHOB	ρB	kg/m^3	lithology	0.3	0.2
Resistivity	MSFL[6	R_{MSFL}	Ωm	Fluids,		
	SFLU[7	R_{SFLU}	Ωm	invasion	0.75	0.6
	LLS[8	R_{LLS}	Ωm	(and		
	LLD[9	R_{LLD}	Ωm	lithology)		
	ILM[10	R_{ILM}	Ωm			
	ILD[11	R_{ILD}	Ωm			
Photoelectric effect	PEF		Ωm	Lithology	0.3	0.2
Gamma radiation	GR	γ	GAPI[12		0.5	0.3
Spectral gamma	K	K	%			
	Th	Th	ppm			
	U	U	ppm			

Table 3. Typical resolution of some wireline logs used in this study.

Notes: [1 Typical values for vertical resolution (m). [2 Typical values for depth of penetration into formation (m). [3 NPHI log actually measures hydrogen index, which is converted to LPU during recording. [4 LPU: Limestone porosity units, porosity in percent with reference to a limestone framework. [5 Sonic velocity is generally recorded as sonic transit time (DT, measured in μs/f), [6 MSFL Micro Spheric Focused Log [7 SFLU: Spheric Focused Log, [8 LLS: Short penetration Laterolog, [9 LLD: Long penetration Laterolog, [10 Medium penetration Induction Log, [11 Deep penetration Induction Log, [12 API gamma radiation units.

within a volume of rock around the borehole (e.g. Hearst *et al*., 1999). True vertical resolution and depth of investigation depend on the property measured, borehole conditions and the tool used (Table 3). Petroleum exploration boreholes penetrating basaltic successions thus provide closely spaced measurements along near vertical profiles, which may be used to characterise the penetrated basalt successions (e.g. Planke, 1994; Helm-Clark *et al*., 2004; Boldreel, 2006). In a later section of this paper we present a scheme for log characterisation of individual units in basaltic successions.

Previous studies of log response from wells in the Northeast Atlantic Volcanic Province

Studies of basalt successions penetrated in exploration and research wells have been published over the last few decades (e.g. Hald and Waagstein, 1984; Keszthelyi, 2002), and downhole logging may contribute to the characterisation of the drilled basalt successions (e.g. Nielsen *et al*., 1984; Buckley and Oliver, 1990; Planke, 1994; Delius, 1995; Boldreel, 2006). The DSDP (Deep Sea Drilling Program), ODP (Ocean Drilling Program) wells form a database of special importance. These wells, are drilled in offshore volcanic successions around the world, are fully cored, and many of them have been extensively logged. The DSDP and ODP wells form the backbone of most recent comprehensive studies of the physical properties of basalts (e.g. Bartetzko *et al*., 2005). The ODP well 642E (Planke, 1994) is presently the most important reference well concerning physical properties and core-log correlation of the extrusive successions of volcanic passive margins. It is drilled into the distal part of the seaward dipping reflector sequence on Vøring Margin, West of Norway. Another important reference well is the Lopra-1/1A well on the Faroe Island (Fig.1; Hald and Waagstein, 1984; Nielsen *et al*., 1984; Kiørboe and Petersen, 1995; Boldreel, 2006; Christie *et al*., 2006). It was drilled to 2167 m (below sea-level) in 1981 and deepened to 3565 m in 1996. It penetrates the Faeroe Lower Basalt Series (base at ca. 2425 m; Ellis *et al*., 2002). A hyaloclastic succession, the Lopra Sequence (Ellis *et al*., 2002; Waagstein,

2006) comprises the lower ca. 1100 m of the well. A fairly complete log-suite was obtained during the deepening of the well. The Lopra 1/1A well is only cored for short intervals but numerous cuttings are available and described in detail (Hald and Waagstein, 1984).

ODP 642E, Vøring Plateau, Norwegian Sea

The ODP well 642E penetrated a ca. 1000 m thick basalt succession. A cyclic log response from basaltic lava flows was observed on the three porosity sensitive logs, neutron porosity (NPHI), γ-γ bulk density (RHOB) and seismic velocity (VP) in a study of wireline logs from ODP well 642E (Planke, 1994). The neutron porosity from ODP642E was processed using an algorithm designed specifically for basaltic rocks (Broglia and Ellis, 1990). In an up to 7 m thick zone below the top of lava beds the neutron porosity decreases (from 0-5 to ca. 50 LPU) while bulk density and seismic velocity increase (ρ_B from ca. 2.2 to max 2.9 g/cm^3; V_P from ca. 3 to max 6 km/s). At the base the neutron porosity increases abruptly within a ca. 1 m thick zone while density and seismic velocity decrease. In thick flows neutron porosity, bulk density and seismic velocity reach nearly constant plateaus in between the upper and lower gradient zone ($\Phi_N \approx 60$ LPU, $\rho_B \approx 2.9$ g/cm^3, $V_P \approx 6$ km/s).

At the base of each lava bed a high resistivities spike (typically in the range 100-1000 Ω) is obtained within the lower gradient zone with the spherically focused resistivity tool (Planke, 1994). Based on our experience artefacts are very common on most resistivity logs, when very large resistivity contrasts are encountered (see also Helm-Clark *et al*., 2004). Therefore we suggest that the R_{SFLU} spikes observed at the base of lava flows might be a shoulder effect caused by a large resistivity contrast at the interface between massive basalt beds and underlying sediments or porous basalt. Although spikes of this character, is a strong tool identifying the base of lava beds, it should be kept in mind that they do not necessarily represent true resistivity.

Correlation with the core allowed Planke (1994) to correlate the upper gradient zone in lava beds with gradually downward decreasing vesicularity. The central zone of lava beds is correlated with massive lava of low vesicularity and with few but large cracks, and the base is correlated with solid (massive?) basalt with few connected cracks. Using the SFLU log, the lower gradient zone is correlated with the (welded) base of flow units (see above).

Lopra-1, Faroe Islands

In Lopra-1/1A, the Faeroe Lower Basalt Series could be divided into units based on a cyclic appearance of the wireline logs showing the physical properties of rocks i.e. sonic (P-, S- and Stonely waves), density (RHOB), neutron porosity (NPHI), resistivity and caliper and in addition gamma-ray was used (Boldreel, 2006). Combining appropriately scaled density, neutron porosity and the two velocity log traces with gamma radiation volcaniclastic intercalations (sediments) were distinguished from lava flows. Based by analogy to the outcrops around the well site and detailed description of cuttings (Hald and Waagstein, 1984) two distinct classes of lava flows were identified, simple lava flows comparable to the lava flows in ODP 642E described by Planke (1994) and compound flow units with several thin (1-5 m) massive zones separated by zones of higher porosity. The massive parts of compound flow units are generally characterised by higher porosity and lower density and sonic velocity than the massive cores of simple lava flows. A further subdivision of simple flows into three parts, a porous crust, a massive core and a thin, porous basal zone is generally apparent, where the basal zone may be absent or thinner than the resolution of the logs (Boldreel, 2006). The log response of lava flows in Lopra-1 are variable and many depart significantly from the log response in ODP 642E described by Planke (1996), and it was suggested that the detailed log response of simple lava flows reflects lava morphology (Boldreel, 2006). Based on abrupt changes in the thorium concentration, measured with the spectral gamma log, lava flows could be grouped into a number of distinct "super units", which is suggested to represent flow fields (Boldreel, 2006).

Well	154/03-1	164/25-1	164/25-1z	205/09-1	209/03-1	209/04-1	209/09-1	164/07-1
Depth range (m)	1184.4-2096.6	1831.9-2818.8	1831.1-3432.1	2619.6-2764.7	1244.2-1735.0	1637.5-2636.1	1172.6-2280.8	2092.9-5089.3
Samples	5986	6476	10506	952	2976	6553	7272	19661
Porosity	NPHI	NPHI	NPHI	NPHI	NPHI	NPHI	NPHI	NPHI
Density	RHOB	RHOB	RHOB	RHOB	RHOB	RHOB	RHOB	RHOB
Velocity	VP	VP	VP	VP	VP	VP	VP	VP
Resistivity	RS, RD(1	MSFL, LLS,LLD ILM,ILD	MSFL, LLS,LLD ILM,ILD	ILM,ILD ILD	SFLU, ILM, ILD	RFOC, RD(1, ILD	SFLU, LLS,	LLS,
Gamma radiation	GR	GR,GRS	GR,GRS	GR,GRS	GR	GR,GRS	GR	GR
Element concentration	K,Th,U	K,Th,U	K,Th,U		K,TH,U		K,TH,U	
Photoelectric effect	PEF	PEF	PEF	PEF				PEF

Table 4. Data used in this study
Notes: (1 RS, RD and RFOC refer to short penetration, deep penetration and focused resistivity logs. Ideally these should give results comparable to short, deep laterolog and spherical focused log respectively.

Data from UK exploration wells

Wireline logs from 7 exploration wells from the eastern part of the Faroe-Shetland Channel and North Rockall Trough have been used for this study. The logs acquired in each well and used for this study are listed in Table 4, and the location of the wells is shown on Figure. 1.

One of the wells, UK164/25-01, was side-tracked above the top of the basaltic succession. The oldest of the investigated wells was logged in 1979 and the youngest in 1997. Several different contractors have been involved in acquisition of the logs. Overall, the acquired data are of similar (fair-good) quality. In all wells the quality of most logs deteriorates in caved intervals, where the true hole diameter exceeds the nominal diameter by more than approximately 50 millimetres. Due to large resistivity contrasts within the basalt succession shoulder effects and other artefacts are suspected on most resistivity logs except the MFSL logs, which are measured using pad mounted electrodes. In the basalt successions of UK209/04-01, the log measurements of the porosity sensitive parameters – neutron porosity, sonic transit time and bulk density – falls on trends clearly deviating from the trends in the other 7 wells. A similar observation is made regarding the sedimentary successions of this well. According to the logging report, tool calibrations were not optimal during logging of this well. It appears that the neutron porosity measurements were corrected using an unspecified algorithm. Neutron porosity data from UK209/04-01 is thus used qualitatively only. To avoid complications arising from imperfect gap compensation, which may be a serious problem (especially in bulk density data, as bulk density compensation are made using undocumented algorithms designed for carbonates and siliciclastic rocks), we have decided to omit all samples where the caving exceeds 50 mm in statistical analyses. This reduces the database by approximately 2.3 % (Table. 1). After picking of bed boundaries, each unit within the volcanic succession in the wells was screened manually, and obvious outliers were flagged. We expect that most of the variability of the early Palaeogene basalts of the Faroe-Shetland Channel is represented by the database we have produced.

Classification of basaltic rocks using downhole logs

Our approach to interpret logs through basaltic successions builds on the experience obtained in previous work (e.g. Nielsen *et al*., 1984; Buckley and Oliver, 1990; Planke, 1994; Helm-Clark *et al*.,

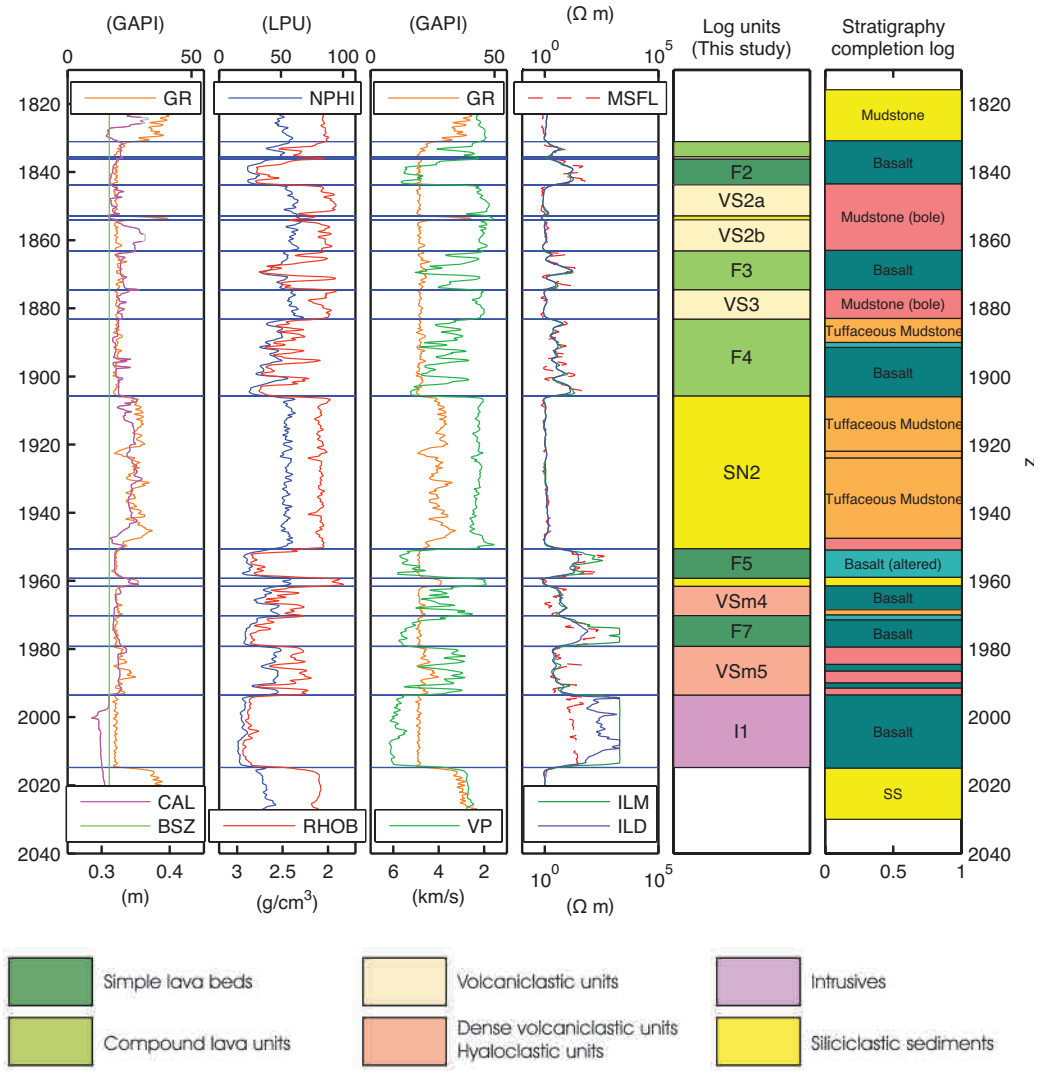

Figure 2. Log interpretation of the volcanic succession in well 164/25-1z. Prefix "F" refers to simple lava beds and compound lava bed, "VS" to volcaniclastic units, "I" to intrusive units and "SN" to siliciclastic units. Description of acronyms for the shown log traces can be found in table 3. For comparison the interpretation from the well completion report is shown in the panel furthest to the right. Vertical scale, 1:2000. Colour coding of the log units is shown below the log panels and refers also to the following log panels.

2004; Boldreel, 2006). First we obtain a sub-division of the basaltic successions into main units using all available data including mud-loggers descriptions of cuttings and sidewall cores (Boldreel, 2006). Based on features typical of each logunit, these may be correlated loosely to lava morphological classes (e.g. Nicholls, 1936; Keszthelyi *et al*., 1999; Keszthelyi, 2002).

The basaltic log units in our classification scheme corresponds with the following lava morphological classes of *simple lava beds*, *compound lava units*, *volcaniclastic units*, *hyaloclastic units*, and *hypabyssal intrusive units*. For enhanced studies on environmental, volcanologic and geody-

namic changes during emplacement of the basalt succession, a more detailed characterisation of the individual units in the basaltic succession is necessary. We define log response characteristics for this purpose. By log response characteristics we mean a characteristic trend/pattern or value found on one or more log traces throughout a unit, within a part of a unit or across the boundary between two units.

1 Picking of basalt units

Using the cross over technique applied to the NPHI and RHOB logs as described by Boldreel (2006), combined with the GR/GRS log this technique was used for preliminary identification of basalt successions in the wells. The agreement with identification based on cutting descriptions is good (Fig.2). All available logs were used to identify individual units within the volcanic succession. Below we describe the general characteristics of the defined basaltic units

1.1 Simple lava beds

On all porosity sensitive log traces simple lava beds are characterised by a distinct asymmetric cyclic log response (Fig. 3). Neutron porosity decreases while density and velocities increase from the upper boundary of the unit towards the core. At the base of the flow porosity increases while density and velocities decrease. Gamma radiation is nearly constant or decreasing slightly downwards throughout the simple lava beds. A positive radiation anomaly may occur at the top of the bed (Fig. 5), but is not ubiquitous. Resitivity logs follows neutron porosity in a qualitative way. In a large number of simple lava flows a separation between the deep and the shallow resistivity is found where the shallow reads higher values than the deep. For induction logs a separation is also seen. However, for tools that not are pad mounted, measured values of resitivity may not be representative of the formation. Helm-Clark *et al.* (2004) recommend that laterologs and induction logs be used with great caution in basaltic successions. In lava beds thicker than about 4 m, distinct asymmetry is generally observed. The absolute gradient, | property/ z|, in the upper part of the unit is less than in the lower part, and the boundary to the underlying unit generally is very sharp (e.g. Planke, 1994; Delius *et. al*., 1995). In the investigated wells the thickest simple lava beds are about 35 m thick, while simple lava beds thinner than 4-5 m are rarely identified. In beds thicker than about 6-8 m an interval with relatively constant properties occur in the core of the unit (Fig. 2). Generally, average density and velocity of thick beds is higher than in thin beds (Fig. 4). Similar observations were made in ODP 642E (Planke, 1994) and in flow units from the Columbia River Basalts (Thodarson and Self, 1998). Planke (1994) suggested that the reason for this is that the lava in flows thinner than about 6 m solidified before all air bubbles had escaped to the upper crust.

A log unit of this class is expected to represent a single flow unit (flow lobe) in the lava morphological sense (Nichols, 1936; Keszthelyi *et al*., 1999). We use the term lava bed because log data do not allow identification of the glassy margins, which surround flow units (Keszthelyi *et al*., 1999). Although we believe this to happen very rarely, it is possible that a log unit interpreted as a simple lava bed actually is comprised by more than one flow unit.

1.2 Hyaloclastic units

In this study the term 'hyalocalstic unit' is used for a class of log units seen in the exploration well UK154/03-01 (Fig.2), which on seismic data is characterised by steeply dipping (20-30°) internal reflectors and thus interpreted as a lava foreset breccia composed dominantly of hyaloclastic basalt (Mushgrove and Michener, 1996; Japsen *et al*., 2005). The hyaloclastic units are characterised by porosity fluctuations of a magnitude of ca. 10 LPU with a period around 10-20 m reflected in all the porosity sensitive logs (Fig. 6). Overall the porosity is slightly higher and the velocity lower than in most volcanoclastic units (Table 1). Careful analysis of the logs (Fig. 6) and cross plots reveals that each hyaloclastic unit rather than being a homogeneous unit characterised by simple correlated fluctuation of properties is composed of a number of intervals each characterised by a distinct property distribution. Hyaloclastic units are thus likely to represent the equivalent of several

flow fields. This is in accordance with observations made from seismic data (Andersen *et al*., 1997; Japsen *et al*., 2005).

We consider the log response observed in the hyaloclastic units in UK154/03-1 as representative of lava foreset breccias (lava deltas, Planke *et al*.,1999), which are a common component of some flood basalt provinces (e.g. Jones and Nelson, 1970; Smythe *et al*., 1983; Gatliff *et al*., 1984; Pedersen, 1985; Planke, 1994). In the context of this paper the term 'hyaloclastic unit' is reserved for thick hyaloclastic units similar to foreset breccias. We will later suggest that hyaloclastic rocks albeit on a smaller scale may be present both in simple lava beds and volcanoclastic units.

1.3 Hypabyssal intrusive units

Hypabyssal intrusive basaltic rocks are common in most of the wells investigated in this study. They are generally characterised by symmetric response on log traces (Figs. 2 and 7), low neutron porosity (ΦN<10-20 LPU), high density, velocities and resistivities ($V_P \approx$5-6 km/s; $\rho_B \approx$2.7-3.0 g/cm^3); R≈10-1000 Ωm), and gamma radiation in the same range as other basaltic rocks (generally below 30 GAPI). Hypabyssal intrusive rocks in the wells from the Faeroe-Shetland region are represented by the highest values of bulk density and seismic velocity observed on the log traces, especially if compared to the neutron porosity. If hypabyssal intrusive units intrude into siliciclastic rocks with high gamma radiation, their boundaries may be picked on sharp gamma deflections at the "top" and "base". However, as with eruptive basaltic rocks a combination of seismic velocity, density and neutron porosity is also recommended to identify hypabyssal units. Velocity, density and resistivity anomalies may frequently be observed in the wallrock above and below sills and are attributed to contact metamorphosis (Planke *et al*., 1999; Smallwood and Maresh, 2002). Dykes are frequently distinguished by a large apparent thickness resistivity signature. In addition the separation between medium and deep inductions logs tends to be of opposite sign in sills and dykes, presumably reflecting the orientation of columnar joints.

1.4 Compound lava units

A compound lava unit is composed of two or more simple lava beds as described above (e.g. Fig. 2, bed F3 and bed F4). Compound lava units are loosely equivalent to the term "compound flow units" as used by Boldreel (2002; 2006), and may be equivalent to compound flow units in a lava morphological sense (Keszthelyi *et al*., 1999). However, first of all a compound lava unit is a convenient way to classify a succession of thin alternating high and low porosity intervals. The individual lava beds in compound lava units are thin with thicknesses less than 5 m. High neutron porosities, low density and seismic velocities, indicative for volcanoclastic units, are rarely documented between individual beds within compound lava units. However, thin veneers of volcanoclastic sediments can not be identified using well logs, and it is assumed that volcanoclastic rocks may be present within compound flow units.

1.5 Volcaniclastic units

Compared to simple lava beds and compound lava units, volcaniclastic units are characterised by high neutron porosity values, while density, seismic velocities and resistivity measurements are low. The log response is quite variable, either blocky on all log traces (e.g. Fig. 2, units VS2a and VS2b), and/or frequently serrated. Less often we see uniformly changing log values on one or more log traces (e.g. Fig. 10). Natural gamma radiation is of the same magnitude or slightly higher than in simple lava beds and compound lava units from the same basalt succession. The level of gamma radiation and the character of the gamma radiation log response in volcaniclastic units may be used for further characterisation of the units. The properties measured by conventional logs are comparable to shaley sediments with low potassium content. Cutting descriptions is therefore important in order to distinguish volcaniclastic units from shaley siliciclastic units. It may also be difficult to distinguish volcaniclastic units from highly vesicular flow tops. Again the cutting descriptions may help. Volcaniclastic may represent either products of explosive volcanic eruptions or volcanic products which has been transported and re-emplaced by

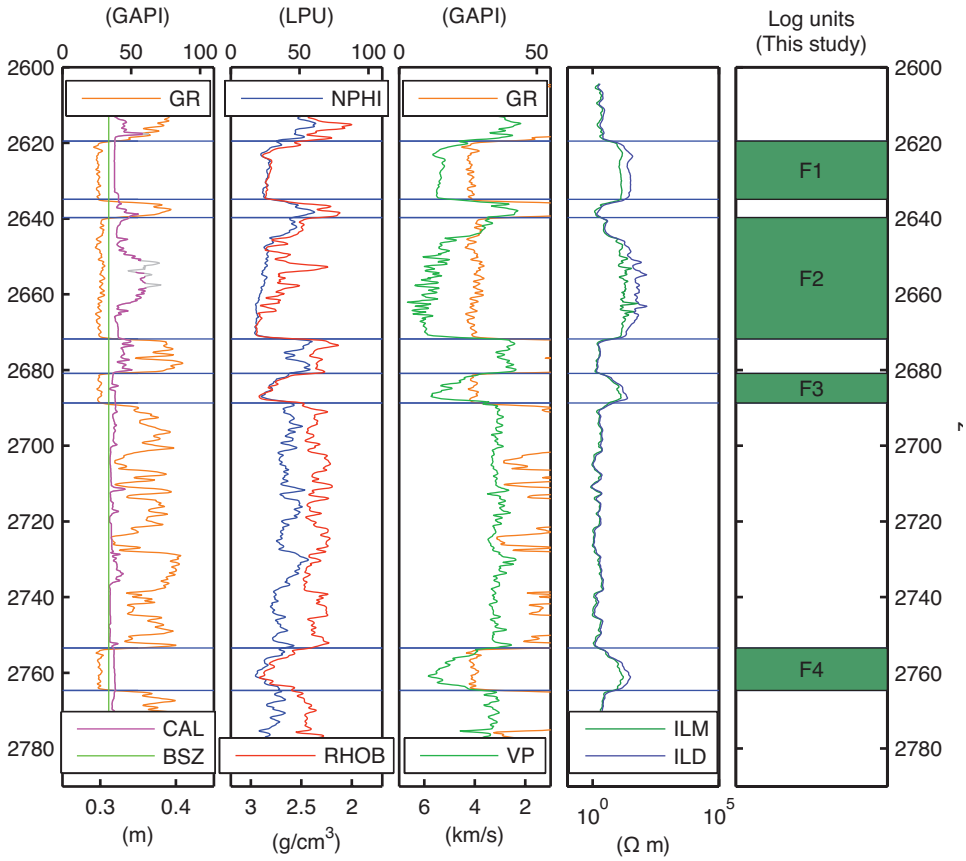

Figure 3. Log response of four simple lava beds identified in well 205/09-01. The lava beds are identical to those identified by Knott *et al*. 1997. Note the distinct difference of the porosity responses (seen on NPHI, RHOB and VP traces) between lava beds F4 and F3 on the one hand and F2 and F1 on the other hand. For colour coding of log interpretation see figure 2 . Description of acronyms for the log traces can be found in table 3. Grey colour on the caliper trace indicate intervals with caving in excess of 0.05 m. Logs are considered less reliable in these intervals. Vertical scale, 1:2000.

sedimentary processes. A detailed analysis of the log response may in some cases be used to indicate the emplacement style of individual units.

2 Intra-unit log shape classification

Log response have morphologic, stratigraphic or petrophysical importance. They are used to improve the characterisation of picked beds. In general terms log shapes in basaltic successions may be thought of as equivalent to intrafacies components (e.g. Single and Jerram, 2004) used for analysis of individual unit in exposed basaltic provinces and the characteristic features proposed by Keszthelyi (2002; Table 3) for analysis of cores through a basaltic succession.

2.1 Porosity responses

Neutron porosity, sonic velocity and bulk density measurements are all sensitive to the pore volume of the logged rock (e.g. Kern and Richter, 1979; Helm-Clark *et al*., 2004). Varying pore volume (vesicularity) within basaltic lava beds is therefore generally reflected by similar trends on porosity sensitive logs (e.g. Figs. 2, 3 and 7). It is the scale and style of variation that are important in identification of these components rather than the actual

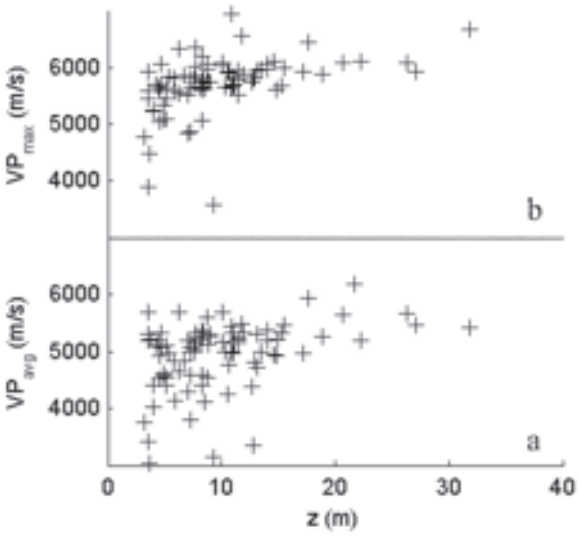

Figure 4. Vertical bed thickness versus seismic velocity of 96 simple lava beds thicker than 4 m. All data from wells in the Faeroe-Shetland Channel. **a**) Average sonic velocity. **b**) Maximum sonic velocity.

value of measurements. This is because hydrous alteration and burial affects also the neutron porosity, sonic velocity and bulk density of basalts (e.g. Boldreel and Andersen, 2006).

In basaltic lava beds the porosity sensitive logs are frequently characterised by gradually downward trends reflecting a gradual porosity decrease in the upper part of the bed, generally with downward decreasing gradient (Fig. 2). This is best observed in beds thicker than about 5 m. This response reflects a fairly continuous (at the resolution of the tool) downward decrease in vesicularity in the upper part of lava flows (Planke, 1994). Inflated pahoehoe lava flows are supposed to be characterised by this type of vesicle distribution.

A stepwise porosity decrease can be sometimes observed in the upper part of lavbed. An upper crust characterised by one or rarely two zones of relatively constant high porosity is seen in some lava beds (Fig. 3). Below the low porosity zone, which rarely is more than 4 m thick, the porosity dependent logs are deflected rather sharply towards low porosity values. This response represents flow tops of high fairly constant vesicularity, possibly "frothy" or brecciated upper crust, above massive core. In some situations it is difficult to distinguish a stepwise porosity decrease in the bed top from an overlying volcaniclastic unit. In these situations, gamma radiation anomalies may be a guide to localise unit boundaries and thus to distinguish stepwise porosity response in bed top from volcaniclastic units.

Many simple lava beds that are more than ca. 6 m thick are generally characterised by constant or slowly changing porosity in the core. The porosity minimum is mostly seen in the lower quarter of the bed (Fig. 3, compare beds F1 and F3). A near constant porosity response in the core is considered representative of lava cores, frequently with downward decreasing vesicularity (e.g. Planke, 1994).

A serrated response is frequently seen on the porosity sensitive log traces (including resistivity logs) in the upper part or throughout lava beds that are thicker than about 6 m (Fig. 5, bed F5). The excursions of the log trace are of an amplitude about 5-10 LPU (some times larger) on the neutron porosity log and of short period (<2 m). Generally the serrated response is characterised by an overall downward porosity decrease. Vertical fluctuation of porosity in the form of vesicle banding is common in basaltic lava flows, and could reflect multiple or stepwise inflation of pahoehoe lava flows (Keszthelyi *et al*., 1999). We suggest that serrated porosity responses in lava beds mostly reflect this vesicle banding. Multiple lava outbreaks in continuously fed lava flows may also be represented by a serrated porosity response.

Most basaltic lava beds investigated in this

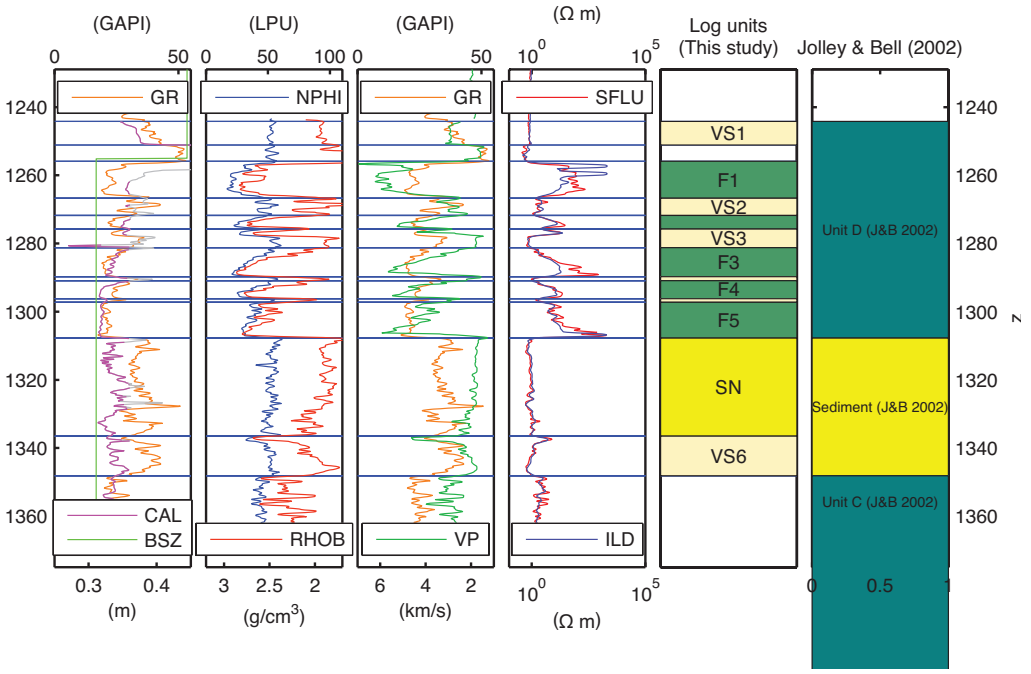

Figure 5. Log interpretation of upper part of the volcanic succession in well 209/03-1. Rightmost panel show stratigraphy according to Jolley and Bell (2002). At depths shallower than 1255 m casing and casing shoe interfere with measurements. Base of VS1 and top of F1 is thus not properly defined. Positive velocity anomaly in top of F1 may be caused by casing shoe. For colour coding of log interpretation see figure 2 . Description of acronyms for the log traces can be found in table 3. Vertical scale, 1:2000.

study are characterised by a narrow zone, ca. 0.5-1 m thick, of high porosity gradient at the base of the lava bed (Fig. 2). Within this zone neutron porosity decrease downward with about 30 LPU, density increase with about 0.5 g/cm^3 and P-wave velocity with about 1 km/s. Resistivity logs may show a similar response with downward resistivity increase of several decades.

On spherically focused resistivity log (SFLU) a narrow low resistivity spike is generally seen, which coincides approximately with the basal zone of the lava bed (Fig. 5). Planke (1994) suggested resistivity spikes of this character are caused by the massive basalt in a welded zone at the base of lava flows. We have observed log response of a similar character recorded with other multi-electrode resistivity tools (e.g. LLS and LLD) and induction tools. This response generally coincides with the base of lava beds as defined from neutron porosity, bulk density and sonic velocity (e.g. Fig. 5).

A zone of relatively high porosity, either nearly constant or continuously increasing downwards, is seen near the bottom of some lava beds (Fig. 3). This response represents a flow base with high vesicularity, possibly a rubbly or brecciated lower crust. A'a flows (especially of distal type) are characterised by a rubbly or brecciated lower crust. However, due to the thickness (>0.5m) of the high porosity bottom zone, we expect that gradational or stepwise porosity increase in the bed bottoms mostly represents hyaloclastic breccias or pillow palagonite complexes (Lyle, 2000), thus reflecting interaction with a wet sediment or emplacement in shallow aquatic environment rather than a'a flows in general.

2.2 Gamma trends and anomalies

The natural gamma radiation from massive basalts is usually less than 40 GAPI (e.g. Versey and Singh, 1989; Buckley and Oliver, 1990; Bartetzko *et al*., 2005). However, flow fields with anomalous

potassium and/or thorium concentrations may be used as stratigraphic markers that can be traced for tens of kilometres (e.g. Versey and Singh, 1989; Buckley and Oliver, 1990). Interbed sediments such as loess may be characterised by increased gamma radiation compared to lava beds and may also be used as stratigraphic markers (Helm-Clark *et al*., 2004). In this study stratigraphic application of gamma radiation anomalies has only been relevant correlating within the Erlend volcanic complex (between wells 209/03-1 and 209/04-1) and between wells 264/25-1 and 264/25-1z, which are less than 50 m apart. However, the response of gamma radiation logs (and spectral gamma radiation logs) may also be used to characterise volcanic products in a basaltic succession and the environment of emplacement.

Narrow positive gamma radiation anomalies about 10-20 GAPI higher than in the adjacent intervals is frequently seen in volcaniclastic sediments just above tops of lava beds (Fig. 11). For anomalies of this type post emplacement alteration (soil formation) is considered the most likely interpretation. In general positive gamma radiation anomalies may be considered to represent prolonged breaks in volcanic activity at the well location.

In many simple lava beds and in composite lava units the gamma radiation decreases downwards in the flow (Fig. 5). The gradient is generally very subtle, just discernible above the general scatter of gamma radiation measurements. In some cases gamma response of this type is correlated with porosity sensitive logs, notably the neutron porosity log. Frequently, a distinct curvature can be observed and the gamma radiation may be estimated by exponential decay,

$$GR(z) \approx GR_{\min} + (GR(z_0) - GR_{\min}) \cdot e^{(z - z_0 / - z_r)},$$

where z_r is a characteristic length, z_0 is the depth to the top of the lava bed, $GR(z_0)$ is the gamma radiation at the top of the lava bed and GR_{min} is a gamma radiation, which is approached asymptotically. In principle GR_{min} is the gamma radiation expected from an unaltered lava bed. In well 164/07-1, where spectral gamma logs were acquired, it is clearly seen that it is the reduced potassium content that is responsible for the downward decrease of gamma radiation in lava beds.

We suggest that decaying gamma radiation gradient in lava bed represent diffusion of potassium downwards into the lava bed. A process which occurs during soil formation as described from exposed basaltic lava flows (e.g. Sheldon, 2003). Assuming that climatic parameters are known, Sheldon (2003) used potassium concentration to estimate the duration of soil formation on lava flows. The individual measurements of gamma radiation in a well are less precise than those that can be obtained by analysis of sampled rock. However, due to the number and systematic samples in downhole logs, it would presumably be possible to use the gamma radiation or potassium logs to estimate the duration of each episode of soil formation observed in the basaltic succession of a well, at least relatively.

As we suggest that decaying gamma radiation gradient in lava bed may be caused by soil formation this trend is considered indicative of sub-aerial emplacement of the basalts.

In most volcaniclastic units, gamma radiation is fluctuating with the amplitude being of the order 10-20 GAPI (peak-trough). A slight negative correlation between gamma radiation on the one hand and bulk density and sonic velocity on the other hand is frequently seen (e.g. Fig. 8). We suggest this is caused by variable concentrations of basaltic and shaley siliciclastic material in the volcaniclastics. Whether the latter represents non-volcanic material or altered volcanic material is not clear to us. We interpret these fluctuations as zones where sedimentary rather than volcanic processes were dominant during emplacement of the unit.

In contrast, the gamma radiation fluctuations are small and the radiation level is not significantly different from the adjacent lava beds (e.g. Figs. 2 and 11), we suggest the unit is composed of almost pure volcanic material and therefore probably emplaced directly by volcanic processes.

In a few volcanic units distinct downward increasing gamma radiation is seen. In accordance with the arguments above, we suggest this response generally should be interpreted as a result of gradual increase of volcanic input during deposition of the unit. These units may thus represent

commencement of volcanism or re-commencement after a major break in volcanic activity. Downward decreasing density and velocity through a volcaniclastic unit may have a similar significance.

Units with this type of response are not necessarily significantly thicker than other volcaniclastic units. But they may have a special stratigraphic significance, as they (if actually representing a break in volcanism) may represent intervals that potentially may be correlated over some distance. Overall, volcaniclastic sediments are expected to have poor reservoir properties (un-stable mineral phases and poor sorting). However, units with this type of response may represent intra-basaltic intervals with some reservoir potential.

In contrast a constant anomalous gamma radiation level from a volcaniclastic unit into the overlying lava bed is a strong indication that the volcaniclastic unit is of eruptive origin and possibly part of the same eruptive unit as the overlying lava bed.

3 Application of wireline log response interpretation to basaltic rocks in exploration wells from the Faeroe-Shetland region

3.1 UK154/03-1, Geikie volcanic complex, North-east Rockall Trough

The well 154/03-1 was drilled through the margin of the Geikie volcanic complex. The well penetrated ca. 900 m thick basaltic rocks in the margin of the Geikie volcanic complex. We divide the basaltic rocks into two successions. The upper succession (ca. 390 m) is comprised by lava beds constituting ca. 70%, and the rest is constituted by volcaniclastic units less than 25 m thick. The lower succession (ca. 480 m) is comprised almost entirely of hyaloclastic units. On seismic data, the hyaloclastic lower succession is seen as prograding sequences, which based on reflectivity character and seismic velocity are interpreted as stacked volcanic foreset breccias (Musgrove and Michener, 1996; Japsen *et al*., 2005). In the lower succession, sediment intercalations with a sharp upper boundary may be identified based on gamma radiation significantly higher (up to between 30 and 50 GAPI; Fig 6, units SN1, -2, -3 and -4). We propose that units like SN1 to SN4 coincide with the boundaries between the stacked progradational sequences observed on seismic data (e.g. Musgrave and Michener, 1996) and suggest they represent sediments deposited during subsidence (due to

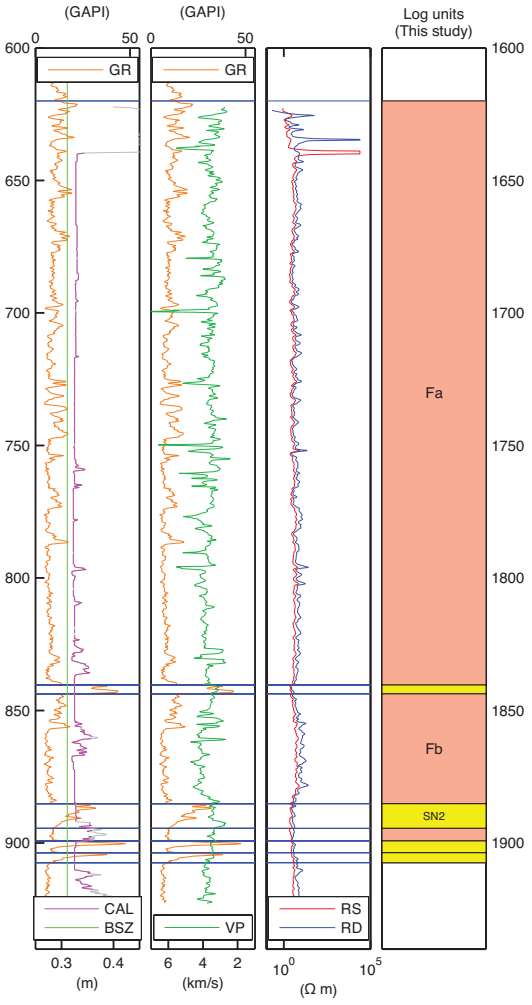

Figure 6. Log interpretation of part of the lower volcanic succession in well 154/03-1. Note the occasional spikes on the porosity sensitive log traces (NPHI, RHOB and VP) within the hyaloclastic units, which otherwise are dominated by relatively low amplitude fluctuations of a period of 10-30 m. Note also the "siliciclastic units" (yellow) at the base of each hyaloclastic unit, and the abrupt gamma radiation change between a "siliciclastic unit" and the overlying hyaloclastic unit. For colour coding of log interpretation see figure 2 . Description of acronyms for the log traces can be found in table 3. Vertical scale, 1:2000.

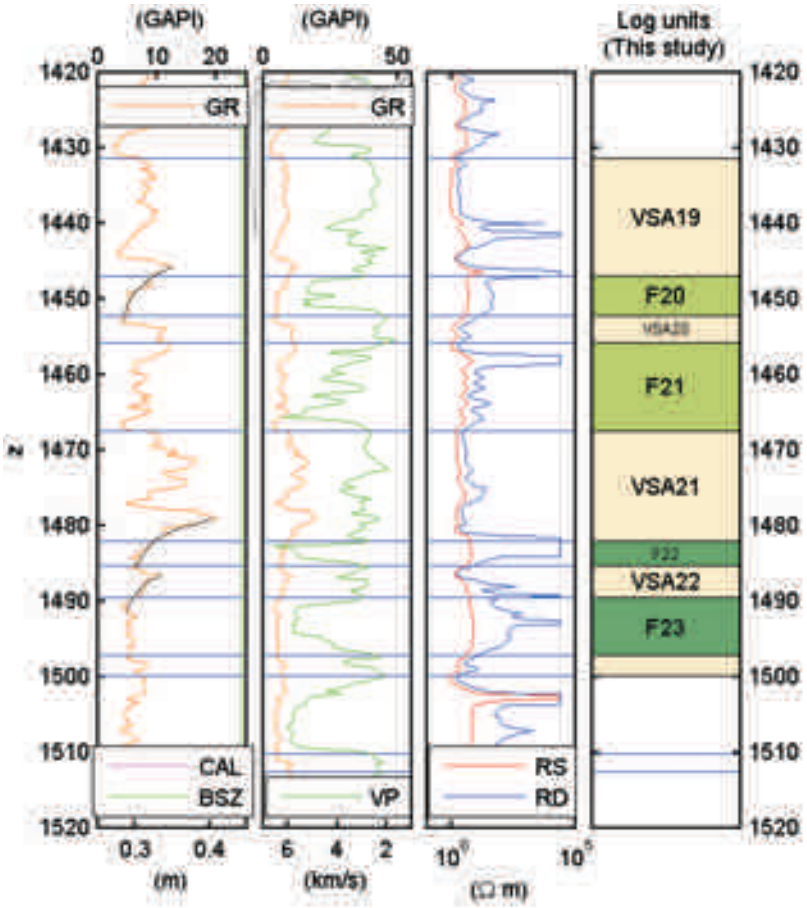

Figure 7. Log interpretation of part of the upper volcanic succession in well 154/03-1. Downward decaying gamma radiation anomalies , are seen in VSA19-F20, VSA21-F22 and VSA22-F23 (highlighted with stippled curves). This is interpreted as the result of diffusion of radioactive isotopes (potassium) during soil formation. For colour coding of log interpretation see figure 2. Description of acronyms for the log traces can be found in table 3. Vertical scale, 1:1000.

load compensation) after emplacement of the underlying hyaloclastic unit. In this way two thicker (ca 225 m and 200) and two thinner (ca. 50 and 5 m) hyaloclastic units are identified. The thinnest unit could by its internal log response be a volcaniclastic unit, as it is too thin to present the features typical of hyaloclastic units. Two thin simple lava beds with stepwise porosity increase in the top and gradational porosity decrease in the bottom of the beds are identified ca. 25 m above the base of one of the thicker hyaloclastic units. Basalt beds with an un-brecciated core are a common feature in hyaloclastic foreset breccias (e.g. Jones, 1966; Jones and Nelson, 1970; Pedersen, 1985). Therefore lava beds with gradational porosity decrease in the bottom are not considered in contradiction of our interpretation of the lower succession in 154/03-1 as hyaloclastic foreset breccias.

The upper volcanic succession was penetrated with a 17.5" (44.45 cm) bit. Neither calliper, neutron porosity nor bulk density were measured in this section of the well. The interpretation of this succession is thus somewhat less detailed and reliable than in the lower succession. Most lava beds are interpreted as compound lava units, possibly representing compound braided systems of flows.

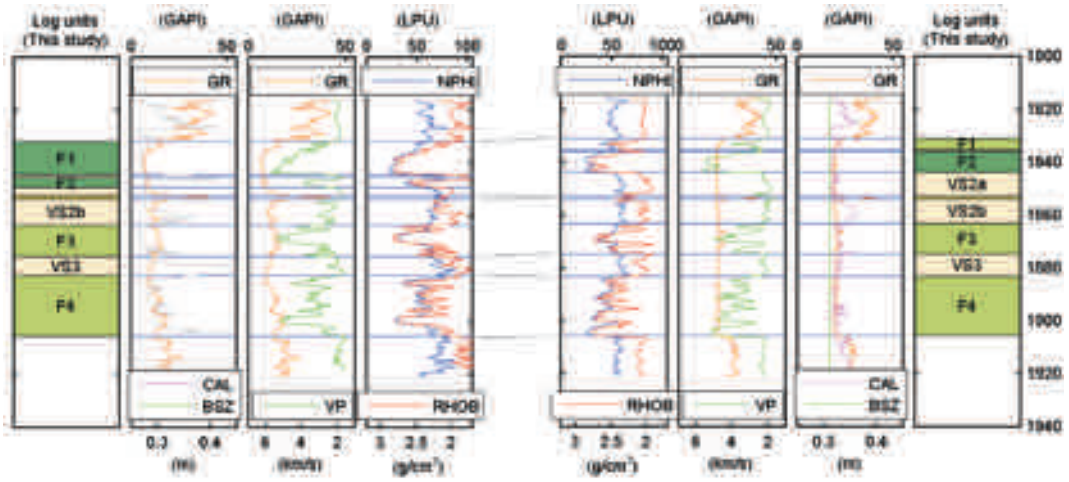

Figure 8. Log traces through sill penetrated in 164/25-1z. Note large separation of induction logs, high density and velocity. Abrupt changes of borehole diameter (CAL trace) is a common feature in boreholes penetrating sills and dykes. Most log traces are affected by this, causing deviations from expected symmetric log responses, most obvious on the NPHI, RHOB and VP traces. For colour coding of log interpretation see figure 2 . Description of acronyms for the log traces can be found in table 3. Grey colour on the caliper trace indicate intervals with caving in excess of 0.05 m. Vertical scale, 1:2000.

Several potential breaks in volcanic activity (soil formation) are indicated by downward decreasing decaying positive gamma radiation anomalies through the upper part of both compound lava units and simple lava beds. (Fig 8). Simple lava beds present in the upper volcanic succession of 154/03-1 are mostly characterised by gradationally velocity decrease (porosity increase) in the top, most having a fairly constant velocity response in the core, while a few have a serrated response in the core. The simple lava beds are thus considered to represent tabular lava flows, a few with multiple porous/vesicular zones, possibly being multiple inflated flow units. Two thicker volcaniclastic units in the lower third of the succession (VSA19 and VSA21; Fig 8) are characterised by gamma radiation in the range 5-20 GAPI, which is fluctuating and slightly correlated with seismic velocity. This indicates that these two units may have been emplaced by sedimentary processes. Volcaniclastic units in the upper half of the upper succession are characterised by smaller gamma radiation fluctuations in the same range as lava beds (5-10 GAPI).

Therefore, we suggest that short lived inundations occurred during emplacement of the upper volcanic succession in 154/03-1 although the emplacement surface generally remained above the sea level throughout emplacement of the upper volcanic. Overall, it appears that both volcanic successions in 154/03-1 were emplaced during continued subsidence. The load of the basalts would be sufficient to explain the amount of subsidence during their emplacement as indicated by the interpretation (between 450 and 700 m). Results from forward modelling of emplacement indicate that a volcanic succession comparable to that seen in 154/03-1 could be emplaced at the margin of a shallow marine basin (or lake) within 0.5 x 10^6 years. This requires viscosity in the compensating mantle comparable to present day viscosity (10^{20} to 10^{21} Pa·s; e.g. Kaufmann and Lambeck, 2000), moderate elastic thickness (ca. 5 km) and appropriate extrusion rates.

3.2 UK164/25-01 and -01z, Northern Rockall Trough

The well 164/25-01 penetrated a ca. 170 m thick volcanic succession comprising two intervals of extrusive basaltic rocks (ca. 80 and 40 m thick)

separated by a 45 m thick interval of tuffaceous mudstones. Due to drilling problems the well was side-tracked and well UK164/25-1z penetrates the same basaltic volcanic succession. At this depth 164/25-1z is displaced horizontally by ca. 30 m from the original well. The analysis of the volcanic succession is mainly based on the data from 164/25-1z as the log data from the original well are of inferior quality due to the hole conditions.

Two simple lava beds are interpreted in the lower extrusive interval. They are both characterised by gradational porosity increase in the top. In the bottom of the beds the porosity response are gradational. However, the bottom zones are thin (ca. 1 m thick). The core of one is characterised as constant porosity response, and that of the other of serrated porosity response. The thin bottom zones with downward increasing porosity could indicate bottom breccias. This in combination with the absence of any indication of soil formation from the gamma radiation propose emplacement in a wet environment. However, a sidewall core from a volcaniclastic unit below is described as "basalt weathered and altered to bole". In the upper interval only one simple lava bed is present. It is characterised by abrupt porosity responses at the bottom indicating a dry substratum during emplacement. The tuffaceous mudstone intercalated between the two intervals of eruptives indicates temporary inundation by the sea or a lake. It thus appears that the volcanic succession in 164/25-1 and 164/25-1z was emplaced during a period when the emplacement surface oscillated around sea level or in an environment where a fairly deep lake (ca. 45 m) could exist. Paleoenvironmental analyses of the tuffaceous mudstone between the eruptive intervals are required to resolve this.

Although the log response from the volcanic units in UK164/25-01 is seriously influenced by the hole condition, it has been possible to correlate units between the original well and the sidetracked well. In the upper 80 m of the volcanic succession (down to 1910 m depth -MD) unit boundaries interpreted in the two wells can generally be tied between the two wells without any problems.

Both qualitatively and quantitatively, there are significant differences between the sections logged in the 164/25-1 and -1z (Fig. 9). Based on all three porosity logs and the resistivity logs, the uppermost lava bed in 164/25-1, F1, appear to have split up into two beds in 164/25-1z, F1a and F1b; the thin but distinct lava bed F2 in 164/25-1

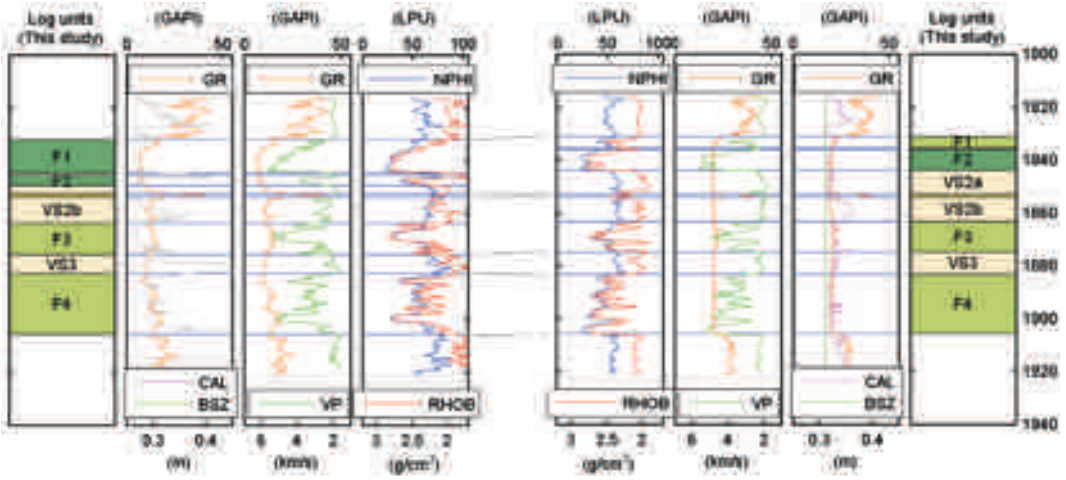

Figure 9. Correlation between the upper part of volcanic succession in boreholes 164/25-1 and 164/25-1z ca. 30 m apart. True lateral changes units are obvious at several depths within the illustrated section (e.g. 1184-1193 m). However, around 1877-1883 m and below 1900 m, cross-well comparison of log responses is of little relevance as borehole conditions in 164/25 did not allow measurement of sufficient quality. For colour coding of log interpretation see figure 2 . Description of acronyms for the log traces can be found in table 3. Grey colour on the caliper traces indicate intervals with caving in excess of 0.05 m. Vertical scale, 1:2000.

is not seen at all in 164/25-1z; the distinct core of the lower bed of the compound lava unit, F3, in 164/25-1z is apparently missing in 164/25-1; also the log response of unit F4 are clearly not the same in the two wells. Although the variable hole diameter in 164/25-1 is expected to have disturbed the measurements, the differences of the volcanic succession between 1830 and 1910 m in the two wells is striking especially, if compared to sediment succession just above, where the hole diameter also is fluctuating considerably.

3.3 UK205/09-01, Faroe-Shetland Channel

Previous studies of the well indicate that Paleocene basaltic lava flows were penetrated in this borehole (e.g. Knox *et al*., 1997; Naylor *et al*., 1999; Ellis *et al*., 2002). Using log data, we found four simple lava beds with a cumulated thickness of 66.5 m. The four lava beds are emplaced in a shaley sediment with high gamma radiation (ca. 40-80 GAPI), and the bed tops and bottoms can be picked accurately (within 25-50 cm) based on a significantly lower natural gamma radiation from the lava beds (ca. 25-30 GAPI).

The lava beds, -F4 and F3-, are characterised by stepwise porosity decrease in the bed top and gradational porosity increase in the bed bottom (best developed on the VP trace; Fig. 3)**.** The bed F2 is characterised by a stepwise porosity decrease in the 5 m thick bed top and high porosity gradient at the bed bottom. The uppermost ca. 16 m thick lava bed, F1, is characterised by high porosity gradient at the base, and near constant porosity in the core. In the top of the bed, the response is a hybrid between the stepwise and gradual porosity decrease (Fig. 3). A ca. 1 m thick zone of near constant porosity is clearly seen in the neutron porosity and bulk density traces. Below this zone porosity decreases along an ellipsoidal trend. The log response of this bed also deviates from that of the three lower beds by a clear porosity minimum about 5 m below the bed top, possibly indicating a lava outbreak or a two-stage inflation process during emplacement of unit F1.

Separation between the induction logs are seen in the cores of all four lava beds in 205/09-1, however, most distinct in the uppermost lava beds ($R_{ILD}/R_{ILM} \approx 5$; Fig. 3). Both invasion of a low resistivity drilling fluid into open fractures in the lava cores and anisotropic fracture distribution with dominantly vertical fractures could cause the observed separation of the induction logs. In surface exposures open fracture systems are common in the cores of basaltic lava flows. Pronounced vertical anisotropy in the form of columnar joint systems are common in tabular lava flows are emplaced on wet sediments (e.g. Lyle, 2000). Resistivity separation in the core of lava beds may thus be an indication of a wet environment.

The occurrence of a positive gamma radiation anomaly in the porous top of lava bed F3 (ca. 5 GAPI above flow average; Fig.3), but in none of the other three beds is interesting. Although this gamma radiation anomaly is subtle, it is clearly not characterised by the exponential decay of gamma radiation, which we in other wells suggest to be an indicator of soil formation. However, we still propose this anomaly could be attributed to early post-depositional alteration of the lava bed enriching the upper part in radioactive isotopes (potassium).

Assuming that blocky gradational porosity response in flow bottoms should be interpreted as brecciation or pillow palagonite complexes, the two lower beds (F4 and F3), were probably emplaced in a shallow water environment or possibly on wet sediments. The two upper lava beds (F2 and F1) are characterised by high porosity gradient at the bottom. It is thus likely that the lava of beds F2 and F1 did not interact to the same degree with wet sediment during emplacement. The difference of the log response in the bed tops of the two upper beds is presumably not a direct effect of lava-water interaction but rather of shear (lava viscosity) in the bed (flow) top, the top of the uppermost bed being less sheared than that below.

The log response of the four simple lava beds observed in 209/05-01 may thus be explained by a shallowing of the depositional emplacement surface relative to the water table. This interpretation is considered to be in general agreement with palynofloras recovered immediately below and between the lava beds, which are described as representative of an aquatic and swamp community (Ellis *et al*., 2004).

3.4 UK209/03-1A, UK209/04-1A and UK209/9, Erlend volcanic complex

Three wells are drilled into the Erlend Volcanic Complex (Chalmers and Western, 1979; Gatliff *et al*., 1984). The volcanic successions in these wells were described using cuttings and sidewall cores as well as wireline logs (Jolley and Bell, 2002). From bottom and up, Jolley and Bell (2002) divided the volcanic successions found in UK209/03-1, UK209/04-1 and UK209/09-1 into four volcanic units. From oldest to youngest these are identified as units Erlend A, B, C and D. A sediment unit is emplaced between unit C and D. All four volcanic units were identified in 209/03-01. In 209/04-1 and 209/09-1 volcanic unit C and D were identified, and the sediment unit between unit C and unit D was not identified in 209/09-1. Based on the palynological analysis Jolley and Bell (2002) found indications of both lateral and temporal changes in the depositional environment and suggested that the depositional environment differed significantly between the three wells.

Using only log data, we have picked unit boundaries slightly different than Jolley and Bell (2002), and we have not been able to identify the unit C and D boundary in 209/09-1. However, our interpretation is still in good agreement with that of Jolley and Bell (2002).

In 209/03-1 we identify unit -A, -B and -C and classify them as compound lava beds, while the thin unit D is comprised dominantly of simple lava beds. Unit A is divided into three separate compound lava units. There is a significant and abrupt increase in separation between neutron porosity and bulk density and a corresponding decrease in seismic velocity passing from unit A into unit B. Overall natural gamma in unit C is higher and more variable than in unit B and most of unit A. We subdivide the ca. 40 m sediments between unit C and D into two units, the lower 15 m having log response of a basaltic sediment, while the upper 25 m have no obvious volcanic signature (Fig. 5). The lack of a distinct volcanic precursor below the lowermost lava bed in unit D could be an indication of a minor hiatus between the sediments and unit D.

In 209/04-1 the volcanic succession is comprised of a mixture of volcaniclastic units, simple lava and a few compound lava units. Near the top and near the bottom sediment units without a clear basaltic signature are intercalated into the volcanic succession. Jolley and Bell (2002) correlate the 40 m sediments between unit C and D in 209/03-01 with ca. 117 m sediments in 209/04-1, which we have picked as combination of volcaniclastic units and sediment units without clear basaltic signature (Figs. 5 and 11). The tie between the two wells would presumably not have been made using only the log interpretation. Gamma radiation in the succession underlying the Erlend sediment unit, (unit C according to Jolley *et al*., 2002) is variable. Some lava beds characterised by a comparable or considerably higher gamma radiation than observed in the same unit in 209/03-1, but most having a lower gamma radiation. Several simple lava beds are characterised by gradational porosity decrease in the bottom indicating emplacement into wet environment, and most volcaniclastic units are characterised by log response indicating emplacement by sedimentary processes. The volcaniclastic unit, below the lowermost lava bed in the succession, appears to represent explosive volcanic products, which we suggest may be associated to the same eruptive event as the overlying lava bed. Overall, the log interpretation indicates that the volcanic succession in 209/04-1, were emplaced in an environment being significantly wetter than the contemporaneous environment in 209/03-1, temporary inundations being likely.

In 209/09-1 the volcanic succession is comprised dominantly of, simple lava and a few compound lava units with intercalations of thin volcaniclastic units. Jolley and Bell (2002) recognise both volcanic unit C and D, but the intra-basaltic sediments are absent in this well. The lava beds in 209/09-1 are all characterised by approximately the same level of gamma radiation (ca. 15 GAPI). The gamma radiation is fluctuation with about ±2 GAPI, and no obvious decaying gamma gradients are observed. This is in contrast to volcanic unit C and D in 209/03-1, where the level of gamma radiation clearly not is the same in the individual lava beds fluctuating between 20 and 30 GAPI.

The interpretation of the logs from the three wells around Erlend volcanic complex shows that careful log interpretation of volcanic successions

can provide a fairly detailed provisional stratigraphy of each well. However, cross-hole correlation between the wells of the volcanic units is not realistic using only log interpretations. Indications of emplacement styles and of down-hole environmental changes observed from the log are overall in fair agreement with the lithological and palynological investigations of cuttings from the wells (Jolley and Bell, 2002).

3.5 164/07-01, Northern Rockall Trough

The well 164/07-01 is located further into the flood basalt province compared to the other investigated wells and penetrated a succession of ca. 1200 m of Eocene basaltic lava beds and volcaniclastics (Archer *et al*., 2005). The well may be more representative for flood basalt provinces than the other wells investigated in this study. In addition to the extrusive basalts the well contains abundant hypabyssal intrusives, mostly sills (Archer *et al*., 2005).

The volcanic succession in 164/07-1 is dominated by volcaniclastic units and simple lava beds typically around 10 m thick. The thickest individual lava beds are around 20-25 m thick. Units of composite lava beds are relatively scarce. Two ca. 50 meter thick units of composite lava beds (2632-2687 m and 2778-2838 m) accounts for nearly half of the penetrated section of composite lava beds in the well. Volcaniclastic units, recognised by relatively high porosity observed on all porosity sensitive logs and generally by a somewhat higher gamma radiation than the lava beds (30-50 versus 20-40 GAPI), are seen between most lava units. Altogether volcaniclastic units accounts for nearly 40% of the complete volcanic succession. However, thickness and relative volumetric importance of the volcaniclastic units varies considerably through the volcanic succession. Some of the thickest volcaniclastic units (>20m) are found in the interval 2342-2588, where volcaniclastic sediments account for 58 % of the succession. In the overlying interval 2213-2342 the volcaniclastic units are thin (ca.1 m) and account for only 12 % of the succession.

A 121 m thick tuffaceous breccia (3207-3328 m) is found above a major unconformity spanning ca. 33 My at the base of the volcanic succession (Archer *et al*., 2005). The breccia contains marine biogenic debris (Archer *et al*., 2005). The upper part of this breccia (Unit VSII, 3207-3295 m; Fig.12) is characterised by a steady upward decrease in gamma radiation, which is caused by a decrease in the concentration of thorium (from 5-1 ppm) and uranium (from 1-0.5 ppm), while the potassium remains constant around 2.5 %. The neutron porosity, bulk density and sonic velocity remain constant throughout this interval. It is thus not likely that the gradual decrease in gamma radiation is the result of gradual increase of basaltic material in the breccia. However, an upward decrease of siliciclastic material with a significant content of heavy minerals and/or of kaolinites would produce a similar gamma radiation response without affecting the porosity response significantly (e.g. Hurst 1990). Both heavy minerals and kaolinites may be considered terrigenous in origin. The upward decreasing gamma radiation in unit VSII could therefore reflect a decrease in the terrigenous component rather than an increase of the igneous component. The source for terrigenous material could have been on highs to the east (e.g. West Lewis Ridge). It thus appears that the onset of volcanism around 164/07-1 was preceded by a relative sea-level fall (in late Cretaceous or Paleocene) followed by a significant relative sea-level rise in Late Paleocene, immediately before or possibly associated with the onset of volcanism. Similar vertical movements have been deduced from investigation of paleo-shorelines on the Rosemary Bank (Boldreel and Andersen, 1994), from denudation studies on the British Isles and from sediment distribution around the British Isles (e.g. White and Lowell, 1997). The large late Cretaceous-late Paleocene hiatus in 164/07-1 indicate that the area of emergent landmass during this period could have been considerably larger than suggested by White and Lowell (1997).

Hyaloclastic breccias within some lava beds in the lower part of the volcanic succession have been reported and the proportion of reddened, oxidised cuttings is increasing upward in the volcanic succession (Archer *et al*., 2005). This indicates a gross relative sea-level fall during emplacement of the volcanic succession (Archer *et al*., 2005). We have found that many (probably most) simple lava beds

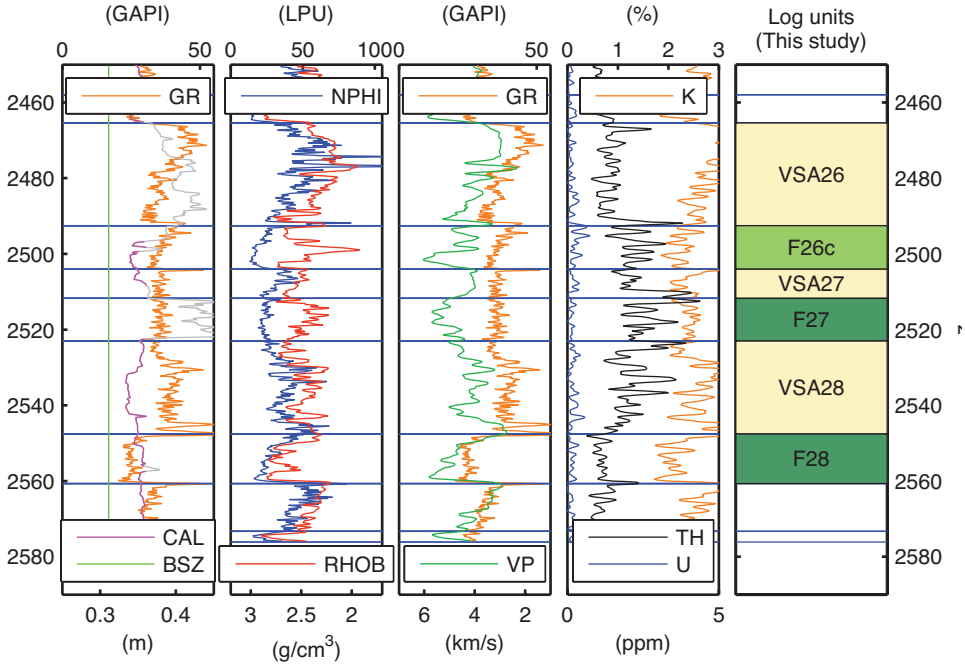

Figure 10. Log interpretation of part of the volcanic succession in well 164/07-1. The compound lava unit F26c and simple lava bed F27 as well as underlying volcaniclastic units are characterised by high thorium concentrations compared to overlying and underlying units. Note considerable caving in upper part of the illustrated section resulting in poor quality on several log traces, especially the RHOB trace. For colour coding of log interpretation see figure 2 . Description of acronyms for the log traces can be found in table 3. Vertical scale, 1:2000.

in the lower three quarters of the volcanic succession is characterised by gradual porosity response at the base, while lava beds with abrupt porosity change at the bottom are dominant in the upper part of the volcanic succession. Based on the interpretation of these log characteristics suggested in this paper, the log interpretation supports the interpretation of Archer *et al.* (2005). Gross relative sea-level rise combined with high frequency relative sea-level fluctuations could be accommodated by load induced subsidence during emplacement of the volcanic succession above viscous mantle. Overall, 150-200 m of final relative sea-level fall is expected due to emplacement of 1200 m of basalt, as found in 164/07-1. This is if we assume constant absolute sea-level and low to moderate elastic strength of the lithosphere in the region, as proposed by Bellingham and White (2000), and no other material movement in the mantel than that induced by the load.

Assuming we can use mantle viscosities obtained from glacial rebound studies (e.g. 10^{19}-10^{20}), complete subsidence after emplacement of a load is predicted to have occurred after ca. 10000 years. The surface of the lava plateau rises during periods with high emplacement rates while it subsides during periods with low emplacement rates. The uppermost lava beds with log responses indicative of emplacement in a wet or aquatic environment is found only ca. 175 m below the top of the lava succession, and all lava beds down to the bottom of the lava succession are characterised by highly porous top zones. The water column during emplacement of the basalts around 164/07-1 was thus never sufficient to suppress the release of volatiles during emplacement of the lava beds. It is thus feasible that the water column never were more than 200 m, and that the youngest lava beds were emplaced just above sea-level. It is therefore not necessary to invoke plume related dynamic up-

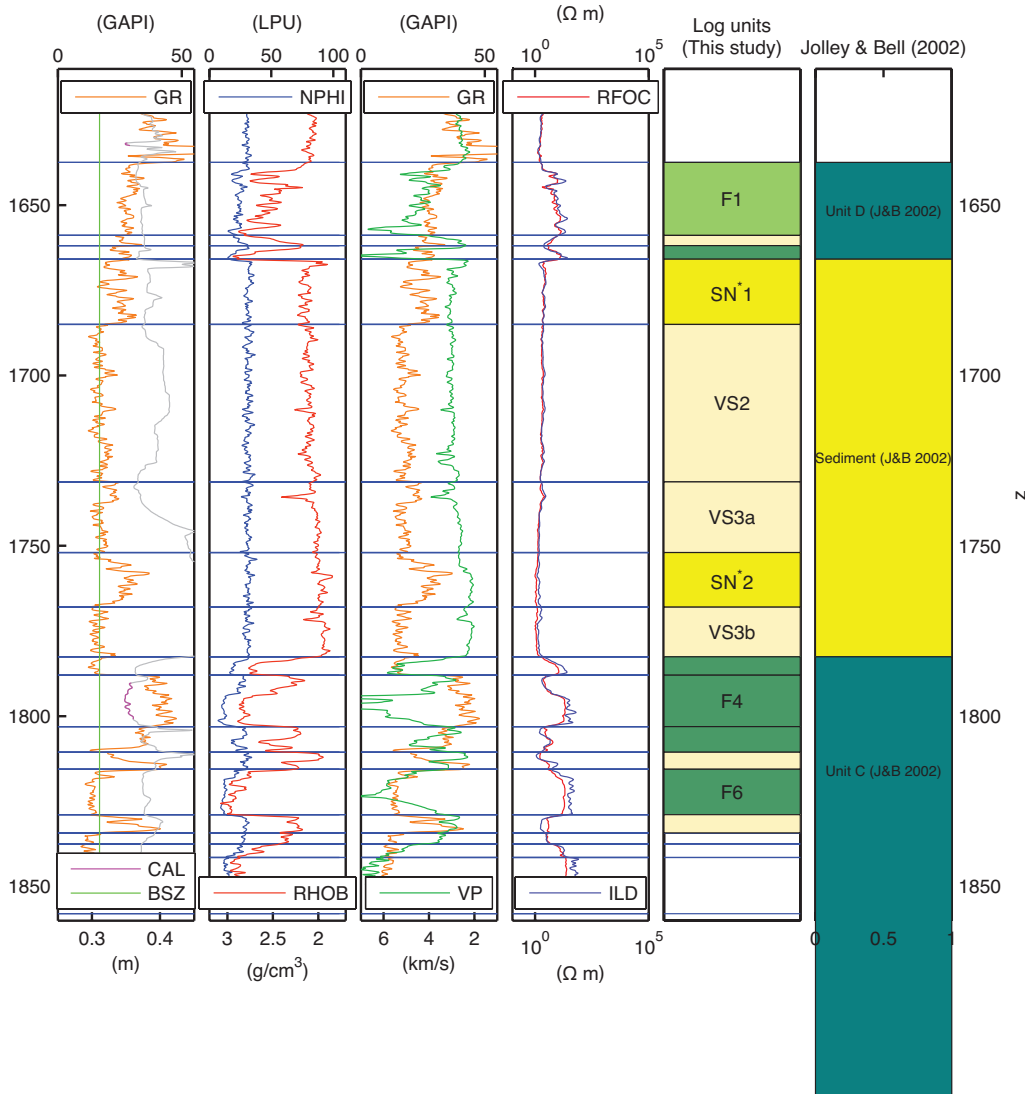

Figure 11. Log interpretation of upper part of the volcanic succession in well 209/04-1. Rightmost panel show stratigraphy according to Jolley and Bell (2002). Note positive correlation between GR and VP traces in unit SN1 possibly indicating this is a siliciclastic sand-shale succession. Caving is significant throughout most of the succession displayed in this figure. Unusual velocity response throughout units F4 and F6 may thus be linked to borehole conditions and compensation. For colour coding of log interpretation see figure 2 . Description of acronyms for the log traces can be found in table 3. Vertical scale, 1:2000.

lift to account for the relative sea-level fall during emplacement of the basalts around 164/07-1.

Decaying gamma radiation anomalies indicative of soil formation are seen in the top of both simple lava beds and compound lava units in this well. However, in the interval 2410-2950 m they are scarce.

Only a few lava beds have distinct chemical signatures based on the radiogenic elements. They are all characterised by a higher level of thorium (2-3 ppm Th) compared to the majority of the lava beds. (1-1.5 ppm Th). Two of the lava beds with high thorium content (F26c and F27) are interbedded with thick volcaniclastic units (Fig 10).

The volcaniclastic units below these lava beds (VSA27 and VSA28) are also characterised by high thorium content. As they are found below the lava bed the volcaniclastic units cannot be erosion products. We suggest that at least these volcaniclastic units represents an initial explosive phase, possibly phreato-magmatic, as the overlying lava beds are characterised by blocky or gradational porosity responses at their bases indicating shallow water, possibly sub-aquatic emplacement (or at least wet conditions). It is likely that many other volcaniclastic intervals found in 164/07-1 represents explosive volcanic products rather than eroded and transported sediments. This may explain the scarcity of fossils from the volcanic succession of 164/07-1 reported by (Archer *et al*., 2005). However, some volcaniclastic units are distinct from the overlying lava beds. These volcaniclastic units are the most likely candidates for intervals with fossils in sufficient abundance to be used for a stratigraphic purpose.

Overall, the lithological interpretation of the wireline logs from 164/07-1 confirms and substantiates the interpretation based on detailed analysis of cuttings and sidewall cores (Archer *et al*., 2005).

Discussion

Only few studies have been published concerning the interrelationship between lava morphology and well data, mostly based on core data or cuttings from the well (e.g. Hald and Waagstein, 1984; Waagstein and Hald, 1984; Keszthelyi, 2002), and even fewer based on wireline logs from the well (e.g. Nielsen *et al*., 1984; Planke, 1994; Delius *et al*., 1995; Boldreel, 2006). In this paper we have demonstrated that basaltic rocks in eight exploration wells drilled in the Faroe-Shetland Channel can be classified into a few major classes based on wireline logs. Style of eruption and environment of emplacement may be characterised. Using the approach outlined in this paper, it should be kept in mind that the geological significance of log shapes is generally not unique. However, it is suggested that the systematic occurrence or disappearance of one or more log characteristics or a class of units in a well may indicate temporal changes in the environment where the basalt was emplaced and/or the style of emplacement. In addition log trends characterising a single unit may allow deductions regarding the nature of individual units.

Results of lithological and palynological analyses of cuttings and sidewall cores from five of the wells used for this study (209/03-1, 209/04-1, 209/09-1, 205/09-1 and 164/07-1) have been published previously (Jolley and Bell, 2002; Ellis *et al*., 2002; Archer *et al*., 2005). Unfortunately the published details of these studies are not sufficient to constrain the log analysis of individual units. However, there is a fair agreement between the log analyses of the wells presented in this paper and the published results of lithological and palynological analyses. It thus appears that log interpretation based on unit classification and analysis of log shapes provides a fast way to get a first approximation of eruption style and environmental changes around the well site during emplacement of a continental flood basalt province.

Systematic interpretation of the logs as indicated in this paper is applicable to wells in Faroe-Shetland area penetrating basalt successions, and presumably to wells in most continental flood basalt provinces. The interpretation should provide information regarding the geological evolution of the basalt succession in the vicinity of the well and regarding the nature of individual units in the well. Compared to other methods for investigating drilled basalt successions log analysis is relatively cheap and fast. However, as it should be evident from this study the results of log interpretation are generally not completely unambiguous. For this reason conclusions from log analysis regarding emplacement style and environment of emplacement should as far as possible be complemented with lithological and paleo-environmental data from other sources (i.e. interpretation of cuttings and cores). In this context, it is important that a previous log analysis may help focus detailed studies at intervals of special relevance.

Combining the analysis of wireline logs along the lines indicated in this paper with results from detailed investigations of flow morphology (e.g. Single and Jerram, 2004) may provide opportunities to create 3D approximations of facies distrib-

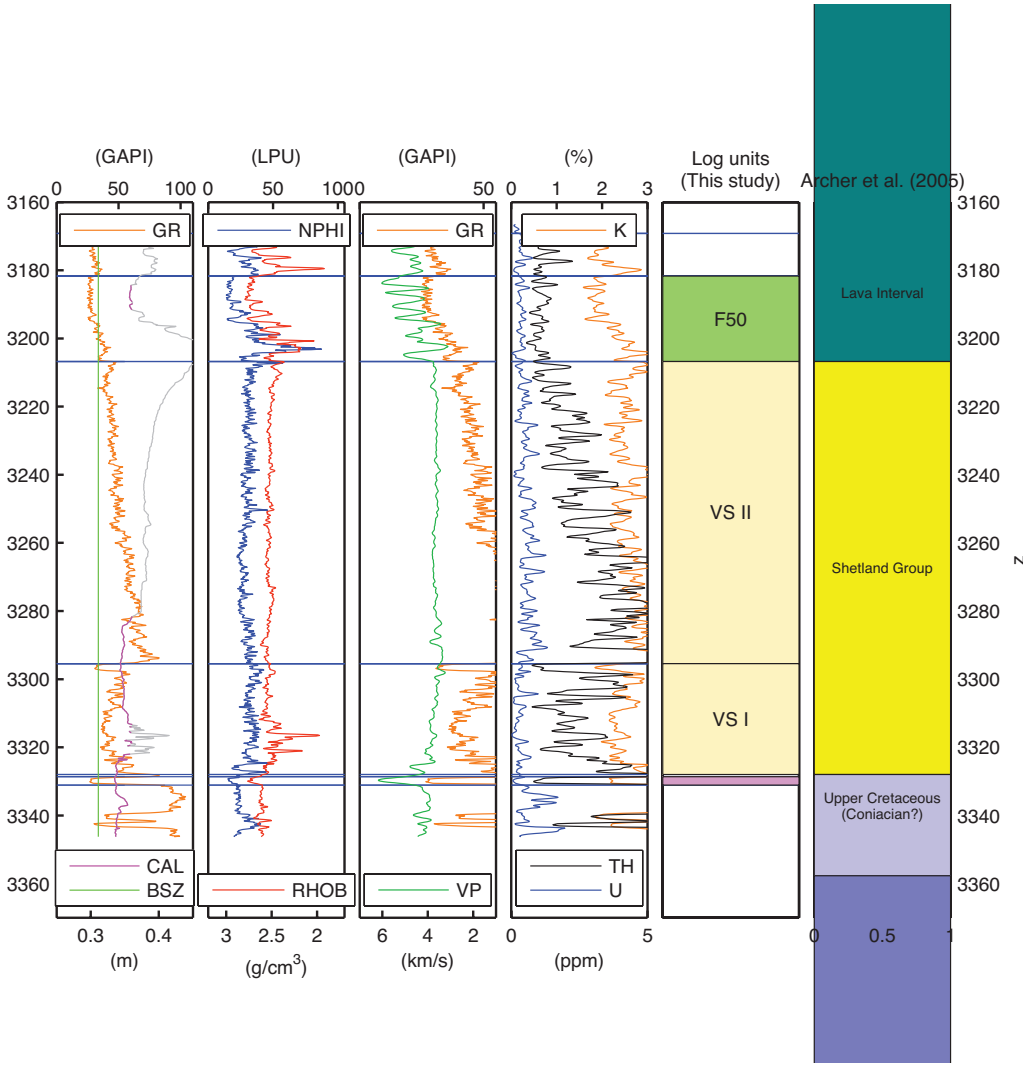

Figure 12. Log traces through Shetland Group in 164/07-1. Note downward decreasing gamma radiation and thorium concentration in upper part of Shetland Group. Rightmost panel show stratigraphy according to Archer *et al.* (2005). For colour coding of log interpretation see figure 2. Description of acronyms for the log traces can be found in table 3. Vertical scale, 1:2000.

utions around wells drilled into continental flood basalt provinces, thus providing a mean to model realistic, but not necessarily true, distributions of physical properties. For instance seismic attenuation in the Faroe Middle Basalt Formation was investigated by Shaw *et al.* (2008) using a 3D property distribution model based on interpretation of a log interval in a shallow well as compound braided basalts. Although model building not is an issue treated in this paper, it is noticed that estimates regarding the intrinsic relationship between properties such as porosity, bulk density, seismic velocities and resistivity in basalts have been published (e.g. Bartetzko *et al.*, 2005). Some estimates have also been made of properties, such as bulk density and seismic velocity, within different intrafacies of

basaltic lava flows (e.g. Single and Jerram, 2004). However, more detailed data concerning the distribution of properties within lava flows are still in demand, particularly quantitative data regarding vesicle and fracture distributions, and their relation to bulk density, seismic velocity, resistivity and permeability.

Acknowledgments

This work is part of the SeiFaBa project funded collectively by oil companies operating in the Faroe Islands sector under a first round licence, the Sindri Group (www.sindri.fo). Thanks are due to the Sindri Group for permission to publish the results. Figures illustrating log response are published with permission from Robertson Research. Thanks to Landmark for issuing a university grant to Department of Geography & Geology, Copenhagen University. A special thank to Ken Hitchen and Paul Egerton, BGS for discussions and support regarding the Geikie volcanic Complex; to Lotte M. Larsen, GEUS, and Simon Passey, Jarðfeingi, for discussions regarding lava morphology; to Asger K. Petersen, University of Copenhagen for discussions concerning the nature of foreset breccias; to Claus Andersen, GEUS, for critical comments and valuable support at different stages of this work.

Thanks to the two reviewer Dr. R. Pechnig and Dr. C.M. Helm-Clark for constructive criticisms and suggestions for improving the paper.

Members of the SeiFaBa research group are Robert S. White, Giovanni Bais (Cambridge University), Michael Worthington, Felicia Shaw (Oxford University) Uni K. Petersen (University of the Faroe Islands) Peter Japsen, Regin Waagstein (GEUS) Lars Gommesen (ØDS), Garry Mavko (Stanford)

References

Archer, S.G., Bergman, S.C., Iliffe, J., Murphy, C.M. and Thornton, M., 2005. Palaeogene igneous rocks reveal new insight into the geodynamic evolution and petroleum potential of the Rockall Trough, NE-Atlantic Margin. *Basin Research* 17: 171-201.

Andersen, M.S., 1988. Late Cretaceous and early Tertiary extension and volcanism around the Faeroe Islands. *In*: Morton, A.C. and Parson, L.M. (eds) *Early Tertiary Volcanism and the Opening of the NE Atlantic*. Geological Society, London, Special Publication 39: 115-112.

Andersen, M.S., Egerton, P. Hitchen, K. and Boldreel, L.O., 1997. Seismic facies analysis of volcanic rocks – a tool in the analysis of thick basaltic successions offshore the British Isles and the Faroes. *Mid-Norwegian Volcanic Margin Conference*, Oslo, 10-11 February 1997.

Bartetzko, A., Delius, H. Pechnig, R., 2005. Effect of compositional and structural variations on log responses of igneous and metamorphic rocks. I: mafic rocks. *In*: Harvey, P.K., Brewer, T.S., Pezard, P.A. and Petrov, V.A. (eds), *Petrophysical properties of crystalline rocks*. Geological Society, London, Special Publications 240: 255-278.

Bellingham, P. and White, N., 2000. A general inverse method for modelling extensional sedimentary basins. *Basin Research* 12: 219-226.

Boldreel, L.O. 2002. Identification and characterization of basalt and sediment units based on wireline logs from the Lopra deep well, Faroe Islands, NE-Atlantic Ocean. *EGS General Assembly XXVII* Nice, France, Abstract EGS02-A-05330.

Boldreel, L.O. and Andersen, M.S. 1994. Tertiary development of the Faeroe-Rockall Plateau based on reflection seismic data. *Bulletin of the Geological Society of Denmark* 41: 162-180.

Boldreel, L.O. 2006. Wire-line log-based stratigraphy of flood basalts from the Lopra1/1A well, Faroe Islands. *In*: Chalmers, J. and Waagstein, R. (eds) *Scientific results from the Lopra-1 borehole, Faroe Islands*. Geological Survey of Denmark and Greenland Bulletin 9: 7-22.

Boldreel, L.O., Andersen, M.S. and the SeiFaBa group 2006. Effect of burial on in situ properties of flood basalt successions in the Faroe-Shetland Region. The Sindri Conference, Tórshavn

Broglia, C. and Ellis, D. 1990. Effect of alteration, formation absorption, and standoff on the response of thermal neutron porosity log in Gabbros and Basalts: examples from Deep Sea Drilling Project-Ocean Drilling Program Sites. *Journal of Geophysical Research* 95: 9171-9188.

Buckley, D.K. and Oliver, D. 1990. Geophysical logging of water exploration boreholes in the Deccan Traps, Central India. *In*: Hurst, A., Lovell, M.A. and Morton, A.C. (eds) *Geological applications of wireline*

logs. Geological Society, London, Special Publications 48: 153-161.

Christie, P., Gollifer, I. and Cowper, D. 2006. Borehole seismic studies of a volcanic succession from the Lopra-1/1A borehole in the Faroe Islands, northern North Atlantic. *In*: Chalmers, J. and Waagstein, R. (eds) *Scientific results from the Lopra-1 borehole, Faroe Islands*. Geological Survey of Denmark and Greenland Bulletin 9: 23-40.

Delius, H., Brewer, T. and Harvey, P.K. 2003. Evidence for textural and alteration changes in basaltic lava flows using variations in rock magnetic properties (ODP Leg 183). *Tectonophysics* 371: 111-140.

Delius, H., Bücker, C.H. and Wohlenberg, J. 1995. Significant log responses of basaltic lava flows and volcanoclastic sediments in ODP Hole 642E. *Scientific Drilling* 5: 217-226.

Eldholm, O. and Grue, K., 1994. North Atlantic volcanic margins: dimensions and production rates. *Journal of Geophysical Research* 99: 2955-2968.

Ellis, D., Bell, B.R., Jolley, D.W. and O'Callaghan, M. 2002. The stratigraphy, environment of eruption and age of the Faroes Lava Group, NE Atlantic Ocean, *In*: Jolley, D. and Bell, B.R. (eds.) *The North Atlantic Igneous Province, Tectonic, Volcanic and Magmatic Processes*. Geological Society, London, Special Publications 197: 253-269.

Gatliff, R.W., Hitchen, K., Ritchie, J.D. and Smythe, D.K., 1984. Internal structure of the Erlend Tertiary volcanic complex, north of Shetland, revealed by seismic reflection. *Journal of the Geological Society*, London: 141: 555-562.

Hald, N. and Waagstein, R. 1984. Lithology and chemistry of a 2 km-sequence of Lower tertiary tholeiitic lavas drilled on Suðuroy, Faeroe Islands (Lopra-1). *In*: Berthelsen,O., Noe-Nygaard, A. and Rasmussen, J (eds) *The deep drilling project 1980-1981 in the Faeroe Islands*. Føroya Fróðskaparfelag, Tórshavn.

Hearst, J.R., Nelson, P.H. and Paillet, F.L. 1999. Well logging for physical properties, 2. edition. John Wiley & Sons, pp 483.

Helm-Clark, C.M., Rodges, D.R. and Smith, R.P. 2004. Borehole geophysical techniques to define stratigraphy, alteration and aquifers in basalt. *Journal of Applied Geophysics* 55(1): 3-38.

Hitchen, K. and Ritchie, J.D., 1987. Geological review of the West Shetland area. *In*: J.D. Brooks and K.W. Glennie (eds) *Petroleum Geology of North West Europe: Proceedings of the third conference*. Graham and Trottman, London: 737-749.

Hurst, A. 1990.Natural gamma-ray spectroscopy in hydrocarbon-bearing sandstones from the Norwegian continental shelf. *In*: Hurst, A., Lowell, M.A. & Morton, A.C. (eds) *Geological applications of wireline logs*. Geological Society, London, Special Publications 48: 211-222.

Japsen, P., Andersen, C., Andersen, H.L. Andersen, M.S., Boldreel, L.O., Mavko, N.G., Mohammed, N.G., Pedersen, J.M., Petersen, U.K., Rasmussen, R., Shaw, F., Springer, N., Waagstein, R. White, R.S. and Worthington, M., 2005. Preliminary results from investigations of seismic and petrophysical properties of Faroes basalts in the SeiFaBa project. *In*: Doré, A.G. and Vinning, B.A. (eds) *Petroleum Geology: North-West Europe and Global Perspectives – Proceedings of 6th Petroleum Geology Conference*. Geological Society, London: 1461-1470.

Jolley, D.W. and Bell, B.R. 2002. Genesis and age of the Erlend Volcano, NE Atlantic Margin, *In*: Jolley, D.W. and Bell, B.R. (eds.) *The North Atlantic Igneous Province, Tectonic, Volcanic and Magmatic Processes*. Geological Society, London, Special Publications 197: 95-110.

Jones, J.G. 1966. Intraglacial volcanoes of south-west Iceland and their significance in interpretation of the marine basaltic volcanoes. *Nature* 212: 586-588.

Jones, J.G. and Nelson, P.H.H., 1970. The flow of basalt lava from air into water-its structural expression and stratigraphic significance. *Geological Magazine* 107: 13-19.

Jørgensen, O. 2006. The regional distribution of zeolites in the basalts of the Faroe Islands and the significance of zeolites as palaeotemperature indicators. *In*: Chalmers, J and Waagstein, R. (eds) *Scientific results from the Lopra-1 borehole, Faroe Islands*. Geological Survey of Denmark and Greenland Bulletin 9: 123-156.

Kaufmann, G. and Lambeck, K. 2000. Mantle dynamics, postglacial rebound and the radial viscosity profile. *Physics of the Earth and Planetary Interiors* 121: 301-324.

Kern, H, and Richter, A., 1979. Compressional and shear wave velocities at high temperatures and confining pressure in basalts from the Faeroe Islands. *Tectonophysics* 54: 231-252.

Keszthelyi, L. 2002. Classification of mafic lava flows from ODP Leg 183. *In*: Frey, F.A., Coffin, M.F., Wallace, P.J. and Quilty, P.G. (eds) *Proceedings of the Ocean Drilling Program*, Scientific Results Volume 183: 1-28.

Keszthelyi, L., Self, S. and Thordarson, T. 1999. Application of recent studies on the emplacement of basaltic lava flows to Deccan Traps. *In*: Subbarao, K.V (ed.) *Deccan Volcanic Province*, Memoir Geological Society of India 43: 485-520.

Kilburn, C.R.J. 1981. Pahoehoe and aa lavas: a discussion and continuation of the model of Peterson & Tilling. *Journal of Volcanology and Geothermal Research* 11: 373-382.

Kiørboe, L. 1999. Stratigraphic relationships of the Lower Tertiary of the Faeroe Basalt Plateau and the Faeroe-Shetland Basin. *In*: Fleet, A.J. and Boldy, S.A.R. (eds) *Petroleum Geology of Northwest Europe: Proceedings of the 5th Conference*. Geological

Society of London: 559-572.

Kiørboe, L. and Petersen, S.A. 1995. Seismic investigation of the Faeroe basalts and their substratum. *In*: Scrutton, R.A., Stoker, M.S., Shimmield, G.B. and Tudhope, A.W. (eds.) *The tectonics, sedimentation and Palaeoceanography of the North Atlantic Region*. Geological Society, London, Special Publication 90: 111-112.

Knox, R.W.O'B., Holloway, S., Kirby, G.A. and Baily, H.E., 1997. Stratigraphic nomenclature of the UK North West Margin. 2. *Early Paleogene lithostratigraphy and sequence stratigraphy*. British Geological Survey, Nottingham.

Lamers, E. and Carmichael, M.M. 1999. The Paleocene deepwater sandstone play West of Shetland. *In*: Fleet, A.J. and Boldy, S.A.R. (eds) *Petroleum Geology of Northwest Europe: Proceedings of the 5th conference*. Geological Society, London: 645-659.

Lyle, P. 2000. The eruption environment of multi-tiered columnar basalt lava flows. *Journal of the Geological Society*, London 157: 715-722.

Musgrove, F.W. and Mitchener, B. 1996. Analysis of the pre-Tertiary rifting history of the Rockall Trough. *Petroleum Geology* 2: 353-360.

Naylor, P.H., Bell, B.R., Jolley, D.W., Durnall, P. and Fredsted, R. 1999. Paleogene magmatism in the Faroe Shetland Basin: influences on uplift history and sedimentation. *In*: Flett, A.J. and Boldy, S.A.R. (eds.) *Petroleum Geology of Northwest Europe: Proceedings of the 5th Conference*. Geological Society, London: 545-558

Nelson, P.H.H. 1966. The James Ross Island Volcanic Group of North-east Graham Land. *British Antarctic Survey Scientific Reports* 54: 1-62.

Nielsen, P.H, Stefánsson, V. and Tulinius, H. 1984. Geophysical logs from Lópra-1 and Vestmanna-1. *In*: Berthelsen, O., Noe-Nygaard, A. and Rasmussen, J. (eds.) *The deep drilling project 1980, 1981 in the Faroe Islands*. Føroya Fróðskaparfelag, Tórshavn: 115-135.

Pedersen, A.K. 1985. Lithostratigraphy of the Tertiary Vaigat Formation on Disko, central West Greenland. *Geological Survey of Greenland Report* 124: 1-30.

Peterson, D.W. and Tilling, R.I. 1980. Transition of basaltic lava from pahoehoe to aa, Kilauea volcano, Hawaii: field observations and key factors. *Journal of Volcanology and Geothermal Research* 7: 271-293.

Planke, S. 1994. Geophysical response of flood basalts from analysis of wireline logs: Ocean Drilling Program Site 642, Vøring volcanic margin. *Journal of Geophysical Research* 99(B5): 9279-9296.

Planke, S., Cerney, B., Bücker, C.J. and Nielsen, O. 1999. Alteration effects on petrophysical properties of subaerial flood basalts: Site 990, Southeast Greenland Margin. *In*: Larsen, H.C., Dunca, R.A., Allan, J.F. and Brooks, K. (eds.) *Proceedings of Ocean Drilling Program*, Scientific Results 163: 17-28.

Richardson, K.R., Smallwood, J.R., White, R.S., Snyder, D. and Maguire, P.K.H. 1998. Crustal structure beneath the Faroe Islands and the Faroe-Iceland Ridge. *Tectonophysics* 300: 159-180.

Richardson, K.R., White, R.S., England, R.W. and Fruehn, J. 1999. Crustal structure east of the Faroe Islands mapping sub-basalt sediments using wide-angle seismic data. *Petroleum Geoscience* 5: 161-172.

Shaw F., Worthington M.H., White R.S., Andersen M.S., Petersen U.K. and the SeiFaBa Group 2007. Seismic attenuation in Faroe Islands basalts. *Geophysical Prospecting* 56: 5-20.

Single, R.T. and Jerram, D.A. 2004. The 3D facies architecture of flood basalt provinces and their internal heterogeneity: examples from the Palaeogene Skye Lava field. *Journal of the Geological Society*, London 161: 911-926.

Sheldon, N.D. 2003. Pedogenesis and Geochemical Alteration of the Picture Gorge Subgroup, Columbia River Basalt, Oregon. *Geological Society of America Bulletin* 115 (11): 1377-1387.

Smythe, D.K., Chalmers, J.A., Skuce, A.G., Dobinson, A. and Mould, A.S. 1983. Early opening history of the North Atlantic -I. Structure and origin of the Faeroe-Shetland Escarpment. *Geophysical Journal of the Royal Astronomical Society* 72: 373-398.

Thordarson, T. and Self, S. 1998. The Roza Member, Colombia River Basalt group. A gigantic pahoehoe lava flow field formed by endogeneous processes?. *Journal of Geophysical Research* 103: 411-445.

Versey, H.R. and Singh, B.K. 1989. Groundwater in the Deccan basalts of the Betwa Basin, India. *Journal of Hydrology* 58: 276-306.

White, N. and Lovell, B. 1997. Measuring the pulse of a plume with the sedimentary record. *Nature* 387(6636): 888-891.

White, R.S. and McKenzie, D. 1989. Magmatism at rift zones: the generation of volcanic margins and flood basalts. *Journal of Geophysical Research* 94: 7685-7729.

Wilmoth, R.A. and Walker, G.P.L. 1993. P-type and S-type pahoehoe: a study of vesicle distribution patterns in Hawaiian lava flows. *Journal of Volcanology and Geothermal Research* 55: 129-142.